
Editors:

Miloš Marjanović, University of Belgrade, Faculty of Mining and Geology

Uroš Đurić, University of Belgrade, Faculty of Civil Engineering

Proceedings of the 6th Regional Symposium on

LANDSLIDES

In the Adriatic-Balkan Region,

[ReSyLAB2024](#), Belgrade, Serbia 15-18th May 2024

Under the auspices of International Consortium
on Landslides (ICL)

University of Belgrade, Faculty of Mining and Geology

May 2024.

Symposium Chairs

Biljana Abolmasov

University of Belgrade, Faculty of Mining and geology
President

Miloš Marjanović

University of Belgrade, Faculty of Mining and geology
Vice president

Uroš Đurić

University of Belgrade, Faculty of Civil Engineering
Secretary

Organizing Committee

Biljana Abolmasov

University of Belgrade, Faculty of Mining and geology

Miloš Marjanović

University of Belgrade, Faculty of Mining and geology

Uroš Đurić

University of Belgrade, Faculty of Civil Engineering

Dragoslav Rakić

University of Belgrade, Faculty of Mining and Geology

Gordana Hadži-Niković

University of Belgrade, Faculty of Mining and Geology

Irena Basarić Ikodinović

University of Belgrade, Faculty of Mining and Geology

Zoran Berisavljević

University of Belgrade, Faculty of Mining and Geology

Dušan Berisavljević

University of Belgrade, Faculty of Mining and Geology

Editors

Miloš Marjanović

University of Belgrade, Faculty of Mining and geology

Uroš Đurić

University of Belgrade, Faculty of Civil Engineering

Miloš S. Marjanović

University of Belgrade, Faculty of Civil Engineering

Jelka Krušić

University of Belgrade, Faculty of Mining and Geology

Ksenija Micić

University of Belgrade, Faculty of Civil Engineering

Tina Đurić

University of Belgrade, Faculty of Mining and Geology

Jovana Janković Pantić

University of Belgrade, Faculty of Mining and Geology

Snežana Bogdanović, Associate

University of Belgrade, Faculty of Mining and Geology

Dragana Slavković

CIP d.o.o., Belgrade,

University of Belgrade, Faculty of Mining and Geology

ISBN -978-86-7352-402-3 – University of Belgrade, Faculty of Mining and Geology

<https://doi.org/10.18485/resylab.2024.6>

Published by: University of Belgrade, Faculty of Mining and Geology

For publisher: Biljana Abolmasov

Print: River Print, Belgrade

Cover design: Marijana Sretković - Slovoslagač

Issued: May 2024, 100 copies

CIP - Каталогизација у публикацији Народна библиотека Србије, Београд

551.4.037(082)

624.131.53(082)

624.138(082)

REGIONAL Symposium on Landslides in the Adriatic-Balkan Region (5 ;
2024 ; Beograd)

Proceedings of the 6th Regional Symposium on Landslides in the Adriatic-Balkan
Region, ReSyLAB, Belgrade, 15-18th May 2024 / editors Miloš Marjanović, Uroš
Đurić. - Belgrade : University of Belgrade, Faculty of Mining and Geology, 2024
(Belgrade : River Print). - 328 str. : ilustr. ; 30 cm

Tiraž 120. - Bibliografija uz svaki rad. - Registar.

ISBN 978-86-7352-402-3

a) Клизишта -- Зборници b) Косине -- Зборници

COBISS.SR-ID 144496393

Scientific Programme Committee and Reviewers Board

Biljana Abolmasov

University of Belgrade, Faculty of Mining and Geology
Belgrade, Serbia

Željko Arbanas

University of Rijeka, Faculty of Civil Engineering, Rijeka, Croatia

Sanja Bernat Gazibara

University of Zagreb, Faculty of Mining, Geology and Petroleum Engineering
Zagreb, Croatia

Julijana Bojadijeva

Ss. Cyril and Methodius University, Faculty of Natural Sciences and Mathematics Skopje, North Macedonia

Sanja Dugonjić

University of Rijeka, Faculty of Civil Engineering, Rijeka, Croatia

Uroš Đurić

University of Belgrade, Faculty for Civil Engineering, Belgrade, Serbia

Luigi Gariano Stefano

CNR IRPI, Italy

Michel Jaboyedoff

University of Lausanne, Institute of Earth Sciences, University of Lausanne, Switzerland

Petra Jagodnik

University of Rijeka, Faculty of Civil Engineering, Rijeka, Croatia

Vedran Jagodnik

University of Rijeka, Faculty of Civil Engineering, Rijeka, Croatia

Mateja Jemec Auflič

Geological Survey of Slovenia
Ljubljana, Slovenia

Milorad Jovanovski

Ss. Cyril and Methodius University, Faculty of Civil Engineering, Skopje, North Macedonia

Martin Krkač

University of Zagreb, Faculty of Mining, Geology and Petroleum Engineering, Zagreb, Croatia

Veljko Lapčević

University of Belgrade, Faculty of Mining and Geology, Belgrade, Serbia

Matej Maček
University of Ljubljana, Faculty of Civil and Geodetic Engineering, Ljubljana, Slovenia

Miloš D. Marjanović

University of Belgrade, Faculty of Mining and Geology, Belgrade, Serbia

Miloš S. Marjanović

University of Belgrade, Faculty of Civil Engineering, Belgrade, Serbia

Svetlana Melentijević

Universidad Complutense de Madrid, Spain

Snježana Mihalić Arbanas

University of Zagreb, Faculty of Mining, Geology and Petroleum Engineering
Zagreb, Croatia

Matjaž Mikoš

University of Ljubljana, Faculty of Civil and Geodetic Engineering, Ljubljana, Slovenia

Jovan Papić

Ss. Cyril and Methodius University, Faculty of Civil Engineering
Skopje, North Macedonia

Dario Peduto

University of Salerno, Department of Civil Engineering, Fisciano, Italy

Josip Peranić

University of Rijeka, Faculty of Civil Engineering, Rijeka, Croatia

Igor Peševski

Ss. Cyril and Methodius University, Faculty of Civil Engineering, Skopje, North Macedonia

Tina Peternel

Geological Survey of Slovenia
Ljubljana, Slovenia

Tomislav Popit

University of Ljubljana, Faculty of Natural Sciences and Engineering
Ljubljana, Slovenia

Vlatko Šešov

Ss. Cyril and Methodius University, Faculty of Natural Sciences and Mathematics
Skopje, North Macedonia

Timotej Verbovšek

University of Ljubljana, Faculty of Natural Sciences and Engineering, Ljubljana, Slovenia

Martina Vivoda Prodan

University of Rijeka, Faculty of Civil Engineering, Rijeka, Croatia

Sabid Zekan

University of Tuzla, Faculty of Mining, Geology and Civil Engineering,
Tuzla, Bosnia and Herzegovina

Cvjetko Sandić

University of Banja Luka, Mining Faculty – Prijedor & Geological Survey of the Republic of Srpska, Zvornik Bosnia and Herzegovina

Foreword

The 6th Regional Symposium on Landslides in Adriatic-Balkan Region (6th ReSYLAB) will be held in Belgrade, Serbia, under the auspices of International Consortium on Landslides (ICL). In the moment when the World is at the turning point, and demanding times and events caused by climate change are in front of landslide scientists, the 6th ReSYLAB is an important event for the regional landslide community but also for ICL and its regional Adriatic-Balkan Network (ABN).

The Adriatic-Balkan Network was established in January 2012 as one of eight regional and thematic ICL networks to promote activities of the ICL and the International Programme on Landslides (IPL) approved at the 10th Anniversary Meeting of ICL held in Kyoto, Japan, in January 2012. The general objective of the ABN is advancing landslide science and its practical application in the region for the benefit of society and the environment. Already next year after ABN establishment, in March 2013, the 1st Regional Symposiums on Landslides in Adriatic-Balkan Region, entitled Landslide and Flood Hazard Assessment, in Zagreb, Croatia, was organized by Croatian Landslide Group, consisted of scientists from University of Zagreb, Faculty of Mining, Geology and Petroleum Engineering, Croatia, and University of Rijeka, Faculty Civil Engineering, Croatia. That was the beginning of ReSYLAB followed by successful symposiums held in Belgrade, Serbia in 2015, Ljubljana, Slovenia in 2017, Sarajevo, Bosnia and Herzegovina in 2019; and in Rijeka, Croatia in 2022, one year moved because of Covid 19 Pandemic.

The Kyoto Landslide Commitment (KLC2020) launched by ICL in 2020 for the global promotion of understanding and reducing landslide disaster risk with one of main priority actions to facilitate and access its progress and fostering through organization of different types of meetings and events at national, regional and global levels has a successful support and contribution through ABN ReSyLAB organizations and sharing ideas, good practices, experiences and policies related with landslide risk reduction in the region. Although the ReSyLAB is the only one of regional symposiums that was continuously sustained, a decrease in regional cooperation within ABN can be observed in the recent years. The ABN needs improvements and strengthening of cooperation and revival of activities in landslide risk reduction between ABN members that will guarantee the further sustainability of ReSyLAB.

The 6th ReSyLAB gathers the scientists from the Adriatic-Balkan region, but also from the other countries throughout Europe, and elsewhere that enables sharing the landslide knowledge divided in five main topics: Landslide remote sensing, monitoring, and early warning; Landslide susceptibility hazard and risk assessment; Climate change and landslides; Testing, modelling and mitigation of landslides; and Landslides in practice – mining and infrastructure. The recent achievements will be presented in series of invited and keynote lectures, thus the world knowledge will be presented in the region, which is especially important for young landslide scientists.

I am very grateful for the effort to organize the 6th ReSyLAB under the auspices of ICL and to publish this valuable publication. I wish the landslide community a very successful meeting and to take an advantage of the opportunity for establishment of new collaborations.



Željko Arbanas

President of International Consortium on Landslides
Rijeka, Croatia

Editorial preface

A great responsibility and even greater honour were put before us some two years ago, in Rijeka (Croatia) where the previous gathering of landslide scientists, researchers, practitioners and enthusiasts from the Adriatic-Balkan Region and beyond took place. We did not have an easy task of outperforming or matching previous organizers, including ourselves from 2015, when very positive and rich feedback was received. In times of expanding needs to communicate experiences and solutions for landslide issues, which are indeed multidisciplinary, we have tried to summon the most esteemed experts to share their wisdom in a series of keynote lectures covering the state-of-the-art landslide topics, followed by invited lectures of established young experts, and last but not the least, our colleagues, landslide researchers from various background, engineering-geological, civil engineering, geotechnical engineering, geodetic engineering, etc. In hope we have met the standards set long ago in this International Consortium on Landslide (ICL) series, and cherished through previous five assemblies, the 6th Regional Symposium on Landslides in Adriatic-Balkan Region (6th ReSyLAB) warmly welcomes authors and participants from 14 countries, with 50 contributions split into five themes:

1. Landslide remote sensing, monitoring, and early warning;
2. Landslide susceptibility hazard and risk assessment;
3. Climate change and landslides;
4. Testing, modelling and mitigation of landslides;
5. Landslides in practice – mining and infrastructure

We will take the opportunity to recollect a decade after the catastrophic landslides and floods that hit the Region in 2014 and adapt the Symposium topics to reflect what has been done in the meantime and what can be expected in the future, with changing climate on one side and intensified infrastructural projects on the other.

We would like to use this opportunity to thank the ICL for providing us with such an efficient framework to extend our connectivity throughout the Region and beyond. We would like to thank the Faculty Dean and ICL Europe vice president prof. Biljana Abolmasov for providing us with needed institutional support in demanding preparations for such an important event. Special thanks go to our keynote and invited lectures and all participants, authors and co-authors for promoting our field with us. We are also very grateful to the scientific board members for taking part in the copious review process and our sponsors for making this possible from a financial point of view. Last, but not least, we would like to thank all our organizing board members, the faculty staff, technical, IT and financial departments, especially members of the Department of Geotechnics and our volunteering students for coming to aid and making this demanding task easier and more worthwhile.



Miloš Marjanović

University of Belgrade
Faculty of Mining and
Geology

Vice president
of the 6th ReSyLAB
Organizing Committee



Uroš Đurić

University of Belgrade,
Faculty of Civil
Engineering

Secretary
of the 6th ReSyLAB
Organizing Committee

Contents

Keynote lectures

Multi-source data analysis in slow-moving landslide-affected built-up environment: case studies in Calabria region (southern Italy)1

Dario Peduto, Gianfranco Nicodemo, Davide Luongo, Settimio Ferlisi, Luigi Borrelli, Diego Reale, Gianfranco Fornaro, Giovanni Gullà

Landslide susceptibility assessment: Chicken or the egg for the risk analysis? 9

Michel Jaboyedoff

Prediction of rainfall-induced landslides in a changing climate: issues and perspectives for regional-scale approaches19

Stefano Luigi Gariano

Seismic Performance Assessments of Embankments27

Kemal Onder Cetin, Anil Yunatci, Bilal Umut Ayhan

Invited lectures

Integral approach in stability analyses for weak anisotropic rocks37

Milorad Jovanovski, Bojan Janevski, Igor Peshevski

High-Precision Landslide Monitoring Using Laser Scanning Technology47

Marko Pejić

Landslide mapping and zonation at national, regional and local scale - Recent experiences from Republic of Macedonia55

Igor Peshevski, Milorad Jovanovski, Dario Peduto, Natasha Nedelkowska, Gjorgi Gjorgiev

Landslide Risks in the Western Balkans Under the Climate Change65

Mirjam Vujadinović Mandić

Determination of the soil-water characteristic curve of the soil by physical modelling tests73

Josip Peranić, Martina Vivoda Prodan, Nina Čeh, Rea Škuflić, Željko Arbanas

Tailings Dam Stability Evaluation using 3D Numerical Modelling 81

Veljko Lapčević, Slavko Torbica

Digital Twin Concept for the Safe and Economic Design and Management of Rock Slopes..... 89

Neil Bar

Landslide remote sensing, monitoring, and early warning

- Interpretation challenges when detecting landslides in flysch environment: examples from visual analysis of LiDAR DTM in the City of Buzet** 99
Petra Jagodnik, Sanja Bernat Gazibara, Federica Fiorucci, Michele Santangelo
- Evaluating the Effectiveness of Deep Learning Algorithms and InSAR Data in Early Warning Systems for Landslide Risk Mitigation**..... 107
Mohammad Amin Khalili, Chiara Di Muro, Luigi Guerriero, Massimo Ramondini, Domenico Calcaterra, Diego Di Martire
- Application of drone photogrammetry in hazard assessment in Međine municipality** 115
Nino Salčin
- Monitoring of the Active Landslide during Excavation of Slopes for the Svračkovo Dam Stilling Basin**121
Nemanja Babović, Dragana Aleksić, Aleksandar Miladinović
- Detection and monitoring of slope movement by using point cloud derived from the SfM technique** 127
Igor Ivanovski, Natasha Nedelkovska, Gose Petrov, Milorad Jovanovski, Toni Nikolovski, Igor Peshevski
- Advanced geospatial solutions for monitoring, modeling and understanding of landslides**133
Ankica Milinković, Goran Stepanović
- Landslide susceptibility assessment of the Teslić municipality, in the Republic of Srpska, B&H**..... 139
Cvjetko Sandić
- Influence of the landslide inventory sampling on the accuracy of the susceptibility modelling using Random Forests: A case study from the NW Croatia**..... 143
Marko Sinčić, Sanja Bernat Gazibara, Mauro Rossi, Martin Krkač, Hrvoje Lukačić, Snježana Mihalić Arbanas
- Large-scale landslide susceptibility models: Examples and conclusions from the modelling of small and shallow landslides in the continental part of Croatia** 149
Sanja Bernat Gazibara, Marko Sinčić, Mauro Rossi, Martin Krkač, Hrvoje Lukačić, Petra Jagodnik, Snježana Mihalić Arbanas
- Landslide susceptibility assessment using Frequency Ratio model for the Polog region, Macedonia**157
Natasha Nedelkovska, Milorad Jovanovski, Igor Peshevski, Natasha M. Andreevska, Gjorgji Gjorgiev
- Žirovac landslide: a case study of the local scale landslide investigation for engineering purposes with its assessment on a regional scale** 163
Davor Marušić

Investigating the factors governing the damage occurrence on buildings exposed to slow-moving landslide risk.....	169
<i>Gianfranco Nicodemo, Dario Peduto, Davide Luongo, Settimio Ferlisi, Luigi Borrelli, Diego Reale, Gianfranco Fornaro, Giovanni Gullà</i>	
Harmonized approach for earthquake - induced landslide susceptibility and risk assessment in Vodno urban area	175
<i>Done Nikolovski, Radmila Salic Makreska, Kemal Edip, Julijana Bojadjieva</i>	
Preliminary landslide hazard map of Serbia	181
<i>Miloš Marjanović, Olivera Kitanović, Saša Todorović</i>	
Assessment of risk scenarios to support landslide studies	187
<i>Giovanna Capparelli, Pasquale Versace, Danilo Spina</i>	
Regional landslide susceptibility assessment: case studies from Greece.....	193
<i>Katerina Kavoura, Natalia Spanou, Emmanuel Apostolidis, Panagiota Kokkali</i>	
Climate change and landslides	
Landslide events in Slovenia 2023: causes and consequences	199
<i>Mateja Jemec Auflič, Jernej Jež, Ela Šegina, Tina Peternel, Andrej Novak, Špela Kumelj, Domen Turk</i>	
Landslide impact on road infrastructure in the Western Balkans	203
<i>Miloš Marjanović, Ivana Stevanović, Danijel Vučković, Aleksandar Bajović, Nedim Begović, Hoxha Nerejda</i>	
Alpine rock slope failures, rockfalls and debris flows in a changing climate and their anticipation	207
<i>Michael Krautblatter</i>	
Testing, modelling and mitigation of landslides	
Rapid 3D rockfall susceptibility assessment of the Orašac rock slope, Croatia	213
<i>Hrvoje Lukačić, Josip Katić, Sanja Bernat Gazibara, Snježana Mihalić Arbanas, Martin Krkač</i>	
Fines content influence on the dynamic slope behavior in small-scale physical models.....	219
<i>Vedran Jagodnik, Davor Marušić, Željko Arbanas, Nina Čeh, Josip Peranić, Martina Vivoda Prodan</i>	
Influence of precipitation and soil conditions on the Krbavčići Landslide reactivation (Istria Peninsula, Croatia)	225
<i>Martina Vivoda Prodan, Josip Peranić, Vedran Jagodnik, Hendy Setiawan, Željko Arbanas</i>	
Debris-flow Susceptibility Assessment in Flow-R: Ribnica River Case Study	231
<i>Ksenija Micić, Miloš Marjanović, Biljana Abolmasov</i>	

Optimization of pipeline design solutions for slope stability in Sakhalin region, Russia	239
<i>Michael Naumov, Denis Gorobtsov, Daria Shubina</i>	
Assessment of landslide stability of ground cuts in Permian sediments of the Urzhum stage in the territory of the Volga uplands (Russia).....	243
<i>Fedor Bufejev, Airat Latypov, Anastasiya Garaeva, Kirill Gudoshnikov, Albert Korolev</i>	
Temperature and rate effects on the residual shear strength of clays: a state of the art.....	247
<i>Gianvito Scaringi, Marco Loche</i>	
Landslides in practice – mining and infrastructure	
Landslide information for land management and planning: Examples from Italy and Croatia.....	253
<i>Paola Reichenbach, Snjezana Mihalić Arbanas, Mauro Rossi, Sanja Bernat Gazibara</i>	
Rock collapse structure on the Liburnian coast (Rijeka Bay, NE Adriatic)	259
<i>Čedomir Benac, Sanja Dugonjić Jovančević, Martina Vivoda Prodan, Lovro Maglić</i>	
Geological-Geotechnical Exploration for the Landslide mitigation Section at the Old Cemetery in Smederevo.....	265
<i>Ivica Tornjanski, Aleksandar Tokin, Nemanja Stanić</i>	
Slope stabilization and erosion control using a Naturally based solution with Biopolymers	271
<i>Aleksandra Nikolovska Atanasovska, Josif Josifovski</i>	
Slope stability back analysis and a proposition for rehabilitation of landslide on the road section Gornji Milanovac – Klatičevo.....	277
<i>Dragana Slavković, Milan Kandić, Ivan Stefanović, Vladimir Filipović</i>	
Addressing Rockfall Challenges in flysch environment - A case study from Greece	283
<i>Themistoklis Chatzitheodosiou, Ioannis Farmakis, George Prountzopoulos, George Stoumpos, Dimitra Papouli, Thomas Thomaidis, Vassilis Marinos</i>	
Geotechnical Conditions, Stability Analysis and Remedial Measures of Višnjička 74 Landslide in Belgrade	291
<i>Uroš Đurić, Sanja Jocković, Miloš S. Marjanović, Veljko Pujević, Ksenija Micić, Zoran Radić, Milena Raković</i>	
Landslide mapping for the regional gas pipeline construction near Priboj (Serbia).....	297
<i>Katarina Andrejev, Miloš Marjanović, Rastko Petrović</i>	
Failure estimation of the Majdanpek open pit east face based on inverse velocity model	303
<i>Miloš Marjanović, Stefan Milanović, Nikola Simić, Lazar Kričak</i>	

Geotechnical conditions of cut 5 on the highway A1, section Gornje Polje-Caričina Dolina	309
<i>Lazar Jovanović, Biljana Abolmasov</i>	
Second phase of Landslide stabilisation on Cut 3, LOT 1, Motorway E75, section Gornje Polje – Caričina dolina	315
<i>Marina Janković, Marija Bakrač</i>	
On the Performance and Related Design Considerations of Geosynthetic Reinforced Soil Structures under Seismic Conditions.....	321
<i>Ehsan Bordbar, Viktor Poberezhnyi, Thomas Hasslacher , Marija Bakrač</i>	
AUTHOR INDEX.....	327

Multi-source data analysis in slow-moving landslide-affected built-up environment: case studies in Calabria region (southern Italy)

Dario Peduto^{(1)*}, Gianfranco Nicodemo⁽¹⁾, Davide Luongo⁽¹⁾, Settimio Ferlisi⁽¹⁾, Luigi Borrelli⁽²⁾, Diego Reale⁽³⁾, Gianfranco Fornaro⁽³⁾, Giovanni Gullà⁽²⁾

1) Department of Civil Engineering, University of Salerno, Via Giovanni Paolo II, 132, 84084 - Fisciano (SA), Italy (dpeduto@unisa.it, gnicodemo@unisa.it, dluongo@unisa.it, sferlisi@unisa.it)

2) Research Institute for Geo-Hydrological Protection (CNR-IRPI), National Research Council of Italy, Via Cavour n. 4/6, 87030, Cosenza, Italy (borrelli@irpi.cnr.it; giovanni.gulla@irpi.cnr.it)

3) Institute for Electromagnetic Sensing of the Environment (IREA – CNR), National Research Council of Italy, Via Diocleziano 328, 80124 Naples, Italy (reale.d@irea.cnr.it; fornaro.g@irea.cnr.it)

Abstract The paper deals with a key step of slow-moving landslide risk analysis such as the vulnerability estimation of the interacting facilities (e.g., buildings, roads) via the exploitation of multi-source multi-temporal data. These latter include information gathered from conventional multi-source (geological, geomorphological and geotechnical) data, which are integrated with non-invasive spaceborne remote sensing monitoring (e.g., Differential Interferometric techniques), in-situ and virtual surveying (e.g., Google Street view imagery). The approach proposed in this work relies on the methodological frameworks developed by the authors within a 20-year multidisciplinary research activity. Two case studies in Calabria region (southern Italy) affected by several slow-moving landslides, which caused damage to the built environment, were selected. The analysis of the available monitoring data allowed i) characterizing slow-moving landslides and ii) generating predictive tools for estimating the degree of loss (inherently related to the expected damage) of the exposed facilities. Once further validated, the proposed circular approach could be part of a procedure for prioritizing building/road (extraordinary) maintenance activities and scheduling/implementing risk mitigation measures.

Keywords slow-moving landslides, circular approach, built-up environment, monitoring/surveying data, damage, risk, buildings, roads.

Introduction

Landslides yearly cause huge losses worldwide in terms of consequences on either people (i.e., injury and life losses) or the built-up environment (i.e., damages of different severity levels to structures and infrastructure).

The analysis of consequences induced by a landslide represents a key step for estimating the risk to which people and/or (infra)structures interacting with a landslide are (or can be) exposed (Fell et al., 2008). Focusing on slow-moving landslides, consequence analysis involves identifying/quantifying the structures (i.e., buildings) and/or the infrastructures (i.e., roads) at

risk as well as estimating their vulnerability (Peduto et al., 2017; Argyroudis et al., 2019). This latter depends on both the landslide intensity (in terms of spatially-distributed parameter related to the landslide destructiveness) and peculiar features of the exposed facilities (e.g., geometry, material properties, state of maintenance, structural and foundation typology for buildings). Therefore, its estimation is a difficult task that entails a thorough knowledge of both the landslide mechanisms (Mavrouli et al. 2014; Peduto et al., 2018) and the behaviour of the exposed elements (Ferlisi et al., 2019) as well as the monitoring of landslide intensity parameters (Peduto et al., 2017).

Nowadays, the technological innovation in monitoring systems (both ground-based or remotely operating) offers the concrete possibility to access unprecedented rich datasets that the landslide community can profitably use for risk analysis purposes. In this regard, the present paper aims at providing an example of how multi-source monitoring/surveying conventional or innovative data can complement with each other to enhance vulnerability analysis and/or forecasting capabilities in the field of landslide consequence analysis.

Proposed approach

The approach proposed to investigate the vulnerability of structures and infrastructures in landslide-affected urban areas includes three main phases (Fig. 1).

The first phase (Phase I) pursues the detection of the elements at risk (i.e. buildings and/or road networks). According to the scale of analysis, quality and resolution of the used data (Ferlisi et al., 2019), they are identified by overlapping base and thematic maps (e.g., built-up area map, DEM, landslide inventory map) with available observations (e.g., optical imagery) and/or monitoring (i.e., provided by conventional or innovative field/remote monitoring techniques) data (Peduto et al., 2018; Greenwood et al., 2019).

In Phase II, a damage severity level (DL) as well as a value of the intensity parameter (IP) are assigned to every identified exposed element. In particular, the DL is

classified based on the analysis of field and/or remote surveys adopting a proper damage ranking. The selected IP (e.g., velocity, settlement or related parameters) is computed based on the quality and resolution of available monitoring data.

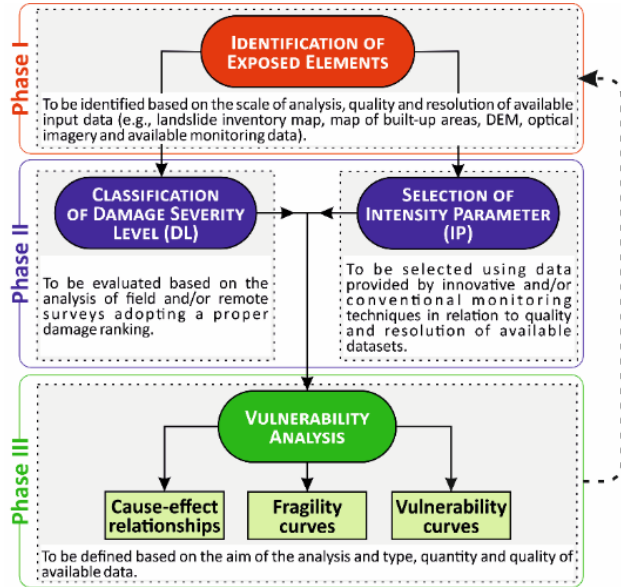


Fig. 1 Flowchart of the proposed approach (Peduto et al., 2021).

In Phase III, the recorded DL and the retrieved magnitude of IP are combined to analyse the vulnerability of the exposed elements.

For this purpose, data are treated based on the aim of the study (i.e., in relation to the scale of analysis), the type (i.e., empirical or numerical) of the analysis, the quantity and quality of available data, via deterministic (i.e., intended to investigate the established relationships between the cause (IP) and effect (DL)) or probabilistic (i.e., aimed at generating consequence forecasting tools such as fragility and/or vulnerability curves) approaches (Ferlisi et al., 2019).

Particularly, DInSAR-derived IP can be first merged with the recorded DLi to retrieve the cause (IP) - effect (DL) relationship; then, according to the procedure described by Peduto et al. (2017, 2018), assuming the log-normal distribution function as probabilistic model, empirical fragility curves providing the conditional probability for a randomly selected building/road section at risk to be in, or exceed, a certain DL when the IP equals a given value can be generated via Eq.(1):

$$P(\text{Damage} \geq \text{DLi} | \text{IP}) = \Phi \left[\frac{1}{\beta_i} \ln \frac{\text{IP}}{\bar{\text{IP}}} \right] \quad (1)$$

where the fragility parameters associated with the standard normal cumulative distribution function $\Phi[\cdot]$ are the median value of the selected intensity parameter ($\bar{\text{IP}}$) and the standard deviation (β_i) of the natural logarithm of the (IP) values.

Then, the vulnerability curve can be used to quantitatively link the expected average level of damage

severity (μ_{DL}) and the IP (Eq.2) considering for each DLi the discrete probability (P_i) retrieved from the previously generated fragility curves with an associated numerical index d_i (ranging from 0 to 1 according to DLi).

$$\mu_{DL}(\text{IP}) = \sum_{i=1}^3 P_i * d_i(2)$$

Finally, using the tangent hyperbolic function (Lagomarsino and Giovinazzi, 2006) as regression model to fit the empirical data, the empirical vulnerability curve, which relates the expected mean level of damage severity (μ_D) to a given exposed element to an IP value, can be derived (Eq. 3).

$$\mu_D = a[b + \tanh(c * \text{IP} + d)] \quad (3)$$

where a, b, c and d are four coefficients determined for the investigated sample of elements at risk using the least mean square method.

Results

Two well-documented case studies in Calabria region (southern Italy) were analysed. As for buildings, the urban centre of the Lungro town, which has been extensively suffering from several slope instabilities that caused damage of different severity to the built-up area, was selected. The SS660 road, which is affected by several ground displacements that over time have caused frequent closures to vehicle traffic, was chosen as test infrastructure. It consists of a 7 m-wide single carriageway with two traffic lanes that represent the main access to Acri town.

Lungro case study

The urban area of Lungro (Fig. 2), located at 650 m a.s.l. in the northern sector of the Calabria region, presents a complex geological context in which the Lungro-Verbicaro Unit dating back to the Middle Trias made up of metapelites and metacarbonates prevails (Gullà et al., 2017). The urban centre is widely affected by slow-moving landslides with either active or dormant state based on geomorphological criteria (Fig. 2a).

Consequently, over the years, several damages (Fig. 2a) were recorded to both masonry buildings – mainly located in the historic centre and its surroundings (Carmine and Lafcantino), made up of 2–3 floors with pebbles, or erratic/irregular stones on shallow foundations – and reinforced concrete buildings up to 5–6 floors mainly located in the San Leonardo area, built since the early 1950–1960s (Peduto et al., 2017, 2018).

Previous studies in the area (Gullà et al., 2017) typified the inventoried slow-moving landslides in six categories (Fig. 2a), through the application of the "aPosIn" procedure that relies on the combination of geological information, geomorphological criteria and both geotechnical and remote displacement monitoring data. These categories differ for geometric and kinematic characteristics, involved soils, and type of movement.

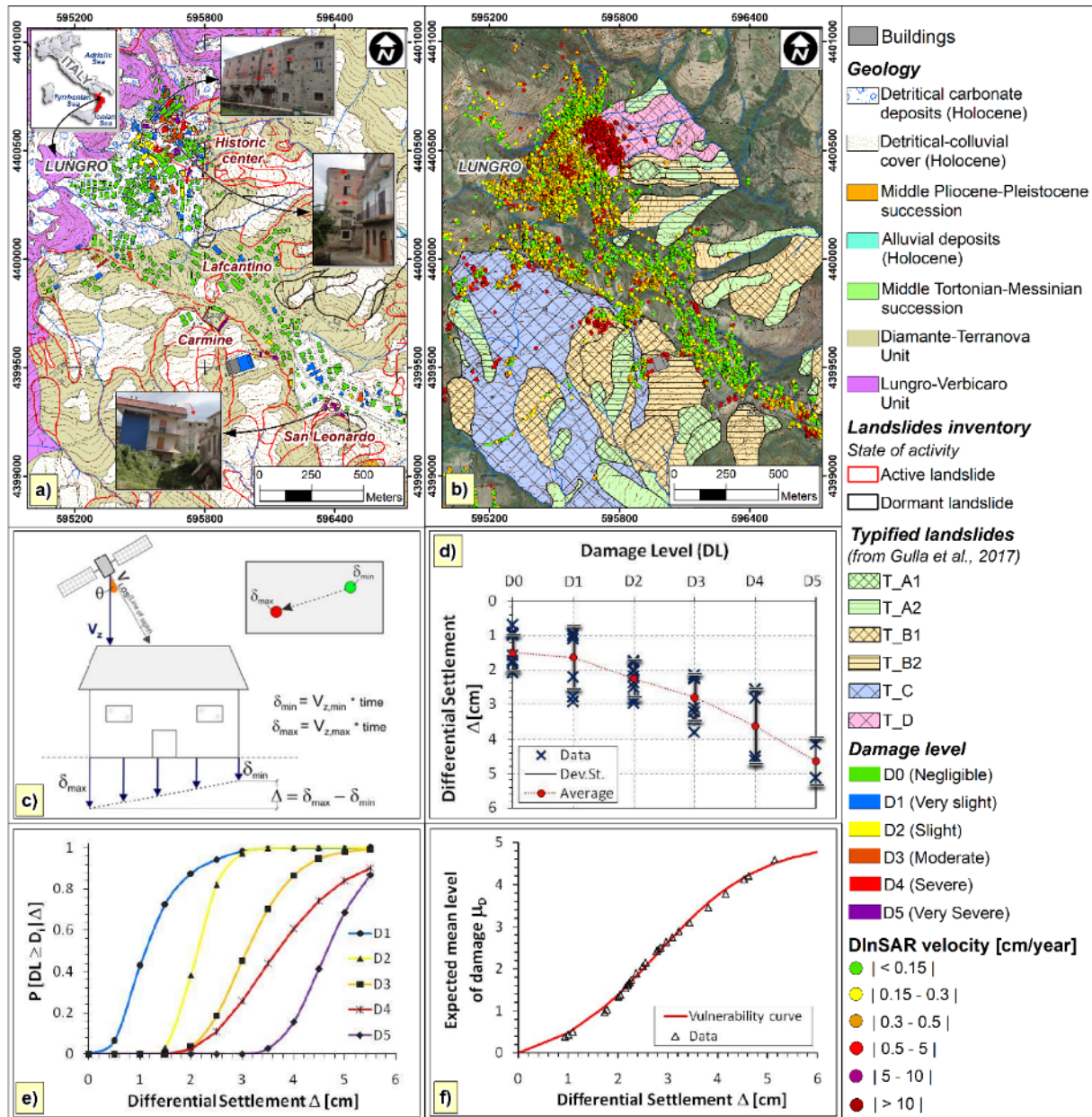


Fig. 2 Lungro case study: a) geological and landslide inventory maps along with their state of activity (modified from Gullà et al., 2017) and building damage map with some examples of crack patterns exhibited by both reinforced concrete and masonry buildings (modified from Peduto et al., 2017); b) map of typified landslides with spatial distribution of DInSAR data acquired by COSMO-SkyMed satellite (ascending orbit, 2012–2014) (modified from Gullà et al., 2017 and Peduto et al., 2018); c) sketch of the DInSAR-derived differential settlement (Δ) of a building; d) damage level (DLi) vs. differential settlements (Δ); e) empirical fragility curves and f) vulnerability curve for masonry buildings in Lungro area (Peduto et al., 2021).

In the area, in addition to deep and surface displacement monitoring data deriving from conventional (inclinometers and GPS) techniques (Gullà et al., 2017; Peduto et al., 2018), innovative monitoring data provided by the interferometric processing of spaceborne synthetic aperture radar images (DInSAR) acquired by Envisat (period August 2003 to January 2010) and COSMO-SkyMed (period October 2012 to April 2014) radar sensors are available. Fig. 2b shows the spatial distribution of the DInSAR coherent pixel velocities derived from the processing of COSMO-SkyMed images on ascending orbit, which were processed according to the SAR tomographic

analysis (Fornaro et al., 2009) which proved to be particularly effective for monitoring built-up areas (Peduto et al., 2017, Nicodemo et al., 2018).

Following the described approach (Fig. 1), in Phase I, single buildings exposed to landslide risk were identified by combining the available input data. Then, in Phase II, both DL and IP were estimated. The former was assigned to each single building (Fig. 2a) based on the data collected via ad-hoc predisposed building fact-sheets (Ferlisi et al., 2015; Peduto et al., 2017) during an extensive in-situ damage survey carried out in October 2015 (including the whole urban area over a total of 540 buildings). The recorded DLs

were categorized by adapting the classification system proposed by Burland et al. (1977) on the basis of the visual interpretation of crack patterns exhibited by the building façades considering six categories (D₀ = negligible; D₁ = very slight; D₂ = slight; D₃ = moderate; D₄ = severe; D₅ = very severe). The IP was assumed as the differential settlement (Δ) computed using the DInSAR data on 49 exposed single buildings (12 of reinforced concrete and 37 of masonry structure) out of 111 total buildings interacting with slow-moving landslides; for this purpose, only those buildings covered by at least two coherent DInSAR benchmarks in both Envisat and COSMO-SkyMed datasets were considered. The DInSAR-derived differential settlement (Δ) was computed as the maximum difference (Fig. 2c) of the cumulative settlements (δ , derived by multiplying the DInSAR velocity along the vertical direction for the observation period of both available SAR datasets) recorded by the DInSAR benchmarks within the building perimeter (Peduto et al., 2017). In the last phase (Phase III), referring to 37 masonry buildings composing a homogeneous sample (i.e., masonry 2-3 floored structures on shallow foundations) and exhibiting all the different damage severity levels (i.e., from D₁ to D₅), the building vulnerability was investigated. First, Fig. 2d shows a generally increasing trend of DL when Δ increases. Then, empirical fragility curves for randomly selected buildings at risk in Lungro town were generated using Eq. 1 (Fig. 2e) by estimating the fragility parameters pertaining to each DLi. Finally, the empirical vulnerability curve (Fig. 2f) was derived by interpolating, using the Eq. 3, the values of the averagely expected damage severity level (μ_{DL}) derived through the adoption of the Eq. 2 with a numerical index di equal to 0.2, 0.4, 0.6, 0.8 and 1 for D₁, D₂, D₃, D₄ and D₅, respectively.

State Road SS660 case study

The study area, located along the western border of the Sila Massif (northern sector of the Calabria region), falls within the middle portion of the Mucone River basin and includes the town of Acri (Fig. 3). The climate is Mediterranean with dry summer and precipitation concentrated during mild winters (Terranova et al. 2007). The area, ranging in elevation from 300 to 900 m a.s.l., is made by high-grade metamorphic rocks of Palaeozoic age, which result intensely weathered (Borrelli et al. 2007; Borrelli et al. 2014). Landslides (Fig. 3a, b) (mainly active and dormant slide-debris flows, debris slides, and rockslides) are widespread along the Mucone River, where the local relief energy, steep slopes, and gravitational landforms are commonly associated with fault zones. Landslides can be distinguished in three categories (i.e. shallow, medium-deep, and deep-seated) based on geomorphological criteria (Borrelli and Gullà 2017), Figure 3b. In addition, a large Deep-Seated Gravitational Slope Deformation of Sackung-type (Serra di Buda DSGSDs) affects the study area (Borrelli and Gullà 2017), Figure 3a,

b. This DSGSD, with a depth equal or higher than 200 m, has a length of about 1.2 km, a width of 3 km and a surface of 3 km². The typical features of this phenomenon, partially covered by shallow, medium-deep and deep landslides, are summit crown-shaped scarps, terrace-like flats, convex slope profiles, and foot protrusions towards the bed of the watercourses. The geomaterials (Fig. 3b) produced by weathering and degraded processes of the gneissic rocks in the study area and in similar geological context can be framed among residual-colluvial soils to saprolitic soils (Cascini and Gullà 1993); their connection with tectonic sub-horizontal structures favour the formation of deep-seated failure surfaces, as in the case of Serra di Buda slow-moving landslide. In Phase I, the road stretch exposed to landslide risk was identified by combining the available input data (Fig. 3a). Then, in Phase II, both IP and DL and were estimated. Particularly, PS velocity values (Fig. 3a) were projected from the LOS to the steepest slope direction following the procedure proposed by Cascini et al. (2010), also fixing a threshold of 4 to the projection coefficient of the 1750 projected PSs for COSMO-SkyMed dataset over the SS660. Then, starting from the landslide inventory map reported in Borrelli and Gullà (2017) and focusing on the Serra di Buda slope, the landslides in the area were typified (Fig. 3b). A multi-temporal analysis of the damage was carried out and the recorded damage was ranked in four increasing DLi (D₀ = negligible; D₁ = slight; D₂ = moderate; D₃ = severe) including both the asphalt pavement (see Ferlisi et al. 2021) and the side retaining structures for the cut-and-fill slope sections of the SS660. Referring to the results of the in-situ survey carried out on 14 December 2021, 69 damaged sections were identified and distinguished according to the severity level recorded to both the asphalt pavement and the side retaining structures. Some photos of the most damaged locations are shown in Fig. 3c. The map in Fig. 3b shows the lengths of the sections with uniform levels of damage that were computed by dividing in two parts the distance between two damaged sections and attributing them the DLi of the closest damaged section in the observation period. The availability of multi-temporal damage data revealed that the damage mainly concentrated in the Serra di Buda rockslide due to its reactivation in 2005 and 2010 (Gullà 2014). In the period 2011 - 2021, a replacement of the road surface was carried out as revealed by the archive photos systematically acquired by the IRPI-CNR. To estimate the IP, first a buffer with a radius of 10 m was drawn around each damaged road section and the PSs located within its perimeter were selected; then, the mean slope velocity of the k_{th} buffer was computed as the root mean square weighted PS velocity along the steepest slope direction (as proposed by Cascini et al. 2013). The cumulative displacement (δ_{slope}) pertaining to k_{th} buffer was assumed as the IP and computed by multiplying the velocity value for the observation period (t).

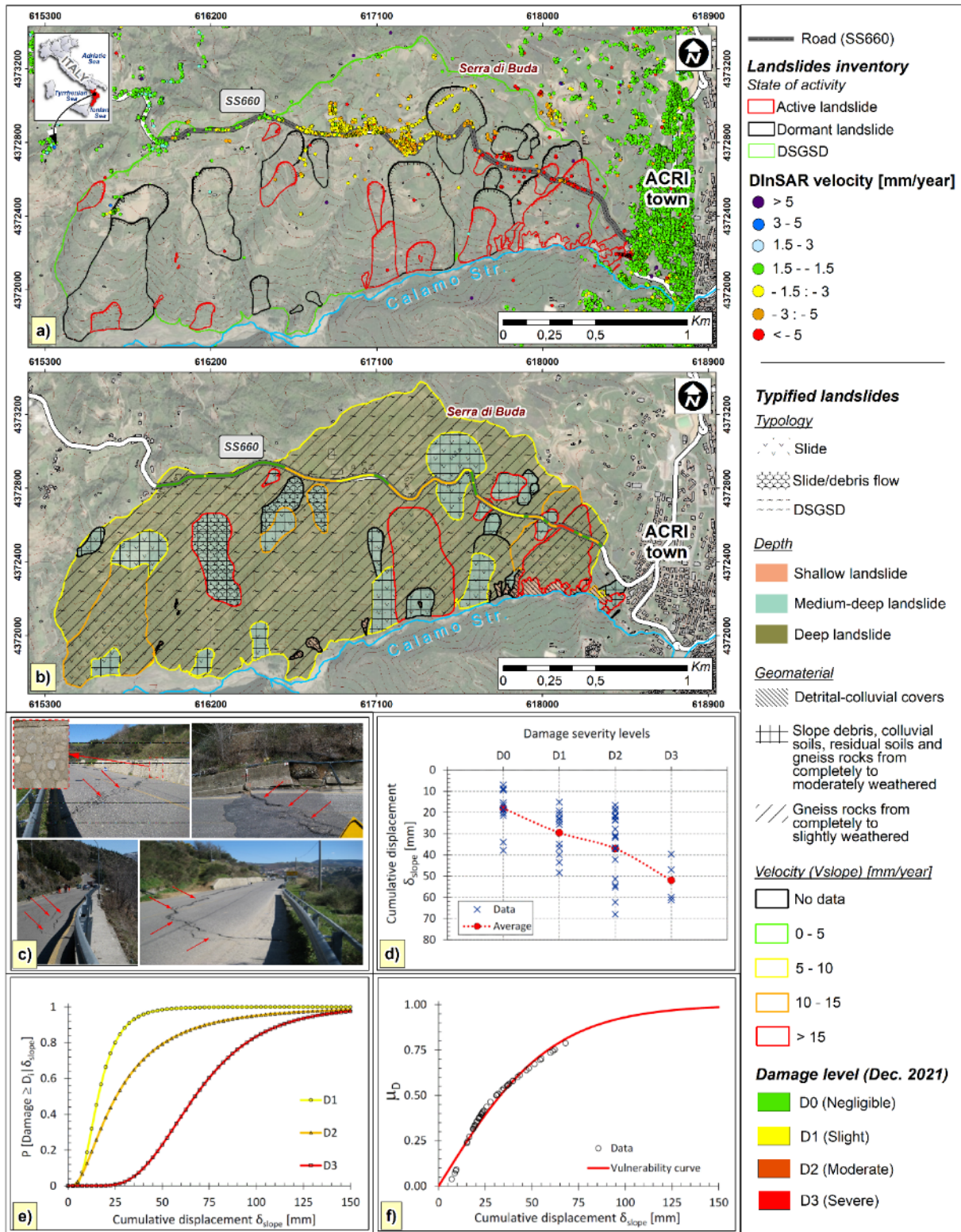


Fig. 3 State Road SS660 case study: a) landslide inventory map with the state of activity (modified from Borelli and Gullà et al., 2017), the analyzed (SS660) road to Aciri town, and spatial distribution of DInSAR data acquired by COSMO-SkyMed satellite (ascending orbit, 2014–2021); b) map of the typified landslides with indication of damage to road; c) some examples of cracks recorded on the asphalt pavement and the side retaining structures during in-situ surveys; d) damage level (DLi) vs. cumulative displacement (δ_{slope}); e) empirical fragility curves and f) vulnerability curve.

Specifically, displacements were cumulated from February 2018 (coinciding with the last repair works to the road) to December 2021. The computed values of δ_{slope} for each

buffer were then associated with the DLi recorded in the survey of 2021. This allowed retrieving the empirical cause-effect relationship shown in Figure 3d.

As expected, the δ_{slope} attains higher values as the damage severity level (DLi) increases, being DLi conservatively assumed as the most severe damage between the one recorded to the road surface and the pertaining retaining structure (if any).

Then, by adopting Eq. 1 with the estimated fragility parameters pertaining to each DLi, the empirical fragility curves were generated (Figure 3e).

Finally, the discrete probabilities (P_i) provided by the empirical fragility curves allowed deriving - according to Eq. 2 - the values of the average expected damage severity level (μ_{DL}), assuming as numerical index d_i the values 0.33, 0.66, and 1 for D1, D2 and D3, respectively.

The interpolation of the latter empirical data through the adoption of Eq. 3 allowed deriving the empirical vulnerability curve shown in Figure 3f.

Discussion and Conclusions

The presented case studies showed that technological innovation of multi-source monitoring/survey data can provide useful contribution to procedures aimed at landslide risk analyses. For instance, Google Street View was proven to be a useful tool for rapid, easy and cost-effective road damage inspections, whereas DInSAR data confirmed to be a well-established complement of conventional displacement monitoring techniques. Both the abovementioned datasets, which are broadly available in archives worldwide, can foster deterministic/probabilistic vulnerability analyses of buildings/roads exposed to slow-moving landslides.

Once further validated, the presented method could be part of a circular approach (Gullà et al., 2021) to help building/road maintenance prioritization and scheduling as well as risk management in slow-moving landslide-affected urban area and extended to other geo-hazards. Nevertheless, the exportability to other areas will require updated landslide inventories, local geotechnical and building/road characteristics to be taken into account to typify representative landslide-damaged buildings/roads in homogeneous geo-lithological contexts.

Acknowledgements

This research was funded by and carried out in the Italian Space Agency (ASI) contract n. 2021-10-U.0 CUP F65F21000630005 MEFISTO—Multi-frequency SAR data processing methods for the hydrogeological instability monitoring.

The activities also fall within the Agreement for scientific cooperation signed by the Italian National Research Council (CNR-IRPI) and the Department of Civil Engineering of the University of Salerno on “Attività di ricerca mirate ad approfondire le conoscenze sulla tipizzazione di movimenti franosi a cinematica lenta e sulla vulnerabilità di strutture e infrastrutture che con essi interagiscono anche mediante l’impiego di tecniche innovative di monitoraggio satellitare e da terra” and the related operative Agreement for Research contribution

signed by the two institutions on the topic: “Analisi quantitativa del rischio da frane a cinematica lenta in aree urbane dell’Appennino Meridionale con l’ausilio di modellazione numerica avanzata e dati di monitoraggio satellitare”.

References

- Argyroudis S A, Mitoulis S A, Winter M G, Kaynia A M (2019) Fragility of transport assets exposed to multiple hazards: State-of-the-art review toward infrastructural resilience. *Reliability Engineering and System Safety*, 191:106567, doi: 10.1016/j.ress.2019.106567.
- Borrelli L, Gullà G (2017) Tectonic constraints on a deep-seated rock slide in weathered crystalline rocks. *Geomorphology* 290: 288–316. <https://doi.org/10.1016/j.geomorph.2017.04.025>
- Borrelli L, Greco R, Gullà G (2007) Weathering grade of rock masses as a predisposing factor to slope instabilities: Reconnaissance and control procedures. *Geomorphology* 87(3): 158–175. <https://doi.org/10.1016/j.geomorph.2006.03.031>
- Borrelli L, Perri F, Critelli S, Gullà G (2014) Characterization of granitoid and gneissic weathering profiles of the Mucone River basin (Calabria, southern Italy). *Catena* 113: 325–340. <https://doi.org/10.1016/j.catena.2013.08.014>
- Burland J B, Broms B B, de Mello V F B (1977) Behaviour of foundations and structures. *Proceedings of the 9th Int. Conf. on Soil Mechanics and Foundation Engineering*, Tokyo. SOA Report, vol. 2, pp. 495–546.
- Cascini L, Gullà G (1993) Caratterizzazione fisico-meccanica dei terreni prodotti dall’alterazione di rocce gneissiche. *Rivista Italiana di Geotecnica*, Anno XXVII, N. 2, Aprile-Giugno 1993, pp.125-147 (in Italian).
- Cascini L, Fornaro G, Peduto D (2010) Advanced low- and full-resolution DInSAR map generation for slow-moving landslide analysis at different scales. *Engineering Geology*, 112(1–4):29-42. <https://doi.org/10.1016/j.enggeo.2010.01.003>
- Fell R, Corominas J, Bonnard Ch, Cascini L, Leroi E, Savage W Z (2008) Guidelines for landslide susceptibility, hazard and risk zoning for land-use planning. *Engineering Geology* 102(3-4):99-111. <https://doi.org/10.1016/j.enggeo.2008.03.014>
- Ferlisi S, Gullà G, Nicodemo G, Peduto D (2019) A multi-scale methodological approach for slow-moving landslide risk mitigation in urban areas, southern Italy. *Euro-Mediterranean Journal for Environmental Integration*, 4:20, doi:10.1007/s41207-019-0110-4
- Ferlisi S, Marchese A, Peduto D (2021) Quantitative analysis of the risk to road networks exposed to slow-moving landslides: a case study in the Campania region (southern Italy). *Landslides* 18:303–319. <https://doi.org/10.1007/s10346-020-01482-8>
- Ferlisi S, Peduto D, Gullà G, Nicodemo G, Borrelli L, Fornaro G (2015) The use of DInSAR data for the analysis of building damage induced by slow-moving landslides. *Engineering Geology for Society and Territory - Landslide Processes*, © Springer International Publishing - Vol. 2. pp. 1835–1839. doi: 10.1007/978-3-319-09057_3_325.
- Fornaro G, Pauciuolo A, Serafino F (2009) Deformation monitoring over large areas with multipass differential SAR interferometry: A new approach based on the use of spatial differences. *Int J Remote Sens* 30(6):1455–1478. <https://doi.org/10.1080/01431160802459569>
- Greenwood W W, Lynch J P, Zekkos D (2019) Applications of UAVs in civil infrastructure. *Journal of Infrastructure Systems*, 25(2):04019002.

- Gullà G (2014) Field monitoring in sample sites: hydrological response of slopes with reference to widespread landslide events. *Procedia Earth and Planetary Science* 9 (2014) 44-53.
- Gullà G, Nicodemo G, Ferlisi S, Borrelli L, Peduto D (2021) Small-scale analysis to rank municipalities requiring slow-moving landslide risk mitigation measures: the case study of the Calabria region (southern Italy). *Geoenvironmental Disasters* (2021) 8:31.
- Gullà G, Peduto D, Borrelli L, Antronico L, Fornaro G (2017) Geometric and kinematic characterization of landslides affecting urban areas: the Lungro case study (Calabria, southern Italy). *Landslides*. 14(1):171–188.
- Lagomarsino S, Giovinazzi S (2006) Macroseismic and mechanical models for the vulnerability and damage assessment of current buildings. *Bull Earthq Eng* 4(4):415-443. <https://doi.org/10.1007/s10518-006-9024-z>
- Mavrouli O, Fotopoulou S, Pitolakis K, Zuccaro G, Corominas J, Santo A, Cacace F, De Gregorio D, Di Crescenzo G, Foerster E, Ulrich T (2014) Vulnerability assessment for reinforced concrete buildings exposed to landslides. *Bull Eng Geol Environ* 73:265– 289. <https://doi.org/10.1007/s10064-014-0573-0>
- Nicodemo G, Peduto D, Ferlisi S, Gullà G, Reale D, Fornaro G (2018) DInSAR data integration in vulnerability analysis of buildings exposed to slow-moving landslides. In: *Proceedings of IEEE International Geoscience and Remote Sensing Symposium (IGARSS 2018)*, València (Spain), 22-27 July, 2018, pp. 6111-6114. <https://doi.org/10.1109/IGARSS.2018.8518808>
- Peduto D, Ferlisi S, Nicodemo G, Reale D, Gullà G (2017) Empirical fragility and vulnerability curves for buildings exposed to slow-moving landslides at medium and large scales. *Landslides*. 14(6):1993–2007.
- Peduto D, Nicodemo G, Caraffa M, Gullà G (2018) Quantitative analysis of consequences induced by slow-moving landslides to masonry buildings: a case study. *Landslides*. 15(10):2017–2030
- Peduto D, Nicodemo G, Nappo N, Gullà G (2021) Innovation in Analysis and Forecasting of Vulnerability to Slow-Moving Landslides. In: Guzzetti F., Mihalić Arbanas S., Reichenbach P., Sassa K., Bobrowsky P.T., Takara K. (eds) *Understanding and Reducing Landslide Disaster Risk*. WLF 2020. ICL Contribution to Landslide Disaster Risk Reduction. Volume 2 “From Mapping to Hazard and Risk Zonation”, pp.441-446. Springer, Cham. https://doi.org/10.1007/978-3-030-60227-7_51, Print ISBN978-3-030-60226-0, Online ISBN978-3-030-60227-7, © Springer Nature Switzerland AG 2021
- Terranova O, Antronico L, Gullà G (2007) Landslide triggering scenarios in homogeneous geological contexts: the area surrounding Acri (Calabria, Italy). *Geomorphology* 87: 250-267 <https://doi.org/10.1016/j.geomorph.2006.09.021>

Landslide susceptibility assessment: Chicken or the egg for the risk analysis?

Michel Jaboyedoff

Risk group - Institute of Earth Sciences, University of Lausanne, GEOPOLIS - CH1015 Lausanne, Switzerland, Address, Country, (michel.jaboyedoff@unil.ch)

Abstract This article explores the complexities of landslide risk assessment, emphasizing the qualitative nature of analysing hazards and consequences. It highlights the necessity for well-defined frameworks to evaluate these risks and the significant role of expert judgment in refining assessments due to inherent uncertainties. The text argues for the development of clear methodologies that stakeholders can understand and accept, incorporating best practices and local knowledge to mitigate legal risks associated with predictive inaccuracies. Additionally, it suggests the use of catastrophe modelling to solve the issues linked with uncertainty.

Keywords Landslide, risk, hazard, susceptibility.

Introduction

Risk management encompasses a more extensive definition of risk than that employed in risk analysis. As per ISO 31000 (2018), risk is conceptualized as:

The “*effect of uncertainty on objectives*”.

This notion includes the potential deviation from anticipated events, which could engender negative impacts, opportunities, or a combination thereof, on predefined objectives. Such objectives may be influenced by a myriad of event types at various process levels. Risk is distinguished by elements likely to yield expected or unexpected outcomes on the objective, coupled with their probability of occurrence. This definition is particularly pertinent to risk in decision-making contexts, such as risk management, where it is often contingent upon factors extrinsic to risk analysis.

Moreover, the above definition acknowledges the possibility of risk leading to positive outcomes, a scenario considerably less frequent in the context of landslides. Decision-making and risk management inherently incorporate uncertainty, which, however, can be quantified through probabilities or qualitative assessments thereof (Aven and Renn, 2009).

It is imperative to recognize that risk definitions are context dependent. In epidemiology, for instance, risk is quantified as the proportion of new disease cases in a specified period relative to the initial healthy population (Rothman, 2012).

The methodology for analysing risks associated with slope movements varies case by case. Typically, a

particular site is examined to assess potential disaster-related costs or the probable number of casualties. Outcomes may be expressed as the probability of event impacts exceeding a defined threshold within a set timeframe, or as temporal frequencies of costs or fatalities. When calculating individual risk of mortality, it is represented as a death rate over time. This mortality risk is frequently juxtaposed with a societal risk acceptability criterion, defined in relation to the size of the affected population (Hung and Wong, 2007). Thus, it is evident that:

“Risk analysis involves applying recipes that may vary based on perspective and available data.”

Identifying the hazard is a primary step, yet quantifying it is often challenging, leading to predominantly qualitative risk assessments, especially when knowledge is limited to susceptibility. The potential impact or vulnerability for given landslide intensities is subject to considerable uncertainty (Galli and Guzzetti, 2007), which means that qualitative assessment is pertinent. In such cases, methodologies like the probability-impact matrix, typically utilized by experts, are beneficial (Haimes, 2009; Porter and Morgenstern, 2013).

Despite its limitations, risk assessment remains a critical tool in decision-making, notably in cost-benefit analyses that guide risk mitigation strategies. Nonetheless, it is essential to acknowledge that risk is not the sole factor in decision-making; socio-economic considerations also play a significant role (Leroi et al. 2005).

The difficulties in quantifying temporal frequency or hazard and consequences are for most landslide risk analyses based on susceptibility, as they are often based on the calibration of both scales.

If the risk framework is clear, the application *sensu stricto* of risk assessment is rarely carried out, and the use of susceptibility is the most commonly used approach. Furthermore, where the hazard can be assessed quantitatively, it may be subject to considerable uncertainty.

Some sections of this document are inspired by a book in preparation in French on landslides (Jaboyedoff et al. in prep.).

Risk Basics

Basic formulas for risk and hazard (frequency)

Considering the magnitude as a quantity describing the volume, surface area, energy, pressure, etc. the landslide's risk quantification for one landslide scenario of magnitude M_i is classically given by (Corominas et al. 2014):

$$R_{ijk} = f(M_i) P(X_j|M_i) \text{Exp}(t|X_j) V_E(I(M_i, X_j)) W(X_j(E_k)) \quad [1]$$

Where $P(X_j|M_i)$ is the probability that an event of magnitude M_i reaches the point X_j , $\text{Exp}(t|X_j)$ is the exposure, which means the probability that the object or the person is located in X_i at the time t of the event, $V_E(I(M_i, X_j))$ is the physical vulnerability of the object E hit by an event of magnitude M_i with an intensity I depending on the location X_j . $W(X_j(E_k))$ is the value of the object E_k located in X_j or the number of units like people, if there is no object in X_j then W is null. $f(M_i)$ is the temporal frequency of a landslide of magnitude M_i or hazard. In fact, the frequency f or hazard H is calculated for a range of magnitude assuming that $\lambda'(M_i)$ is the frequency density and $\lambda(M_i)$ the cumulative of the temporal frequency to exceed M_i , for a range of magnitude $M_i \pm \Delta M$ it comes:

$$f(M_i) = H(M_i) = \int_{M_i - \Delta M}^{M_i + \Delta M} \lambda'(m) dm \quad [2]$$

knowing that it is not possible to know the time separating two events of the same magnitude; this can only be done by classes of values or using the directly $\lambda(M)$. The relationship between temporal frequency and return period is given by (Hungry et al. 1999):

$$\lambda(m \geq M) = \frac{1}{T(m \geq M)} \quad [3]$$

where $\lambda(m \geq M)$ is the frequency of events of magnitude greater than or equal to M , i.e. a cumulative frequency. The intensity is used to evaluate vulnerability, but often the event frequency is related to the source of the hazard of magnitude M_i and not to the intensity of the event at a given location X . A typical example is the rockfall hazard given by volumes of the source area, but it fragmented along the path (Farvacque et al. 2019; Lanfranconi et al. 2023 Ruiz-Carulla et al, 2016). When the vulnerability V concerns people, it can equal to lethality or a function of the vulnerability of the buildings including injuries (Li et al. 2010).

Relationship Frequency - Probability

The classic example is the distribution of landslide volumes. If $f(M_i)$ is quantified, then the probability that during a period Δt , n events will occur for a class of

magnitude M_i using the Poisson distribution, provided that these events are independent:

$$P(n, \Delta t) = \frac{(f(M_i)\Delta t)^n}{n!} e^{-f(M_i)\Delta t} \quad [4]$$

The temporal frequency should not be confused with the probability, because some phenomena have a frequency greater than 1, whereas the probability cannot exceed one, which is a common mistake. So, it is only when $T \gg 1$ is large that the probability of an event per unit of time so:

$$P \approx \frac{1}{T} \quad [5]$$

In that case the probability of an event not occurring in a year is close to $(1-P)$, and therefore the probability of at least one event occurring in d years is classically given by:

$$P(n \geq 1, d) \approx 1 - \left(1 - \frac{1}{T}\right)^d \quad [6]$$

But this formulation depends on the unit of time, because for $T = d = 1$ we get 100%, but respecting the hypothesis $T \gg 1$, for 8760 hours in a year we get 63.2%. It is therefore preferable to use the Poisson distribution by evaluating the probability that there is no event (Corominas et al. 2014):

$$P(n \geq 1, d) = 1 - P(0, d) = 1 - \frac{(f(M_i)d)^0}{0!} e^{-\lambda_i d} = 1 - e^{-f(M_i)d} \quad [7]$$

In fact, we can show that the two formulations are equivalent. In case of multiple events with reconstruction, the use of Poisson's law for $n = 1, 2, \dots, n$ maybe used, if significant. For small frequency the $P \approx f$, there is less than 2% difference for a ratio $f/\Delta t = f/T > 25$. To perform a full risk calculation class of magnitude must be used and formally integration or a summation must be performed over M_i, X_j , (implicitly $f(M_i)$) and E_k :

$$R_{total} = \sum_{i=1}^n \sum_{j=1}^m \sum_{k=1}^q R_{ijk} \quad [8]$$

Second form of risk

An alternative way to present risk is to give a probability of occurrence given by the above formula and the damage or cost:

$$C(E, X_j, M_i) = \text{Exp}(t|X_j) V_p(I(M_i, X_j)) W(E, X_j) \quad [9]$$

This gives the possibility to create graphs such as consequences-frequency or frequency exceedance. Which is typically $f-N$ or $F-N$ curves (Farmer, 1967; Ale, 2008). The matrix usually represents C versus P or f , but if P is used the period d must be indicated, which is often omitted.

Matrix approach

It is obvious that the F-N curves are a direct transcription of risk equation, it is rather easy create when all the terms of the risk formula are knows. But they present some drawbacks concerning the risk acceptability and tolerability limits, which is not well established for F-N and for the non-cumulative version f-N, they depend on the domain they are applied, at le level of a country or in a local context (Ale et al. 2015).

In addition, the frequencies are not easily accessible like for earthquakes or flooding by their repetitive nature, using respectively Gutenberg-Richer law (Gutenberg and Richter, 1956) or Gumbel’s law (Gumbel, 1941). This is also true for the damage estimations. In both case probabilities can be used to assess which class of frequency or damage it belongs.

The methodologies encompassed by Consequences-Frequency Matrices (CFM) are designed to facilitate risk assessment through the hierarchical classification of various hazards (UK-CO, 2017) (Fig. 1). This approach is particularly tailored for individual case studies, addressing key inquiries as posited by Haimes (2008): namely, identifying potential failings, as well as their respective probabilities and repercussions. Concurrently, industrial and insurance sectors implement a systematic process for Risk Filtering, Ranking, and Management (RFRM), which is an efficient and effective identification, prioritization, and administration of risks (Krause et al. 1995; Haimes, 2008; Jaboyedoff, 2023):

1. Scope definitions: what are the problems?
2. Creation of a group of experts concerned by each level of the analyzed risky system.
3. Hazard identification, i.e. identification of potential events and their scenarios
4. Risk filtering and ranking in several sub-stages which implies to establish frequency (probability) and impact classes and their corresponding limits (in loop with point 5)
 - 1.1. Use decision trees to select for C and f or H
 - 1.2. Place in risk matrix
5. Establish a ranking.
6. Risk management, including the quantification of the potential risk reduction, which necessitates the understanding of causes and effects
7. Finalization of decision-making process
8. Refinement of the process with the feedback

The CFM must in principle follow certain rules. Cox (2008) highlights an inconsistency in the color-coded risk scale, particularly due to the ambiguity in classifying risks positioned at the boundaries of different categories (Fig. 1). For instance, a data point situated at the juncture of three distinct risk classes may exhibit considerable classification variability. A mere unitary alteration in the axis values could potentially result in a shift of two entire class levels, thereby indicating a significant discrepancy in risk categorization. This phenomenon underscores the

inherent challenges in maintaining a consistent and accurate risk assessment framework when utilizing colour-based scales.

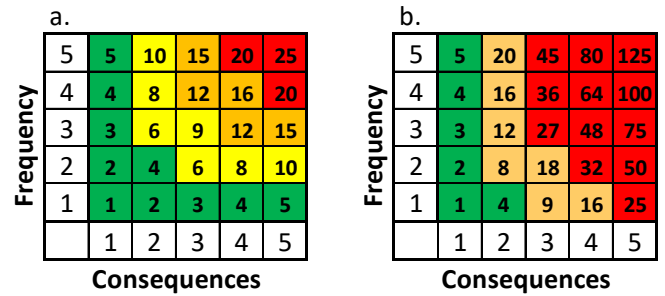


Figure 1 The illustration of 5 × 5 risk matrices presents two distinct configurations: firstly, a hyperbolic risk scale encompassing four classes (a), and secondly, a model incorporating risk aversion, characterized by a reduction to three classes (b). This comparative analysis underscores the variability in risk matrix structures and the impact of scaling and class alterations on risk assessment (modified form Jaboyedoff, 2023).

Example of hazard consequences values

Numerous exemplars of risk matrices exist within the risk domain. Porter and Morgenstern (2013) proposed a matrix for landslide risk assessment being particularly noteworthy (Fig. 2). This matrix provides the order of magnitudes of frequency and the different types of impacts delineating impacts across various domains such as Health and Safety, Environmental, and Social & Cultural factors. It underscores the imperative of maintaining fixed categories for likelihood estimation. However, it allows for the scaling of consequence metrics to align with specific objectives, such as adjusting for the scale of an enterprise or its associated bankruptcy risks. This adaptability renders the matrix a versatile tool in risk assessment.

Defining the classes of consequences and frequency or probability

To choose the membership to a class of consequences or frequency, several strategies can be used. It can be based on a set of indicators with weight which provide a value for one or for both scales as for geotechnical and geomorphic indicators used for quick clays risk analysis (Lacasse et Nadim, 2009).

Decision trees are fundamental tools for the analysis of risks or hazards (Leroueil et Locat, 1998; Haimes, 2008; Lacasse et al. 2008). These methodologies are adept at providing class values for either one or both axes in risk assessment frameworks. The employment of dichotomous branching, as advocated in the context of pandemic analysis by ECDC (2011), is preferred due to the enhanced ease in decision-making it offers. For instance, the frequency or return period (T_i) can be inferred through the process illustrated in Fig. 3, which is dependent on climatic variables, although specific quantitative values are not specified.

Multi-hazard Risk Evaluation Matrix (SAMPLE)																	
For the Qualitative Assessment of Natural Hazards																	
Likelihood Descriptions			Indices			Probability Range			Risk Evaluation and Response								
									VH	Very High	Risk is imminent; short-term risk reduction required; long-term risk reduction plan must be developed and implemented						
Event typically occurs at least once per year			F			Almost certain			>0.9			H	High	Risk is unacceptable; long-term risk reduction plan must be developed and implemented in a reasonable time frame. Planning should begin immediately			
												M	Moderate	Risk may be tolerable; more detailed review required; reduce risk to As Low As Reasonably Practicable (ALARP)			
Event typically occurs every few years			E			Very Likely			0.1 to 0.9			L	Low	Risk is tolerable; continue to monitor and reduce risk to As Low As Reasonably Practicable (ALARP)			
												VL	Very Low	Risk is broadly acceptable; no further review or risk reduction required			
Event expected to occur every 10 to 100 years			D			Likely			0.01 to 0.1			L	Low	Risk is tolerable; continue to monitor and reduce risk to As Low As Reasonably Practicable (ALARP)			
												VL	Very Low	Risk is broadly acceptable; no further review or risk reduction required			
Event expected to occur every 100 to 1,000 years			C			Possible			0.001 to 0.01			VL	Very Low	Risk is broadly acceptable; no further review or risk reduction required			
												VL	Very Low	Risk is broadly acceptable; no further review or risk reduction required			
Event expected to occur every 1,000 to 10,000 years			B			Unlikely			0.0001 to 0.001			VL	Very Low	Risk is broadly acceptable; no further review or risk reduction required			
												VL	Very Low	Risk is broadly acceptable; no further review or risk reduction required			
Event is possible but expected to occur less than once every 10,000 years			A			Very Unlikely			<0.0001			VL	Very Low	Risk is broadly acceptable; no further review or risk reduction required			
												VL	Very Low	Risk is broadly acceptable; no further review or risk reduction required			
Likelihood Descriptions			Indices			Probability Range			1	2	3	4	5	6			
									Incidental	Minor	Moderate	Major	Severe	Catastrophic			
Health and Safety			No impact			Slight impact; recoverable within days			Minor injury or personal hardship; recoverable within days or weeks			Serious injury or personal hardship; recoverable within weeks or months			Fatality or serious personal long-term hardship		
Social & Cultural			Negligible impact			Slight impact to social & cultural values; recoverable within days or weeks			Moderate impact to social & cultural values; recoverable within weeks or months			Significant impact to social & cultural values; recoverable within months or years			Partial loss of social & cultural values; not recoverable within the lifetime of the project		

Figure 2 Illustration of a risk matrix, devised by BGC Engineering Inc. and proposed to the Geological Survey of Canada, is presented as a Sample Qualitative Risk Evaluation Matrix (Porter and Morgenstern, 2013).

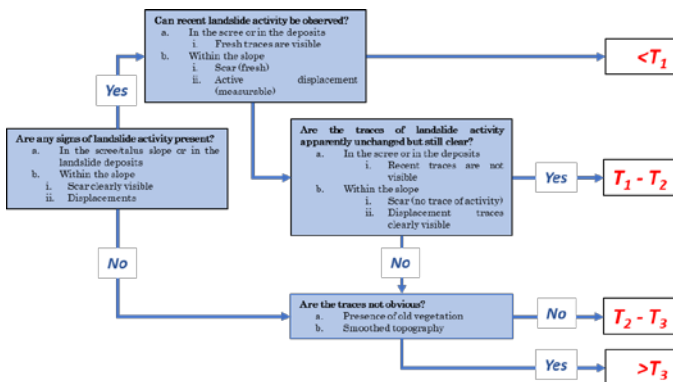


Figure 3 Example of a decision tree to determine the return period.

For the consequences scale, implementing a decision tree to determine the class categories is a feasible method. This approach is exemplified in the case of a landslide threatening a road, as shown in Fig. 4.

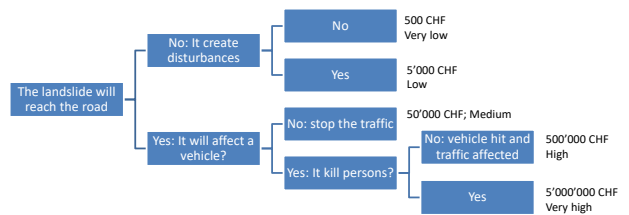


Figure 4 illustrates a decision tree used to ascertain the consequence levels for the Pont Bourquin landslide in Switzerland (from Jaboyedoff, 2023).

Alternatively, experts can be consulted to assign the probability of falling into each class on the scale. This method, as suggested by Vengeon et al. (2001), involves setting the frequency through a probability-delay matrix for landslide failures. This technique is applicable to both consequence assessment and frequency determination.

Temporal frequency and its estimates

Temporal frequencies can be analysed in several ways, in particular using inventories with event chronologies (Jaboyedoff et al. in prep.). But when the data are not sufficient or regional, the lack of local temporal is compensated for data with other information. This

information can be weighted to create a local frequency or susceptibility scale. In the case of more detailed studies, seasonality can be integrated.

This involves assessing the temporal frequency for areas ω_i of the territory Ω (from a single landslide to an entire region) for a magnitude class $M_j \pm \Delta M$ which, on average, can be broken down into three terms (modified from Guzzetti et al. 2005):

$$\lambda(\Omega, M_j, t, \omega_i) = \lambda_r(\Omega, t) \times f_r(M_j) dM \times PS(\Omega, \omega_i) \quad [10]$$

so (λ_r, Ω, t) is the frequency of landslides in a region Ω at time t . t can be omitted, as the dependency is there simply to highlight the possible seasonal variability. From a practical point of view, we can estimate the temporal frequency for a given region Ω by:

$$\lambda_r(\Omega) = \frac{N_0(\Omega)}{\Delta t} \quad [11]$$

where $N_0(\Omega)$ is the number of landslides that have occurred during a period Δt , per unit area, or not. $f_r(M_j) dM$ corresponds to the relative distribution of magnitudes equal to M_i given that :

$$\int_{M_0}^{M_{max}} f_r(M) dM = 1 \quad [12]$$

This formulation can be replaced by a discrete formulation, i.e. a sum of probabilities for several scenarios of different magnitudes. Finally, $PS(\Omega, \omega_i)$ is the probability of an event occurring within a given perimeter ω_i of Ω , which may be the landslide itself or zones of

identical susceptibility. $PS(\Omega, \omega_i)$ corresponds to a standardised susceptibility scale, i.e. a weighting that can be derived from different types of analysis, for example: counting of criteria favourable to the triggering of landslides (Hantz et al. 2003), regression on these parameters, probabilistic analysis, a neural network, etc. If we assume that s_i is a susceptibility value for one class among n susceptibilities, of m surfaces a_j^i of class i , of any scale, then for a given class $PS(\Omega, \omega_i)$ we have :

$$PS(\omega_i) = \frac{s_i \sum_{j=1}^m a_j^i}{\sum_{i=1}^n s_i \sum_{j=1}^m a_j^i} \quad [13]$$

With

$$\sum_{i=1}^n PS(\omega_i) = 1 \text{ et } \Omega = \sum_{i=1}^n \omega_i = \sum_{i=1}^n \sum_{j=1}^m a_j^i \quad [14]$$

Examination of all the variables shows that it is often difficult to estimate them all, and that some are often fixed at 1, which amounts to ignoring them. Many studies use only values of $PS(\Omega, \omega_i)$, s_i or ω_i and/or expert opinions which produce scales of susceptibility in the broadest sense ranging from *negligible*, for example, through *low*, *medium* and *high* to *very high*. Others are based on the distribution of magnitudes f_r such as volumes, with or without the use of λ_r , or simply by choosing a single class of volume i.e. $f_r(M_j) dM = 1$, $PS = 1$, and λ_r per unit area. This shows the great diversity possible in the assessment of "hazard", or susceptibility. It can exist in very different forms.

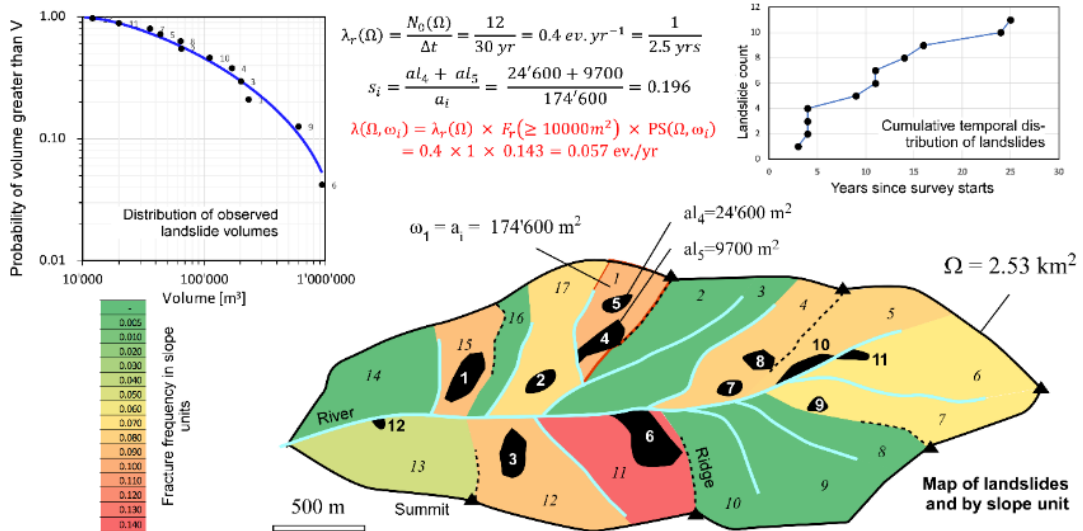


Figure 5 Synthetic illustration of the calculation of the temporal frequency of landslides (in grey) per slope unit. Here, in fact, by simplification, $PS(\Omega, \omega_i)$ is equal to the ratio of the surface area of landslides on a slope unit to the total surface area of all landslides, since the choice to quantify s_i by the ratio of the total surface area of landslides a_j to that of a unit a_i is based on this assumption.

The Fig. 5 and Table 1 show a synthetic example of such an approach. Based on an inventory of landslides in a catchment area that is subdivided into slope units (bounded by rivers and ridges; Carrara et al. 1991; Guzzetti et al. 2005). To simplify matters, the susceptibility s_i is calculated as the ratio of the surface area of the landslides to the surface area of the units containing them, $f_r(M_j) dM = 1$ for all M_j as only one class of volumes above $10^4 m^3$ is considered, and PS and λ are calculated according to the formulae set out above. In a true statistical analysis, none of the values of s_i would be zero.

Table 1 Calculation of non-zero frequencies per slope unit of Fig 5.

i	$\omega_i = a_i$ [m ²]	Surf. landslides [m ²]	s_i	$f_r(v \geq 10^4 m^3)$	PS(ω_i)	$\lambda(\omega_i)$
1	174'600	34'300	0.196	1	0.143	0.057
4	255'500	21'000	0.082	1	0.087	0.035
5	222'600	18'500	0.083	1	0.077	0.031
6	347'300	5'600	0.016	1	0.023	0.009
7	253'000	5'900	0.023	1	0.025	0.010
11	343'900	80'000	0.233	1	0.333	0.133
12	332'100	27'700	0.083	1	0.115	0.046
13	337'500	4'000	0.012	1	0.017	0.007
15	160'400	30'600	0.191	1	0.127	0.051
17	269'800	12'700	0.047	1	0.053	0.021
				Total	1.000	0.400

λ_T is often estimated based on historical inventories, observations of signs of activity, or expert opinion. Dating using C¹⁴ or cosmogenic nuclides, etc. is possible, but difficult to implement on a regional basis; however, analysis using dendrochronology and observations of damage to trees provides interesting results, particularly for debris flows and boulder falls (Stoffel et al. 2010) (Fig. 6).

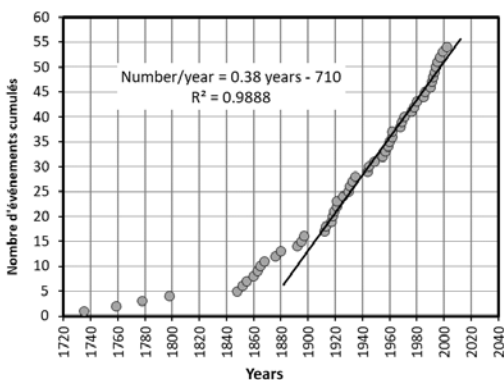


Figure 6 Debris flow activity in the Geisstriftbach (Switzerland), based on observations of tree damage and dendrogeomorphology. From 1910 onwards, the trees were sufficiently well preserved to show stationary activity, with an average of one event every 2 or 3 years (based on data from Stoffel et al. 2010).

Examples

Assessing risk based on matrix approach

As an example of matrix approach for risk analysis, Cardinali et al. (2002). They established a hazard map in Umbria region (Italy). They obtained risk at objects for the area of Rotecastello village. They used first a matrix to assess the landslide intensity (Fig. 7a) by crossing velocities and volumes, which provided a ranking of intensity. The landslide frequency was estimated using four classes, based on the number of landslide events (of the same type) observed within each Landslide Hazard Zone (low 1 event over 60 years, ..., very high > 3 ev./60 yrs.). The landslide hazard (LHZ) matrix was obtained by crossing intensity and frequency (Fig. 8).

a.

Volume [m ³]	Expected landslide velocity		
	Fast moving landslide	Rapid moving landslide	Slow moving landslide
	Boulder falls and rock avalanches	Debris-flow	Slide
< 0.001	Slight		
0.001 to 0.5	Medium		
0.5 to 500	High	Slight	
500 to 1.0E+04	High	Medium	Slight
1.0E+04 to 5.0E+05	High	High	Medium
5.0E+05 to 6.0E+06	Very High	Very High	High
> 6.0E+06	Very High	Very High	Very High

b.

Landslides intensity	Elements at risk					
	High population density	Low population density	Industries	Animal farms	Sports facilities	Cemeteries
Light	Falling rocks	A	A	A	A	A
	Debris flow	A	A	A	A	A
	Landslide	A	A	A	A	A
Medium	Falling rocks	F	F	F	F	F
	Debris flow	F	F	F	F	F
	Landslide	F	F	F	F	F
High	Falling rocks	S	S	S	S	S
	Debris flow	S	S	S	S	S
	Landslide	S	S	S	S	S
Very high	Falling rocks	S	S	S	S	S
	Debris flow	S	S	S	S	S
Landslide	S	S	S	S	S	

Figure 7 (a) Landslide intensity matrix based on volumes and velocities, for 3 main types of landslides. (b) Impact of landslides on infrastructures expected for elements at risk. A = superficial (low) damage; F = functional (or medium) damage; S = structural (or total) damage. Intensities are shown in (a) (modified from Cardinali et al. 2002).

The vulnerability was defined based on the intensity scale for each type of landslides for many types of objects (Fig. 7b). As the LHZ matrix is linking frequency and intensity and as the intensity and damage increase it can be considered as a risk matrix (Fig. 8). But observations showed that were not all fitting the scale. Indicating that uncertainty was not included.

Estimated landslide frequency	Landslide intensity			
	Light (1)	Medium (2)	High (3)	Very high (4)
Low (1)	1 1	1 2	1 3	1 4
Medium (2)	2 1	2 2	2 3	2 4
High (3)	3 1	3 2	3 3	3 4
Very high (4)	4 1	4 2	4 3	4 4

Figure 8 Interpretation of the theoretical LHZ matrix of Carinali et al. (2002) in terms of risk: the yellow correspond to low risk, orange to medium, red to high and purple to very high. Note that there is no contact between three classes.

Assessing risk based on indicators

Norway has implemented a straightforward methodology for risk zoning in the context of sensitive clays, as developed by Lacasse and Nadim (2009). This method involves assigning weights w_{a_i} to various indicators S_{a_i} to derive the susceptibility to landslide which means that it is only based on PS estimations. The hazard is categorized into 4 classes S_{a_i} : null, low, medium, and high levels, based on a weighted system accounting for 8 parameters, i.e. topography, geotechnical properties, dynamic conditions like erosion, human activity, historical landslide occurrences, etc.

Similarly, consequences are evaluated on a scale S_{c_j} from not serious to very serious (0-3), considering 7 factors such as loss of life, property damage, and economic or social impacts which are weighted by w_{c_j} .

The risk index (R_i) is calculated for different zones by multiplying the susceptibility index (S_i) and the consequences index (C_i), using a formula that combines the weighted sums of hazard and consequence indicators (Figure 9):

$$R_i = S_i \times C_i = \left(\sum_{i=1}^8 w_{a_i} \times S_{a_i} \right) \times \left(\sum_{j=1}^7 w_{c_j} \times S_{c_j} \right) \quad [15]$$

This methodology categorizes R_i into five distinct classes ranging from very low to very high. It enables the creation of risk maps through a consequence-susceptibility diagram (Figure 9b), aiding in risk assessment. Associated actions range from geotechnical investigations to mitigation measures. This risk assessment approach is part of a broader spectrum of methods that integrate hazard, impact, and risk estimates, using various parameters and can be adapted to statistical or artificial intelligence methods.

Uncertainty of the frequency estimations

The magnitude- frequency relationship for rockfalls instability sources failure hazard can be characterized using power law frequency cumulative distributions (Hungr et al. 1999; Dussauge et al. 2003; Hantz et al. 2020):

$$F_s(v_s \geq V) = a_s V^{-b_s} \quad [16]$$

In this equation, a_s denotes the frequency of volumes exceeding a specified threshold, reflecting the active nature of a region (Figure 10). The b_s -value in the equation

is indicative of the frequency of encountering larger volumes which correspond to $\lambda(M_i)$ described above.

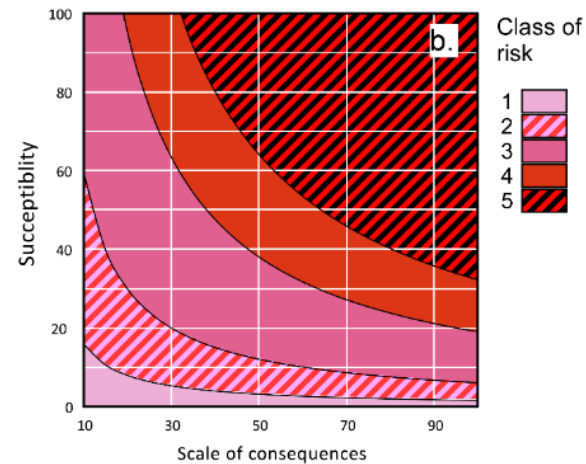
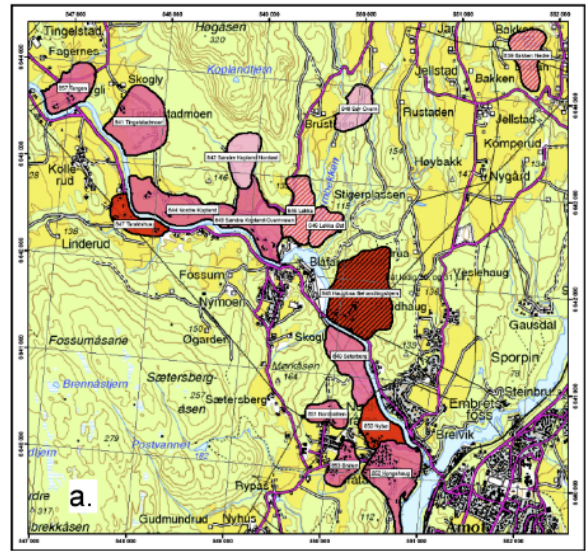


Figure 9 a. Landslide risk map for sensitive clays in the Modum region of Norway (from Lacasse and Nadim, 2009). b. Risk classes in a consequence-hazard or susceptibility diagram (based on the criteria of Lacasse and Nadim, 2009)

The frequency distribution approach, currently a principal method for quantifying hazard in terms of both diffuse failures and released propagated blocks, is not without its limitations. One significant drawback is the potential for substantial uncertainty. The power law used in this approach can be fitted using linear least squares regression or the maximum likelihood estimation (MLE) method, as noted by Dussauge et al. (2003). However, the reliability of this fitting is contingent upon the number of data points available. Despite achieving a perfect fit ($R^2 = 1.0$) with a reasonable dataset, simulations based on the derived power law will likely yield a lower R^2 , indicating inherent uncertainty in such a frequency distribution.

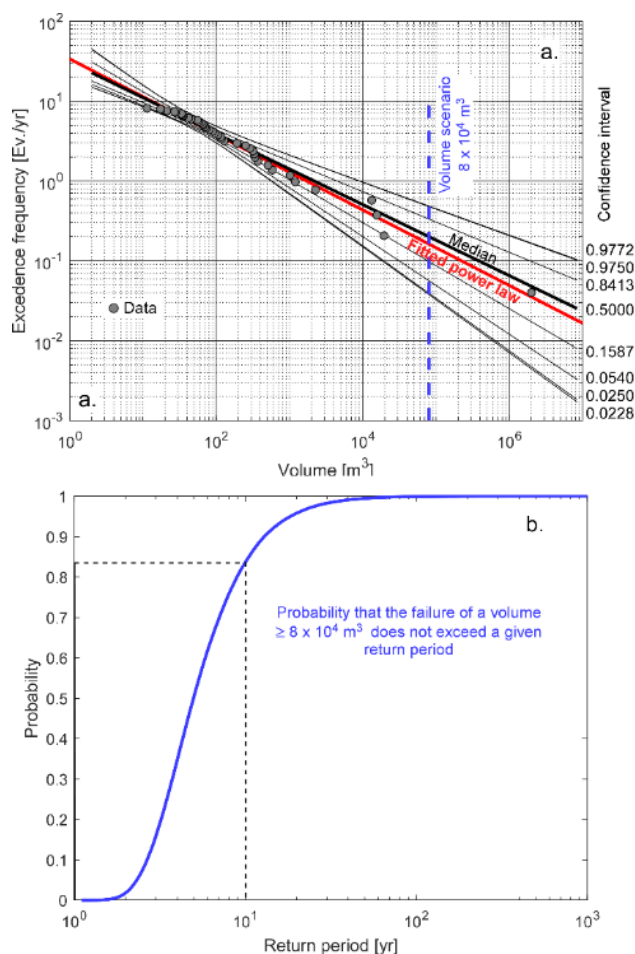


Figure 10 (a) Confidence intervals for the power law, derived from one million Monte Carlo simulations for 42 events. The original data from the La Brenva scar in Italy are represented by grey dots. (b) The probability that a volume equal to or larger than $8 \times 10^4 m^3$ will not exceed a certain return period (adapted from Fei et al. (2023)).

To ascertain the probability of a specific volume occurring within a given return period T , one can conduct simulations based on the fitted power laws. Repeated fittings across these datasets will yield a range of T -values for any given volume, as demonstrated by Fei et al. (2023) and illustrated in Figure 10b. For example, there is an 83% likelihood that an event with a volume equal to or greater than $8 \times 10^4 m^3$ will have a return period of less than 10 years, highlighting the inherent uncertainty in predicting specific volume occurrences.

Discussion and conclusions

The delineation of risk encompasses multiple facets, elucidated through diverse examples, indicating that risk frequently emanates from a qualitative analysis of two primary dimensions: hazard and consequences. Thus, the appraisal of risk is customarily conducted by experts within the domain. However, the imperative for establishing well-defined guidelines and frameworks for the evaluation of hazards, impacts, and consequentially, risk, is paramount (Corominas et al. 2014). Such a process necessitates meticulous attention towards its formulation,

facilitating the quantification of risk to inform decision-making processes. It is essential that stakeholders, encompassing both institutional and private entities, possess the capacity to reconstruct, comprehend, and endorse the methodology employed in deriving the outcome (Corominas et al. 2014). Furthermore, the assessment scale should embody the epitome of current best practices, incorporating extant data and regional expertise. Absence of adherence to these principles significantly escalates the potential for legal disputes in instances of predictive inaccuracies (Griffiths, 1999).

Even in scenarios where risk can be quantitatively evaluated with a degree of precision, such as in rockfall events through simulation techniques and the analysis of rockfall sources failure frequencies, a substantial level of uncertainty persists (Fei et al. 2023). This uncertainty necessitates that final evaluations are frequently refined by domain experts, underscoring the indissoluble link between susceptibility and risk assessments. This principle equally pertains to the evaluation of vulnerability. As a result, the employment of catastrophe modeling (CAT models) (Mitchell-Wallace et al. 2017), which incorporate uncertainty to generate an exceedance probability curve (Macciotta et al. 2016; Jaboyedoff et al. 2021), represents a potential strategy for navigating the inherent paradox presented by the inseparability of susceptibility, vulnerability, and risk assessments.

References

- Ale B. 2008, Risk: an introduction: the concepts of risk, danger and chance. Routledge, Taylor and Francis group, 134 p.
- Ale, B. Burnap, P. & Slater, D. 2015. On the origin of PCDS – (Probability consequence diagrams). Safety Science, 72, 229-239, doi: <https://doi.org/10.1016/j.ssci.2014.09.003>.
- Aven, T. & Renn, O. 2009. On risk defined as an event where the outcome is uncertain. Journal of Risk Research, 12, 1-11, doi: 10.1080/13669870802488883.
- Cardinali, M. Reichenbach, P. Guzzetti, F. Ardizzone, F. Antonini, G. Galli, M. Cacciano, M. Castellani, M. & Salvati, P. 2002. A geomorphological approach to the estimation of landslide hazards and risks in Umbria, Central Italy. Natural Hazards and Earth System Sciences, 2, 57-72, doi: 10.5194/nhess-2-57-2002.
- Carrara, A. Cardinali, M. Detti, R. Guzzetti, F. Pasqui, V. & Reichenbach, P. 1991. GIS techniques and statistical models in evaluating landslide hazard. Earth Surface Processes and Landforms, 16, 427-445, doi: <https://doi.org/10.1002/esp.3290160505>.
- Corominas, J. van Westen, C. Frattini, P. Cascini, L. Malet, J.P. Fotopoulou, S. Catani, F. Van Den Eeckhaut, M. Mavrouli, O. Agliardi, F. Ptilakis, K. Winter, M.G. Pastor, M. Ferlisi, S. Tofani, V. Hervás, J. and Smith, J.T. 2014. Recommendations for the quantitative analysis of landslide risk. Bulletin of Engineering Geology and the Environment, 73(2): 209-263.
- Cox LA Jr. 2008' What's wrong with risk matrices? Risk Analysis, 28, 497-512.
- Dussauge, C. Grasso, J.-R. & Helmstetter, A. 2003. Statistical analysis of rockfall volume distributions: Implications for rockfall dynamics. Journal of Geophysical Research: Solid Earth, 108, doi: 10.1029/2001jb000650.

- ECDC, 2011, European centre for Disease Prevention and Control: Operational guidance on rapid risk assessment methodology. Stockholm, ECDC, 68p.
- Farmer, F.R. 1967. Siting criteria-a new approach. Containment and Siting of Nuclear Power Plants. Proceedings of a Symposium on the Containment and Siting of Nuclear Power Plants.
- Farvacque, M. Lopez-Saez, J. Corona, C. Toe, D. Bourrier, F. & Eckert, N. 2019. How is rockfall risk impacted by land-use and land-cover changes? Insights from the French Alps. *Global and Planetary Change*, 174, 138-152, doi: 10.1016/j.gloplacha.2019.01.009.
- Fei, L. Jaboyedoff, M. Guerin, A. Noël, F. Bertolo, D. Derron, M.-H. Thuegaz, P. Troilo, F. & Ravel, L. 2023. Assessing the rock failure return period on an unstable Alpine rock wall based on volume-frequency relationships: The Brenva Spur (3916 m a.s.l. Aosta Valley, Italy). *Engineering Geology*, 323, 107239, doi: <https://doi.org/10.1016/j.enggeo.2023.107239>.
- Galli, M. & Guzzetti, F. 2007. Landslide Vulnerability Criteria: A Case Study from Umbria, Central Italy. *Environmental Management*, 40, 649-665, doi: 10.1007/s00267-006-0325-4.
- Griffiths, J.S. 1999. Proving the occurrence and cause of a landslide in a legal context. *Bulletin of Engineering Geology and the Environment*, 58, 75-85, doi: 10.1007/s100640050070.
- Gumbel, E.J. 1941. The Return Period of Flood Flows. *The Annals of Mathematical Statistics*, 12, 163-190.
- Gutenberg, B. & Richter, C.F. 1956. Earthquake magnitude, intensity, energy, and acceleration: (Second paper). *Bulletin of the Seismological Society of America*, 46, 105-145, doi: 10.1785/bssa0460020105.
- Guzzetti, F. Reichenbach, P. Cardinali, M. Galli, M. & Ardizzone, F. 2005. Probabilistic landslide hazard assessment at the basin scale. *Geomorphology*, 72, 272-299, doi: <https://doi.org/10.1016/j.geomorph.2005.06.002>.
- Haimes, Y.Y. 2008, 'Risk Modeling, Assessment, and Management'. 3rd Edition. John Wiley & Sons, 1009 p.
- Hantz, D. Vengeon, J.M. & Dussauge-Peisser, C. 2003. An historical, geomechanical and probabilistic approach to rock-fall hazard assessment. *Natural Hazards and Earth System Sciences*, 3, 693-701, doi: 10.5194/nhess-3-693-2003.
- Hantz, D. Colas, B. Dewez, T. Lévy, C. Rossetti, J.-P. Guerin, A. & Jaboyedoff, M. 2020. Caractérisation quantitative des aléas rocheux de départ diffus. *Rev. Fr. Geotech.* 2.
- Hungr, O. & Wong, H. 2007. Landslide risk acceptability criteria: are FN plots objective. *Geotechnical News*, 25, 47.
- Hungr, O. Evans, S.G. & Hazzard, J. 1999. Magnitude and frequency of rock falls and rock slides along the main transportation corridors of southwestern British Columbia. *Canadian Geotechnical Journal*, 36, 224-238, doi: 10.1139/t98-106.
- ISO 2018. Risk management—principles and guidelines. ISO 31000:24
- Jaboyedoff, M. 2023. Consequence: Frequency Matrix as a Tool to Assess Landslides Risk. In: Alcántara-Ayala, I. Arbanas, Ž. Huntley, D. Konagai, K. Mihalić Arbanas, S. Mikoš, M. V. Ramesh, M. Sassa, K. Sassa, S. Tang, H. & Tiwari, B. (eds.) *Progress in Landslide Research and Technology*, Volume 2 Issue 2, 2023. Springer Nature Switzerland, Cham, 137-153.
- Jaboyedoff, M. Choanji, T. Derron, M.-H. Fei, L. Gutierrez, A. Loiotine, L. Noel, F. Sun, C. Wyser, E. & Wolff, C. 2021. Introducing Uncertainty in Risk Calculation along Roads Using a Simple Stochastic Approach. *Geosciences*, 11, doi: 10.3390/geosciences11030143.
- Jaboyedoff M. Locat J. Merrien V. Michoud C. (in prep): Mouvements de terrain. PPUR. (a French treaty about landslides)
- Krause, J.-P. & R. Mock, Gheorghe A.D. 1995, Assessment of Risks from Technical Systems: Integrating Fuzzy Logic into the Zurich Hazard Analysis Method. in: *International Journal of Environment and Pollution (IJEP)* 5 (2-3), 278-296.
- Lacasse, S. & Nadim, F. 2009. Landslide Risk Assessment and Mitigation Strategy. In: Sassa, K. & Canuti, P. (eds.) *Landslides – Disaster Risk Reduction*. Springer Berlin Heidelberg, Berlin, Heidelberg, 31-61.
- Lacasse, S. Eidsvik, U. Nadim, F. Høeg, K. and Blikra, L.H. 2008. Event Tree analysis of Åknes rock slide hazard. IV Geohazards Québec, 4th Canadian Conf. on Geohazards. 551-557.
- Lanfranchi, C. Frattini, P. Sala, G. Dattola, G. Bertolo, D. Sun, J. & Crosta, G.B. 2023. Accounting for the effect of forest and fragmentation in probabilistic rockfall hazard. *Natural Hazards and Earth System Sciences*, 23, 2349-2363, doi: 10.5194/nhess-23-2349-2023.
- Leroi, E. Bonnard, C. Fell, R. & McInnes, R. 2005. Risk assessment and management. *Balkema*, 159-198. Porter, M. and Morgenstern, N. 2013. *Landslide Risk Evaluation – Canadian Technical Guidelines and Best Practices related to Landslides: a national initiative for loss reduction*; Geological Survey of Canada, Open File 7312, 21 p. doi:10.4095/292234
- Leroueil, S. & Locat, J. 1998. Slope movements: geotechnical characterisation, risk assessment and mitigation. *Proc. 11th Danube-European Conf. Soil Mech. Geotech. Eng. Porec, Croatia*, 95–106. Also published in *Proc. 8th Congress Int. Assoc. Eng. Geology, Vancouver*, 933-944, *Balkema, Rotterdam*.
- Li, Z. Nadim, F. Huang, H. Uzielli, M. & Lacasse, S. 2010. Quantitative vulnerability estimation for scenario-based landslide hazards. *Landslides*, 7, 125-134, doi: 10.1007/s10346-009-0190-3.
- Macciotta, R. Martin, C.D. Morgenstern, N.R. & Cruden, D.M. 2016. Quantitative risk assessment of slope hazards along a section of railway in the Canadian Cordillera—a methodology considering the uncertainty in the results. *Landslides*, 13, 115-127, doi: 10.1007/s10346-014-0551-4.
- Mitchell-Wallace, K. Jones, M. Hillier, J. & Foote, M. 2017. *Natural catastrophe risk management and modelling: A practitioner's guide*. John Wiley & Sons.
- Porter, M. and Morgenstern, N. 2013. *Landslide Risk Evaluation – Canadian Technical Guidelines and Best Practices related to Landslides: a national initiative for loss reduction*; Geological Survey of Canada, Open File 7312, 21 p. doi:10.4095/292234
- Rothman, K.J. 2012. *Epidemiology: an introduction*. Oxford university press.
- Ruiz-Carulla, R. Corominas, J. & Mavrouli, O. 2016. A fractal fragmentation model for rockfalls. *Landslides*, 14, 875-889, doi: 10.1007/s10346-016-0773-8.
- Stoffel, M. Bollschweiler, M. Widmer, S. & Sorg, A. 2010. Spatio-temporal variability in debris-flow activity: a tree-ring study at Geisstriftbach (Swiss Alps) extending back to AD 1736. *Swiss Journal of Geosciences*, 103, 283-292, doi: 10.1007/s00015-010-0014-4.
- UK-CO (Cabinet Office) 2017. National Risk Register Of Civil Emergencies, retrieved from https://assets.publishing.service.gov.uk/government/uploads/system/uploads/attachment_data/file/644968/UK_National_Risk_Register_2017.pdf
- Vengeon, J.-M. Hantz, D. & Dussauge, C. 2001. Prévisibilité des éboulements rocheux. Approche probabiliste par combinaison d'études historiques et géomécaniques. *Revue française de géotechnique*, 143-154.

Prediction of rainfall-induced landslides in a changing climate: issues and perspectives for regional-scale approaches

Stefano Luigi Gariano

CNR-IRPI (Italian National Research Council – Research Institute for Geo-Hydrological Protection), via Madonna Alta 126, Perugia, Italy, stefanoluigi.gariano@cnr.it

Abstract Global warming is unequivocal. An increase in the frequency and magnitude of intense rainfall events was observed in several areas of the World and more changes are expected. This has major implications for operational landslide prediction, given that the effects of climate change on landslides are difficult to determine and to predict. As a matter of fact, regional-scale landslide early warning systems, usually based on rainfall-related prediction tools and susceptibility zonation, need to consider these effects and the related variations. In Italy, where landslides are mainly triggered by intense and/or prolonged rainfall, several investigations were carried out for the prediction of rainfall-induced landslides, for the implementation of landslide early warning systems and for the evaluation of the role of climate and environmental changes (mostly rainfall and land use) on landslide activity, occurrence, and frequency. In this contribution, a brief overview of the defined methods, models and tools is presented. Special emphasis is placed on the definition of rainfall thresholds defining the minimum triggering conditions for the initiation of shallow landslides, given their usability in regional and national warning systems and in the evaluation of changes in the triggering conditions of the landslides. Issues and perspectives of regional-scale analyses of the ongoing and expected effects of climate change on rainfall-induced landslides are discussed.

Keywords landslides, rainfall, climate change, climate projections, landslide prediction, rainfall thresholds, Italy

Introduction

According to the last report of the International Panel on Climate Change (IPCC 2023), human-caused climate change is already affecting many weather and climate extremes in every region across the globe. This has led to widespread adverse impacts and related losses and damages to nature and people.

The last annual report of the International Disaster Database (CRED 2023) recorded 387 natural disasters worldwide in 2022 that affected 185 million individuals and caused 30,704 deaths, with economic losses that totalled around 223.8 billion US\$. A partial estimate for 2023 counted a 30% increase in the number of deaths (compared to 2022) due to climate-related events (i.e., floods, wildfires, cyclones, storms, and landslides) and a 60% rise in the number of deaths from landslides, globally.

The Global Fatal Landslide Database lists 4862 non-seismic landslides that caused 55 997 deaths worldwide in the period 2004-2016 (Froude and Petley 2018). In a European survey, 849,543 landslides were mapped in 20 national inventories (Herrera et al. 2018). Within Europe, Italy experiences a large number of landslides and related damage, with more than 622,000 landslides mapped by the Italian Institute for Environmental Protection and Research, covering about 8% of the national territory (<https://idrogeo.isprambiente.it/app/>). According to the last Polaris report by the Research Institute for Geo-Hydrological Protection of the Italian National Research Council (CNR-IRPI), between 1973 and 2022, landslides caused 144,806 people homeless or evacuees, 1077 deaths, 10 missing and 1443 injured persons in all the 20 administrative Italian regions (Bianchi and Salvati 2023; <https://polaris.irpi.cnr.it/>). Some severe rainfall events hit the Italian territory in 2022 and 2023, triggering thousands of landslides and causing dozens of victims (e.g., Donnini et al. 2023; Romeo et al. 2023; Ferrario and Livio 2024).

Individual landslides do not affect wide areas as floods, megafloods, and earthquakes; however, they are numerous and they occur frequently in hilly and mountainous areas. Landslides are complex and very diversified phenomena whose ranges of measures encompass different orders of magnitude (Guzzetti et al. 2012). Given the high spatial and temporal variability of the landslides, climate (and its change) can affect them in multiple ways and at different temporal and geographical scales (Gariano and Guzzetti 2016). The landslide response to climate change varies depending on the landslide type and size, and on the local stability or instability conditions. The response is different for first-time shallow failures and for the reactivation of large deep-seated landslides. Overall, the increase in frequency and intensity of the rainfall events may result in a change in the frequency, abundance, and location of rapid and very rapid landslides, mostly shallow slides and debris flows, which are the primary cause of landslide casualties, and therefore deserve particular attention. Nevertheless, these issues are often neglected in the operational prediction of rainfall-induced landslides (Gariano and Guzzetti 2022).

According to many literature reviews, Italy had a pivotal role in the preparation of a relevant number of studies in the topics of rainfall-induced landslide prediction (mostly with rainfall thresholds, Guzzetti et al. 2008; Chae et al. 2017; Segoni et al. 2018; Gariano et al. 2020a; Gonzalez et al. 2024), susceptibility assessment

(Reichenbach et al. 2018), and early warning (Piciullo et al. 2018; Guzzetti et al. 2020), as well as in the evaluation of the role of climate and environmental changes (mostly rainfall and land use) on landslides (Crozier 2010; Gariano and Guzzetti, 2016, 2022; Jakob 2021).

In this paper, a brief overview of methods and models for the prediction of the occurrence and activity of rainfall-induced landslides in a changing climate is presented, with an eye for regional-scale, empirical analyses.

Background

Main approaches to evaluate the relationships between rainfall and landslides

The relationships between rainfall and landslide occurrence/activation are generally modelled using two approaches (Guzzetti et al. 2022): physically-based (or deterministic) and empirical (or statistical). The first approach relies on numerical models and necessitates an extensive collection of precise hydrogeological and geotechnical variables to compute a factor of safety, which indicates the ratio between the local resisting and driving forces. The latter approach involves the statistical analysis of past rainfall conditions linked to landslide initiation, obtained by combining rainfall series with the dates at which slope movements occurred or were activated. To distinguish between conditions that likely trigger or do not trigger landslides, empirical relations have to be established using threshold values or functions. In most cases, the analysis results in the calculation of rainfall thresholds for landslide initiation.

Main approaches to evaluate the role of climate change on landslides

Three main approaches are employed to assess the role of climate change on the occurrence, frequency, and activity of landslides (Gariano and Guzzetti 2016, 2022): (i) the implementation of numerical climate and landslide models, i.e. the use of rainfall projections, generated by downscaled and bias-corrected global climate models, as input to slope stability and landslide hazard models of different types (modelling approach); (ii) the execution of empirical analyses of landslides and climatic (mostly rainfall and temperature) records, usually over a period that last from 30 to around 100 years, attempting at assessing geographical and temporal variations in landslides activity (empirical approach); (iii) the study of paleo-evidences of landslides, proxy climate indicators, and climate data, in a time range that covers the period from 40,000 BP to the 20th century. In recent years, there has been a significant rise in the amount of studies that have used a modelling approach to examine the relationships between landslides and climate at the basin, regional, and national scales (Gariano and Guzzetti 2022; Gariano and Rianna 2024). In some cases, the empirical and the modelling approaches were successfully coupled.

Landslide prediction in a changing climate

Empirical rainfall thresholds: definition and usability

Empirical rainfall thresholds have become the most used tools to analyse the triggering conditions of slope failures and to predict the possible occurrence of a landslide or of a population of landslides in a given area (Segoni et al. 2018; Guzzetti et al. 2020; Gonzalez et al. 2024).

Among the diverse methods adopted to calculate thresholds, the frequentist method (Brunetti et al. 2010; Peruccacci et al. 2012) has become the most used worldwide. This method is based on a frequency analysis of the empirical rainfall conditions that have resulted in known landslides in a given period and in a given area. The threshold is modeled by a power law relationship between cumulated event rainfall E (in mm) and the rainfall duration D (generally in hours, also in days), according to equation [1]:

$$E = (\alpha \pm \Delta\alpha)D^{(\gamma \pm \Delta\gamma)} \quad [1]$$

where α is the intercept (the scaling parameter) and γ is the slope (the scaling exponent) of the curve, and $\Delta\alpha$ and $\Delta\gamma$ are the uncertainties associated with α and γ , respectively. The method allows the calculation of objective and reproducible thresholds at different non-exceedance probabilities, and the uncertainties associated with the threshold parameters. The 5% non-exceedance probability thresholds is usually calculated, as a reference with previous works.

To define reliable thresholds, a large amount of accurate spatial and temporal information on landslides induced by rainfall in a given study area (generally collected in a catalogue, e.g. Peruccacci et al. 2023) is needed. A tool for the objective and reproducible identification of the rainfall conditions likely responsible for landslide triggering and the calculation of frequentist rainfall was implemented using the R open-source software and is freely downloadable (Melillo et al. 2018). Details on the methods and tools needed to define rainfall thresholds with the frequentist method can be found in Guzzetti et al. (2022) and references therein.

Using a catalogue of 2309 rainfall events responsible for the occurrence of shallow landslides in Italy between 1996 and 2014, national and regional thresholds for climate and meteorological domains in the Italian territory were defined by Peruccacci et al. (2017). In particular, five classes distinguished by a progressive average annual precipitation were considered and the frequentist rainfall thresholds for the landslides that occurred in each area were calculated. A key observation was that regions with higher mean annual precipitation values were characterized by higher and steeper thresholds. In more rainy areas, the landscape requires a greater amount of rainfall to trigger landslides, compared to less rainy areas with comparable environmental conditions. This finding suggests that the landscape adapts to the rainfall patterns prevalent in the area. A relevant implication is that when

and where the weather regimes undergo a transformation as a consequence of global warming, the thresholds are anticipated to change, and the operational prediction systems (mostly based on thresholds) will also necessitate corresponding adjustments.

Frequentist rainfall thresholds can be also used to assess the variations in the landslide-triggering conditions over long periods, both in the past and in the future (using landslide-climate simulations), as described below.

Changes in landslide-triggering conditions: a look at the past

Adopting an empirical approach at the regional scale, the variations in the occurrence of rainfall-induced landslides in Calabria region, southern Italy, in the 90-year period 1921-2010 were analysed (Gariano et al. 2015). In particular, using a catalogue of 7000 landslides and daily rainfall data recorded by 318 rain gauges, 1466 rainfall events with landslides (REs) were reconstructed in the investigated period. A rainfall event with landslides was defined as the occurrence of one or more landslide during or shortly after a rainfall event. Fig. 1 shows the flowchart and data used in to reconstruct the REs and their temporal and spatial distribution.

The dataset was split in three 30-year sub-periods (1921-1950, 1951-1980, and 1981-2010) and the changes in the spatial and temporal distribution of the REs, as well as the changes in the landslide-triggering rainfall conditions and in the impact of the landslides to the population were evaluated. For the spatial analyses, the municipality boundaries were used as units of analysis; for the assessment of the landslide impact to the population, the number of REs in each municipality was ratioed to the

number of inhabitants per municipality measured by national censuses conducted in 1951, 1981, and 2011.

Changes in the geographical and the temporal distributions of the REs were observed, with a particular concentration of the events in the late winter and early spring in the recent-most 30-year period. A rise of approximately 40% in the population living in municipalities with increased impact posed by the landslides was observed; this was ascribed to a confluence of climate-related and societal transformations in the region over the investigated period.

The landslide-triggering rainfall conditions were evaluated calculating the duration (*D*) and the cumulated rainfall (*E*) of the REs that occurred in each of the three defined 30-year periods. Lower values of the average and maximum cumulated event rainfall that have resulted in landslides were observed in the recent-most 30-year period 1981-2010 than in the previous periods. This can be considered a proxy of an increased vulnerability of the territory, which need less rainfall to trigger a landslide than in the past.

An update of that work is here proposed, with the calculation of the frequentist, landslide-triggering rainfall thresholds for several 30-year periods defined using a moving window with a 5-year step, rather than only for the three separated 30-year periods. This results in thirteen periods and, consequently, thirteen thresholds, allowing a more precise evaluation of the changes. Tab. 1 lists the mean values of *D* and *E* for the rainfall events that have induced landslides in the thirteen 30-year periods and the equations of the related thresholds. Fig. 2 shows the thirteen thresholds and Fig. 3 shows the how the threshold parameters change over time.

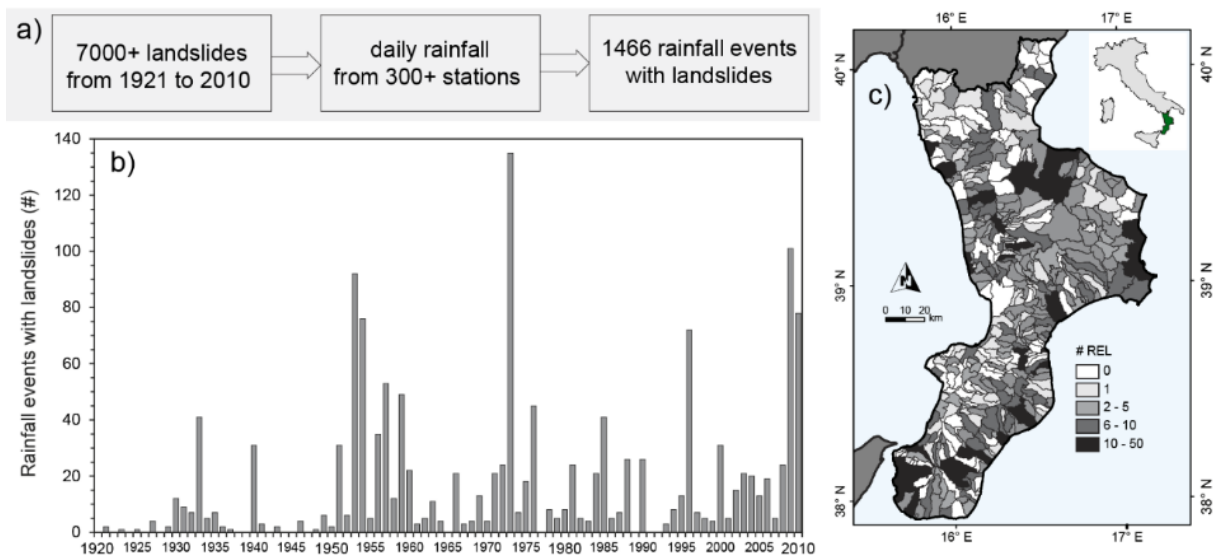


Figure 1 a) Flowchart and data used for the reconstruction of the rainfall events with landslides (REs). b) Temporal distribution of the 1466 REs occurred in Calabria region, Italy, from 1921 to 2010. c) Geographical distribution of the REs in the municipalities of the Calabria region. Modified from Gariano et al. (2015).

Table 1 Parameters of the *ED* frequentist thresholds at 5% non-exceedance probability calculated for different 30-year periods in Calabria region, southern Italy. Key: Threshold equations according to eq. [1]; *D*, rainfall duration (in days); *E*, cumulated event rainfall (in mm).

Period	Threshold equation	Mean <i>D</i> (day)	Mean <i>E</i> (mm)
1921-1950	$E = (11.1 \pm 1.4)D^{(0.93+0.05)}$	7.3	232.1
1926-1951	$E = (12.1 \pm 1.1)D^{(0.87+0.04)}$	6.8	282.5
1931-1960	$E = (15.5 \pm 1.3)D^{(0.77+0.04)}$	7.9	253.2
1936-1965	$E = (17.2 \pm 1.5)D^{(0.72+0.04)}$	7.8	242.9
1941-1970	$E = (15.8 \pm 1.4)D^{(0.75+0.04)}$	7.9	240.5
1946-1975	$E = (16.1 \pm 1.4)D^{(0.73+0.04)}$	7.5	236.3
1951-1980	$E = (15.3 \pm 1.2)D^{(0.75+0.04)}$	7.2	225.7
1956-1985	$E = (15.6 \pm 1.4)D^{(0.74+0.04)}$	7.0	196.0
1961-1990	$E = (14.1 \pm 1.4)D^{(0.76+0.05)}$	6.4	182.7
1966-1995	$E = (14.4 \pm 1.5)D^{(0.74+0.05)}$	6.2	180.9
1971-2000	$E = (15.5 \pm 1.5)D^{(0.69+0.05)}$	5.7	176.4
1976-2005	$E = (15.2 \pm 1.4)D^{(0.66+0.05)}$	5.4	145.7
1981-2010	$E = (16.0 \pm 1.2)D^{(0.66+0.04)}$	6.6	167.2

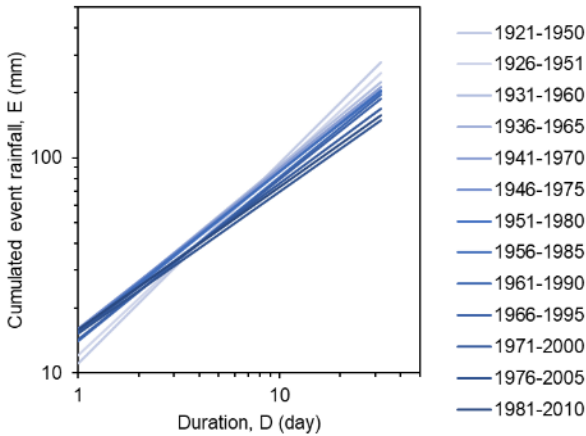


Figure 2 *ED* rainfall thresholds defined for thirteen 30-year moving windows from 1921 to 2010 in Calabria region, southern Italy. The regions of uncertainty of the thresholds are not shown.

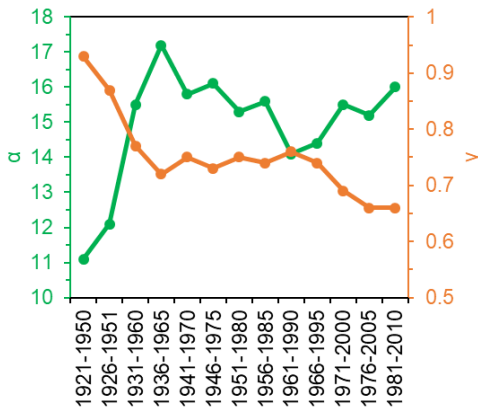


Figure 3 Values of the parameters of the frequentist thresholds defined for thirteen 30-year moving windows from 1921 to 2010 in Calabria region, southern Italy.

A slight decrease in the mean values of the duration of the landslide-triggering rainfall events and a marked decrease in the mean values of the cumulated rainfall can

be observed, indicating a trend in the increase of the propensity of the landscape to generate landslides, even with less rain needed. Moreover, an increase in the α parameter and a decrease in the γ parameter during time is clearly visible. The thresholds become higher and less steep in the recent years, meaning that, in the study area, the landslide-triggering rainfall events of short durations were characterized by higher cumulated rainfall, i.e. they became more intense.

The same approach described in Gariano et al. (2015) was applied in Umbria, a region in Central Italy (Gariano et al. 2021), to investigate changes in the spatial distribution and temporal occurrence of 453 rainfall-induced landslides that occurred from 1928 to 2001. Landslide-triggering rainfall thresholds can be defined also in this case by adopting the frequentist approach. However, due to a lower number of RELs in the first part of the observation period, reliable thresholds can be defined only for the period 1971-200. Tab. 2 lists the mean values of *D* and *E* for the rainfall events that have induced landslides in five 30-year periods and the equations of the five related thresholds. Landslide-triggering rainfall events underwent changes in characteristics over the observation period also in this area. Specifically, the landslides occurred in the recent most period were triggered by rainfall events with on average lower cumulated rainfall and shorter duration, especially during the winter and early spring seasons. The propensity of this area to generate landslides has also increased with time. Moving forward through time, the landslide-triggering rainfall thresholds became flatter also in this area.

Table 2 Parameters of the *ED* thresholds at 5% non-exceedance probability calculated for five 30-year periods in Umbria region, central Italy. Key: Threshold equations according to eq. [1]; *D*, rainfall duration (in days); *E*, cumulated event rainfall (in mm).

Period	Threshold equation	Mean <i>D</i> (day)	Mean <i>E</i> (mm)
1951-1980	$E = (14.8 \pm 1.7)D^{(0.47+0.06)}$	4.3	80.3
1956-1985	$E = (14.5 \pm 1.3)D^{(0.48+0.06)}$	4.2	76.1
1961-1990	$E = (14.4 \pm 1.0)D^{(0.46+0.05)}$	4.2	72.5
1966-1995	$E = (15.6 \pm 1.0)D^{(0.44+0.05)}$	3.7	72.6
1971-2000	$E = (16.8 \pm 1.0)D^{(0.41+0.04)}$	3.6	77.6

The results obtained in both cases may seem contrasting at first glance. However, such findings indicate that, in the studied areas, on the one hand the mean values of the cumulated rainfall associated with landslides were lowering, suggesting that less rainfall was needed to trigger landslides in the recent-most years than in the past. On the other hand, the distribution (in the *D-E* space) and the characteristics of landslide-triggering conditions, which shapes the threshold curves, was changing over time. In particular, the short-term landslide-triggering rainfall conditions became characterized by higher cumulated rainfall in the recent-most years, while the ones with long durations had lower cumulated rainfall. These findings can be relevant for scientific purposes and

practical applications, e.g. land planning and design of operational systems for landslides prediction.

Other examples in which rainfall thresholds, either empirical or physically-based, were used to evaluate past and future changes in landslide triggering conditions in Italy can be found in Rianna et al. (2017, 2020), Alvioli et al. (2018), Sangelantoni et al. (2018).

Changes in landslide-occurrence: a look towards the future

A well-populated historical catalogue of rainfall events with landslide like the one collected in Calabria region is also useful to define a calibration set for climatic models, in order to evaluate possible future landslide projections. Indeed, using the recent part of the catalogue of RELs occurred in Calabria (specifically the last 30-year period 1981–2010, which lists information about 600 landslides) and daily rainfall measurements in the same period, empirical correlations between landslide occurrence and two climate variables assumed to be proxies for landslide activity, i.e. mean annual rainfall and seasonal cumulative rainfall, were defined (Gariano et al. 2017). A good correlation was found between the mean annual rainfall and the number of rainfall events with landslides.

Combining this correlation laws with mid-term (2036–2065) projections of the mean annual rainfall obtained for two climate scenarios (i.e., Representative Concentration Pathways RCP4.5 and RCP8.5), future scenarios for possible landslide occurrence in the region were defined. In particular, the CMCC_CM (Scoccimarro et al. 2016), with a horizontal resolution of about 80 km, was used as Global Circulation Model in the simulation chain. Moreover, a dynamical downscaling through the COSMO_CLM model (Bucchignani et al. 2015) at 8 km resolution was adopted.

Results outlined an increase in landslide occurrence in the future period 2036–2065, in both scenarios: +21.2% for the “mid-way” RCP4.5 scenario and +45.7 for the more pessimistic RCP8.5 scenario. This experiment showed that the empirical and the modelling approaches can be successfully combined. Furthermore, using projections of population data for the year 2065, the variations in the impact of RELs on the population of the region of Calabria in the future period 2036–2065 were assessed using the same methods proposed in Gariano et al. (2015). A relevant increase in the landslide impact to the population was modelled for both climate scenarios. Such changes can be due to either changes in the number of the rainfall-induced landslides and in the number of the exposed elements (only population in this case).

Since a catalogue of landslides that caused damage to citizens, properties, and infrastructures was used for these works, the obtained results can be useful for societal and land planning, and the definition of actions for landslide risk management in the study area.

The role of land use/cover in landslide occurrence

The evaluation of the role of land use/cover on landslides is a remarkable topic (e.g. Sidle and Ochiai 2006). The effects of climate change on vegetation, soil, land use and

land cover, together with the associated feedback processes, contribute to more intricate interactions within an already challenging assessment.

An assessment of spatial and temporal variations in landslide occurrence at regional scale under the effect of land use/cover changes was also conducted in Calabria region (Gariano et al. 2018). The complete record of landslides that were recorded in the region from 1921 to 2010, together with land use/cover maps from 1956 (from the Italian National Research Council and the Italian Touring Club) and 2000 (from CORINE land cover project), and future estimates of projected land use/cover changes at 2050 (an ensemble of 32 simulations from the LUC@CMCC model; Santini and Valentini, 2011) were employed. Empirical relationships linking the observed land use/cover variations to landslide occurrence were defined. The modelling findings indicated that landslide occurrence increased across the majority of the regional territory. However, it was observed that land use changes that imply agricultural practices and land management that can mitigate landslide occurrence had positive local effects. Regarding the future, the landslide projections conditioned to the land use/cover change ensemble reveal an overall, modest increase in landslide occurrence in all scenarios. An increase in the number of landslides due to land use/cover variations was projected in 291 municipalities in Calabria (71%), with 4 municipalities where the increase is expected to exceed 50%. In this case, too, the results may suggest a join in the climate and social factors involved.

Other examples in which land use/cover and their changes were considered to evaluate past and future changes in landslide occurrence in Italy can be found in Reichenbach et al. (2014), Lonigro et al. (2017), Persichillo et al. (2017), and Pisano et al. (2017).

Discussion and perspectives

The majority of the research works that attempted to assess how the observed and expected climatic and environmental changes might affect landslides looked at case studies in Europe. Most basin-, regional-, and national-scale studies model the links between landslides and climate using empirical and statistical analyses (Gariano and Guzzetti 2022; Gariano and Rianna 2024).

In this contribution, a brief overview on the possible use of empirical analyses and models for the quantitative evaluation of the impact of climate change on landslide at the regional scale is presented, with a focus on applications in Italy, which is the country with the largest number of applications and case studies on this topic.

The use of an empirical approach has pros and cons. The primary advantage is the possibility to apply the same method to different study areas where similar data is available, so allowing a quantitative comparison of the results. Moreover, an empirical approach can be effectively combined with a climate modelling chain, to evaluate not only the changes in the past but also the expected future variations.

A relevant issue in the adoption of the climate modelling chain (Rianna et al. 2014; Gariano and Guzzetti 2016) is the selection of the global circulation models, of the technique to downscale to a regional model, of the bias correction methods and of the concentration scenario. The selection of only “extreme” scenarios is not advisable, while the adoption of ensembles guarantee more reliable results (Jakob 2021). Furthermore, considering that an increasing number of countries are now requiring the reduction of carbon emissions by a given time horizon, if the current policies remain as ambitious until 2100, the “business-as-usual” scenario (RCP 8.5) is not the most probable outcome, but rather an extreme possibility. For this reason, it should not always be used as the worst-case scenario in modelling applications; conversely the use of more realistic scenarios could lead to more effective policy-making (Hausfather and Peters 2020).

A downside of any empirical approach is the need of a sufficiently long series of data, which is even more important in the evaluation of spatial and temporal variations in landslide activity due to global changes. An incomplete or poorly extended series of climate and landslide records limits the possibility to properly evaluate the impact of the climate and environmental changes on landslide frequency and distribution (Crozier 2010). Regardless of the approach used to model the relationships among rainfall and landslides (and their changes), accurate and complete records of landslides and their consequences, preferably collected with common standards and procedures, are needed for modelling purposes. The catalogues used in the works discussed here (Gariano et al. 2015, 2017, 2018, 2021) can be considered accurate and complete with regard to rainfall-induced landslides that have caused damage to people, property, and infrastructure in the study areas, and have been reported by relevant information sources. Moreover, a sufficiently long series of climate records (at least 30 years,) is necessary to effectively eliminate interannual fluctuations and anomalies, while still capturing longer-term climate patterns.

A key question in the application of a model at the regional scale is the choice of the unit of analysis. In the works described in this contribution, the municipality boundaries were selected as reference spatial unit, to evaluate spatial changes, assess landslide impact, assign a land use/cover class. This choice enabled an effective matching between environmental and socio-economic data. However, the methods discussed in this contribution can be applied adopting different units of analysis.

A noteworthy issue is that the rainfall thresholds defined using long series of past landslide and rainfall data to evaluate their spatial and temporal variations, as in the cases here presented, should not be applied to operational landslide prediction. Utilizing data series that span extensive periods of time (especially in the past) imply the use of rainfall data with coarse temporal resolution (e.g. daily rainfall series), which is proved to be a cause of high uncertainty and underestimation of landslide-triggering

rainfall thresholds (Gariano et al. 2020b), hampering their application in operational landslide early warning systems.

The evaluation of uncertainties in landslide prediction or in the evaluation of the role of climate change on landslide activity is frequently overlooked. Despite the relevant improvements achieved in the recent years in all components of the landslide-climate modelling chain, significant epistemic and aleatory uncertainties are expected to persist. Their evaluation (and communication) is crucial. The quantification and the reduction of the uncertainties in landslide projections can be achieved improving the methods for landslide modelling, and using ensembles of climate projections, which is more common now than in the past.

An important challenge in assessing the impact of climate change on landslides is the limited overlap between the temporal (short and long term) and geographical (local, regional, global) scales of climate analysis and landslide phenomena (Gariano and Guzzetti 2016; 2022). This discrepancy makes modelling and extrapolation increasingly complex. It should be remarked that simple inferences linking climate change to an increase in landslide activity can be erroneous (Jakob 2021). The complexity of the situation prevents the definition of a single approach suggesting the way of a multidisciplinary, holistic approach (Picarelli et al. 2016). Quantitative, regional-scale analyses in which historical and modelling approaches are combined to evaluate the impact of observed and projected rainfall variations on the frequency or magnitude (or both) of landslides of various types and in different physiographical settings could lead to reliable results and reduce all the inherent uncertainties.

In addition, in the evaluation of strategies for the mitigation of landslides risk in a changing world, it should be taken in mind that climate and its variations have a significant influence on both environmental and socio-economic elements, with several feedback mechanisms (Pasini et al. 2018). Climate change has an influence on both landslide activity and landscape vulnerability (e.g. due to changes in land use); the exposure of population and infrastructure to landslides is closely linked to the socio-economic conditions of the affected regions. In some cases, variations in environmental or socio-economic factors could have impacts on landslides even higher than climate change. Such issues are also crucial in the definition of effective adaptation measures.

Conclusions

The evaluation of the effects of climate and environmental changes on landslides is, and will remain, a relevant and noteworthy research topic, which requires appropriate funding and political support. With good efforts, the prediction of rainfall-induced landslides in a changing environment is feasible and can help reduce landslide hazard and risk. Rigorous approaches, either empirical or physically-based, should be based on accurate and complete (as much as possible) landslide records and climate series, with the aim of reducing the uncertainties

in the modeling results. Regional-scale analyses, looking at both the (observed) past and the (projected) future, provide comprehensive insight into the relationship between climate change and landslides, which can have useful implications for decision-making and the design of adaptation strategies.

A comprehensive and interdisciplinary strategy is needed to understand and quantify the impact of climatic factors and their changes on landslides, especially in the assessment of landslide hazard and risk.

Acknowledgements

The work described here is the outcome of the studies I began during my PhD and continued during my research activities, thanks to the collaboration of many colleagues. I would like to thank in particular Maria Teresa Brunetti, Fausto Guzzetti, Massimo Melillo, Silvia Peruccacci, Olga Petrucci, and Guido Rianna, whose contributions were crucial for the realization of this work.

References

- Alvioli M, Melillo M, Guzzetti F, Rossi M, Palazzi E, von Hardenberg J, Brunetti MT, Peruccacci S (2018) Implications of climate change on landslide hazard in Central Italy. *Science of the Total Environment*. 630:1528–1543. <https://doi.org/10.1016/j.scitotenv.2018.02.315>
- Bianchi C, Salvati P (2023) Rapporto Periodico sul Rischio posto alla Popolazione italiana da Frane e Inondazioni. Anno 2023, Istituto di Ricerca per la Protezione Idrogeologica (IRPI), Consiglio Nazionale delle Ricerche (CNR) <https://doi.org/10.30437/report2023> (in Italian)
- Bucchignani E, Montesarchio M, Zollo AL, Mercogliano P (2015) High-resolution climate simulations with COSMO-CLM over Italy: performance evaluation and climate projections for the 21st century. *International Journal of Climatology* 36(2):735–756. <http://dx.doi.org/10.1002/joc.4379>
- Brunetti MT, Peruccacci S, Rossi M, Luciani S, Valigi D, Guzzetti F (2010) Rainfall thresholds for the possible occurrence of landslides in Italy. *Natural Hazards and Earth System Sciences* 10:447–458. <https://doi.org/10.5194/nhess-10-447-2010>
- Donnini M, Santangelo M, Gariano SL, Bucci F, Peruccacci S, Alvioli M, Althwaynee O, Ardizzone F, Bianchi C, Bornaetxea T, Brunetti MT, Cardinali M, Esposito G, Grita S, Marchesini I, Melillo M, Salvati P, Yazdani M, Fiorucci F (2023) Landslides triggered by an extraordinary rainfall event in Central Italy on September 15, 2022. *Landslides* 20:2199–2211. <https://doi.org/10.1007/s10346-023-02109-4>
- Chae B-G, Park H-J, Catani F, Simoni A, Berti M (2017) Landslide prediction, monitoring and early warning: a concise review of state-of-the-art. *Geosciences Journal* 21:1033–1070. <https://doi.org/10.1007/s12303-017-0034-4>
- CRED (2023) 2022 Disasters in numbers Centre for Research on the Epidemiology of Disasters, Brussels. https://cred.be/sites/default/files/2022_EMDAT_report.pdf
- Crozier MJ (2010) Deciphering the effect of climate change on landslide activity: a review. *Geomorphology* 124:260–267. <http://dx.doi.org/10.1016/j.geomorph.2010.04.009>
- Ferrario MF, Livio F (2024) Rapid Mapping of Landslides Induced by Heavy Rainfall in the Emilia-Romagna (Italy) Region in May 2023. *Remote Sensing* 16(1):122. <https://doi.org/10.3390/rs16010122>
- Froude MJ, Petley DN (2018) Global fatal landslide occurrence from 2004 to 2016. *Natural Hazards and Earth System Sciences* 18:2161–2181. <https://doi.org/10.5194/nhess-18-2161-2018>
- Gariano SL, Guzzetti F (2016) Landslides in a changing climate. *Earth-Science Reviews*. 162:227–252. <https://doi.org/10.1016/j.earscirev.2016.08.011>
- Gariano SL, Guzzetti F (2022) Mass-Movements and Climate Change. *Treatise on Geomorphology* (Second Edition). 5:546–558. <https://doi.org/10.1016/B978-0-12-818234-5.00043-2>
- Gariano SL, Petrucci O, Guzzetti F (2015) Changes in the occurrence of rainfall-induced landslides in Calabria, southern Italy, in the 20th century. *Natural Hazards and Earth System Sciences*. 15:2313–2330. <https://doi.org/10.5194/nhess-15-2313-2015>
- Gariano SL, Rianna G, Petrucci O, Guzzetti F (2017) Assessing future changes in the occurrence of rainfall-induced landslides at a regional scale. *Science of the Total Environment*. 596-597:417–426. <https://doi.org/10.1016/j.scitotenv.2017.03.103>
- Gariano SL, Petrucci O, Rianna G, Santini M, Guzzetti F (2018) Impacts of past and future land changes on landslides in southern Italy. *Regional Environmental Change*. 18:437–449. <https://doi.org/10.1007/s10113-017-1210-9>
- Gariano SL, Segoni S, Piciullo L (2020a) Advances in rainfall thresholds for landslide triggering in Italy. In: *Applied Geology*. Springer, pp. 247–263. https://doi.org/10.1007/978-3-030-43953-8_15
- Gariano SL, Melillo M, Peruccacci S, Brunetti MT (2020b) How much does the rainfall temporal resolution affect rainfall thresholds for landslide triggering? *Natural Hazards* 100:655–670. <https://doi.org/10.1007/s11069-019-03830-x>
- Gariano SL, Verini Supplizi G., Ardizzone F., Salvati P., Bianchi C., Morbidelli R., Saltalippi C (2021) Long-term analysis of rainfall-induced landslides in Umbria, central Italy. *Natural Hazards* 106(3):2207–2225. <https://doi.org/10.1007/s11069-021-04539-6>
- Gariano SL, Rianna G (2024) Modelling approaches to evaluate the role of climate change in landslide activity in Europe, EGU General Assembly 2024, Vienna, Austria, 14–19 Apr 2024, EGU24-14725, <https://doi.org/10.5194/egusphere-egu24-14725>
- Gonzalez FCG, Cavacanti MDCR, Nahas Ribeiro W, Mendonça MB, Haddad AN (2023) A systematic review on rainfall thresholds for landslides occurrence. *Heliyon* 3(10):e23247. <https://doi.org/10.1016/j.heliyon.2023.e23247>
- Guzzetti F, Peruccacci S, Rossi M, Stark CP (2008) The rainfall intensity-duration control of shallow landslides and debris flows: an update. *Landslides* 5:3–17. <https://doi.org/10.1007/s10346-007-0112-1>
- Guzzetti F, Mondini AC, Cardinali M, Fiorucci F, Santangelo M, Chang K-T (2012) Landslide inventory maps: New tools for an old problem. *Earth-Science Reviews* 112:42–66. <https://doi.org/10.1016/j.earscirev.2012.02.001>
- Guzzetti F, Gariano SL, Peruccacci S, Brunetti MT, Marchesini I, Rossi M, Melillo M (2020) Geographical landslide early warning systems. *Earth-Science Reviews* 200:102973. <https://doi.org/10.1016/j.earscirev.2019.102973>
- Guzzetti F, Gariano SL, Peruccacci S, Brunetti MT, Melillo M (2022) Rainfall and landslide initiation. In *Morbidelli R (Ed.) Rainfall - Modeling, Measurement and Applications*, Elsevier, pp. 427–450. <https://doi.org/10.1016/B978-0-12-822544-8.00012-3>
- Hausfather Z, Peters GP (2020) Emissions – the ‘business as usual’ story is misleading. *Nature* 577:618–620. <https://doi.org/10.1038/d41586-020-00177-3>
- Herrera G, Mateos RM, Garcia-Davalillo JC, Grandjean G, Poyiadji E, Maftai R, Filipciuc T-C, Jemec Aulfic M, Jež J, Podolszki L, Trigila A, Iadanza C, Raetzo H, Kociu A, Przyłucka MKułał M, Sheehy M, Pellicer XM, McKeown C, Ryan G, Kopacková V, Frei M, Kuhn D, Hermanns RL, Koulermou N, Smith CA, Engdahl M, Buxó P, Gonzalez M, Dashwood C, Reeves H, Cigna F, Liščák P, Pauditš P,

- Mikulenias V, Demir V, Raha M, Quental L, Sandic C, Fusi B, Jensen OA (2018) Landslide databases in the Geological Surveys of Europe. *Landslides* 15:359–379. <https://doi.org/10.1007/s10346-017-0902-z>
- IPCC (2023) Climate Change 2023: Synthesis Report. Contribution of Working Groups I, II and III to the Sixth Assessment Report of the Intergovernmental Panel on Climate Change [Core Writing Team, H. Lee and J. Romero (eds.)]. IPCC, Geneva, Switzerland, 184 pp., doi: 10.59327/IPCC/AR6-9789291691647
- Jakob M (2022) Landslides in a changing climate. In: Davies T, Rosser N, Shroder F (Eds.) *Landslide Hazards and Disasters Series, Second Edition* 505–579. <https://doi.org/10.1016/B978-0-12-818464-6.00003-2>
- Lonigro T, Gentile F, Polemio M (2017) The influence of climate variability and land use variations on the occurrence of landslide events (Subappennino Dauno, Southern Italy). *Italian Journal of Engineering Geology and Environment*, 85–92. <https://doi.org/10.4408/IJEGE.2017-01.S-08>
- Melillo M, Brunetti MT, Peruccacci S, Gariano SL, Roccati A, Guzzetti F (2018) A tool for the automatic calculation of rainfall thresholds for landslide occurrence. *Environmental Modelling & Software* 105:230–243. <https://doi.org/10.1016/j.envsoft.2018.03.024>
- Pasini A, Mastrojeni G, Tubiello FN (2018) Climate actions in a changing world. *The Anthropocene Review* 5(3):237–241. <https://doi.org/10.1177/2053019618794213>
- Persichillo MG, Bordoni M, Meisina C (2017) The role of land use changes in the distribution of shallow landslides. *Science of the Total Environment* 574:924–937. <https://doi.org/10.1016/j.scitotenv.2016.09.125>
- Peruccacci S, Brunetti MT, Luciani S, Vennari C, Guzzetti F (2012) Lithological and seasonal control of rainfall thresholds for the possible initiation of landslides in central Italy. *Geomorphology* 139–140:79–90. <https://doi.org/10.1016/j.geomorph.2011.10.005>
- Peruccacci S, Brunetti MT, Gariano SL, Melillo M, Rossi M, Guzzetti F (2017) Rainfall thresholds for possible landslide occurrence in Italy. *Geomorphology* 290:39–57. <https://doi.org/10.1016/j.geomorph.2017.03.031>
- Peruccacci S, Gariano SL, Melillo M, Solimano M, Guzzetti F, Brunetti MT (2023) The ITALian rainfall-induced Landslides Catalogue, an extensive and accurate spatio-temporal catalogue of rainfall-induced landslides in Italy. *Earth System Science Data* 15:2863–2877. <https://doi.org/10.5194/essd-15-2863-2023>
- Picarelli L, Comegna L, Gariano SL, Guzzetti F, Mercogliano P, Rianna G, Santini M, Tommasi P (2016) Potential climate changes in Italy and consequences on land stability, in Ho K, Lacasse S, Picarelli L (eds) *Slope Safety Preparedness for Impact of Climate Change*, pp. 151–198, CRC press, ISBN 9781138032309
- Piciullo L, Calvello M, Cepeda JM (2018) Territorial early warning systems for rainfall-induced landslides. *Earth-Science Reviews* 179:228–247. <https://doi.org/10.1016/j.earscirev.2018.02.013>
- Pisano L, Zumpano V, Malek Z, Roskopf CM, Parise M (2017) Variations in the susceptibility to landslides, as a consequence of land cover changes: A look to the past, and another towards the future. *Science of the Total Environment* 601–602:1147–1159. <https://doi.org/10.1016/j.scitotenv.2017.05.231>
- Reichenbach P, Busca C, Mondini AC, Rossi M (2014) The influence of land use change on landslide susceptibility zonation: the Briga catchment test site (Messina, Italy). *Environmental Management* 54:1372–1384. <https://doi.org/10.1007/s00267-014-0357-0>
- Reichenbach P, Rossi M, Malamud BD, Mihir M, Guzzetti F (2018) A review of statistically-based landslide susceptibility models. *Earth-Science Reviews* 180:60–91. <https://doi.org/10.1016/j.earscirev.2018.03.001>
- Rianna G, Zollo AL, Tommasi P, Paciucci M, Comegna L, Mercogliano P (2014) Evaluation of the effects of climate changes on landslide activity of Orvieto clayey slope. *Procedia Earth and Planetary Science* 9:54–63. <http://dx.doi.org/10.1016/j.proeps.2014.06.017>
- Rianna G, Reder A, Mercogliano P, Pagano L (2017) Evaluation of variations in frequency of landslide events affecting pyroclastic covers in Campania region under the effect of climate changes. *Hydrology* 4(3):34. <https://doi.org/10.3390/hydrology4030034>
- Rianna G, Reder A, Pagano L, Mercogliano P (2020) Assessing Future Variations in Landslide Occurrence Due to Climate Changes: Insights from an Italian Test Case. In: Calvetti F, Cotecchia F, Galli A, Jommi C (eds) *Geotechnical Research for Land Protection and Development*. CNRIG 2019. *Lecture Notes in Civil Engineering*, vol 40. Springer, Cham. https://doi.org/10.1007/978-3-030-21359-6_27
- Romeo S, D’Angiò D, Fraccica A, Licata V, Chiessi V, Amanti M, Bonasera M (2023) Investigation and preliminary assessment of the Casamicciola landslide in the island of Ischia (Italy) on November 26, 2022. *Landslides* 20:1265–1276. <https://doi.org/10.1007/s10346-023-02064-0>
- Sangelantoni L, Gioia E, Marincioni F (2018) Impact of climate change on landslides frequency: the Esino river basin case study (Central Italy). *Natural Hazards* 93:849–884. <https://doi.org/10.1007/s11069-018-3328-6>
- Santini M, Valentini R (2011) Predicting hot-spots of land use changes in Italy by ensemble forecasting. *Regional Environmental Change* 11:483–502. <https://doi.org/10.1007/s10113-010-0157-x>
- Scoccimarro E, Gualdi S, Bellucci A, Zampieri M, Navarra A (2016) Heavy precipitation events over the Euro-Mediterranean region in a warmer climate: results from CMIP5 models. *Regional Environmental Change* 16:595–602. <http://dx.doi.org/10.1007/s10113-014-0712-y>
- Segoni S, Piciullo L, Gariano SL (2018). A review of the recent literature on rainfall thresholds for landslide occurrence. *Landslides* 15:1483–1501. <https://doi.org/10.1007/s10346-018-0966-4>
- Sidle RC, Ochiai H (2006) *Landslides: Processes, Prediction, and Land Use*. In: *Water Resources Monography Series* 18. AGU, Washington, DC. <https://doi.org/10.1029/WM018>

Seismic Performance Assessments of Embankments

Kemal Onder Cetin^{(1)*}, Anil Yunatci⁽²⁾, Bilal Umut Ayhan⁽³⁾

1) Middle East Technical University, Department of Civil Engineering, Ankara, Türkiye, +(90) (312) 210 2418
(kemalondercetin@gmail.com, ocetin@metu.edu.tr)

2) GeoDestek, Ankara, Türkiye

3) Istanbul Bilgi University, Department of Civil Engineering, Istanbul, Türkiye

Abstract Steps followed during seismic design and performance assessments of embankments include: i) seismic hazard assessments, ii) pseudo-static stability evaluations and the determination of seismic coefficient k , iii) allowable permanent deformations. For earthfill and rockfill dams and embankments, there exists a consensus regarding the selection of a 50 % probability of exceedance in 100 years hazard level for operation basis earthquake levels. The dam subjected to this shaking level is expected to behave elastically or almost elastically. However, for dams classified under "high" and "very high" risk, international codes suggest a seismic assessment which adopts a 10,000-year return period hazard level for safety evaluation earthquake, whereas national guidelines at regions of higher seismicity often recommend ground motions having lower return period ($T_r= 2475$ years) in practice. For transport infrastructure embankments and retaining structures, until recently, 475-year return period ground motions have established the design practice. However, after AASHTO (2006), 1,000-year return periods have started to be adopted as the basis for design. The corresponding seismic coefficient is applied to the critical block using the least favorable combinations to model earthquake shaking in both horizontal and vertical directions. The use of a predetermined constant seismic coefficient as a fraction of maximum acceleration, e.g.: half of maximum acceleration, is commonly proposed in practice, nevertheless it is shown that selection criteria shall be based on allowable displacement, critical block geometry, earthquake moment magnitude (or duration), and other relevant factors. It was noted that the seismic coefficient commonly used in outdated literature, corresponding to 0.5 of the maximum acceleration, aims to target permanent displacements in the order of 1.5-2.5 cm. A wide range of permissible permanent displacement values is defined in the literature. For dams, the stability of the dam body was concluded not to be significantly jeopardized when permanent displacements are below 1-1.5 meters (3-5 feet). For transport infrastructure embankments or natural slopes, permissible permanent displacement values range from 5 to 10 cm.

Keywords geostructures, earthfill and rockfill dams, retaining structures, seismic hazard assessment, deterministic analysis, seismic coefficient (k)

Introduction

The engineering evaluations for dynamic response of geo-structures such as natural or engineered slopes, soil-rock fills, transport infrastructure embankments and dams involve four assessment steps, as shown in Tab. 1. Firstly, design basis seismic hazard levels are identified to quantify the demand. The second step involves identifying their dynamic responses under seismic hazard levels. The third step assesses whether the response characteristics including induced-stresses, -strains, and -displacements, align with acceptable performance levels. If the desired performance level is exceeded, the evaluation proceeds to discuss improvement measures for existing structures or revisions of the design for the ones to be constructed.

Table 1 Seismic Performance Assessment Steps of Embankments and Slopes

Definitions
1. The Assessment of Seismic Hazard Level
2. Seismic Response Analyses: Pseudo-static vs. Dynamic
3. The Assessment of Seismically induced Deformations and Displacements: Allowable Deformation/Displacement Criteria
4. Mitigation Solution: If Needed

In this manuscript, current widely used engineering criteria for evaluating seismic hazard levels will be briefly discussed. As part of response assessments, the historical development of semi-static (pseudo-static) analyses, which serve as the initial stability assessment stage in the design under seismic loads, will be addressed. Special attention will be given to the discussion of estimating the seismic coefficient, " k ", as functions of permanent deformations and displacements. Due to the complexity of the subject, discussions about evaluations related to dynamic response analyses will be excluded herein. A compilation of permissible deformation criteria available in the literature will be presented. The discussions on rehabilitation, and design revision measures, which constitute the fourth assessment stage, will also be deferred to another study. Following a brief overview of the historical advancements in the evolution of seismic design methods for embankments and slopes, the manuscript will provide discussions aligned with the outlined scope.

Historical progress in seismic design and performance evaluations

Embankments, including dams and transport infrastructures, have been designed with consideration for earthquake loads since the 1930s. In fact, embankments and slopes were among the first structures to be designed with seismic loading criteria compared to other engineering structures. The first dynamic analysis of an earthfill dam was conducted by Mononobe et al. in 1936. The dam body was represented by an infinitely long symmetric triangular linear elastic section resting on a rigid foundation (Mononobe et al., 1936; Seed and Martin, 1966). In this method, seismic forces acting on the dam body are determined by the product of the weight of the critical block and the seismic coefficient "k." The typical seismic coefficient values used at that time ranged from 0.10 to 0.15. During these analyses, when the safety factor drops below 1.0, the embankment is inaccurately classified as "close to failure." Ambraseys (1960) cautioned against relying on a predetermined constant seismic coefficient, advocating for the selection of the seismic coefficients based on seismic response analyses. Although semi-static analyses account for the embankment's inertia and the hydrodynamic effects of water loads on stability, they fall short in analyzing the combined interaction of the embankment body mass, foundation site conditions, water bodies, and earthquake shaking, and thus fail to reflect these interactions in the results.

In summary, the early practice in 1960s has evolved into multidimensional dynamic response analyses considering the multiple earthquake levels and using the soil-rock constitutive models based on effective stress. These advancements have shifted the approach from engineering judgement and experience-based assessment to pseudo-static analyses, and ultimately, two- or three-dimensional dynamic response analysis in current practice. Determining the seismic hazard (earthquake scenario) levels that serve as the foundation for these analyses has also evolved and has now reached its partially mature state. The next section will provide a brief summary of this evolution.

Seismic hazard assessment framework

There exists a considerable amount of randomness in the source properties of the earthquake process, namely the magnitude, location and time of occurrence. Variation of ground motion intensity along the distance from source to the site of interest also contains randomness. The basic logic behind probabilistic seismic hazard assessment is assigning a probability distribution for every random variable in the process. The probabilistic seismic hazard methodology, as described in Cornell (1968) integrates all the probabilities from each random variable, to come up with the rate of exceedance for a selected value of ground motion intensity.

Probabilistic seismic hazard analysis has often been compared and contrasted with deterministic methods of hazard calculations. While the scope of this paper is

beyond flourishing this discussion; it is considered beneficial to briefly make a reasonable interpretation, in order to make a proper selection among the methods. McGuire (2001) discusses the role of probabilistic and deterministic methods in decision making purposes, in which the study distills to the major conclusion stating that both probabilistic and deterministic methods have a role in seismic hazard and risk analyses performed for decision-making purposes. These two methods can complement one another to provide additional insights to the seismic hazard or risk problem. Depending on the seismotectonic setting, indicating whether the total hazard is to be controlled by a single source, a fault segment with in-depth characterized properties or the performance criteria of the structure as well as the project scope, one method may have priority over the other. In many applications, use of hazard disaggregation to gain insight about the dominating set of scenarios based on the results obtained using the probabilistic framework is a common approach in practice.

Deterministic approach

The deterministic approach fundamentally covers the identification of each active earthquake source (faults), assigning a scenario earthquake magnitude, which is a function of the geometrical characterization of the associated fault segment anticipated to undergo independent rupture, closely or loosely supported by recorded seismicity data, also often coupled with closest source to site distance. The resulting magnitude – distance pair, along with additional input parameters controlling a varying number of effects, including but not limited to source mechanism and local site effects, forms the input for the empirical strong ground motion parameter estimation models. These intensity prediction models also contain their own model uncertainties and the median ground motion obtained from the independent earthquake scenario, or 84% (median+1 standard deviation in normal distribution) for embankment dams in the high and highest risk class can be calculated as a basis for design. The scenario that produces the largest value among all studied sources, assuming mutually exclusive and totally independent ruptures, is selected as the design ground motion level. This approach is called deterministic because the earthquake magnitude, source to site distance and the number of standard deviations to be added to the median estimate are considered as the only possible combination of variables in the calculations. For those interested in performance of critical structures, the question that comes to mind is whether a higher hazard (shake) will occur than what is obtained with the selected criteria in the deterministic scenario.

When adequacy of the median moment magnitude obtained from the fault rupture geometry, or the level of danger posed by ground movements with 1 standard deviation added to the median value is questioned by the designer, a "worst case scenario" is sought; in which applying a higher number of standard deviations, in the order of "2" on the calculated median ground motion

intensity levels is brought into discussion. While the worst-case scenarios may indicate progress to a higher level of confidence, it often introduces conditions in which the project evolves into an unmanageable status in terms of fiscal constraints and engineering practice in seismically active regions, while not rationally quantifying the risk of failure of the structure and justifying target performance levels. Ground motion intensity levels, exceeding median + 2 standard deviation estimates at a particular spectral period (either peak components or spectral) has been frequently addressed after large magnitude events, which evokes the discussion of establishing performance-based criteria coupled with a fully probabilistic framework in which uncertainties due to ground motion intensity estimation and structural demands can be seamlessly blended and quantified.

Probabilistic Approach

The basic methodology of probabilistic seismic hazard assessment (PSHA) involves calculating the frequency of specified level of ground motion (either their peak or spectral values) will be exceeded at the location of interest. In a PSHA, the annual rate of events (annual rate of exceedance), ν , that produces a ground motion intensity parameter, let's pick spectral acceleration, S_a , that exceeds a specified level, z , at the site is calculated. The inverse of ν corresponds to the definition of return period. The calculation of the annual frequency of exceedance “ ν ” involves, i) the rate of earthquake of various magnitudes, ii) rupture dimensions of earthquakes, iii) the location of the earthquakes relative to the site, and iv) attenuation of the ground motion from the earthquake rupture to the site. The general expression for a selected “linearly characterized” source is presented in Equation 1.

$$\begin{aligned} \nu_i(S_a > z) &= N_i(M_{min}) \int_{RL=0}^{RL_{max}} \int_{E_x=0}^1 \int_{m=M_{min}}^{M_{max}} \int_{\epsilon=\epsilon_{min}}^{\epsilon_{max}} f_{RL_i}(m, RL) f_{E_x}(m, E_x) f_m(m) f_{\epsilon}(\epsilon) P(S_a > z | m, r(RL, E_x), \epsilon) dRL dE_x dmd\epsilon \quad [1] \end{aligned}$$

$P(S_a > z | m, r(RL, E_x), \epsilon)$ is the probability of exceedance of the specified ground motion level for the given magnitude and distance, $f_i(m)$ and $f_i(r)$ are the probability density functions for the magnitude and distance for that source. The integration is carried out for every possible magnitude value between M_{min} and M_{max} , and source to site distance values corresponding to the magnitude of interest. $N_i(M_{min})$ is the annual rate of earthquakes having magnitudes greater than or equal to M_{min} . In Equation 1, ϵ is the number of standard deviations above or below the median ground motion, $f_{\epsilon}(\epsilon)$ is the probability density function for ϵ ; which is essentially the standard normal distribution. RL is the rupture length, and E_x is the location of rupture along the fault length, “o” and “1” representing both ends of the fault. Unlike area source idealization, site to source distance is now a function of rupture dimension and location of rupture along the fault. More complicated forms of the hazard integral are possible by introducing additional variables to be randomized. Fig. 1 illustrates the basic steps involved in PSHA.

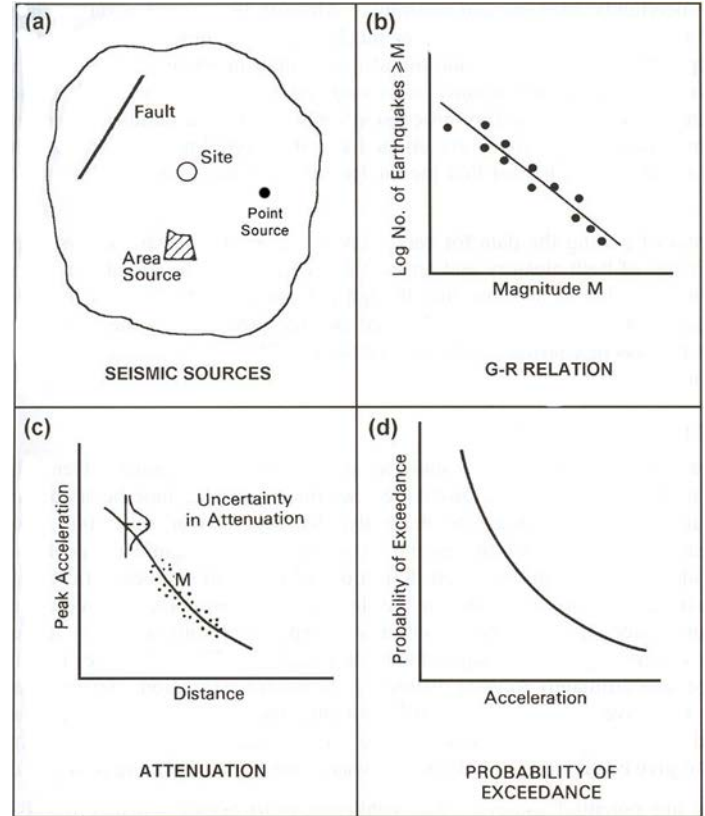


Figure 1 Basic steps of PSHA (Modified from Finn et al., 2004)

Whether calculated by deterministic or probabilistic methods, the response (performance) expected from the dam, or slopes in general varies under different calculated seismic hazard levels. In order to point out these differences, the seismic hazard scenarios frequently referred to in national and international specifications and the performance levels that the embankment or slope is expected to provide within the scope of these scenarios will be summarized in the next section.

Design basis seismic intensity levels

The Operating Basis Earthquake (O.B.E.), widely referred to in dam engineering, defines the level of strong ground motion that the embankments or dams are likely to be exposed to during its operational lifespan. Generally, considering that dams are typically designed for a lifespan of 100 years, there is a general consensus within the scope of O.B.E. evaluation that a level corresponding to a 50% hazard level over 100 years, equivalent to a strong ground motion event with a return period of 144 years, would be adequate (for example: ICOLD Bulletin 72, Revision 2010; FEMA 2005; Turkish Dam Agency, DSI Guide No: 1, 2012). The expected performance level from a dam structure exposed to O.B.E. level is defined as either the structure sustaining no damage or any damage being at sufficiently low levels as not to interrupt the operational activities of the structure. The prompt and economical repair of potential low-level damage is also among the expectations. Determining the O.B.E. level is more of an economically driven criterion for the operation rather than a safety-related assessment, so it may be governed by the

preferences of investors than regulatory and approving public institutions (Wieland, 2005).

However, a more speculative scenario emerges when determining the hazard levels that form the basis for the design or safety of the structure. Within this context, in the literature, one encounters the maximum design earthquake (M.D.E.) and, more recently, definitions such as the safety-evaluation earthquake (S.E.E.) replacing this terminology in relation to the design process compatible with multiple hazard levels. When determining the safety-oriented earthquake level, a more complex scenario arises compared to the relatively consensual definition of the O.B.E., recommending the use of probabilistic evaluation levels ranging from the 475-year (10% in 50 years) design earthquake level to the 10,000-year (1% in 100 years) level. In addition to this differentiation, there are contradictions regarding which scenario will be considered if deterministic and probabilistic analysis results do not overlap. Some sources suggest selecting the lower of the deterministic and probabilistic hazard analysis results (Turkish Dam Agency, DSI Guide No: 1, 2012), while others suggest selecting the higher (ICOLD Bulletin 72, 2010).

Despite all this differentiation and complexity, it is clear that the new definitions have been introduced, along with efforts to classify embankment types, heights, and the dimensions of the impact in case of damage, somewhat assist in deciding the level of risk to be undertaken. However, especially when compared with national and international standards in determining safety-oriented hazard levels, serious differences and disagreements are observed. Particularly, for embankments classified under high and very high-risk groups, there is inconsistency between defining the safety-oriented earthquake (S.E.E.) level identified through probabilistic studies with earthquake scenarios corresponding to a recurrence period of 2,475 years and the recommendation of 10,000-year recurrence periods by the ICOLD Bulletin 72, 2010 revision. In regions, where seismic hazard levels are extremely high, determining S.E.E. levels corresponding to lower recurrence periods may sometimes support project feasibility by reducing maximum ground acceleration values calculated at levels compatible with 10,000-year recurrence periods to more reasonable levels of 1.5-2.0 g. However, the safety of these relatively lower recurrence levels needs to be debated.

At this stage, it is crucial to emphasize the necessity of establishing a common language between the project owner and the geoscientist or earthquake engineer. In this relationship, the party assuming the risk should clearly articulate the risk, and the decision on which safety criteria will be acceptable should not solely rest on the hazard assessor's mind. Today's accumulation of knowledge has evolved to enable decisions to be made based on the behavior (response) of the structure rather than solely on the forces that will affect the structure.

For conventional transport infrastructure embankments and slopes, the selection of design earthquake recurrence periods is less complex compared

to hydraulic structures. In international literature, until 2006, recurrence periods of 475 years, corresponding to a 10% exceedance probability in 50 years, were used as the basis for design. After the AASHTO LRFD Bridge Design Specifications (2006), this recurrence period has been increased to the order of 1,000 years. This change has been accepted not only for bridges but also for key components of transportation systems, including highway embankments, fills, and retaining structures. In national specifications, however, earthquake scenarios corresponding to recurrence periods of 475 years have continued to be used as the basis of design for transport infrastructure embankments, fills, and retaining structures.

Assessing seismic coefficient, k in a performance-based design framework

Semi-static analysis methods, which are still widely used in the preliminary evaluation stage of embankment engineering analyses today, were the sole analysis method used in the seismic design of many existing ones built in the 1960s and earlier. As shown in Fig. 2, in this analysis method, the seismic forces acting on the dam body are determined by the product of the weight of the critical block, W , and the seismic " k " coefficient. The seismic coefficient is applied to the critical block using the least favorable combinations to model earthquake shaking in both horizontal and vertical directions. Typical seismic coefficient values used during that time ranged from 0.10 to 0.15. If the safety factor fell below 1.0, the embankment was inaccurately classified as "close to failure." Ambraseys (1960) suggested that the seismic coefficient, k , should be determined based on seismic response analyses and highlighted the limitations of using a fixed k value. Despite considering the inertia of the embankment mass and hydrodynamic forces (if there is any), pseudo-static analyses are insufficient for assessing the combined interaction of the embankment body mass, site conditions, earthquake, and reservoir, in case of dams, and may therefore not accurately represent their effects.

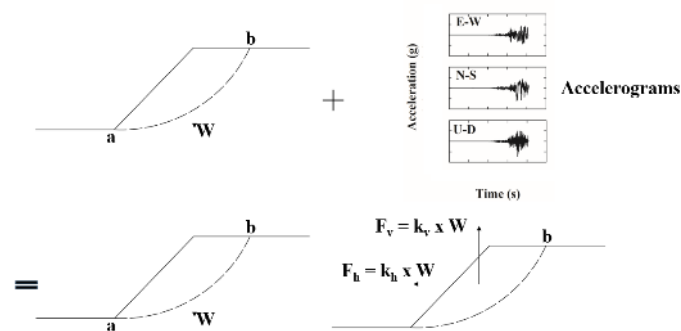


Figure 2 Pseudo-static analysis for embankments and slopes

Seed and Martin (1966) emphasized the need to select the seismic coefficient, k , based on dynamic response analyses and considering the stiffness of the material constituting the embankment body, rather than choosing fixed values. They determined the acceleration and stress variations in the embankment using the

Mononobe sliding beam method and viscoelastic response analyses. This allowed the stresses occurring on the sliding planes of the dam to be converted into equivalent seismic coefficients that varied across the dam body and over time. It was observed in all examples studied during that period that the seismic coefficient did not exceed a value of 0.4. However, no relationship was established between the maximum ground acceleration and the seismic k coefficient. Marcuson (1981) pointed out the relationship between the seismic coefficient and maximum ground acceleration, suggesting that an appropriate semi-static k coefficient should be selected at levels ranging from one-third to one-half of the calculated maximum ground acceleration considering the amplification or reduction effects consistent with local soil conditions in the embankment area. Similarly, after conducting numerous analyses using the Newmark method, Hynes-Griffin and Franklin (1984) concluded that if the safety factor exceeded 1.0 in semi-static stability analyses using a seismic k coefficient selected at one-half of the maximum ground acceleration/ g , the expected deformations in embankment dams would be minimal and acceptable. Additionally, there is a limitation on the use of semi-static analyses in dam types where an increase in pore water pressure in the foundation soils of the embankment body may occur during an earthquake, disregarding a potential strength loss of up to 15-20% during earthquakes.

Despite their widespread use, semi-static analysis methods are now limited to the preliminary design stage due to their inherently irrational goal of converting repetitive motion, such as earthquakes, into equivalent static loads, resembling empirical structures. Often, when the safety factor falls below 1.0 during analysis, inaccurate conclusions are drawn, such as the critical dam mass being renewed and sliding completely downhill. However, under a repetitive and constantly changing (transient) load like an earthquake, inertia forces cannot always be applied in the same direction, changing with every millisecond of the earthquake. Thus, a rigid block that becomes unstable at any moment during the earthquake will stabilize again when the direction of the inertia force changes or

diminishes due to the earthquake continuing. Furthermore, a block sliding downhill may move upward due to a subsequent earthquake in the opposite direction, potentially partially compensating some of the permanent deformations that occurred downhill in the previous seconds of the earthquake. Based on these observations, Newmark (1965) proposed that earthquakes' effects on dams should be examined in terms of deformations rather than minimum safety factors or equivalent seismic coefficients. Newmark and derivative methods were developed based on the assumption that when the shear stresses acting on the sliding plane exceed the shear strength, the critical mass block begins to slide. The acceleration level at which sliding is triggered is called the yield acceleration level. The displacement of the rigid block can be obtained by taking the double integral of the acceleration-time data above the yield level. The validity of the method has been confirmed using recorded displacement data from the La Villita Dam in Mexico, which is frequently exposed to high seismic levels (Elgamal et al., 1960). It should be noted that the Newmark method can be applied to dam bodies consisting of low-sensitivity fill materials that do not produce significant strength loss (less than 20% loss) under earthquake loads and do not produce significant pore water levels.

Makdisi and Seed (1977) demonstrated through numerical analyses, which, by today's standards, might be considered limited in number but represented serious efforts given the technology available at the time, that the seismic coefficient, k , could be determined through the interaction of dam height, depth of the critical block, maximum crest acceleration, and allowable displacement parameters. As shown in Fig. 3, after determining the maximum crest acceleration, the maximum seismic coefficient value, k_{max} , is found using a ratio determined by dividing the critical block depth, " y ," by the dam height, denoted as ' h .' Then, the ratio obtained by dividing the seismic coefficient value, k_y , which triggers sliding and produces a safety factor of 1.0 in semi-static analyses, by k_{max} , is used to determine the expected post-seismic permanent horizontal displacement levels in the dam.

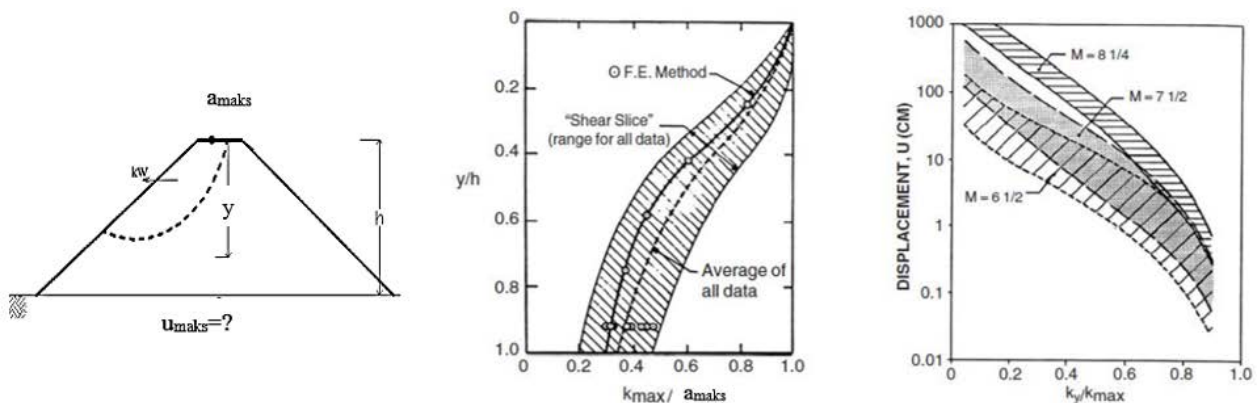


Figure 3 Assessing seismic coefficient, k , as per Makdisi and Seed (1977)

Makdisi and Seed's analysis method relies on several key input parameters, one of which is determining the maximum crest acceleration value. As presented by Kavruk (2003) and elsewhere, accelerations intensify at the crest of embankments to levels 1.5-4.0 times higher compared to the maximum rock ground accelerations. Taking into account that this amplification varies widely depending on factors such as dam rigidity, height, and seismic record characteristics, it is assumed that the maximum rock ground acceleration will amplify by a factor of about 2.0. With this assumption, seismic coefficient values corresponding to for circular failure surfaces passing from the toe of embankments, allowable

displacement, moment magnitude, and y/h values for a safety factor of 1.0 can be obtained, as presented in Tab. 2. As shown in this simple calculation sequence, the primary parameters influencing the selection of the seismic coefficient are typically the allowable displacement criterion, earthquake moment magnitude, and depth of the critical sliding block. While selecting the seismic coefficient at levels around 0.4-0.6 of the maximum rock ground acceleration, as suggested in some specifications and design guidelines, may generally be somewhat compatible or on the safer side, as demonstrated in Tab. 2, this approach may occasionally result in unsafe outcomes for shallower embankments.

Table 2 The $k_g/a_{max-rock}$ ratios varying with permanent lateral displacement, the moment magnitude of the event and y/h

Permanent Displacement (cm)	Moment Magnitude, M_w					
	6.50		7.50		8.25	
	$y/h=1$	$y/h=0.6$	$y/h=1$	$y/h=0.6$	$y/h=1$	$y/h=0.6$
2.5	0.41	0.64	0.44	0.69	0.53	0.83
10	0.24	0.38	0.33	0.52	0.45	0.70
30	0.12	0.19	0.24	0.37	0.38	0.60
60	0.08	0.13	0.17	0.27	0.33	0.52

The main purpose behind summarizing the equivalent seismic coefficients based on the work of Makdisi and Seed (1977) as presented in Tab. 2, is not to necessarily recommend the use of these values in preliminary quasi-static stability analyses, but to emphasize the necessity of selecting the equivalent seismic coefficient based on allowable displacement, critical block geometry, earthquake moment magnitude (or duration), and other relevant factors. After considering increased permissible (acceptable) permanent displacement levels, it becomes feasible to analyze and design the embankment with lower equivalent seismic coefficients. It should be noted that the seismic coefficient commonly used in outdated literature, corresponding to 0.5 of the maximum ground acceleration, aims to target permanent displacements at approximately 1.5-2.5 cm levels.

Semi-empirical models for permanent slope displacements

As part of performance assessment of seismically induced natural and embankment slopes, significant research efforts have been focused on assessing permanent displacements. Newmark's sliding block (NSB) concept (Newmark, 1965) has been frequently used by engineers to assess the performance of slopes under earthquake loading. As one of the first attempts, Ambraseys and Menu (1988) proposed a predictive model using 50 strong ground motion recordings. Their equation tried to predict the NSB displacement using the ratio between yield acceleration and PGA. After this, there have been various researchers (Yegian et al., 1991; Jibson, 1993; Ambraseys and Srbulov, 1994; Ambraseys and Srbulov, 1995; Crespellani et al., 1998) who tried to estimate the NSB displacement with various functional forms including additional ground motion

intensity measures. However, these models were still utilizing a database with a limited number of ground motions. Therefore, the variability (i.e., standard deviation) in their predicted means was still high. To decrease such variability, Jibson et al. (1998) proposed a model using a relatively larger dataset consisting of 555 strong ground motion recordings from 13 events. However, in this time, aleatory variability in the predictions is increased. Since then, several predictive models have been proposed, some of which are presented in Tab. 3.

These predictive models link the intensity of shaking with permanent displacements, supporting the earlier conclusion that seismic coefficient k is governed by permanent displacements allowed for embankment or natural slopes. This necessitates discussions on allowable permanent displacements for slopes.

Allowable permanent displacements criteria for slopes

First and foremost, it should be emphasized that defining permissible displacements for embankments necessitates considering at least two different earthquake scenarios. Expectations for the operational earthquake level revolve around the embankment being able to continue its operational activities without interruption following this earthquake scenario. In this case, it is evident that the seismic response of the dam body should remain within elastic limits. Considering typical modulus reduction relationships based on unit deformation for materials like sand, clay, and rock, it can be noted that the elastic or nearly elastic limits correspond roughly to shear strains (unit deformations) in the ranges of 10^{-4} to 10^{-3} % for sands and clays, and 10^{-3} to 10^{-2} % for rocks. Similarly, for rock, the elastic behavior limit can be selected as 10^{-3} %. From hydraulic structures point of view, when considering the safety earthquake scenario, it is important to remember

that the expectation is for the dam not to lose its ability to retain water. Therefore, the issue to be discussed is the determination of permissible permanent displacements that correspond to this scenario. A wide range of permissible permanent displacement values is defined in the literature under the safety earthquake scenario.

Although related to factors such as dam height, zoning, filter thickness, and the strength and stiffness behavior of materials, it can be said that the stability of the dam body will not be significantly threatened when permanent displacements are below 1-1.5 meters (3-5 feet).

Table 3 A summary of some sliding block permanent displacement predictive models

Model	Eq. model	Functional form	Designated application	Number of records
Rigid	Newmark (1965)	$D_N = 3 \frac{PGV^2}{PGA} \left(\frac{a_c}{PGA}\right)^{-1}$	Earth dams and embankments.	4
	Ambraseys and Menu (1988)	$\log(D_N) = 0.90 + \log\left[\left(1 - \frac{a_c}{PGA}\right)^{2.53} \left(\frac{a_c}{PGA}\right)^{-1.09}\right]$	Ground and slopes	50
	Jibson (2007)	$\log(D_{N(cm)}) = 0.215 + \log\left[\left(1 - \frac{a_c}{PGA}\right)^{2.341} \left(\frac{a_c}{PGA}\right)^{-1.438}\right]$	Natural slopes	2270
		$\log(D_{N(cm)}) = -2.71 + \log\left[\left(1 - \frac{a_c}{PGA}\right)^{2.335} \left(\frac{a_c}{PGA}\right)^{-1.478}\right] + 0.424M$		
		$\log(D_{N(cm)}) = 2.401\log I_a - 3.481\log a_c - 3.23$		
		$\log(D_{N(cm)}) = 0.5611\log I_a - 3.833\log a_c - 1.474$		
	Saygili and Rathje (2008)	$\log(D_{N(cm)}) = 5.52 - 4.43\left(\frac{a_c}{PGA}\right) - 20.93\left(\frac{a_c}{PGA}\right)^2 + 42.61\left(\frac{a_c}{PGA}\right)^3 - 28.74\left(\frac{a_c}{PGA}\right)^4 + 0.72\ln(PGA)$	Natural slopes	2383
		$\log(D_{N(cm)}) = -1.56 - 4.58\left(\frac{a_c}{PGA}\right) - 20.84\left(\frac{a_c}{PGA}\right)^2 + 44.75\left(\frac{a_c}{PGA}\right)^3 - 30.5\left(\frac{a_c}{PGA}\right)^4 - 0.64\ln(PGA) + 1.55\ln(PGV)$		
Alfredo and Christian (2013)	$\log(D_N) = -0.1 - 4.3\left(\frac{a_c}{PGA}\right) + \log\left(\frac{I_a T}{PGA}\right)$	-	-	
Bray and Travasarou (2007)	$\log(D_N) = -0.22 - 2.83\ln(k_c) - 0.333(\ln(k_c))^2 + 3.04\ln(a_c) + 0.566\ln(k_c)\ln(a_c) - 0.244(\ln(a_c))^2 + 0.278(M - 7)$	Earth and waste slopes	1376	

It should be noted that permanent displacements exceeding 3 meters (approximately 10 feet) are considered unacceptable for embankment dams, and even in cases where displacements exceed these levels, the calculated values may not be reliable due to limitations in analysis methods and structural models. Permanent displacements between 1.5 and 3.0 meters constitute a gray area, indicating the need for careful analysis and potentially reassessment. It should be recognized that these assessments are general and rough recommendations in the literature, and it is possible to encounter examples of dam performance that do not conform to these limits, whether stable or unstable. Instead of a wholesale approach, it is imperative that the analysis and evaluation of results be conducted by specialized engineers tailored to the specific project.

For transport infrastructure embankment or natural slopes, the decision is less complex. Depending on the importance and intended use of the retaining structure, permissible permanent displacement values for slopes typically range from 5 to 10 cm.

Summary and conclusion

The analysis stages followed in determining the dynamic behavior of embankments and natural slopes consist of four analysis stages. The first stage involves determining the seismic hazard levels that will form the basis for the

design or performance evaluations of the structure. The second stage deals with the calculation of the dynamic response behavior of the structure under these seismic hazard levels, and during this stage, the response characteristics (stress, strain, displacement, etc.) are examined to determine whether they are consistent with the expected or allowable performance levels, which constitutes the third stage. In the final stage, if the determined performance is not compatible with acceptable levels, improvement measures for existing ge-structures or revision measures for structures in the design phase are discussed.

In this manuscript, the first analysis stage focuses on summarizing the current national and international criteria for determining seismic hazard levels, highlighting their agreements and differences. The second stage covers a discussion on pseudo-static (or semi-static) analyses, which represent the initial stability assessment stage for geotechnical structures under seismic loads in their historical development process. Particularly, emphasis is placed on the seismic coefficient "k," which is a fundamental input parameter for pseudo-static analyses. Due to the complexity of the subject and the page limit of the paper, evaluations related to dynamic response analyses have been deferred for another study. In the scope of the third evaluation stage, a compilation of available permissible deformation criteria from national

and international literature has been made, addressing not only the compatibility and discrepancies between these criteria but also their shortcomings. Justified by the same reasoning for excluding dynamic response analyses from the paper, the fourth evaluation stage concerning improvement and section revision measures has also been reserved for another study. A detailed discussion on seismic hazard assessment framework, selecting the design basis seismic intensity levels, and corresponding seismic coefficient k values, was provided. Currently available semi empirical models for assessing permanent seismic slope displacements are evaluated. Followings are the major findings and conclusions of these discussions:

- The deterministic seismic hazard assessment involves the identification of active earthquake sources (faults), assigning a scenario earthquake magnitude, which is a function of the geometrical characterization of the associated fault segment anticipated to undergo independent rupture.
- The resulting earthquake magnitude – distance pair forms the input for the empirical strong ground motion parameter estimation models.
- The median ground motion obtained from the independent earthquake scenario, or 84% (median+1 standard deviation in normal distribution) for critical embankments located in the high and highest risk class are selected as design basis scenario.
- In probabilistic seismic hazard assessment (PSHA), the frequency of specified level of ground motion (either their peak or spectral values), exceeding certain thresholds are assessed for the location of interest.
- The annual rate of events (annual rate of exceedance), ν , that produces a ground motion intensity parameter, that exceeds a specified level, z , at the site is calculated. The inverse of ν corresponds to the definition of return period.
- The Operating Basis Earthquake (O.B.E.), widely referred to in dam engineering, defines the level of strong ground motion that the embankments or dams are likely to be exposed to during its operational lifespan.
- Considering that dams are typically designed for a lifespan of 100 years and conventional transport infrastructure embankments for 50 years, there is a consensus within the scope of O.B.E. evaluation that a level corresponding to a 50% hazard level over 100 or 50 years, equivalent to a strong ground motion event with a return period of 144 and 72 years, would be adequate.
- For hydraulic structures (dams) classified under high and very high-risk groups, there is inconsistency between defining the safety-oriented earthquake (S.E.E.) level identified through probabilistic studies with earthquake scenarios corresponding to a recurrence period of 2,475 years and the recommendation of 10,000-year recurrence periods by the ICOLD Bulletin 72, 2010 revision.
- For conventional transport infrastructure embankments and slopes, the selection of design earthquake recurrence periods is less complex compared to dams. In international literature, until 2006, recurrence periods of 475 years, corresponding to a 10% exceedance probability in 50 years, were used as the basis for design.
- After the AASHTO LRFD Bridge Design Specifications (2006), this recurrence period has been increased to the order of 1,000 years. This change has been accepted not only for bridges but also for key components of transportation systems, including highway embankments, fills, and retaining structures. In national specifications, however, earthquake scenarios corresponding to recurrence periods of 475 years are still used as the basis for highway embankments, fills, and retaining structures.
- In semi-static analysis methods, which are still widely used in the preliminary evaluation stage of embankments, the seismic forces acting on the dam body are determined by the product of the weight of the critical block, W , and the seismic "k" coefficient.
- The seismic coefficient is applied to the critical block using the least favorable combinations to model earthquake shaking in both horizontal and vertical directions. Typical seismic coefficient values used during that time ranged from 0.10 to 0.15.
- Ambraseys (1960) cautioned against relying on a predetermined constant seismic coefficient, advocating instead for the selection of the seismic coefficients based on seismic response analyses.
- Although semi-static analyses account for the embankment's inertia and the hydrodynamic effects of water loads on stability, they fall short in analyzing the combined interaction of the embankment body mass, foundation site conditions, water bodies, and earthquake shaking, and thus fail to reflect these interactions in the results.
- The equivalent seismic coefficient is shown to be selected based on allowable displacement, critical block geometry, earthquake moment magnitude (or duration), and other relevant factors.
- It was noted that the seismic coefficient commonly used in outdated literature, corresponding to 0.5 of the maximum ground acceleration, aims to target permanent displacements at approximately 1.5-2.5 cm levels. This conclusion was also supported by available sliding block permanent displacement predictive models.
- A wide range of permissible permanent displacement values is defined in the literature under the safety earthquake scenario for dams. Although related to factors such as dam height, zoning, filter thickness, and the strength and stiffness behavior of materials, it can be said that the stability of the dam body will not be significantly threatened when permanent displacements are below 1-1.5 meters (3-5 feet).

- Permanent displacements between 1.5 and 3.0 meters constitute a gray area, indicating the need for careful analysis and potentially reassessment. It should be recognized that these assessments are general and rough recommendations in the literature, and it is possible to encounter examples of dam performance that do not conform to these limits, whether stable or unstable.
- For transport infrastructure embankment or natural slopes, the decision is less complex. Depending on the importance and intended use of the retaining structure, permissible permanent displacement values for slopes typically range from 5 to 10 cm.

As the final remark, for dynamic assessment of embankments and natural slopes, seismic hazard assessment framework is recommended to be closely followed to evaluate multiple design scenarios with variable acceptable performance definitions. As part of preliminary design, pseudo-static analyses are widely performed to assess the performance of these geo-structures, during which seismic coefficient k , is recommended to be selected considering the geometry and the rigidity of the failure block, earthquake shaking characteristics and allowable permanent displacements. During these analyses, when the safety factor drops below 1.0, the embankment or slope should not be inaccurately classified as "close to failure." Despite considering the inertia of the embankment mass, pseudo-static analyses are insufficient for assessing the combined interaction of the embankment body mass, site conditions, earthquake, and reservoir (in case of dams), and may therefore not accurately represent their interaction. Thus, when these interactions are critical, pseudo-static assessments are recommended to be complemented by effective stress based dynamic response evaluations.

References

- AASHTO (2006), AASHTO LRFD Bridge Design Specifications, Washington, DC, USA.
- Alfredo U., Christian J.T., (2013). Sliding displacements due to subduction-zone earthquakes. *Engineering Geology*, 166, 237-244.
- Ambraseys, N.N. (1960). On the seismic behaviour of earth dams: Proceedings of the Second World Conference on Earthquake Engineering, Tokyo and Kyoto, Japan, v.1, p. 331-358
- Ambraseys, N.N., Menu, J.M, (1988). Earthquake-induced ground displacements. *Earthquake Engineering & Structural Dynamics* 16(7), 985-1006.
- Ambraseys, N.N., Srbulov, M. (1994). Attenuation of earthquake-induced ground displacements. *Earthquake Engineering & Structural Dynamics*, 23(5), 467-487.
- Ambraseys, N.N., Srbulov, M. (1995). Earthquake-induced displacements of slopes. *Soil Dynamics and Earthquake Engineering*, 14(1), 59-71.
- Anderson, D.G., Martin, G.R., Lam, I.P., Wang, J.N., (2008). Seismic Analysis and Design of Retaining Walls, Buried Structures, Slopes and Embankments, NCHRP Report 611, Washington, D.C.
- Bray, J.D., Travasarou, T., (2007). Simplified procedure for estimating earthquake-induced deviatoric slope displacements. *Journal of Geotechnical & Geoenvironmental Engineering*, 133(4), 381-392.
- Cetin, K. O., Yunatçı, A. A., Bilge, H. T. Importance of seismic hazard analysis in design of dam structures: a comparative assessment of design guidelines, 2nd National Dam Safety Symposium, Eskişehir, Türkiye, September, 2012 (in Turkish).
- Cornell, C.A., (1968). Engineering Seismic Risk Analysis. *Bulletin of the Seismological Society of America*, 58(5), 1583-1606.
- Crespellani, T., Madaia, C., Vannuchi, G., (1988). Earthquake destructiveness potential factor and slope stability. *Géotechnique*, 48(3), 411-419.
- Turkish Dam Agency, DSİ Guide No: 1, (2012). Guide to seismic parameter selection in dam design. Dams Congress, November, 2012, Ankara, Türkiye.
- Elgamal, Ahmed-Waeil M., Scott, R.F., Succarieh, M.F., Yan, L., (1990). La Villita dam response during five earthquakes including permanent deformations. *J. Geotech. Engrg, ASCE*, 116(10):1443-1462.
- FEMA (2005). Federal Guidelines for Dam Safety, Earthquake Analyses and Design of Dams, May 2005.
- Finn, W.D.L., Onur, T., Ventura, C.E. (2004). Microzonation: Developments and Applications, in *Recent Advances in Earthquake Geotechnical Engineering and Microzonation*, Ed. Atilla Ansal, Kluwer Academic Publishers, pp. 5-8.
- Hynes-Griffin, M.E., Franklin, A.G., (1984). Rationalizing the Seismic Coefficient Method. Miscellaneous Paper No. GL-84-3, U.S. Army Engineer Waterways Experiment Station, Vicksburg, Mississippi.
- ICOLD Bulletin 72, (2010 Revision), Selecting Seismic Parameters for Large Dams Guidelines, ICOLD 2010.
- Jibson, R.W., (1993). Predicting earthquake-induced landslide displacements using Newmark's sliding block analysis. *Transportation research record*, 1411, 9-17.
- Jibson, R.W (2007). Regression models for estimating coseismic landslide displacement. *Engineering Geology*, 91(2-4), 209-218.
- Kavruk, F., (2003). Seismic Behavior of Embankment Dams. MS thesis, Middle East Technical University, Ankara, Türkiye.
- Makdisi, F. I., Seed, H. B., (1977). UCB/EERC-77/19, Earthquake Engineering Research Center, University of California, Berkeley, 1977-08, 65 pages (480.2/M21/1977)
- Marcuson W. F., (1981). Seismic Design and Analysis of Embankment Dams: The State of Practice. The Donal M. Burmister Lecture.
- McGuire, R. K. (2001). Deterministic vs. probabilistic earthquake hazards and risks. *Soil Dynamics and Earthquake Engineering*, 21, 377-384.
- Mononobe, N., Takata, A., Matumura, M., (1936). Seismic stability of the earth dam. *Trans. 2nd Congress on Large Dams*, Washington, D.C. Q. VII, pp.435-444
- Newmark, N.M., (1965). Effects of earthquakes on dams and embankments. *Géotechnique*, 15(2):139-160.
- Saygili G., Rathje, E.M., (2008). Empirical predictive models for earthquake-induced sliding displacements of slopes. *Journal of Geotechnical & Geoenvironmental Engineering*, 134(6), 790-803.
- Seed, H.B., Martin, G.R., (1966). The seismic coefficient in earth dam design. *J. Soil Mech. and Found. Div., ASCE*, 92(SM3):25-58.
- Wieland, M., (2005). Review of Seismic Design Criteria of Large Concrete and Embankment Dams. 73rd Annual Meeting of ICOLD, Tehran, Iran, May 1-6, 2005, Paper No. 012-W4.
- Yegian, M.K, Marciano, E.A., Ghahraman, V.G, (1991). Earthquake-induced permanent deformations: probabilistic approach. *Journal of Geotechnical Engineering*, 117(1), 35-50.

Integral approach in stability analyses for weak anisotropic rocks

Milorad Jovanovski^{(1)*}, Bojan Janevski⁽²⁾, Igor Peshevski⁽³⁾

1) University Ss. Cyril and Methodius, Faculty of Civil Engineering, Skopje, blvd. Partizanski odredi 24, MKD, +38970236962
jovanovski@gf.ukim.edu.mk

2) Civil Engineering Institute "Makedonija", Skopje, Drezdenska 52, MKD

3) University Ss. Cyril and Methodius, Faculty of Civil Engineering, Skopje, blvd. Partizanski odredi 24, MKD

Abstract Slope stability in weak rock masses is a practical problem where the anisotropy, weathering, and inhomogeneity must be incorporated adequately in geotechnical models for stability analyses. Such media are susceptible to local or global instabilities expressed as wedge, planar, or rotational mode of failure, depending on combinations of slope elements, discontinuity orientation, block sizes, and other factors in the rock masses. Often, even in cases with extensive field investigations, some uncertainties still exist, thus it is a challenging task to compromise between the economy and the reliability of the solution. With an idea to underline some open questions, we are presenting experiences gathered through phases of investigation, design, and construction for several large infrastructural projects on the Macedonian road network. An extensive data basis is collected for weak rock mass parameters, modes of failure, and methods for rock mass stabilization for over 80 deep cut sections. The well-known limit equilibrium, kinematic, and empirical methods are used in certain analyses. Some of the results are presented in partially modified diagrams from known Q-slope in correlation with the Slope Mass Rating method. Some diagrams with values from calculations of the factor of safety and probability of failure are also presented. An attempt is made to incorporate also some findings related to different design approaches. Analyses indicate that it is necessary to combine results from stability analyses with tolerable levels of risk. Here, consequence classes and geotechnical categories defined in Eurocode 7 are correlated with values of the so-called reliability index. The findings lead to the conclusion, that interaction and integration of technical, economic, and social aspects as well as involving different perspectives are necessary in the process of rock slope risk management. Some arising open questions and some recommendations for further development of the methodology are also presented.

Keywords anisotropic rocks, analytical methods, integral approach, empirical methods, slope stability, reliability index

Introduction

There are many guidelines for design of cut slopes in rocks, but rarely do they anticipate the material anisotropy and

discontinuity. It is a well-known fact that weak rock masses are complex media, where anisotropy and inhomogeneity often play an important role in forming geotechnical and calculation models. ISRM (1981) classified the weak rock mass in categories: R₀ when Uniaxial Compressive Strength (UCS) has values UCS < 1, R₁ when UCS = 1-5 MPa and R₂ for a range of UCS = 5-25 MPa. Usually, weak rocks are also highly anisotropic. In practice, for intact rocks, several classes of index of anisotropy I_d are defined (Saroglou et al., 2007). Such media are susceptible to local or global instabilities expressed in different modes of failure depending on combinations of two main elements in interaction – rock mass states and properties (especially discontinuity orientations and block sizes) in relation to artificial engineering structures and their elements. When dealing with slope stability problems in weak rock masses, this problem becomes very complex, because there are a lot of uncertainties even in cases with extensive field investigations, problems of relaxation because of excavation influences etc.

With an idea to underline some important questions and dilemmas, experiences gathered from several large infrastructural projects on the Macedonian road network are presented. Namely, in the past decade, the A₂ motorway from Kicevo-Ohrid, the express road near the town Kriva Palanka to the Bulgarian border, and express roads from town Stip to Kocani and to Radovis were in construction, in a heavy geological environment with impressive cut heights. An extensive database is collected for weak rocks for physical and mechanical properties, rock mass classes, modes of failure, methods for stabilization and other problems from over 80 deep cuts.

The authors believe that a presentation of observed phenomena and problems in construction can be interesting for the scientific community, with an idea of some of the findings, to be incorporated in practice in future projects.

Analysed area

The presented case histories are in different areas of the country. The position of the analysed cases is presented in Fig.1. from where it is visible that the subject road sections are located in different geotectonical units. The geological conditions of the areas certainly influenced a lot on the stability conditions in specific ways during the construction phases.

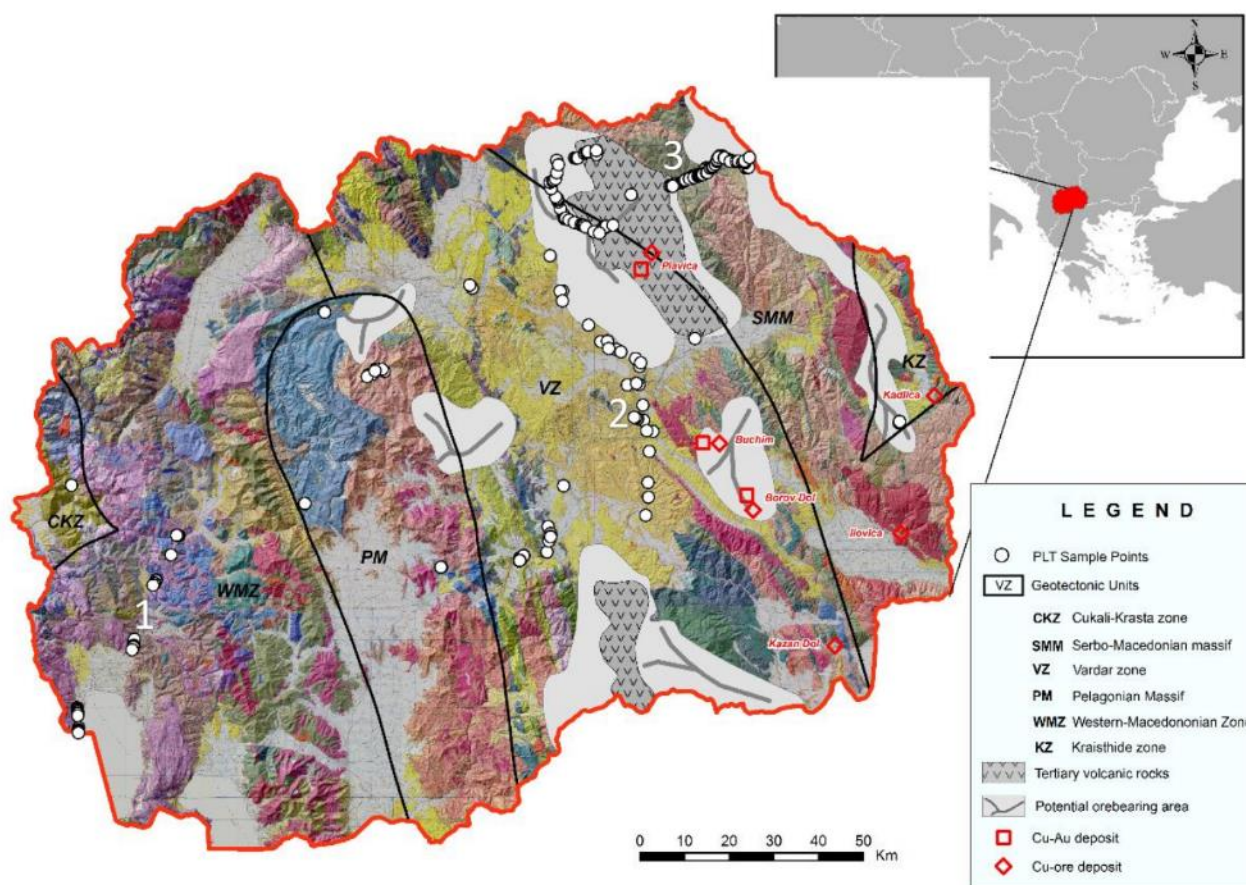


Figure 1. Main geotectonic units in the country and schematical position of the analysed infrastructural projects. 1 – area of highway from Kicevo to Ohrid; 2 – area of express roads from Stip to Kocani and Stip to Radovis; 3 – area of express road from Kriva Palanka to the Bulgarian border.

The Section for the highway from Kicevo to Ohrid is placed in the so-called Western-Macedonian zone (WMZ in Fig.1). It is represented by very complex tectonics, with a multitude of folded and faulted structures. It is mostly composed of a phyllitic low-grade metamorphic complex. Its lower parts are dominated by volcanic sedimentary rocks and its upper part by a terrigenous-carbonate formation. Along the highway route, about 53 cut slopes are analysed. The majority of the cuts are with heights of more than 30 m and several of the cuts are even higher than 100 m. The terrain predominantly consists from phyllites and schists (sericite, quartz-sericite and graphitic). The anisotropic rocks are low-grade metamorphic rocks of Palaeozoic age, folded, tectonically disturbed and affected by the processes of surface degradation. The heterogeneity of the rock formations is manifested through often transformation from one rock type to another, both in horizontal and vertical direction. The positive aspect in terms of stability is the foliation dip angles, which vary in the range from 10° – 50° , with predominant dipping into the hill slope.

The express roads from Stip to Kocani and from Stip to Radovis are placed in the Vardar zone (VZ). This zone is also known as an area with complex tectonic structure, that includes fragments from the Precambrian Earth crust, Palaeozoic volcanic-sedimentary complexes, Mesozoic

magmatism and in the areas of roads, Eocene flysch complexes. Along the express roads route, about 17 cut slopes are analysed. Some of them are constructed in areas of the Eocene flysch complex, built up dominantly from marles and sandstones in rhythmic sequences. Some of the cuts are with heights of more than 20 m. The main element of anisotropy is related to properties parallel and perpendicular to sedimentary planes.

The Serbian-Macedonian massif (SMM) is an area, where the construction of the express road Kriva Palanka to the Bulgarian border takes place. It is characterized by the presence of Precambrian and Riffey-Cambrian complexes. In the area of the road, quartz-sericite schist formations are dominant. The anisotropy is mainly connected with foliation, but very often, along the route of 10 higher cuts, the changes in rock mass properties and weathering state are expressed on short distances.

It should be considered, that as a result of the various changes in each stage of geologic development, the rocks will exhibit very variable behaviour during the construction, especially related to the rock mass parameters. Fig. 1 also shows the approximate spatial distribution of analysed intact rock samples in total, around 1200 samples have been analysed (Peshevski et al., 2019). Just to illustrate the effect of anisotropy even at the range of volume for intact rocks, some correlations obtained from testing of the Point Load Strength Index

perpendicular and parallel to main structural planes, are presented in Tab. 1.

Table 1. Correlations of the point load index for samples tested parallel and normal to foliation/bedding for some dominant rock types (part of the table from Peshevski et al., 2019).

Established correlation	Project	Rock type
$J_s(n)=1.4127*J_s(p)+1.4169$ $r^2=0,8083$	Zones of highway Kicevo-Ohrid	Quartz- sericite schists
$J_s(n)=2,7199*J_s(p)+0.6445$ $r^2=0,915$	Cuts in Flysch	Marls are dominant
$J_s(p)=0.4382J_s(n)+0.3931$ $r^2=0,8266$	KrivaPalanka – Deve Bair	Albite-sericite schists

From Tab. 1 it can be seen that the coefficient of correlation r^2 has usually high values, but the correlations vary a lot depending on the rock type. This certainly has an effect on the anisotropy of the shear strength at the rock mass level.

Applied methods in the stability analyses

In the slope stability calculations, the intention shall be to apply adequate geotechnical models when choosing the most appropriate method for the analysis. In the selected sections, based on local conditions, all main known approaches are used, depending on kinematic conditions at certain zones, scale effect, orientation of the main structural elements and slope dimensions.

As a supporting empirical method, in some cases, the Slope Mass Rating System – SMR (Romana, 1995) and/or the Q-slope system, developed by Barton and Bar (2015) are used. The Q-slope method is presented in Eq. 1.

$$Q_{slope} = \frac{RQD}{J_n} \left(\frac{J_r}{J_a} \right)_O \frac{J_{wice}}{SRF_{slope}} \quad [1]$$

The first four parameters (RQD, J_n , J_a , and J_r) in the equation remain unchanged from the original Q-system (Barton, Lien and Lunde, 1974), while important changes are related to the discontinuity orientation factor (O), environmental and geological condition number (J_{wice}), and the strength reduction factor (SRF_{slope}).

Global stability analyses are prepared using the Limit Equilibrium Methods (LEM) i.e. the methods of Bishop, Spencer and Morgenstern-Price in the program Slide.

Methods developed for the analyses of planar or wedge failure type by E. Hoek and J.W. Bray 1974 are also used, combining them with kinematic analyses, when slope and discontinuity elements produce such conditions.

In some cases, the Finite Element Method (FEM), or Eurocode 7 suggested approaches are also used, but detailed explanations overcome the frame of this article.

The concept of the traditional factor of safety definition is extended whenever possible using the theory of probability and reliability with approaches of Reliability-Based Design (RBD). The fundamental difference between the RBD and the deterministic approach is in the fact that the uncertainty of parameters can be quantified through their probability distribution function. The benefit of this type of analysis is in cases when some of the material parameters cannot be precisely defined or they vary within some range. This is often a case when, the rock mass is highly weathered and fractured, characterized with anisotropy and discontinuities. The probability of failure (PF) is defined by the relation shown in Eq. (2).

$$PF = \frac{N_f}{N_s} * 100\% \quad [2]$$

Where N_f is the number of analyses with a safety factor less than 1.0 and N_s is the total number of samples defined before the calculation.

The reliability index is another commonly used measure of slope stability. This index is an indication of the number of standard deviations which separate the mean factor of safety from the critical factor of safety ($FS=1.0$). It can be calculated assuming either a normal or log-normal distribution of the results. If the factors of safety are normally distributed, then the following equation is used to calculate the reliability index (β), as shown in Eq. (3).

$$\beta = \frac{\mu-1}{\sigma} \quad [3]$$

Where μ is the mean factor of safety and σ represents the standard deviation of the factor of safety. There are options to calculate the Reliability Index also with a log-normal distribution.

Shortly, it can be noted, that there are a variety of methods available. They can be used with adequate success and they can give a reliable result if only they are applied to models that present the physical conditions in the field, which are always expressed in a unique way.

The presentation of different modes of failure for the analysed cases is illustrated in Fig. 2, Fig. 3 and Fig. 4.



Figure 2. View of some of the representative cuts, along the route of the A2 motorway, section Kicevo – Ohrid: a) 3+400 – 3+961; b) 14+990 – 15+310 c) 11+745 – 12+140; d) 12+340 – 12+600; e) 13+327 – 13+576; f) 15+690 – 16+114; g) 13+770 – 14+000; h) 17+740 – 18+200.

In Fig. 2, several cases from the highway Kicevo to Ohrid are presented, and each of them has some specifics. The global failure occurred on the first two cuts (Fig. 2a, Fig. 2b), local failure on the second two cuts (Fig. 2c, Fig. 2d), the next two cuts (Fig. 2e, Fig. 2f) have only minor (local) deformations and the last two cuts (Fig. 2g, Fig. 2h) have no deformations. The instabilities on the first two cuts (Fig. 2a, Fig. 2b) occurred a few months after excavation, while the local failures (wedges) on the second two cuts (Fig. 2c, Fig. 2d), occurred a few weeks after excavation of the subject berms.

In Fig. 3a and 3b, several cases from expressways from Stip to Kocani and from Stip to Radovish are presented. Here, the dominant role in slope stability is the orientation of the bedding planes in relation to the slope elements. In every case, when the slope has a higher dip angle, typical planar failures occur often, even in a case when some anti-erosion measures are applied (Fig 3b).

In Fig. 3c and 3d typical examples of several cases from the express road from Kriva Palanka to the Bulgarian border show, that failure mechanisms depend not only on the orientation of planes of weakness but also on the zones with different grades of weathering. It can be concluded, that a lot of cases and variations of problems are possible, and to solve them, a high level of theoretical and practical knowledge is essential in the formulation of reliable calculation models. The key element in the analyses is that a multi-disciplinary approach and step-by-step procedures are always necessary, with a main point, that the geotechnical and calculation model must be based on conceptual geological and engineering-geological models. Several typical examples are presented in Fig. 4, Fig.5, Fig.6, Fig. 7 and Fig. 8.

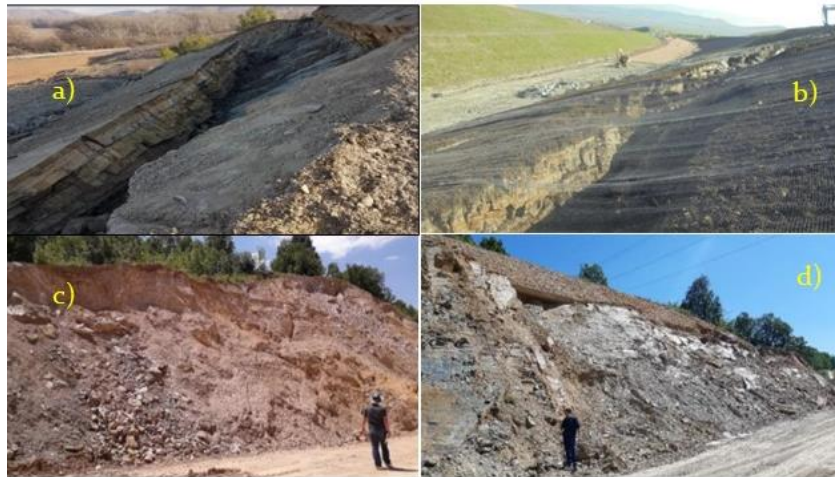


Figure 3. a) Cut in Eocene flysch deposits with kinematic conditions for plane failure along bedding planes at the express road from Stip to Radovich; b) cut at km 2+700 at express road Stip-Kocani; c) and d) Different types of failure at cuts along route of express road from Kriva Palanka to the Bulgarian border: upper section – rotational failure in soil debris at cut 5+900 – 6+100.

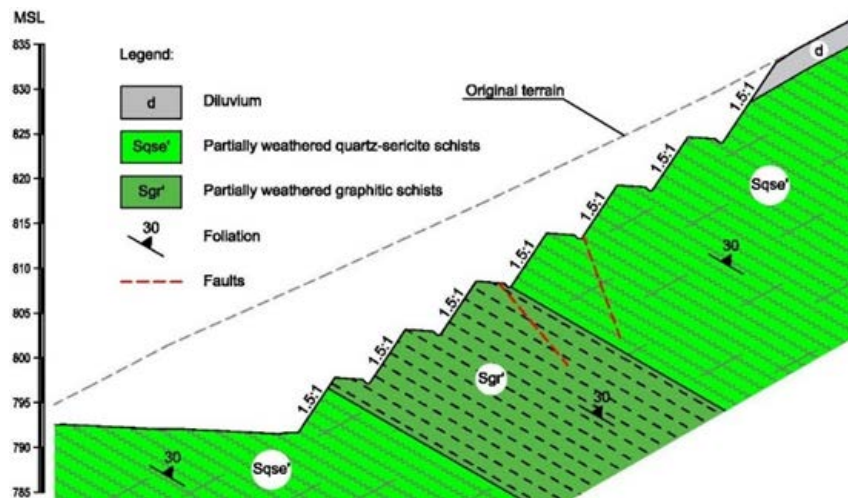


Figure 4. Geological model for one of the cuts at the highway from Kicevo to Ohrid in highly anisotropic weak rocks with favourable foliation orientation.

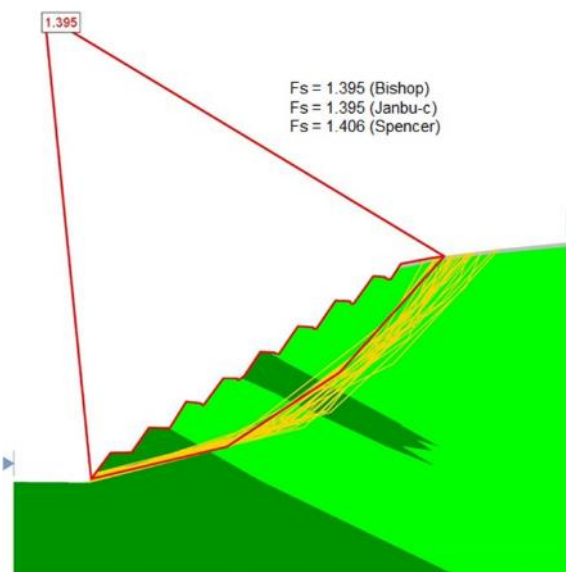


Figure 5. Calculation model for stability analyses with LEM for one of the cuts from Kicevo to Ohrid, which is appropriate for such cases in order to define global stability.

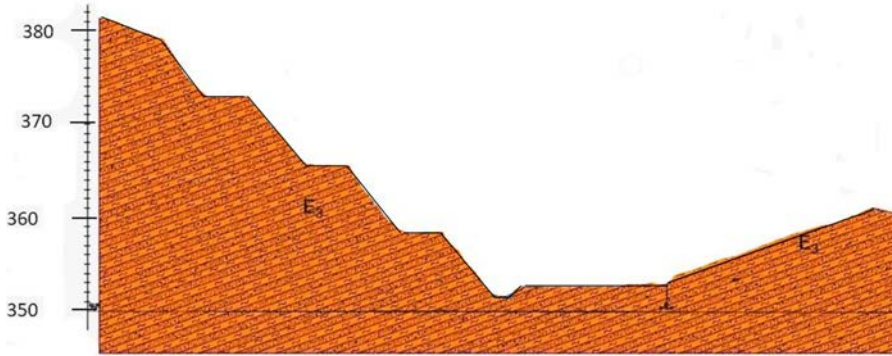


Figure 6. Geological model for a cut at km 2+700 (section from Stip to Kocani) in weak anisotropic Eocene flysch deposits, illustrating a case with favourable orientation of bedding planes at the left side and unfavourable bedding planes orientation for the right side that produces kinematic conditions for planar failure.

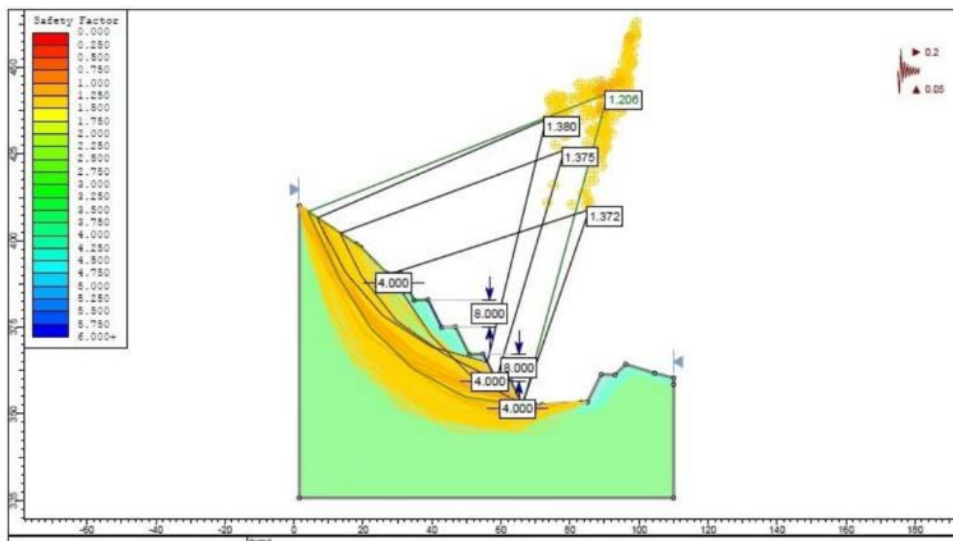


Figure 7. Calculation model for stability analyses with LEM method for left side of the cut at km 2+700.

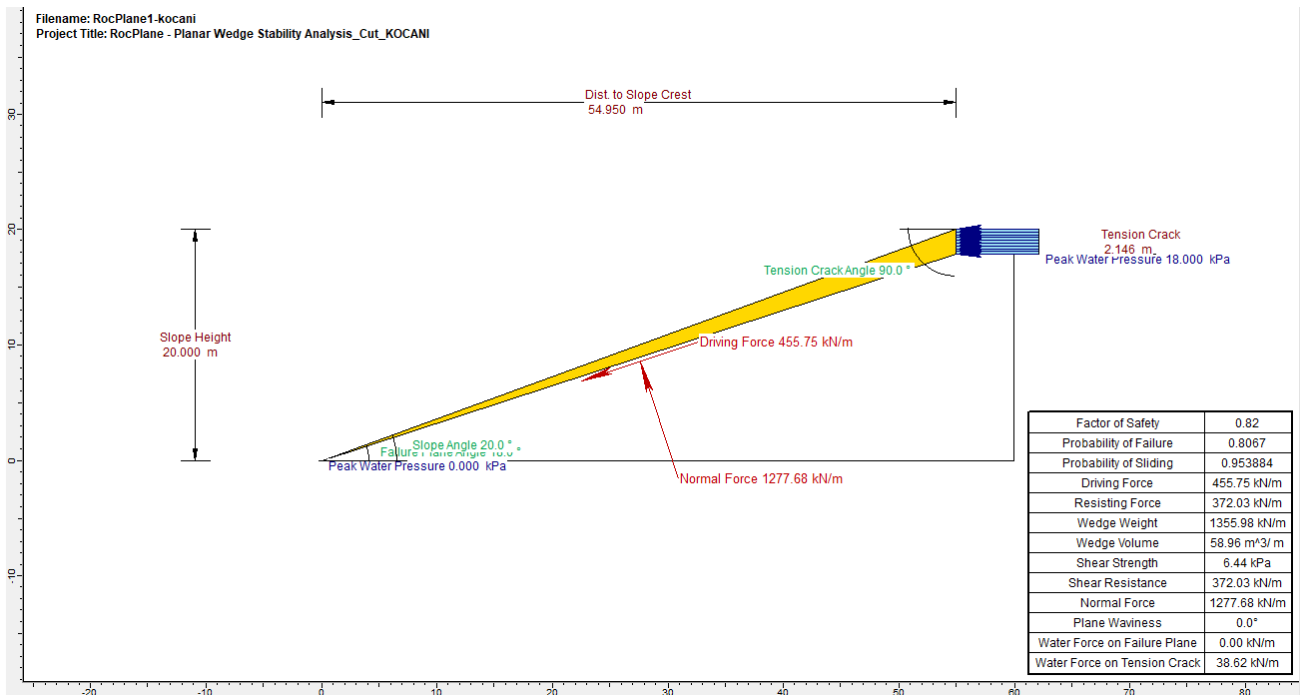


Figure 8. Calculation model for planar failure at the right side of the cut at km 2+700 using Eurocode 7, Design Approach 3.

Suggested methodology for integral approach

The presented results indicate that, in practice, every case is unique, and needs adequate attention in model preparations. The fact is that there are many guidelines for the design of slopes in rocks, including weak rock masses. Anyhow, there are still a lot of open questions to be analysed. The difficulty in determining the long-term stable slope geometry arises from the geological uncertainties within the rock mass. Although some methodological approaches can take into account these uncertainties, a major drawback that remains is the difficulty in defining an acceptable (adequate) level of risk.

This can be solved if only we use some integration of knowledge from several engineering and other disciplines. The integrated approach assumes that the problem shall be analysed from several perspectives, not always strictly related to geotechnical engineering. For example, in rock engineering problems, input from structural geology in rock mechanics is very important.

It is very obvious that the main step is to produce reliable geological and engineering-geological models, where the separation of quasi-homogeneous zones per necessary parameters for analytical or numerical analyses is necessary. The design model should incorporate slope protection methods, actions and resistance. All elements shall be analysed by an adequate geotechnical calculation model. After problem definition in critical zones, typical phases of the slope stability and slope protection program based on adequate investigation and design process shall be applied. Methodology must include a back-analysis of the past failures, prognosis failure modes, estimation of rock strength along joints etc. In brief, the methodology is based on the application of several interrelated phases, using the following approaches (Jovanovski et al, 2017):

- Analyses of possible kinematic modes of failure;
 - Statistical analyses in order to define the probability distribution functions;
 - Defining the factor of safety (Fs), probability of failure (PF) and reliability index (RI);
 - Analytical and/or numerical analysis;
 - Definition of the risk from sliding or rockfalls;
 - Cost-benefit analyses;
 - Definition of the acceptable level of risk (ALR);
- Integration of all findings.

For example, the risk level can be proposed using ideas presented in Fig. 9. The upper portion of the diagram presents a combination of the values of mean factor of safety and the probability of failure. The down portion presents a combination of the probability of failure and the potential economic losses in the event of an incident. In the diagrams, there are zones considered with broadly acceptable (BA), acceptable (A), conditionally acceptable (CA) and non-acceptable (NA) level of risk. The zone NA indicates an unacceptable level of risk and must be avoided or reduced, irrespective of the benefits.

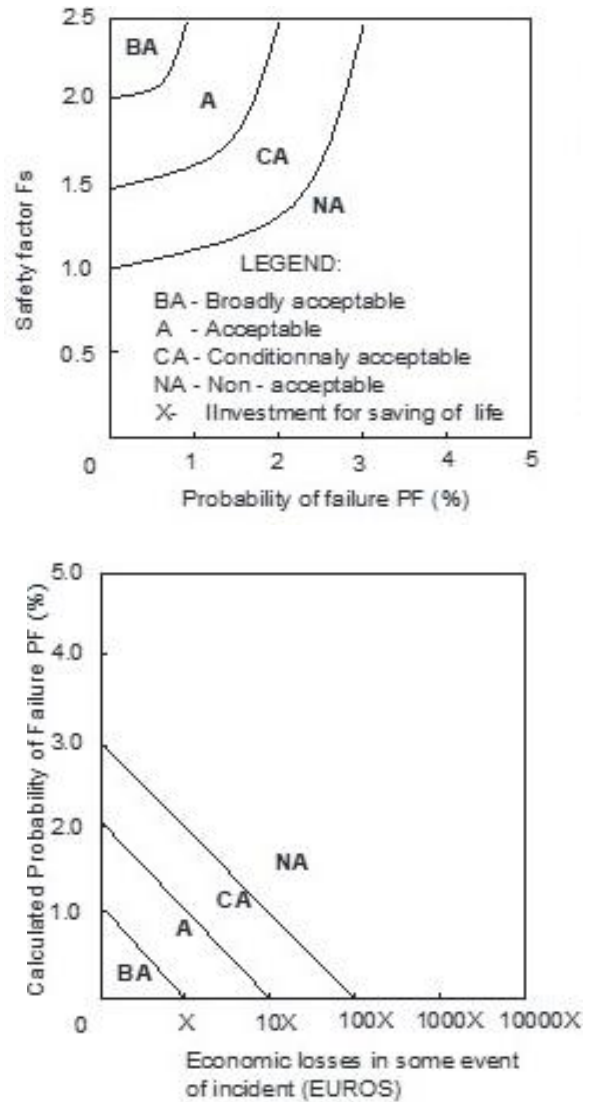


Figure 9. One concept for defining an acceptable level of risk. Upper section: mean value for the factor of safety vs. probability of failure; down section: probability of failure vs. potential economic losses in the event of incidents (Jovanovski et al, 2017).

Within the CA region, the risks may be tolerated, but here there are possibilities for some optimization of solutions. The value X in the right diagram portion includes possible economic and life loss impacts. In different countries, such values can be adopted using the country's GDP, values from insurance companies and other specifics in each country, but explanations overcome the frame of this article.

Every time when possible, it is good to combine methods and not to use only one approach. For example, in Fig. 10, a correlation is established between the results from Q-slope and SMR analyses. In Fig. 11, a combination of empirical and analytical methods is presented. Such combinations can give us the possibility to find some „weak points” or confirmation approaches with cross-checking of findings.

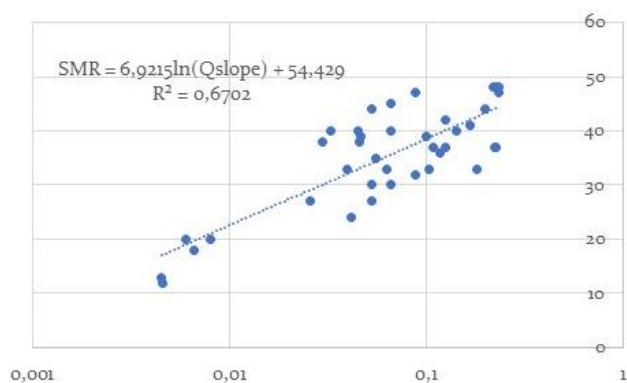


Figure 10. Correlation between the values of SMR and Q-slope for a cut at the express road from Kriva Palanka to the Bulgarian border.

If we compare the correlation from Fig. 10, we can only underline, that recommendations from Q-slope methods are usually related to stable slope angle, but without supporting structures, while SMR for categories with lower values typical for weak rock masse, usually suggests applying some protective measures.

The circles in Fig. 11 represent the Q-slope value and obtained factors of safety in the software package Slide in a parallel way. Circles refer to the global stability and the factors of safety obtained with Slide software, or results for local instabilities defined for wedge mode of failure with software package Swedge. According to the results, it is clear that the cuts with failures are quite deep in the unstable zone of the Q-slope stability chart. Also, for these two cuts, the values of the factor of safety against forming surface wedges are smaller than 1.0 which confirms the failures. The global factor of safety does not indicate a failure (which in rock slopes is not common) but it is not satisfactory either.

Some additional ideas in the methodology are based on the findings from the highway from Kicevo to Ohrid. The summary of the results from the deterministic and probabilistic slope stability analyses for all of the cuts is shown in Tab. 2.

Table 2. Summary of the slope stability analyses (Janevski et al,2021).

Cut information	No. of cuts	Safety factor	Reliability index	Probability of failure [%]
Failure occurred	15	1.06 – 1.26	1.27 – 1.98	1.5 – 9.8
Minor deformation	15	1.08 – 1.43	1.71 – 3.05	0.3 – 4.9
No deformation	23	1.39 – 1.69	2.40 – 5.50	0.0 – 1.0

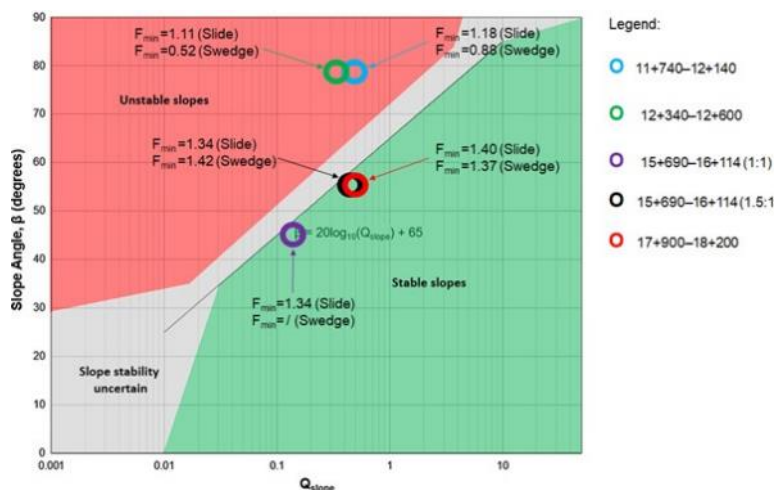


Figure 11. Q-slope stability chart (Barton and Bar 2015, 2017) for the subject cut slopes and their corresponding factors of safety obtained with LEM in Slide and Swedge (Janevski et al.,2020).

The results for the cuts with failure which initially were considered to be stable, show a factor of safety greater than 1.0, reliability index less than 2.0 and probability of failure less than 10%. Hence, this can be a motivation for further improvements of the methodology and redefine the possible uncertainties of the cut slopes in weak rocks.

Some open questions

Presented findings show that the problem of stability in weak rocks is very complex, and needs a lot of attention. In fact, newer approaches related to the reliability design methods and the probability analyses, indicate that there are still some open questions.

New trends that should be followed in the near future in preparation for the next Eurocode 7 generation shall also incorporate term consequence classes CC [10]. In Table 3, we present ideas for further analyses, in the form of recommended values for weak rock slopes. A summarised simple diagram is presented in Fig. 12. If we want to reach the acceptable zone (A) defined in Fig. 9, and if we want to achieve the desired value of RI=5, we must invest more resources in the remediation of the slopes. Some additional open questions can arise, related to values of Disturbance factor D in analytical and numerical analyses (Fig.13 and Fig.14).

Table 3. Authors suggestions for a value for Reliability Index and Probability of Failure for rock slopes in weak rocks related to Consequence's Classes in Eurocode 7.

Consequence Class	Reliability index	Probability of failure [%]
Lower CC1	1.27 – 1.98	1.5 – 9.8
Normal CC2	1.71 – 3.05	0.3 – 4.9
Higher CC3	2.40 – 5.50	0.0 – 1.0

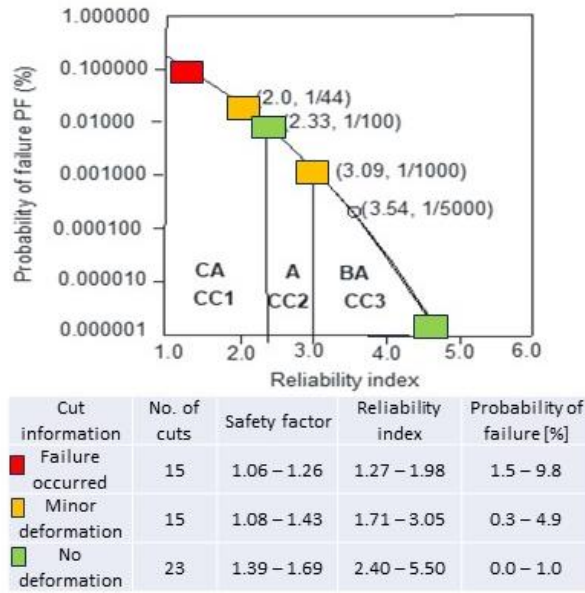


Figure 12. Diagrams presenting consequence classes from Eurocode 7, reliability index and value for the probability of failure and the level of risk from Fig.9.

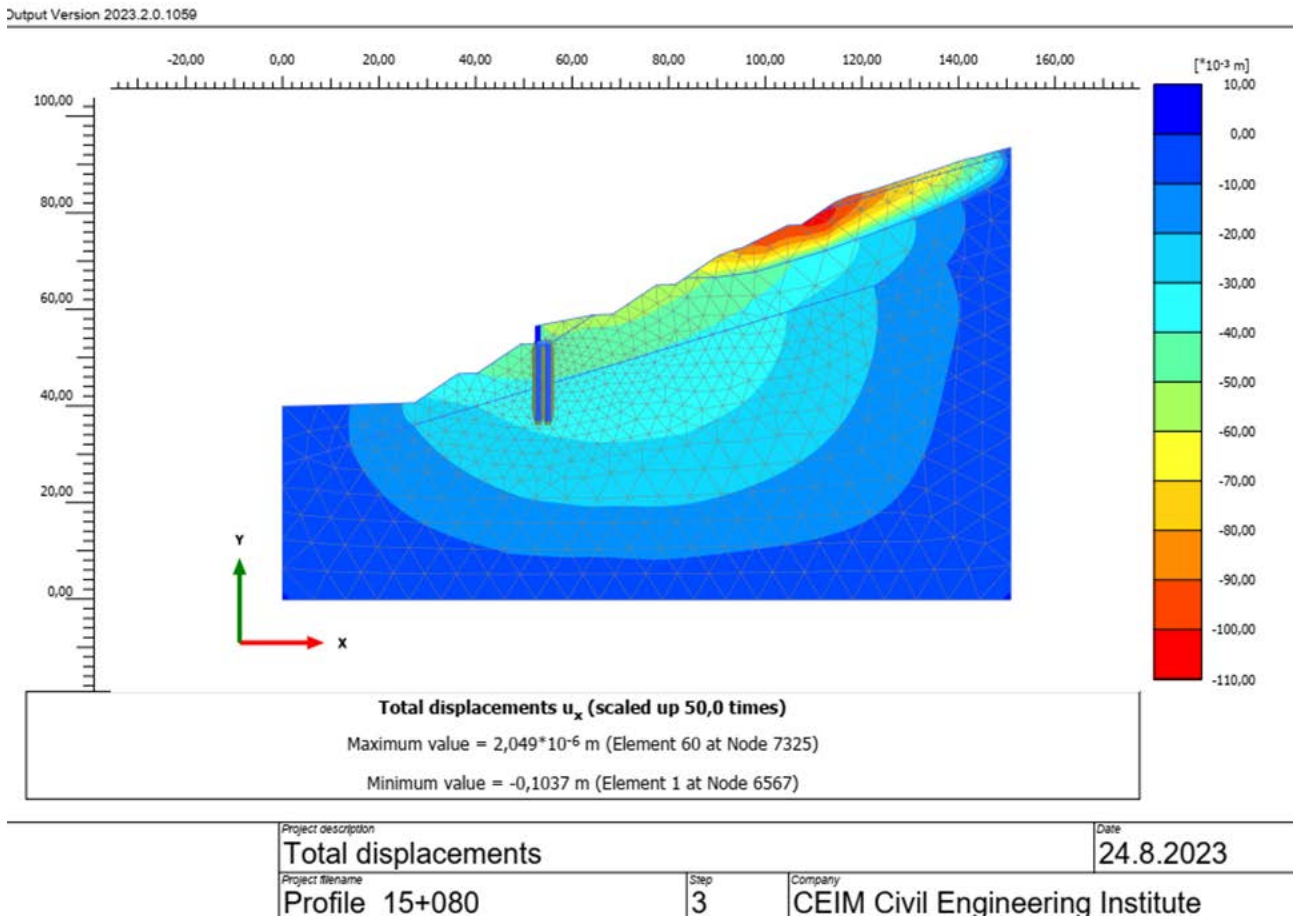


Figure 13. Numerical analyses for a cut slope at highway from Kicevo to Ohrid using the Plaxis software.

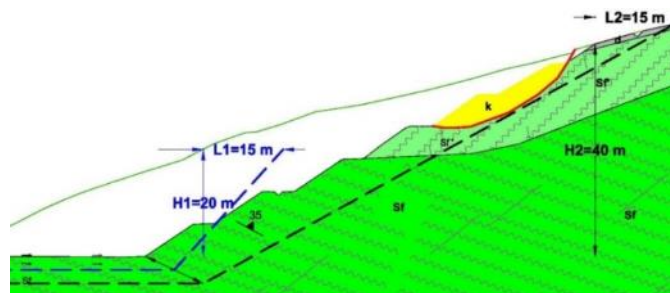


Figure 14. Geological section illustrating two possible solutions for the cut presented in Fig. 13, using reinforced concrete structure (blue colour) or unloading of slope and delineation of disturbance zone (blue for the first solution, black for the second solution).

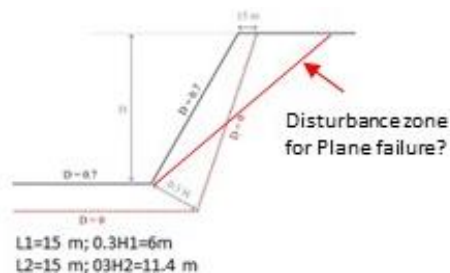


Figure 15. Diagram for defining the disturbance zone of slopes. <https://www.rocscience.com/help/slide2/tutorials/tutorials-overview/damage-regions-generalized-hoek-brown>

A lot of discussions can be opened if such recommendations for disturbance factor D and if the interpretation of disturbance zone for different slope heights can be similar for slope crest. Certainly, such recommendations cannot be valid when planar failure is the dominant failure mode (Fig. 15).

Finally, as an idea for further analyses, in weak rock mass media, we can underline a problem in the interpretation of rock bridge influences in assuming shear strength and coefficients of normal (K_n) and shear stiffness (K_s) along sliding surfaces, in a process of relaxation of rock mass during excavation, etc. These aspects are highlighted as an area for further scientific analyses, with one main goal – to get closer to the real mechanical behaviour of weak rocks during construction.

Conclusions

The article highlights some specific aspects of the stability behaviour of weak rock masses. The main conclusion is that the optimal way to assess the stability condition of slopes is to combine different tools and techniques and to choose which one suits best for the selected case. The given analyses show that all experiences and practices can be useful in developing some new ideas, despite the fact that each case is unique and has to be considered in terms of a particular set of circumstances. Solutions should be based upon detailed analyses, but also on engineering judgement guided by practical and theoretical studies of rockfall risks and stability of the slopes. The authors believe that the presented experiences can help in establishing an effective way for the protection of rock slopes susceptible to different modes of failure.

Acknowledgements

The authors are grateful for the support of the Rocscience company, for using the software for educational and scientific purposes.

References

- Barton, N., Lien, R. and Lunde, J. (1974) Engineering Classification of Rock Masses for the Design of Tunnel Support. *Rock Mechanics*, 6, 189-236.
- Barton N, Bar N (2015) Introducing the Q-slope method and its intended use within civil and mining engineering projects. Proc. Eurock 2015 & 64th Geomechanics Colloquium, Salzburg, 7–10 October 2015, Austrian Society for Geomechanics, 157–162.
- Bar, N. & Barton, N. (2017) The Q-Slope Method for Rock Slope Engineering. *Rock Mechanics & Rock Engineering* 50(12): 3307–3322
- Fengchang B., Lei X., Mengyang Z., Chao X., Yuan C (2022) Numerical Investigation of the Scale Effects of Rock Bridges. *Rock Mechanics and Rock Engineering*. URL: <https://doi.org/10.1007/s00603-022-02952-2>.
- Franzen, G; Garin, H.: (2021) Eurocode 7 – an updated framework to ensure reliable geotechnical solutions, 18th Nordic Geotechnical Meeting, IOP Conf. Series: Earth and Environmental Science
- Hoek E. and Bray, J.W. 1974. *Rock Slope Engineering*. London: Instn Min. Metall.
- ISRM (1981), “Rock characterization testing and monitoring”. Pergamon Press, Oxford.
- Janevski B, Jovanovski M (2020) Comparative assessment of slope stability in weathered schists using Q-slope and LEM. ISRM International Symposium Eurock 2020, Trondheim, Norway.
- Jovanovski, M.; Peshevski I.; Papic J.; Abazi S (2017) An approach for slope protection on the access road to arch dam “Sveta Petka” in Republic of Macedonia. Naucnikup, Geoxpo, Sarajevo 2017.
- Jovanovski M, Peshevski I, Uzunov D, (2023). Integral approach in rockfall risk analyses. Proceedings from Symposium, GEOEXPO20123, Mostar, DOI: 10.35123/GEO-EXPO, 2023.
- Martin D., (2023) 9th Müller Award Lecture, ISRM International Congress on Rock Mechanics, Salzburg. URL: <https://isrm.net/news/show/653>.
- Peshevski I., Jovanovski M., Velinov (2019) Point load database of the Republic of N.Macedonia. 14th ISRM Congress, Sao Paulo, Brasil.
- Romana M (1995) The geomechanical classification SMR for slope correction. In: Proceedings of the 8th ISRM congress on rock mechanics vol 3, Tokyo, 25–29 September 1995, pp 1085–1092.
- Saroglou H., Tziambaos (2007) Classification of anisotropic rock masses. Conference: Proc. 11th Int. Congress of Rock Mechanics At: 191-196, Volume: 1

High-Precision Landslide Monitoring Using Laser Scanning Technology

Marko Pejić

University of Belgrade, Faculty of Civil Engineering, Department of Geodesy and Geoinformatics, Bulevar kralja Aleksandra 73, Serbia, +381658331164 (mpejic@grf.bg.ac.rs)

Abstract Landslides represent geological phenomena that pose significant threats to infrastructure safety. In response to the need for more advanced monitoring techniques in terms of accuracy and reliability of spatial data, this paper undertakes an examination of recent advancements in geodetic technologies, specifically focusing on the application of state-of-the-art laser scanning (LS) techniques. This article deals with laser scanning techniques capable of providing a high-quality point cloud necessary for more advanced landslide analysis. Paper explores Terrestrial Laser Scanning (TLS), Mobile Laser Scanning (MLS) and Unmanned Aerial Vehicles Laser Scanning (UAVLS), emphasizing their potential in achieving optimal quality of spatial data for landslide analysis.

Recent developments in LS technologies have improved the field of geodetic monitoring, enabling surveyors to measure detailed three-dimensional data with high accuracy and in the same time with high spatial resolution and low data noise. TLS, conducted from ground-based stations, MLS from ground moving vehicles and UAVLS provide complementary perspectives, facilitating a better understanding of landslide dynamics.

The approach employed in rockfall monitoring using LS techniques is multifaceted. The paper underscores the significance of achieving millimetre-level precision of a single point and in the same time high spatial resolution and low data noise typical for LS. Data processing techniques include advanced point cloud registration, georeferencing, 3D modelling and analysis,

The application of laser scanning is demonstrated through two case studies. The first involves a seven-year monitoring campaign of a rocky slope near Ljig, Serbia, utilizing TLS technology. This method ensures precise and detailed three-dimensional surveying for a reliable assessment of rockfall dynamics. In the second case study, erosion monitoring at Devils' Town in southern Serbia employs an approach integrating TLS and UAV photogrammetry. This strategy provides overall and targeted insights into erosional processes, showcasing the versatility of 3D surveying in terrain monitoring.

Keywords Landslide Monitoring, Geodetic Techniques, Laser Scanning (LS), Terrestrial Laser Scanning (TLS), Mobile Laser Scanning (MLS), Unmanned Aerial Vehicles Laser Scanning (UAVLS), Rockfall Dynamics.

Introduction

Enhancing the functional characteristics of laser scanners and developing corresponding software algorithms have created the essential prerequisites to meet two basic quality requirements within a comprehensive process of measurement and data processing. The first requirement pertains to point accuracy from the measurement sample, representing the positional accuracy of each point in the measurement sample commonly referred to as a point cloud. The second requirement concerns the ability to interpret the recorded object as a whole, often associated with the spatial resolution of the point cloud. In the context of LS technology, both requirements are largely satisfied, marking a significant improvement in overall data quality compared to traditional geodetic observation methods (Pejić, 2022).

The optimal surveying method in geotechnics should be applied in accordance with the characteristics and composition of the object being surveyed, considering the dynamics of potential movements. When it comes to landslides as objects of geodetic measurement, optimal geodetic methods are often those offering greater potential for territorial coverage in a short time, consequently resulting in higher spatial uncertainty. This primarily pertains to landslides such as debris flow, mudflow, earthflow, etc. Geodetic methods like aerial photogrammetry, satellite imagery, and similar approaches can be employed in such cases. However, high-precision laser scanning technology, primarily utilizing TLS, finds its place for rocky formations that require geotechnical analysis of scanned rock surfaces and rockfall monitoring (Abellán et al.). Therefore, this study will focus on objects of that specific nature. The primary objective of geodesy in rock formation surveying and monitoring is to provide geometric information essential for subsequent geotechnical analyses.

LS devices conduct measurements with a certain measurement uncertainty, and the scanned data is three-dimensional (3D), referred to as a point cloud (Figure 1a.). An additional attribute, in the form of return intensity for each point, can be associated with the point cloud (Figure 1b). This intensity value mostly depends on the object's reflectivity and such attribute is part of the laser measurement system. In practice, it is common for each scanned point to be associated with RGB (Red Green Blue) values based on an integrated CCD (Charged Coupled Device) sensor and corresponding optics, which can be

integral or external component of LS instrument (Figure 1c) (Pejić, 2022).

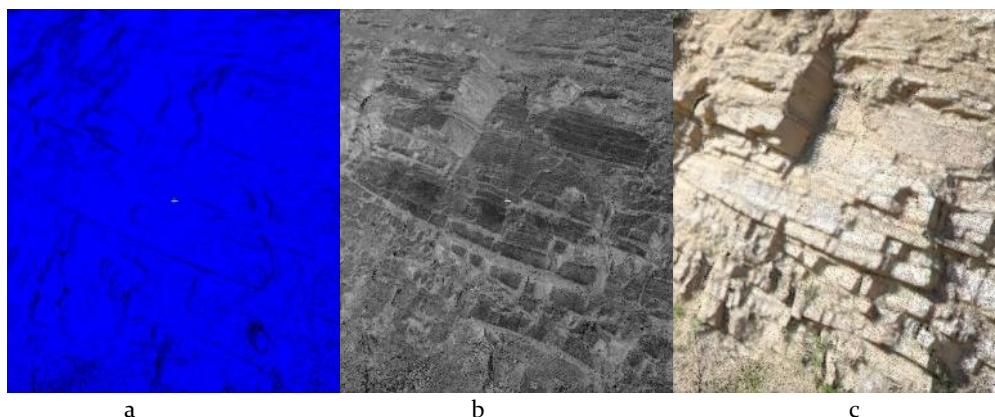


Figure 1 Point cloud. Lacking additional attributes (a.), accompanied by the attribute of backscattered radiation intensity (b.), and incorporating the attribute of RGB values (c.).

Considering that light travels at an almost constant speed through a medium, the distance can be determined based on the time it takes for light to return to the detector. These systems are known as Time of Flight (TOF) systems. TOF measurements can also be achieved indirectly through phase measurements of continuous waves by amplitude modulation of the continuous wave (AMCW – Amplitude-Modulated Continuous Wave) or frequency modulation of the continuous wave (FMCW – Frequency-Modulated Continuous Wave).

The triangulation method involves forming a triangle using two known angles (exit and entrance) and a constant baseline, from which the distance to the object can be determined. The range and accuracy of LS largely depend on the methodology of distance determination. The triangulation method is used for very close distances, the phase measurement methods for measurements from close to medium distances, and the pulsed TOF measurement method for medium to large distances. Figure 2 illustrates the uncertainty and working range of laser rangefinders in LS systems, classifying them based on their application areas.

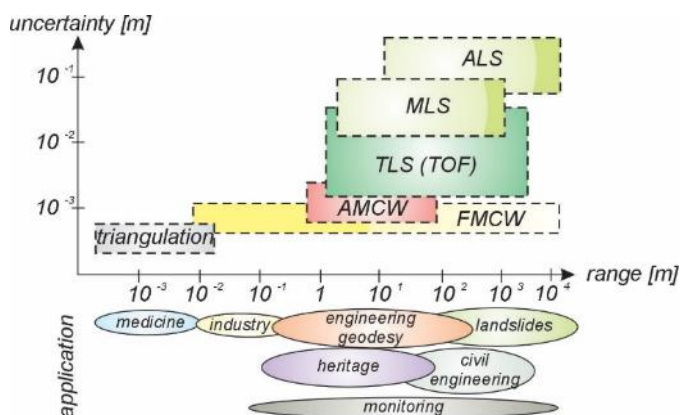


Figure 2 Distance determination, application, working range, and uncertainty of LS systems (after Schulz, 2007)

When it comes to LS technology, it is important to mention that this term can include devices that are stationary (TLS) or placed on mobile platforms such as MLS and ALS (airborne LS) devices. As these instrument moves during measurements, the system must have additional devices which define the positions and inclinations of the instrument in real-time. However, due to the fact that the instrument is on an unstable platform, despite the use of complex sensors, the quality of scanning data with respect to positional accuracy and data noise is typically lower for such instruments. These instruments are usually oriented towards applications where positional accuracy is not the primary priority.

A Mobile Laser Scanning (MLS) system integrates a laser scanner unit for three-dimensional point cloud acquisition, Global Navigation Satellite System (GNSS) for precise positioning, an Inertial Measurement Unit (IMU) to sense and record angular rate and acceleration, cameras for synchronized high-resolution imaging, a dedicated data storage and processing unit to manage acquired data, a reliable power supply for uninterrupted operation, a control and navigation system for overall system management, and communication Interfaces to facilitate data transfer and system control. The synchronized integration of these components enables MLS systems to dynamically acquire precise geospatial information during motion, making them essential for applications such as topographic mapping and geohazard assessment (Singh et al., 2021). MLS are often mounted on a vehicle moving along roads or terrain.

Unmanned Aerial Vehicle (UAV) mapping, a rapidly advancing field in geospatial sciences, involves the use of drones equipped with remote sensing instruments to capture data for mapping applications. These drones, acting as aerial platforms, carry a variety of sensors such as RGB or multispectral cameras or LiDAR scanners, GNSS and IMU. The workflow includes planning, data acquisition, and post-processing, resulting in data essential for environmental monitoring. Very recent technological developments have enabled UAV to

integrate laser scanners, achieving flight durations and measurement precision suitable for engineering applications (Liu at all, 2019.)

The accuracy and reliability of data acquired by MLS or UAVLS is still far from the level achieved by TLS. Nevertheless, the spatial coverage that can be scanned in a short time is very large (Guisado-Pintado at all, 2019.). Additionally, inaccessible areas for humans are not a challenge especially for UAV systems.

Laser Scanning Method in Geodetic Engineering

Surveying measurements, such as tachymetry, GNSS, photogrammetry, and precise leveling, have traditionally been widely used in engineering. Precise leveling is extensively employed for height transfers and will not be further discussed in the context of LS.

In engineering applications, tachymetry, photogrammetry, and GNSS can be considered compatible methods compared to LS. These methods can provide 3D data of complex objects. Additionally, radar interferometry holds a significant place in modern engineering geodesy for determining digital elevation models, scanning, or deformation monitoring at large distances from the observed object (Zogg, 2008).

Tachymetry is a polar method for determining the 3D coordinates of a predefined point on an object using a total station (TS). Measurement accuracy is typically high only when targeting a standard prism, while measurement frequency is low. The range of TS in engineering varies from a few centimeters to several hundred meters. Tachymetry enables transferring and marking the horizontal and vertical positions of points on the ground (staking out).

GNSS measurements in geodesy provide 3D position, time, and receiver movement speed as results. In engineering, selected points on the object are measured using this method, along with vectors between two or more receivers in relative positioning procedures.

Photogrammetry is a method that determines the position of points on an object based on one or more images. It is an indirect measurement method, where data on the radiation intensity of the object are collected using a passive sensor (CCD camera), usually in the visible part of the spectrum. The fundamental data is the pixel, and the record is a digital image. Typical accuracy ranges from less than one millimetre to several decimetres, with a range from several centimetres to several hundred meters (Zogg, 2008). A photogrammetric camera can be stationary or mounted on a moving platform. Given that the image acquisition occurs within a brief exposure period, the geometric reconstruction of pixel positions in space may obviate the need for camera integration with inertial and positional systems. This characteristic renders photogrammetry a cost-effective.

Terrestrial radar interferometry (ground-based interferometric synthetic aperture radar – GB-InSAR) is a modern polar measurement method based on radar technology. It measures distance based on electromagnetic waves in the microwave part of the spectrum. Measurements are realized on a grid or profile by linear movement of the radar interferometer along a track and/or rotation around the vertical axis. It is applied in terrain deformation monitoring. Temporal resolution is measured in minutes, making this method suitable for early warning systems. The range is up to several kilometres, with submillimetre-level precision. Terrestrial radar interferometry effectively detects surface changes related to mass movement, detecting slow and fast displacements in rock walls, and assessing qualitatively fast and episodic processes like rockfall (Caduff at all, 2015). The drawback of radar interferometry is relatively poor spatial resolution compared to LS systems. The spaceborne aspect of InSAR involves the deployment of radar-equipped satellites in orbit around the Earth. These satellites emit radar signals towards the Earth's surface, and the signals are reflected back to the satellite's antenna.

The LS method does not completely belong to polar measurement methods, photogrammetric methods, or any other method. It can be considered a distinct method of geodetic measurement, and LS represents a specialized discipline within geodetic surveying.

Photogrammetry and laser scanning share common characteristics in terms of high detail (density) of collected geometric data and additional information about the intensity of the reflected radiation. If the reflection intensity is a result of the object's own reflectivity, it can be a parameter in content classification processes. Often, an RGB value can be assigned to a scanned point for easier interpretation of content. This information is collected by a digital camera, which is an integrated or additional part of most TLS devices, although it is not inherently part of LS technology. This visual information is usually not accessed for measurement purposes, primarily serving visual interpretation of point clouds.

The basic principle of determining coordinates using TLS technology does not differ from the principle that has been used in geodesy for a long time thanks to classical instruments. TLS instrument has a similar technical solution to total station instrument, regarding certain components, such as the main instrumental axes, collimation, compensators, etc. Coordinates are determined using a polar geodetic method, with the measurement of the slope distance, horizontal and vertical direction of individual points on the object.

LS, photogrammetry, and radar interferometry represent post-processing methods, meaning measurement results must be processed and interpreted after measurement realization. These methods are also called indirect methods, unlike direct methods such as tachymetry or GNSS, which can provide real-time results

without the obligatory need for post-data processing. Direct measurement methods enable surveying procedures such as staking out. (Zogg, 2008).

LS in precise landslide monitoring and analysis - examples

In this section, the practical value of laser scanning data in geotechnical analyses of landslides will be demonstrated. Special emphasis will be placed on techniques capable of providing high-reliability data for geometric interpretation. This is particularly crucial when observing rocky structures adjacent to infrastructure elements, as their stability often demands thorough analysis and monitoring.

Rock slope Ljig monitoring and analysis

LS monitoring systems, particularly TLS, can be employed to observe suspicious rock faces over extended periods, either seasonally, annually, or even daily. This approach yields systematic data that enhances comprehension of the prefailure and failure stages and facilitates the correlation of these stages with triggering conditions. The research focuses on these precursory indicators, advocating for the standardization of monitoring parameters in rockfall management. While this study presents a singular example of isolated rockfall, entire rock slope will be analysed in greater depth in the near future (Marjanovic et al, 2021).



a



b

Figure 3 TLS point cloud of experimental site. a: S1, S2 and S3 represent scanner station. Objects 1 to 6 represents scanning targets (a). Detail of a rock slope with an associated attribute of radiation intensity value

The site of interest is located along IB22 highway, a corridor with high traffic frequency near Ljig in Serbia ($44^{\circ} 12' 02''$ N; $20^{\circ} 14' 35''$ E), featuring a height of 30 m and a length of 60 m, with an approximate 60° slope (Figure 3).

Originally engineered as a road cut, the exposed rock face has undergone significant deformations. Despite its relatively active slope, the insignificant rockfall volume and runout led to the slope being left unprotected.

Comprising a flysch complex dominated by brittle sandstone banks and marly-shales, the slope poses stability concerns. Over seven years of TLS monitoring (from 2013. to 2019.) source areas are identified, but runouts were unrecorded due to swift clean-ups by the Public Enterprise Roads of Serbia. Back-analysis involved comparing TLS scanning epochs, determining block size, and assessing rock properties. Results indicate one source area as potentially critical, with trajectories reaching the road. Calculations show manageable energies and forces, suggesting feasible remediation measures. Rock bouncing and fragmentation effects are mitigated by the slope's characteristics (Marjanovic et al, 2021).

The primary acquisition technique involves the Leica Scan Station P20, a TOF TLS scanner with a laser beam width of 2.6 mm and a single-point 3D uncertainty of up to 3 mm/50 m. It collects points within a range up to 100-120 m, providing 3D coordinates and intensity values (I) for each point. Colour information is obtained either from the internal scanner camera or external high-definition camera for enhanced results.

The initial years of rockslope monitoring were experimental, marked by irregular and less systematic data acquisition. This experience aided in optimizing the long-term TLS observation procedure. The main goal was to ensure nearly identical measurement conditions and establish a standard procedure, determining spatial and temporal resolution, timing, and other crucial acquisition parameters. Procedures are standardized with an annual frequency. The optimal acquisition time is early spring on a cloudy but dry day for consistent lighting and minimal vegetation interference. Three scanning stations are used for near-full data coverage, with 5-8 evenly distributed scanner targets for reliable registration. Scanning parameters are set for a spatial resolution of at least 3 cm over the entire rock face. Additionally, a full $360^{\circ}/270^{\circ}$ field of view enables reliable cloud-to-cloud data registration. (Marjanovic et al, 2021).

The georeferencing of registered point clouds from all epochs is performed using surface matching algorithms, with the reference epoch being 2013. The standard deviation of the coordinate transformation in registration and georeferencing procedures is up to 3 mm. Leica Cyclone software is used for data processing, segmentation, and point cloud resolution unifying. The CloudCompare software plug-in CANUPO classifier eliminates remaining vegetation points for each epoch. Deformation analysis involves calculating cloud-to-cloud differences between successive scanning epochs and the "zero-2013" point cloud.

Over the period from 2013 to 2019, a total of seven scanning epochs were performed and analysed in accordance with the described procedure.

The Figure 4 shows an example illustrating the quantities and locations of rockfalls between spring 2013 and 2016. The analysis was conducted using Leica Cyclone 3DR software.

For a more comprehensive geotechnical analysis of landslides and the cause-and-effect mechanisms, refer to (Marjanovic et al, 2021).

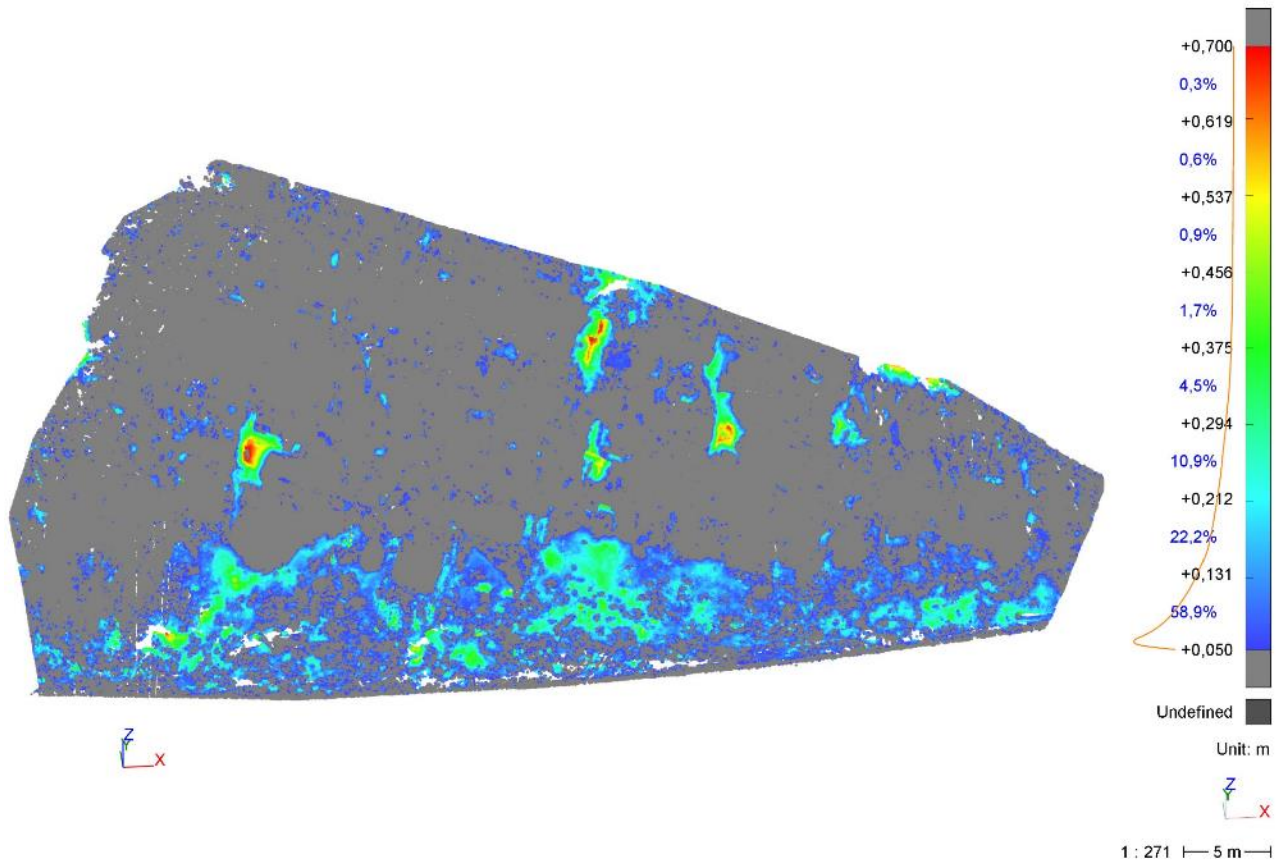


Figure 4 Example Cloud-to-cloud difference computed using Leica Cyclone 3DR software. Epoch 2016-2013.

Devils' town erosion monitoring

The erosion monitoring focuses on Devils' Town, a unique natural site in southern Serbia, shaped by water and wind over millennia. It is a UNESCO-listed protected heritage site managed by Planinka, the Municipality of Kuršumljija, and the Institute for Nature Conservation of Serbia. Increased human interest and activity on the site have led to observed erosional changes in the pillars, highlighting the need for a comprehensive understanding.

The Devils' Town site is part of the larger Lece volcanic complex in southern Serbia, spanning about 700 km². Formed over millions of years, this extensive stratovolcano experienced both violent and peaceful eruptions, leaving geological evidence of calderas and volcanic activity. The area, now featuring hot springs like Prolom Spa, Kuršumljija Spa, and Sijarinjska Spa, showcases the aftermath of extensive volcanic history.

Erosional processes have obscured the once-visible calderas, but the geological legacy persists. Notably, violent eruptions produced lahars and pyroclastic flows, crucial for understanding the authenticity of the Devils' Town site.

The project titled DEMONITOR, which specifically deals with the erosion of these rocky formations, has been approved as a three-year grant by the Ministry of Science of the Republic of Serbia. It utilizes advanced surveying methods such as TLS, UAV photogrammetry and satellite InSAR, as well as geophysical techniques, to quantify erosion dynamics, rockfall occurrences, weathering rates, and ground subsidence. Building on a successful 1-year pilot, the project aims to not only depict changes but predict rates and trends, facilitating the design of preventive measures for the permanent conservation of the site.



Figure 5 A point cloud generated through UAV photogrammetry at the Devils' Town site. Epoch 2017-2018.

The complex interplay of erosional processes and volcanic rock has yielded a diverse array of noteworthy landforms, colloquially termed "the Devils" and scientifically acknowledged as the "badlands" (Figure 5). The host rock represents a vestige of an ancient pyroclastic flow, characterized by loose and friable material prone to erosion. Over extended periods of time, the cumulative effects of weathering and erosion have intricately carved nearly 200 pillar-like structures, reaching heights of up to 15 meters and diameters spanning 6 meters.

During the pilot monitoring project, two measurement epochs were conducted in the autumns of 2017 and 2018. Data for the broader area of the Devils' Town site were collected using UAV photogrammetry, providing an overview of the general terrain morphology beyond the pillar-like forms. For a detailed analysis of the erosion of the figures themselves, TLS data were utilized. Measurements were performed using the Leica ScanStation P20 scanner, based on a pre-defined surveying methodology. The objective was to optimize all measurement parameters to ensure the necessary resolution, measurement uncertainty, and a consistent coordinate system for all future measurements. The achieved accuracy of the point cloud is within a few millimetres in absolute terms for TLS and in the order of centimetres for the photogrammetric method.

The pivotal outcomes of the aforementioned pilot project indicate ability to identify annual changes specifically between 2017 and 2018, quantifying and illustrating them (see Fig. 6). The annual change rate is concerning, encompassing detached small rock fragments from the pillar bodies and incisions at their bases caused

by linear erosion (red areas indicate changes > 14 cm). Some preliminary findings have been partially published in Đurić et al, 2018.

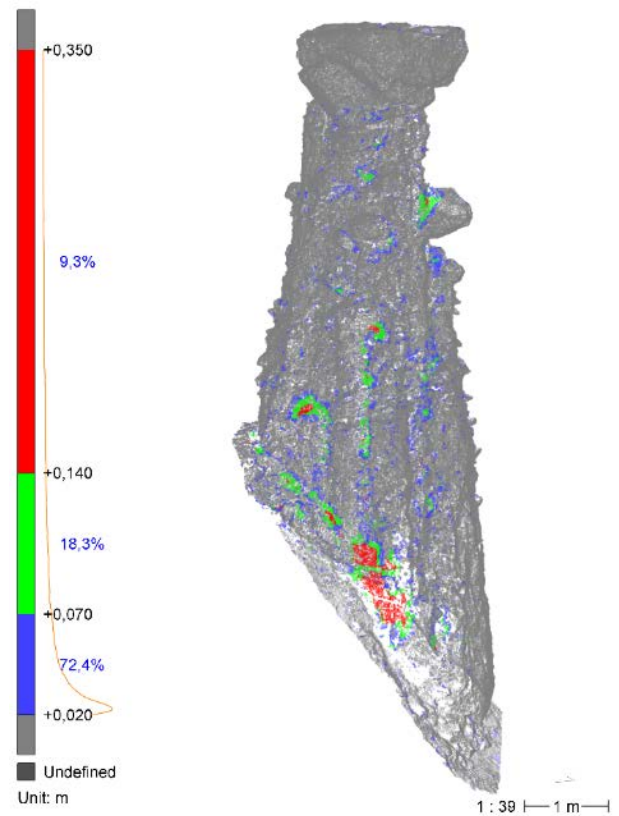


Figure 6 Identified erosion in the landform known as "Barjaktar" between the years 2017 and 2018. Computed in Leica Cyclone 3DR software.

Preliminary analyses of the point cloud of the earth feature known as "Barjaktar" (Figure 7) have indicated that its andesite cap (Figure 7b) has a mass of approximately 3,4 tons, significantly larger than the mass estimated based on visual observation.

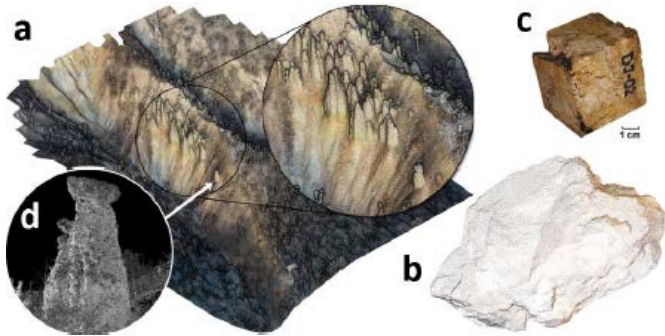


Figure 7 a) point cloud from the wider area, b) a point cloud of the andesite cap of the "Barjaktar" figure obtained by TLS, c) a sample of the andesite rock taken from an accessible location (with similar properties to the rock cap) near the "Barjaktar," used for measuring bulk density, required for the estimation of the cap mass, d) the "Barjaktar" scanned by TLS (Đurić et al, 2018).

Conclusion

LS has integral role in geodetic engineering, specifically for the high-precision landslide monitoring. The demand for precise and reliable spatial data in the analysis of geological phenomena, especially in the context of landslides is a critical imperative. The examination of recent developments in laser scanning techniques reveals their potential to provide detailed three-dimensional data marked by notable precision, high spatial resolution, and low data noise.

The practical applications of laser scanning in rockfall monitoring, as exemplified through case studies such as the seven-year rock slope monitoring near Ljig, Serbia, demonstrate the efficacy of laser scanning in capturing the progression of rockfalls. Furthermore, the erosion monitoring of Devils' Town exemplifies the integration of other surveying methods, such as UAV photogrammetry or UAV LS, providing a comprehensive approach to quantify erosion dynamics, predict rates, and enhance conservation.

In essence, LS emerges as a powerful tool in geodetic engineering, providing a reliable spatial data source that contributes to the broader understanding of landslide dynamics. Designing parameters of scanning experiment, their processing, and analysis, with the aim of reaching reliable conclusions during rockfall monitoring and analysis, represents a crucial step.

Acknowledgements

Supported by the Ministry of science, technological development and innovation of Serbia, Project number: 7515.

References

- Abellán, A., Oppikofer, T., Jaboyedoff, M., Rosser, N., Lim, M., Lato, M. (2014) Terrestrial laser scanning of rock slope instabilities. *Earth Surface Processes and Landforms*, 39. <https://doi.org/10.1002/esp.3493>.
- Caduff, R., Schlunegger, F., Kos, A., Wiesmann, A. (2015) A review of terrestrial radar interferometry for measuring surface change in the geosciences. *Earth Surface Processes and Landforms*, 40, 208 - 228. <https://doi.org/10.1002/esp.3656>.
- Đurić, U., Pejić, M., Marjanović, M., Đurić, D., Krušić, J. (2018) Monitoring of erosion in the area of Đabolja Varoš: Project "Međa". In *Knjiga apstrakata/17. Kongres geologa Srbije, Vrnjačka Banja, 17-20. maj 2018. Book of abstracts/17th Serbian Geological Congress, Vrnjačka banja, Maz 17-20, 2018. Vol. 2 (pp. 780-785). Srpsko geološko društvo, Beograd.*
- Guisado-Pintado, E., Jackson, D., Rogers, D. (2019) 3D mapping efficacy of a drone and terrestrial laser scanner over a temperate beach-dune zone. *Geomorphology*. <https://doi.org/10.1016/j.geomorph.2018.12.013>.
- Liu, C., Liu, X., Peng, X., Wang, E., Wang, S. (2019) Application of 3D-DDA integrated with unmanned aerial vehicle-laser scanner (UAV-LS) photogrammetry for stability analysis of a blocky rock mass slope. *Landslides*, 1-17. <https://doi.org/10.1007/s10346-019-01196-6>.
- Marjanovic, M., Abolmasov, B., Berisavljevic, Z., Pejic, M., Vranic, P. (2021) Pre-failure deformation monitoring as rockfall prediction tool. In *ISRM EUROCK (pp. ISRM-EUROCK)*. ISRM. <https://doi.org/10.1088/1755-1315/833/1/012197>
- Pejić, M. (2022) *Terestričko lasersko skeniranje u inženjerstvu. Građevinski fakultet, Akademska misao. (ISBN: 978-86-7466-932-7), 152p.*
- Singh, S., Raval, S., Banerjee, B. (2021) Automated structural discontinuity mapping in a rock face occluded by vegetation using mobile laser scanning. *Engineering Geology*, 285, 106040. <https://doi.org/10.1016/j.enggeo.2021.106040>.
- Zogg, H.M. (2008) *Investigations of High Precision Terrestrial Laser Scanning with Emphasis on the Development of a Robust Close-Range 3D-Laser Scanning System. Dissertation. Institute of Geodesy and Photogrammetry, ETH Zurich, Switzerland.*

Landslide mapping and zonation at national, regional and local scale - Recent experiences from Republic of Macedonia

Igor Peshevski^{(1)*}, Milorad Jovanovski⁽²⁾, Dario Peduto⁽³⁾, Natasha Nedelkovska⁽⁴⁾, Gjorgi Gjorgiev⁽⁵⁾

1) Ss. Cyril and Methodius University in Skopje, Faculty of civil engineering, Skopje, blvd. Partizanski odredi 24, peshevski@gf.ukim.edu.mk

3) Dario Peduto, Department of Civil Engineering, University of Salerno, Italy, Via Giovanni Paolo II, 132 - 84084 Fisciano (SA),

4) Geohydroconsulting Ltd., Skopje, Manapo 7

5) Ss. Cyril and Methodius University in Skopje, Faculty of civil engineering, Skopje, blvd. Partizanski odredi 24

Abstract The paper presents an overview of recent landslide mapping and zonation projects in Macedonia at different scales. On national level, the most recent study is a national scale susceptibility mapping performed within a geohazards study - part of the spatial plan of Macedonia. Due to limitations with regards to landslide characterization and a relatively poor landslide database, the rather simple arbitrary polynomial approach was applied. Lithology, terrain slope, rainfalls, earthquake acceleration and land use were considered causal factors for landslide development. Two susceptibility models, with different return periods for maximum expected earthquake acceleration according to Eurocode 8, were produced. The results are compared with previously performed studies and certain conclusions and recommendations for further activities were drawn. The second part of the paper is dedicated to regional and local scale mapping case studies, most of which are done for the Polog region. Several techniques for landslide susceptibility mapping had been applied, such as LiDAR semi-automated susceptibility mapping, frequency ratio method, arbitrary polynomial method, DInSAR “hotspot” detection. Depending on data availability, different datasets were used for the specific methods. Based on results of the landslide susceptibility mapping, the landslide hazard and risk for a number of most critical locations was assessed at a local scale. These locations were considered for design of remedial measures. Namely, the preliminary remediation designs were made, consisting of at least two possible solutions per location. The solutions were then subjected to a cost-benefit analysis, upon which the final design was done for the most feasible one. Solutions are now being implemented. Some other regional and local scale assessments are presented only briefly in the paper.

Keywords landslide, zonation, national, regional, local, Macedonia

Introduction

Landslides in Republic of Macedonia have been investigated for a long period. First “extensive” landslide mapping, has been performed during the time of Yugoslavia.

Namely, between 1960 and 1980, in frame of the basic geological mapping for the entire territory of the country at 1 : 100,000 scale, over 150 landslides were detected. Unfortunately, only the landslide polygons are now available, while the associated data on the landslides characteristics have been lost. After this period, the landslides had been treated sporadically, mostly during the construction of large infrastructure projects. The Geological survey and the large construction companies had great capacity in investigating and remediating the landslides. With the downfall of these entities, the landslide problems had become harder to tackle. Moreover, the procedures and laws related to the landslide management have delayed the interventions, usually leading to obstacles in the use of public infrastructure for unreasonable long periods. Due to limited budgets, municipalities have even more difficulties in landslide remediation. In some cases with obvious life threatening risk being overlooked. First attempt to present the landslide threats on national level was done by Jovanovski in 2010. Peshevski (2015) performed a regional landslide susceptibility mapping for the Polog region. Milevski et al.(2019) produced an AHP susceptibility map for Macedonia. UNDP sponsored a project related to landslide risk reduction for Polog region, where some local scale analyses were performed (Jovanovski et al. 2021). Case studies for earthquake-induced landslide hazard in local and regional contexts were presented by Bojadzieva et al. (2018 and 2022). Nedelkovska (2023) performed a multi-method susceptibility assessment of the Polog region. In 2023 Peshevski et al. performed a national scale susceptibility mapping framed within the national spatial plan.

National scale studies

Jovanovski(2010) presented an overview map of landslide locations in Macedonia (Fig.1). The main idea of the paper was to stress the most critical regions threatened by landslides and to propose more specific geographic regions for which detailed studies should be performed. Some data for larger landslide risk assessment also for the surroundings was presented. This paper stressed the need

for a more systematic approach in the landslide hazard and risk mapping in Macedonia.

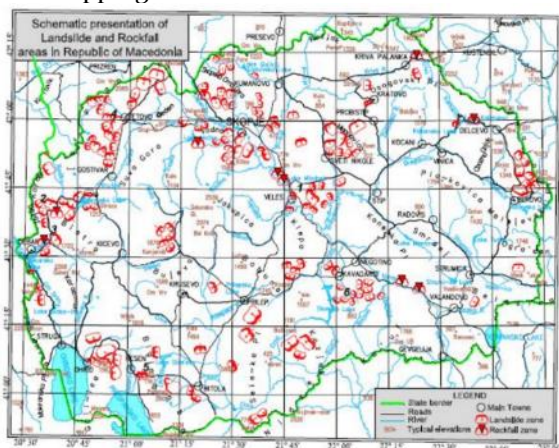


Figure 1 Schematic presentation of landslide and rockfall areas in the country (Jovanovski 2010).

Peshevski(2015) prepared a landslide inventory map of Macedonia consisting of over 300 occurrences (Fig. 2). The level of data available for each landslide ranges from very detailed to very poor - even unknown location (i.e. only from spoken information). The final map consisted of 255 landslide occurrences.

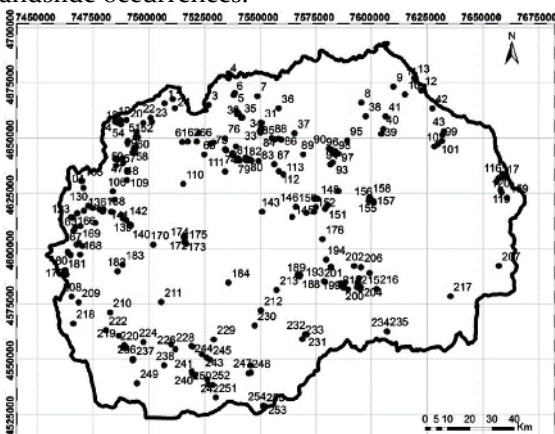


Figure 2 Landslide inventory map of the Republic of Macedonia (Peshevski 2015).

Milevski et al. (2019) performed statistical and expert based susceptibility modelling on a national scale (Fig. 3). Authors applied combination of Frequency Ratio and Analytic Hierarchy Process modelling. Lithology, slope, plan curvature, precipitation, land cover, distance from streams and distance from roads, had been selected as landslide preconditioning factors. The authors considered this approach to be very useful and practical in case of poor landslide inventory.

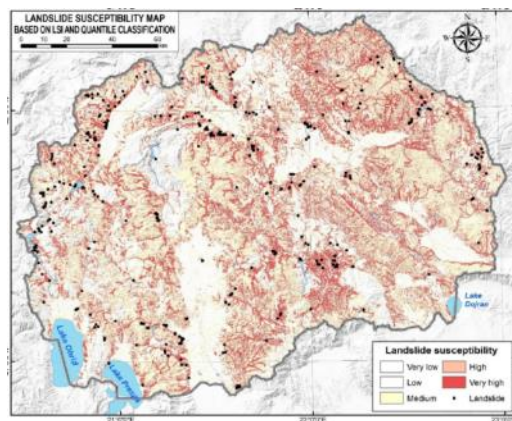


Figure 3 Landslide susceptibility map based on LSI and Quantile classification, Milevski et al. (2019).

Then, in the frames of the Geohazards study for the Spatial plan of Republic of Macedonia for planning period 2021-2040, Peshevski et al. (2023) applied the heuristic arbitrary polynomial approach. This method was previously applied at a regional level for the Polog region and gave satisfactory results (see in Peshevski 2015). Particularly, the geology, slope, precipitation, expected seismic acceleration according to Eurocode 8 for return periods of 95 and 475 years, and land use were assumed as landslide preconditioning factors. Adopted ratings for each conditioning factor are presented in the following tables and graphs.

Table 1 Maximum possible rating according importance of the conditioning parameter.

Classification parameter	Rating
Lithological type	3
Slope	3
Precipitation	2
Seismic zoning per Eurocode 8	1
Land use	1
Maximum possible rating	10

The data for lithology was taken from the Basic geological map of Macedonia at 1:200,000 scale. Lithological units were zoned according the potential for development of landslides. Five groups were delimited, by empirically assigning values ranging from 0 up to 3. In total, 161 lithological units were classified. The number of units clearly implies to the uncertainty of any used susceptibility model, no matter what type of methodology is used. This means that when dealing with regional and local scale landslide zoning, future studies should pay a lot of attention in defining the soil and rock geotechnical properties. For this goal, extensive geotechnical studies should be performed, while the gathered data should be statistically analyzed. Groundwater monitoring should be also performed.

The rating of slope is defined using a polynomial interpolation method, where the following graph was used (Fig. 4).

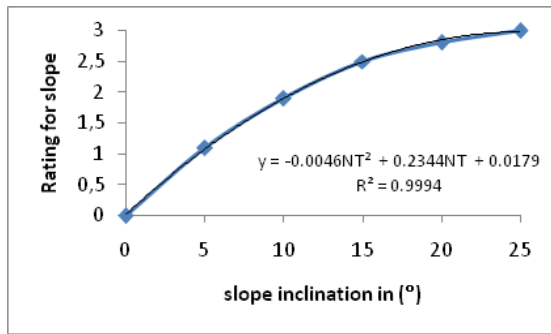


Figure 4 Slope rating adoption according polynomial interpolation.

Values of rating for precipitation, seismic acceleration and land use are respectively presented in Table 2 through Table 5.

Table 2 Ratings according to average precipitation (arbitrarily adopted).

Precipitation (mm/year)	Rating
400-500	0,1
500-600	0,2
600-700	0,3
700-800	0,4
800-900	0,8
900-1000	1,0
1000-1250	1,5
>1250	2,0

Table 3 Rating according to agR in units of the gravitational acceleration $1q= 9.81m/s^2$ for type A of soil - return period 95 years. According MKC-EH1998-1/2004-Eurocode 8.

Maximum ground acceleration (agR)	Rating
Z1 (0.05 g)	0,1
Z2 (0.1 g)	0,2
Z3 (0.15 g)	0,35

Table 4 Rating according to agR in units of the gravitational acceleration $1q= 9.81m/s^2$ for type A of soil - return period of 475 years. According MKC-EH1998-1/2004-Eurocode 8.

Maximum ground acceleration (agR)	Rating
Z1 (0.1 g)	0,2
Z2 (0.15 g)	0,35
Z3 (0.20 g)	0,65
Z4 (0.25 g)	0,85
Z5 (0.30 g)	1,0

Table 5 Ratings according to land use.

Land use type (Corine-CLC 2018)	Rating
1.Forest areas	0,1
2.Pastures	0,3
3.Agricultural areas	0,6
4.Artificial areas	0,9
5.Bare rock	1,0

Every specific combination of these evaluation factors is related to different degree of susceptibility to

landsliding. The sum of individual ratings gives the total rating of landslide susceptibility (Eq.1):

$$TLSR = LTR + NTR + GVR + IR + ZPR \quad [1]$$

where:

- TLSR – total landslide susceptibility rating
- LTR – value of rating for lithological type
- NTR – value of rating for slope inclination
- GVR – value of rating for precipitation
- IR – value of rating for seismic acceleration
- ZPR – value of rating for land cover

The maximum value of TLRS is 10, and the minimum is 0.3. After performing the algorithm and obtaining the TLRS value, the terrain susceptibility to landsliding is reclassified in 5 classes (applying the appropriate mathematical classification model Jenks natural breaks).

Final susceptibility maps are presented in Fig.5 and Fig.6, while details can be found in Peshevski et al. (2023).

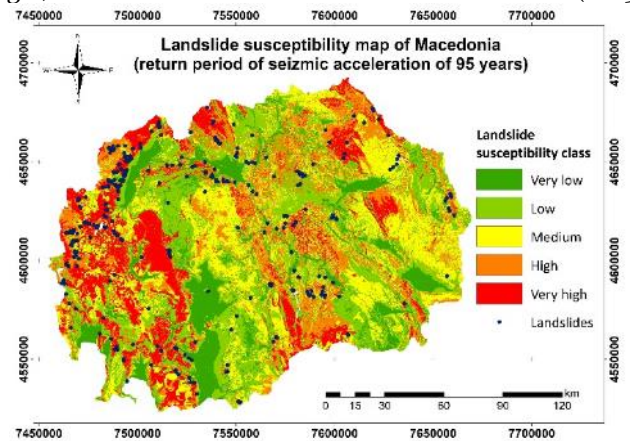


Figure 5 Landslide susceptibility map of Macedonia, for return period of seismic acceleration of 95 years (Peshevski et al. 2023).

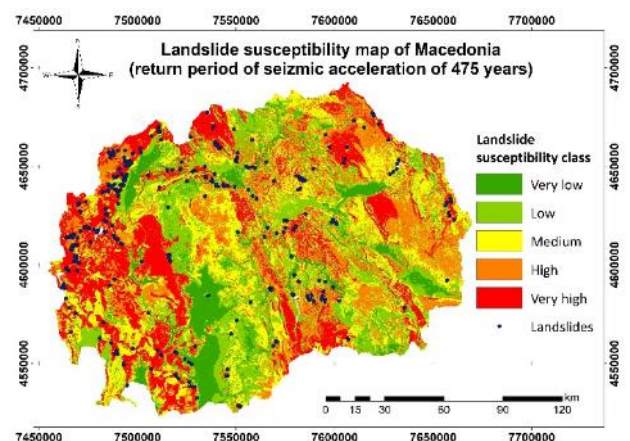


Figure 6 Landslide susceptibility map of Macedonia, for return period of seismic acceleration of 475 years (Peshevski et al. 2023).

All of the national susceptibility models considered above have their limitations and advantages, but main conclusion is that they are correlating between each other. Therefore, future studies should focus more on the regional and local scale landslide zonation.

Regional scale mapping for Polog region

As seen from national scale mapping examples, the Polog region seems that should be considered as the most prone to landslides. In fact, almost 2/3 of registered landslides in the country are located in this region. First attempt to perform susceptibility zoning of Polog was by done by Peshevski et al. in 2015 and 2019. The above mentioned arbitrary polynomial method was applied, where the landslide inventory was formed predominantly by use of historical data and Google Earth imagery.

More recently, Nedelkovska (2023) performed again an assessment of the landslide susceptibility for the region by using the Frequency Ratio (FR) model. It is worth to mention that on this occasion, the existing landslide inventory for the region was upgraded by two methods that were applied for the first time in Macedonia. Namely, Differential Interferometry Synthetic Aperture Radar (DInSAR) remote sensing method was applied to indicate “unstable” zones (Fig.7). The second method is the Light Detection And Ranging (LiDAR) which was used to generate DEM of the terrain in different resolutions and detect some landslide scars by visual approach (Fig.8). In addition to this, the LiDAR was also applied in a semi-automatic approach for Scarp Identification and Contour Connection Method (SICCM) (Fig.9) as proposed by Bunn et al. 2019. Then, twelve landslide conditioning factors were generated for landslide susceptibility modelling: slope, elevation, aspect, plane curvature, profile curvature, roughness, distance to roads, lithology, distance to faults, rainfalls, distance to rivers and land use/land cover. Frequency Ratio (FR) values were used to produce the Landslide Susceptibility Index (LSI), based on which the study area was divided in five zones of relative landslide susceptibility. Validation was done by calculation of the so-called R-index. The results showed that the FR is reliable method for landslide susceptibility assessment. Final map prepared in scale 1:100,000 is shown in Figure 10. More details in Nedelkovska, 2024 (in print).

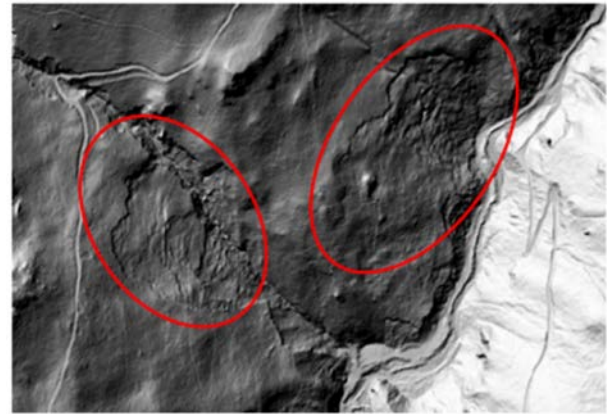


Figure 8 Detection of landslide scars from LIDAR survey, Nedelkovska 2023.

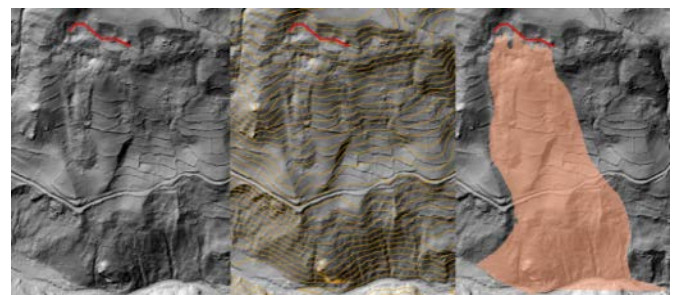


Figure 9 Example of the process for landslide zones modeling by SICCM.

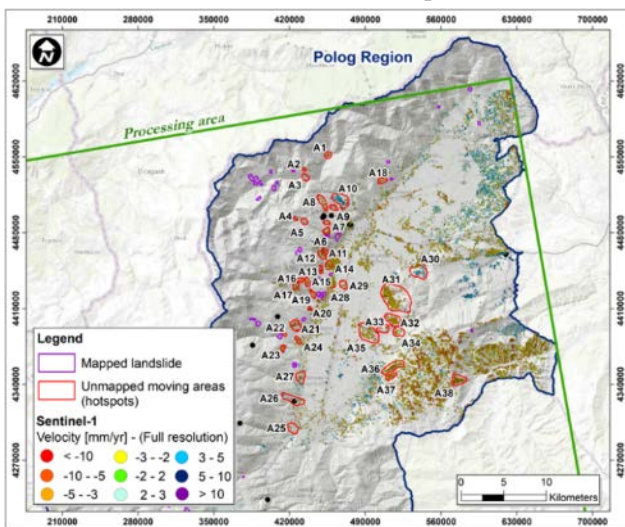


Figure 7 Map of indicated “unstable” zones using Sentinel DInSAR data at low resolution.

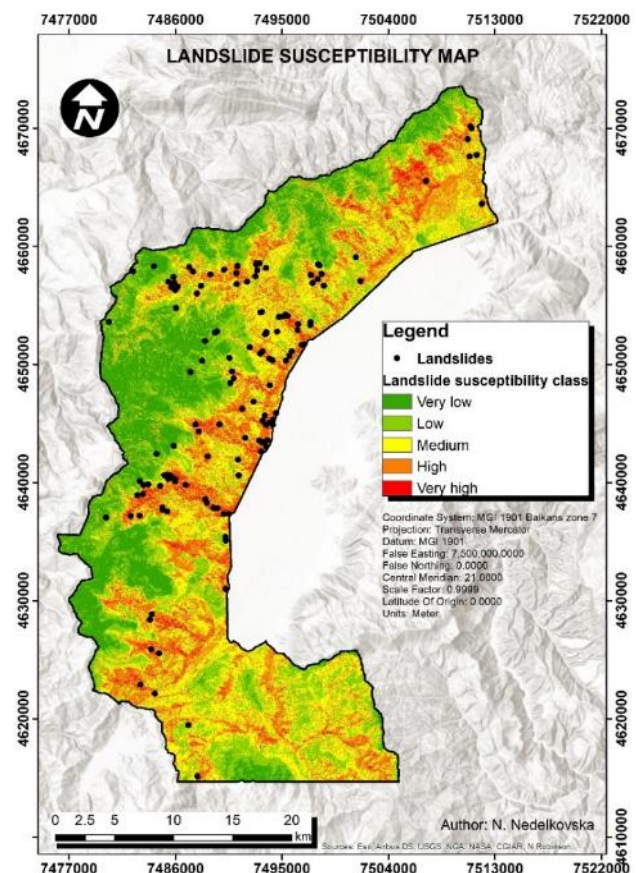


Figure 10 Final landslide susceptibility map obtained by FR model, Nedelkovska 2023.

Landslide hazard and risk assessment

Upon finalization of the regional susceptibility maps and the field collection of data, the next logical step for Polog region was to attempt and define the landslide hazard (and risk) for the most critical locations. To this aim, in first instance a combination of the approaches by Larsen et al. 2010, Ikeya 1981, SedNetNZ 2015 as well as own expert analysis was applied. The goal of these methods is to assess the sediment yield from landslides, which is one form of expression of the landslide hazard.

As a first step, the landslides of interest were analyzed in respect to how close they were to a particular main stream or tributary and which part of the landslide is possible to be reactivated during an extreme rainfall event was assessed. After the “landslide selection”, in the following stage a total landslide volume through the landslide area was defined, in a semi-empirical manner. The findings of Larsen et al. (2010) were used as a starting point, with certain calibrations performed for landslides with known quantity of detached material in historical events, specific active area, depth, etc. Each landslide was considered thoroughly and appropriate coefficients were adopted. In order to assess the landslide volume, the following empirical equations were applied:

For shallow landslides:

$$V_L = 0.2 - 0.5 * L_a^{1.1-1.3} \quad [2]$$

For deep landslides:

$$V_L = 0.2 - 0.5 * L_a^{1.3-1.6} \quad [3]$$

where:

- V_L - landslide volume (m³)
- L_a - landslide area (m²)
- 0.2-0.5 and 1.1-1.6 empirical coefficients suggested by Larsen et al. (2010) (in most cases we have used the most optimistic coefficients: 0.2 for both shallow and deep landslides, usual exponent of 1.1 for shallow and 1.3 for deep landslides).

In the next stage the expected landslide run out distance was defined, by using the formula of Ikeya (1981):

$$L = 8.6 * (V_L * \tan\theta)^{0.42} \quad [4]$$

where:

- θ - landslide slope in degrees
- L- run out distance (m).

We note that this equation is generally intended for the assessment of run out distance of debris flows and shallow landslides. However, due to scarcity of data from past events, it was also considered as acceptable for deep landslides. We consider this approach as conservative in predicting mass quantities.

In following step, the sediment delivery ratio (SDR) was assessed. This parameter is defined as the sediment yield from an area divided by the gross erosion of that same area. In general terms, SDR is expressed as a percentage and represents the efficiency of the watershed in moving soil particles from areas of erosion to the point where sediment yield is measured. In this case, SDR is considered as the percentage of landslide sediment yield from the total landslide volume, according to the approach of Chiuet al. (2019).

$$SDR = (L - D) / L \quad [5]$$

where:

- D (m) - distance between the centre of the landslide area and the nearest downslope stream channel
- L (m)- Landslide migration distance is the maximum possible moving distance of the sediment produced in a newly added landslide area.

From the literature it was found that SDR varies in different regions, in the range between 80-100% for short landslides directly connected to the stream channel below, and from 20-80% for landslides with gentle slope. According to the SedNetNZ study (2015), for shallow landslides, the average value of SDR is about 0.5.

The SDR was first calculated for all selected upstream landslides in each watershed, according to the above equation. In addition, the quantity of material, which has been removed (cleaned) from the respective watershed main stream at its outlet to the plain, was known for several cases, a data which served as benchmark to see if the calculated SDR was appropriate.

Finally, calculation of the possible landslide sediment yield for each particular landslide and every subwatershed of the region was performed. It is worth to mention that there was no possibility to make further calibration, in the sense of whether the material stops upstream in the sub-watershed where the landslide belongs. Therefore, the quantities obtained are presented only as preliminary, and more precise assessment should be done upon detailed in situ investigations and geotechnical and hydrological monitoring. Some examples of the calculated expected sediment load are presented in Table 6.

Table 6. Event based landslide sediment yield assessment (some examples).

Land slide tab ID	Depth of landslide	Assumed area that can be activated (m ²)	Calculated volume (m ³)	Sediment delivery ratio (SDR)	Landslide sediment yield (m ³)
1002	Shallow	7.564	3695	0.57	2.122
1	Shallow	44.615	23029	0.171	4.452
17	Shallow	86.946	54.225,62	0.089	4.845
015*	Deep	30.000	132.217	0.5	66.108
1001	Deep	117.640	489.699	0.083	40.647
009	Shallow	110.721	70.742	0.24	17.111

Fig. 11 presents an excerpt of the final map of landslide hazard for the so called Poroj watershed.

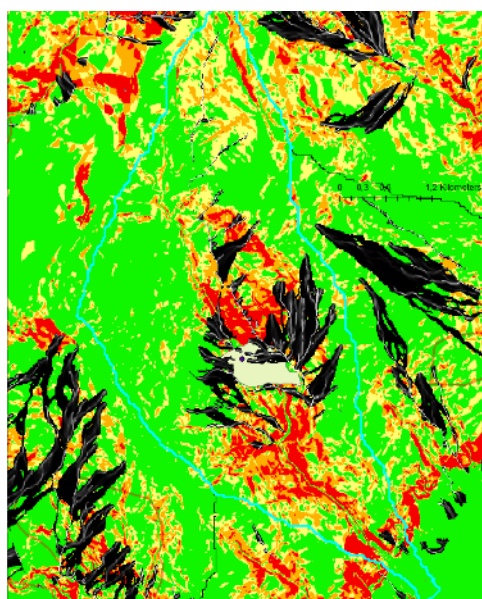


Figure 11 Integral landslide hazard in the Poroj watershed. Legend: Pale blue-watershed border; pale green polygon-Gjermo landslide; black zones-expected debris flow runout zones (obtained by Flow-R software); yellow to red colored zones-landslide susceptibility classes.

Besides the ability to obtain a sense of the quantity of landslide generated sediment yield in extreme events, the temporal component remains undefined. This means that even if the quantity of material to reach the stream can be assessed with certain level of confidence, the dynamics of the occurrence during an extreme rainfall event can't be defined fully. In some cases, we can have extreme rapid movement of an entire landslide and transformation in debris flow, while in other there can be slow gradual erosion of the landslide continuing for days and even weeks. In the latter case, the same total amount of sediments might reach the local stream, however with smaller quantities being transported within a longer period. Since there is no data for registered fast debris flows or blockage of rivers due to landslides in the region for a period from 1970-2020 and even before, these

estimations should be taken with great precaution and revised once monitoring data becomes available.

Preliminary risk assesment

Besides the fact that there was a lack of data to perform regular risk analyses at a local level in the period of 2020, the typical risk formula was applied:

$$R=H*(E*V) \quad [6]$$

where:

- R– risk (total damages due to landsliding)
- H – landslide hazard
- E – elements exposed to landslide hazard (population & goods)
- V – vulnerability of exposed elements.

In this sense, we can consider the following analyses as a preliminary or relative risk assessment.

Namely, due to the relatively poor knowledge on the frequency of landsliding, which is a prerequisite for risk assessment, the rules that were applied to perform relative risk were set up empirically. By analyzing all landslides from the database and taking into account the build-up area, the prioritisation Tab. 7 was created. Using these criteria, the final list of landslides considered for conceptual design development is presented in Tab. 8.

Table 7 Landslide prioritisation criteria and points for relative risk ranking (values in table are prioritization ranking points).

Prioritisation criteria	Very low	Low	Medium	High	Very high
1. Ability of landslide to threaten settlements or critical infrastructure	1	5	10	15	20
2. Landslide has the potential to dam a river with potential for outburst flow	1	5	10	15	20
3. Landslide might directly transform into flow with long travel distance and affect lowland areas	1	5	10	15	20
4. Relative size of landslide in comparison to other landslides in the inventory	1	5	10	15	20
5. Information for landslide hazard from municipalities	1	5	10	15	20

Table 8 Prioritization list of Landslides considered for conceptual design development.

Location	Priorit. points	Landslide type	Subject of hazard
1. Gjermo and Poroj	100	Deep landslide	Part of village of Gjermo & possible outflow of debris toward Tetovo. River damming is not excluded.
2.Bozovce	80	Complex slide	Entire village of Bozovce under risk of debris-flow
3.School in Pirok	71	Translatory sliding	Elementary school and several houses under risk.
4.Jelovjane landslide	66	Complex slide	Part of village Jelovjane, past event recorded large damages and resettlement.
5.Landslide near el. hydro power plant	60	Rock slide	Risk for busy local road.
6.Landslide on road Senokos – Lomnica	47	Rockfall and translatory sliding	On several locations along the road with possibility for blockage of the road.
7.Damped material in Senokos	41	Complex slide	Possibility to affect several houses below dump zone.
8.Jegunovce – Staro selo	36	Rockfall	Risk to village below rock outcrop, road to Ljuboten peak.
9.Jegunovce– Road to Ljuboten peak	31	Rock slide	Risk to block the road to Ljuboten peak.
10.Dolna Leshnica	27	Landslide	Possibility to block local road to Gorna Leshnica and houses.

Two possible remediation solutions were then developed for almost all of the analysed cases. Depending on each separate case, solutions were from various nature: setting up of a geotechnical monitoring system, planting vegetation and terracing of the terrain, gabion walls, support walls, rockfall barriers, dewatering. Appropriate stability analyses were performed to confirm the reliability of the proposed solutions. Finally, a bill of quantity was prepared for all of the considered cases. Due to the character of the paper, these analyses are not presented here, while further below in the text details on the developed solution for the case of Gjermo landslide are provided.

For all of these landslides risk analyses by use of software RAMMS were performed (Fig. 12), with scenarios of not undertaking and undertaking the possible designed remediation measures. This enabled performing the cost-benefit analyses that followed, as a subsequent logical step.

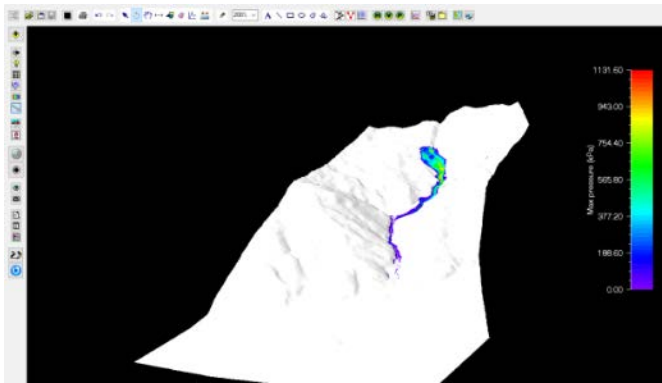


Figure 12 Example of RAMMS simulation for Gjermo landslide.

The risk analysis consisted of considering the following elements:

- Landslide area and volume,
- Expected run out distance,
- Elements at risk (No of affected houses),
- Total houses area,
- No of houses in low landslide risk,
- No of houses in medium landslide risk,
- No of houses in high landslide risk,
- Affected critical infrastructure,
- Length of affected road infrastructure,
- Directly affected population,
- Total affected population.

After the simulations, Benefit-Cost Analysis (BCA) were performed. Main purpose of the benefit-cost analysis was to use the project cash flow forecasts to calculate suitable net return indicators. A particular emphasis was placed on three financial indicators:

- Net Present Value (NPV),
- Internal Rate of Return (IRR),
- Benefit-Cost Ratio (B/C).

In the preparation of the BCA the following main input parameters and assumptions were used:

- reference time horizon of 25 years, including one “0-year” as project implementation period, while all other capital expenditures and benefits take place from year 1 onward;
- it is assumed that if no mitigation measures are applied at the sites (Do nothing scenario), at least one landslide event with assessed/ modeled severity would occur over the 25-year period;
- all analyzed alternative technical solutions pertaining to the same landslide site, result in accomplishment of equal level of benefits (avoided damages and losses);
- discount rate of 3.5%;
- all costs are VAT free;
- all benefits and costs are valued at constant prices (2020);
- all calculations are in MKD denars.

A residual value at the end of the analyzed 25-year period was applied, as a proxy of the value of all subsequent project costs and benefits.

The categories of landslide mitigation benefits assessed in this analysis are:

- Avoided direct property damage (e.g. houses, buildings, roads, bridges, etc.);
- Avoided direct business interruption loss (e.g. damaged industrial and commercial facilities);
- Avoided infrastructure repair costs (as a consequence of the landslide event);
- Avoided environmental damage (increased flooding caused by the landslide);
- Avoided/reduced societal losses (monetary losses as a results of working population not being able to go to work for several days due to blocked roads, etc.).

The investment costs for implementation of the landslide mitigation efforts at the analyzed sites for all alternative solutions were estimated based on input from the engineering analysis as described above. Maintenance costs required for the continuous functioning of the applied technical landslide remediation solutions (infrastructure), including labor, equipment maintenance and repair, replacements, etc., were also considered.

The results showed that the analyzed landslide sites in CBA terms varied to a large extent (Tab. 9). However, except for two sites – Senokos-Lomnica and Jegunovce-Staro selo, which had negative NPV values and B/C values (below 1) –the interventions were in general economically viable, which confirmed the benefits that would accrue from the investments outweigh the costs incurred.

From the CBA it was concluded that the projects will generate sustained beneficial socio-economic impact, perceived above all in reduced risk of landslide damages and losses for the local population. Therefore, in following stage further developments of the landslide remediation activities were carried out. These consisted of more detailed field investigations, engineering geological mapping, drilling, geotechnical testing etc. Then advanced basic designs were developed for some of the landslides, while some are still in discussion and design phase. Further comments are presented below.

Table 9 Summary of BCA results.

Location	Landslide type	Investments (MKD) Alternatives		B/C ratio		NPV alternative	IRR alternative
		A1	A2	A1	A2		
Gjermo, Poroj river	Deep landslide	37.333.906		7.6		282.055.585	46%
Bozovce	Complex slide	5.862.142		32.3		246.039.306	230%
School in Pirok	Translatory sliding	10.003.635	4.632.188	1.5	2.8	13.234.122	20%
Jelovjane	Complex slide	997.100		27.7		50.656.946	277%
HPP in Pena watershed	Rock slide	5.078.880	4.636.880	1.5	1.5	3.035.098	8%
Senokos-Lomnica	Rockfall and translatory sliding	7.050.290	6.088.966	0.5	0.6	-2.268.303	0.1%
Jegunovce	Rock slide	5.002.250	10.126.990	2.4	1.0	8.782.042	15%
Jegunovce-Staro selo	Rockfall	5.036.200	4.688.450	0.6	0.6	-2.272.381	-1%
Dolna Leshnica	Landslide	2.326.250	3.819.115	1.8	1.2	2.241.677	10%
Settlement near Senokos	Complex slide	5.251.000	2.065.532	3.8	8.3	18.835.757	54%

Risk assesment methodology for Basic design

The first of the case studies presented in Tab. 9, the Germo landslide and Poroj river watershed, are presented here as an example of a Basic design study. To support the decisions for the design, the risk assessment methodology had to be upgraded on higher level.

The catchment area of Poroj River river is with highest altitude of 2376 m (Fig. 13). There are two villages in the catchment area: the village of Poroj down at the transition from mountain to plain area, as well as the village of Gjermo at an elevation of about 1070 m. In terms of rainfalls, the study area is characterized by the highest annual average rainfall in the country, in the range 600 - 1250 mm/year.

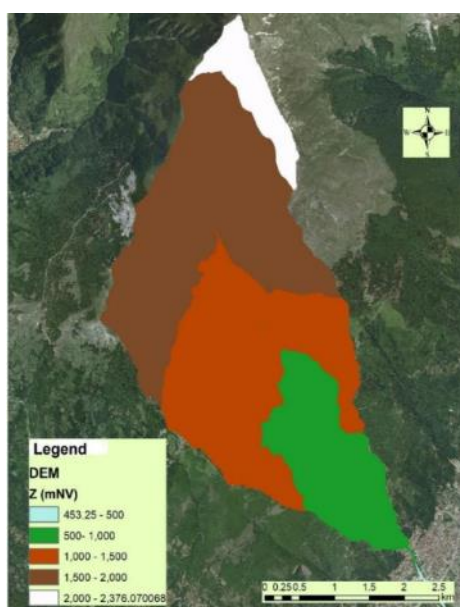


Figure 13 Elevation distribution of the Poroj river watershed.

One of the most important elements of the catchment area is the existence of deep landslide at the area of village Gjermo.

The applied methods related to holistic approach for risk assessment, so the following steps were performed:

- review of all previous data and knowledge for the study area;
- use of methods for detecting and characterizing the unstable phenomena;
- preparation of shallow landslide susceptibility (relative hazard) models;
- calculation of slope stability of Gjermo landslide and definition of probability of failure;
- assumptions of exposed elements at risk and possible consequences;
- preparation of risk map;
- suggestion of measures for further development of design documents for protection from flooding and landslides.

In this paper we only briefly present the component of risk map preparation. The risk assessment process consisted in the determination of the expected damages and losses from possible fast reactivation of landslide Gjermo. The simple methodology is used in forming of risk matrix, as a combination of 5*5 consequences (C) and probability of failure class (S), as presented in Fig.14.

Classes of probability of landslide failure S	S ₅	Yellow	Red	Red	Red	Red
	S ₄	Yellow	Yellow	Red	Red	Red
	S ₃	White	Yellow	Yellow	Yellow	Yellow
	S ₂	White	White	White	Yellow	Yellow
	S ₁	White	White	White	White	White
		C ₁	C ₂	C ₃	C ₄	C ₅
Classes of consequences C						

Figure 14 Risk matrix used for preparation of risk map combining the classes of consequences (C) expressed as socio-economic costs and classes of probability of landslide failure (S); red colour is for areas with high landslide risk; orange for areas with medium landslide risk; white for areas with low landslide risk.

The consequence analysis considered the total affected population, possible damages on houses, possible number of people killed, possible damage on road infrastructure, several small Hydro Power Plants (HPP), environmental consequences, requirement of remediation, remedial costs etc. Landslide probability is assessed using variation of input parameters in some range, in order to see the effects on variation on the Safety Factor and Probability of Failure.

As a final product from all analyses, a simple risk map was prepared. In its preparation, adequate calculations of socio-economic costs and a comparative analysis of relevant probability and consequences classes were carried out (Fig. 15).

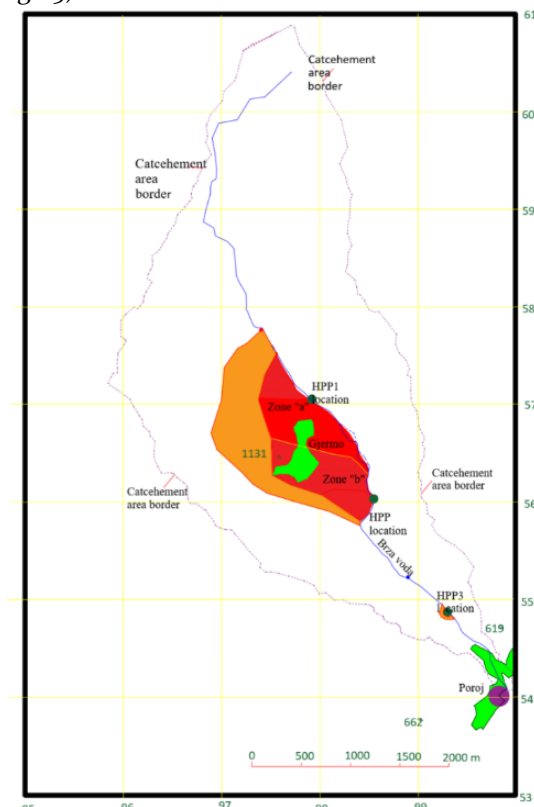


Figure 15 Risk map for Poroj River watershed. Legend: landslide risk 1.orange-medium, 2.red-high, 3.white-low, green colour-settlement area

Conclusions

Recent experiences dealing with the assessment of landslide susceptibility, hazard and risk in Macedonia are positive. Application of new tools and methods made it possible to raise the level of confidence in the produced susceptibility models on national level. By this time, it can be said that the main regions in which landslide problems are present and can be expected in the future are relatively well defined, and they should be a subject of more detailed analyses at a regional and watershed level. For some areas, sub-watershed analyses will be of tremendous importance. In this sense, we consider that the presented Polog projects can serve as a good starting guide for other regions and watersheds in the country. In order to create positive conditions for such analyses in systematic way, i.e for improved overall treatment of the landslide risk in general terms, certain actions should be taken on different levels. These should include capacity building of institutions, law changes, establishing of geohazards database, installing geotechnical monitoring systems for defined landslides, educating and attracting larger number of students in the field of landslides, awareness rising of the population and decision makers in general.

Acknowledgements

The authors like to acknowledge the support to UNDP (Office branch in Macedonia), Swiss Development and Cooperation (SDC), International consultant Markus Zimmermann from Switzerland, Dr. Gianfranco Nicodemo from Salerno University, and Danco Uzunov from Pointpro Skopje.

The presented work also includes the results of the Agreement For Research Funding (n. 4858 year 2019) between the Faculty of Civil Engineering of the Ss. Cyril and Methodius University in Skopje (R.N. Macedonia) and the Department of Civil Engineering of the University of Salerno (Italy) entitled: “Analysis and interpretation of remote sensing data (Differential Interferometric Synthetic Aperture Radar) for geotechnical studies pursuing the detection, mapping, and geometric and kinematic characterization of slope instabilities over the Polog Region (R.N. Macedonia)”, funded by United Nations Development Programme (UNDP) for the R.N. Macedonia on “Feasibility Study on Basin Scale Sediment Management Options for the Polog Region 41/2019 55510”.

References

Bojadjieva J, Sheshov V, Bonnard C (2018) Hazard and risk assessment of earthquake-induced landslides—case study. *Landslides*. 15(1): 161-171.

Bojadjieva J, Sheshov V, Edip K, Shalic R, Stojmanovska M, Apostolska R, Fotopoulou S, Pitilakis D, Shkodrani N, Babaleku M, Bozzoni F, di Meo A (2022) Harmonized approach for mapping the earthquake-induced landslide hazard at the cross-border region between North Macedonia, Greece and Albania. *Proceedings of 5th Regional symposium on landslides in Adriatic-Balkan Region, Landslide modeling and application*. pp.119-124.

- Bunn MD, Leshchinsky BA, Olsen MJ, Booth A, (2019) A simplified, object-based framework for efficient landslide inventorying using LIDAR digital elevation model derivatives. *Remote Sensing*. 11(3):303.
- Chiu YJ, Lee HY, Wang TL, Yu J, Lin YT, Yuan Y, (2019) Modeling sediment yields and stream stability due to sediment-related disaster in Shihmen Reservoir Watershed in Taiwan. *Water*. 11(2): 332.
- Ikeya H. (1981) A method of designation for area in danger of debris flow. In: *Erosion and Sediment Transport in Pacific Rim Steeplands*; IAHS Publ.: Christchurch, New Zealand. pp. 576-587.
- Jovanovski M, (2010) Landslide and Rock Fall occurrences and processes in R. Macedonia. Croatia–Japan project on risk identification and land-use planning for disaster mitigation of landslides and floods in Croatia, 1st Project workshop „International experience“, 22-24 November 2010. Dubrovnik, Croatia.
- Jovanovski M, Peshevski I, GjorgievGj, Nedelkovska N, Nicodemo G, Reale D, Fornaro G, Peduto D (2021) Landslide characterization in the Polog Region (R.N. Macedonia) by innovative and conventional methods. *Rivista Italiana di Geotecnica*. 4:7-31.
- Larsen I, Montgomery D, Korup O, (2010) Landslide erosion controlled by hillslope material. *Nature Geoscience*. 3: 247-251.
- Milevski I, Dragicevic S, Zorn M, (2019) Statistical and expert-based landslide susceptibility modeling on a national scale applied to North Macedonia. *Open Geosciences*. 11(1): 750-764.
- Mueller U, Dymond R, (2015) SedNetNZ modelling of soil erosion in Northland. Landcare Research, Landcare Search Contract Report LC2424, prepared for Northland Regional Council.
- Nedelkovska N, (2023) Contemporary methods for detection and characterization of terrain unstable phenomena. Doctoral thesis, University Ss. Cyril and Methodius, Faculty of civil engineering, Skopje.
- Peshevski I, (2015) Landslide susceptibility modeling using GIS technology. Doctoral thesis, University Ss. Cyril and Methodius, Faculty of civil engineering, Skopje.
- Peshevski I, Jovanovski M, Abolmasov B, Papić J, Marjanović M, Đurić U, Haque U, Nedelkovska N, (2019) Preliminary regional landslide susceptibility assessment using limited data. *Geologica Croatica*. 72(1): 81-92.
- Peshevski I, Jovanovski M, Papić J, Josifovski J, GjorgievGj, Malijanska N, (2023) Landslide susceptibility mapping on national level in scale 1:200000 – chapter in frames of Geohazards study, National spatial plan 2021-2040 (in preparation).

Landslide Risks in the Western Balkans Under the Climate Change

Mirjam Vujadinović Mandić

University of Belgrade, Faculty of Agriculture, Belgrade, Nemanjina 6, Serbia, mirjam@agrif.bg.ac.rs

Abstract Under the global warming impact, the Western Balkans region has experienced a mean temperature increase exceeding the global average, of about 1.4°C rise over the last 60 years. Depending on global efforts to reduce greenhouse gasses emissions, further warming of the region could vary from 1.7 to 4°C. Alongside the temperature rise, the Western Balkans countries have seen change in inter-annual and distribution of precipitation, as well as an increase in frequency and severity of the extreme weather and climate events. Changes in climate characteristics are increasing the risks from natural disasters such as floods, droughts, wildfires, and landslides, and emphasize the need for risk assessment of such events in future periods in order to prevent catastrophic consequences and preserve lives and assets. In this study analysed are changes in the precipitation patterns and intensity distribution by the end of the 21st century using the results of an ensemble of eight regional climate models from the EURO-CORDEX database, under the RCP4.5 and RCP8.5 IPCC scenarios. The results showed increase in the average number of days with heavy precipitation events, especially in the mountains and hilly parts of the region. Besides, more frequent, longer, and severe drought events and heatwaves, and the changes in vegetation and land use, further diminish the natural capacity to mitigate landslide risks, intensifying the overall vulnerability across the region. Projected increase of landslides risks indicates the need to incorporate future climate change impact assessments into the risk management strategies, land-use planning, and infrastructure development across the Western Balkans region.

Keywords climate change, landslides, risk assessment, precipitation, natural disasters

Introduction

Although human activities such as urbanisation and infrastructure development, deforestation, and in general land degradation is considered as the important factor of the land disturbance (Jakob, 2022) these natural disasters are further intensified by the changed patterns and increased intensity of precipitation caused by the climate change. The Western Balkans (WB) region, characterised by its diverse topography, is prone to landslides that may pose a significant risk to human lives, infrastructure, and the environment. At the same time, WB is recognised as a region where temperature increases at the rate above the

global average (Vukovic and Vujadinovic Mandic, 2018), bringing quicker and more intensive changes than in many other parts of the world.

Over the last two decades WB has experienced a large number of extreme weather events (TNC SRB 2024, TNC MNE 2020, FNC BIH 2021, FNC MKD 2023, FNC ALB 2022), including intensive rainfall, floods and flash floods, and prolonged droughts, which all may contribute to the intensifying slope instability and increasing frequency and magnitude of landslides in the region.

According to the IPCC Assessment Report 6 (IPCC, 2021) further warming, precipitation changes and intensification of extreme weather events is expected to continue, if not worsen, in the forthcoming decades. Therefore, there is a need for further strengthening of knowledge on the link between climate characteristics and landslides in the region in order to assess and map future vulnerabilities and risks, develop effective early warning systems, and adaptation measures and strategies in order to mitigate the adverse impacts.

This study aims to assess the changes in precipitation patterns and intensity over WB by the end of the century in order to estimate changes in future levels of landslide risks in the region.

Methods and materials

An ensemble of high-resolution regional climate models (RCMs) was used for assessment of future climate change in WB. Data on daily temperature and precipitation were taken from eight RCMs from the EURO-CORDEX database (Jacob et al. 2014), which were proven to be able to reproduce past climate feature across the region. The names of selected RCMs and their driving global climate models (GCMs) are given in the Tab. 1.

Table 1 Global (GCM) and regional (RCM) climate models used in the ensemble.

GCM	RCM
ICHEC-EC-EARTH	CLM-CCLM4-8-17
ICHEC-EC-EARTH	DMI-HIRHAM5
ICHEC-EC-EARTH	KNMI-RACMO22E
MOHC-HadGEM2-ES	CLM-CCLM4-8-17
MOHC-HadGEM2-ES	KNMI-RACMO22E
MPI-M-MPI-ESM-LR	CLM-CCLM4-8-17
MPI-M-MPI-ESM-LR	MPI-CSC-REMO2009_r1
MPI-M-MPI-ESM-LR	MPI-CSC-REMO2009_r2

Climate change is assessed under the two most commonly used Relative Concentration Pathways (RCP) scenarios of greenhouse gas (GHG) emissions, RCP4.5 and RCP8.5. Scenario RCP4.5 predicts peak of GHG emissions around the year 2040 and gradually decline afterwards, while RCP8.5 foresees continuous increase of the emissions by the end of the century (van Vuuren et al. 2011). Projected climate conditions of two future periods, the mid-century (2046-2065) and end-of-century (2081-2100), are compared to the climate conditions of the referent period (1986-2005).

The assessment is performed on a high-resolution grid (about 12 km regular latitude/longitude grid) over the WB region, i.e. Albania (ALB), Bosnia and Herzegovina (BIH), Montenegro (MNE), North Macedonia (MKD) and Serbia (SRB).

Results and discussion

Change in temperature

Mean annual temperature averaged across WB is expected to continuously increase by the end of the century, according to both considered scenarios. Under the RCP4.5 median value of the mean annual temperature will increase by 1.6°C by the mid-century (min/max range of change from 0.4 to 2.6°C) and by 2°C by the end of the century (min/max range of change from 0.8 to 3.1°C), compared to the referent period. Warming under the RCP8.5 is more pronounced, and it will reach 2.1°C (min/max range of change from 1.1 to 3.5°C) by the middle and 4.4°C (min/max range of change from 3.3 to 5.5°C) by the end of the century. Ranges of projected changes under the two scenarios mostly overlap until the 2080's, when they begin to diverge and complete diverge by the end of the century, when the minimum warming estimate according to RCP8.5 exceeds the maximum estimate according to RCP4.5. Spatial distribution of the median value of mean annual temperature anomaly is given in Fig. 1.

1.

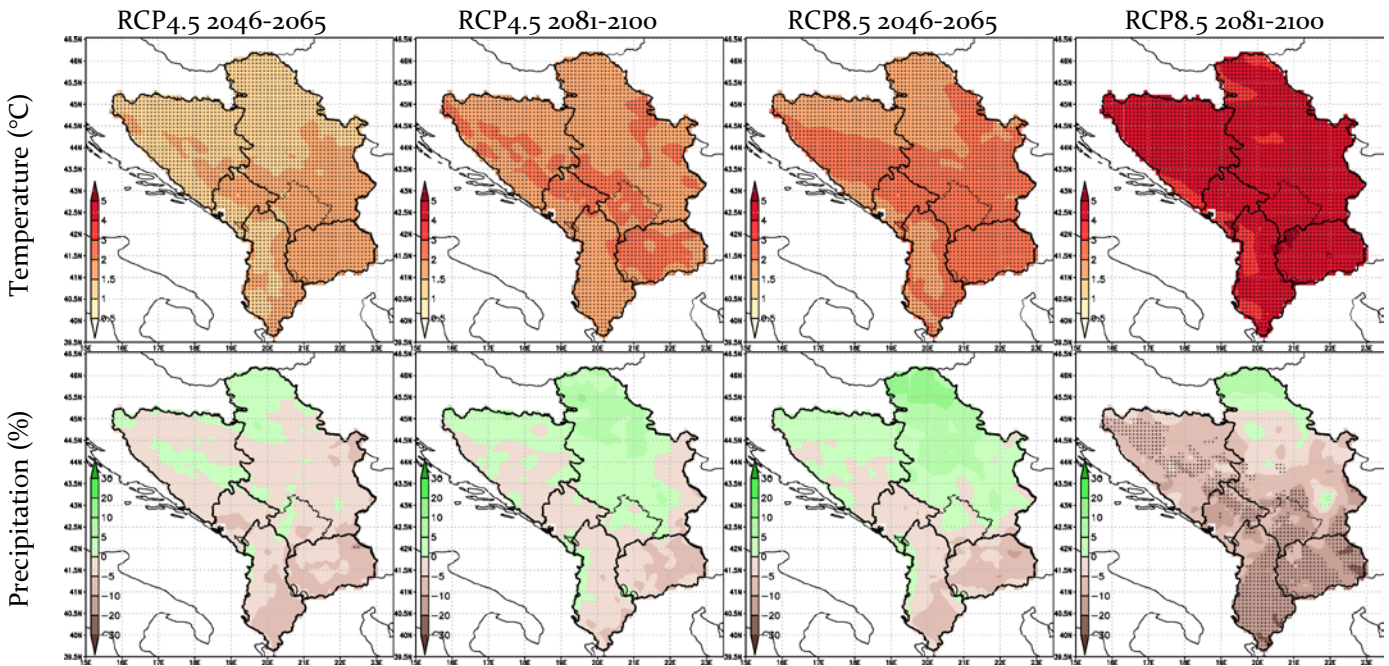


Figure 1 Mean annual temperature and precipitation anomalies for mid-century (2046-2065) and end-of-the-century (2081-2100) periods, under RCP4.5 and RCP8.5 scenarios, compared to referent period (1986-2005). Black dots denotate statistically significant change.

Seasonal changes of the median value of the mean temperature show that spring (MAM, March-April-May) warms the least, followed by winter (DJF, December-January-February) and autumn (SON, September-October-November), while summer (JJA, Jun-July-August) warms the most in both periods and under both scenarios.

The least winter warming is found along the coast. Mean maximum temperatures increase more than mean minimum temperatures. Ranges of median values of the mean seasonal changes across the region are shown in Tab. 2, while spatial distribution of summer change is presented in Fig 2.

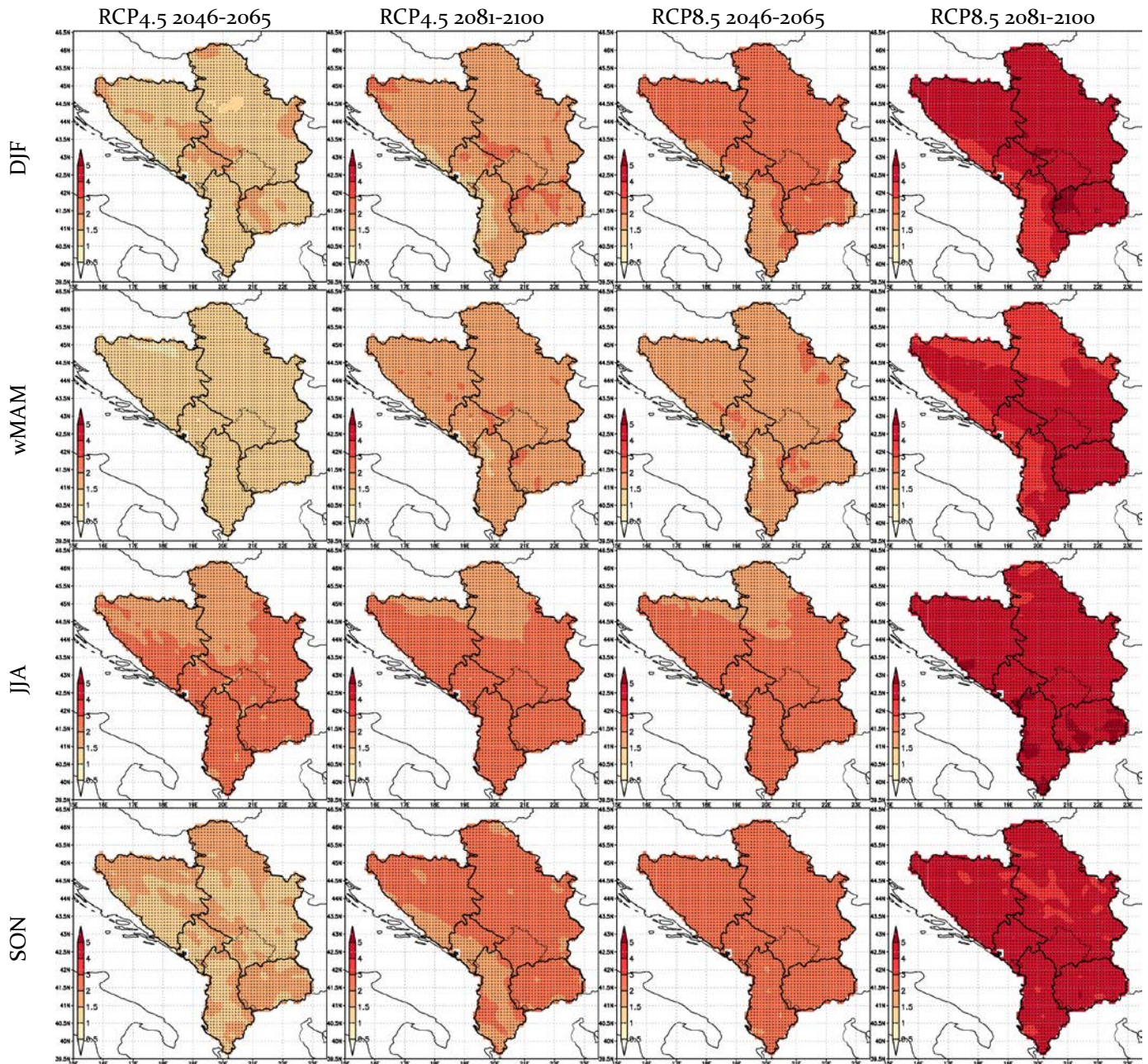


Figure 2 Mean seasonal temperature anomalies (°C) for mid-century (2046-2065) and end-of-the-century (2081-2100) periods, under RCP4.5 and RCP8.5 scenarios, compared to referent period (1986-2005). Black dots denote statistically significant change.

Table 2 Range of median value of mean seasonal anomaly (°C) across WB, for mid-century and end-of-the-century periods, under RCP4.5 and RCP8.5, compared to the referent period.

Season	Mid-century		End of century	
	RCP4.5	RCP8.5	RCP4.5	RCP8.5
winter	1-2°C	1.5-3°C	1-3°C	3-6°C
spring	1-1.5°C	1.5-2°C	1.5-2°C	3-5°C
summer	1.5-3°C	1.5-3°C	1.5-3°C	3-6°C
autumn	1.5-2°C	1.5-3°C	1.5-3°C	3-5°C

Change in annual and seasonal precipitation

Unlike the temperature, change in annual precipitation is not uniform across WB. Generally, northern parts of the region could have somewhat more precipitation in average, while southern parts could have a slight decrease

on annual level (Fig. 1). These changes are mostly within the range from -10% to +10% comparing to the referent period, and therefore they could be considered as a part of a natural climate variability. However, notable changes are expected in inter-annual distribution of precipitation. Seasonal precipitation changes are presented in Fig. 3.

Increase in winter precipitation is expected across the region in both future periods and under both scenarios. This change is the greatest in northern and central parts of SRB and BIH, northern MNE, and central parts of ALB and MKD. Besides the winter precipitation increase, it is important to note that due to warming of the season there will be less snowfall and shorter snow cover retention, especially in lower altitudes.

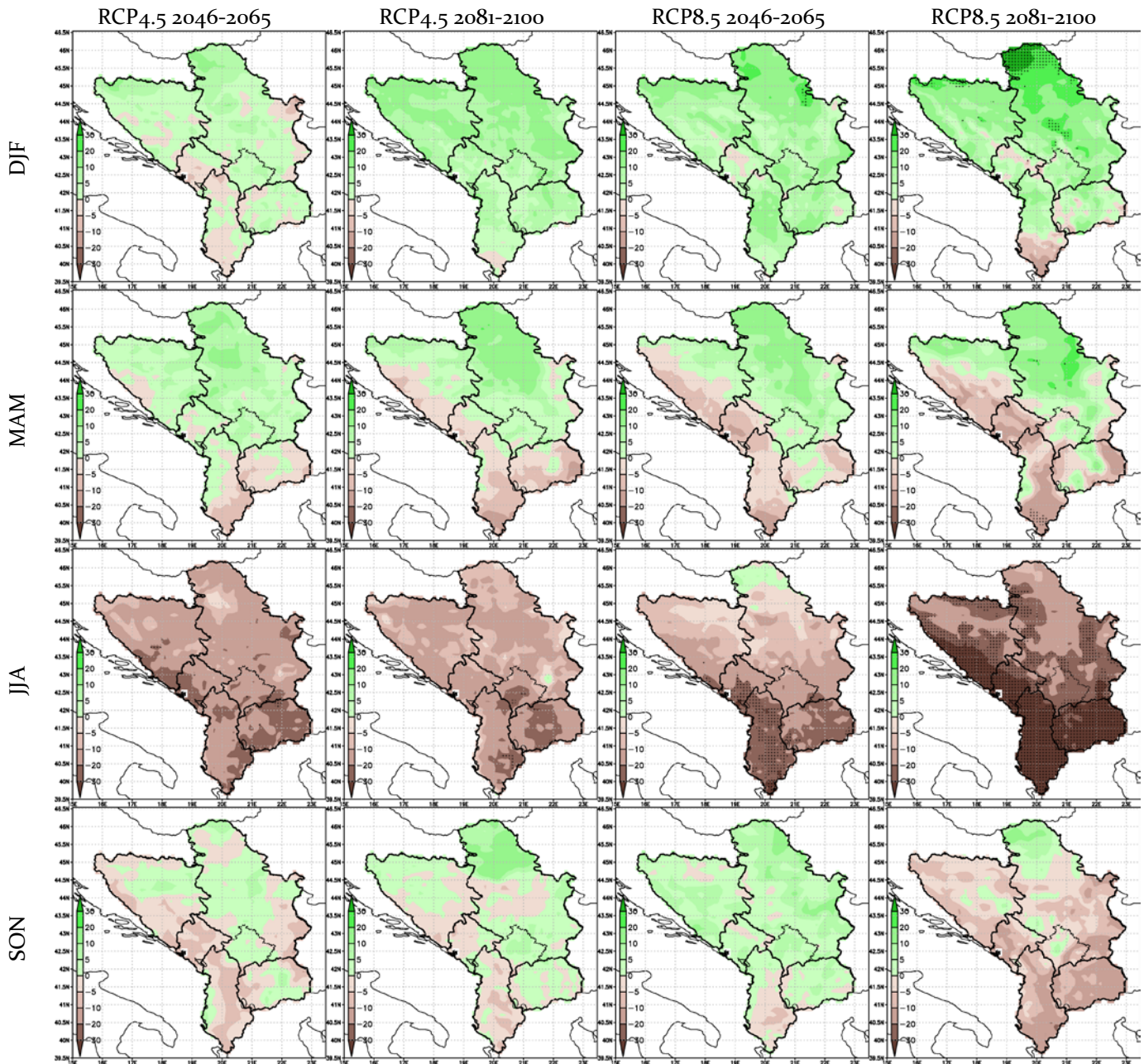


Figure 3 Mean seasonal precipitation anomalies (%) for mid-century (2046-2065) and end-of-the-century (2081-2100) periods, under RCP4.5 and RCP8.5 scenarios, compared to referent period (1986-2005). Black dots denotate statistically significant change.

Spring precipitation is expected to increase over SRB, northern and eastern BIH, coastal ALB, central MKD and northern MNE (only under RCP4.5). Frequent episodes of warm weather may trigger fast snow melting. If such event coincides with high spring rainfall or comes after the high winter rainfall, it could cause saturation of slopes, increase in groundwater levels and increase risk of landslides.

Summer is the season with pronounced precipitation deficit projected all over the region. The expected decrease ranges between 10 and 20%, locally up to 30% in parts of ALB, MKD and the coastline. Under RCP8.5 by the end of the century projected summer precipitation shortfall is the largest and it exceeds 30% in the southern part of WB (ALB, MKD, MNE, and south and southwestern BIH),

while in other regions it is mainly between 10 and 20% compared to the referent period. Very high summer temperatures combine with droughts stress vegetation, impacting, among other, root growth which in turn provides less stabilization for slopes. Reduced soil moisture content and/or depletion of groundwater levels weakens cohesion between soil particles, creates cracks and change soil properties influencing its ability to absorb and retain water, which increase surface runoff and erosion. Prolonged droughts and high temperature increase the risk of wildfires which removes vegetation leaving slopes more prone to landslides during later rainfall events.

Autumn precipitation changes are nonuniform across the region. Generally, increase could be expected in the largest part of SRB, MKD, coastal ALB, and north and central BIH. At the end of the century under RCP8.5 precipitation decrease is projected in almost all WB, except for northern SRB and locally in eastern BIH and southern and western SRB.

Change in precipitation intensity

With the atmosphere warming, it is expected to have more intensive precipitation events. Such events are associated with high uncertainties within the climate models, since they mainly come from convective processes which have spatial scales below the horizontal resolution of RCMs.

However, the tendencies of increased number of intensive precipitation events, as well as increase in maximum 1-day and 5-days accumulated precipitation have been observed all over WB.

Number of days with precipitation above 20 mm, which are found to may increase landslide risks in the region, is projected to increase on an annual level all over the region, especially in SRB, BIH, northern MNE, central and western MKD, and coastal and eastern ALB. The largest increase in the accumulated water in such events is expected in the northern and southern SRB, northern and eastern BIH, northern and western MKD and eastern ALB.

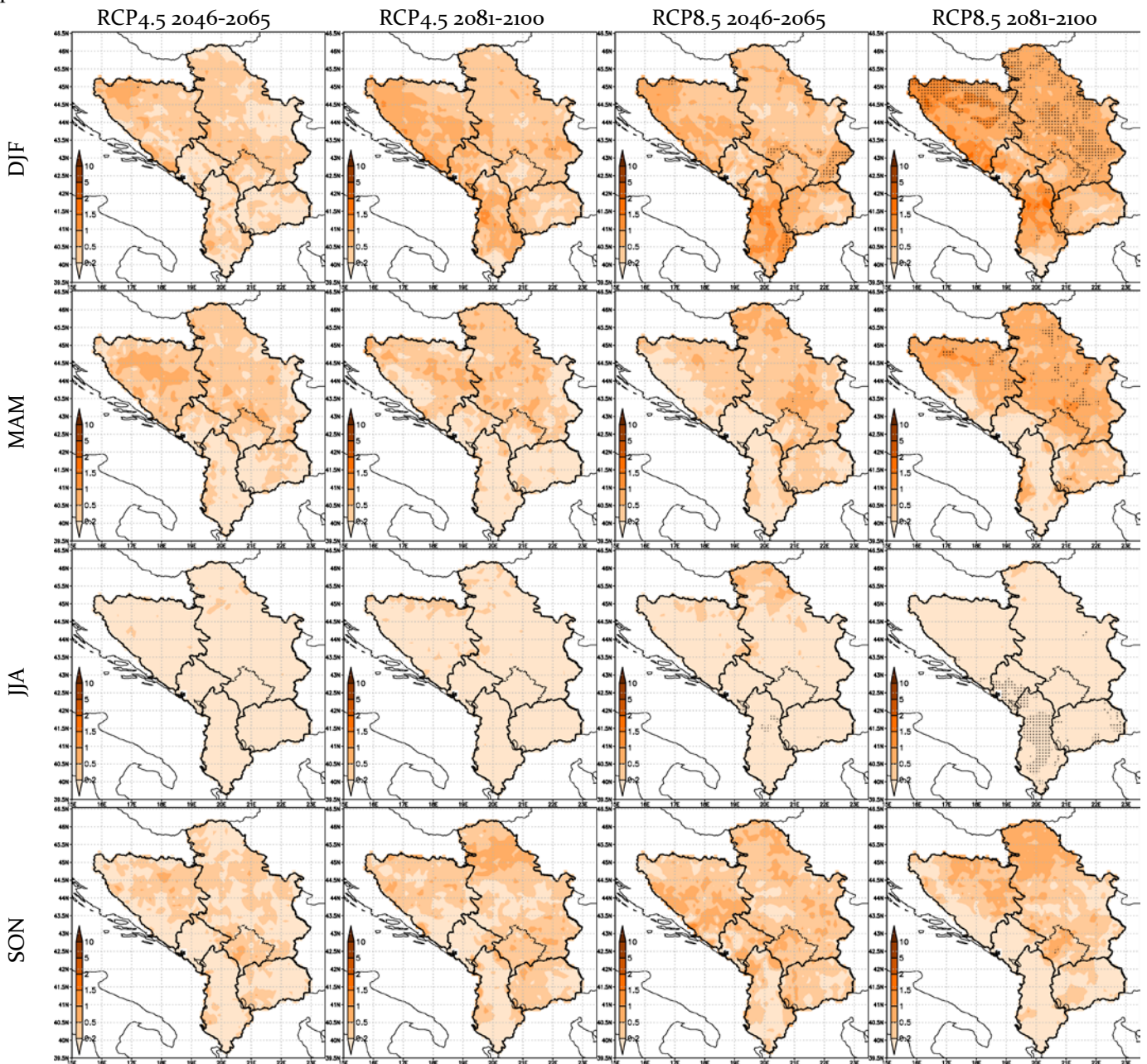


Figure 4 Seasonal change in number of days with precipitation above 20 mm (days) for mid-century (2046-2065) and end-of-the-century (2081-2100) periods, under RCP4.5 and RCP8.5 scenarios, compared to referent period (1986-2005). Black dots denote statistically significant change.

Seasonally, the highest increase in number of days with precipitation above 20 mm is expected in winter across the mountain region of BIH, SRB, MNE and ALB. In spring and autumn, the largest increase in number of such days across SRB, northern and eastern BIH, coastal ALB and western MKD. In summer, increase of such days is smallest, with less than 1 additional day per season, in average. Seasonal changes in number of days with precipitation above 20 mm are presented in Fig. 4.

The expected increase of water amount accumulated in events with precipitation above 20 mm is the largest (above 30%) in winter across SRB, BIH, MKD, northern

MNE and eastern and western ALB. In spring, affected are the same region, but within slightly smaller areas compared to winter. In autumn the largest increase is expected in northern BIH, northern and southern SRB, central MKD, and northern MNE. In summer season, decrease in amount of accumulated water in heavy precipitation events is expected in most parts of the region, while the increase is projected in the northern parts of SRB and BIH, and locally in eastern, central and western SRB. Seasonal changes in water accumulated in events with precipitation above 20 mm are presented in Fig. 5.

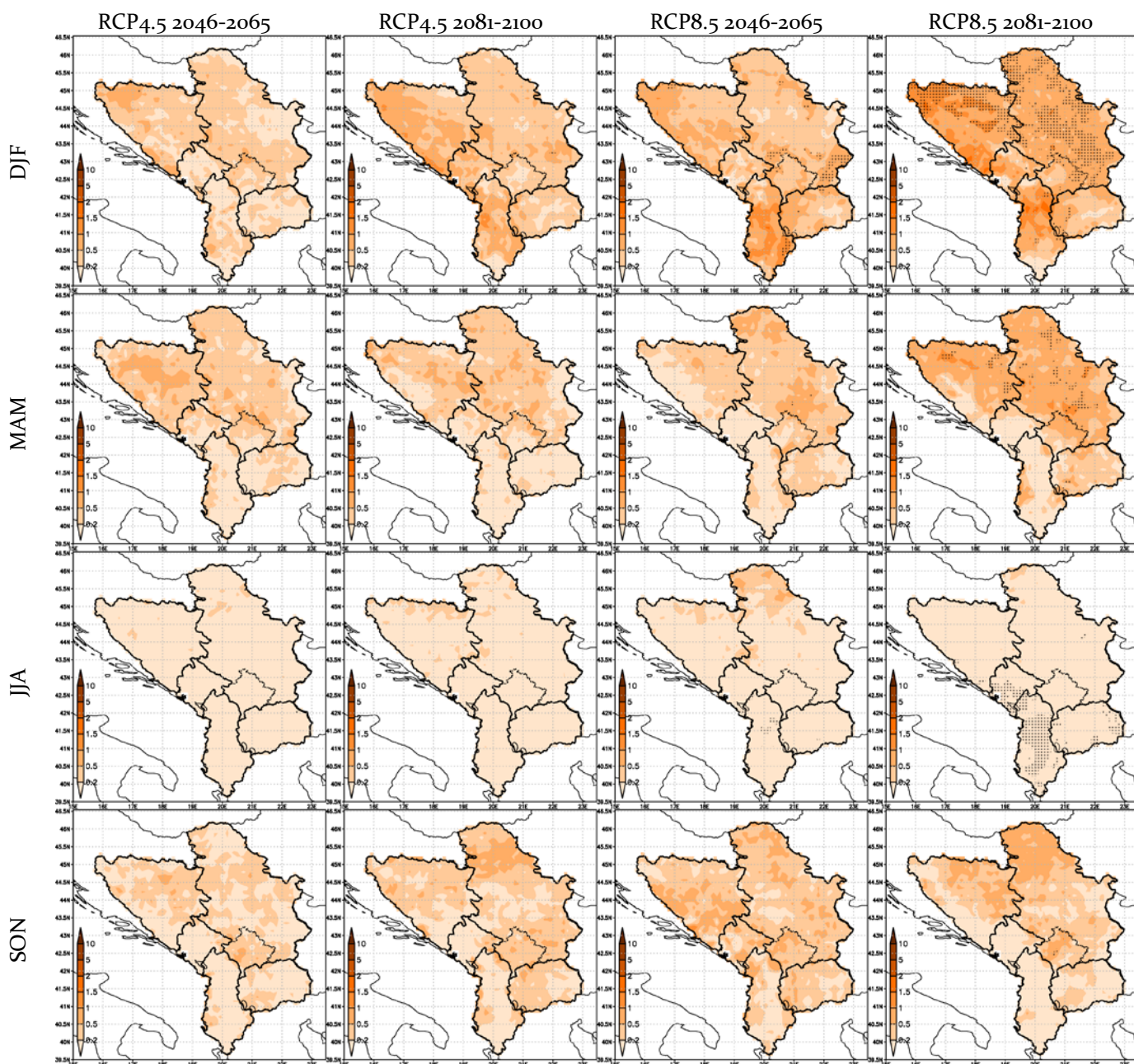


Figure 5 Seasonal change in water accumulated in events with precipitation above 20 mm (%) for mid-century (2046-2065) and end-of-the-century (2081-2100) periods, under RCP4.5 and RCP8.5 scenarios, compared to referent period (1986-2005). Black dots denote statistically significant change.

Conclusions

Temperature rise, change in seasonal precipitation patterns, intensification of heavy precipitation events, and overall increased climate variability, will increase risks in the landslides-prone areas across the WB region. Beside the direct effect of increased intensive precipitation events and amount of water in such events, other climate-related factors, such as summer droughts, high temperature, wildfires, land degradation, overlap of snowmelt and increased spring precipitation periods could also expand the risk across the areas that are currently not susceptible to landslides. Rate of the expected changes depends on the success of mitigation efforts implemented on a global level, while the direction of the changes is unequivocal.

In addition to the climate changes impacts, shifts of vegetation dynamics and land use practices may influence region's natural capacity to mitigate landslide risks and increase overall vulnerability.

Assessment of the future climate change impacts needs to be systematically integrated into risks management strategies within the region, land-use planning and infrastructure development, and used as basis for developing and prioritizing adaptation measures. Such measures could include, among other, development or strengthening of early warning systems (providing timely alerts and increasing preparedness), increasing infrastructure resilience (both in planning and maintenance) and vegetation management (restore or maintain vegetation cover to enhance slope stability and mitigate erosion), which will all increase readiness of citizens and authorities and contribute to the development of a climate resilient society, environment and infrastructure.

References

- FNC ALB (2022) The Fourth National Communication of Albania on Climate Change. pp 336
- FNC BIH (2021) Fourth National Communication of Bosnia and Herzegovina Under the United Nations Framework Convention on Climate Change. pp 221
- FNC MKD (2023) Fourth National Climate Change Communication of North Macedonia. pp 276
- IPCC (2021) Summary for Policymakers. In: *Climate Change 2021: The Physical Science Basis. Contribution of Working Group I to the Sixth Assessment Report of the Intergovernmental Panel on Climate Change.* Masson-Delmotte V, Zhai P, Pirani A, Connors S L, Péan C, Berger S, Caud N, Chen Y, Goldfarb L, Gomis M I, Huang M, Leitzell K, Lonnoy E, Matthews J B R, Maycock T K, Waterfield T, Yelekçi O, Yu R, Zhou B (eds.) Cambridge University Press, Cambridge, United Kingdom and New York, NY, USA, pp. 3–32, doi:10.1017/9781009157896.001
- Jacob D, Petersen J, Eggert B, Alias A, Christensen O B, Bouwer L M, Braun A, Colette A, Deque M, Georgievski G, et al. (2014) EURO-CORDEX: New high-resolution climate change projections for European impact research. *Regional Environmental Change*. 14: 563-678.
- Jakob M (2022) *Landslides in a changing climate. Hazards, Risks and Disasters (Second Edition).* Davies T, Rosser N, Shroder J F (eds). Elsevier, Amsterdam, Netherlands (ISBN 9780128184646). pp 505-579.
- TNC MNE (2020) Montenegro Third National Communication on Climate Change. pp 297
- TNC SRB (2024) The Third National Communication of the Republic of Serbia to the United Nations Framework Convention on Climate Change. pp 82
- Van Vuuren D P, Edmonds J, Kainuma M, Riahi K, Thomson A, Hibbard K, Hurtt G C, Kram T, Krey V, Lamarque JF, et al. (2011) The representative concentration pathways: An overview. *Climatic Change*, 109, 5.
- Vukovic A, Vujadinovic Mandic M (2018) Study on climate change in the Western Balkans region. Nikcevic R. (ed.) Regional Cooperation Council, Sarajevo, Bosnia and Herzegovina (ISBN 9789926402099), 76p.

Determination of the soil-water characteristic curve of the soil by physical modelling tests

Josip Peranić^{(1)*}, Martina Vivoda Prodan⁽¹⁾, Nina Čeh⁽¹⁾, Rea Škuflić⁽¹⁾, Željko Arbanas⁽¹⁾

1) University of Rijeka, Faculty of Civil Engineering, Rijeka, Radmile Matejčić 3, Croatia, +385 51 265 943 (josip.peranic@gradri.uniri.hr)

Abstract An increasing number of studies published in the last decade show that physical model experiments are becoming an increasingly popular and more available tool in the study of various problems, such as rainfall infiltration, surface runoff, hydromechanical response of soils and slopes, slope stability, effectiveness of remediation measures, hydraulic barriers, the impact of vegetation on slope stability, etc. The soil water characteristic curve (SWCC), which relates soil suction to soil moisture content, is one of the most important features in unsaturated soil mechanics. Together with the hydraulic conductivity function, it plays a crucial role in the transient rainfall infiltration process and thus has major influence on stability of slopes exposed to rainfall. However, numerous studies have shown that the direct measurement of unsaturated hydraulic parameters using conventional laboratory methods can be difficult, expensive, time-consuming, and involve many uncertainties. This is especially present for fine-grained soils, where unsaturated soil property functions cover a wide range of soil suction that these soils may typically exhibit, and where measurements necessary to determine SWCC typically require the combination of different measurement techniques and equipment. On the other hand, measurements in uniformly graded, coarse soils can be challenging due to the typically highly nonlinear and steep shape of the SWCC, where only a few kPa of soil suction can distinguish between saturated and residual soil moisture conditions. This study presents some preliminary results on determining the SWCC of a uniformly graded sand using a specifically designed physical modelling tests. A 30 cm high slope inclined at 35 degrees and instrumented with soil moisture and pore water pressure sensors was subjected to different simulated rainfall intensities to investigate whether the data on steady-state seepage conditions could be used for hydraulic characterisation of a slope material. The preliminary results indicate that the method is not only useful for this application, but that the approach is useful for the investigation of hydraulic hysteresis and its effects on soil moisture and pore water pressure conditions as well, which also affect slope stability.

Keywords physical modelling, landslides, rainfall infiltration, soil-water characteristic curve, unsaturated soil

Introduction

Claiming numerous victims and causing enormous economic losses in various geological and climatic contexts, landslides represent one of the most devastating geohazards in the world. Although they are often triggered by earthquakes, snowmelt, volcanic or human activity, rainfall infiltration, especially during exceptional rainfall events, is by far the most common triggering factor for landslides worldwide. Considering that, as the consequences of climate change become more pronounced, extraordinary rainfall events are increasingly becoming a common phenomenon, it is not surprising that more and more studies are pointing to the link between changes in precipitation characteristics caused by climate change and the frequency and magnitude of rainfall-induced landslides.

While the physical mechanism of how rainfall infiltration affects the stability of shallow landslides by reducing soil suction (e.g. Montrasio et al. 2016; Toll et al. 2016; Chen et al. 2018; Ebel et al. 2018; Marino et al. 2020), or how the rise in groundwater level associated with prolonged and heavy rainfall can cause slopes to become unstable due to increased pore water pressure (e.g. Comegna et al. 2013; Peranić et al. 2021; Pedone et al. 2022; Tagarelli and Cotecchia 2022; Peranić and Arbanas 2022), predicting the exact location and timing of landslide occurrence remains a major challenge for the landslide scientific community. The complexity of the problem arises from the fact that there are many factors and processes that influence the stability state of a slope, most of them being interrelated and essentially inseparable. Therefore, more and more studies are recognising the need for an interdisciplinary approach to understanding and mitigating the hazards posed by rainfall-induced landslides (e.g. Crozier 2010; Bogaard and Greco 2016).

The soil water characteristic curve (SWCC), which relates soil moisture to soil suction, represents a fundamental feature in unsaturated soil mechanics. In the context of the stability of slopes exposed to rainfall infiltration, it can be considered as a means of providing a link between the hydrological conditions in a slope and its mechanical aspects, i.e. slope stability. In other words, it enables a coupling between the hydraulic response of a slope, which is usually reflected in transient, seepage-induced soil moisture changes resulting from a complex interaction between the surface soil in the unsaturated

part of a slope, the atmosphere and the vegetation, and the mechanical response, i.e. how the soil-moisture changes affect stress conditions, the deformations and the available shear strength of a slope. In general, these changes can be caused by both positive (downward) and negative (outward) net fluxes, depending on the interplay between evapo(transpi)rational demands and rainfall conditions on a slope. Due to hysteresis effects, modelling such processes typically requires defining sets of hydraulic parameters that are representative of the drying and wetting processes, i.e. defining the drying and wetting branches of the SWCC. Possible hydraulic paths that the soil can undergo depending on the acting boundary conditions should be constrained by the main drying and wetting branches of the SWCC. Together with the hydraulic conductivity function (HCF) and the rainfall properties, the SWCC plays a decisive role in the transient rainfall infiltration process and thus has a major influence on the stability of slopes exposed to rainfall.

However, direct measurement of SWCC using conventional laboratory methods can be challenging, expensive, time-consuming, and, include a great number of uncertainties (e.g. Ridley and Borland 1993; Oliveira and Fernando 2006; Cresswell et al. 2008). This is particularly present for fine-grained soils, where the unsaturated soil property functions cover a wide range of soil suction that these soils may typically exhibit, and where measurements to determine SWCC typically require the combination of different measurement techniques and equipment (Peranić et al. 2018). On the other hand, measurements in uniformly graded coarse soils can be challenging due to the typically highly nonlinear and steep shape of the SWCC, where only a few kPa of soil suction can distinguish between saturated and residual soil moisture conditions (Peranić et al. 2022; Crescenzo et al. 2024). This study encompasses such types of soil materials.

The study presents some of the preliminary results and experiences in determining the soil-water retention properties of a uniformly graded fine sand using specifically designed physical model tests. A 30 cm high and 35-degree inclined slope model instrumented with the soil moisture and pore water pressure sensors was subjected to increasing and decreasing simulated rainfall intensity to obtain data on steady-state seepage conditions that can be used to hydraulically characterise the slope material. The preliminary results indicate that the approach presented is not only useful for the hydraulic characterisation of the soil, but that the data collected during the experiment could also be useful for studying the effects of hydraulic hysteresis on soil moisture and pore water pressure conditions, i.e. its effects on the stability of slopes exposed to rainfall infiltration.

Methodology

The experimental setup includes a platform for testing slope models exposed to simulated rainfall conditions, a rainfall simulator and a comprehensive monitoring system

that allows the hydraulic and mechanical response of the model to be monitored. The platform itself consists of steel elements and transparent Plexiglass side walls. The flume itself is 1.0 m wide, while the upper, inclined and lower segments of the platform are 0.3, 1.4 and 0.8 m long. The geogrid is usually attached to the bottom of the platform, which is made of impermeable steel plates with the aforementioned dimensions, to prevent slippage of the installed soil material. The rotating hinge connection between the plates and the adjustable height of the steel columns supporting the upper part of the slope enable construction of slope models with desired inclination angles, for example from less than 20 to more than 45 degrees. The transparent Plexiglass side walls are 50 cm high and make it possible to observe the wetting front advancement during the test, as well as the movements at the side of the model. A three-level system of drainage lines inserted through the front-facing Plexiglass wall in the lower part of the flume, allows the water level condition in the model to be controlled during the test and fast drainage of the flume after a test is completed. The rainfall simulator comprises of three independent sprinkling branches that deliver water from the main control block. Each of the branches is equipped with different axial-flow full-cone nozzles, so that the system can generate different rainfall patterns and a wide range of rainfall intensities, depending on the working pressure and spray nozzle(s) used. More details about the platform and the rainfall simulator can be found in Pajalić et al. (2021) and Peranić et al. (2022). Several details about the platform are shown in Fig. 1.

Model build-up and instrumentation

The soil considered in the study, a uniformly graded fine sand (Tab. 1), was used for the construction of two slope models. In both cases, the dry sandy soil was thoroughly mixed with tap water to achieve a targeted gravimetric water content of 2%. Then the predefined amount of soil was placed into the platform and compacted in 5 layers according to Ladd's under-compaction method (Ladd 1974) to build the 30 cm high sandy slope model with homogenous conditions in terms of the initial porosity and moisture, as much as possible. From Tab. 1, the targeted initial porosity of 0.44 corresponds to 50% of the relative density of the sandy soil encompassed in the study. The compaction was carried out in a way that the number of finished (i.e. compacted) soil layers always increased from the lower to the upper part of the slope in order to ensure the stability of a model during the construction.

The first slope model was built directly on the impermeable steel plate, with the slope's toe extending to the end of the flume. However, moulding of the groundwater level in the lower part of the slope during the infiltration stage of the test resulted in most of the monitored points being submerged or taking too long to reach steady-state conditions for the applied rainfall intensity, especially at higher rainfall intensities in the later phase of the test. Therefore, to improve the drainage

conditions in the model, the second model was built in the same way, but with 5 cm of gravel placed on the impermeable bottom of the flume before the sandy material was built in and compacted. A geosynthetic was laid on top of the gravel to prevent washout of fine sandy material

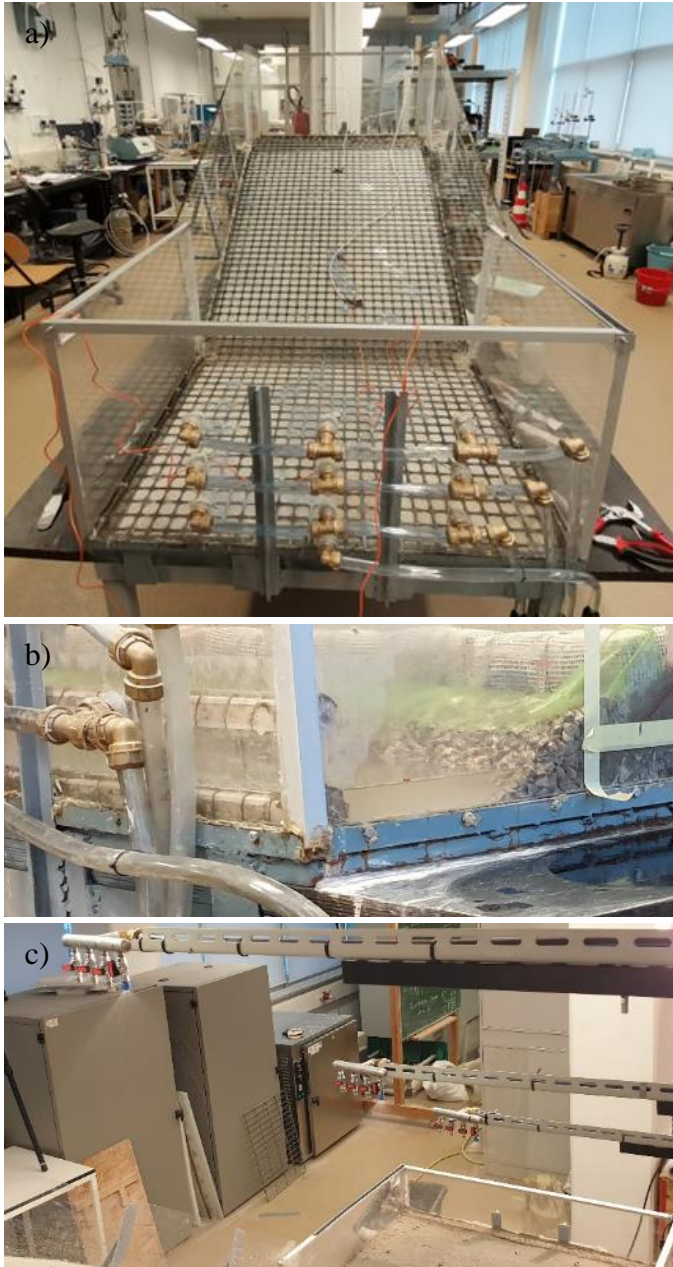


Figure 1 Some details about the testing platform: a) Empty platform prepared for model build-up with geogrid attached to the bottom steel plates and drainage elements in the lower segment of the flume; b) The use of drainage valves to control the boundary conditions (water level) during the experiment considered in the presentation; c) Three branches of the rainfall simulator during the experiment.

Table 1 Properties of the uniformly graded fine sand considered in the study.

Parameter	Symbol	Value	Unit
Specific gravity	G_s	2.7	(/)
Particle size	D_{10}	0.19	(mm)
Particle size	D_{60}	0.37	(mm)
Uniformity coefficient	C_u	1.95	(/)
Min./max. void ratio	e_{min}/e_{max}	0.64/0.91	(/)/(/)
Targeted init. porosity	n_i	0.44	(/)
Targeted init. relative density	D_i	50	(%)
Targeted init. (gravimetric) water content	w_i	2	(%)
Hydraulic parameters*			
saturated hydraulic cond.	k_s	3.3e-4	(m/s)
SWRC parameters	α	0.82	(kPa)
	n	2.7	(/)

*best-fit parameters obtained by numerical inverse modelling (Crescenzo et al., 2024)

into the coarser material during the rainfall infiltration. In addition, the geometry of the model was modified so that it terminates as an “infinite slope” at the bottom, to avoid or postpone rise in groundwater level and saturation of the monitored points in the sloping part of the model. This proved to be beneficial for the purpose of the investigation of hydraulic characteristics of the tested material, as it allowed a longer testing time and achievement of steady-state conditions for the monitored points, even with a relatively high rainfall intensity applied. The gabion wall was installed at the bottom of the slope to ensure that the toe of the slope would not be eroded during prolonged testing time and high rainfall loads applied. The two slope models at the start of the test are shown in Fig. 2. For the sake of brevity, only the results of the second, i.e. “the infinite slope” model are included in this paper.

After the building of the models was completed, the slope models were instrumented to monitor their hydraulic and mechanical response. Changes in soil moisture were monitored using TEROS 10 and TEROS 12 theta probes, while TEROS-31 mini-tensiometers (METER Group AG, Munich, Germany) enabled the measurement of pore water pressure in the positive and negative domain (i.e., soil suction). A central part of the slope model was vertically cut at three different locations, where three measurement profiles were established: one for the upper part (U-profile), and two profiles along the inclined part of the model, one in the upper part (I^U-profile) and one in the lower part (I^L-profile). The position of the profiles in the inclined part of the model was defined to be at one third of the floor plan section length. The sensors were then pushed into the slope model at the depths corresponding to the junction of layers formed during model build-up stage. Care was taken to ensure that minimum disturbance of the soil material was introduced, and that good hydraulic contact was established between the sensor unit and the surrounding soil (Fig. 3). In this way, a total of 18



Figure 2 Models with a 35-degree inclination built from clean, uniformly-grained fine sand at the beginning of the test: The case with impermeable bottom boundary condition and the slope's toe reaching the end of the flume (upper photo); The "infinite" slope model over a 5 cm thick layer of gravel to improve drainage conditions - the case considered in this study (lower photo).

sensors were installed within the slope model along three measurement profiles, as shown in Fig. 4.

A range of measurement techniques, such as photogrammetric equipment for multi-temporal landslide analysis of image sequences obtained from a pair of high-speed stereo cameras, terrestrial laser scanning, structure-from-motion (SfM) photogrammetry surveys, as well as accelerometers, strain gauges, etc. (for more details see Arbanas et al. 2020, 2022; Pajalić et al. 2021; Čeh et al. 2022) can be used to monitor the surface and/or displacements within the slope model. While these are usually crucial for investigating different aspects of landslide triggering mechanisms or different stages of landslide activity, this is not the case for the study presented here. The specific aim of the study, i.e. the investigation of the unsaturated hydraulic properties of the soil, which undergoes negligible volumetric deformations during the rainfall infiltration (Crescenzo et al. 2024), where the stability of the slope and the absence of larger shear deformations is the condition required for proper data analysis, the

geodetic and geotechnical parts of the monitoring related to the displacements of the model essentially represent a tool that only checks the condition of negligible soil deformations during the test. In this case, no coupling between pore water pressure and soil deformations is required. Therefore, pins with marker points were placed on the surface of the model and a continuous monitoring of the 3D coordinates of the reference points was performed during the tests using the optical non-contact 3D measurement system ARAMIS 4M (GOM mbH, Braunschweig, Germany) only for the first model (upper photo in Fig 2). While further details on the measurement system can be found elsewhere (Pajalić et al. 2021; Čeh et al. 2022; Peranić et al. 2022), the results on the mechanical response of the models are irrelevant for the present study and thus are excluded from this presentation.

Once the slope model was built and instrumented with monitoring equipment, the model was covered with nylon to prevent loss of soil moisture through evaporation until the test was started. All sensors were connected to corresponding data logging units and appropriate recording intervals were selected.

Testing conditions

Starting from the initial (known) soil moisture and pore water pressure conditions, the slope model was subjected to a range of rainfall intensities until steady-state conditions were observed for the monitored points. Given the purpose of the study, rapid drainage of the sandy slope model was desirable. Therefore, the drainage valves were constantly open to prevent any pore water pressure build-up in the slope, i.e. to maintain the rainfall infiltration process through the model in partially saturated conditions.

Starting from relatively dry, i.e. near-to residual soil moisture conditions, the test was initiated with the relatively low rainfall intensity of 36.9 mm/h, which was kept constant for 66 minutes. As no further changes in pore water pressure and volumetric water content were observed, the working pressure and nozzles were combined so that the rainfall intensity was approximately doubled in the following test phase. The rainfall intensity was maintained at 78.6 mm/h until the 148th minute of the



Figure 3 Detail of the installation of the soil moisture sensor and the mini-tensiometer at the monitored point I¹-6.

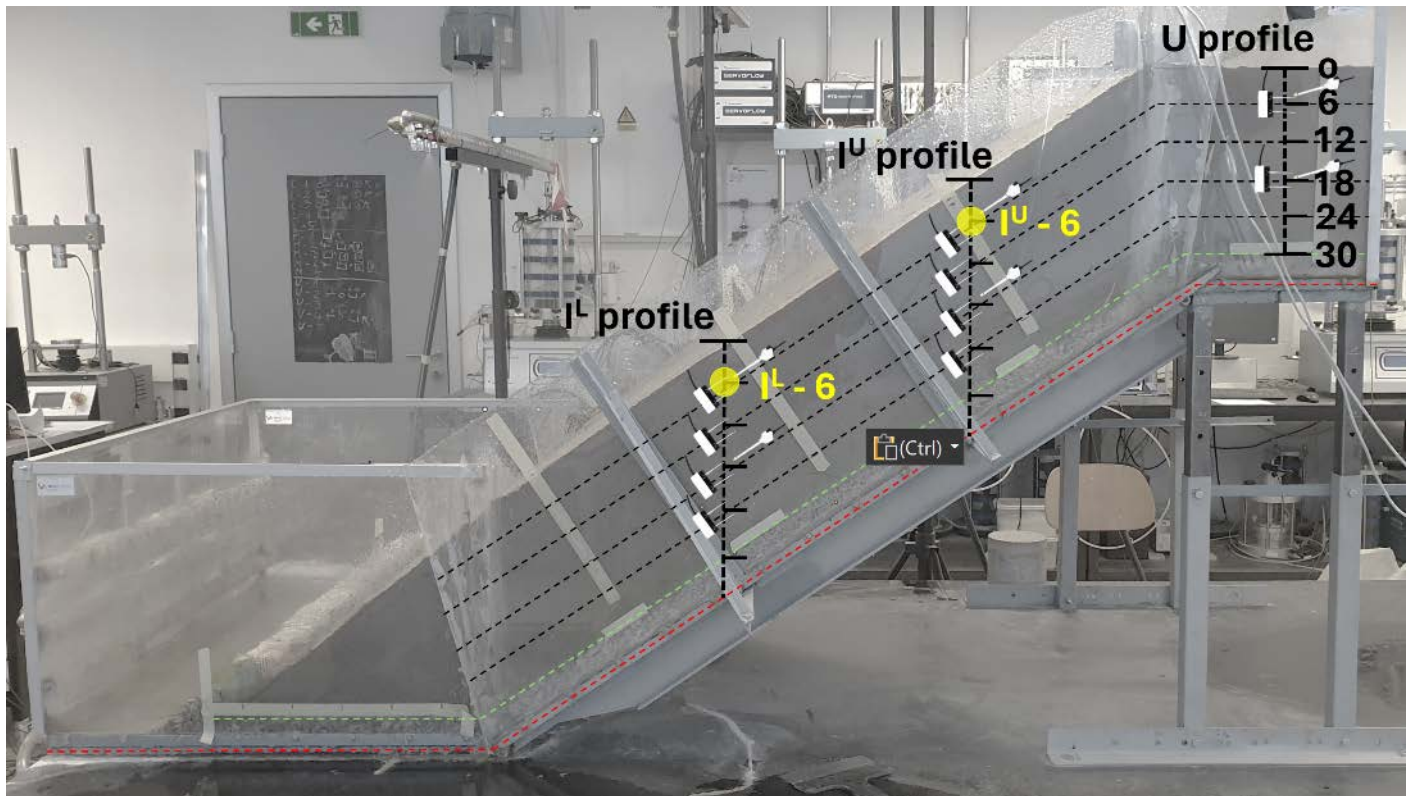


Figure 4 Schematic representation of the measurement profiles and the points at which the hydraulic response was measured in terms of volumetric water content (θ) and pore water pressure (u). The two uppermost measurement points, for which the data on soil suction and volumetric water content are presented in the study, are outlined in yellow.

test. Again, steady-state conditions were established under the applied (constant) rainfall conditions so that the intensity of the simulated rainfall was again approximately doubled and maintained at 157.2 mm/h until the 180th minute of the test. Finally, the rainfall intensity was reduced to the starting value, i.e. 36.9 mm/h and was kept constant until the hydraulic equilibrium at the monitored points was observed.

After 306 minutes of the test the rainfall was stopped, and the first stage of the test was declared completed. However, the collection of the data from the hydraulic monitoring system was continued during the drainage stage of the slope in the following weeks. Finally, the second stage was carried out a few weeks later to test the model's response to extremely high rainfall intensity. In this case, the rainfall intensity of 300.3 mm/h was maintained for 34 minutes when the test was stopped as traces of slope failure have started to appear. The rainfall conditions for the two test stages considered in the study are summarised in Fig. 5.

Results and Discussion

The measured volumetric water content and pore water pressure values (i.e., matric suction in this case) for the U^L-6 and I^L-6 monitored points (locations in Fig. 4) are shown in Fig. 6. Some interesting points are discussed and outlined in the following part.

After the onset of rainfall, it takes about 10 minutes for the wetting front to reach monitored points and for theta probes and mini-tensiometers to register changes in volumetric water content and soil suction. While the readings on change in soil moisture appear to be more diffuse and the time to reach steady-state conditions is more than 20 minutes, an abrupt decrease in soil suction is observed in the data collected with the mini-tensiometers, and a much shorter time to reach constant reading values. In any case, from the 40th minute of the test, both monitored points appear to reach hydraulic equilibrium and constant readings for both soil moisture and suction. In the following phase of the test, the increase in soil moisture and pore water pressure seems to be immediate with the increase in rainfall intensity from 36.9 to 78.6 mm/h and steady-state conditions are established much faster for both monitored points. A very similar response is observed for the test period around the 148th minute when the rainfall intensity was further increased to 157.2 mm/h. It is interesting to note that despite the increase in rainfall intensity from 37 to 157 mm/h, soil suction remained unchanged, with the difference between the steady-state conditions for the two rainfall intensities being less than 0.3 kPa. The volumetric water content increased from about 0.22 to 0.26 with the same increase in rainfall load.

An interesting observation can be made for the drying response of the monitored points, which was

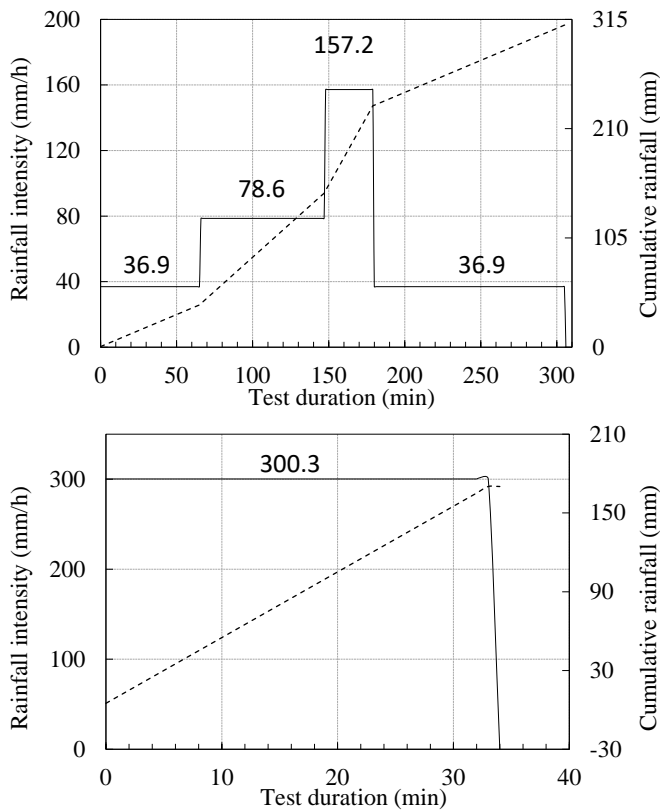


Figure 5 Rainfall conditions applied in the first (top) and the second (bottom) stage of the test.

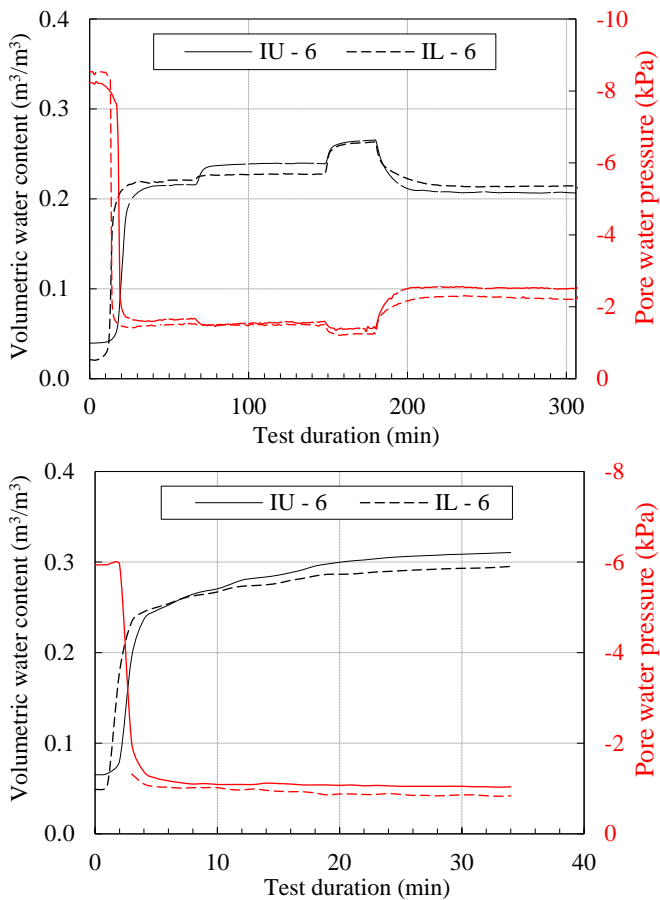


Figure 6 The volumetric water content and the pore water pressure (i.e. matric suction) for the monitoring points U^l-6 and I^l-6 (see Fig. 4) in the first (upper diagram) and second (lower diagram) stage of the test.

induced by the reduction in rainfall intensity from the 180th minute of the test. Now the response appears to be much slower, both in terms of soil moisture and change in soil suction, with both instrumented points approaching equilibrium conditions over the following 20 minutes or more. Unlike the steady-state volumetric water content conditions, which closely correspond to those from the first phase of the test, soil suction is evidently higher in the case where steady-state conditions are achieved by reducing rainfall intensity rather than by increasing it.

The data from the second stage of the test provides an interesting insight into the hydraulic response of the soil when exposed to an extremely high rainfall intensity of 300 mm/h. After allowing the slope model to drain freely for an extended period of time, the second test stage of the test begins with relatively dry conditions, although the soil suction value appears to be slightly lower than in the previous case. The wetting front has reached the monitored points much faster now, with changes in soil moisture and suction values observed within a minute or two after the rainfall was started. Again, similar considerations could be made regarding the diffuse nature of the changes in soil moisture and the abrupt changes in soil suction as before, although it is unclear whether the equilibrium volumetric water content conditions were reached by the end of the test, as it appears to increase slowly but steadily even after the 20th minute of the rainfall application. However, an important observation is that even with a rainfall intensity of 300 mm/h, the negative pore water pressure, i.e. soil suction, was still maintained at the monitored points.

All previously presented pairs of volumetric water content and soil suction are plotted in Fig. 7 with the soil suction in logarithmic form – a plane typically used to present SWCC. In the same figure, the SWCC obtained for the same soil by numerical modelling of small-scale slope model subjected to rainfall according to the methodology proposed by Crescenzo et al. (2024) is shown in a continuous black colour. The hydraulic paths that the monitored points undergo during the first stage of the test are summarised in Fig. 8 together with the SWCC branches obtained. While a detailed discussion on the SWCC branches, shown in dashed red (drying) and blue (wetting) lines, as well as the data presenting the hydraulic paths of the monitored points is beyond the scope of this presentation, it is worth noting the fit between the SWCC branches and the obtained data, while the wetting branch obtained by Crescenzo et al. (2024) falls close to the data obtained for the wetting path, albeit slightly more to the wet side.

These preliminary results suggest that the physical slope model tests could be useful not only for the hydraulic characterisation of the soil, but also for the investigation of a range of problems associated with rainfall-induced landslides.

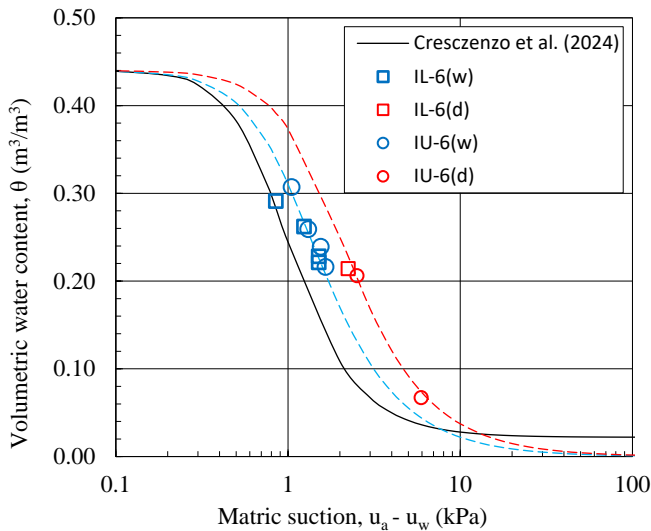


Figure 7 Steady-state volumetric water content and soil suction data obtained for the monitored points on the drying (red markers) and wetting (blue markers) paths, together with the SWCC numerically determined by Crescenzo et al. (2024).

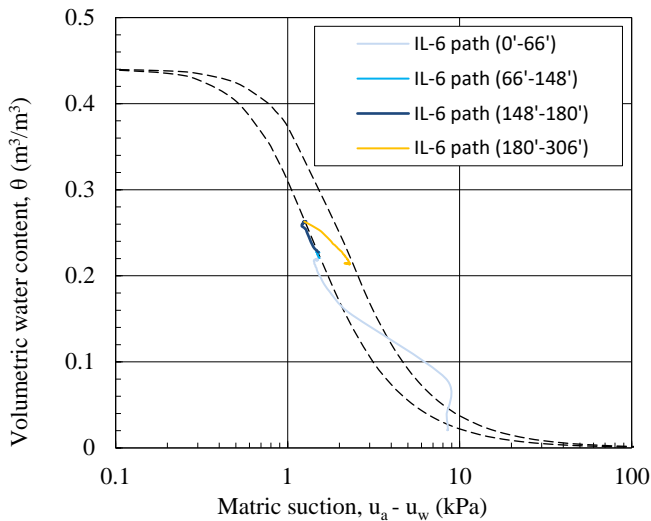


Figure 8 The hydraulic paths reconstructed for the monitored points during the first stage of the test, together with the branches obtained from the data presented.

Conclusions

In this study, some preliminary results and experiences were presented on the possible use of physical slope model tests to determine a SWCC of the uniformly graded sand. The study involved the 30 cm high, 35-degree inclined slope equipped with soil moisture and pore water pressure sensors and subjected to various simulated rainfall intensities. While these preliminary results suggest that the approach could be very useful to investigate different aspects of the hydraulic response of slopes exposed to a rainfall, e.g. for soil hydraulic characterisation, as well as to gain insight into the hysteretic hydraulic response of slopes and how this might influence the stability conditions of the slope, some aspects of the presented approach that could be improved were also discovered.

For example, using the very limited data presented in the study (for brevity, data from only two monitored points were included in the presentation), it is evident that for a soil under consideration, the possibility of applying a wider range of rainfall intensities, particularly those that would cover parts of the SWCC where residual conditions along the wetting path approach, or applying high rainfall intensities where the SWCC would approach saturated soil moisture conditions, would be extremely valuable to the approach.

In addition, the study considered a soil that undergoes negligible volumetric deformations when soil moisture (i.e. suction) changes occur. If the approach is to be generalised to fine-grained soils, where hydromechanical coupling would be required to obtain an adequate hydraulic characterisation of such soils, the approach should also use the geodetic and part of the geotechnical monitoring system, which would provide the data that would allow quantification of the deformations induced in different phases of a test. Additional considerations need to be made to distinguish between the various possible SWCCs that the approach could yield depending on the initial soil moisture conditions or hydraulic conditions to which the soil is generally exposed during the test.

Finally, the different responses observed under different rainfall conditions have direct impact on the stability state of a slope exposed to rainfall. However, the rainfall to which slopes are exposed in the field are much more complex and exhibit strong temporal and spatial variations (Peranić and Arbanas 2022). These are some of the aspects that should be further investigated to improve understanding and modelling capabilities and mitigate the hazard posed by rainfall-induced landslides.

Acknowledgements

This research was funded by the Croatian Science Foundation under the Project IP-2018-1503 *Physical modelling of landslide remediation constructions behaviour under static and seismic actions (ModLandRemSS)*. This work has been supported by the International Consortium on Landslides under the IPL-256: *Investigation of landslide initiation caused by rainfall infiltration using small-scale physical and numerical modeling (ILIRIM)* and IPL-269: *Landslide Initiation, Evolution and Remediation: Physical and Numerical Modeling (LIEREM)* projects. This work has been partially supported by the University of Rijeka project uniri-mladi-tehnic-22-62. These supports are gratefully acknowledged.

References

- Arbanas Ž, Jagodnik V, Peranić J, et al (2020) Physical Model of Rainfall Induced Landslide in Flume Test : Preliminary Results. In: Proceedings of the ECPMG 2020. pp 115-122.
- Arbanas Ž, Peranić J, Jagodnik V, et al (2022) Impact of gravity retaining wall on the stability of a sandy slope in small-scale physical model. In: Peranić J, Vivoda Prodan M, Bernat Gazibara S, et al. (eds) Landslide Modelling & Applications: Proceedings of the 5th Regional Symposium on Landslides in the Adriatic-Balkan Region. Faculty of Civil Engineering, University of Rijeka and Faculty of Mining, Geology and Petroleum Engineering, University of Zagreb, Rijeka, pp 193–200
- Bogaard TA, Greco R (2016) Landslide hydrology: from hydrology to pore pressure. Wiley Interdisciplinary Reviews: Water 3
- Čeh N, Peranić J, Jagodnik V, et al (2022) Digital image correlation and the use of high-speed cameras for 3D displacement monitoring in 1g small-scale landslide models. In: Proceedings of the 5th ReSyLAB 'Landslide Modelling & Applications. pp 181–186
- Chen P, Lu N, Formetta G, et al (2018) Tropical storm-induced landslide potential using combined field monitoring and numerical modeling. Journal of Geotechnical and Geoenvironmental Engineering. [https://doi.org/10.1061/\(ASCE\)GT.1943-5606.0001969](https://doi.org/10.1061/(ASCE)GT.1943-5606.0001969)
- Comegna L, Picarelli L, Bucchignani E, Mercogliano P (2013) Potential effects of incoming climate changes on the behaviour of slow active landslides in clay. Landslides. <https://doi.org/10.1007/s10346-012-0339-3>
- Crescenzo L, Peranić J, Arbanas Ž, Calvello M (2024) An approach to calibrate the unsaturated hydraulic properties of a soil through numerical modelling of a small-scale slope model exposed to rainfall. Acta Geotech. <https://doi.org/10.1007/s11440-023-02170-2>
- Cresswell HP, Green TW, McKenzie NJ (2008) The Adequacy of Pressure Plate Apparatus for Determining Soil Water Retention. Soil Science Society of America Journal 72:. <https://doi.org/10.2136/sssaj2006.0182>
- Crozier MJ (2010) Deciphering the effect of climate change on landslide activity: A review. Geomorphology 124
- Ebel BA, Godt JW, Lu N, et al (2018) Field and Laboratory Hydraulic Characterization of Landslide-Prone Soils in the Oregon Coast Range and Implications for Hydrologic Simulation. Vadose Zone Journal. <https://doi.org/10.2136/vzj2018.04.0078>
- Ladd RS (1974) Specimen Preparation and Liquefaction of Sands. Journal of the Geotechnical Engineering Division 100:. <https://doi.org/10.1061/ajgeb6.0000117>
- Marino P, Santonastaso GF, Fan X, Greco R (2020) Prediction of shallow landslides in pyroclastic-covered slopes by coupled modeling of unsaturated and saturated groundwater flow. Landslides. <https://doi.org/10.1007/s10346-020-01484-6>
- Montrasio L, Schilirò L, Terrone A (2016) Physical and numerical modelling of shallow landslides. Landslides 13:. <https://doi.org/10.1007/s10346-015-0642-x>
- Oliveira OM, Fernando FAM (2006) Study of Equilibration Time in the Pressure Plate
- Pajalić S, Peranić J, Maksimović S, et al (2021) Monitoring and data analysis in small-scale landslide physical model. Applied Sciences (Switzerland). <https://doi.org/10.3390/app11115040>
- Pedone G, Tsiampousi A, Cotecchia F, Zdravkovic L (2022) Coupled hydro-mechanical modelling of soil–vegetation– atmosphere interaction in natural clay slopes. Canadian Geotechnical Journal 59:. <https://doi.org/10.1139/cgj-2020-0479>
- Peranić J, Arbanas Ž (2022) The influence of the rainfall data temporal resolution on the results of numerical modelling of landslide reactivation in flysch slope. Landslides 19:2809–2822. <https://doi.org/10.1007/s10346-022-01937-0>
- Peranić J, Arbanas Ž, Cuomo S, Maček M (2018) Soil-Water Characteristic Curve of Residual Soil from a Flysch Rock Mass. Geofluids 2018:1–15. <https://doi.org/10.1155/2018/6297819>
- Peranić J, Čeh N, Arbanas Ž (2022) The Use of Soil Moisture and Pore-Water Pressure Sensors for the Interpretation of Landslide Behavior in Small-Scale Physical Models. Sensors 22:7337. <https://doi.org/10.3390/s22197337>
- Peranić J, Mihalić Arbanas S, Arbanas Ž (2021) Importance of the unsaturated zone in landslide reactivation on flysch slopes: observations from Valići Landslide, Croatia. Landslides 18:3737–3751. <https://doi.org/10.1007/s10346-021-01757-8>
- Ridley AM, Borland JB (1993) A new instrument for the measurement of soil moisture suction. Geotechnique 43:. <https://doi.org/10.1680/geot.1993.43.2.321>
- Tagarelli V, Cotecchia F (2022) Coupled hydro-mechanical analysis of the effects of medium depth drainage trenches mitigating deep landslide activity. Eng Geol 297:. <https://doi.org/10.1016/j.enggeo.2021.106510>
- Toll DG, Md Rahim MS, Karthikeyan M, Tsaparas I (2016) Soil-atmosphere interactions for analysing slopes in tropical soils in Singapore. Environmental Geotechnics. <https://doi.org/10.1680/jenge.15.00071>

Tailings Dam Stability Evaluation using 3D Numerical Modelling

Veljko Lapčević^{(1)*}, Slavko Torbica⁽²⁾

1) University of Belgrade – Faculty of Mining and Geology, Đušina 7, Belgrade, Serbia (veljko.lapcevic@rgf.bg.ac.rs)

2) Owl and Fox – Mining Consultants, Cara Dušana 67/3, Belgrade, Serbia

Abstract The disposal of tailings represents a significant engineering challenge in the mining industry, primarily due to the vast volume of material involved and the potential environmental risks. As such, the assessment of tailing dam stability is a critical component of the engineering process, alongside design considerations. Terrain topography plays a pivotal role in both design and stability assessment; flat terrains generally simplify these processes. In contrast, complex terrain conditions necessitate a design that accommodates spatial constraints, which in turn makes stability assessment more intricate and demanding.

Traditionally, 2D limit equilibrium and stress-strain analyses have been the standard, offering reliability for simpler design scenarios. However, for more complex designs, these traditional methods fall short due to complex boundary conditions that significantly impact the stability of tailing dams. These complex conditions can only be accurately assessed through 3D analysis. This paper delves into a comparative study of 2D versus 3D limit equilibrium and stress-strain analyses in tailings dam design and stability assessments.

Beyond the complex boundary conditions inadequately captured by 2D analysis, the distribution of pore pressure within the dam material also undergoes significant variations, which 3D methods can more accurately account for. The advantages of 3D analysis become particularly evident in the identification of risks associated with the intricate designs of tailing dams. Neglecting these complexities and resorting to oversimplified methods for stability assessments can escalate environmental risks, potentially leading to dire consequences. Thus, this paper underscores the importance of adopting advanced techniques in managing the stability risks of tailing dams in complex geological settings.

Keywords tailings dam, stability, numerical methods

Introduction

Tailings dams are engineered structures designed for storing by-products of mineral processing in the mining industry. These by-products, known as tailings, consist of a mixture of fine particles, water, and various chemicals used in the processing. The mixture is transported to a designated area for deposition, where excess water is removed using hydrocyclones. The coarser sand material is then utilized to construct the dam, which serves the purpose of containing the remaining material within the pond. However, these processes and the tailings dams themselves pose significant environmental risks. Historical records document catastrophic events (Morgenstern et al, 2016), with the Brumadinho dam disaster in Brazil being one of the most recent and notable examples.

Tailings dam design varies based on the terrain where it is planned to be located. In flat areas, construction is straightforward and easy to manage throughout the production process. However, more complex terrains, such as hilly areas and valleys, necessitate intricate designs and management strategies. As a result, stability evaluation becomes significantly more critical with complex designs (Vick, 1990). Until recently, stability evaluations were performed using available 2D tools that relied on the finite element method and the limit equilibrium method. Planar analysis, however, has substantial limitations in capturing the boundary conditions of the structure being analyzed. It requires the identification and analysis of numerous cross-sections for stability, especially in cases requiring complex designs. The adoption of 3D tools, which are increasingly becoming standard in engineering practice, allows for the analysis of complex structures as whole entities. This approach considers both the mechanical behavior and the influence of water levels, offering a more comprehensive analysis. This paper is dedicated to showcasing the use of 3D numerical modeling in assessing the stability of tailings dams. It elaborates on the creation and validation of a 3D model designed specifically to mimic the intricate systems of tailings dams. Through an exploration of the strengths and weaknesses of 3D numerical modeling in the context of tailings dam stability evaluations, this paper aims to enrich the domain of tailings dam safety. Its goal is to lay the groundwork for the creation of more precise and dependable forecasting tools, thereby advancing safer tailings management methodologies.

Preliminary considerations

Figure 1 illustrates a tailings dam situated in a valley, highlighting the location of a typical cross-section used for evaluating planar stability. This representation significantly simplifies the actual construction, a critical point to bear in mind as evident from the figure itself. Figure 2 depicts the material structure, showing that the initial dam is constructed from rock material, followed by layers of sand, with the majority of the volume comprising tailings. Owing to the nature of the tailings discharged from the flotation plant and the segregation of material fractions during operation, a transitional zone between

the sand and tailings (mud) has been identified (Duncan et al, 2014).

The stability evaluation involves assessing the slope stability across various cross-sections that are representatively defined. These cross-sections must be delineated in a way that captures the essential features of the structure. There is a potential risk if too few sections are selected, leading to the omission of critical parts of the tailings dam from the analysis. Apart from the slope itself, failure could also result from sliding over the ground rock mass or from the failure of the ground itself.

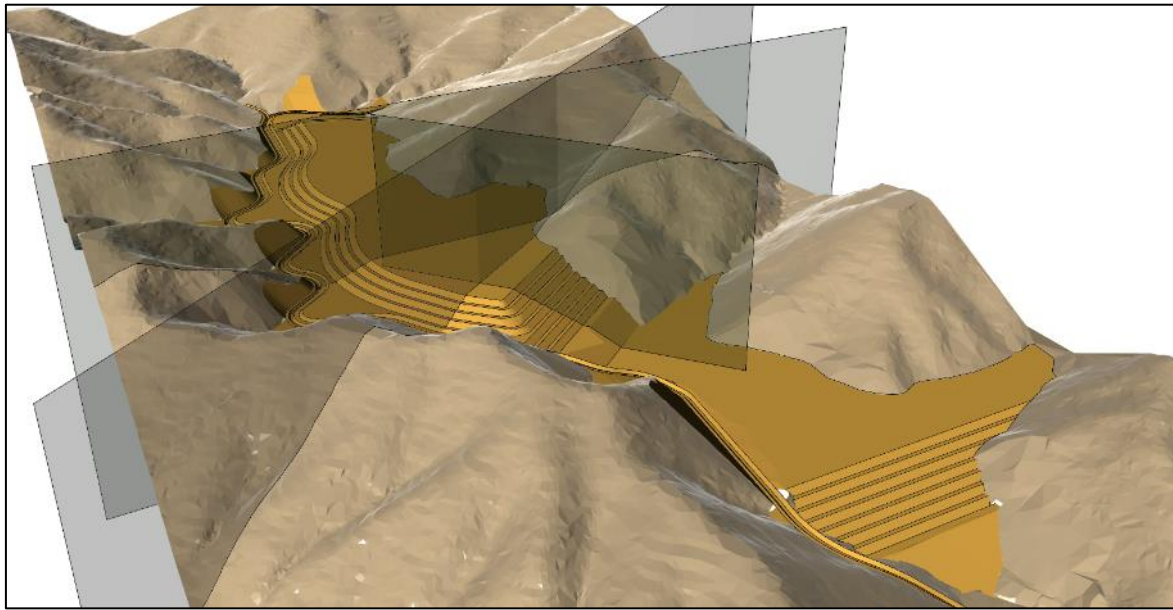


Figure 1 Tailing dam construction

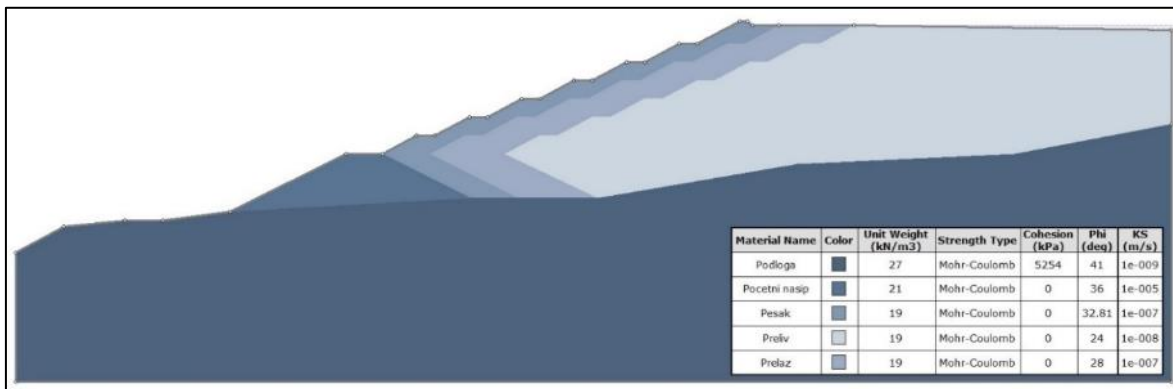


Figure 2 Geomechanical cross section used for 2D models

Figure 2 illustrates the geomechanical cross-section utilized for creating the 2D models, with the results of the limit equilibrium model shown for simplicity. The same figure also details the material properties used in the analysis. To depict the worst-case scenario, the model simulates conditions where the pond is at its maximum water level.

The critical Factor of Safety (FOS) identified using Limit Equilibrium Method (LEM) modeling occurs in cross section 1, with a critical water level resulting in a FOS value of 1.197 (Figure 3). This example serves as a reference to highlight the differences between 2D and 3D modeling approaches. Rocscience Slide (Rocscience, 2023) was used in this case.

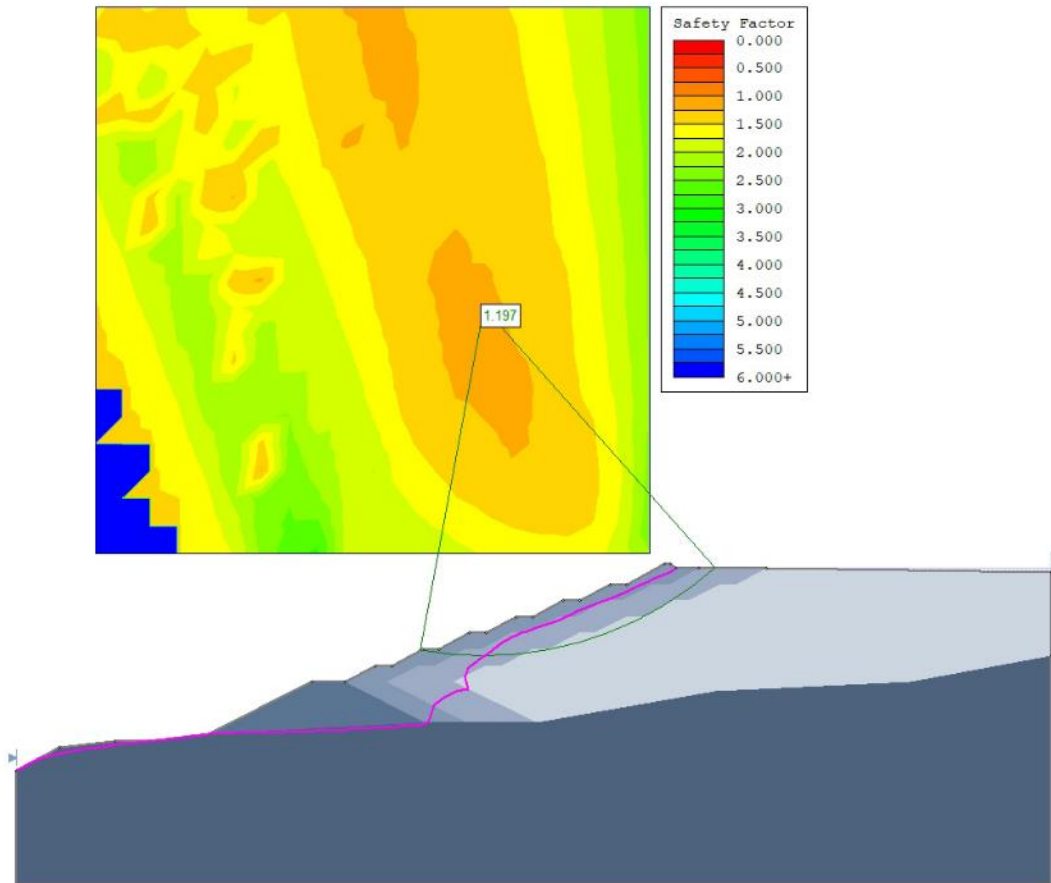


Figure 3 FOS for 2D LEM model

3D approach of modelling tailing dam stability

Planar models greatly simplify the representation of tailing dams, especially in scenarios where the terrain's configuration is a key factor. Complex structures, like the one shown in Figure 1, are inherently three-dimensional problems when evaluating stability due to their complex boundary conditions. The planar representation of such structures overlooks the boundary conditions that are crucial to stability assessments. Consequently, the Factor of Safety (FOS) values calculated using two-dimensional (2D) and three-dimensional (3D) models show significant differences.

To assess the stability of tailing dams, available 3D tools rely on stress-strain analysis using finite element method (FEM) and 3D limit equilibrium. This discussion covers the application of both methods.

3D FEM stability analysis

Rocscience RS3 (Rocscience, 2023) offers an outstanding tool for three-dimensional stress-strain analysis using the finite element method, and it is showcased to demonstrate its capabilities in evaluating the stability of tailing dams, as depicted in Figure 1. The model is constructed and illustrated in Figure 4, with the hatched area indicating the critical position of the water level within the pond, or scenarios where the water level reaches the dam itself. This step also establishes the boundary conditions necessary for calculating the pore pressure distribution within the model. Figure 5 displays the model's discretization along with its mechanical boundary conditions.

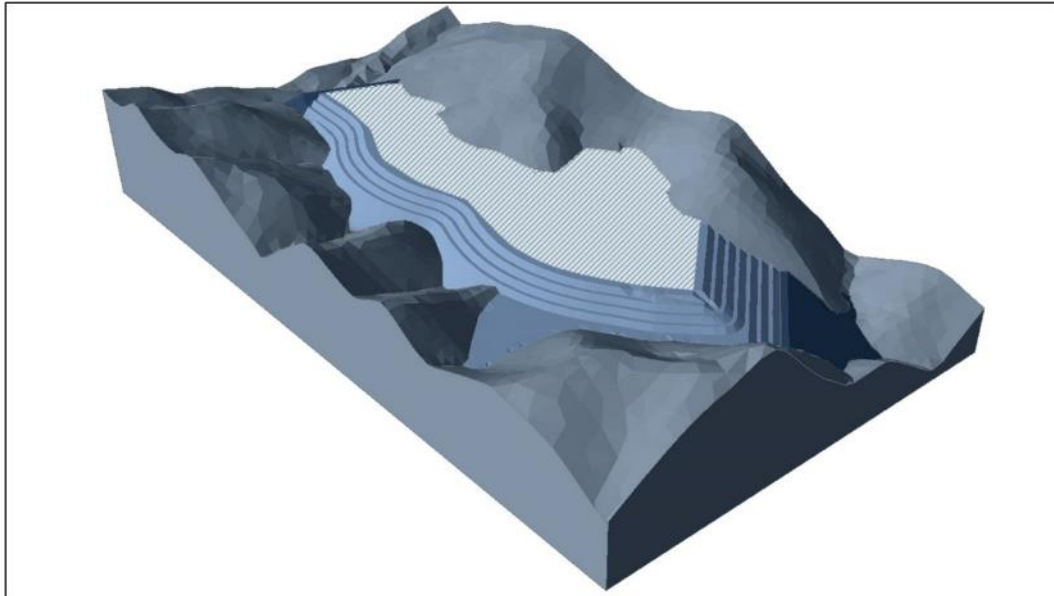


Figure 4 3D finite element model

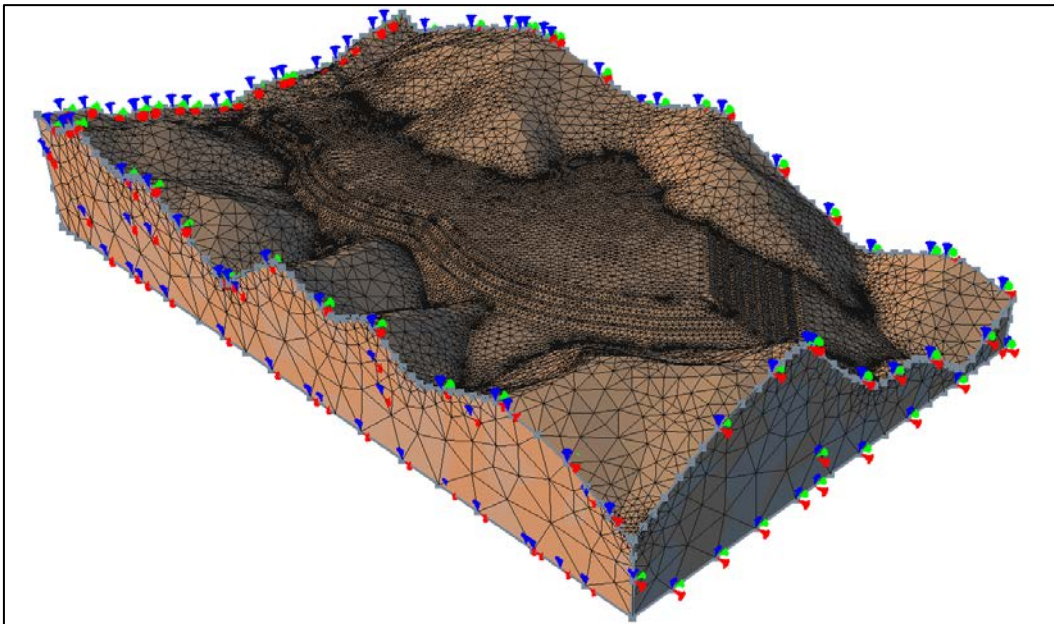


Figure 5 3D finite element mesh and boundary conditions

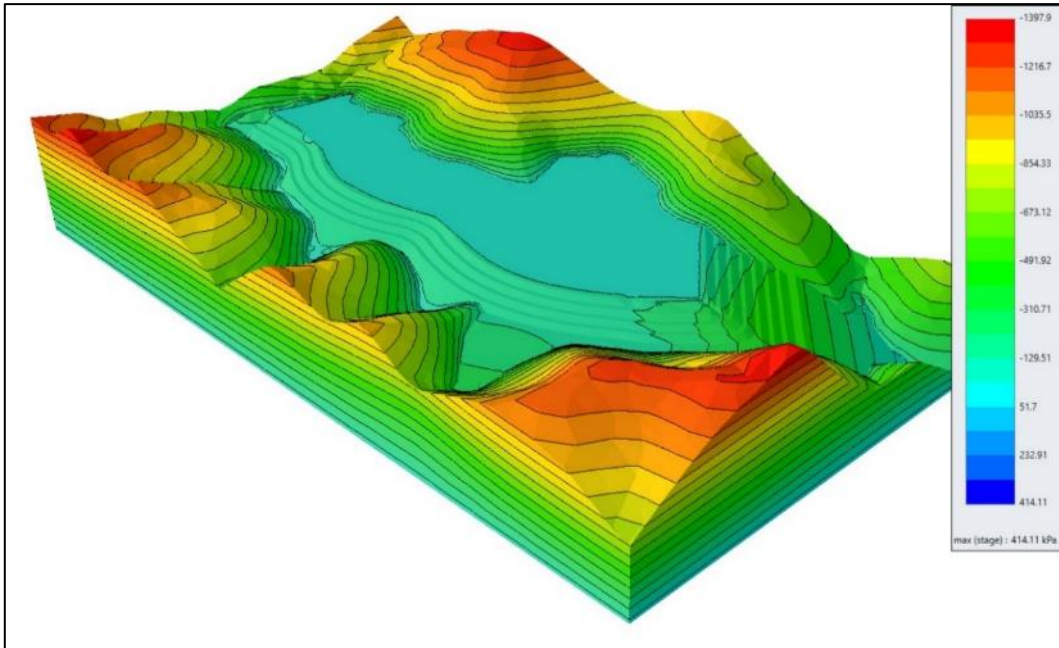


Figure 6 Pore pressure distribution within the model

Following the establishment of the model's geometry and the definition of boundary conditions for mechanical analysis, the strength reduction procedure also includes defining water level conditions. This is essential for determining the spatial distribution of pore pressure within the tailing dam and the pond. The first step involves presenting the pore pressure distributions, as shown in Figure 6.

The distribution of pore pressure is affected by both the construction of the tailing dam and the configuration of the surrounding terrain. Knowing the groundwater level within the surrounding rock mass enables the assessment of how water from the rock mass and the pond will interact, from an environmental perspective.

The main method used to determine the Factor of Safety (FOS) is strength reduction, and the results shown in Figure 7 highlight a clear distinction in areas where zones of increased displacements may occur, illustrating the shape of the failure body. In this case, the critical FOS is 2.25, which is significantly higher than the FOS value determined by 2D analysis. The primary reason for this difference is the boundary conditions; in 3D models, there is significantly higher resistance. This effect is particularly pronounced in constructions with irregular dam shapes, as demonstrated by the example provided.

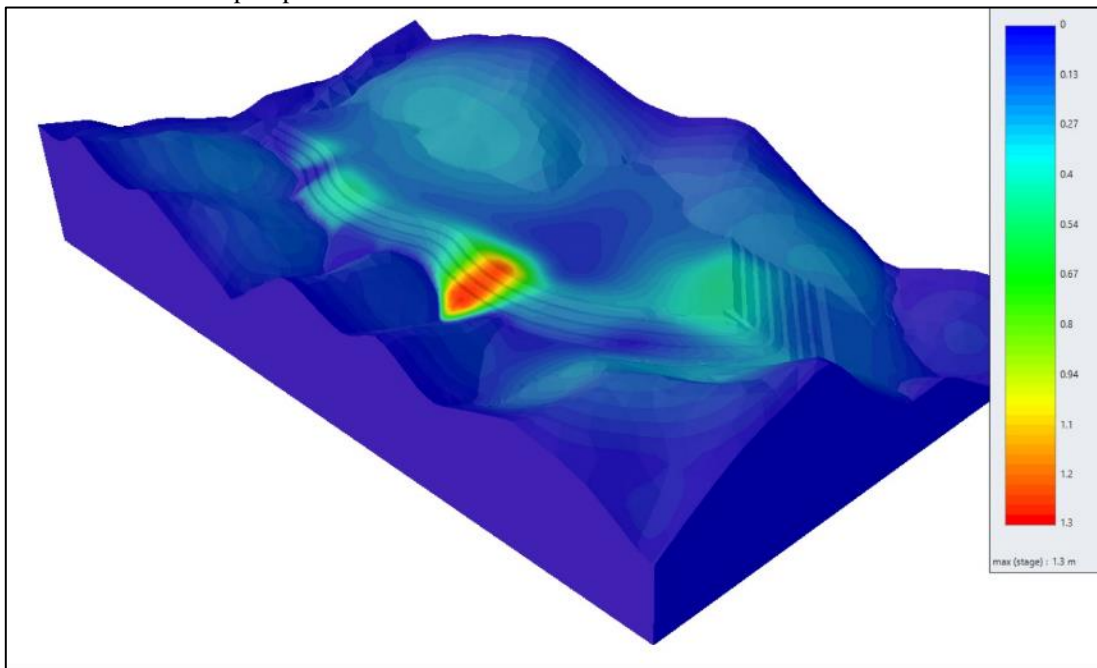


Figure 7 Resulting displacements after strength reduction procedure

In addition to identifying the critical failure body, it is observed that other locations within the model also exhibit increased displacements. Although these areas do not undergo progressive failure, it is beneficial to recognize them as potential risks. Evaluating these areas separately during the design and production phases is crucial for a comprehensive risk assessment.

3D limit equilibrium analysis

The analysis was conducted on the same geometry used for Finite Element Method (FEM) analysis, utilizing the Slide3 package (Rocscience, 2023). These software packages are compatible, allowing for the exchange of model files between them. However, a limitation of Slide 3 is that pore pressure calculations must be imported from RS3.

Unlike RS3, where the strength reduction procedure identifies the failure body, Slide3 performs a search across the model. It assumes a set of potential failure bodies and evaluates their stability one by one. This search is conducted within the model's boundaries, generating a series of spherical or elliptical surfaces for evaluation. The analysis results, presented in Figure 8, show that the failure body identified as critical corresponds to the one

identified using FEM analysis in terms of position, shape, and dimension. In this case, the Factor of Safety (FOS) is 2.31 (Bishop). The volume of the failure is 90,000 cubic meters, with a smaller body contained within it having a volume of 16,000 cubic meters and a FOS of 1.58.

An important aspect of the limit equilibrium approach is accurately identifying the critical location where failure may occur and conducting an appropriate search. Inadequate searching could result in overlooking potentially unstable locations, thereby increasing the risk of misinterpreting the stability of the entire structure.

3D limit equilibrium analysis often results in higher Factor of Safety (FOS) values compared to the 2D approach. Given that the 3D approach is relatively new, it is prudent to exercise caution in its application until comprehensive validation has been conducted.

The accuracy of the limit equilibrium approach is known to be sensitive to the density of the search network, necessitating extra caution in this area. Gradually increasing the density of the search network is a wise strategy for optimizing computational costs. This principle also applies to Finite Element Method (FEM) analysis, where the size of the elements and the density of the mesh directly affect the accuracy of the results.

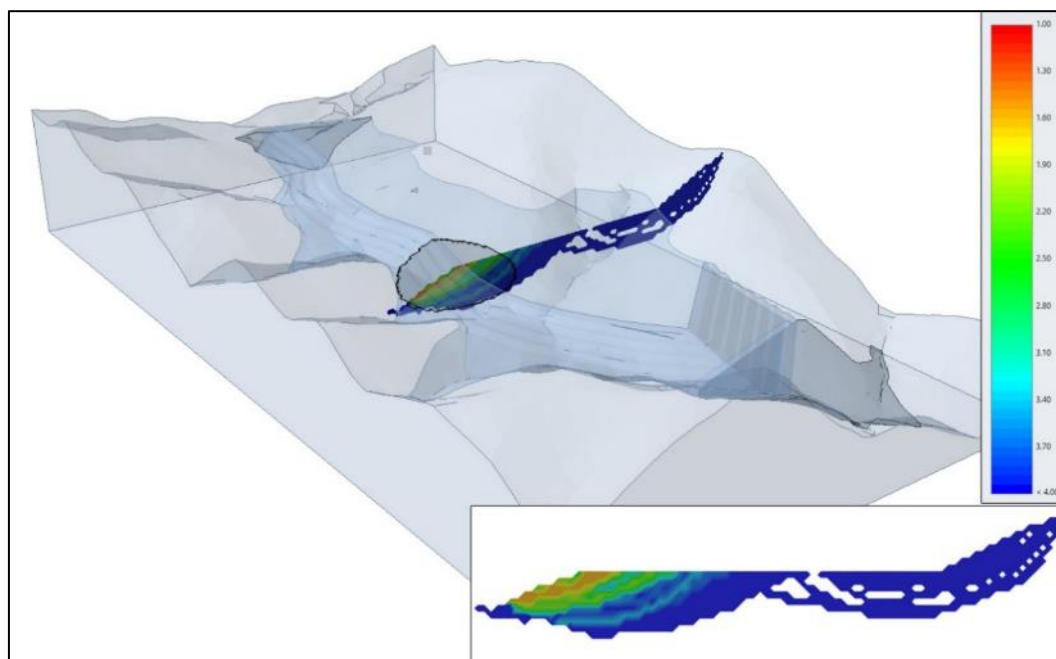


Figure 8 Results of 3D limit equilibrium analysis

Conclusion

Designing and evaluating the stability of tailings dams are critical engineering tasks that require meticulous attention to detail to prevent catastrophic events. The complexity of the design can significantly affect the complexity of the stability evaluation process. In scenarios where the terrain configuration leads to a complex design, only a 3D modeling approach can offer a comprehensive understanding of the structure's mechanical behavior. The 2D approach, on the other hand, necessitates the evaluation of numerous cross-sections. The selection of their locations must be informed by an understanding of the critical points in the design. As a result, there is a risk of overlooking these critical points when choosing a representative cross-section for analysis.

On the other hand, 3D analysis is considerably more complex and requires a significantly longer time for modeling and evaluating results. For instance, preparing the model mesh in the Finite Element Method (FEM) approach can be time-consuming for complex designs. However, once the model is set up, evaluating the critical aspects of the structure's stability becomes straightforward.

This paper demonstrates the application of 3D numerical tools (RS3 and Slide3) and how they can be utilized in the process of identifying critical aspects within the tailings dam. It is evident that the Factor of Safety (FOS) values obtained are significantly higher than those derived from 2D tools, thus highlighting the need for careful consideration before finalizing design decisions.

The typical approach discussed here involves evaluating several cross-sections using 2D models, which requires assuming the location of critical areas. However, if these areas are identified using a 3D approach, they can be further analyzed with 3D tools.

The comparison between the Finite Element Method (FEM) and the Limit Equilibrium Method (LEM) approaches showed that both methods identified the same areas of the structure as critical, with negligible differences.

References

- Duncan, J. Michael, Wright, Stephen G., Brandon, Thomas L., (2014) Soil Strength and Slope Stability. John Wiley & Sons, Inc., Hoboken, New Jersey.
- Morgenstern, N R, Vick, S G, Viotti, C B, Watts, B D, (2016). Fundão Tailings Dam Review Panel, Report on the Immediate Causes of the Failure of the Fundão Dam 25 August 2016. Cleary Gottlieb Steen and Hamilton.
- Rocscience Inc. (2023). RS3 (4.031) [Software]. Available from <https://www.rocscience.com>.
- Rocscience Inc. (2023). Slide2 (9.028) [Software]. Available from <https://www.rocscience.com>.
- Rocscience Inc. (2023). Slide3 (3.022) [Software]. Available from <https://www.rocscience.com>.
- Vick, Steven G., (1990) Analysis of Tailings Dams. BiTech Publishers Ltd.

Digital Twin Concept for the Safe and Economic Design and Management of Rock Slopes

Neil Bar^{(1,2)*}

1) Gecko Geotechnics LLC, Kingstown, Saint Vincent and the Grenadines, neil@geckogeotech.com

2) Budapest University of Technology and Economics, Department of Engineering Geology & Geotechnics, Budapest, Hungary

Abstract Technological improvements including the routine use of aerial photogrammetry, semi-automatic rock mass characterization, three-dimensional slope stability modelling and ground-based radar monitoring (i.e. mapping, modelling and monitoring) can now be rapidly applied to develop a continuously improving digital twin in parallel to a rock slope excavation sequence for civil and mining engineering projects. This is critical for reconciling the effectiveness of geotechnical models for predicting future slope stability (or instability) by reducing uncertainty in ground conditions as excavations progress. This paper presents a framework and case studies to describe the application of a manual digital twin approach with multiple layers of monitoring. Monitoring systems used to manage safety risks were developed in response to uncertainties in ground characterization and limitations in slope stability analysis and design, i.e., to address known or perceived residual risks prior to excavation. Fast data collection and analysis permits comparison of the three-dimensional model with observed slope conditions as a form of reconciliation and allows for critical geological structures to be added to the geotechnical model as excavations progress.

Keywords slope stability, empirical methods, 3D analysis, photogrammetry, monitoring, digital twin

Introduction

Rock slope failures on man-made and natural slopes include slope instability, rock falls and landslides, as well as debris flows and shallow landslides in weathered rock.

Socioeconomic consequences of rock slope failures include direct costs such as removing the failed rock debris and stabilizing the slope, and a wide range of indirect costs. Indirect costs may include:

- Civil engineering: potential losses of life, damage to vehicles and injury to passengers on highways and railways, traffic delays, business disruptions, loss of tax revenue due to decreased land values, and flooding and disruption of water supplies where rivers are blocked by slides
- Mining engineering: potential losses of life, damage to mining equipment and injury to mine personnel, mine production delays, impairment or sterilization of

mineral resources, reputational damage, and mine or mining company closure.

Between 2004 and 2016, a total of 55,997 fatalities were recorded globally from 4,862 individual, non-seismic slope failures including landslides (Froude and Petley, 2018). Slope failure occurrence triggered by human activity such as construction, illegal mining and hill cutting is increasing. Froude and Petley (2018) identified that the majority of landslides that were not initiated by rainfall or earthquakes, were triggered by human activity such as:

- Mining (232 multi-fatality; 67 single fatality events)
- Construction (170 multi-fatality events; 140 single fatality events)
- Illegal hill cutting (60 multi-fatality events; 27 single fatality events).

In both civil and mining engineering projects, it is practically impossible to assess the stability of rock slope cuttings and benches in real-time, using analytical approaches such as kinematics, limit equilibrium or FEM/DEM (numerical) modelling. The rate of excavation advance is usually too fast for this.

Since rock slopes are excavated in existing and natural geological formations, which usually have limitations with respect to site investigations, significant uncertainty and variability inevitably exists in the estimation or calculation of resting forces. Uncertainty in slope design primarily stems from the inherent natural variability of ground conditions, i.e. geological and engineering geological uncertainty and anomalies (Hoek and Diederichs, 2006). Figure 1 describes rock slope design uncertainty associated with the geotechnical components and is based on a similar concept for tunnelling scenarios by Paraskevopoulou and Boutsis (2020).

The idea of a “digital twin” was born at NASA in the 1960’s as a “living model” of the Apollo mission (Allen, 2021). In response to Apollo 13’s oxygen tank explosion and subsequent damage to the main engine, NASA employed multiple simulators to evaluate the failure and extended a physical model of the vehicle to include digital components. This “digital twin” was the first of its kind, allowing for a continuous ingestion of data to model the events leading to up to the accident for forensic analysis and exploration of next steps. A digital twin can simply be described as ‘the simulation of the physical object itself to predict future states of the system’ (Gabor et al. 2016).

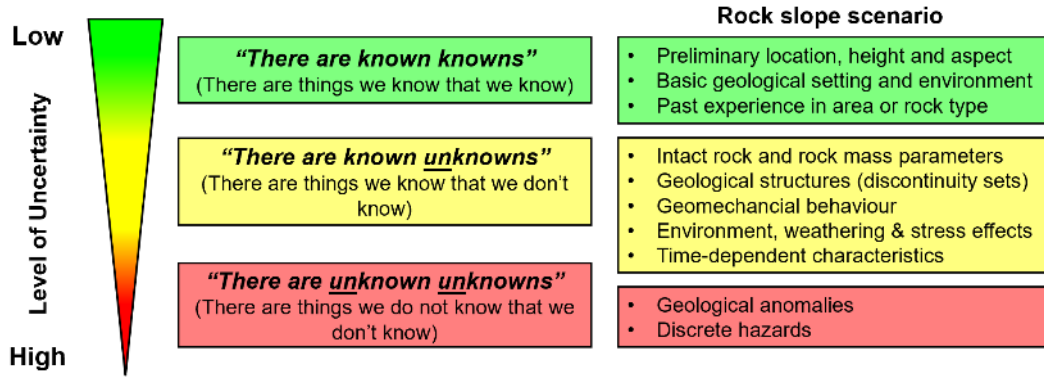


Figure 1 Design uncertainty in association with the geotechnical engineering components for a rock slope scenario

Continuous technological improvements for mapping including aerial photogrammetry and laser scanning, modelling (faster 3D analysis techniques) and monitoring (e.g. satellite InSAR and ground-based radar) facilitate the development and routine updating of digital twin models for rock slope stability (Bautista et al. 2023). As excavations progress and geological and geotechnical data becomes available, digital twin models are updated to reduce uncertainty and improve design reliability.

This paper discusses the key elements required for developing and applying a digital twin approach for the design and management of rock slopes.

Frameworks for the Design of Rock Slopes

Rock slope design has been considered an iterative process in civil and mining engineering projects for 50 years since Hoek and Londe (1974) developed the closed-loop framework shown in Figure 2.

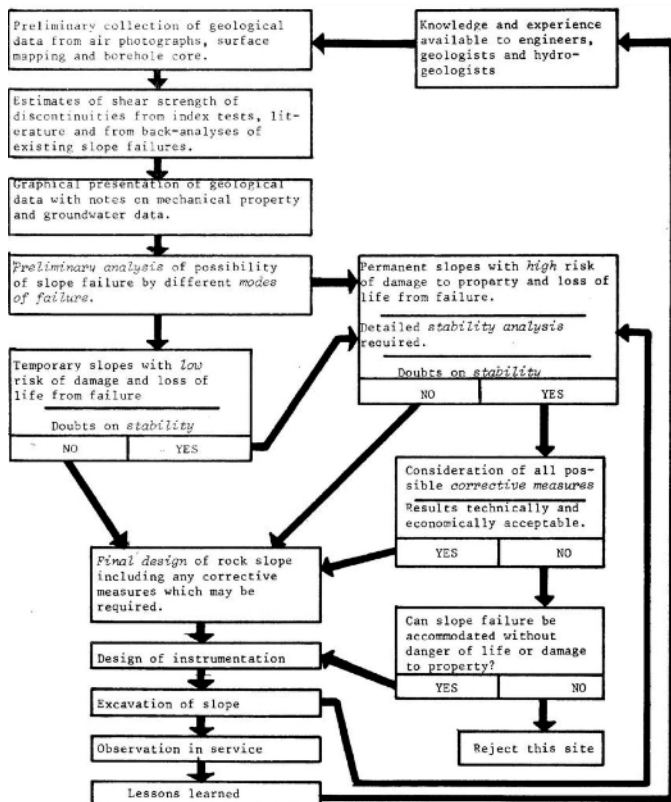


Figure 2 Rock slope design flow chart (Hoek and Londe, 1974)

The flow chart in Figure 2 has a robust initial design process, which is followed by monitoring and observing slope performance during excavation, and feeding back observations, lessons learned and new data into improving the design. Similar frameworks for the design of rock slopes have been adopted in civil and mining engineering with guidance provided by Wyllie and Mah (2004).

In the late 2000's, divergence occurred between rock slope design in civil and mining engineering applications with the development of guidelines for open pit slope design (Read and Stacey, 2009) as part of the mining industry funded LOP Project. This was followed by an update to rock slope engineering guidance for civil engineering applications by Wyllie (2018).

The resultant slope design process in Figure 3 for open pits by Read and Stacey (2009) includes an iterative process for considering mine planning and risk evaluation prior to excavation. However, unlike its predecessors, Figure 3, does not have a clear feedback loop for improving and optimizing the design based on monitoring, new data, slope performance, etc.

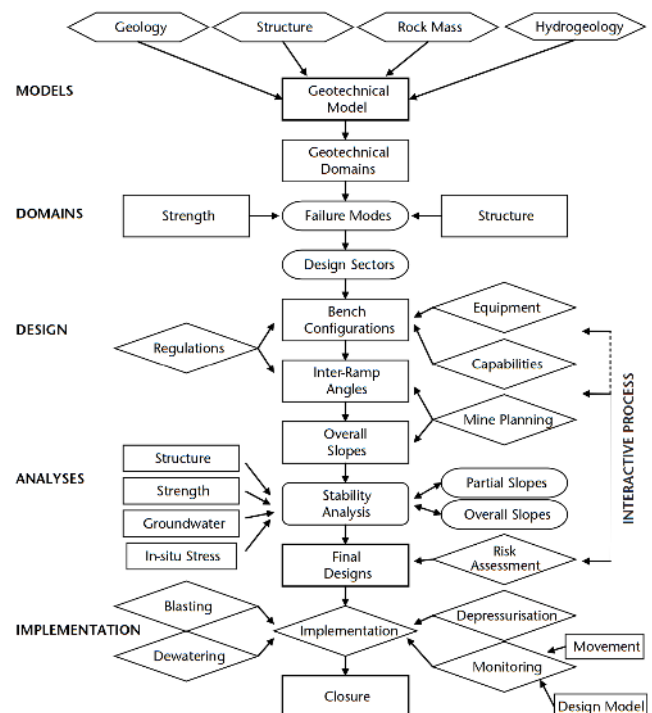


Figure 3 Open pit slope design process (Read and Stacey, 2009)

Rock slope design and management in civil and mining engineering applications are quite different in terms of:

- The design life of a civil engineering slope could be in excess of 100 years, whilst a slope in an open pit mine could range from a few months to a year or two in the case of individual benches and inter-ramp slopes, to several years for larger slopes.
- Risk exposure in civil engineering slopes involves the public (e.g. several thousands of people or more per day on roads, highways and railways) with very little or no access control and without routine monitoring instrumentation. In open pit mining, access is strictly controlled (e.g. typically less than 100 mine workers per day) with several options for additional control measures including monitoring instrumentation.
- Prior to design, site investigations for civil engineering slopes may be limited to outcrop mapping and little or no drilling for understanding subsurface conditions. On the contrary, mineral deposits are extensively drilled to understand the economical feasibility of deposit extraction. Arguably there should be a lower level of uncertainty in a mining engineering project than in civil engineering; however, geological and geotechnical conditions around a mining project are often significantly more complex.

Despite the abovementioned differences, uncertainty related risks described in Figure 1 effect the safe and economic design and management of rock slopes in both civil and mining engineering projects in a similar manner.

By adopting the framework for slope design and management in Figure 4, uncertainty and risk can be reduced and proactively managed through a continuous improvement process that manages safety and has capacity to optimize slope design to add economic value.



Figure 4 Continuous Improvement Framework for Safe and Economic Rock Slope Design and Management

The continuous improvement framework in Figure 4 can be incorporated into a Ground Control Management Plan (GCMP) or Slope Management Plan (SMP) with detailed processes for each component. By way of example, various elements of the ‘Geotechnical Model’ could be described in further detail, as could the process for their development and their limitations:

- Lithological, weathering and alteration model
- Structural model (major, medium and minor)
- Rock mass model
- Groundwater (pore pressure) model.

Understanding the limitations of a geotechnical model and rock slope design can be used to define the risks.

Hazard and Risk Definition

Ground failure and fall of ground are terms used to generalize various geotechnical hazards in surface mines, including (Bar et al. 2022):

- Rock slope failure: sub-bench, bench scale and larger failures, landslides, etc. (e.g. plane failure, wedge, toppling, step-path or complex failure mechanism, etc.).
- Rock fall: single or multiple rocks or boulders moving down a slope.

For rock slopes, the above hazards are associated with safety (public or mining), economic, environmental and reputational risks.

Risk Management Framework

Critical control measures are the equipment, systems, procedures, and policies that an organization uses to prevent injuries and death (Ross, 2017).

Figure 5 presents a framework of five critical control measures that can be used for managing fall of ground risks (Bar et al. 2022).



Figure 5 Fall of Ground Risk Management Critical Control Measures

Critical Control Measures

The use of multiple control measures provides redundancy for ensuring safety in the event that one control measure becomes ineffective, safety is maintained through the others.

By implementing the five critical control measures in Figure 5 as part of a GCMP or SMP, the continuous improvement framework for the safe and economic design and management of rock slopes (Figure 4) is followed during excavation.

Rock fall risks can be managed using Safe Operating Practices and Design Execution. By way of example, prescribed standoff distances may be used for personnel on foot to reduce their exposure to rock fall risks, and rock slopes can be excavated and scaled to remove loose rocks and debris that have a potential to fall (Bar et al. 2022).

Rock slope failure safety risks are managed through a combination of Slope Monitoring and Response using instrumentation such as radar and prisms to identify instabilities and remove personnel from the line-of-fire prior to collapse (Bar et al. 2022). Geotechnical Design and Reconciliation, and Water Management also contribute significantly by reducing the likelihood of failure.

Economic risks associated with rock slope failures are primarily reduced by Geotechnical Design and Reconciliation, which requires the use of the continuous improvement framework in Figure 4. This process helps reduce uncertainty in the geotechnical model and better understand potential failure modes as study phases and excavations progress. Water Management to enable and maintain slope depressurization assists in improving stability and facilitates slope optimization in wet climates and below the water table.

Failure Modes

Rock slope failures are rarely circular, spherical or ellipsoidal. In a recent review of over 500 rock slope failures in open pit mines, rock mass and circular failure modes accounted for only 10% and 8% of the database, respectively (McQuillan and Bar, 2024). The vast majority and remaining 82% were structurally-driven failures such as planar, wedge, toppling or step-path mechanisms.

For the design of rock slopes, it is critical to ensure that reasonable failure modes are investigated based on the geotechnical model. Quite simply, assessing for rotational (circular or near-circular) failure modes is considered inadequate in the context of real world, physical outcomes.

Since most failure modes in rock slopes are structurally-driven and may involve one or more geological faults or other persistent singularities, which are almost certainly oblique (i.e. not perfectly parallel) to the slope, stability should be assessed in three dimensions (3D). Rock slope failure modes should be assessed using 3D analysis method in a geotechnical design review process in the case of any of the following conditions (McQuillan and Bar, 2023):

- Non-linear slope geometry.
- Spatially or laterally varying geological and hydrogeological conditions.
- Spatially varying material strengths, including anisotropic material behaviour in the same unit.
- Singularities and persistent geological structures, striking and intersecting up to 50° from the slope orientation.
- Highly variable 2D results within close spatial proximity to each other.

Digital Twin Processes

The continuous improvement framework in Figure 4 is compatible with the digital twin concept; where input parameters (e.g. geotechnical model) are routinely updated as additional information becomes available during design stages.

Assessing rock slope failure modes, stability analysis and design using a digital twin can be undertaken using different levels of complexity from empirical methods to analytical approaches and numerical models.

Empirical Methods

Empirical methods can be used to evaluate the stability of excavations at the rate of excavation.

Methods such as slope mass rating, SMR (Romana, 1985; 1995), and Q-slope (Bar and Barton, 2017) can be used to quickly assess the stability and expected performance of slopes and provide advice on appropriate slope angles using design charts.

When geo-referenced, these empirical methods can serve as rudimentary digital twins, which can be updated several times per day as excavations progress.

Analytical and Numerical Methods

Compared with empirical methods, analytical and numerical approaches require more time for data collection, analysis & interpretation (site investigations), geotechnical model updates (e.g. developing wireframes for new geological faults) and 3D slope stability analysis.

Aerial photogrammetry and laser scanning have a pivotal role in large area rapid data collection for understanding geological structure and its potential impact on slope stability. Bar et al (2020) and Bautista et al (2023) demonstrate how aerial photogrammetry can be used to update a structural model for major and medium faults in a local area in less than a day, i.e. enabling a geotechnical model and 3D slope stability analysis update immediately thereafter.

Similarly, slope deformation monitoring data showing unexpected movements can be used to initiate a geotechnical model update and review of 3D slope stability analyses (Bautista et al 2023), i.e. initiate a digital twin update following the continuous improvement framework in Figure 4.

3D Slope Stability Models – Basis of Digital Twin

A 3D slope stability model can be considered the basis of a modern digital twin, or as the simulation of the physical rock slope in a mining or civil engineering excavation and its future state. Commonly used 3D stability analysis approaches include limit equilibrium method (LEM), finite element method (FEM), finite difference method (FDM) and distinct element method (DEM).

Planning Long-Term Excavations – Hazard Identification

A large coal mine in the Americas that operates multiple open pits simultaneously was planning an expansion of one of these pits, which was 3 x 4.5 km in size with pit slope heights reaching 300 m. These pits exploit over 50 individual coal seams within an interbedded stratigraphical sequence comprising sandstone, siltstone and claystone.

Table 1 presents material properties adopted for the 3D LEM models using Slide3 software (Figure 6). The rock mass and defect properties are well understood after several decades of site investigations, previous 2D LEM analyses and mining activities. The rock masses are moderately anisotropic with an anisotropy index (R_c) ranging from 3 to 4 (Ramamurthy, 1993). Directionally dependent shear strengths were applied to account for the anisotropy formed by continuous bedding planes as described by Bar and Weekes (2017). For 3D LEM analysis, a linear transition from bedding to rock mass shear

strength was applied with parameters A and B set to 15° and 30°, respectively (i.e. the 3D LEM model applies bedding shear strengths within 15° of the bedding plane orientation, and then linearly transitions to rock mass strength).

The structural geology is quite simple with minor folding of the stratigraphic sequence. Despite the simplicity, shears have developed on the contacts of the coal and its adjacent units as a result of folding. These shears present themselves in the form of thin, very weak clay seams. These are considered in the slope stability models as weak layers or interfaces.

The groundwater model was developed based on vibrating wire piezometers (VWPs). It assumes a 3D phreatic surface equal to the ground or excavation surface and uses H_u coefficients to assign pore pressures to match actual data observed in the VWPs.

The 3D LEM model was tested on existing slopes and predicted two multi-bench failures as shown in Figure 7. The upper modelled failure had actually occurred and was identified with the radar, whilst the lower had not occurred, indicating a reasonable model output with potential for some degree of conservatism.

The 3D LEM models were used to forecast stability conditions for the life-of-mine (long-term excavations) design considering the excavation sequence at different time steps to identify potential hazards and their significance as shown in Figure 8.

Table 1 Rock Mass, Defect and Pore Pressure Properties for coal mine

Material	γ kN/m ³	UCS MPa	Rock Mass			Discontinuity		Anisotropy			Groundwater H_u
			GSI	m_i	D	c' kPa	ϕ' °	R_c	A	B	
Sandstone	25	27	60	13	0 - 0.7	0	27	4.0	15	30	0.79 - 0.88
Siltstone	24	13	51	11	0 - 0.7	0	21	3.1	15	30	0.79 - 0.88
Claystone/Shale	24	10	46	7	0 - 0.7	0	15	3.5	15	30	0.79 - 0.88
Coal	14	15	51	16	0 - 0.7	0	23	3.0	15	30	0.79 - 0.88
Clay Seam	-	-	-	-	-	10	15	-	-	-	0.85 - 1.00
Fault Zone	20	-	-	-	-	20	22	-	-	-	0.85 - 1.00

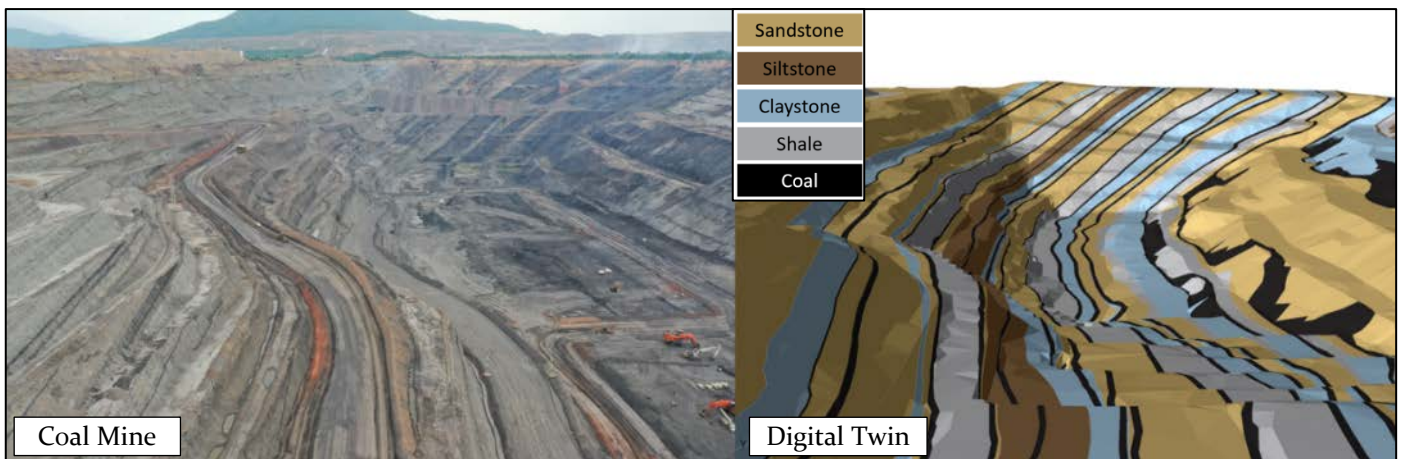


Figure 6 Photograph of coal mine slopes (reality) versus 3D LE model geometry developed in Slide3 software (digital twin) by Rocscience Inc (note: phreatic surface and clay seam interfaces not shown for clarity).

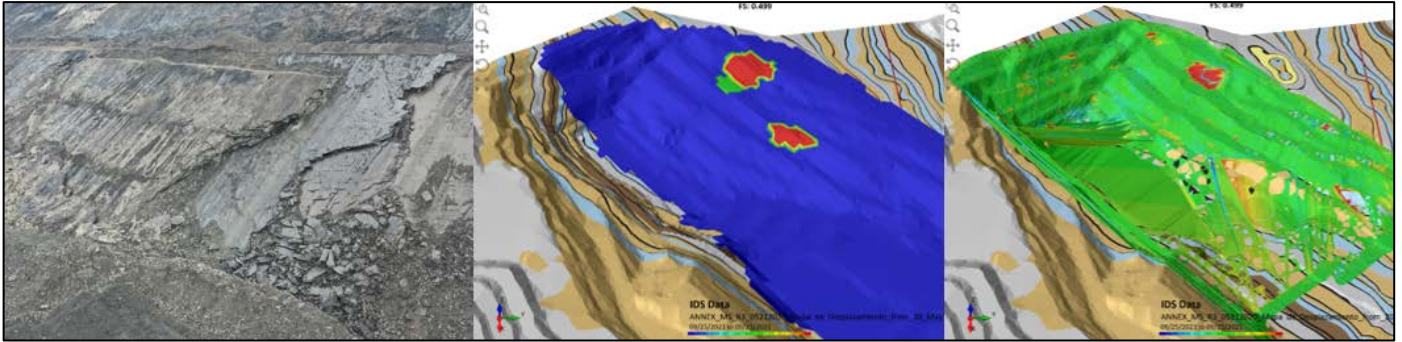


Figure 7 Left to right: Photograph of 30m high failure; 3D LE model outputs (Factor of Safety map: red indicates $FoS < 1$): two multi-bench failures; IDS radar data showing the deformation hotspot associated with the failure in the photograph.

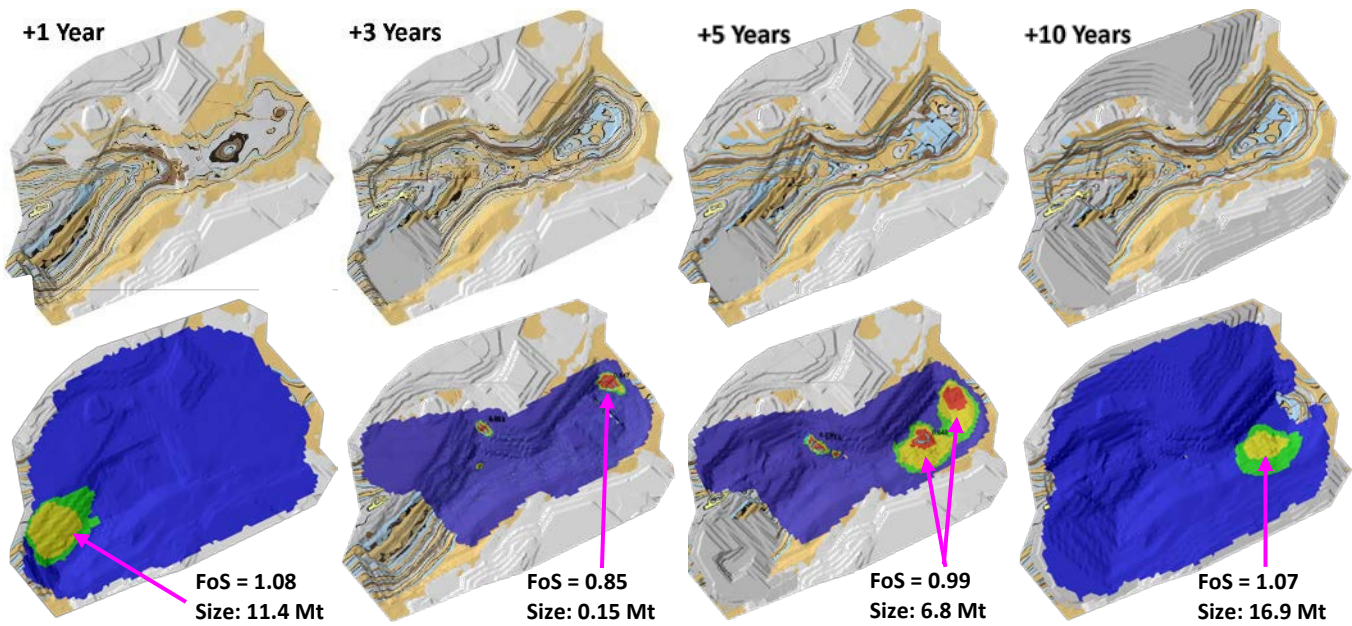


Figure 8 Top: Mine design time horizons with pit progressing from west to east, dumps enlarging and an in-pit dump being constructed. Bottom: Lowest FoS areas and size of modelled failure mechanisms.

For the near future, 1 to 3 years, a relatively large volume low FoS area ($FoS \approx 1.1$) was identified as well as a few small volume potential failures ($FoS < 1$). These risks can be managed either through minor design changes, which will result in reduced coal recovery, or risk acceptance and the use of the monitoring and response control measure to continue as planned.

Later in the mine plan, between 3 and 10 years, significantly larger failure volumes were identified ($FoS < 1$). Such failures (>6 million tonnes) would have significant consequences that are likely to impact the economic feasibility of the pit and need to be managed through design (e.g. shallower slope through unloading and additional overburden removal, or a step-in and loss in coal recovery). However, since these risks are several years away, there is time available for additional site investigations and analysis to further refine the geotechnical model and minimize the impacts of the design changes.

Assessing Optionality – Risk versus Reward

A large gold mine in the Americas that operates a single, large open pit, which is 3 x 2 km in size with pit slopes reaching 300 m. The pit is hosted within highly anisotropic and weak Carbonaceous Sediments, which overly various, relatively isotropic volcanic and volcanoclastic rocks.

The Carbonaceous Sediments are up to 100 m thick in the upper portion of the slope and have been host to several ductile slope instabilities, generally involving sliding on bedding planes and sub-parallel faults.

Several of the instabilities within the Carbonaceous Sediments have been back analysed using 3D LEM, FEM and FDM models to derive and calibrate material properties shown in Table 2.

3D LEM models were used as a digital twin due to their ease of updating for the purpose of assessing optionality. Future slope designs with different inter-ramp slope angles (IRA) ranging from 16 to 33° for the Carbonaceous Sediments were assessed (Figures 9 & 10).

Table 2 Rock Mass, Defect and Pore Pressure Properties for gold mine

Material	Rock Mass					Discontinuity		Anisotropy			Groundwater H _u
	γ kN/m ³	UCS MPa	GSI	m _i	D	c' kPa	φ' °	R _c	A	B	
Carbonaceous Sediments	26 - 27	<10 - 18	35 - 50	8	0 - 0.7	6 - 8	12 - 18	2 - 3	15	30	0.69 - 1.00
Volcanics	27 - 28	30 - 70	50 - 60	10	0 - 0.7	-	-	-	-	-	0.61 - 0.85
Fault Zone	24	-	-	-	-	2 - 7	17 - 24	-	-	-	0.85 - 1.00



Figure 9 Assessing Optionality: Different IRA within Carbonaceous Sediments using simplified slope design geometry

Five 3D LEM models were developed in Slide3 software to assess the stability of each different conceptual IRA slope design within the Carbonaceous Sediments from Figure 9.

Figure 10 presents 3D LEM model results showing FoS (Factor of Safety) and potential failure volumes in Mt (million tonnes). These optionality assessments illustrate potential risks (low FoS) and consequences (failure volumes) which can be used in a semi-quantitative risk assessment.

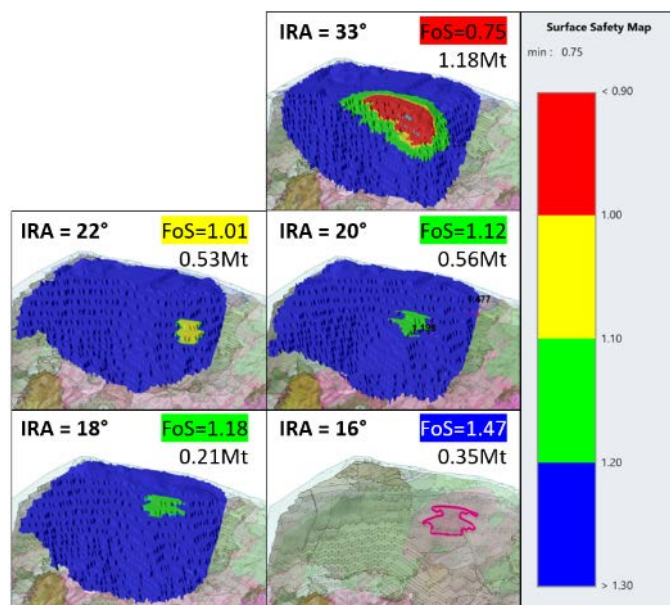


Figure 10 Optionality Assessments of Risk (FoS and Potential Failure Volume) versus Reward (IRA) using 3D LEM (Slide3)

Based on the optionality assessments in Figure 10, a slope design may be chosen based on the risk appetite of the project, and the availability and robustness of critical

control measures (Figure 5) required to manage potential safety and economic consequences.

Hazard Management – Slope Depressurization

A large copper mine in Central Asia that operates a single, large open pit, which is 2.5 x 2 km in size with pit slope heights reaching 400 m.

The pit is hosted in relatively isotropic intrusive and volcanic rocks; however, it has a series of persistent fault sets as shown in Figure 11. These fault sets, in combination with pore pressure have the potential to form unstable wedges that can impact inter-ramp slopes on future pit stages.

3D LEM models were used as a digital twin to understand potential failure mechanisms and the impact of pore pressure on slope stability for future design stages (Bar and Zlobin, 2024). The 3D LEM models were also validated using 3D FEM (RS3 software by Rocscience) to check for complex failure mechanisms, including toppling associated with some of the fault sets.

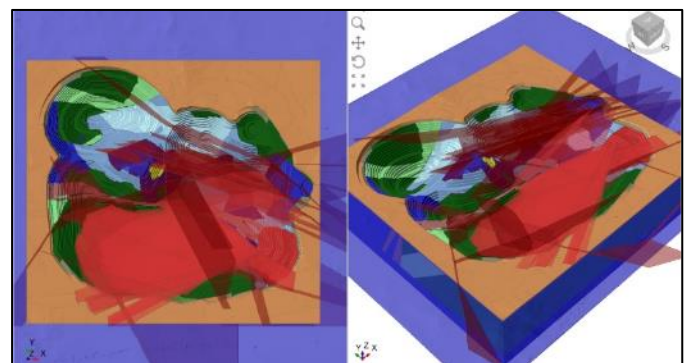


Figure 11 Geological faults (red) intersect pit slopes and groundwater table (blue) in 3D LEM model (Slide3)

Figure 12 identifies three wedges with a low FoS (<1) using 3D LEM for the future south wall under current pore pressure conditions, which are understood from a network of VWP (vibrating wire piezometers). Currently the slopes are not actively dewatered or depressurised, i.e. water reporting to the bottom of the pit is captured in sumps and pumped out.

With a 25% reduction in pore pressure, which can be achieved through either targeted horizontal drains, vertical pumping wells, or a combination of both; Figure 13 demonstrates a significant improvement in FoS whereby two of the three wedges are stabilized. These negate the need for a shallower slope angle, which would result in significant additional excavation costs.

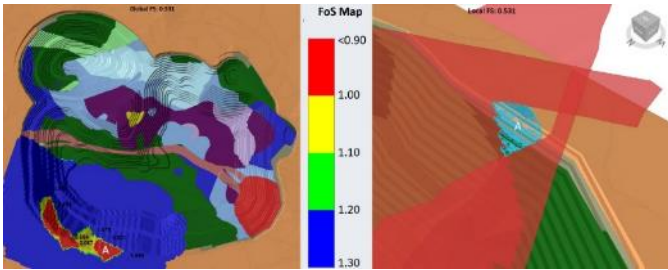


Figure 12 3D LEM model identifying 3 wedges on future south wall with $FoS < 1.0$ with current pore pressure conditions.

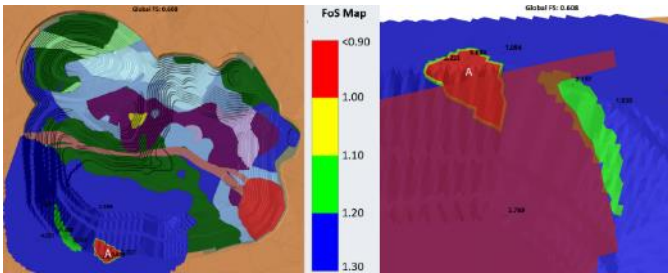


Figure 13 3D LEM model identifying only 2 wedges with improved FoS on future south wall with 25% reduction in pore pressure

A 3D FEM model was utilized to validate the failure mechanisms identified by 3D LEM, and confirmed the wedge risk on the south wall as shown in Figure 14. It also identified a ductile deformation with movement upward along faults on the central north slope in response to unloading from excavation. No toppling mechanisms were identified elsewhere in the proposed slope design.

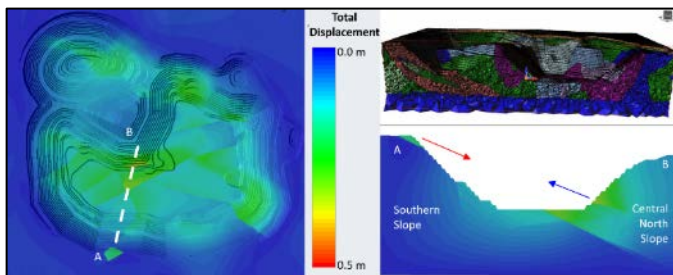


Figure 14 3D FEM model validating wedge mechanism on future south wall from 3D LEM models (Bar & Zlobin, 2024).

Key Findings and Future Developments

Rock slopes can be managed safely and excavation costs can be optimized by adopting a framework with multiple critical control measures as well as a digital twin to continuously improve the design as ground conditions become apparent.

The use of digital twins, particularly combining both empirical and analytical and numerical methods, facilitates the routine application of processes to reduce uncertainty in rock slope engineering. It also helps identify and manage many (but possibly not all) ‘unknown unknowns’ (geological anomalies or discrete geological faults – e.g. non-daylighting faults). The digital twin process can incorporate:

- Mapping: acquisition and analysis of structures mapped from in-pit face mapping, laser scanning and aerial photogrammetry as excavations progress.
- Modelling: the basis of a digital twin: developing and updating of three-dimensional LEM, FEM, FDM or DEM slope stability models to predict and reconcile slope performance.
- Monitoring: acquisition and review of real time, ground-based, interferometric synthetic aperture radar (Gb-InSAR) with full pit coverage for safety and model validation.

Depending on resourcing for a project, digital twins can be updated for various time horizons including long-term designs (life-of-mine, or life-of-project), individual pushbacks, 2-year plans and even quarterly plans for large open pit mines.

In its current form the digital twin process remains a relatively manual process; however, it is envisaged with ongoing improvements in technology and software integration, the digital twin process for rock slope design and risk management will be automated by 2030.

The use of a digital twin concept for the safe and economic design and management of rock slopes should see a return to similar practices in civil and mining engineering applications.

Acknowledgements

The author would like to acknowledge Dr Alison McQuillan, Mr Geoffrey Weekes, Mr Phil de Graaf, Dr Reginald Hammah, Dr Thamer Yacoub, Dr Andreas Gaich, Dr Markus Pötsch, Dr Niccolò Coli, Mr Juan Carlos Cobián, Mr Marco Arrieta, Dr German Zlobin, Mr Nurk Teleu and Mr Bayuprima Adiyansyah for their collaboration on various projects pertaining to 3D rock slope appraisal and digital twin development.

References

- Allen, B.D. (2021) Digital Twins and Living Models at NASA. Proceedings of the ASME Digital Twin Summit, 3-4 November 2021, Online, 40p.
- Bar, N., Cobián, J.C., Bautista, M., Mojica, B., Coli, N., Preston, C., Ribeiro, R., Bueno, G. and Lopes, L. (2022) Brittle and Ductile Slope Failure Management. Proceedings of Slope Stability 2022, 17-21 October 2022, Tucson, United States of America, 17p.
- Bar, N. and Barton, N. (2017) The Q-slope method for rock slope engineering. *Rock Mechanics and Rock Engineering*. 50(12): 3307-332.
- Bar, N., Kostadinovski, M., Tucker, M., Byng, G., Rachmatullah, R., Maldonado, A., Pötsch, M., Gaich, A., McQuillan, A. and Yacoub, T. (2020) Rapid and robust slope failure appraisal using aerial photogrammetry and 3D slope stability models. *International Journal of Mining Science and Technology*. 30: 651-658.
- Bautista, M., Cobián, J.C., López, J., Bar, N., Coli, N., Coppi, F., Gaich, A., Pötsch, M., Baumgartner, M. and McQuillan, A. (2023) Developing a Digital Twin: A Semi-Brittle Slope Failure Case Study from Pueblo Viejo Gold Mine. Proceedings of the 15th ISRM Congress 2023 and 72nd Geomechanics Colloquium, 9-14 October 2023. Salzburg, Austria. pp. 2874-2879.
- Bar, N. and Weekes, G. (2017) Directional shear strength models in 2D and 3D limit equilibrium analyses to assess the stability of anisotropic rock slopes in the Pilbara Region of Western Australia. *Australian Geomechanics Journal*. 52(4): 91-104.
- Bar, N. and Zlobin, G. (2024) Geotechnical design of slopes and risk control in Aktogay open pit mine (ГЕОТЕХНИЧЕСКОЕ ПРОЕКТИРОВАНИЕ ОТКОСОВ КАРЬЕРА «АКТОГАЙ» (КАЗАХСТАН) И УПРАВЛЕНИЕ РИСКАМИ). In Russian. *Gornyi Zhurnal*. 2024(1): 89-94.
- Froude, M.J. and Petley, D.N. (2018) Global fatal landslide occurrence from 2004 to 2016. *Natural Hazards and Earth System Sciences*. 18(8): 2161–2181.
- Gabor, L., Belzner, M., Kiermeier, M.T., Beck, A. and Neitz, A. (2016) A Simulation-Based Architecture for Smart Cyber-Physical Systems. Proceedings of the 2016 IEEE International Conference on Autonomic Computing (ICAC), 17-22 July 2016, Würzburg, Germany. pp. 374-379.
- Hoek, E. and Diederichs, M.S. (2006) Empirical estimation of rock mass modulus. *International Journal of Rock Mechanics and Mining Sciences*. 43(2): 203-215.
- Hoek, E. and Londe, P. (1974) The design of Rock Slopes and Foundations. General Report for the Third Congress of the International Society for Rock Mechanics, Denver, United States of America, 78p.
- McQuillan, A. and Bar, N. (2023) The necessity of 3D analysis for open-pit rock slope stability studies: Theory and practice. *Journal of the Southern African Institute of Mining and Metallurgy*. 123(2): 63-70.
- McQuillan, A. and Bar, N. (2024) Forecasting Open Pit Slope Failure Runout Distances. *Journal of the Southern African Institute of Mining and Metallurgy*.
- Paraskevopoulou, C. and Boutsis, G. (2020) Cost Overruns in Tunnelling Projects: Investigating the Impact of Geological and Geotechnical Uncertainty Using Case Studies. *Infrastructures*. 5(9): 73.
- Ramamurthy, T. 1993. Strength, Modulus Responses of Anisotropic Rocks. *Comprehensive Rock Engineering*, Volume 1: 313-329.
- Read, J.R.L. and Stacey, P.F. (2009) Guidelines for Open Pit Slope Design. CSIRO Publishing, Collingwood, 511p.
- Romana, M. (1985) New adjustment ratings for application of Bieniawski classification to slopes.. Proceedings of ISRM International Symposium on the Role of Rock Mechanics in Excavations for Mining and Civil Works, Zacatecas Mexico, pp. 49-53.
- Romana, M. (1995) The geomechanical classification SMR for slope correction. Proceedings of the 8th ISRM Congress on Rock Mechanics 3, 25-29 September 1995, Tokyo, Japan. pp. 1085-1092.
- Ross, B. (2017) Rise to the Occasion: Lessons from the Bingham Canyon Manefay Slide. Society for Mining, Metallurgy & Exploration Inc. (SME), Englewood, 369p.
- Wyllie, D.C. (2018) *Rock Slope Engineering Civil Applications*, Fifth Edition. CRC Press, Boca Raton, 620p.
- Wyllie, D.C. and Mah, C.W. (2004) *Rock Slope Engineering Civil and Mining*, Fourth Edition. Spon Press, London, 456p

Interpretation challenges when detecting landslides in flysch environment: examples from visual analysis of LiDAR DTM in the City of Buzet

Petra Jagodnik^{(1)*}, Sanja Bernat Gazibara⁽²⁾, Federica Fiorucci⁽³⁾, Michele Santangelo⁽³⁾

1) University of Rijeka, Faculty of Civil Engineering, Rijeka, Radmile Matejčić 3, Croatia, +38551265959 (petra.jagodnik@gradri.uniri.hr)

2) University of Zagreb, Faculty of Mining, Geology and Petroleum Engineering, Zagreb, Croatia

3) Research Institute for Geo-Hydrological Protection, Perugia, Italy

Abstract This paper presents examples of interpretation challenges in unambiguous landslide detection arising from the visual interpretation of 0.3 m LiDAR DTM in the City of Buzet (20 km²), Croatia. The study area is within the Istrian Flysch, for which the large-scale geomorphological landslide inventory mapping was performed for the first time. First, we present distinctive concave forms detected along the hillslopes and discuss whether they represent landslides or not. Furthermore, we present examples of the geomorphological convergence between the landslides and erosional features formed along gully channel walls. Finally, we show examples of Badlands topography on LiDAR DTM derivatives and point to the similarity of these phenomena with landslide features.

Keywords landslide detection, visual interpretation, LiDAR DTM, geomorphological convergence, landslides in flysch, City of Buzet

Introduction

Landslide inventory maps document the extent of landslides in a territory, providing information about the spatial distribution, types, pattern, recurrence and statistics of landslides (Guzzetti et al. 2012). Inventory maps are commonly prepared by the visual interpretation of LiDAR (Light Detection and Ranging) Digital Terrain Model (DTM) morphometric derivatives (Scaioni et al. 2014), especially in area covered by dense forests (e.g., Ardizzone et al. 2007; Van den Eeckhaut et al. 2007; Razak et al. 2011), by detecting the geomorphic expression of landslide features (Soeters and van Westen 1996). Given that landslide inventories are essential input data for subsequent analyses in landslide research, e.g., landscape evolution (Guzzetti et al. 2008; Bibentyo et al. 2024) or susceptibility modelling (van Westen et al. 2006), the quality of the landslide map, controlled by its accuracy and certainty of the presented information, is a critical issue. Accuracy of a landslide inventory depends on geographical and thematic correctness of the information shown on the map, as well as on its completeness, i.e. the proportion of mapped landslides compared to the ground truth (Guzzetti et al. 2012). While geographic accuracy depends on the type and resolution of the interpreted imagery, completeness of the landslide map may strongly vary due

to the interpreter's skills and experience at detection and classification of slope failures.

Distinguishing landslides from other specific geomorphic expressions becomes challenging task even for highly experienced interpreters when mapping is carried out in geologically complex settings, especially if an area is affected by multiple geomorphological processes. In that case, errors in landslide detection may arise either from geomorphologic convergence between landslides and other geological processes (Hart et al. 2012) and certain surface deposits (Antonini et al. 2002), or if the landslide topography has been dismantled (Jagodnik et al. 2020). In terrains characterized by mechanically weak lithology, e.g., siliciclastic rocks, weathering processes and high erodibility of bedrock favor the superimposition of the signature of various denudational forms (Ciccacci et al. 2008).

Most of the landslide research based on the visual interpretation of LiDAR DTM commonly present examples of the typical landslide topography identified on DTM derivatives (e.g. Petschko et al. 2015; Görum 2019). On the other hand, there is a lack of studies focusing on the interpretation difficulties in landslide mapping on LiDAR DTM derivatives. In this paper we present and discuss the challenges in landslide detection and mapping specific for the flysch environment, based on the experience of the visual interpretation of 0.3 m LiDAR DTM in the City of Buzet (Bernat Gazibara et al. 2023; Jagodnik et al. 2023). The study area is terrain in Istrian Flysch, composed of a rhythmical alternation of hemipelagic marls and turbidities (Marinčić et al. 1996). Although landslides frequently occur in the Istrian Flysch (Arbanas et al. 2014), no systematic landslide inventory mapping has been carried out so far. The research was conducted within the frame of scientific research project "Methodology development for landslide susceptibility assessment for land-use planning based on LiDAR technology" (LandSlidePlan, HRZZ IP-2019-04-9900).

Study area

The study area (20 km²) is in the northern Istria, in Croatia. It is the part of the City of Buzet, between the Mirna River Valley in the north and the Butoniga water reservoir in the south (Fig. 1). The terrain predominantly consists of Middle Eocene clastic sedimentary rocks (Fig. 1a), also

known as Istrian Flysch, super-positioned on the Palaeogene *Globigerina* marls, and foraminiferal limestone (Pleničar et al. 1969). Flysch deposits can be stratigraphically divided into the lower and upper units (Marinčić et al. 1996; Bergant et al. 2003). The lower flysch unit is composed of a rhythmical alternation of marls and carbonates (i.e. breccias, conglomerates and bioclastic arenites), while in the upper flysch unit thin layers of carbonate-siliciclastic turbidity sediments are deposited. According to Petrinjak et al. (2021), carbonate megabeds composed of lithoclasts from the underlying limestone can be found in different stratigraphic positions within the flysch succession. The estimated total thickness of Istrian Flysch is 350 m.

averaging 0°C, and no dry season. Mean annual precipitation is 1,200-1,300 mm (Zaninović et al. 2008).

Due to low durability of flysch bedrock (Gulam et al. 2018) and intensive weathering processes (Vivoda Prodan et al. 2017), slopes are typically covered by Quaternary superficial deposits (Dugonjić Jovančević and Arbanas 2012). There is an interplay between mass movements and linear erosion, resulting in numerous active landslides (Arbanas et al. 2014), gullies (Jagodnik et al. 2023), and Badlands (Gulam et al. 2014; Bostjančić et al. 2023). So far, more than 1,100 landslides have been identified in the study area (Jagodnik et al. 2023), and the landslide inventory mapping is still in progress. Landslides mostly occur in gullies and low-order valleys, as well as on terraced hillslopes and slope segments with concentrated surface runoff, e.g. near roads. They are predominantly small to medium-sized debris slides and earth slides, caused by rainfall and/or human activity (Arbanas et al. 2007). Sliding mostly occur along the contacts between superficial deposits and bedrock, or within the weathered flysch (Dugonjić Jovančević and Arbanas 2012). Deep seated landslides were also identified; with certain phenomena being large, very old and relict (Jagodnik et al. 2023).

Landslide inventory map

LiDAR datasets

The LiDAR data used in this study were acquired in the framework of the LandSlidePlan scientific project. Airborne laser scanning was performed in March 2020, at an average altitude of 700 m a.s.l., with an average point density of 16,09 pt./m², thus resulting in average point spacing of 0.18 cm. The classified Point Cloud ground bare-earth points were interpolated using kriging interpolation method, and the DTM was generated at a spatial resolution of 0.3 m.

Visual interpretation of LiDAR DTM derivatives

For the landslide detection and mapping, the following morphometric datasets were derived from the DTM: (i) hillshade maps, using the sun azimuth angles 315° and 45°, and the sun elevation angles of 45°; (ii) slope map; (iii) and contour line maps, created with 1-m; 2-m; and 5-m contour intervals. Additional topographic information was available from two official state maps: (i) the digital orthophoto (DOF) from year 2020, at a resolution of 0.5 m; and (ii) the Croatian Base Map (CBM) at a scale of 1:5,000.

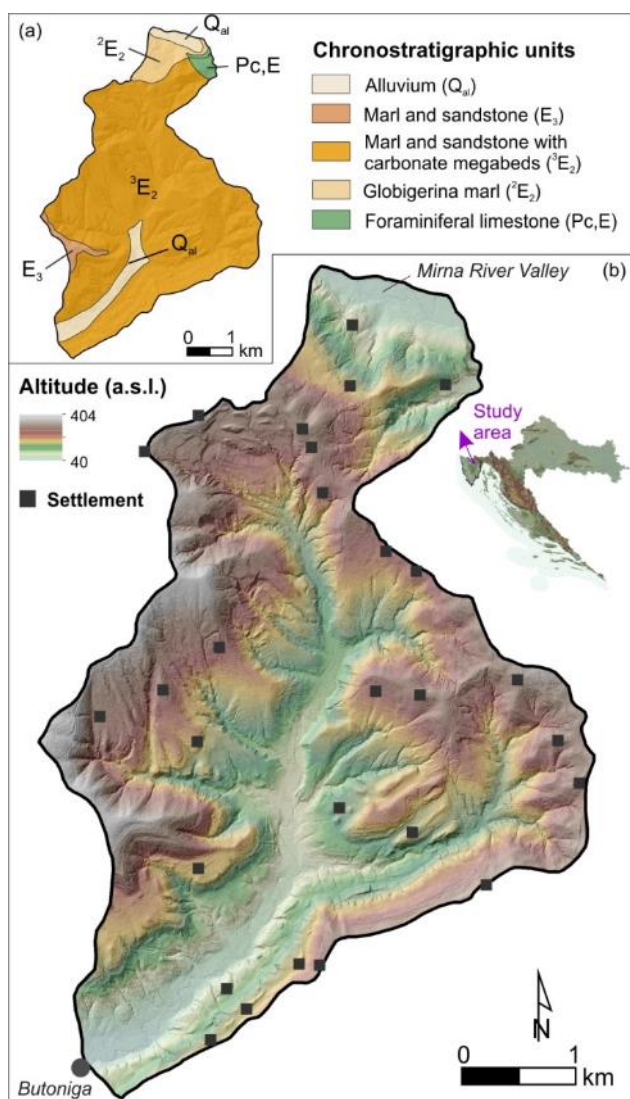


Figure 1 Study area in the City of Buzet: (a) simplified geologic map (after Pleničar et al. 1969); and (b) relief map.

The relief is hilly and moderately dissected (Fig. 1b). Predominant slope angles range from 13° to 32°. Prevailing elevations range from 100 to 300 m a.s.l.. Approximately 55% of the area is covered by forests, while ~40% is an agricultural area (Sinčić et al. 2022). The climate is temperate with hot summers, the coldest months

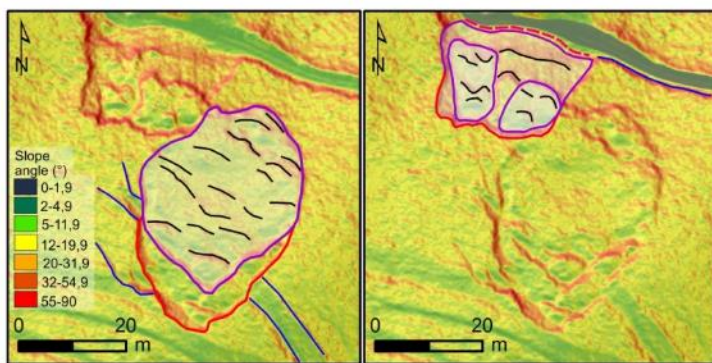
In general, landslide detection relies on the identification of a set of photographic/radiometric and morphologic evidence that characterizes an anomaly within the lateral continuity of the other landscape features (e.g., the morphological trace of bedding, scarps; Santangelo et al., 2022). Landslide identification on LiDAR DTM data relies on a reduced set of evidence, as no radiometric information is available, which increases the level of uncertainty. On the other hand, the use of DTM derivatives may help enforcing the set of evidence to detect and map landslides. Figure 2 shows an example of evidence collected on a slope where the lateral continuity of extended linear features is suddenly interrupted by an area characterized by a concave-convex topographic profile, a coarser texture, and a larger scale roughness compared to the surrounding area. All these elements converge towards the identification of a landslide with little uncertainty. In cases where such set of evidence is poorer, uncertainty is higher. It must be stated here that collecting such elements is not only a matter of the images portraying the landslide features, but also a matter of the

capability and experience of the interpreter to spot them and relate them to produce a sort of multivariate expert model in their mind.

In this phase of landslide inventory mapping, two levels of confidence of interpretation were distinguished: high, and low. Thereby, the high level of confidence implies that the landslide morphological signature is obvious on DTM derivatives (Fig.3). On the other hand, the low level of confidence implies either: (i) that the landslide topography is poorly expressed on DTM derivatives; (ii) or that part of a landslide is not visible; or (iii) that the topography of the observed phenomenon is clearly expressed on DTM derivatives, but there is a doubt depending on the interpreter's experience.

In the study area, most of the challenges in the identification and mapping of landslides are related to distinguishing landslides from other similar geomorphic expression observable on LiDAR DTM derivatives. Characteristic examples are presented and discussed in the following section.

VISUAL APPEARANCE OF TOPOGRAPHY ON LiDAR DTM DERIVATIVES



MAIN LANDSLIDE EVIDENCE

- **Landslide scarp:**
Concave topography delimited by a scarp that has an arcuate shape downslope. Strong evidence of the interruption of the lateral continuity of linear elements outside the boundary. Presence of a possible secondary scarp that has no continuity outside.
- Landslide deposit:**
Mainly convex and hummocky topography. Coarser texture and larger scale roughness than outside. Presence of linear elements (possible secondary scarps) not continuing outside.
- - - **Landslide toe:**
The deposit slightly covering the road.
- **Internal linear elements:** Not present outside.
- **External elements not present inside:**
Interruption of the lateral continuity of geological and geomorphological elements.
- Road**

Figure 9 Example of the collection of main landslide evidence converging towards the identification of a landslide with high level of confidence. The hillshade map is overlapped by the semi-transparent (30% transparency) slope map.

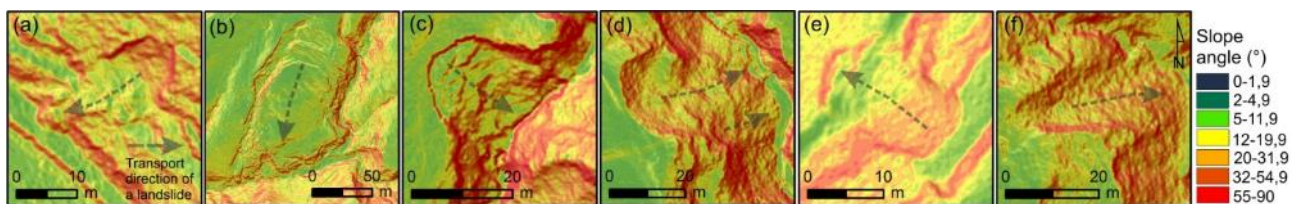


Figure 3 Examples of the landslides identified with high level of confidence in interpretation. Landslide boundaries are not presented for easier recognition of the landslide topography on LiDAR DTM derivatives. In all examples, the hillshade map is overlapped by the semi-transparent (30% transparency) slope map.

Challenges in landslide detection on LiDAR DTM: characteristic examples

Concave forms along hillslopes: landslides or not?

Figure 4a presents distinctive hillslope topography in the study area, characterized by linear features of agricultural terraces and bedding of competent flysch lithology. Most of the terraced landscape is now abandoned and covered by dense forests, thus there are favourable conditions for the land degradation (Tarolli et al. 2019). Here, numerous concave forms resembling landslide crowns and flanks are expressed on DTM derivatives. However, the anthropic elements are usually regular and rectilinear, whereas the bedding in this area appears continuous and does not show local variations both in attitude and in thickness. Landslides cause local interruption of anthropic elements and local variations in the continuity of bedding traces. In detail, the observed feature is considered a landslide (continuous red line in Fig. 4b) if the disturbance of linear hillslope element is evident, together with the evidence of distinctive toe topography. Other morphologies similar to landslide crowns and flanks are uncertain to be landslides (presented by red dashed line in Fig. 4b), especially if associated with persistent bedding (pointed by black arrows in Fig. 4b). Moreover, landslide accumulation zones in such cases were usually not detected. Such phenomena could be considered to represent evidences of erosional fluting formed at slope segments with concentrated runoff along the structural discontinuities.

Morphological features similar to landslide crowns (presented by blue dashed line in Fig. 4b) were also detected around gullies, which often form on the hillslopes

near roads. Although they can easily be misinterpreted as landslides, they actually represent features of the gully head. In the study area, there are numerous similar morphological expressions observed, especially around the soft gully margins (Brooks et al. 2019) of more complex and older gully systems.

Concave scarps in gullies

Figure 5 presents examples of landslide identification within gullies. More than 300 gullies of different types and evolution states are identified in the study area, comprising more than a half of the total number of identified landslides (Jagodnik et al. 2023). The most challenging identification of landslides was precisely within gully landforms, since there are distinctive morphologies that share little apparent difference between each other on LiDAR DTM derivatives but have been formed by different geomorphological processes.

Many landslides in gullies are interpreted with high level of confidence if their features are preserved and clearly expressed on DTM derivatives (Fig. 5a). The landslide mapping was also facilitated by the fact that the landslide crown usually coincides with the gully edge, while the landslide toe reaches the gully thalweg (Jagodnik et al. 2020). However, many gullies in the study area have a specific appearance on DTM derivatives (Fig. 5b) with numerous ridges and concavities that appear like zones of landslide crowns and depletion (pointed by blue arrows in Fig. 5d). The DOF analysis (Fig. 5c) indicated that such gullies have characteristics of the B-type calanchi landforms (Rodolfi and Frascati 1979). Landslides within them were delineated only in the cases when all features were detected on DTM derivatives (Fig. 5d), but the level of interpretation confidence is often low

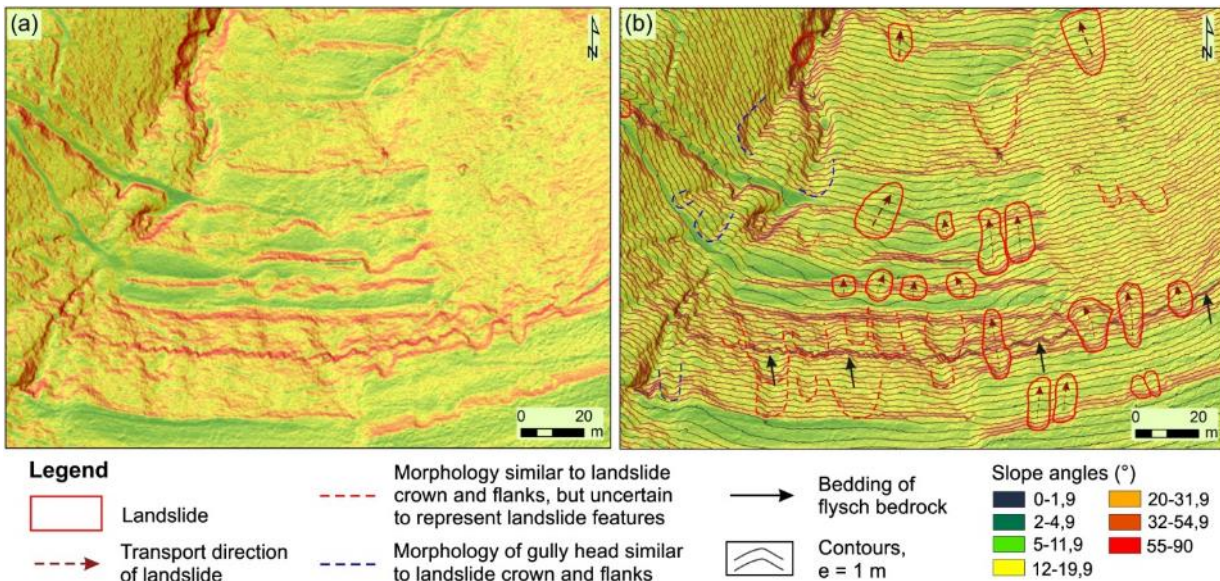


Figure 4 Example of the distinctive topography of flysch hillslopes in the study area, with landslides and concave forms resembling landslide features: (a) without, and (b) with interpretation. The hillshade map is overlapped by the semi-transparent (30%) slope map.

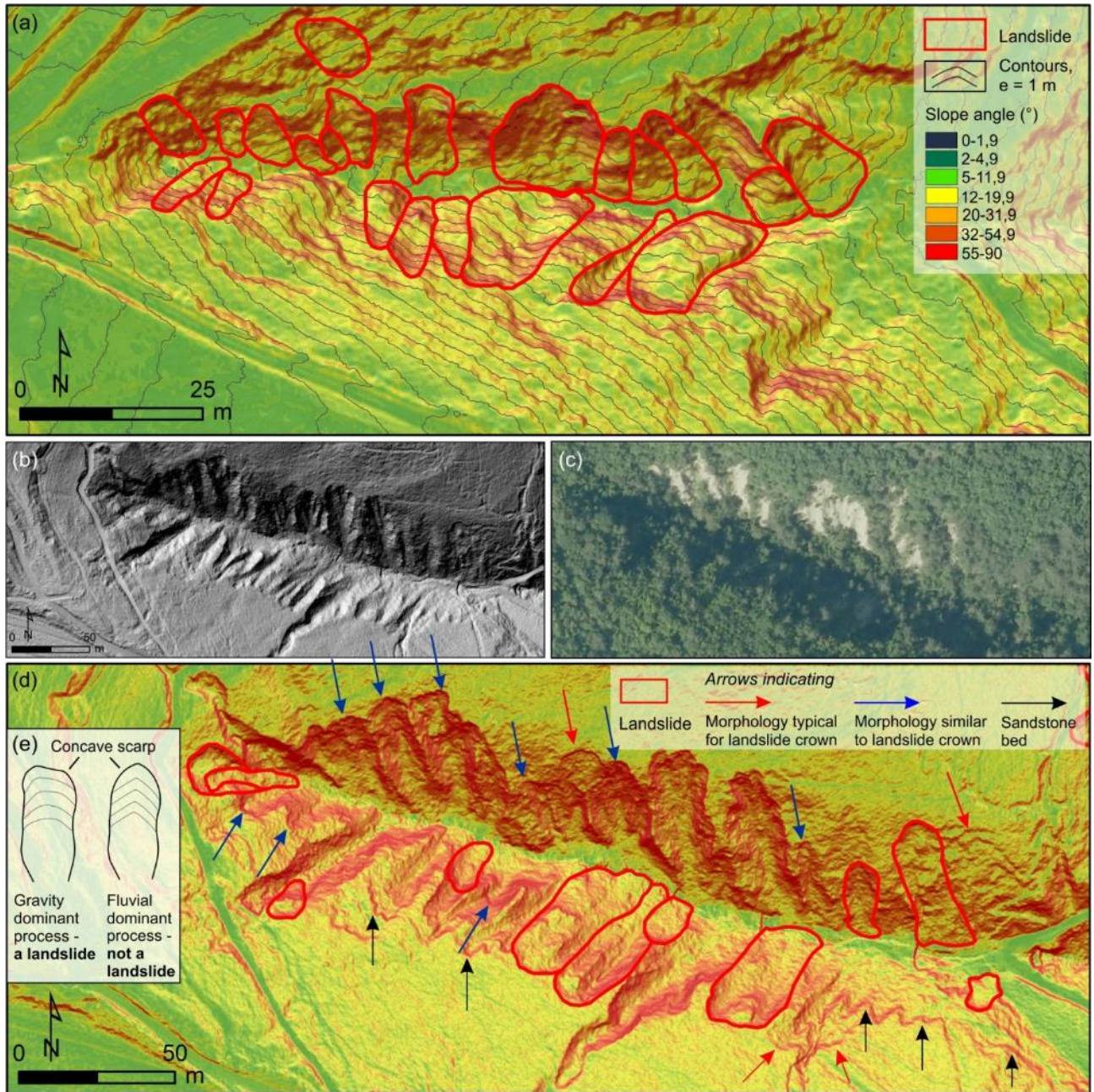


Figure 5 Identification and mapping of landslides within gullies: (a) examples of landslides identified with high level of confidence; (b) example of distinctive topography of gully landforms having characteristics of the B-type calanchi (Rodolfi and Frascati 1979) on the hillshade map; and (c) on the digital ortophoto (DOF); (d) examples of geomorphological convergence between the morphologies typical for landslide crowns and erosional concave scarps, with identified landslides; and (e) the pattern of contour lines reflecting the dominant formative process of a concave phenomenon.

On the opposite, where only the concave scarps are expressed but not the landslide deposit, care must be taken not to misinterpret them as landslides. Still, there is a doubt as to whether some of these phenomena are traces of debris flows formed along gully walls, with toes being removed by the active gully erosion. For a more reliable distinguishing of the dominant process forming similar phenomena, more detailed analysis of the pattern of contour lines reflecting the shape of a concave scarp should be performed (Fig. 5e).

Badland or landslide phenomenon?

Figure 6 presents examples of the valley topography associated to badlands and landslide occurrences in the study area, as well as the example when a badland phenomenon was initially misinterpreted as a landslide. Clearly observable landslides, identified with high confidence, are pointed by red arrows in Fig. 6d.

During the preliminary visual analysis of the hillshade map (Fig. 6a), topographic contour lines on CBM (Fig. 6b), and DOF (Fig. 6c), the phenomenon marked by number 1 was first identified as a landslide with a small

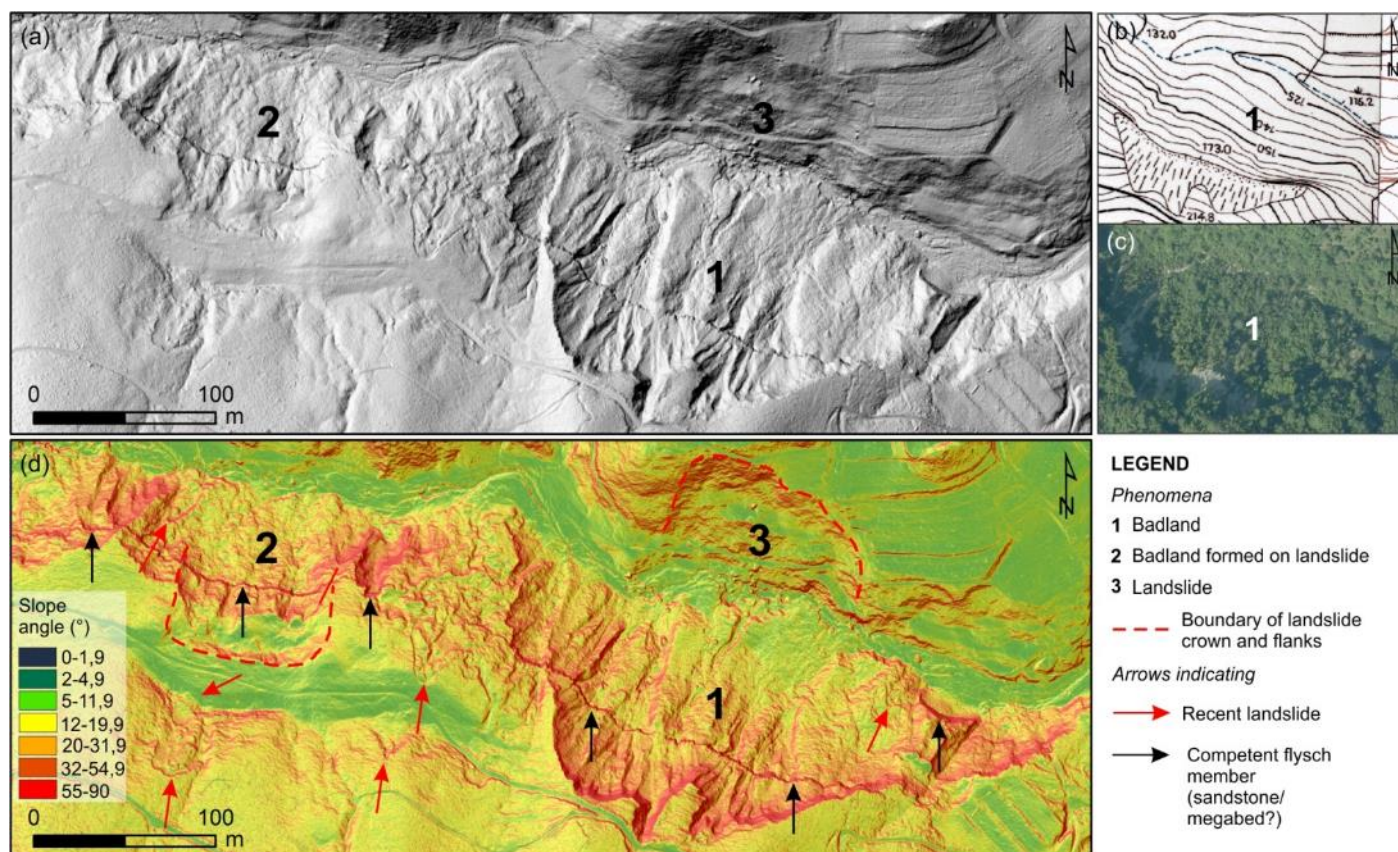


Figure 6 Example of the topography associated to Badlands and landslides: (a) appearance of the observed phenomena marked by numbers 1, 2, and 3 on the hillshade map; (b) appearance of the phenomenon marked by number 1 on the Croatian Base Map (CBM) 1:5,000; and (c) on the DOF; appearance of the observed phenomena marked by numbers 1, 2, and 3 on the slope map, with points to recent landslides and bedding of flysch bedrock.

badland formed within the depletion zone. The landslide was primarily assumed by the arcuate shape and steep slope angles distributed along the head segment visible on the slope map (Fig. 5d), as well as the sharp flanks, and the accumulated material that pushed the watercourse at the foot slope. However, a more detailed analysis of other topographic features, especially the linear features of bedding persistence of competent flysch members (pointed by black arrows in Fig. 5d), identified the phenomenon as the A/B-type of badland (Rodolfi and Frascati 1979), having a typical horse-shoe appearance with sharp edges still present, and the valley bottom filled by earth-flow deposits covered by vegetation. Several small recent landslides are identified along the surface of the badland phenomenon 1.

Similar badland topography was also observed in the case of the phenomenon marked with number 2, which was formed along the body of an older landslide. A deep-seated landslide, acting as the host phenomenon of the badland formation, is indicated by the topography specific for landslide crown, main scarp, and head visible on the slope map (dashed red line in Fig. 5d). The topography of adjacent deep-seated landslide identified in the presented environment is marked by number 3 in the figure.

Conclusions

Based on the experience in the visual interpretation of 0.3 m LiDAR DTM of the study area in the City of Buzet in Istria (Croatia), and the presented examples, we conclude that the difficulties in landslide detection in flysch environment mostly arise from their similarity to erosional forms. The most challenging was to distinguish the topography of particular landslide features, i.e. crowns and flanks from numerous concave scars formed by linear erosion along gully channel walls. Yet, many landslides within certain gullies have been identified with high level of confidence, in the cases when all landslide features could have been detected on LiDAR DTM derivatives. In order to more reliably distinguish the landslides from morphologically similar erosional forms, a detail analysis of the pattern of contours reflecting the shape of a concave form is recommended. In general, using a wide and rigorous set of evidence, and a reproducible procedure to detect landslides is essential, as it limits both omission and commission errors, positively impacting the completeness, i.e., statistical representativeness of the final inventory and, hence, its quality.

Acknowledgements

This research was funded by the Croatian Science Foundation under the project Methodology development for landslide susceptibility assessment for land-use planning based on LiDAR technology (HRZZ IP-2019-04-9900, HRZZ DOK-2020-01-2432). It was partially supported by the project of the University of Rijeka Landslides and erosion as associated geological hazards in flysch environment (uniri-iskusni-tehnic-23-191). These supports are gratefully acknowledged.

References

- Antonini G, Ardizzone F, Cardinali M, Galli M, Guzzetti F, Reichenbach P, (2002) Surface deposits and landslide inventory map of the area affected by the 1997 Umbria–Marche earthquakes. *Bollettino della Societa Geologica Italiana*. 121(2): 843–853.
- Arbanas Ž, Grošić M, Goršić D, Griparić B, (2007) Landslides remedial works on small roads of Istria. *Proceedings of the 4th Croatian Roads Congress*. p.38.
- Arbanas Ž, Jovančević S D, Vivoda M, Mihalić Arbanas S, (2014) Study of Landslides in Flysch Deposits of North Istria, Croatia: Landslide Data Collection and Recent Landslide Occurrences. *Landslide Science for a Safer Geoenvironment*. Springer International Publishing, Cham. pp. 89-94.
- Ardizzone F, Cardinali M, Galli M, Guzzetti F, Reichenbach, P (2007) Identification and mapping of recent rainfall-induced landslides using elevation data collected by airborne LiDAR. *Natural Hazards and Earth System Sciences*. 7(6): 637–650.
- Bergant S, Tišljarić J, Šparica M, (2003) Eocene carbonates and flysch deposits of the Pazin Basin. *Field trip guidebook of 22nd IAS meeting of sedimentology*, 17-19 September 2003. Opatija, Croatia. pp. 57-63.
- Bernat Gazibara S, Jagodnik, P, Lukačić, H, et al., (2023) Landslide and soil erosion inventory mapping based on high-resolution remote sensing data: a case study from Istria (Croatia). *Progress in Landslide Research and Technology*, Vol. 2. Springer International Publishing, Cham. pp. 363-375.
- Bibentyo T M, Dille A, Depicker, A, et al., (2024) Landslides, bedrock incision and human-induced environmental changes in an extremely rapidly formed tropical river gorge. *Geomorphology*. 449: 109046.
- Bostjančić I, Gulam V, Frangen T, Hećej N, (2023) Relation between relief and Badland spatial distribution in the Paleogene Pazin Basin, Croatia. *Journal of Maps*. 19:1: 2163196.
- Brooks A, Thwaites R, Spencer J, Pietsch T, Daley, J (2019) *A Gully Classification Scheme to Underpin Great Barrier Reef Water Quality Management: 1st Edition*. Report to the National Environmental Science Program. Reef and Rainforest Research Centre Limited, Cairns. 123 pp.
- Ciccacci S, Galiano M, Roma M A, Salvatore, M C, (2008) Morphological analysis and erosion rate evaluation in badlands of Radicofani area (Southern Tuscany – Italy). *Catena*. 74: 87-97.
- Dugonjić Jovančević S, Arbanas Ž, (2012) Recent Landslides on the Istrian peninsula, Croatia. *Natural Hazards*. 62:1323-1338.
- Görum T, (2019) Landslide recognition and mapping in a mixed forest environment from airborne LiDAR data. *Engineering Geology*. 258, 105155.
- Gulam V, Pollak D, Podolszki L, (2014) The analysis of the flysch badlands inventory in central Istria. *Geologia Croatica*. 67/1: 1-15.
- Gulam V, Gajski D, Podolszki L, (2018) Photogrammetric measurement methods of the gully rock wall retreat in istrian badlands. *Catena*. 160: 298-309.
- Guzzetti F, Ardizzone F, Cardinali M, Galli M, Reichenbach, P, (2008) Distribution of landslides in the Upper Tibet River basin, central Italy. *Geomorphology*. 96:105-122.
- Guzzetti F, Mondini A C, Cardinali M, Fiorucci, F, Santangelo, M, Chang, K T, (2012) Landslide inventory maps: new tools for an old problem. *Earth-Science Reviews*. 112: 42-66.
- Hart M W, Shaller P J, Farrand G T, (2012) When Landslides are Misinterpreted as Faults: Case Studies from the Western United States.
- Jagodnik P, Jagodnik V, Arbanas Ž, Mihalić Arbanas S, (2020) Landslide types in the Slani Potok gully, Croatia. *Geologia Croatica*. 73/1:13-28.
- Jagodnik P, Bernat Gazibara S, Sinčić M, et al. (2023) Landslides, gully erosion and badlands as associated geological hazards in flysch environment – analysis of geomorphological inventories and LiDAR DTM at a large scale. *Proceedings of the 6th World Landslide Forum-Abstract Book*. Florence, Italy. p. 110-110.
- Marinčić S, Šparica M, Tunis G, Uchman A, (1996) The eocene flysch deposits of the Istrian peninsula in Croatia and Slovenia. *Regional, stratigraphic, sedimentological and ichnological analysis*. *Annales*. 9:139-156.
- Petschko H, Bell R, Glade T, (2015) Effectiveness of visually analyzing LiDAR DTM derivatives for earth and debris slide inventory mapping for statistical susceptibility modeling. *Landslides*. 13(5): 857–872.
- Petrinjak K, Budić M, Bergant S, Korbar, T, (2021) Megabeds in Istrian Flysch as markers of synsedimentary tectonics within the Dinaric foredeep (Croatia). *Geologia Croatica*. 74/2: 99-120.
- Pleničar M, Polšak A, Šikić D, (1969) *Osnovna geološka karta SFRJ 1:100000, list Rovinj L33-100* [Basic geological Map of SFRJ 1:100000, Rovinj sheet – in Croatian]. Institut za geološka istraživanja, Zagreb; Savezni geološki zavod.
- Razak K A, Straatsma M W, van Westen C J, Malet J-P, de Jong S M, (2011) Airborne laser scanning of forested landslides characterization: terrain model quality and visualization. *Geomorphology*. 126: 186–200.
- Rodolfi G, Frascati F, (1979) *Cartografia di base per la programmazione degli interventi in aree marginali (area rappresentativa della Val D’Era)*. *Annali Ist. Per lo Studio e la Difesa del Suolo*, vol. 10.
- Santangelo M, Cardinali M, Bucci F, Fiorucci F, Mondini A C (2022) Exploring event landslide mapping using Sentinel-1 SAR backscatter products. *Geomorphology*. 397: 108021.
- Scaioni M, Longoni L, Melillo V, Papini M, (2014) Remote Sensing for Landslide Investigations: An Overview of Recent Achievements and Perspectives. *Remote Sensing*. 6(10): 9600-9652.
- Sinčić M, Bernat Gazibara S, Krkač M, Lukačić H, Mihalić Arbanas S, (2022) The Use of High-Resolution Remote Sensing Data in Preparation of Input Data for Large-Scale Landslide Hazard Assessment. *Land*. 11:1360.
- Soeters R, van Westen C J, (1996) Slope instability recognition, analysis, and zonation. Turner, A K, Schuster, R L (eds.): *Landslides, Investigation and Mitigation*. Transportation Research Board, Special Report 247, Washington D.C., USA (ISBN 0-309-06151-2). 129-177.
- Van den Eeckhaut M, Poesen J, Verstraeten G, Vanacker V, Nyssen J, Moeyersons J, Van Beek L P H, Vandekerckhove L, (2007) Use of LiDAR-derived images for mapping old landslides under forest. *Earth Surface Processes and Landforms*. 32: 754–769.
- van Westen C J, van Asch T W J, Soeters R, (2006) Landslide hazard and risk zonation – why is it still so difficult? *Bulletin of Engineering Geology and the Environment*. 65: 167-184.
- Tarolli P, Rizzo D, Brancucci G, (2019) *Terraced Landscapes: Land Abandonment, Soil degradation, and Suitable Management*.

World Terraced Landscapes: History, Environment, Quality of Life,
Chapter 12. Springer. 195-210.

Vivoda Prodan M, Mileusnić M, Mihalić Arbanas S, Arbanas Ž, (2017)
Influence of weathering processes on the shear strength of
siltstones from a flysch rock mass along the northern Adriatic
coast of Croatia. *Bulletin of Engineering Geology and the
Environment*. 76/2: 695-711.

Zaninović K, Gajić-Čapka M, Perčec Tadić, M, et al., (2008) *Klimatski
atlas Hrvatske 1961-1990, 1971-2000* [Climate atlas of Croatia – in
Croatian]. Državni hidrometeorološki zavod, Zagreb (ISBN 978-
953-7526-01-6). 200p.

Evaluating the Effectiveness of Deep Learning Algorithms and InSAR Data in Early Warning Systems for Landslide Risk Mitigation

Mohammad Amin Khalili^{(1)*}, Chiara Di Muro⁽¹⁾, Luigi Guerriero⁽¹⁾, Massimo Ramondini^(2,3), Domenico Calcaterra⁽¹⁾, Diego Di Martire^(1,3)

1) Federico II University of Naples, Department of Earth, Environmental and Resource Sciences, Monte Sant'Angelo Campus, Naples, Italy, mohammadamin.khalili@unina.it, +393444137462

2) Federico II University of Naples, Department of Civil, Architectural and Environmental Engineering, via Claudio 21, Naples, Italy

3) SINTEMA Engineering srl, viale Maria Bakunin 14, Naples, Italy

Abstract Landslides are a significant natural hazard that can cause severe damage to infrastructure and impact local communities' safety and prosperity. Accurate and reliable prediction of deformation caused by landslides is crucial to implementing effective disaster management strategies that can mitigate the risk of landslides and their impact on communities and provide an accurate early warning system. This study proposes a comprehensive approach to cumulative deformation induced by landslide prediction in the Caiazzo hamlet (southern Italy), a critical area that has experienced significant landslides that have impacted settlements and infrastructure. The study uses a CNN-LSTM algorithm with Spatio-Temporal dependency to predict cumulative deformation caused by landslides, employing geological, geomorphological, and geospatial data as predisposing factors. These factors include elevation, slope, aspect, Topographic Wetness Index (TWI), Stream Power Index (SPI), geology, flow direction, curvature, Normalized Difference Vegetation Index (NDVI), and land use. The Permanent Scatterer Interferometry (PSI) technique was applied on 132 and 143 SENTINEL-1A ascending and descending tracks, respectively, to obtain cumulative deformation data as labels, providing an extensive data set that allowed for accurate and reliable prediction of landslide deformation. The proposed CNN-LSTM algorithm integrates convolutional neural networks (CNNs) and long short-term memory (LSTM) networks to learn the spatio-temporal dependencies between landslides' predisposing factors and their cumulative deformation. This approach allows the algorithm to capture the complex relationships between the predisposing factors and the occurrence of landslides, resulting in accurate and reliable understanding of landslide kinematics and providing early warning system accurately. The close match between predicted and observed cumulative deformation indicates that the CCN-LSTM model effectively captures the complex relationships between the various factors contributing to cumulative deformation prediction. Our finding illustrates more than 70% of predicted deformation with less than 2 mm error and 90% with less than 5 mm error after prediction. Overall, the proposed algorithm's superior performance in predicting cumulative deformation caused by landslides highlights

the potential of deep learning algorithms to enhance landslide prediction and disaster management strategies.

Keywords Landslide prediction, CNN-LSTM algorithm, Spatio-Temporal dependency, Deep learning, Early Warning System, PSI technique

Introduction

The Landslides are one of the most pervasive natural hazards globally, posing a significant threat to human lives, infrastructure, and ecosystems (Di Martire et al., 2015). These geological phenomena, characterized by the downward and outward movement of slope-forming materials, are triggered by various factors that can significantly vary across different geographical locations. These triggers include intense precipitation, seismic activities, volcanic eruptions, anthropogenic actions such as deforestation, urban development, and alterations in land use (Calò et al., 2009). The complexity and interplay of these triggers necessitate a sophisticated approach to understanding, predicting, and managing landslide risks (Bravo-López et al., 2022).

Focusing on the Caiazzo hamlet in southern Italy, this area exemplifies a region highly susceptible to the devastating effects of landslides (Sammartini et al., 2019). The lithological setting, characterized by weak geological materials coupled with the region's geotechnical properties, such as soil composition and water content, significantly contributes to slope instability. This instability is further exacerbated by human activities and climatic factors, leading to morphodynamic events that have historically impacted the local communities and infrastructure. The landslides in Caiazzo, encompassing both active and dormant phases, manifest predominantly as rotational and translational slides and Earth flows (Carannante et al., 2010).

The advent of remote sensing technologies, particularly Multi-temporal Interferometric Synthetic Aperture Radar (MT-InSAR), has revolutionized the monitoring and analysis of landslides. Among the techniques derived from MT-InSAR, the Permanent Scatterer Interferometry (PSI) technique stands out for its precision in detecting and measuring ground

displacement over time (Hooper, 2008). SENTINEL1-A satellite imagery equipped with Synthetic Aperture Radar (SAR) is particularly advantageous in landslide studies. SAR's ability to penetrate cloud cover and its independence from daylight conditions make it an invaluable resource for continuously monitoring Earth's surface changes, including the subtle displacement preceding or indicating landslide activity (Potin et al., 2016).

Predicting the cumulative deformation caused by landslides is crucial for the timely implementation of disaster management and mitigation measures (Khalili et al., 2023a). This prediction is inherently challenging due to the need for integrating diverse and complex datasets, encompassing spatial data on predisposing factors and temporal data on landslide cumulative deformation. Machine Learning Algorithm (MLA) has been applied in various ways to predict landslides accurately and rapidly (Gan et al., 2019). It includes Decision Trees, Random Forests (Hong et al., 2016), and Support Vector Machines (Liu et al., 2021), which are extensively used to detect landslides. However, most time-series prediction applications prefer Deep Learning Algorithms (DLAs) over traditional statistical models. Yet, they cannot describe the behaviour of multivariate time series. DLAs can analyze datasets with multiple dimensions by integrating numerous processing layers, extracting learning features, and nonlinear dependencies (Khalili et al., 2023b; Li et al., 2020). Recent advances in the field have shown that DLAs can be used as a model for predicting deformation (Hajimoradlou et al., 2020).

The introduction of Convolutional Neural Networks (CCN) and Long Short-Term Memory (LSTM) networks marks a significant advancement in the field of landslide prediction (Greff et al., 2017; Zarándy et al., 2015). CCNs are adept at processing spatial data, including geospatial data (predisposing factor), to identify patterns and features indicative of landslide susceptibility. On the other hand, LSTMs excel in analyzing time-series data, making them ideal for modeling the temporal progression of landslide cumulative deformations based on historical and real-time data.

Our study proposes a novel approach that synergizes the spatial data processing capabilities of CCN with the temporal data (cumulative deformation) modeling strengths of LSTM. This integrated CCN-LSTM model is designed to harness the full potential of both neural network architectures, thereby providing a more accurate and reliable prediction of landslide-induced cumulative deformations in the Caiazzo hamlet. By doing so, this research addresses the existing challenges in accurately predicting landslides and contributes to the development of more effective early warning systems and disaster management strategies.

Case Study

Caiazzo is a municipality of Campania region (Italy) located in the Caserta province, in the northern part of the regional territory, at 200 m a.s.l. According to the CARG Project (Geological Cartography of Italy), the area is mainly characterized by coarse sandstones, conglomerates, and microconglomerates, which belongs to Caiazzo Sandstones Unit. Such formation is also composed by marly-silty intercalations and chaotic deposits alternate with extra-basial elements (olistostroms) consisting of limestone and marly limestone referable to scaly clays. These rocks alternate with eluvial and colluvial deposits (Holocene-Current), which are silty-sandy deposits of a pyroclastic nature with calcareous clasts and silty-clayey deposits with arenaceous or calcareous-marly clasts. In the northern sector of the urban center Pietraraja Formation (Tortonian) of Matese-Taburno-Camposauro Unit outcrops, it consists of stratified clayey-silty marls and subordinate fine sandstones. While, in the southern sector Casalnuovo-Casoria Unit outcrops, including levels of laminated cinerites passing through a level of pumices in a cineritic matrix (Pleistocene Sup. - Holocene).

From a geomorphological and structural point of view, Caiazzo area is characterized by a landscape with reliefs with medium-low slopes (less than 20°), consisting of arenaceous-marly-clay lithostratigraphic units, and areas at lower altitudes characterized by Quaternary eluvial-colluvial deposits. The arenaceous hilly reliefs are in stratigraphic (Scarsella, 1971) and tectonic (Pescatore et al., 1971) relationship with the underlying formations. These lithologies have low resistance to erosion, so although some tectonic structures (normal faults NE-SW) are present, they do not have significant structural morphologies. The slopes are concave-convex, and they are characterized by linear erosion valleys and landslide bodies of various typologies and sizes (Carannante et al., 2010).

The lithological and geotechnical characteristics of the investigated area contribute to the instability of the hilly slopes. They are affected by gravitational phenomena, marked by different morphodynamic events. Specifically, they involve the terrigenous units of Caiazzo and consist of active and quiescent landslides (Carannante et al., 2010), mainly rotational and translational slides and earth flows. The landslides involving arenaceous slopes are in total 140, they include 99 rotational/translational slides, 20 mass creep, 17 soil creep, 3 falls and 1 undefined landslide (Fig. 1). Many of them have a complex style and consist of slide evolving to flows, that overtake 1000 m. As could be seen, this area is characterized by a large number of mass movements which affect urban center and rural zones, therefore, they represent a danger for structures and infrastructures, in particular in the eastern sector of the town.

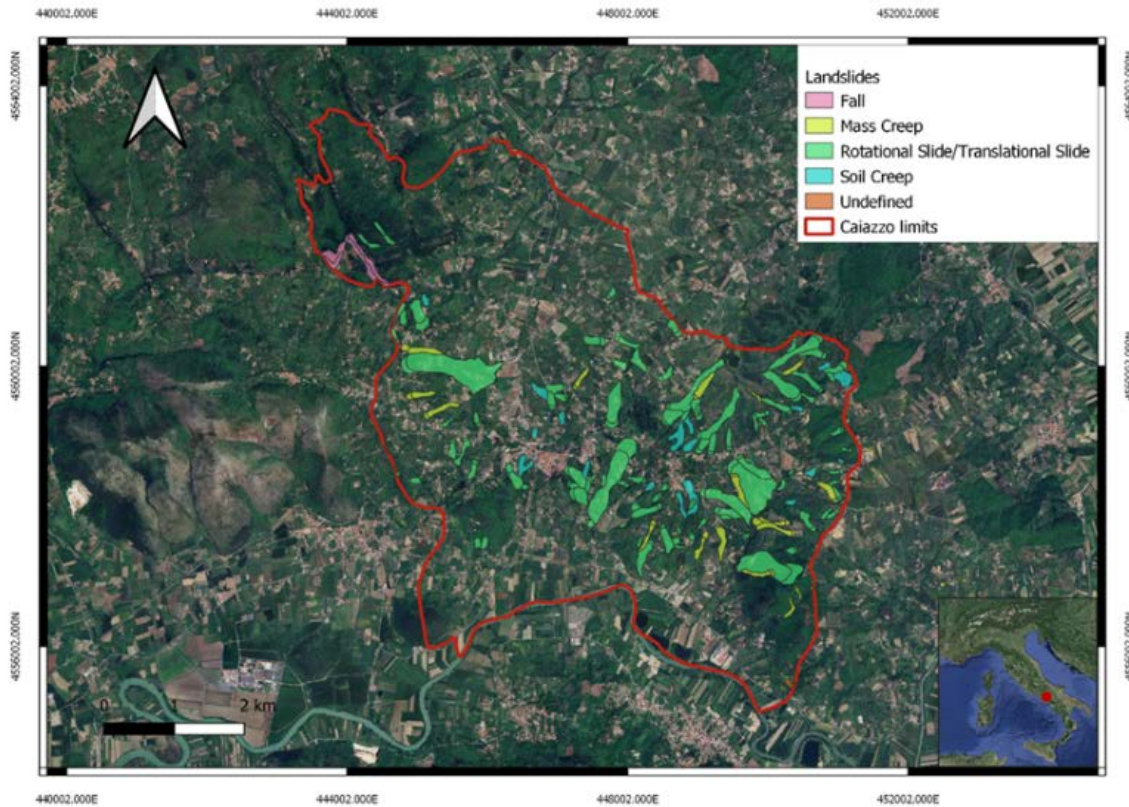


Figure 1 Landslides inventory map of Caiazzo municipality.

Material

SAR Data Acquisition

Synthetic Aperture Radar (SAR) data have emerged as indispensable tools in natural disaster analysis, particularly landslide detection and monitoring. SAR's unique advantages, including its all-weather, day-and-night operation capabilities and its sensitivity to ground movement, make it ideal for observing and analyzing Earth's surface changes over time. This study utilizes SAR data from the SENTINEL1-A satellite, part of the Copernicus program managed by the European Space Agency (ESA), which provides comprehensive coverage and detailed images essential for monitoring landslide-prone areas (Potin et al., 2016).

The SAR data for the Caiazzo hamlet were acquired from the SENTINEL1-A satellite, focusing on ascending and descending tracks to capture comprehensive deformation patterns across different times and viewpoints. A total of 132 ascending and 143 descending tracks from 14/01/2017 to 25/11/2021 and from 16/01/2017 to 27/11/2021, respectively, were analyzed to ensure a robust dataset for accurate cumulative deformation analysis as temporal data for training and predicting by LSTM algorithms.

Predisposing Factors

In the context of landslide prediction, predisposing factors are critical elements that contribute to the likelihood of landslide occurrence. These factors, derived from geological, geomorphological, and geospatial data, provide a foundation for understanding the conditions

under which landslides are most likely to occur. This study incorporates a comprehensive set of predisposing factors, including elevation, slope, aspect Topographic Wetness Index (TWI), Stream Power Index (SPI), geology, flow direction, curvature, Normalized Difference Vegetation Index (NDVI), and land use. Each factor plays a vital role in the landslide prediction model, contributing to accurately assessing landslide susceptibility.

The study makes use of primary geological, geospatial, and geomorphological data, including:

i) To understand the geological background, A geological map of the Caiazzo hamlet with a scale of 1:50,000.

ii) A Digital Elevation Map (DEM) of the case study with a 20-meter pixel resolution, primarily utilized to investigate the topographic and geomorphological features of the Caiazzo hamlet, such as elevation, slope, flow direction, aspect, curvature, Topographic Wetness Index (TWI), and Stream Power Index (SPI).

iii) Landsat7 ETM+ took remote sensing images with a 30-meter resolution for bands 1 to 7 to discuss the climatic and environmental characteristics of the Caiazzo hamlet. This data is used to acquire the normalized differential vegetation index (NDVI) and land use type.

Methods

Permanent Scatterer Interferometry (PSI) technique

Permanent Multi-temporal Interferometric Synthetic Aperture Radar (MT-InSAR) is a sophisticated technique that analyzes phase differences in SAR images over time to detect ground deformations. This approach offers

unparalleled precision in measuring surface movements, which is essential for monitoring geological hazards. MT-InSAR's capability to capture data under any weather conditions and its broad area coverage make it an invaluable dataset for understanding and predicting natural disasters, including landslides and earth subsidence (Ferretti et al., 2001; Hanssen and Ferretti, 2002).

Permanent Scatterer Interferometry (PSI) is a specialized subset of MT-InSAR that focuses on the identification and monitoring of stable reflection points or permanent scatterers over time. This method enhances the accuracy of deformation measurements in urban or rocky terrains, where two-pass InSAR might face challenges due to coherence loss. PSI's ability to provide long-term deformation trends with millimeter-level accuracy is critical for assessing structural stability and ground movements, offering vital data for infrastructure planning and risk assessment (Hooper, 2008).

A Digital Elevation Model (DEM) with a cell resolution of $20\text{m} \times 20\text{m}$ and a multi-looking factor of 1×1 in range and azimuth is used for this technique in this study. The SUBSIDENCE software developed at Universitat Politècnica de Catalunya implemented the Coherent Pixels Technique and was used to apply the PSI method (Blanco-Sánchez et al., 2008). The software processed the co-registered images and selected all possible interferogram pairs (including 456 for ascending track and 428 for descending) with spatial baselines lower than 100 meters. It used a Temporal Phase Coherence threshold of 0.7. Finally, the deformation rate map along the line of sight (LoS) and time series of cumulative deformation was calculated.

Convolutional Neural Networks (CNNs)

Convolutional Neural Networks (CNNs) represent a class of deep neural networks highly effective at processing data with a grid-like topology. A fundamental concept in CNNs is their ability to learn spatial hierarchies of features automatically and adaptively from input data. This is achieved through convolutional, pooling, and fully connected layers (Zarándy et al., 2015).

Our paper explores using CNNs to identify and learn spatial patterns from predisposing factors related to landslide occurrences. By treating each predisposing factor as a separate channel (similar to the RGB channels in color images), we can feed a multi-dimensional array into the CNN, where each layer is designed to detect patterns and features indicative of potential landslide hazards automatically. Through convolutional and pooling layers, the CNN condenses this spatial information into a high-level feature vector that encapsulates the critical spatial dependencies among these predisposing factors. This vector serves as a compact yet rich representation of the input data, which is then used by the LSTM network to predict landslide cumulative deformations by considering the temporal evolution of these spatial features. This approach allows us to leverage the strengths of CNNs in processing visual data and in any

domain where understanding spatial relationships is critical to making accurate predictions.

For the CNN component of our study, we calibrate and tune an array of hyperparameters to ensure optimal extraction and learning of spatial patterns from the predisposing factors associated with landslides. These hyperparameters, set before the training phase, play a pivotal role in defining the architecture and learning dynamics of the CNN. Key hyperparameters for our CNN include the number of convolutional layers (12 layers), the number of filters (initial layer = 64 and deeper layer = 256) in each convolutional layer, and the size of these filters (3×3). We chose ReLU as an activation functions enabling it to learn complex patterns. Pooling layer configurations, specifically the selection of max pooling and their respective kernel sizes (2×2), dictate the Downsampling strategy, affecting the model's sensitivity to feature localization. The dropout rate (0.3) is another crucial hyperparameter that prevents overfitting by randomly omitting a subset of features during training. Lastly, the learning rate and optimization algorithm (Adam) are fine-tuned to balance the speed and stability of the learning process.

Long Short-Term Memory (LSTM)

LSTM networks are a special kind of Recurrent Neural Network (RNN) architecture designed to overcome the limitations of traditional RNNs in capturing long-term dependencies. LSTMs are particularly adept at remembering information for extended periods, thanks to their unique structure, which includes memory cells and multiple gates (input, output, and forget gates). These components work together to regulate the flow of information, allowing the network to retain or discard data based on its relevance to the task at hand. This capability makes LSTMs highly effective for various sequence prediction problems (Greff et al., 2017; Khalili et al., 2023b).

In our paper, we leverage LSTM's prowess in handling time-series data to model the temporal aspect of landslide deformation, explicitly focusing on cumulative deformation data obtained from ascending and descending tracks. The cumulative deformation data, characterized by its sequential nature over time, serves as an ideal input for the LSTM network, allowing it to learn the temporal patterns and dependencies inherent in the deformation process. By training separate LSTM models on datasets from ascending and descending tracks, we aim to capture the nuances and variances in deformation patterns that might be specific to the direction of satellite observation. This dual approach enables a more comprehensive understanding of landslide dynamics, potentially improving prediction accuracy by integrating insights from both perspectives. Each LSTM model is trained on a sequence of past deformation measurements to predict future deformation, utilizing the LSTM's capacity to learn from long-term sequences to anticipate changes in landslide behaviour over time in ascending and descending separately.

In our research, optimizing and fine-tuning hyperparameters for the LSTM component are critical to accurately modeling the temporal dynamics of cumulative landslide deformation. Key hyperparameters for the LSTM include the number of hidden layers and the number of units (or neurons) in each layer, which dictate the model's capacity to learn from the data. Typically, we experiment with one to three hidden layers containing 50 to 200 units, balancing model complexity with computational efficiency. The learning rate, another crucial hyperparameter, is carefully selected to ensure convergence without overshooting, with initial values set at 0.001. The optimizer's choice, Adam, is made to effectively minimize the loss function, considering their ability to adapt learning rates based on the history of gradients. Dropout rates are applied within the LSTM layers, 0.3, to prevent overfitting by randomly omitting a subset of the features during training. The sequence length, or the number of times steps the LSTM looks back on, is six time steps of cumulative deformation, ensuring the model captures relevant temporal patterns without noise. Batch size is another parameter adjusted for efficient training, 64, balancing the trade-off between training speed and memory constraints. These LSTM hyperparameters are iteratively refined through validation and cross-validation, aiming to achieve a model that generalizes well to unseen data while accurately capturing the temporal patterns in cumulative deformation and predicting the cumulative deformation in a specific time.

Proposed CNN-LSTM Algorithm

In our study, we propose a novel CNN-LSTM hybrid model that leverages the strengths of CNNs and LSTM networks to accurately predict landslide cumulative deformations by effectively capturing both spatial and temporal dependencies. The CNN component is a powerful feature extractor, processing predisposing factors such as slope, aspect, etc, to identify relevant spatial patterns and interactions. These extracted high-level spatial features are then passed onto the LSTM component, which is adept at modeling time-series data (ascending and descending cumulative deformation). The LSTM uses these features to learn the temporal dynamics of cumulative deformation, considering the sequential nature of the data and its historical progression. This synergistic combination allows our model to understand how spatial configurations evolve, leading to more accurate and insightful predictions of landslide occurrences. By integrating CNN's spatial analysis capabilities with LSTM's temporal dependency modeling, our CNN-LSTM architecture offers a comprehensive approach to landslide prediction, effectively harnessing the complex interplay between the various factors influencing landslide dynamics.

Results and Discussion

Fig 2a represents the cumulative deformations on 25/11/2021 for the ascending track, and Fig 2b represents the last predicted epoch for cumulative deformations on the same date, to help understand how the proposed prediction model (CCN-LSTM) works. The model correctly predicted positive and negative deformation amounts and locations, with a mean absolute error of 0.29. Fig 3a and b also show a good agreement between actual and predicted cumulative deformation on 27/11/2021, with a mean absolute error of 0.34.

Figs. 2 and 3 demonstrate that our model provides an excellent fit to the observed data, indicating its ability to predict cumulative deformation accurately and reliably and, thus, the risk of landslides in the studied area. The close match between the predicted and observed cumulative deformation shows that the CCN-LSTM model effectively captures the complex relationships between the various factors contributing to cumulative deformation prediction, such as geological, geomorphological, and geospatial data types. These figures highlight the potential of the CCN-LSTM model as a valuable tool for predicting cumulative deformation and the risk of landslides, which can inform decision-making and disaster response efforts.

The Bland-Altman plot presented herein is a graphical method to assess the agreement between the cumulative deformation predicted by our model and the observed deformation data. On the y-axis, the differences between the observed and predicted values are plotted against their mean on the x-axis, providing a direct visualization of the prediction error distribution.

The plot is color-coded to represent different ranges of actual cumulative deformation, with distinct colours denoting the intervals as specified: less than -2 mm, between -2 mm to 2 mm, and greater than 2 mm. This colours scheme enables a quick visual correlation between the magnitude of cumulative deformation and the associated prediction error. Horizontal lines are drawn at ± 2 mm and ± 5 mm to denote the acceptable error thresholds. According to the analysis encapsulated by the plot, a substantial majority of the data points—represented by their spread along the zero line—fall within the ± 2 mm error margin, consistent with the assertion that over 70% of the deformation predictions are within this range. Furthermore, when considering the wider ± 5 mm margin, the data points enveloped by this criterion rise to 90%, underlining the robustness of the predictive model. The distribution of points across the plot reveals a clustering around the mean difference line, which indicates a high accuracy level in the predictions across the range of cumulative deformation values. Points outside the ± 5 mm bounds are few, suggesting that the prediction errors are generally minor, and the model's performance is dependable. Tab 1 presents the proposed algorithms' evaluation metrics for ascending and descending tracks. Two key metrics assess the model's performance: the Root Mean Square Error (RMSE) and the R-squared (R^2) score.

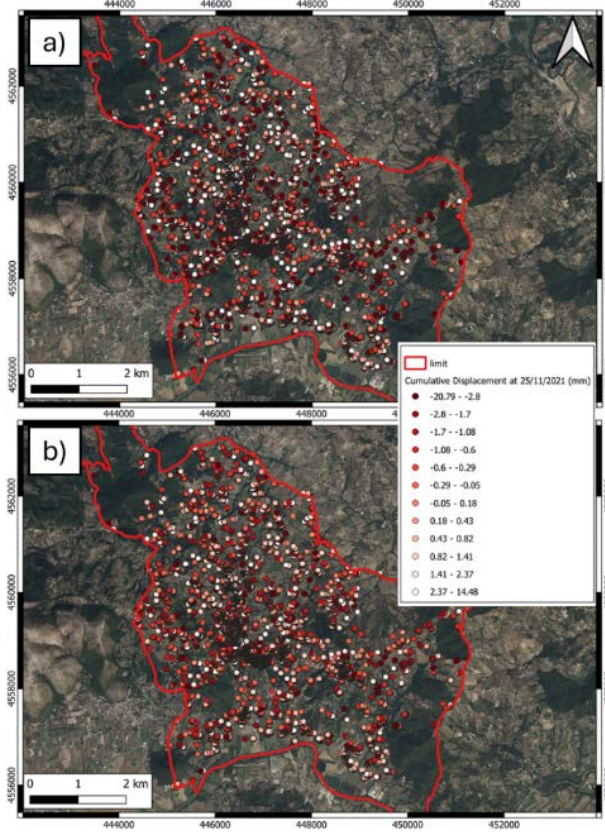


Figure 2 Location and map of deformation by a) PSI technique and b) CCN_LSTM (Unit: MM) in ascending track.

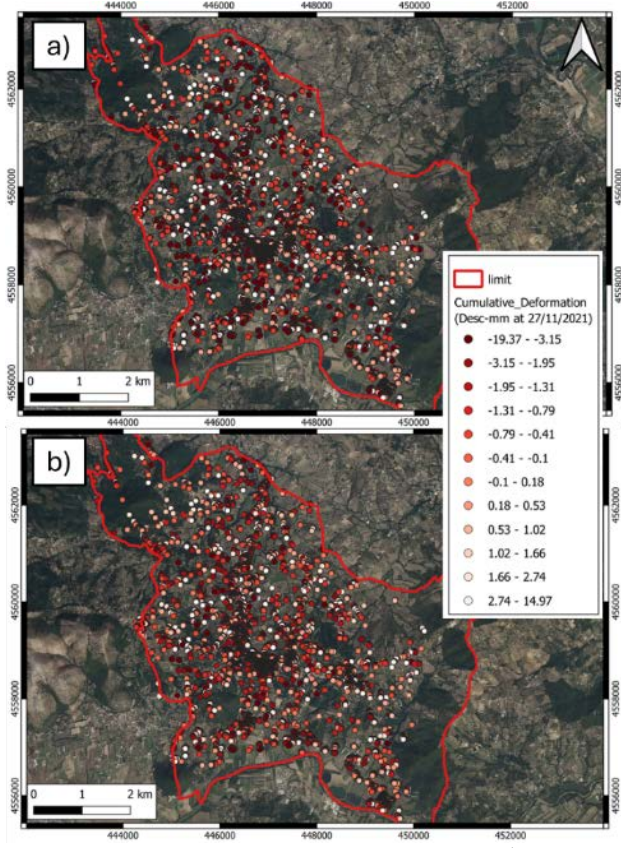


Figure 3 Location and map of deformation by a) PSI technique and b) CCN_LSTM (Unit: MM) in descending track.

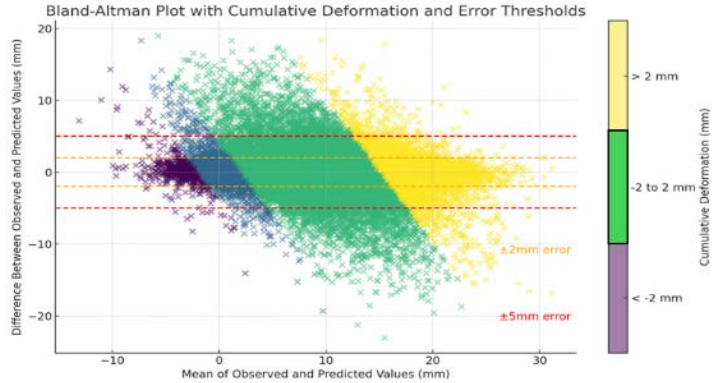


Figure 4 Bland-Altman plot showing prediction accuracy for cumulative deformation, with over 70% of predictions within $\pm 2 \text{ mm}$ error and 90% within $\pm 5 \text{ mm}$ error.

RMSE: This metric measures the average magnitude of the errors between the predicted values by the model and the actual values. It's beneficial because it gives more weight to significant errors, making it sensitive to outliers. A lower RMSE value indicates a better fit of the model to the data. According to the table, the CNN-LSTM model applied to the ascending track data has an RMSE of 0.26, suggesting it predicts cumulative deformation with relatively small errors. The descending track data's RMSE is slightly higher at 0.32, indicating more significant average prediction errors.

R² Score: Also known as the coefficient of determination, the R² score measures the proportion of the variance in the dependent variable that is predictable from the independent variables. It indicates the model's goodness of fit. An R² score of 1 indicates perfect prediction, while a score of 0 would mean that the model fails to accurately predict the outcome any better than simply using the mean of the actual values. The CNN-LSTM model achieves an R² score of 0.88 for the ascending track, which is relatively high, suggesting that the model accounts for a significant proportion of the variance in the cumulative deformation. For the descending track, the R² score is 0.79, which is still substantial but indicates a slightly lesser ability of the model to explain the variance in the data compared to the ascending track.

Table 1 Evaluation metrics for the proposed algorithms.

Model	RMSE	R ² Score
CNN-LSTM in Ascending Track	0.26	0.88
CNN-LSTM in Descending Track	0.32	0.79

The model demonstrates commendable precision in estimating cumulative deformation, with a notably lower RMSE for the ascending track data. This suggests that the model is slightly more effective in capturing the intricate spatial-temporal dynamics when analyzing data from ascending tracks, potentially due to variations in the satellite's observational geometry or differences in the environmental characteristics captured in each track type.

Conclusion

In conclusion, the comprehensive evaluation of the CNN-LSTM model through quantitative metrics and the Bland-Altman plot analysis has substantiated its ability to accurately predict cumulative deformation from SAR data across ascending and descending tracks. The model exhibited notable precision in its predictions, as evidenced by the low RMSE values and high R^2 scores, particularly for the ascending track data. This level of accuracy is crucial for developing reliable early warning systems for landslides, which can significantly mitigate the risk to infrastructure and communities in vulnerable areas. The Bland-Altman plot further affirmed the model's consistency in prediction accuracy, highlighting its potential applicability in real-world scenarios where precise and reliable predictions are paramount.

Moving forward, it is imperative to address the slight disparity in model performance between ascending and descending tracks, potentially by integrating additional data sources or refining the model architecture better to capture the unique characteristics of each track type. Future research could also explore the integration of more diverse environmental variables and apply advanced Artificial Intelligence algorithms to enhance the model's predictive power. Ultimately, the goal is to refine and adapt the model to serve as a cornerstone in proactively managing landslide risks, contributing to the safety and resilience of affected communities worldwide.

References

- Blanco-Sánchez, P., Mallorquí, J.J., Duque, S., Monells, D., 2008. The Coherent Pixels Technique (CPT): An Advanced DInSAR Technique for Nonlinear Deformation Monitoring, in: Camacho, A.G., Díaz, J.I., Fernández, J. (Eds.), *Earth Sciences and Mathematics: Volume 1, Pageoph Topical Volumes*. Birkhäuser, Basel, pp. 1167–1193. https://doi.org/10.1007/978-3-7643-8907-9_10
- Bravo-López, E., Fernández Del Castillo, T., Sellers, C., Delgado-García, J., 2022. Landslide Susceptibility Mapping of Landslides with Artificial Neural Networks: Multi-Approach Analysis of Backpropagation Algorithm Applying the Neuralnet Package in Cuenca, Ecuador. *Remote Sens.* 14, 3495. <https://doi.org/10.3390/rs14143495>
- Calò, F., Ramondini, M., Calcaterra, D., Parise, M., 2009. Analysis of slow - moving landslides by means of integration of ground measurements and remote sensing techniques 7404.
- Carannante G., Cesarano M., Pappone G., Putignano M.L., Santangelo N., Casciello E., Ferrarini F., Aucelli P., De Vita P., 2010. Note illustrative della Carta Geologica d'Italia alla Scala 1:50000 - Foglio 431 Caserta Est, ISPRA – Istituto Superiore per la
- Di Martire, D., Ramondini, M., Calcaterra, D., 2015. Integrated monitoring network for the hazard assessment of slow-moving landslides at Moio della Civitella (Italy). *Rendiconti Online Soc. Geol. Ital.* 35, 109–112.
- Ferretti, A., Prati, C., Rocca, F., 2001. Permanent scatterers in SAR interferometry. *IEEE Trans. Geosci. Remote Sens.* 39, 8–20. <https://doi.org/10.1109/36.898661>
- Gan, B.-R., Yang, X.-G., Zhou, J.-W., 2019. GIS-based remote sensing analysis of the spatial-temporal evolution of landslides in a hydropower reservoir in southwest China. *Geomat. Nat. Hazards Risk* 10, 2291–2312. <https://doi.org/10.1080/19475705.2019.1685599>
- Greff, K., Srivastava, R.K., Koutník, J., Steunebrink, B.R., Schmidhuber, J., 2017. LSTM: A Search Space Odyssey. *IEEE Trans. Neural Netw. Learn. Syst.* 28, 2222–2232. <https://doi.org/10.1109/TNNLS.2016.2582924>
- Hajimoradlou, A., Roberti, G., Poole, D., 2020. Predicting Landslides Using Locally Aligned Convolutional Neural Networks, in: *Proceedings of the Twenty-Ninth International Joint Conference on Artificial Intelligence*. pp. 3342–3348. <https://doi.org/10.24963/ijcai.2020/462>
- Hanssen, R.F., Ferretti, A., 2002. Parameter estimation in PS-InSAR deformation studies using integer least-squares techniques 2002, G62A-06.
- Hong, H., Pourghasemi, H.R., Pourtaghi, Z.S., 2016. Landslide susceptibility assessment in Lianhua County (China): A comparison between a random forest data mining technique and bivariate and multivariate statistical models. *Geomorphology* 259, 105–118. <https://doi.org/10.1016/j.geomorph.2016.02.012>
- Hooper, A., 2008. A multi-temporal InSAR method incorporating both persistent scatterer and small baseline approaches. *Geophys. Res. Lett.* 35. <https://doi.org/10.1029/2008GL034654>
- Khalili, Mohammad Amin, Guerriero, L., Pouralizadeh, M., Calcaterra, D., Di Martire, D., 2023a. Monitoring and prediction of landslide-related deformation based on the GCN-LSTM algorithm and SAR imagery. *Nat. Hazards*. <https://doi.org/10.1007/s11069-023-06121-8>
- Khalili, M. A., Guerriero, L., Pouralizadeh, M., Calcaterra, D., Di Martire, D., 2023b. PREDICTION OF DEFORMATION CAUSED BY LANDSLIDES BASED ON GRAPH CONVOLUTION NETWORKS ALGORITHM AND DINSAR TECHNIQUE. *ISPRS Ann. Photogramm. Remote Sens. Spat. Inf. Sci.* X-4-W1-2022, 391–397. <https://doi.org/10.5194/isprs-annals-X-4-W1-2022-391-2023>
- Li, H., Xu, Q., He, Y., Fan, X., Li, S., 2020. Modeling and predicting reservoir landslide displacement with deep belief network and EWMA control charts: a case study in Three Gorges Reservoir. *Landslides* 17, 693–707. <https://doi.org/10.1007/s10346-019-01312-6>
- Liu, R., Peng, J., Leng, Y., Lee, S., Panahi, M., Chen, W., Zhao, X., 2021. Hybrids of Support Vector Regression with Grey Wolf Optimizer and Firefly Algorithm for Spatial Prediction of Landslide Susceptibility. *Remote Sens.* 13, 4966. <https://doi.org/10.3390/rs13244966>
- Pescatore T., Sgrosso, I., Torre M., 1971. Lineamenti di tettonica e sedimentazione nel Miocene dell'Appennino campano-lucano. *Mem. Soc. Natur. In Napoli, suppl. al Boll.* 80, 337-408, Napoli.
- Potin, P., Rosich, B., Grimont, P., Miranda, N., Shurmer, I., O'Connell, A., Torres, R., Krassenburg, M., 2016. Sentinel-1 Mission Status, in: *Proceedings of EUSAR 2016: 11th European Conference on Synthetic Aperture Radar*. Presented at the Proceedings of EUSAR 2016: 11th European Conference on Synthetic Aperture Radar, pp. 1–6.
- Sammartini, M., Camerlenghi, A., Budillon, F., Insinga, D.D., Zgur, F., Conforti, A., Iorio, M., Romeo, R., Tonielli, R., 2019. Open-slope, translational submarine landslide in a tectonically active volcanic continental margin (Licosa submarine landslide, southern Tyrrhenian Sea). *Geol. Soc. Lond. Spec. Publ.* 477, 133–150. <https://doi.org/10.1144/SP477.34>
- Scarsella F., 1971. Note illustrative della Carta Geologica d'Italia, Foglio 172 Caserta – Servizio Geologico d'Italia, 1-123, Roma.
- Zarándy, Á., Rekeczky, C., Szolgay, P., Chua, L.O., 2015. Overview of CNN research: 25 years history and the current trends, in: *2015 IEEE International Symposium on Circuits and Systems (ISCAS)*. Presented at the 2015 IEEE International Symposium on Circuits and Systems (ISCAS), pp. 401–404. <https://doi.org/10.1109/ISCAS.2015.7168655>

Application of drone photogrammetry in hazard assessment in Međine municipality

Nino Salčin

Hidrozaod DTD, Novi Sad, Petra Drapšina 56, nino.salcin@hidrozavodddtd.rs

Abstract: After heavy rainfall at the beginning of September 2023 in the municipality of Međine, 6 km southwest of Mostar, debris flow appeared, which caused minor material damage to the surrounding buildings. Immediately after the appearance of the **debris flow**, a wider area of 160 ha was recorded using a drone to analyze the hazard, which, over time, contributed to the formation of the alluvial fan on which the site is located. The recording was done with the DJI Mini 2 drone, and the resulting photos were further processed with different software. Agisoft Metashape generated a point cloud, a 3D terrain model, an orthophoto, and a digital terrain elevation model (DEM) based on 337 photographs. The DEM image was used in further analysis within the FlowR software to obtain a debris flow simulation. An orthophoto was used to validate the simulation.

Keywords drone, model, debris flow

Introduction

Geological hazards represent one of the main threats to urban and rural populated areas, especially in hilly and mountainous regions. Many settlements are built in areas that are subject to geological hazards. The settlement of Međine, with about 200 inhabitants, was built on an alluvial fan. Debris flows, and floods periodically occur on alluvial fans, which puts the population and material goods at risk during periods of heavy rainfall. Human activity and changes in climatic conditions can lead to increased risk, where extreme temperatures and periods without precipitation, followed by extreme rainfall, are increasingly common. In November 2023, a debris flow formed after heavy rain, which caused material damage to the buildings.

After the occurrence of the debris flow, the terrain was photographed with an unmanned aerial vehicle to obtain photos to generate a 3D terrain model, a Digital Elevation Model (DEM), and an Orthomosaic, which were used for hazard analysis in the Flow-R program.

Geological structure

According to the geotectonic rezoning of Bosnia and Herzegovina, three large structural-facies units were distinguished: the Inner Dinarides, the Transition Zone, and the Outer Dinarides (M. Mojičević, J. Papeš, S. Čičić, 1984.)

The area of interest for this paper is part of the structural-facies macro unit of the Outer Dinarides, which was formed on the Mesozoic carbonate platform. Geotechnically, it expresses the greater part of Herzegovina, southwestern Bosnia, and part of western Bosnia. In the belt of the Outer Dinarides, compressional fold structures, anticlines, synclines, extensive thrusts, and reverse and horizontal shear faults prevail. Numerous pull-apart basins, positive and negative "flower" structures, are genetically linked to fault zones. The lithological composition of the Dinarides is dominated by a thick series of micro tectonically cracked Mesozoic limestones, limestones with dolomite inlays, and dolomite.

The area of interest belongs to the geological map sheet Mostar K33-24, which covers an area of 1498 km² between coordinates 17°30' to 18°00' east longitude and 43°20' to 43°40' north latitude according to Greenwich. The most significant part of the terrain belongs to the high mountains of Herzegovina: Čvrsnica, Prenj, Čabulja, Velež, and Plasa, which have a Dinaric direction and are characterized by a complete absence of vegetation. Towards the south, the high Herzegovinian mountains pass into the surface with an average height of about 1000 m. A particular morphological unit is represented by karst fields, Bijelo polje, Rudno polje, Blidinje jezero, smaller karst fields around Lištica, and Mostarsko blato in the southern part of the field, where the site of interest is located. Mostarsko blato is located west of Mostar and represents a typical periodically flooded karst field.

According to the geological composition of the wider area, Cretaceous sediments are the most dominant, represented by massive and layered limestones and dolomites, which lie concordantly over the Jurassic sediments. The Lower and Upper Cretaceous have been established, but in the research area relevant to this work, the Cretaceous sediments of the Cenomanian and Turonian are present.

Limestones and dolomites of the Cenomanian lie concordantly over the Lower Cretaceous; larger parts were isolated in the area of mountain Čabulja, Velež, and Jasenjane, and smaller parts were found around Crnač and Lištica. In Lištica, which flows through the Mostarsko blato, dolomites dominate compared to limestone. The thickness of separated sediments is around 250m.

Sediments of the Turonian age lie concordantly over Cenomanian limestones and dolomites. They are

represented on the mountains of Čabulja, Velež, Jasenjin, Varda, and Bogdola, and smaller parties were observed north and northeast of the list. Dolomites are finely crystalline, and smaller amounts of microcrystalline calcite are present in addition to dolomite crystals. The thickness of the mentioned sediments is around 400m.

Alluvial sediments are found in the Lištica valley, represented by fine and coarse gravel, less often by sand, which occurs in uneven stratification with frequent sandy clays. Also present are proluvial deposits, which represent formations built from clastic material created by the action of occasional linear flows, and torrents, where the erosion is intense and short-lived. This process often causes accompanying phenomena, such as landslides and landslides. The conditions for creating proluvial deposits are heavy rainfall, pronounced relief, and abundant yield of eroded material. Deposits are often deposited in fans at the foot of mountain echoes, at the outlet of smaller streams on the alluvial plains of larger rivers, and the like. These morphological forms are frequent in arid and semiarid areas, where there is rare but very abundant and heavy rainfall. Typical fans vary in length from decameters to kilometers, and their thickness ranges from meters to decameters.

The fan's general characteristic is the material's non-roundness and weak attachment to the gradation sorting from the root to the periphery of the cone. The gradational deposition of material occurs due to the decrease in the kinematic energy of the flow so that at the root of the fan, there are primarily pieces of rock, coarse-grained pebbles. At the same time, finer-grained deposits, such as gravel and sand, are found in the lower parts, and the smallest sediments are present on the peripheral parts of the fan.

Geomorphological features

According to A. Leprica (2018), the Mostarsko blato represents a neo-tectonically lowered valley, dominantly characterized by accumulation processes. Geomorphologically, it was reshaped within fault-predisposed pull-apart basins. Based on the results of geological analyses, it was established that the slopes of larger fields in the karst and some valley extensions in the Outer Dinarides were filled with Neogene lakes that communicated with each other. Today, the Mostarsko blato is a periodically flooded field where lacustrine and bar sediments are deposited to cover the lowest parts of the field. And form today's peatland. The wider area is made of carbonate rocks, limestone, and dolomite, which are quite susceptible to physical and chemical surface decomposition.

Physical and chemical decomposition are closely related and act together, but the intensities are usually different. Limestones and dolomites, as monomineralic rocks, are not subject to thermal decomposition. Still, the crystallization of salt and freezing of water leads to the physical decomposition of rocks, creating and expanding cracks that enable more intense chemical decomposition.

The main agents of chemical decomposition are water, oxygen, carbonic acid, and organic acids. Chemical alteration leads to a decrease in the mechanical strength of the rock so that the physical decay is facilitated and intensified, which again leads to an increase in the chemical decay and to the complete decay of the rock and its erosion. In the process of karst erosion, carbonic acid is the most important, created by dissolving carbon in water, thus increasing the solvent power of water by about 100 times. It should be taken into account that although dolomites are carbonate rocks, they are much less sensitive to chemical decomposition than limestone, about 20 times less.

Karst areas with many dilapidated and decomposed rocks are suitable for denudation, in which loose soil and decomposed rock are washed away underwater, leaving bare rocks (Figure 1). The intensity of denudation depends on the amount of precipitation, the terrain's slope, the soil's composition, and the vegetation cover.



Figure 1 - Aerial photograph of Medine

Slope processes develop on terrains covered by intense physical and chemical erosion. For this paper's case, the proluvial process and proluvial deposits are essential. Proluvial deposits represent clastic formations formed by torrential flows, and the conditions for their formation are heavy rainfall, pronounced relief, and an abundant yield of destroyed material.

Climate characteristics

The temperature of this area is characteristic of the northern hemisphere and the area of moderate latitudes. The average annual temperature has a regular development; the warmest month is August, and the coldest is December. In the summer months, it is not uncommon for temperatures to exceed 40°C; the coldest month is January, with an average temperature of 5°C, and the hottest month is July, with an average temperature of 26°C. Mostar has a relatively dry season from July to September, and the rest of the year is humid with a mild

climate. The highest temperature in Mostar was measured on July 31, 1901. year and was 46.2°C.

Next to temperature, precipitation is the most critical climate element. Cyclonic precipitation prevails in Herzegovina, and Herzegovina belongs to the Mediterranean pluviometric regime characterized by distinct winter maximum and summer droughts.

The debris flow formed in November after daily rainfall of 31.3 mm, although it should be taken into account that although the measured interval was 24 hours, the rainfall lasted only a few hours. The Federal Hydrometeorological Institute of Bosnia and Herzegovina provided data on the amount of precipitation.

Formation of the debris flow

After heavy rainfall, debris, decay, and soil suddenly moved under the action of water. This is a proluvial process where the agent is the kinetic energy of occasional linear flows. The erosive effect of the flow that occurred in Medine was immediate. It caused the movement of rubble, the volume measured in m³, and created a ravine.



Figure 2 - Ravine created by debris flow and deposited material

The material was transported along the ravine, 650m, then moved 250m through the settlement, and as the flow lost its kinetic energy, the material was sorted by size.

The factors that caused erosion are:

- precipitation, November 3, 2023. year were so and so, which contributed to the increase in the kinetic energy of the flow
- the absence of vegetation enabled easy washing of materials from the slopes, their transport, and disposal on the lower parts of the terrain.

In conversation with the locals, I learned that in the 1950s, a debris flow that was larger than the watershed in 2023 was formed. This caused significant material damage to the buildings. In recent years, part of the construction material from the damaged buildings has been found in the bottom of the fan, covered with a thin layer of humus.

Specific remedial measures can be taken to prevent the occurrence of such water bodies, which include reducing erosion, shortening the length of material transport, and building an anti-flood barrier.

Research methods

The methods used to process the investigation area are remote sensing methods, which, in the narrower sense, include analyzing and interpreting images of parts of the Earth's surface, whether taken from the ground, air, or space. One of the widely used remote sensing methods is digital photogrammetry.

Photogrammetry is an optical technique based on the stereo principle, that is, on the existence of parallax between two recording positions. Parallax represents an apparent change in the object's position relative to the background due to the difference in the observation position or due to the rapid movement of the observer. In the photogrammetric analysis, recordings of the visible part of the spectrum and a high-resolution camera are used, whereby the recordings are performed with an overlay to achieve a stereo effect.

By applying digital photogrammetry, 3D models of the object of interest, in this case, the terrain, can be obtained using digital images. Footage can be obtained in different ways, such as by using other platforms like helicopters, airplanes, or drones.

The geometry of the shot is reconstructed based on the recognition of the same object on two or more different shots (that's why it is necessary to perform a recording with an overlay), and based on the geometry of the camera lens, knowledge of the position from which the recording was made and the stereo effect, the x,y,z coordinates of the recognized object are obtained of the object. The procedure is repeated until sufficient points are reconstructed to form a 3D terrain surface.

The main goal of photogrammetry is to determine the geometrical dependence between the object and the photograph and collect information about the object from the picture. Digital photogrammetry involves processing all types of images, passive (obtained by an optical system) or active (obtained by an active system), taken from any platform, be it a pocket camera, drone, airplane, or satellite.

Aerial photography was used to write this paper. Aerial photography can be done vertically or obliquely. In vertical images, the optical axis is perpendicular to the horizontal plane. In oblique shooting, the camera's optical axis coincides with the horizontal plane at an angle smaller than 90 degrees. Decreasing this angle increases the area of the recorded terrain and the deformations that appear on the video due to the perspective, which is not uniform. Parts of the terrain closer to the camera are much less deformed than areas further away. In vertical images, deformations also occur, which are evenly distributed and grow from the center of the image to its periphery. Although oblique shots cause deformations when recording, the same part of the terrain must be recorded twice from two different positions. There must be a certain convergence angle between the axes, meaning that at least one axis must have an oblique position about the horizontal plane. The requirements are contradictory, but

a solution is easily reached by recording the terrain with overlapping shots so that the part where the shots are overlapped is recorded twice from two different positions. The required overlay during recording should be a minimum of two-thirds of the image because an overlap of 50% of the image surface does not provide sufficient certainty that each point of the terrain will be captured twice from two different positions.

Research results

The research area covers an area of 160ha and was recorded with a DJI Mini 2 drone for photogrammetric analysis of the area, dated November 4, 2023. immediately after the start of the flow, the recording was made. Three hundred twenty-seven photos with mutual overlap >60% were taken.

In the Agisoft Metashape program, a 65 million-point cloud was generated based on previously taken photos. The point cloud was later used to generate the 3D terrain model shown in Figure 3.



Figure 3 – 3D model of research terrain

Subsequently, the point cloud was filtered in Agisoft Metashape and CloudCompare. With the help of the CloudCompare program, vegetation removal from point clouds was also performed, in addition to filtration. The Agisoft Metashape program also generated an orthophoto of the area, which includes the area above the site, the site itself, and part of the karst field. The resolution of the orthophoto image is 12 cm and clearly shows the area affected by the debris flow, Figure 4. In addition to the orthophoto, a digital terrain elevation model (DEM) with a resolution of 24 cm was also generated, Figure 5.



Figure 4 – Ortofoto of research terrain

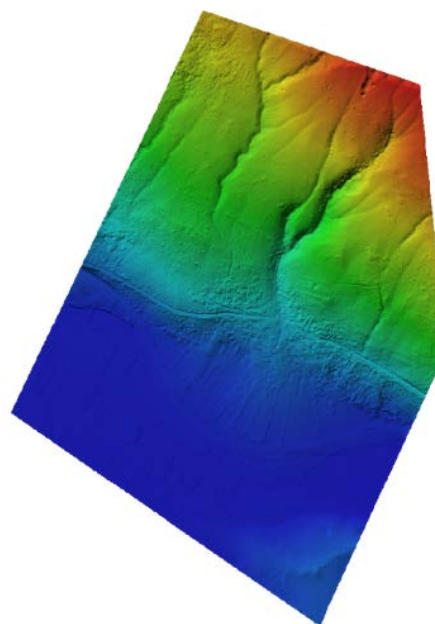


Figure 5 – Digital Elevation Model of research terrain

Using the Flow-R program, the debris flow simulation was made. The modified Holmgren algorithm (1994) was used as the direction algorithm, and the Perla et al. (1980) function was used as the friction loss function. Iterations were performed with different parameters until the result corresponded to the actual situation in the field. If the simulation result is compared with the orthophoto image, it can be concluded that the simulation is valid. Also, by changing the parameters, the very creation of the fan on which Medine is located can be shown.



Figure 6 – Result of Flow-R simulation

Conclusion

The rapid advancement of technology has led to drones for commercial service, providing outstanding footage that can be used for a variety of purposes for little money. On the recordings obtained by the DJI Mini 2 aircraft, which are subsequently processed in various software, a spatial analysis of the terrain can be done, accompanied by animations and photo documentation, which is of satisfactory quality even for professional use. With a high-quality analysis and interpretation of the results, suggestions can be made for protection against natural disasters and improvement of urbanization. Still, it is also essential for the user to recognize insufficient initial data and interpret them well.

Acknowledgements

I would like to thank my mentor, Prof. Dr Miloš Marjanović, for his help and support during the writing period. Also, I thank the Federative Hydrometeorological Zavod for providing me with valuable data on the amount of precipitation, and special thanks to all the residents of Međine who helped me during field research.

References

- Čičić S., Mojićević M., Papeš J., (1984) Geologija Bosne i Hercegovine, Knjiga II.- Geoinženjering, Sarajevo str. 315
- Duplančić Leder T., Leder N.(2018) Određivanje površinske temperature tla grada Mostara satelitskim metodama,, Fakultet građevinarstvom arhitekture i geodezije, Split str 68
- Francioni M., Simone M., Stead D., Sciarra N., Mataloni G., Calamita F. (2019) A new fast and low-cost photogrammetry method for the engineering characterization of rock slopes
- Lepirica A. (2013) Geomorfologija Bosne i Hercegovine, Sarajevo str 16, 24, 25
- Mojićević M., Laušević M. (1973) Tumač za list Mostar K 33-24, Osnovna geološka karta 1:100 000, Socijalistička Federativna Republika Jugoslavija, Beograd str 5, 7, 11, 23, 25-29
- Nenadović D., Bogićević K. (2010) Geologija kvartara, Beograd str. 125-126
- Petrović R., Čupkoović T., Marković M. (2001) Daljinska detekcija, Beograd str 43-45
- Regodić M. (2008) Daljinska detekcija kao metod prikupljanja podataka o prostoru
- Timičić D. Klimatske značajke Mostara, Danijela Motrišta br. 57-58, glasilo Matice hrvatske Mostar, str. 156, 158, 163, 164
- ШАНЦЕР Е. В. (1966) Очерки учения о генетических типах континентальных осадочных образований. Недра, Москва

Monitoring of the Active Landslide during Excavation of Slopes for the Svračkovo Dam Stilling Basin

Nemanja Babović ^{(1)*}, Dragana Aleksić ⁽¹⁾, Aleksandar Miladinović ⁽¹⁾

1) Energoprojekt-Hidroinženjering, Geology, hydrogeology, geophysics, geodesy, GIS and roads, Belgrade, Bulevar Mihajla Pupina 12, nbabovic@ephydro.com

Abstract The Svračkovo dam site is located in western Serbia, on the Veliki Rzav River, 8 km upstream of Arilje town. About 26 million m³ reservoir capacity shall be formed by construction of an embankment dam with a clay core - 60 m high and with the dam crest elevation of 423.60 masl. The narrow area of the dam site and appurtenant structures comprises an area of about 0.4 km². For the requirements of construction of the stilling basin, i.e. the outlet from the diversion tunnel on the left abutment, bench slopes from access roads S₁ and S₃ are excavated. During excavation of slopes beneath the access road S₃, contemporary scars resulting from terrain movement were detected on the upper access roads and in the vicinity. In addition to investigation works, geodetic surveys were also carried out for the purpose of landslide monitoring in conditions of ongoing remedial measures.

Keywords Svračkovo, investigation works, geodetic surveys

Introduction

The main purpose of the „Svračkovo“ dam construction is a certain, sustainable water supply to the broader area of this part of the Republic of Serbia, encompassing the towns of Arilje, Požega, Užice and Ivanjica (Fig. 1).

In addition to its basic hydrotechnical purpose, this structure is designed as a hydropower facility, too, so that apart from water supply, its function will be to generate electric power as well (HPP Svračkovo).



Figure 1 Geographic position of the Svračkovo dam

By construction of the first access road to the construction site in 2010, the works related to the execution of the HPP Svračkovo structure commenced. For the requirements of construction of the stilling basin, i.e. the outlet from the diversion tunnel on the left abutment, bench slopes from the access roads S₁ and S₃ are excavated. The access road S₃ is hypsometrically lower (~elevation masl) than the access road S₁ (~elevation masl). During excavation of slopes beneath the access road S₃, contemporary scars resulting from terrain movement were detected on the upper access roads and in the vicinity. Active scars on the terrain have been identified almost at the peak elevations of the terrain above the road S₁ (Fig. 3).

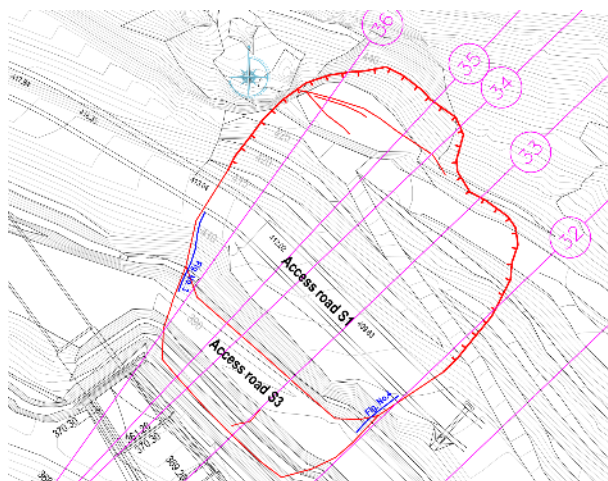


Figure 2 Active scars on the terrain

The boundaries of contemporary geodynamic phenomena, which are presented in Fig. 2, have been geodetically surveyed. The frontal scar of the landslide was identified up to the peak elevation of 420 masl, in the zone of limestone blocks. Lateral landslide scars were clearly identified on already executed slopes covered with shotcrete. The gap of the lateral landslide scars on shotcrete is even up to several cm, Fig.3 and Fig. 4.



Figure 3 Active scars on the terrain



Figure 4 Active scars on the terrain

The presented landslide is one of the two major landslides registered at this site during execution of excavation works for the stilling basin. The other, downstream landslide, is described in detail within the earlier submitted paper at the 5th Regional Symposium on Landslides, Rijeka, 2022.

Upon detection of contemporary geodynamic phenomena on the terrain, extensive measures of investigation works with appropriate computational analyses of terrain stability were implemented.

Presentation of the Results of Geological/Geotechnical Field Investigations

Within the investigation procedure for the requirements of remediation of the activated landslide, detailed engineering-geological mapping of the slopes of service-construction access roads, exploratory drilling of 7 boreholes to the depth of 50 m, and geo-electric probing of terrain were carried out. Based on the analysis of obtained data and investigation results, it was concluded that the narrower investigation area is built up of Lower Triassic and Middle Triassic sedimentary rocks, and Quaternary formations, Fig. 5.

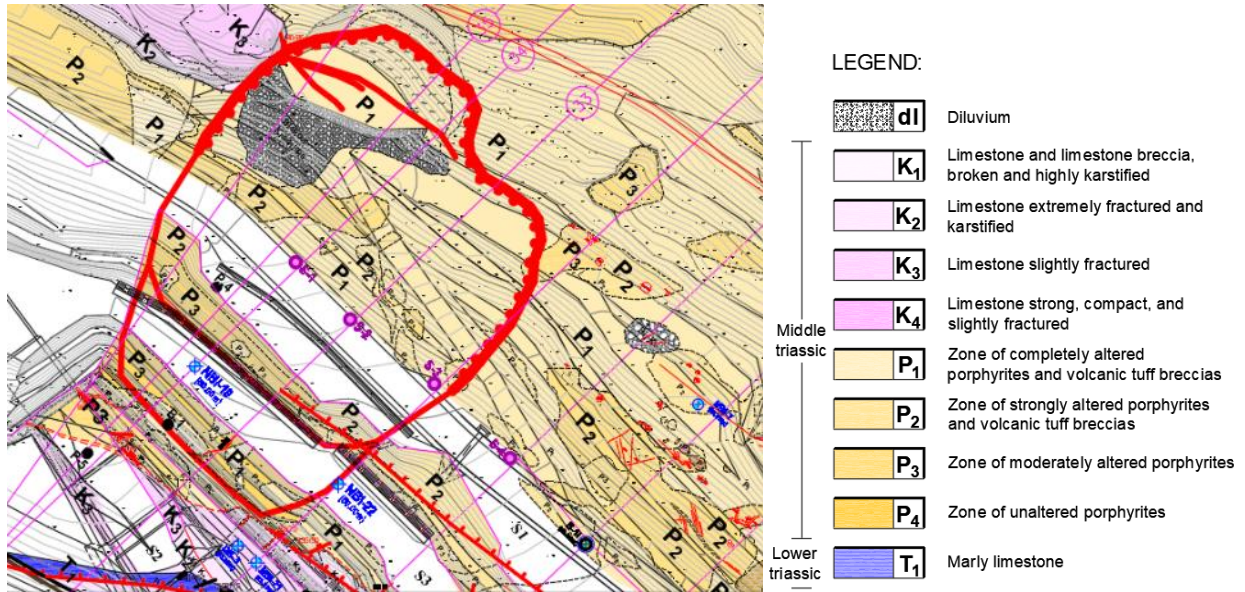


Figure 5 Engineering geological map of the investigation area

The **Lower Triassic rocks** are relatively poorly exposed, outcropping is identified along the riverbed edge and sporadically in the proximity of access roads. It is represented by *bioturbatic formation* composed of marly limestones of pronounced laminated structure. The rock mass is of medium to low strength, with pronounced fracture systems, their walls being smooth and flat. On the Basic Geological Map of SFRY (Brkovic and Malesevic 1977), it was believed for a long time that the Lower Triassic sediments were in a normal relationship with the Middle Triassic sediments, all until the extensive investigation procedure conducted for the requirements of remediation of this instability. In fact, during execution of access roads to the higher exploratory boreholes NBI-10 and NB-4, it was noted on fresh outcrops that the Lower Triassic sediments were in a reverse relationship with the Middle Triassic sediments. The contacts have mild slopes, with mandatory presence of a thin layer of hydrothermal altered rocks of red colour in the contact zone. This data indicates to high pressures during the block overthrust of older geological formations over younger ones. The described procedure is also identified in the exploratory drilling cores. The expert confirmation of such a geological composition of terrain in conditions of intensive block overthrust was supported by the results of the executed investigation procedure, and documented within the structural-tectonic Study (Trivić, 2019). Based on the mentioned study, block overthrusts are generally dipping northeast, with mean statistical dip elements EPkr 21/44. In Fig.6, the Lower Triassic sediments are marked T₁.

Middle Triassic sediments spatially dominate in the investigation area, and are composed of limestones of sparite structure, massive texture, partly or completely

recrystallized, in some places irregularly dolomitized, and in some places with lenticular intercalations of sedimentary breccias. The slopes structured of massive limestone are steep, and in some places turn into vertical sections, which was noted immediately above the frontal scar of the active landslide. On limestone outcrops, sets of fractures stand out, dividing the rock into monoliths of different dimensions. According to the degree of jointing and degree of karstification, the massive limestones are divided into four media:

- K₁ – Limestone and limestone breccia, broken and highly karstified;
- K₂ – Limestone, extremely fractured and karstified;
- K₃ – Limestone, slightly fractured;
- K₄ – Limestone, strong, compact and slightly fractured.

In Fig. 6, massive limestones are marked K₁ to K₄.

Porphyrites are present in the central and southwest part of the investigation area. Their genesis is associated to submarine-type volcanism in synsedimentary conditions. These volcanic rocks, according to most authors, represent a product of the Triassic rift area. On the Basic Geological Map, sheet Užice (Mojsilovic and Baklaic 1977), they are treated as an integral part of the volcanogenic-sedimentary unit where it was noted that they appear in the form of porphyritic tuffs, breccias and porphyrites, alternating with crystalloclastic tuffs. Based on additional petrologic tests, it was determined that these exact volcanogenic-sedimentary rock masses are present at this location. Porphyrites are volcanic rocks formed by lava outflow, thus they are initially of higher strength than the volcanic tuff-breccias, and in addition to that, the volcanic tuff-breccias, as softer rocks, are more susceptible to the process of hydrothermal alterations. Chloritization

and calcitization were registered on most samples from volcanic tuff-breccias, and sericitization on one sample.

Based on the degree of alteration, these volcanic-sedimentary rock masses are divided into four categories:

- P₁ – Zone of completely altered porphyrites and volcanic tuff-breccias;
- P₂ – Zone of strongly altered porphyrites and volcanic tuff-breccias;
- P₃ – Zone of moderately altered porphyrites;
- P₄ – Zone of weakly altered and unaltered porphyrites.

It may be stated that the zones of completely (P₁) and partly altered porphyrites (P₂) are mixed with tuff breccias, provided that the processes of hydrothermal alterations have masked the mutual geological transitions and boundaries. The processes of chloritization, calcitization, and especially sericitization, play the key role in the rock material degradation. On representative samples from these materials, very low values of physical-mechanical properties were obtained.

It may be concluded on the basis of conducted geological analyses that the sliding planes are formed on unfavourable systems of fracture sets (EPsm₁ – 225/68) in weakened geological zones of completely altered porphyrites with tuff-breccias, Fig. 6.

Fracture systems EPsm₁ with mean dip elements 225/68 are assessed a very unfavourable set of fractures in terms of slope stability. The spatial position of the strike of these fracture sets is almost parallel to the strike of executed slopes. Apart from the foregoing, the fractures of this set are slickenside and undulatory along the angle of dip, so that they may form very unfavourable sliding planes in relation to other fracture sets.

Slope Stabilization Measures in the Active Landslide Zone

Based on conducted computational analyses of terrain stability in operating conditions, two terrain stabilization phases have been defined.

Terrain stabilization Phase I – reduction of the slope inclination, i.e. slope relief in the form of removal of overburden and moved rock material. Slope relief was performed from elevation ~445 masl to the access road S₁, approximate terrain elevation 410 masl. About 25 000 m³ of rock material was removed. The slopes are executed at 1:1 gradient with berm width up to 3 m. The newly executed slopes are supported by three layers of shotcrete, 2 reinforcing meshes and passive anchors up to 10 m long. In Fig.8, this remediation measure is marked blue.

Terrain stabilization Phase II – systematic anchoring of terrain using pre-stressed anchors, under the access road S₁:

- Geotechnical pre-stressed anchors in the zone of road S₁ – the total of 12 anchors, 25 m long each, at the mutual horizontal distance of 4 m.

- Geotechnical pre-stressed anchors on road S₃ – the total of 36 anchors, 25 m long each, in two rows at the mutual horizontal distance of 4 m
- Geotechnical pre-stressed anchors from elevation 375 masl – the total of 36 anchors, 25 m long each.
- Geotechnical pre-stressed anchors from elevation 369.20 masl – the total of 36 anchors, 25 m long each, in two rows, at the mutual horizontal distance of 4 m.

The length of geotechnical anchors is 25.0 m, while the anchoring section is 10 m long. The maximum pre-stressing force is 1300 kN. In Fig. 6, this remediation measure is marked green.

The works on execution of this terrain stabilization phase were performed in the period from January 2016 to the end of 2017. For the requirements of continuous monitoring of works, and slope monitoring during execution of the envisaged remediation works, benchmarks were systematically executed on the slope. The benchmarks were executed in the broader zone of works and continuously monitored during execution of the terrain remediation.

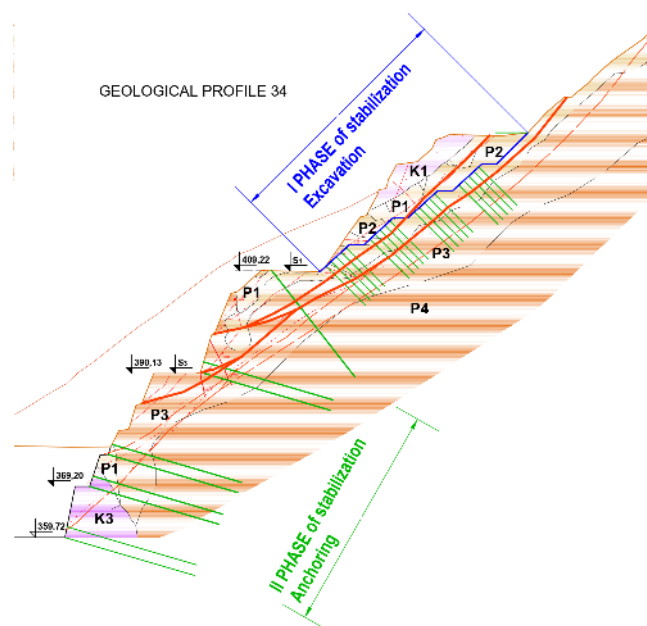


Figure 6 Geological profile 34 with indicated terrain stability measures

Monitoring of the Slope Above the Stilling Basin

In the landslide zone, the total of 25 points are monitored. Out of the total number of monitoring points, 17 points are designed on the landslide itself, and the rest outside this zone in order to observe and monitor the broader area.

The basic 2D and 1D landslide monitoring network consists of 7 points: S₁, S₂, S₃, S₄, S₅, S₉ and S₁₂. Materialization of network points is performed by setting up concrete columns with the height, from tread, of about 1.30 m above the ground surface. The coordinate system in the basic 2D and 1D network is the state reference system.

To determine the horizontal displacement of monitored points, the conventional method was selected, measuring the following quantities: horizontal directions, vertical angles and diagonal distances. For measurement of horizontal directions, the method of measurement in both faces was applied, and the number of rounds of directions was three. Measurement of diagonal distances is to be performed in both positions of the telescope KL and KD. Measurements to determine the vertical displacements of points on the landslide in 1D network were performed by the method of trigonometric levelling. Based on the measurement of all quantities in the basic 2D and 1D network of the specified parameters, the definite values of directions, distances and height differences were calculated.

The basic 2D and 1D network were first adjusted as free ones, and then the fixed points were determined and re-adjustment with minimum trace was performed to the given (fixed) points of the 2D and 1D network.

For each control series, fixed points of the basic 2D and 1D network were determined. The analysis of fixed points in the basic 2D and 1D network was performed by one of the verified methods in the deformation analysis (Pelzer method).

The measurement was performed using an instrument with measurement uncertainty as follows:

- For horizontal and vertical directions 1"
- For distances $(1+1 \cdot 10^{-6} \cdot L)$ mm, (L in mm)

Total displacement of control points is calculated in relation to the zero measurement executed in December 2015. In the period from February 2016 to August 2017, 12 control series were executed. The value of detectable displacement is smaller than 1 cm, both for horizontal and vertical movements. Assessments of unknown parameters with accuracy assessment and size of detectable displacement at the test rating of 0.80 are presented in the table.

Table 1 Results of laboratory tests in a large scale

No.	Control point	my [mm]	mx [mm]	dpy [mm]	dpx [mm]	mh [mm]	dph [mm]
1	S1, S2, S3, S4, S5, S9 and S12	0.7	0.8	3.0	3.1	1.6	6.2
2	1 to 8	0.7	0.9	2.8	3.5	1.2	4.7
3	9 to 17	0.8	1.0	3.0	4.3	1.2	4.7
4	18 to 25	1.7	1.9	6.8	7.9	1.7	6.5

Wherein:

- my – Mean error in determining the coordinates on Y axis
- mx - Mean error in determining the coordinates on X axis
- mh – Mean error in determining the heights
- dpy – Detectable displacement size on Y axis
- dpx – Detectable displacement size on X axis

- dph – Detectable displacement size on Z axis

The values of changes in movement for the period February 2016 – July 2016 are presented on Fig. 7.

date	02/2016			03/2016			04/2016			05/2016			06/2016			07/2016			
CONTROL POINT	V-IV SERIA			VI-V SERIA			VII-VI SERIA			VIII-VII SERIA			IX-VIII SERIA			X-IX SERIA			
	DVY (mm)	DVX (mm)	DZ (mm)	DVY (mm)	DVX (mm)	DZ (mm)	DVY (mm)	DVX (mm)	DZ (mm)	DVY (mm)	DVX (mm)	DZ (mm)	DVY (mm)	DVX (mm)	DZ (mm)	DVY (mm)	DVX (mm)	DZ (mm)	
1	-2	0	1	-4	-3	-1	-2	-3	1	-1	-1	0	1	1	1	0	0	-1	2
2	-4	-2	0	-18	-18	0	-17	-16	1	-11	-11	-2	-2	-3	-1	-3	-2	1	
3	-2	-1	0	-10	-14	0	-9	-13	1	-5	-8	1	1	-2	0	0	-2	1	
4	-2	1	0	-14	-14	-4	-17	-16	0	-7	-8	-2	0	-1	0	0	-1	1	
5	-2	1	-1	-13	-18	-7	-16	-22	-2	-5	-7	-1	0	-1	0	0	1	0	
6	-4	-1	0	-16	-21	1	-18	-24	4	-11	-12	1	-1	-2	0	-3	-5	1	
7	-4	-2	-1	-22	-25	2	-25	-25	4	-14	-16	1	-4	-5	0	-3	-2	1	
8	-5	-4	0	-17	-17	3	-17	-17	4	-10	-9	2	-1	-1	1	4	3	0	

Figure 7 Changes in horizontal and vertical movements

Wherein:

- DVY – Change of movement on Y axis between two series.
- DVX – Change of movement on X axis between two series.
- DZ – Change of movement on Z axis between two series.

Fig. 8 shows the summary of vectors of total horizontal and vertical movements obtained after the sixteenth control series in August 2017.

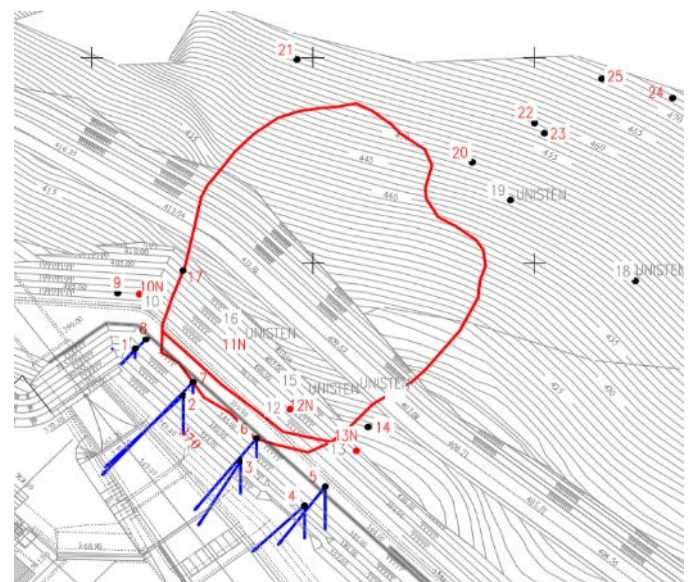


Figure 8 Total horizontal and vertical movements – August 2017

LEGEND:

- Total vertical movements – sixteenth measurement series – August 2017
- Vector of total horizontal movements – sixteenth measurement series – August 2017

Analysis of the Monitoring Results

As mentioned in the preceding chapter, for the requirements of slope monitoring first the benchmarks 1-25 were installed, on which the zero measurements were performed in December 2015. Surveying benchmarks with serial numbers from 1 to 4 and from 5 to 8 are positioned on the slopes above the road S₃, so that they are not damaged during slope remediation and, consequently, they were monitored for the longest time. The results of

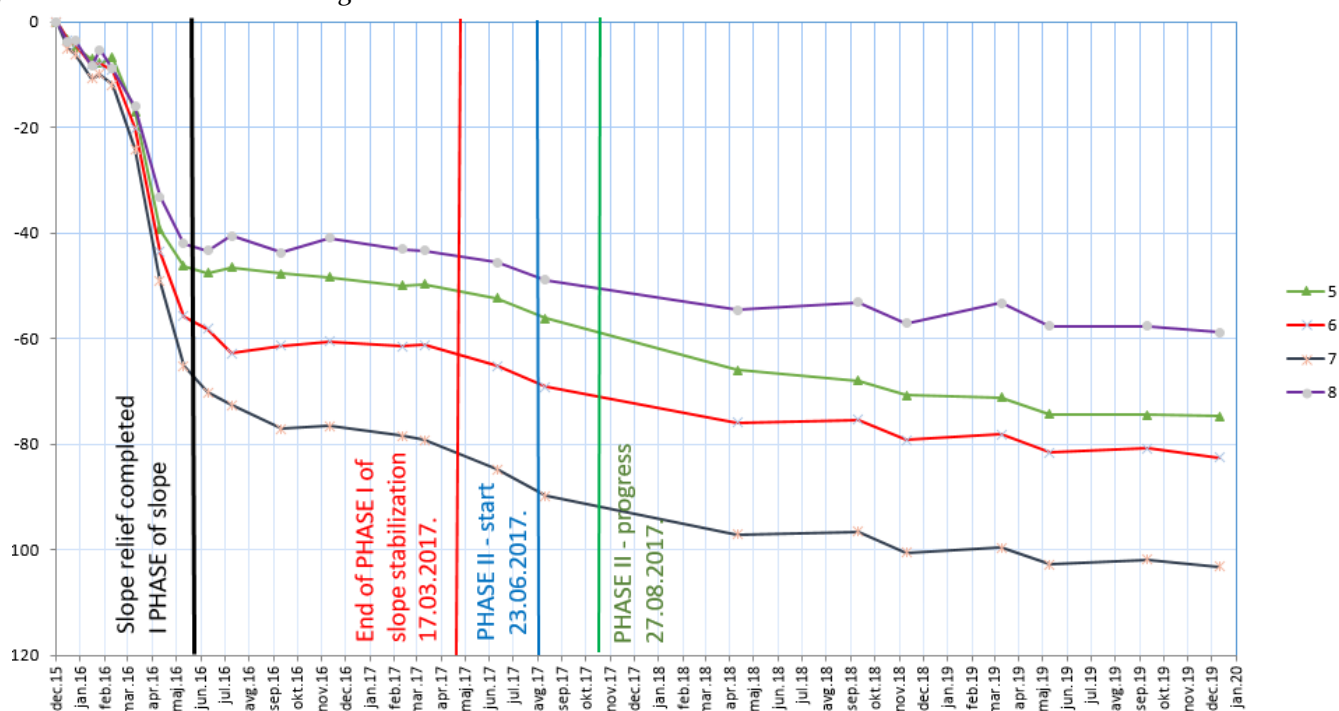


Figure 9 Moving of the benchmark on the landslide in the X direction – II row

Conclusion

For the requirements of stabilization of slopes above the stilling basin, dedicated geological investigations were carried out. Based on conducted investigations, structural analyses were made for the requirements of stabilization of the slope above the stilling basin. The slope remediation design defines two terrain stabilization phases.

Terrain stabilization Phase I – reduction of the slope gradient, i.e. slope relief in the form of removal of the overburden and moved rock material.

Terrain stabilization Phase II – systematic terrain anchoring using pre-stressed anchors, under the access road S₁.

The works on execution of these two terrain stabilization phases were performed in the period from January 2016 to the end of 2017.

For the requirements of continuous monitoring of works, slope monitoring during execution of envisaged slope remediation works, surveying benchmarks were systematically executed and monitored during the remediation works.

the monitoring of surveying benchmarks 1 to 4 and 5 to 8 are almost analogous, therefore Fig.No.11 shows the movements on x axis on benchmarks 5 to 8.

The largest movements took place until May 2016, when the removal of overburden above the road S₁, PHASE I, was completed. Gradually, in line with the progress of landslide remediation progress, the movements diminished, resulting in the benchmark movement of mm order of magnitude from April 2018 to September 2019.

After analysis of displacements detected on surveying benchmarks, it was concluded that the largest movements took place until May 2016, when the removal of overburden over the road S₁, PHASE I, was completed. Gradually, in line with the progress of landslide consolidation, the movements diminished, resulting in the benchmark movement of mm order of magnitude from April 2018 to September 2019.

Acknowledgements

The authors would like to thank the Public Water Management Company “Srbijavode”, for supporting us during the field investigations and approving of the publishing of the presented data.

References

- Brkovic T, Malesevic M (1977) Basic Geological Map, Sheet Čačak 1:100 000 – K34-05, Institute for Geological and Geophysical Investigations, Belgrade, SFRY.
- Mojsilovic S, Baklaic D (1977) Basic Geological Map, Sheet Titovo Užice 1:100 000 – K34-04, Institute for Geological and Geophysical Investigations, Belgrade, SFRY.

Detection and monitoring of slope movement by using point cloud derived from the SfM technique

Igor Ivanovski^{(1)*}, Natasha Nedelkovska⁽²⁾, Gose Petrov⁽³⁾, Milorad Jovanovski⁽⁴⁾, Toni Nikolovski⁽¹⁾, Igor Peshevski⁽⁴⁾

1) Strabag AG, Skopje, Mirče Acev 2, MK-1000 Skopje, Republic of North Macedonia, igor.ivanovski@strabag.com

2) Geohydroconsulting Ltd., Skopje, Manapo

3) Faculty of Natural and Technical Sciences, "Goce Delčev" University in Štip

4) Ss. Cyril and Methodius University in Skopje, Faculty of Civil Engineering, Skopje, blvd. Partizanski odredi 24

Abstract The paper presents an example of the detection and monitoring of slope movements by using a 3D point cloud obtained from the low-cost, remote, and precise SfM (Structure from Motion) technique. SfM is a photogrammetric range imaging technique for estimating three-dimensional structures from two-dimensional image sequences that may be coupled with local motion signals. Its algorithm detects common feature points in multiple images and uses them to reconstruct the movement of those points throughout the image sequence. The analysed instability represents one part of the cut 4 at km 11+620 to km 12+244 on A2 Expressway Kriva Palanka-Stracin, section Dlabochica-Chatal (Republic of Macedonia). The rockslide developed at the beginning of the cut 4 excavation, in a medium of albite-epidote-chlorite schists. The surveying was performed with a low-altitude camera drone - Phantom 4 RTK, the Pix4D software was used for processing the SfM recordings, while the analyses were done in the CloudCompare software. Four point cloud sets were analyzed in relation to the initial (the reference) one acquired before the detected movements. Multi-temporal geomorphic changes in the rockslide area were identified by comparing the SfM-derived point clouds in pairs. 3D distances were estimated with the multi-scale model-to-model cloud comparison for each pair of point clouds. The results show that the displacements on the slope range up to 70 cm. Also, the 5-month observation period shows that the rockslide is not settled and there are certain movements, especially in its upper part. The obtained results show that the application of SfM for the detection and monitoring of displacements seems to be a beneficial technique for such purposes because of its swiftness, the high detail of prospecting, and the possibility of determining minimal movements.

Keywords SfM technique, displacement, rockslide, point cloud

Introduction

Among the many geological hazards, landslides have the widest distribution and cause considerable losses to the national economy and property. The stability of the road cuts directly affects the local traffic and the safety of life and property of the surrounding residents (Montgomery 1994, Harabinova 2017, Shariati et al. 2021).

Monitoring of loose rocky slopes along the roads is quite important. This aspect is relevant for Macedonia during the construction, reconstruction, and exploitation of the roads, especially since many roads are built in mountainous areas.

In terms of in-situ measurement and monitoring, many scholars have used monitoring devices such as displacement sensors, inclinometers, and pore water pressure sensors, combined with IoT technology and GNSS technology to monitor slopes (Moradi et al. 2021). These monitoring devices improve monitoring efficiency (Olabode et al. 2022). However, this type of sensor equipment is point-based monitoring and cannot achieve comprehensive coverage of the slope. The monitoring data comes from various scattered sensors, and there is little relevant monitoring information for non-sensor installation points (Zhou et al. 2020).

SfM (Structure-from-Motion) (Westoby et al. 2012), is now a powerful method for 3D reconstruction and point-cloud generation. SfM applications, such as Smart3DCapture, PhotoScan, and Pix4D, are popular for professional and/or non-professional operators of photogrammetry. These systems directly process a sequence of images and generate point clouds. Each point has a colour index originating from the colour of an original image pixel. By photographing loose rock and the surrounding environment, SfM software can calculate a point cloud which can realize a quantitative estimation of rock movement (Kazuo et al. 2016).

Here we present an example of monitoring slope failure mechanisms during the construction of A2 Expressway Kriva Palanka-Stracin, by using Unmanned Aerial Vehicles (UAV) and SfM photogrammetry. UAVs are an effective tool in landslide risk management,

allowing rapid collection of imagery and production of high-resolution photomosaics to safely evaluate rockslide deformation and activity. UAVs combined with SfM photogrammetry have emerged as a new approach in recent studies for landslide monitoring (Brook et al. 2020). The efficiency of SfM algorithms has been demonstrated in multiple studies for landslide monitoring (Lucieer et al. 2014).

Various papers have been published elaborating examples of predicting rockfall assessments using point clouds (Marjanović et al. 2021), (Rosser et al. 2007), (Janeras et al. 2017), (Xiao et al. 2023). Systematic application of these methods can provide excellent information for managing rockfall-prone slopes.

This research aims to implement already available datasets that were obtained for another purpose for this site, here processed in the context of monitoring and predicting the movement of a rockslide during road construction. The goal is to present a low-cost and fast new approach that replaces the classic field surveying. Considering that the known methods are used for monitoring already occurred instabilities, the application of SfM represents the earliest form of constant monitoring and detection of possible rockslides.

Study area

The study area represents one part of the cut at chainage km 11+635 to km 12+191 on the A2 Expressway Kriva Palanka-Stracin, section Dlabochica-Chatal, close to village Petralica. The rocks in this part of the alignment by their mineralogical composition can be distinguished in different lithological units, depending on the dominant minerals. However, according to the similar structural, textural, and physico-mechanical characteristics all rocks are classified as green schists. During the field geological mapping, the schists were further distinguished as albite-epidote-chlorite schists, which are characterized by a schistose structure, at some parts quite fractured, folded, and tectonized especially at the contact parts with fresher and stronger albite-epidote-chlorite schists.

With the start of the construction activities, a major rockslide occurred on the right side, at the beginning of the cut (Fig. 1). After the remediation of this part, another local rockslide occurred in the approximate same area, which is the subject of this paper (Fig. 2). The monitoring of this part of the cut using drone surveillance and the SfM technique enabled comparison and estimation of the scale of movement of the rockslide.

The processes of surface weathering of the rocks change the composition and setting of the rock mass and lead to the destruction of the rock into fine debris and larger rock fragments. These engineering geological processes are anthropologically caused, i.e. they occurred after undertaking construction activities for the alignment of the road and construction of the cut.



Figure 1 Aerial view of the cut: the studied area before the rockslide occurrence is marked with a red circle.



Figure 2 The initial stage of the rockslide (01.02.2023).

On the other hand, the morphology of the terrain, precipitation, oxygen, CO₂, temperature oscillations, ice, and the steep inclination of the slopes also contribute to the occurrence of rockslides. The surface weathering of the rocks is expressed along the entire length of the cut slope and is most pronounced on the contact parts between the schists and the fault structures. At the currently constructed slopes, the first two are made with an inclination of 1:2 (26.6°), and the third (the one where the rockslide occurred) is excavated with an inclination of 1:1.5 (33.7°). Because of the gravitational conditions, there is the occurrence of falling of small rock fragments and in some instances of larger quantities of rock material. The unfavourable dip elements of the foliation on the right side of the cut, tectonic fracturing, intersection of fault structures with the foliation, and perpendicular fractures to the foliation, as well as precipitation, are significant factors for the creation of this state.

In the subsequent period, the dimensions of this rockslide increased, as a result of which additional amounts of material were falling off the slope (Fig. 3).



Figure 3 Rockslide state on 27.09.2023.

Used methods, hardware, and software

The traditional methods are based on physical access to the rock surface. Since the 2000s, remote sensing techniques have been applied to several fields, particularly

to the characterization of rocky slopes (Riquelme et al 2021). The scientific community has shown a growing interest in the extraction of information on discontinuities from remote sensing-derived datasets (Ivanovski et al. 2023).

Structure from Motion introduced by Ullman (1979), is a photogrammetric range imaging technique for estimating three-dimensional structures from two-dimensional image sequences that may be coupled with local motion signals. It requires a digital camera and, if needed, a Remotely Piloted Aircraft System (RPAS). It can provide a 3D point cloud (3DPC) that can be further analyzed by appropriate software.

In our case, this technique has been performed using a low-altitude camera drone - Phantom 4 RTK (enterprise.dji.com). It belongs to Low-Altitude Unmanned Aerial Vehicles which is employed to capture the ortho and oblique images during the flight. (Fig. 4a). The photo size is 5742 x 3648 pixels with horizontal and vertical resolution of 72 dpi.

Before scanning the area with the camera mounted on the drone, at least four reference points should be visibly marked which are surveyed with high precision GPS device. In our case, when using the drone, it is connected in real-time with NTRIP MAKPOS reference stations in Macedonia that send corrections to the drone. Due to the operating range that is specially intended for our alignment, it is necessary to set control points to obtain the necessary accuracy, whereby the model would correspond to the project on which the expressway is being worked.

With the SfM technique using the drone, the entire area was recorded by navigating the drone to take pictures and record all visible surfaces (Fig. 4b). When recording, the drone positions itself using its coordinates.

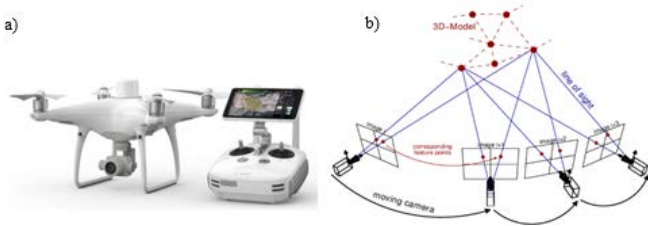


Figure 4 a) Drone b) Principles of SfM method.

There are several approaches and algorithms to reconstruct camera orientation and geometry from images. Currently, one of the most used methods is based on the employment of Structure-from-Motion (SfM) algorithms. These algorithms belong to the computer vision research field and together with stereo-reconstruction techniques provide the opportunity to create accurate 3D models from images without prior information about the location of image acquisition, or about the camera parameters used to perform the acquisition (Verhoeven 2013).

With the SfM method, the 3D scene geometry and camera motion are reconstructed from a sequence of 2D

images which are taken by a camera that moves around the scene. The SfM algorithm detects common feature points in multiple images and uses them to reconstruct the movement of those points throughout the image sequence. With this information, the locations of those points can be calculated and visualized as a 3D point cloud.

Four different surveys are made and four point cloud sets are prepared for this research: The point cloud acquired before detected movement is the reference point cloud. During five months, four photogrammetric surveys were made on 13.12.2022, 20.01.2023, 21.02.2023, and 16.05.2023.

Multitemporal geomorphic changes in the rockslide area were identified by comparing the SfM-derived point clouds in pairs. 3D distances were estimated with the multiscale model-to-model cloud comparison for each pair of point clouds.

Two different software were applied. Pix4D mapper version 4.8.3 is commercial software specialized for photogrammetry (pix4d.com). It was used for the photos received from drone imaging to be turned into a point cloud. CloudCompare version 2.11.0 is an open-source software that was used for the processing of 3D point clouds.

During the processing of the obtained images in Pix4D, a visualization of the exact positions of the camera while the photos were taken is obtained (Fig. 5).

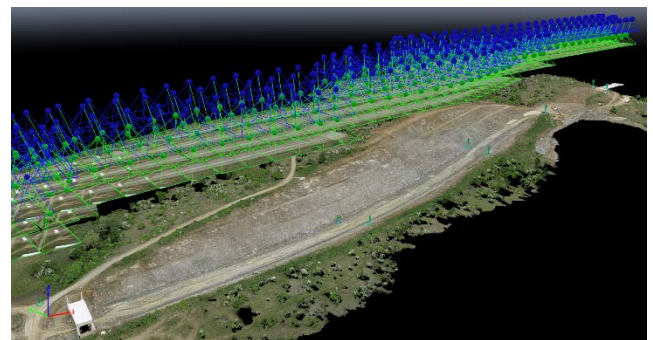


Figure 5 Positions of the camera while surveying.

Very high-density point clouds can be extracted from these photos, but to be able to work properly, an optimal point density number was chosen. In this case point cloud density is set to 5-7cm. With the complete processing, the model is obtained, i.e., four different point clouds (Fig. 6). The resulting model was saved in .xyz, extension. The number of points for these four surveys is between 510.034 to 655.834 depending on the conditions when the survey was done.



Figure 6 Point clouds derived from four different surveys.

Results

The study area represents a small part of the entire cut 4, i.e. area of 100m by 60m.

The CloudCompare tool Cloud-to-Cloud (C2C) Distance is used to compute the distances between two selected point clouds. Before displaying the tool dialog, it is necessary to select the reference cloud, and the comparative one. The older cloud would always be the reference one (www.cloudcompare.org).

For each C2C distance computation method, CloudCompare software computes four values for the distance, which are: the maximum distance, average distance, mean distance, and the standard deviation. In this case, that data are not used because of the changes due to cut excavation in the surrounding parts of the rockslide, a factor that influences the complete statistics. The detection of the largest differences is done manually using the tool *Point picking*. The entire visible area that shows changes due to the comparison doesn't represent the real positions of the material that has been moved (the size of the rockslide). Choosing bulk data for C2C distances can gain false information due to redepositing of some material, i.e., changes of a type that some part that showed differences in one time of surveying, in other time can be redeposited and with that to falsely represent that there is no movement. So manual point picking addresses the positions that in reality suffered the most changes.

The bright colours in the middle of the image indicate that there are some changes when comparing the first two surveys. The bright colours at the edges of the area indicate differences due to excavation that was done in the surrounding area between the two surveys (Fig. 7). The rockslide was detected first time on 01.02.2023. When using the surveys from the period before the rockslide, i.e. surveys 1 and 2, and using survey 1 as a reference, it can be easily detected that there was some kind of movement before the visual detection of the rockslide.

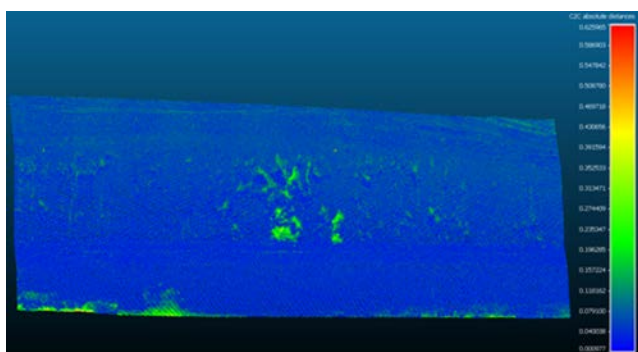


Figure 7 Comparison between the first and second surveys.

The biggest change in positions between the first two surveys is 28 cm, and mostly in the range of 0-8 cm (Fig. 8a). It can be noticed that there are small differences around the study area, because of the small difference in positioning of the two point clouds (up to 3 cm) and from the erosion that was present at the cut. Apart from the fact that this type of rockslide is already observed, using

Cloudcompare, displacements can be measured in different places of the rockslide, with the largest displacement being 59 centimetres (Fig. 8b).

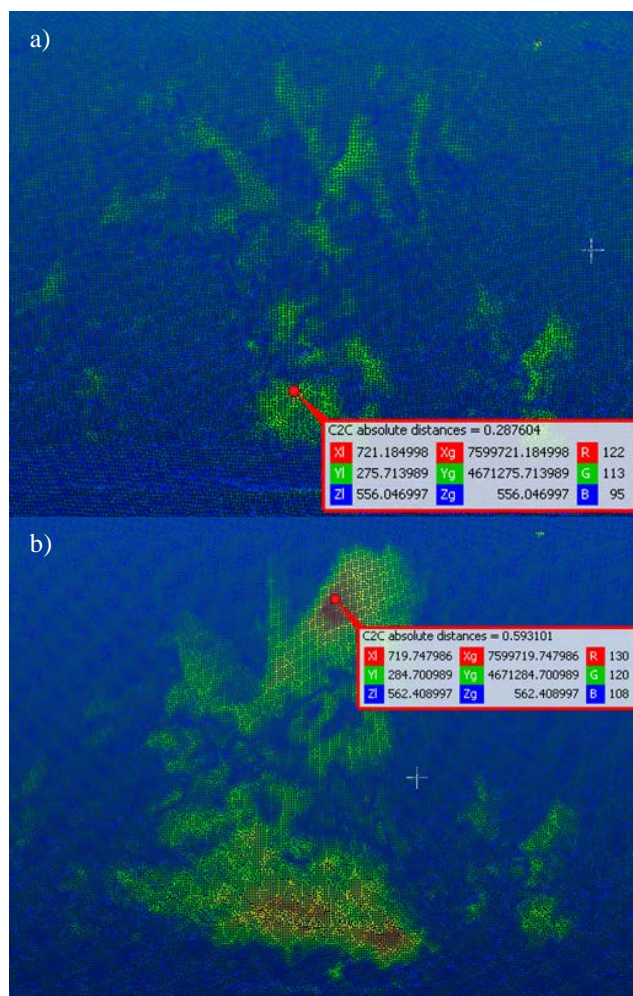


Figure 8 a) Absolute distances between first and second survey (up) b) Absolute distances between first and third survey.

When comparing the first survey with the survey that was taken after the occurrence of the rockslide (the third survey), it can be said that the greater difference between the two clouds of points in the part of the researched area is already noticeable (Fig. 9). When comparing the first with the last survey (Fig. 10), it can be noticed that the differences between the two point clouds are larger and that they are spread over a larger area.

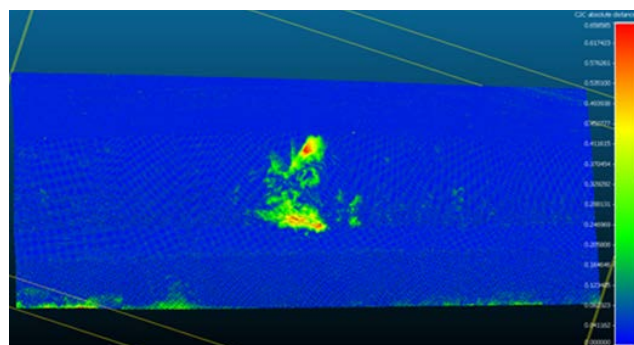


Figure 9 Comparison between the first and third survey

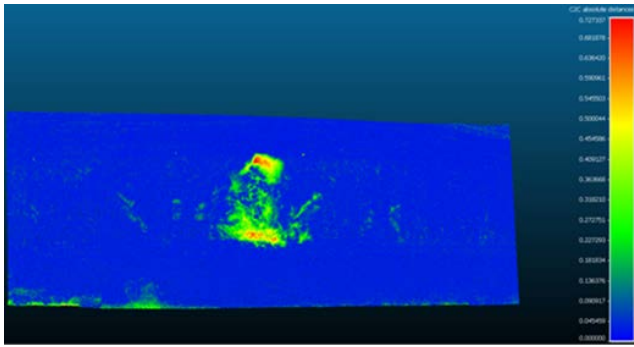


Figure 10 Comparison between the first and fourth surveys.

The maximum observed distance is 70 cm (Fig. 11a).

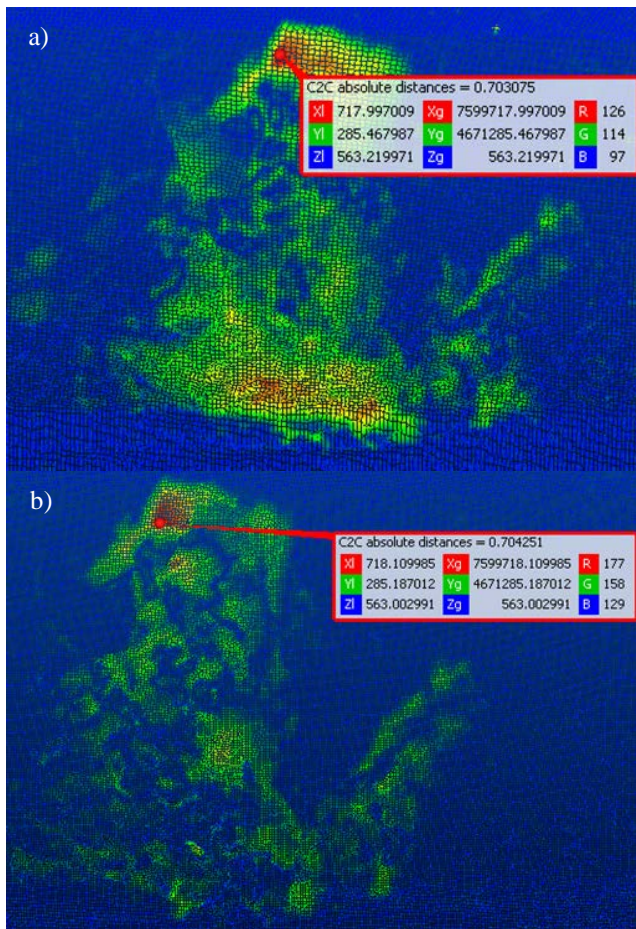


Figure 11 a) Absolute distances between first and fourth survey; b) Absolute distances between third and fourth survey.

It is noticeable that the absolute maximum distance of the two point clouds is increasing but it is also noticeable that the shape of the rockslide is changing especially in the upper part of the area. This is because of the permanent erosion and rockslides throughout the cut and redeposition of the rocky material. The real activity of the rockslide is in the upper part.

From this comparison, it can be noted that by comparing two images taken after the occurrence of the rockslide, in 5 months from one survey to the other, it is not settled and there are still certain movements, especially in its upper half. For this period, the largest distance between these two recordings is 70 cm (Fig. 10b).

It is clear that the maximum distance is the same as comparing the changes from the initiation of the rockslide. However, it can be seen that due to constant erosion and rockslides, there is redepositing of the rocky material on the slope, which is changing the shape of the rockslide. The part with maximum absolute change has narrowed its gap due to redeposition and erosion.

After the analysis, it can be concluded that movements are greatest in the part where the actual sliding occurred (along the foliation of the schist), i.e. in the upper part of the slope. The lower part of the rockslide endures changes mostly due to redepositing the rocky material from the upper parts.

Because this comparison provides reliable data that there is still movement on that part of the slope, the same technique can be applied to the entire cut where periodic recordings can be used for a quick and constant insight into the possible dangers of slope instabilities.

Figure 12 shows the differences between the recordings done on 13.12.2022 and 16.05.2023. In blue are the parts where there were no changes during that period. In red are the parts of the cut where changes have occurred.

It is most noticeable in the part of the rehabilitation of the slopes and the part of the road construction, positions where excavation was carried out in the meantime, as well as in the periphery where there is a change in the vegetation. In the part of the slopes and berms, it can be noticed the occurred change, the rockslide on the third slope on the right side of the cut (marked with the white arrow).

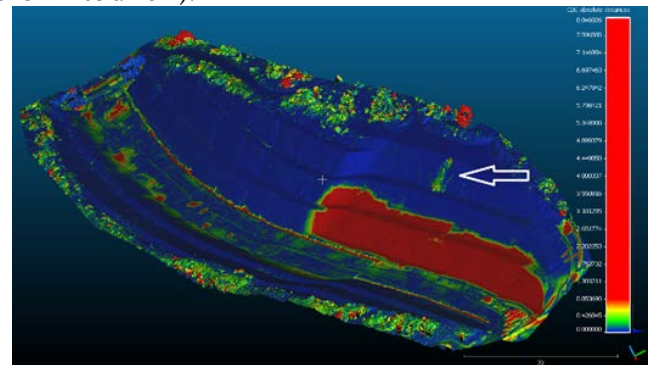


Figure 12 Terrain changes for 5 months.

With constant monitoring of the entire cut, early detection of any unwanted occurrences of slopes is possible.

Conclusions

The example presented in this paper is about a small local rockslide, but it should be taken into account that the same methodology can quite well give information about the occurrence of other types of movement, or the initiation of planar or wedge-shaped failures.

This methodology does not represent an implementation of the latest innovations in technology, but rather the application of several software and hardware solutions that have been used in engineering for

years. However, this is a practical example of the application of this methodology on site and its direct engagement during the construction of civil structures, such as an expressway. Using this type of prospecting/monitoring, there is a possibility to determine the occurrence of rockslides at an early stage, and thus to undertake appropriate measures, which would increase the safety of labour and machinery operating in a certain area, as well as during exploitation of the road.

There are several procedures for detecting this kind of phenomenon, all of which give similar results in terms of dimensions and the speed of the changes. The most standard is the visual one, where almost always, after the occurrence of a certain hazard, the solution to the problem is approached. From the presented in this paper, it is obvious that even before the visual detection, there are ways to determine possible minor or major changes, and thus the possibility of preventing or minimizing major damage and increasing the safety of the area.

This can be an example of introducing a procedure for slope monitoring using recordings that are used for other purposes in the construction process as in this case for the calculation of quantities for performed earthworks. This does not incur new costs, it increases the detail of prospecting, replaces the slow in-situ inspection with computer processing, and finally gains greater reliability because it is proven that this method can determine even the smallest processes during the occurrence of rockslides.

However, it should be borne in mind that the use of this method should be approached carefully. Changes in vegetation, or advances in excavation, should be considered before accessing analyses of this type. Also, a good knowledge of geological predisposition and processes combined with a strong geotechnical background is crucial for proper result interpretation.

References

- Brook M, Tunnicliffe J, (2020). Rapid, cost-effective 3D monitoring of urban landslide displacements using UAV-Structure from Motion (SfM) (3714483), Research report for www.eqc.govt.nz, paper number 3809 (EQC 18/762).
- Harabinova S (2017) Assessment of slope stability on the road. *Procedia Eng* 190:390–397.
- Ivanovski I, Nedelkovska N, Petrov G., Jovanovski M., Nikolovski T. (2023) Comparison between traditional and contemporary methods for data recording in structural geology. *Journal Geologica Macedonica* (37):119-133.
- Janeras M, Jara J A, Royán M J, Vilaplana J M, Aguasca A, Fàbregas X, Gili J, and Buxó P, (2017) Multi-technique approach to rockfall monitoring in the Montserrat massif (Catalonia, NE Spain). *Eng. Geol.* (219):4–20.
- Kazuo O, Satoko H, Toko T, (2016) Detection of slope movement by comparing point clouds created. *The International Archives of the Photogrammetry, Remote Sensing and Spatial Information Sciences*, Volume XLI-B5, 2016 XXIII ISPRS Congress, 12–19 July 2016, Prague, Czech Republic
- Lucieer A, Jong SMD, Turner D, (2014) Mapping landslide displacements using Structure from Motion (SfM) and image correlation of multi-temporal UAV photography. *Progress in Physical Geography* 38:97-116.
- Marjanović M, Abolmasov B, Berisavljević Z, Pejić M, Vranić P, (2021) Pre-failure deformation monitoring as rockfall prediction tool. *IOP Conf. Series: Earth and Environmental Science* 833 (2021) 012197.
- Montgomery DR, (1994) Road surface drainage, channel initiation, and slope instability. *Water Resour Res* 30:1925–1932.
- Moradi S, Heinze T, Budler J, et al (2021) Combining site characterization, monitoring and hydromechanical modeling for assessing slope stability. *Land* 10:423.
- Olabode OP, San LH, Ramli MH, (2022) Geophysical and geotechnical evaluation of landslide slip surface in a residual soil for monitoring of slope instability. *Earth and Space Science*, 9, e2022EA002248.
- Riquelme A, Tomás R, Cano M, Pastor JL, and Jordá-Bordevore L, (2021) Extraction of discontinuity sets of rocky slopes using iPhone-12 derived 3DPC and comparison to TLS and SfM datasets. *IOP Conf. Ser.: Earth Environ. Sci.* 833 012056
- Rosser N, Lim M, Petley D, Dunning S and Allison R 2007 Patterns of precursory rockfall prior to slope failure. *Jour. of Geoph. res.* 112 F04014
- Shariati M, Fereidooni D, (2021) Rock slope stability evaluation using kinematic and kinetic methods along the Kamyaran-Marivan road, west of Iran. *J. Mt. Sci.* (2021) 18(3): 779-793
- Ullman S, (1979) The interpretation of structure from motion. *Proceedings of the Royal Society of London.* 203(1153): 405–426.
- Verhoeven G, Sevara C, Karel W, Ressel C, Doneus M, Briese C, (2013) Undistorting the Past: New Techniques for Orthorectification of Archaeological Aerial Frame Imagery. In: C. Corsi, B. Slapsak and F. Vermeulen, ed., *Good Practice in Archaeological Diagnostics*, 1st ed. Springer International Publishing Switzerland, pp.31-67.
- Westoby MJ, Brasington J, Glasser NF, Hambrey MJ, Reynolds JM, (2012) Structure-from-Motion Photogrammetry: A Low-Cost, Effective Tool for Geoscience Applications. *Geomorphology* 179: 300–314.
- Xiao G, & Nie, Wen & Geng, Jiabo & Yuan, Canming & Zhu, Tianqiang & Zheng, Shilai (2023) Road slope monitoring and early warning system integrating numerical simulation and image recognition: a case study of Nanping, Fujian, China. *Stochastic Environmental Research and Risk Assessment* 37:1-17.
- Zhou X, Xu Q, Zhao K et al, (2020) Research on calibration method of discrete element mesoscopic parameters based on neural network landslide in Heifangtai, Gansu as an example. *Chinese J Rock Mech Eng* 39:2837–2847.
- <https://enterprise.dji.com/phantom-4-rtk/specs> [Last accessed: 16.01.2024].
- École Polytechnique Fédérale de Lausanne (EPFL) Computer Vision Lab in Switzerland – Pix4D mapper. Available online: pix4d.com [Last accessed: 16.01.2024].
- https://www.cloudcompare.org/doc/wiki/index.php/Cloud-to-Cloud_Distance [Last accessed: 16.01.2024].

Advanced geospatial solutions for monitoring, modeling and understanding of landslides

Ankica Milinković^{(1)*}, Goran Stepanović⁽¹⁾

1) Vekom Geo, Beograd, Todora Dukina 61, Serbia, +38163277763 (ankica.milinkovic@vekom.com)

Abstract Landslide represents a geological event in which there is a sliding or shifting of soil, usually resulting from factors such as rainfall, earthquakes, erosion, changes in water levels, climate change, and/or human activities. Especially with the prevalent challenges of climate change, the risk of landslides becomes exceptionally high, emphasizing the need for response and preventive action in terms of crisis management. Humans strives for understanding, prediction, and preventive action to minimize potential hazards and damages from such risks. This paper demonstrates the description of advanced technologies, namely the integration of various technologies into unified automated systems, for effective monitoring, modeling, and understanding of landslides. By integrating these technologies, precise monitoring of geological changes, quick identification of potential hazards, and detailed modeling of relevant factors are enabled. An overview of the general approach to the architecture of monitoring systems will be provided, including the basic components of integrated geodetic and terrestrial radar sensors, as well as a practical example where such an approach has had necessary application.

Keywords monitoring, geodetic technologies, terrestrial radar, landslides.

Introduction

Landslides are one of the most dangerous and destructive natural hazards, capable of causing significant damage to the environment, economy, infrastructure, and human lives. The speed of landslide movement varies from slow material displacement in millimeters or centimeters per year to sudden avalanches of large volumes of debris (Pradhan, S. P. et al., 2019). To effectively manage the risks associated with the occurrence and activity of landslides in the short and long term, it is evident that data from various sources need to be combined and analyzed. Integrating data from different sources leads to the representation of parameters that control the event and contribute to the classification of their impact on the evolution of the phenomenon. Modern monitoring techniques can provide very precise and reliable data on deformations caused by soil displacement even in real-time. Furthermore, they enable increased speed, affordability, and overall quality of landslide monitoring. Viewed from the perspective of integrating different technologies, a holistic approach to

landslide monitoring is often provided, enabling better understanding and adequate response to potential hazards. Scientific and technological advances in recent decades have made available the necessary tools for conducting monitoring, modeling, understanding, and mitigating landslide-related crisis events. Never before have scientific and practical communities had access to such a wide variety of powerful tools for monitoring and modeling landslides on different aspects. However, geoscientific understanding of landslide processes and mass movement remains crucial for the adequate interpretation of all collected results provided by monitoring and modeling tools, and for their use in designing mitigation measures (Corsini A, Borgatti L, (2019).

In this paper, the geodetic techniques will be mentioned in the review of data and information that they can provide. It is important to note that each techniques has its own advantages and limitations, which may be imposed by the area of interest itself, and thus each individual project requires a certain degree of personalization and optimization.

Monitoring system architecture

The common elements of a monitoring system typically include the structure (object, area of interest being monitored), sensors, data collection systems, mechanisms for data transmission and recording, data management tools, and tools for data interpretation and diagnosis (system identification, structural model updating, condition assessment, prediction of remaining parameters indicating future behavior). This concept is widely applied to various forms of crisis areas or objects, especially as countries worldwide face ever greater challenges of risk moments. Particularly when it comes to damages caused by geological phenomena, it is important to note that there are phases of increasing severity that require knowledge of the following characteristics:

- Determining the existence of damage to the environment affected by the crisis phenomenon,
- Locating damage,
- Identifying types of damage,
- Quantifying the severity of damage.

In these cases, signal processing and statistical classification are necessary to convert field sensor data into information about potential corrective and preventive measures.

The mentioned approach can be more simply characterized by four main components, which include monitoring sensors that generate raw measurements at defined intervals, a 24/7 power supply with backup power, a communication device to facilitate data transmission, and software for monitoring displacements and reporting movements. If the previous approach were narrowed down to a specific application and illustration in a landslide, various fields of interest that need to be included in the monitoring architecture would be considered. These can include: geotechnical sensors, geodetic instrumentation and automated monitoring instruments, meteorological sensors, data loggers, data transmission systems, data analysis software, management and diagnostic systems, warnings, deep learning, and prediction of future scenarios. Each monitoring project is different and unique, it means that monitoring solutions combine diversity and flexibility in adapting to project requirements, regardless of the environment or object requiring monitoring. Whether it is human activity or a natural process, proven solutions are needed to provide the highest level of safety, performance, and sustainability. In order to mitigate the landslide hazard, several landslide monitoring techniques have been developed over the last decades. Broadly, these can be categorized into remote sensing, photogrammetric, geodetic, geotechnical, geophysical, wireless sensor networks (WSN) and the Internet of Things (IoT) (Thirugnanam H, Uhlemann S, Reghunadh R, Ramesh M.V., Rangan V.P., 2022)

Here it will be focused on reviewing and analyzing the application of geodetic solutions for landslide monitoring, with an approach to creating, combining, and integrating multidimensional approaches into tailored solutions adapted to specific project needs. In addition to the geodetic approach, certain projects also require integration with radar terrestrial systems and/or geotechnical sensors, leading to the creation of absolute or total monitoring approaches. Monitoring data from ground-based radars are used to give a holistic view of the unstable area. Remediation and early warning strategies are commonly based on continuous monitoring of the slope displacement which can give crucial information on the dynamics and evolution of the landslide (Eberhardt, E., Watson, A.D. and Loew, S., 2008). Integrating data from different sources is leading to the depiction of the eventcontrolling parameters and the delineation of their effect on the phenomenon's evolution (Botsialas K., Røyve V, Falomi A, Meloni F., Boldrini N Bellotti F., Leoni L., Coli N., 2021). Whether it is monitoring to provide information to experts for early warning of natural hazards such as landslides, seismic, and volcanic activity, information for potential fault prediction, or data after events for studies and better understanding, the hardware-software concept must be purposeful, compatible, and reliable. The priority is on monitoring real-time information, with automated report generation. Special reports with inverse velocity, hazard, and displacement maps, as well as speed limit checks, provide additional insight into mass land acceleration, increasing the risk of failure. Since

components of geodetic monitoring can stem from various approaches, such as GNSS systems, LiDAR, InSAR, total stations, and leveling instruments, as well as photogrammetry, this paper will further explore one example of a system composed of a total station and a radar terrestrial system as key measuring equipment. The architecture is based on the concept of total monitoring developed by the companies Leica Geosystems AG and IDS GeoRadars.

Geodetic and radar monitoring architecture

The complexity of monitoring projects often lies in installation and configuration part of the monitoring project. This is often a cumbersome process, which requires special equipment and expertise. Another challenge is surely missing or low-quality data, a situation that significantly increases the risk of not capturing movements in critical moments. What could cause this? Basically anything from instrument issues, communication issues, power outages. In response to the identified risks and challenges, Leica Geosystems has developed a monitoring system based on Edge computing technology and networked communication.

IoT is the networking of smart objects, commonly referred to as things, enabling interoperability and intelligent communication with services and applications in the cloud using Internet standards. IoT facilitates the inclusion of everyday objects as virtual representations, where people and objects interact with each other as equals. Such inclusivity can provide greater penetration and understanding of the environment, aiding in addressing societal issues, including disaster monitoring and early warning, more effectively than before (Thirugnanam H, Uhlemann S, Reghunadh R, Ramesh M.V., Rangan V.P., 2022). Based on this rationale, the company Leica Geosystems has developed a monitoring system that relies on Edge technology within the IoT communication framework.

The latest technological advancements in the geodetic terrestrial monitoring solution address potential issues to provide continuous and uninterrupted data flow, which in practice includes the Leica Nova TM60 total station for monitoring, the Leica ComBox60 communication device with built-in monitoring software, and Leica GeoMoS Edge, enabling autonomous functions and local data storage using "EdgeConnect" technology. This provides a secure IoT connection between field monitoring sensors and the office software Leica GeoMoS Monitor.

The Leica TM60 total station is designed with several characteristics specific to monitoring with automatic measurements, in variable environmental conditions, and over long distances. These innovations help ensure continuous, comprehensive data collection. Equipped with Leica Captivate software and ATRplus technology, the TM60 automatically adjusts measurement settings to current environmental conditions and ensures that targets are automatically measured at distances of up to 3,000 meters, much further than traditional total stations.

Additionally, ATRplus recognizes and rejects non-target reflections, such as headlights or sunlight, to focus on the correct tracking prisms. The TM60 is equipped with a Piezo-drive system for uninterrupted long-term operation, as well as a Leica PinPoint EDM rangefinder for distance measurement accuracy and an optional camera for inspection and remote positioning and photodocumentation. Another tracking-specific innovation with the TM60 is the AutoLearn application, which quickly detects, measures, and learns all targets in a defined area. Automatic point learning speeds up the initial setup of monitoring projects and the integration of additional prisms while eliminating human errors, thereby minimizing the risk of insufficient coverage of all planned measurement points.

The specialized monitoring software, GeoMoS Monitor, acts as a server and can be installed on a personal computer or a virtual machine. Depending on project requirements and security standards, connectivity to field devices is achieved either via EdgeConnect cloud technology or within the local area network (LAN). Since various factors can disrupt this connection, it's crucial that field components can operate autonomously without a continuous connection to the office software. This is achieved through GeoMoS Edge, a data collection software component embedded in Leica M-Com communication devices. Utilizing EdgeComputing technology, GeoMoS Edge executes a measurement cycle pre-configured in GeoMoS Monitor, calculates the quality of raw measurement data, initiates repeated measurements, and delivers data to GeoMoS Monitor. With the Leica ComBox60, measurement cycles proceed uninterrupted based on the last available configuration, even during power and/or communication outages. This is possible due to the internal battery, which serves as a secondary power source and can supply power to monitoring sensors for hours or even days depending on the measurement frequency. These measurements are stored locally until communication with the server is reestablished, eliminating gaps in data.

Experience shows that transferring measurements from the field to the office is a critical step in the monitoring process, and therefore, the monitoring system must provide a quality solution in this regard. Data transmission protocols must meet the highest security requirements due to the sensitivity of monitoring data and the overall security of the server's local network. However, robust security measures involving complex IT configurations often require a significant amount of time and money. On the other hand, EdgeConnect technology simplifies this process while maintaining the necessary security levels. The integrated GeoMoS Edge enables a secure IoT connection in the cloud between the field and the office. EdgeConnect's "smart" procedure manages communication between GeoMoS Monitor and Leica M-Com communication devices using standard, open HTTPS ports, enabling configuration without additional IT modifications. Once connected, GeoMoS Monitor takes

ownership of the device, making data loss, tampering, or theft impossible. The user has full control over the device and can transfer it from one project to another, simultaneously removing IT complexity from monitoring installation, reducing costs, and significantly shortening the time to start the monitoring phase.

One advantage of such a monitoring solution structure is the provided autonomous control over hardware and software, with the ultimate goal of ensuring data completeness and reliable information about movements in the monitored area. Another advantage is the possibility of integration with radar or geotechnical sensors into a unified solution. From radar devices to crack gauges, each instrument or sensor adds value to the solution if used correctly. In most monitoring projects, the integration of at least two technologies will generally be applied. Configuration, measurement, and data acquisition can be very simple but also time-consuming if automated solutions are not available. This may involve many complex cables or data logging solutions. However, the data they provide is highly valuable for analysis; therefore, the primary goal of the solution involves a wireless network that integrates measurement data from various sensors, avoiding complex cable installations and applying automated readings with wireless transport.

In the context of landslide applications, the role of ground-based radar systems is recognized in practice, among which the Hydra-G device stands out as part of the IDS Hydra family, comprising rapid monitoring radars designed for early warning and real-time measurement of submillimeter displacements. With a scanning range of up to 800 meters, the system employs advanced radar technology with high precision and resolution, relying on ArcSAR (rotation of the system around its centre point) technology that provides spatial resolution in centimeters and delivers updated displacement information every 30 seconds. Additionally, there is an optical and infrared HD camera enabling real-time visual inspection of monitored areas. Data obtained from radar scanning are further projected onto a 3D model of the scene, formed using built-in laser technology. The leading Hydra Guardian software offers a simple yet enhanced tool for visualization and interpretation of radar data, as well as analysis of trends in structural and slope movements. Furthermore, SurfScan serves as specialized software for analyzing real displacements and deformations.

The combination of radar and geodetic monitoring for landslides involves integrating data from radar-based systems, with traditional geodetic monitoring techniques like total stations and GNSS. This integrated approach allows for a more comprehensive understanding of landslide behavior, including detecting surface deformations and movements over time with high spatial resolution provided by radar systems, while also providing precise positioning and monitoring of key points using geodetic instruments. By combining radar and geodetic monitoring, researchers and engineers can gain insights

into the dynamics of landslides, identify potential risks, and implement effective mitigation measures.

Case study

For practical application of the solution described here, a case study conducted by Leica Geosystems and InfoTop will be presented, focusing on a landslide of toxic mass from a slope landfill as an example. The example will depict monitoring after a landslide occurred due to the intense movement of several thousand meters of material from the landfill on the slope. This event took place in northern Spain, and despite the material damage caused by blocking traffic on the highway, it also claimed two human lives Fig.1. The primary task was to carry out remediation and cleaning of the mass while preemptively responding to any potential further movements.



Fig 1. The Landslides slope

The landslide dragged thousands of cubic meters of material - some of them toxic and flammable - from the landfill, which occupied an area 30 meters wide and about four meters high (Fig2).



Fig.2. landslide mass

Emergency services needed to quickly assess the stability of the slopes to initiate rescue operations. They were working in a hazardous and unstable environment

and required an alert system to notify them if the waste material shifted again. It was a challenging installation. Due to the hazards on-site, the monitoring system had to be completely remote, without manual measurements. It could only be installed within 400 - 800 meters of the landslide, and more importantly, it had to operate 24/7 without operator presence. In terms of speed, the data collected by the system had to be automatically processed, with reports generated and sent to stakeholders for interpretation. For coordination with the distributed team, data had to be accessible from anywhere. Ultimately, the monitoring system had to be configured to send real-time alerts to technicians via SMS and email.

Faced with these conditions, an automated monitoring solution was implemented, combining total stations with radar. Two Leica Nova TS60 total stations were installed, with mobile communication provided by a Leica ComGate10 router using 4G technology via a virtual private network (VPN). The total stations conducted measurements using a series of over 100 prisms placed in the field. Positioned on concrete pillars, one total station was placed next to the radar, while the other was positioned in an area near the landfill to measure prisms not visible from the first station. The measurements were then managed by the Leica GeoMoS software installed on a virtual cloud infrastructure, Fig 3.

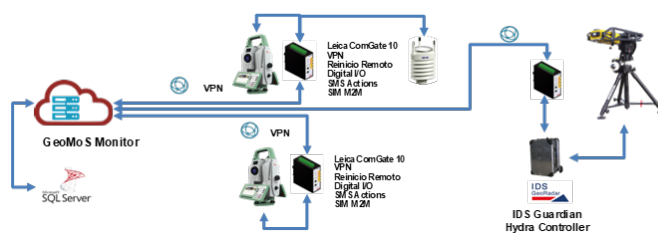


Fig.3. Architecture of monitoring system

In addition, an IDS HYDRA-G – remote sensing monitoring system based on radar technology – was installed to give a continuous measurement sweep. With 120 degrees of coverage horizontally and 30 degrees vertically, this covered most of the danger zone, except for areas hidden by vegetation. Designed for early warning and real-time measurements of sub-millimetric displacements in cut-slopes, the HYDRA-G provided real-time data of movements, transmitted to the IDS Guardian software for interpretation and alarm management, Fig4, Fig 5.



Fig.4. Combination setup radar technology and geodetic technology

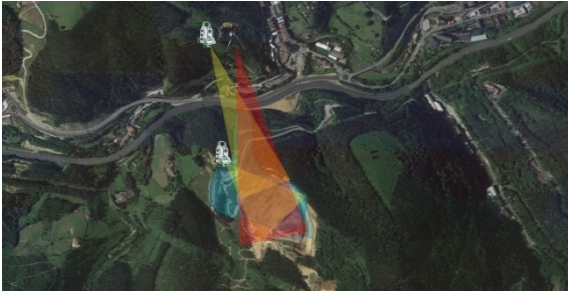


Fig 5. coverage of the landslide with total stations and radar system

The radar system allowed movements to be identified across hectares in seconds by comparing consecutive measurements through interferometry (the interference of waves) over a large distance range, detecting movements of $\pm 0.1\text{mm}$ at up to 800m. While highly sensitive, it can only monitor within its line of sight. Not all areas of the landslide allowed radar measurement due to its inclination and parts being hidden by vegetation.

Therefore, multiple total stations covered any blind spots and measured prisms in both the radar coverage and shadowed areas. The prism data helped the engineers and geologists understand each area's true movement, building an exact picture of the 3D movements taking place. Geodetic measurements are a prerequisite for ensuring geotechnical safety by monitoring the impassibility of not exceeding the critical states defined for the slopes of the landfill, they make it possible to monitor the uniformity of settlement of the facility, and on their basis it is possible to model the directions of future displacements and deformations of the facility, which are of fundamental importance in planning the target land management after completion of reclamation works. Geodetic data also provide information on the dimensions, surface area and volume of the facility and their variability over time, (Pasternak, G. 2022). These highly complementary technologies provided a combination of speed from radar detection with reliable spatial information on the movements via total station measurements. Leica Geosystems and IDS GeoRadar technology and software form Hexagon Geosystems' monitoring solution.

The Leica GeoMoS and IDS Guardian data processing software allowed experts to automate the system so that the data could be instantly and remotely shared with specialists for interpretation. GeoMoS Now! is web interface that made it possible for the geologists to analyse the situation from any location, 24/7. The system was also configured with a series of real-time alerts that sent warnings immediately if the configured thresholds were exceeded.

Conclusions

Monitoring techniques are of paramount importance, especially when there is a need to predict landslide events and thus allow time for safe evacuation with early warning signs indicating failures in monitoring unstable slopes.

Additionally, monitoring facilitates the study of various mitigation techniques and the effectiveness of soil stabilization, enabling geological or geotechnical experts to accurately model slope deformations, thereby protecting people and infrastructure with minimal disruption. Projects present unique challenges, and different hardware-software solutions are applied according to their needs. Besides the example described in this paper, monitoring requirements may necessitate the use of other technologies, where following list provides examples of components that have justified practical application in monitoring various types of geohazards.

Leica Geosystems solutions:

- Leica MS60 MultiStation for 3D measurement, imaging & scanning
- Leica ComBox60 power & communications controller with GeoMoS Edge
- Leica GeoMoS Monitor data acquisition & computation software
- Leica GeoMoS Now! data analysis & visualisation software / service
- Leica Geosystems AS11 / GM30 GNSS absolute 3D monitoring
- Leica GPR112 monitoring prisms measuring 3D structural displacements
- Leica GMX910 smart antenna tracking position via post-processing & GNSS Spider
- Remote image capture / live video stream of embankment via TPS telescope camera
- Remote detection of surface deformation using fully automated 3D laser patch scanning technology via MS60 and GeoMoS
- Leica VADASE for rapid autonomous GNSS displacement onboard GM30

Integrated 3rd party solutions:

- Wireless smart data hub for geotechnical sensors
- Geotechnical sensor data import into Leica GeoMoS via AnyData
- Wireless tilt sensors to monitor slope
- Wireless interface with locally connected water level sensor / IPI / borehole extensometers
- Wireless sensor tilt measurement for verticality of wall

Interferometric Radar solutions:

- IBIS-FM EVO,
- HYDRA-G,
- IBIS-FS,
- RockSpot

Monitoring is necessary to report dangerous events in hazardous areas by providing measurement information as early as possible when a landslide occurs, to inform about the magnitude of movement so that every danger can be immediately assessed. Landslides can block, damage, or destroy transportation links and critical infrastructure, besides endangering lives. Therefore, an automatic early warning system is essential to provide information for mitigating the risks of such hazards. Pre/post-event records are crucial for aiding in understanding why landslides occur. Additionally, during

remediation, it is essential to have as realistic supervision of the event as possible to measure subsequent movements and future monitoring of soil collapse.

Monitoring provides real-time information on slope movements and enables fact-based decision-making, facilitating swift and crucial decisions to ensure the highest level of safety and effective risk management.

Acknowledgements

This paper has been made possible thanks to the available monitoring solutions developed by Leica Geosystems AG. The authors of this paper respect the copyrights and integrity of the responsible individuals who have implemented the described Case Study project (Bruna D.F, Michelle Zeller M). This paper has been created as a summary of technologies and example of good practice publicly published on the website of Leica Geosystems AG. As the general representative of Leica Geosystems AG for Serbia, the company Vekom Geo provides all types of hardware-software and technical support in the development, implementation, and application of monitoring solutions.

References

- Botsialas K., Røvdde V, Falomi A, Meloni F., Boldrini N Bellotti F., Leoni L., Coli N., (2021) The integrated usage of ground-based and satellite SAR, along with 3D structural modelling in Titania: creating a link between short and long - term slope stability hazard management. *Mechanics and Rock Engineering, from Theory to Practice IOP Conf. Series: Earth and Environmental Science* 833 (2021) 012143 IOP Publishing doi:10.1088/1755-1315/833/1/012143
- Corsini A, Borgatti L, (2019) Mountain Landslides: Monitoring, Modeling, and Mitigation. *Geosciences*, 9, 365; doi:10.3390/geosciences9090365.
- Eberhardt, E., Watson, A.D. and Loew, S., 2008 Improving the interpretation of slope monitoring and early warning data through better understanding of complex deepseated landslide failure mechanisms. *Landslides and Engineered Slopes* pp.39-51
- Pradhan S.P., Vishal V., Singh T.N., (2019) *Landslides: Theory, Practice and Modelling*. Buettner A., Springer Cham (Electronic ISSN 978-3-319-77377-3) 313p.
- Pasternak, G. (2022). Geodetic monitoring of geotechnical structures displacements: a case study of Radiowo landfill site in Warsaw. *Acta Sci. Pol. Architectura*, 21 (2), 75–83, doi: 10.22630/ASPA.2022.21.2.16
- Thirugnanam H, Uhlemann S, Reghunadh R, Ramesh M.V., Rangan V.P., 2022, Review of Landslide Monitoring Techniques With IoT Integration Opportunities, *IEEE journal of selected topics in applied Earth observations and remote sensing*, VOL. 15, 2022.
- Bruna D.F, Michelle Zeller M., The benefit of combining technologies; the detection speed of radar and the reliability of interpretation of movements via measurements from total stations. <https://leica-geosystems.com/case-studies/monitoring/monitoring-a-landslide-recovery-operation>, ©2024 Leica Geosystems AG - Part of [Hexagon](#)

Landslide susceptibility assessment of the Teslić municipality, in the Republic of Srpska, B&H

Cvjetko Sandić

Geological Survey of the Republic of Srpska, Zvornik, Vuka Karadžića 148b, Bosnia and Herzegovina, c.sandic@geozavodrs.com

Abstract This paper presents the landslide susceptibility assessment of the Teslić municipality. The paper also presents information on engineering geological properties and landslides in this area, based on field data collection and input into the digital GIS cadaster of landslides. Landslides are a common phenomenon in this area, but they are poorly treated in the spatial planning documentation. Landslides are mostly shallow, with a depth of up to 2 m, and they are most often activated in areas of intense human activity, in areas of roads and by the river courses. Landslide susceptibility assessment was performed, after the field registration and the establishment of a digital cadaster of landslides, in polygonal form. All influential factors were taken into account, such as lithology, slope, precipitation, distance to watercourses, land use, aspect and curvature. Modelling was performed using the multi-criteria AHP method in the scale of 25x25 m.

Keywords landslide, database, susceptibility, Teslić

Introduction

Landslides represent one of the most significant modern geological processes in the world (Glade et al., 2004; Guzzetti, 2005; 2020). Landslides represent a very complex problem that is common within the territory of the Republic of Srpska, B&H (Sandić, 2015). The municipality of Teslić is one of the municipalities in the Republic of Srpska, where this problem is very pronounced.

Through field mapping in the last year, 128 occurrences of landslides were registered on the field and entered into the database. Landslides which were mapped in detail, according to the Cruden and Varnes classification (1996) and actual instructions and the Rulebook for entering data into the digital landslide cadastral (Official Gazette of Republic of Srpska No. 113/22).

Study area

The municipality of Teslić is located in the western part of the Republic of Srpska, i.e. in the central part of Bosnia and Herzegovina (Fig. 1). Teslić is one of the largest municipalities in the Republic of Srpska. It covers an area of 846 km².

According to earlier research, this area was characterized as prone to landslides, with large material damages in the previous period (Mitrović& Sandić, 2011; Sandić, 2015).

The geological setting is very complex, but diabase - chert formation and Oligo-Miocene complex of conglomerate, marl and clay, have the largest share in the percentage of registered landslides. It is very important to mention the very pronounced engineering and human activity in most of the municipality. It is also the reason for the activation of a large number of landslides.

Landslides are mostly shallow, with a depth of up to 2 m. Sliding occurs when contact between the decomposed cover and the underlying rock mass. The cover is mostly clayey-sandy (52%) and debris type (48%), (Sandić & Leka, 2023).



Figure 1 Geographical position of the Teslić municipality.

Applied Methodology

The development of methodologies for landslide susceptibility, hazard and risk assessment, dates back to the 70's of the XXI century (Nilsen et al., 1979), intensively continued and applied during the nineties (Aleotti & Chowdhury, 1999), and today become the "main tool" used in the combat against these natural disasters, primarily in spatial planning (AGS, 2007; Cascini, 2008; Fell et al. 2008; Anderson & Holcombe, 2013; Abolmasov, 2016).

Preparing the landslide susceptibility maps generally includes the following steps: preparing a detailed inventory of the landslides present in the study area, and the identification of the conditions and processes controlling them as well as the triggering factors (Sandić et al., 2017).

The landslide susceptibility assessment and map for the Teslić municipality were generated according to the Analytical Hierarchy Process (AHP) principles (Saaty 2003). The first step was to determine the causative

factors and their relative-normalized importance, considering the scale of the landslide susceptibility map.

For modelling seven main parameters were identified such as: lithology (L), slope (S), slope aspect (A), slope curvature (C), land cover (LU), distance to water boundaries (W) and average historical precipitation (P).

Table 1 Causative parameters (factors), parameters class and their weighting factor (WF).

L	Lithological unit	WF
al	Alluvial sediments; River terrace	1
J	Jurassic igneous and metamorphic rocks	2
T ₂	Limestones	3
² T, J	Marly limestones, cherts, clays, sandstones	4
J, K	Marls and limestones	5
J, K	Breccias, clays, marls, sands, clays, gravels	6
T _{2,3} ; J	Layered marls, coal, clay, sand	7
Pl, Q; dpr	Conglomerates, gravel, sand, gravels, clays, cherts	8
M	Marls, sandstones, conglomerates, tuffs, coal	9
Ol, M	Sandstones, marls, conglomerates, clays, coal	10
S	Slope (°)	WF
1	>30	4
2	0-5	5
3	5-10	6
4	20-30	7
5	15-20	9
6	10-15	10
P	Precipitation (mm/year) - average	WF
1	<900	5
2	900-1000	6
3	1000-1100	8
4	>1100	10
W	Distance to water boudaries (m)	WF
1	>1000	3
2	800-1000	7
3	500-800	8
4	200-500	9
5	0-200	10
LU	Land Use (Category)	WF
1	Forests and natural areas	2
2	Shrubs and/or grassy plant cover	4
3	Agricultural areas, pastures, bushes	5
4	Urban area	8
A	Aspect	WF
1	Flat	1
2	E; SE; S; W	3
3	SW	6
4	N; NE;NW	9
C	Curvature	WF
1	(-1) - 1	1
2	(-18,12) - (-1)	3
3	1 - 37,06	6

All parameters were modelled as a grid (raster) in a GIS environment. AHP was selected as a suitable procedure for multi-criteria modelling with rasters, and analysis of spatial data on landslides and other influencing factors (Marjanović, 2013).

Each parameter class was evaluated and their relationships were weighted (Tab 1).

The modelling procedure was generally done by comparing the above causative parameters in terms of importance for the development of the landslide process based on expert judgment. It should be emphasized that the data on the spatial distribution of landslides represent the key and most important information needed for the creation of this type of map. Each parameter included in the analysis was validated (checked) with spatial data on landslides.

Table 2 Landslide susceptibility AHP matrix for Teslić municipality.

AHP	L	S	P	W	LU	A	C	
L	1	2	5	5	6	7	8	
S	0,5	1	4	4	5	6	8	
P	0,2	0,25	1	2	3	4	6	
W	0,2	0,25	0,5	1	2	3	4	
LU	0,16	0,2	0,33	0,5	1	2	4	
A	0,14	0,16	0,25	0,33	0,5	1	3	
C	0,12	0,12	0,16	0,25	0,25	0,33	1	
Σ	2,3	3,9	11,2	13,1	17,7	23,3	34	
AHP	L	S	P	W	LU	A	C	Sr
L	0,43	0,50	0,44	0,38	0,33	0,30	0,23	0,376
S	0,21	0,25	0,35	0,30	0,28	0,25	0,23	0,271
P	0,08	0,06	0,08	0,15	0,17	0,17	0,17	0,130
W	0,08	0,05	0,04	0,07	0,11	0,12	0,11	0,090
LU	0,07	0,05	0,03	0,03	0,05	0,08	0,11	0,064
A	0,06	0,04	0,02	0,02	0,02	0,04	0,08	0,044
C	0,05	0,03	0,01	0,01	0,01	0,01	0,02	0,025
Σ	1	1	1	1	1	1	1	1

A corresponding equation of landslide susceptibility was developed through the AHP matrix (Tab 2) as a:

$$LS = 0,376xL + 0,271xS + 0,130xP + 0,094xW + 0,060xLU + 0,044xA + 0,025xC \quad [1]$$

wherein:

- LS-Landslide susceptibility
- L-Lithological data
- S-Slope angle data
- P-Precipitation data
- W-Distance to watercourses
- LU-Land use data
- A-Slope aspect
- C-Slope curvature

For each parameter included in the analysis, analytical maps were made, according to the adopted criteria, i.e. weighting factors values (Fig. 2, part a-g).

As we can see from Eq. 1 and Tab. 2, lithological data has the greatest influence on modelling (Fig. 2, part a). During the field mapping of landslides, engineering-geological mapping of the terrain was carried out, which produced a map on a scale of 1:25000. Weighting factors were assigned by overlapping with the registered landslides. Higher weighting factors were assigned to units with a higher number of registered landslides.

A similar procedure was applied to the rest of the causative factors: slope (Fig. 2, part b), precipitation (Fig. 2, part c), distance to water boundaries (Fig. 2, part d), land cover (Fig. 2, part e), slope aspect (Fig. 2, part f), and slope curvature (Fig. 2, part g).

Results and conclusion

A landslide susceptibility map was obtained through a procedure carried out in a GIS environment (Fig. 2, part h). The map has been divided (reclassified) into five (5) classes, from very low to very high class of susceptibility.

The analysis of the obtained results showed that most landslides were activated in the "high" and "very high susceptibility" categories and that they occupy 21% and 3% of the territory of the Teslić municipality (Fig.3). This somewhat coincides with the opinion that about 30% of the territory of Teslić municipality has high landslide susceptibility.

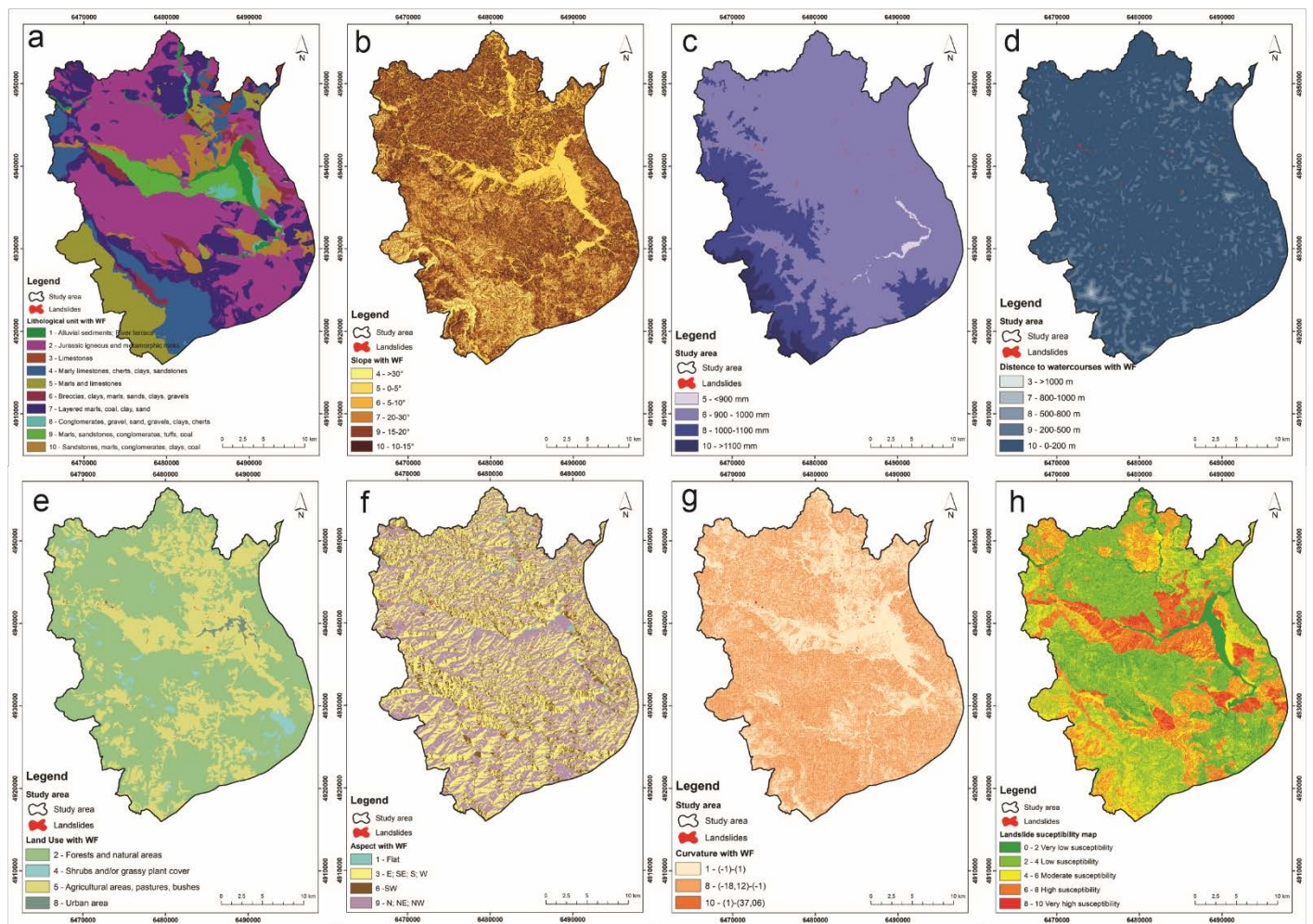


Figure 2 Causative (triggering) parameters (a-g), and landslide susceptibility map (h).

Given that the Teslić municipality, in the past, did not have planned exploration in the area of landslide susceptibility and systematic mitigation, this can serve as a basic assessment. First of all, this refers to zones with a high class of susceptibility in which preventive action should be taken. Although it can be said that these assessments are in the beginning in the Republic of Srpska, it is necessary to include them as an obligation in spatial planning documents on national and local levels. With the development of new techniques, it is necessary to increase their precision and level of detail.

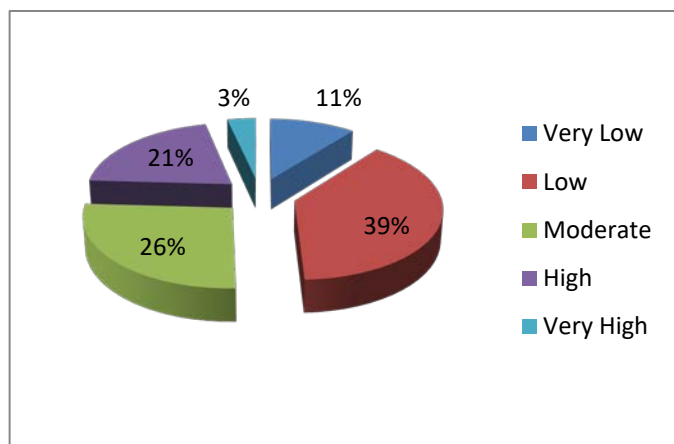


Figure 3 Susceptibility percentage by class.

References

- Abolmasov, B. (2016). Landslide risk assessment in Bosnia and Herzegovina. UNDP in B&H. Sarejevo. p. 82.
- Aleotti, P., Chowdhury, R. (1999). Landslide Hazard Assessment: Summary Review and New Perspectives. *Bulletin of Engineering Geology and Environment* 58: 21-44.
- Anderson, M.G. & Holcombe, E. (2013). *Community-Based Landslide Risk Reduction: Managing Disasters in Small Steps*. Washington, D.C.: World Bank. License: Creative Commons Attribution CC BY 3.0. 385p. ISBN 978-0-8213-9456-4. DOI 10.1596/978-0-8213-9456-4.
- Australian Geomechanics Society (AGS). (2007). *Guideline for landslide susceptibility, hazard and risk zoning for land use planning*, Australian Geomechanics, Vol 42 No 1, March 2007. 13-36. ISSN 0818-9110.
- Cascini, L. (2008). Applicability of landslide susceptibility and hazard zoning at different scales. *Engineering Geology*, 102 (3-4): 164-177.
- Cruden, D.M, Varnes, D.J (1996). Landslide types and processes. In: Turner AK, Schuster RL (eds) *Landslide investigation and mitigation*, Special Report 247, Transportation Research Board, National Research Council, National Academy Press, Washington, D.C. 1996, Chapter 3: 36-75.
- Fell, R., Corominas, J., Bonnard, C., Cascini, L., Leroi, E., Savage, W.Z. (2008). Guidelines for landslide susceptibility, hazard and risk zoning for land use planning. *Bulletin of Engineering Geology* 102 (3,4): 85–98.
- Glade, T., Anderson M., Crozier M. (eds.) (2004). *Landslide Hazard and Risk*; John Wiley & Sons Ltd, The Atrium, Southern Gate, Chichester, West Sussex PO19 8SQ, England. (ISBN: 0-471-48663-9) p. 793.
- Guzzetti, F., Stark, C. and Salvati, P. (2005). Evaluation of Flood and Landslide Risk to the Population of Italy. *Environmental Management* 36 (1): 15-36.
- Guzzetti, F., Gariano, S.L., Peruccacci, S., Brunetti, M.T., Marchesini, I., Rossi, M., Melillo, M. (2020). Geographical landslide early warning systems. *Earth Sci. Rev.* 200, 102973.
- Marjanović, M. (2013). *Conventional and Machine Learning Methods for Landslide Assessment in GIS*, Palacky University in Olomouc, Faculty of Science, Department for Geoinformatics. Olomouc-Belgrade. pp. 204. ISBN 978-80-244-4169-6.
- Mitrović, D., Sandić, C. (2011). Landslides in the Republic of Srpska. *Proceedings of the 2nd Project workshop-Monitoring and analysis for disaster mitigation of landslides, debris flow and floods*. 15-17 December 2011, Rijeka, Croatia. Croatia-Japan Project on Risk Identification and Land-Use Planning for Disaster Mitigation of Landslides and Floods in Croatia. pp.138-141.
- Nilsen, T.H., Wright, R.H., Vlastic, T.C., Spangle, W.E. (1979). Relative slope stability and land-use planning in the San Francisco Bay region, California. U.S. Geological Survey Professional Paper 944: 96.
- Saaty, T.L., (2003). Decision – making with the AHP: Why is the principal eigenvector necessary. *European Journal of Operational Research*, Volume 145. pp. 85-91.
- Sandić, C. (2015). Damages and consequences of landslides, after the floods in 2014. in the Republic of Srpska, *Proceedings of 2nd Regional Symposium on Landslides in the Adriatic-Balkan Region - 2nd ReSyLAB 2015*, Faculty of Mining and Geology, Belgrade, Serbia, pp. 251-254. ISBN 978-86-7352-296-8
- Sandić, C., Leka, K. (2023). Landslides on the territory of Teslić Municipality, *Proceedings of 3rd Geological congress of Bosnia and Herzegovina with International participation*, Neum, B&H, pp. 335-347. ISSN 1840-4073 (In Serbian).

Influence of the landslide inventory sampling on the accuracy of the susceptibility modelling using Random Forests: A case study from the NW Croatia

Marko Sinčić^{(1)*}, Sanja Bernat Gazibara⁽¹⁾, Mauro Rossi⁽²⁾, Martin Krkač⁽¹⁾, Hrvoje Lukačić⁽¹⁾, Snježana Mihalić Arbanas⁽¹⁾

1) University of Zagreb, Faculty of Mining, Geology and Petroleum Engineering, Pierottijeva 6, 10000 Zagreb, Croatia (msincic@rgn.hr)

2) Research Institute for Geo-Hydrological Protection, Italian National Research Council (CNR IRPI), Via della Madonna Alta 126, 06128 Perugia, Italy

Abstract The quality of landslide susceptibility maps depends on the quality of the input data, i.e. the spatial resolution and accuracy of the landslide conditioning factor maps and the completeness and accuracy of the landslide inventory map. For the pilot areas (40 km²) in NW Croatia, a detailed landslide mapping was done based on visual interpretation of high-resolution LiDAR DTM. This study aims to test the relevance of landslide inventory completeness and sampling on the landslide susceptibility model. Moreover, by analysing different scenarios, i.e. different ratios of landslides for model training and validation and sampling of landslide location and morphological conditions, we aim to provide new insight into the need for detailed landslide mapping for large-scale susceptibility modelling, as well as the impact on the landslide susceptibility map. Landslide susceptibility modelling was performed based on 5 m pixel-based analysis and Random Forests machine learning method. The landslide susceptibility analysis consists of nine scenarios that were defined considering the percentage of landslide polygons in the inventory for model training ($S_1 = 90\%$, $S_2 = 80\%$, $S_3 = 70\%$, etc.). Furthermore, three more scenarios were defined based on sampling strategy, i.e. original terrain inside landslide polygon, smooth terrain inside landslide polygon and original buffer around landslide boundary. Landslide susceptibility performance was measured with the Area Under the ROC Curve (AUC) metric. The results are part of the scientific research project “Methodology development for landslide susceptibility assessment for land-use planning based on LiDAR technology” (LandSlidePlan, HRZZ IP-2019-04-9900). The purpose of comparing landslide susceptibility models is to define the most suitable methodology for application in the Croatian spatial planning system at the local level.

Keywords landslide susceptibility modelling, sampling strategy, landslide inventory, large-scale, random forests

Introduction

Landslide susceptibility presents the spatial element of a landslide occurrence (Guzzetti et al. 2005), further

resulting in zonation maps which depict homogenous areas of an equal degree of susceptibility (Fell et al. 2008), whose applicability is welcomed in spatial and urban planning (Mihalić Arbanas et al. 2023). As identified in a recent and most comprehensive review paper Reichenbach et al. 2018, researchers in statistically-based susceptibility modelling are eager to experiment with parameters, leading to certain conclusions about each of the suggested steps for developing landslide susceptibility assessments. Namely, mapping units (Jacobs et al. 2020), statistical models, (Chen et al. 2017), inventory types (Guzzetti et al. 2012) and landslide conditioning factors (LCFs) (Gaidzik and Ramirez 2021) are some of the topics of interest. Considering sampling strategies (i.e. the scope of this research), stable areas are often discussed in recent years (Fu et al. 2023), but the most common approach is still random sampling. Similarly, polygon sampling (Farooq and Akram 2021) and point sampling (Hemasinghe et al. 2018) remain the two most common landslide sampling strategies. Süzen and Doyuran, 2004 introduced seed cells as areas which sample undisturbed terrain, i.e. settings prior to the landslide occurrence, whereas several comprehensive comparisons of landslide sampling strategies are given in Hussin et al. 2016. Most researchers opt for a larger training over validation landslide dataset, e.g. Lucchese et al. 2021, whereas an equal amount of stable and unstable areas is usually ensured (Xi et al. 2022).

The objective of this research is to provide preliminary information about the influence of landslide sampling strategies using a representative and LiDAR (Light Detection and Ranging) based landslide inventory. Two approaches are defined in a large scale 5 m pixel analysis using Random Forests (RF) to model small and shallow landslides. Namely, the amount of training landslides is tested in Podsljeme zone pilot area, varying from 10 to 90% with a 10% increment resulting in nine scenarios. On the other hand, in Hrvatsko Zagorje pilot area, two scenarios based on capturing undisturbed terrain approach are defined alongside one regular polygon sampling scenario as a reference point. For each of the 12 models, Area Under the Curve (AUC) is

calculated, followed by a discussion and drawing out conclusions about the two approaches in the two pilot areas in NW Croatia.

Study area

For large-scale landslide susceptibility modelling, two pilot areas approximately 20 km² in size each were selected to investigate the landslide inventory completeness and sampling strategies of unstable areas. Namely, Podsljeme zone and Hrvatsko Zagorje are located in NW Croatia (Fig. 1), being a part of the Pannonian basin where small and shallow landslides commonly occur in soil and soft rock. Both pilot areas are predominantly hilly with steep slopes (Sinčić et al. 2022a; Bernat Gazibara et al. 2023a) where intensive rainfall and snowmelt are considered the main triggering factors for landslide occurrence, recorded as Multiple-Occurrence Regional Landslide Events (MORLE) (Bernat et al. 2014a,b). Administratively, the Podsljeme zone is an urbanized part of the City of Zagreb, unlike the Hrvatsko Zagorje pilot area, which belongs to the rural parts of the City of Lepoglava and the Bednja Municipality in the Varaždin County. Previous landslide susceptibility assessments conducted in the pilot areas include Bernat Gazibara et al. 2023a in Podsljeme zone and Krkač et al. 2023 and Bernat Gazibara et al. 2023b in Hrvatsko Zagorje.

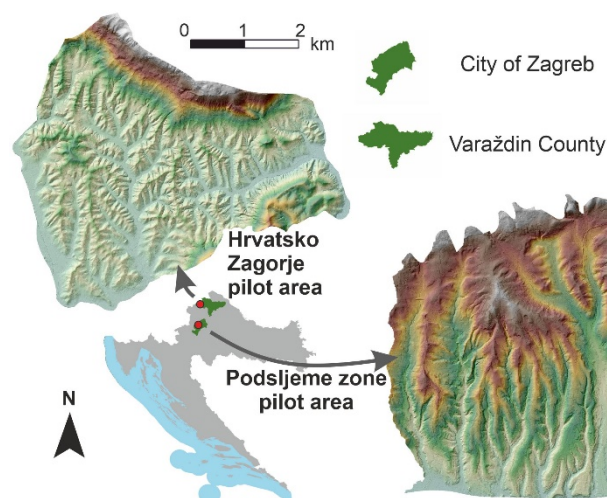


Figure 1 Podsljeme zone and Hrvatsko Zagorje pilot areas, located in NW Croatia (modified after Bernat Gazibara et al. 2022)

Material

Landslide and thematic data represent the two necessary input datasets for statistically-based landslide susceptibility modelling and should be acquired according to the scope of the analysis (Reichenbach et al. 2018). Acquiring a representative landslide inventory map for large-scale landslide susceptibility modelling of small and shallow landslides commonly located in vegetated areas is challenging, leaving LiDAR as the optimal remote sensing approach (Razak et al. 2011). Namely, for both pilot areas airborne laser scanning was performed, resulting in approximately 30 cm average point spacing of bare earth

ground points (Bernat Gazibara et al. 2022). After thorough mapping of the high-resolution digital terrain model (DTM) derivatives followed by field verification, representative polygon based landslide inventory maps are presented in Bernat Gazibara et al. 2019 and Krkač et al. 2022 for Podsljeme zone and Hrvatsko Zagorje, respectively. With an approximate landslide density of 33 per square kilometre in the Podsljeme area and 45 in Hrvatsko Zagorje, landslide management in terms of a landslide susceptibility assessment is imperative (Mihalić Arbanas et al. 2023).

Considering the scale of the analysis, great attention was given to developing LCFs of appropriate spatial accuracy. Namely, a variety of different data sources were considered, leading to specific procedures in preparing certain LCFs, e.g. improving geological and anthropogenic LCFs (Sinčić et al. 2022a). Scarce of thematic data can often be the case for undeveloped regions, leaving remote sensing data such as LiDAR point cloud and orthophoto imagery as an affordable and appropriate solution. On the other hand, free and available datasets are often used in small-scale and can be of good use for regional landslide susceptibility assessments (Sinčić et al. 2022b). Driven by experience and preliminary research, a final list of LCFs used for two pilot areas is given in Table 1, grouped as geomorphological, hydrological, geological or anthropogenic.

Table 1 List of used LCFs in Podsljeme zone and Hrvatsko Zagorje pilot areas.

LCF group	Landslide conditioning factor (LCF)	Podsljeme zone	Hrvatsko Zagorje
Geomorphological	Elevation*	YES	YES
	Slope*	YES	YES
	Aspect*	YES	YES
	Landform curvature*	NO	YES
Hydrological	Proximity to drainage network	YES	YES
	Site exposure index*	NO	YES
	Integrated moisture index*	NO	YES
	Compound Topographic index	YES	NO
	Proximity to streams	YES	NO
Geological	Soil/rock type	YES	YES
	Proximity to geological contact	YES	YES
	Proximity to faults	YES	NO
Anthropogenic	Land use	YES	YES
	Proximity to land use contact	NO	YES
	Proximity to traffic infrastructure	NO	YES

*DTM based LCFs, smoothed for S₅ scenario

Methodology

General susceptibility modelling workflow

After acquiring relevant landslide and thematic data, landslide susceptibility modelling requires certain parameters to be selected in each of the modelling steps. Namely, a 5 m pixel is selected as a mapping unit (Bernat Gazibara et al. 2023b) for Random Forests (RF) machine learning algorithm. A pixel based analysis is commonly used in landslide susceptibility assessments (Reichenbach et al. 2018), whereas RF as a method was introduced in Breiman 2001, followed by numerous applications in susceptibility modelling (e.g. Catani et al. 2013 and Sandić et al. 2023), and nowadays often analysed in algorithm review papers as a successful method choice (Merghadi et al. 2020). As most of the data processing and evaluation metrics were conducted jointly in ArcMap 10.8 and Microsoft Excel, the “*Statistics and Machine Learning Toolbox*” (The MathWorks, Inc., 2021) in MATLAB software was used to perform the RF method. Moreover, it should be stated that LCF collinearity was tested prior to the susceptibility modelling by using a Pearson’s R absolute value of 0.5 as the cut-off threshold to ensure no collinearity presence. The latter was performed in R software, using an open-source software LAND-SUITE (Rossi et al. 2022). As we experiment with different sampling strategies, we opted for an equal comparison strategy as commonly used fitting and predictive performance would not result in objective conclusions. Namely, for each landslide susceptibility model, a curve is plotted by defining cumulative landslide area against cumulative susceptibility area with a 0.01 interval of probabilistic value to calculate AUC. As defined in Chung

and Fabbri 1999 and Chung and Fabbri 2003, this is used to measure success and prediction rate (e.g. in bivariate analysis Moazzam et al. 2020 and Sinčić et al. 2022b) by examining training and validation landslides, respectively. In our case, all landslides will be examined to emphasize applicability on a local scale, i.e. measuring classification capabilities of the models for all mapped landslides only. Moreover, this metric is the basis for the zonation method applicable in the Croatian local scale spatial planning system (Bernat Gazibara et al. 2023a). In both pilot areas, the equal procedure to define stable pixels is as follows. By removing training landslides from the pilot area, an extent where stable pixels can be generated is defined, ensuring unbiased sampling. Namely, the stable pixels are generated randomly and as single units, in an equal amount as there are unstable pixels in the training landslide dataset. On the other hand, unstable pixel sampling differs greatly from model to model and is explained in detail separately for each pilot area.

Podsljeme zone pilot area

All landslide polygons in the Podsljeme zone are firstly split randomly into ten equal-in-size sets. Then, scenario S₁ is defined by using nine sets for training (i.e. 90%), followed by using eight sets (i.e. 80%) for training in scenario S₂, etc., up to scenario S₉ which uses only one set (i.e. 10%) for training the model. Scenarios S₁ to S₉ define the nine models derived in the Podsljeme zone with the purpose of testing landslide inventory representatives and its possibility to yield satisfactory results with a limited training landslide.

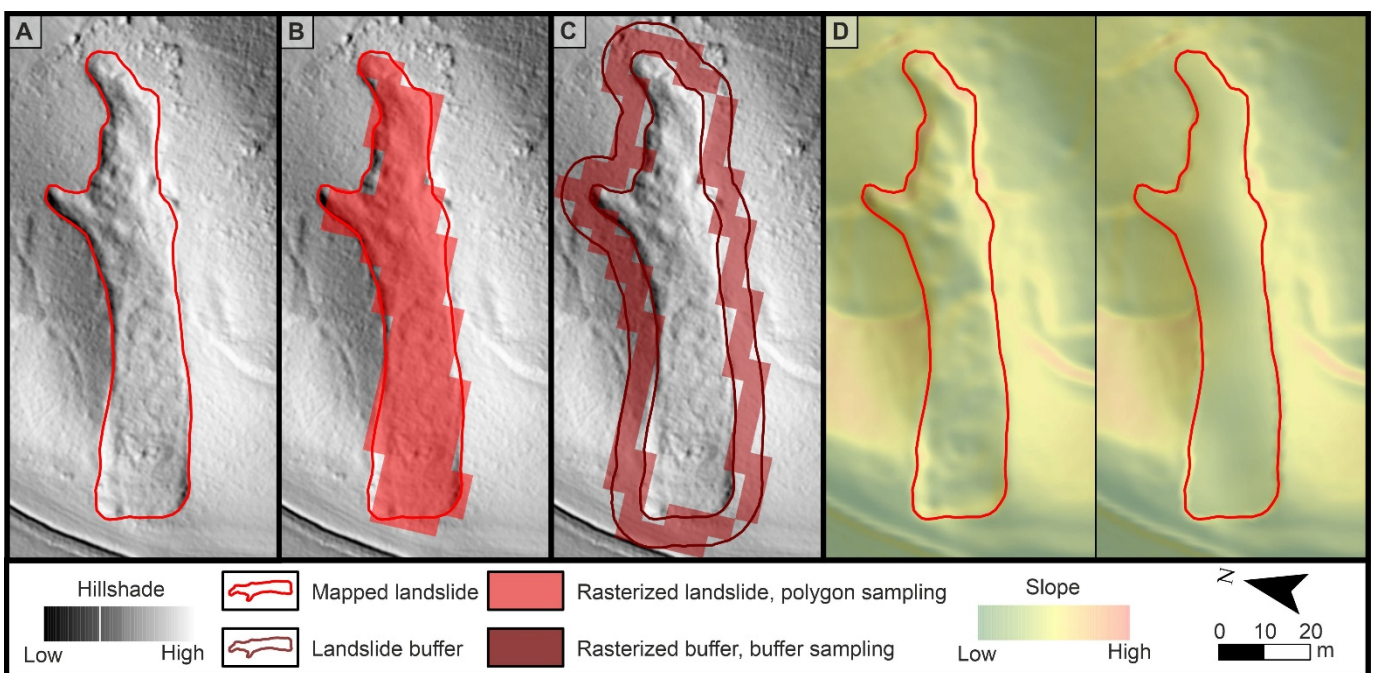


Figure 2 An example of mapped landslide (A) and sampling methodologies for scenarios S_P (B), S_B (C) and S_S (D) in the Hrvatsko Zagorje pilot area.

Hrvatsko Zagorje pilot area

The landslide inventory is split into two equal sets, using one half differently to train the model in each of the three scenarios in Hrvatsko Zagorje. The first scenario S_P samples rasterized polygons (“P”), as does the second scenario S_S . However, in the S_S scenario, DTM based LCFs are smoothed (“S”) at all landslide locations prior to the modelling. By buffering (“B”) a 6.25m zone around the landslides, a sampling zone for scenario S_B is defined, using exclusively the rasterized pixels from the buffered zone. Smoothened LCFs for S_S scenario are noted with an asterisk (*) in Table 1, whereas Fig. 2 illustrates the described sampling methodology. Commonly used strategy as in scenario S_P serves for comparison (a reference point), whereas scenarios S_S and S_B aim to capture the geomorphologically undistributed terrain conditions, i.e. prior to landslide occurrence.

Results and discussion

Testing nine different amounts of landslides included in training the model ranging from 10 to 90% was tested in the Podsljeme zone. Namely, the AUC results are as follows: S_1 -0.98, S_2 -0.97, S_3 -0.96, S_4 -0.95, S_5 -0.94, S_6 -0.92, S_7 -0.91, S_8 -0.89 and S_9 -0.86 (Fig. 3). Surprisingly, results indicate excellent performance in all scenarios when measuring the classification capabilities for all landslides. A general declining trend in AUC values is evident as the amount of training landslides decreases, i.e. from 90% (S_1) to 10% (S_9). As this is not surprising, however, even a rigorous S_9 scenario managed to yield high AUC, indirectly pointing to very high predictive performance of the model. We argue that the presented results are due to the systematic and complete mapping which resulted in a representative landslide inventory. Thus, we highlight the benefits and emphasize the capabilities of such a landslide inventory map even in rigorous landslide susceptibility modelling. Moreover, compared to approximately 0.86 AUC values for fitting and predictive performance in Bernat Gazibara et al. 2023a where 50% of the landslide were used for training, an evident increase in performance is noted. Namely, scenario S_5 using 50% of training landslides in this study resulted in 0.94 AUC values, likely due to the use of machine learning instead of bivariate methodology. Different findings are found in the Hrvatsko Zagorje where S_P , S_S and S_B scenarios resulted in 0.88, 0.89 and 0.80 AUC values, respectively (Fig. 3). The minimal change in scenario S_S is not surprising as a small portion of the study area was altered, whereas a significant decrease to 0.80 in scenario S_B is undoubtedly a drastic decrease in model performance. Compared to previous landslide susceptibility assessments, i.e. Krkač et al. 2023 and Bernat Gazibara et al. 2023b, a significant increase is seen in S_P and S_S scenarios, likely due to the application of the RF method. In both cases, we reckon that a more detailed analysis is necessary to deliver a complete and comprehensive conclusion about the sampling scenarios, whereas in this research, we identified preliminary model

behaviour for the given settings. For instance, measuring the variability, fitting and predictive performance (individually), as well as zoning the model (and analysing it qualitatively) into an applicable map for local scale application remains a task out of the scope of this research.

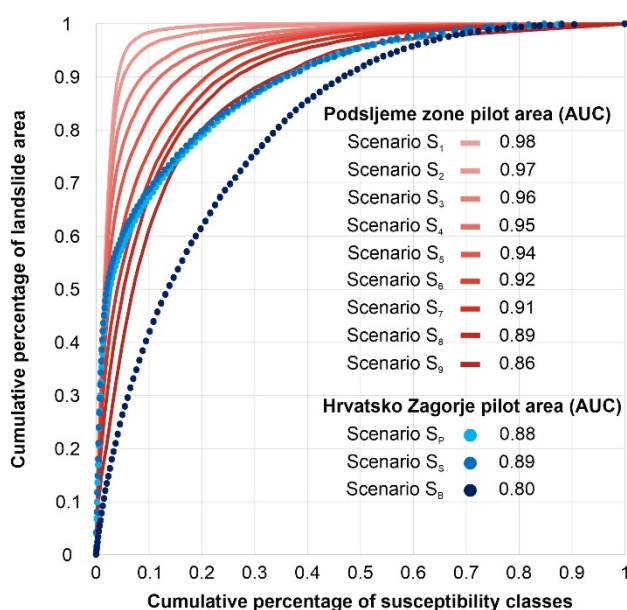


Figure 3 Calculated AUC values for scenarios in Podsljeme zone and Hrvatsko Zagorje pilot areas.

Conclusions

This study aimed to preliminary investigate the landslide inventory sampling in landslide susceptibility modelling of small and shallow landslides present in NW Croatia. One approach was tested in the Podsljeme zone where landslide training amount was reduced from 90 to 10% in nine equal steps. In the Hrvatsko Zagorje we opted for common polygon sampling, smoothing the DTM derived LCFs at landslide locations and buffering the landslides as two scenarios simulating undistributed terrain conditions, i.e. prior to landslide occurrence. In both pilot areas, used landslide inventories are representative and mapped based on high resolution DTM derivatives, used in combination with reliable LCFs for a 5 m pixel based analysis by applying the RF algorithm. Furthermore, AUC which considered all landslides was calculated, serving as a metric unifying fitting and predictive performance.

Generally, satisfactory results were achieved in both pilot areas for all defined scenarios, with generally better results in the Podsljeme zone. Scenario S_B is the only scenario which yielded significantly lower AUC values, i.e. 0.80 and can be considered as a less favorable strategy. On the other hand, using smoothed DTM derived LCFs led to an insignificantly AUC increase compared to the S_P scenario. The most interesting finding in Podsljeme zone is that using only 10% of landslides for training can yield an AUC of 0.86. For both cases, using additional metrics and assessing the models qualitatively considering possible zoning methods is likely to unveil more

significant differences in the sampling strategies. Compared to previous landslide susceptibility assessments in the study area, a general increase in AUC is noted, likely due to the RF method.

A further approach considering the experiment in the Podsljeme zone could be splitting the pilot area spatially, unlike randomly as in this research. Similarly, simultaneously experimenting with stable and unstable area sampling in the Hrvatsko Zagorje pilot area is likely to yield new insight into the sampling strategies, as it is uncommon in the literature.

Acknowledgements

This research has been fully supported by the Croatian Science Foundation under the project ‘Methodology development for landslide susceptibility assessment for land-use planning based on LiDAR technology’, LandSlidePlan (HRZZ IP-2019-04-9900, HRZZ DOK-2020-01-2432) and by Institutional project 31980036 ModKLIZ, co-funded by the Faculty of Mining, Geology and Petroleum Engineering.

References

- Bernat S, Mihalić Arbanas S, Krkač M (2014a) Inventory of precipitation triggered landslides in the winter of 2013 in Zagreb (Croatia, Europe). *Proceedings of World Landslide Forum 3*, 2-6 June 2014. Springer, Cham. pp. 829-836.
- Bernat S, Mihalić Arbanas S, Krkač M (2014b) Landslides triggered in the continental part of Croatia by extreme precipitation in 2013. *Proceedings of the XII IAEG Congress*, 15-19 September 2014. Springer, Heidelberg. pp. 1599–1603.
- Bernat Gazibara S, Krkač M, Mihalić Arbanas S (2019) Landslide inventory mapping using LiDAR data in the City of Zagreb (Croatia). *Journal of Maps* 15:773–779. <https://doi.org/10.1080/17445647.2019.1671906>.
- Bernat Gazibara S, Sinčić M, Krkač M, Lukačić H, Mihalić Arbanas S (2023a) Landslide susceptibility assessment on a large scale in the Podsljeme area, City of Zagreb (Croatia). *Journal of Maps* 19:1. <https://doi.org/10.1080/17445647.2022.2163197>.
- Bernat Gazibara S, Mihalić Arbanas S, Sinčić M, Krkač M, Lukačić H, Jagodnik P, Arbanas Ž (2022) LandSlidePlan -Scientific research project on landslide susceptibility assessment in large scale. *Proceedings of the 5th regional symposium on landslides in Adriatic-Balkan Region*, 23-26 March 2022. University of Rijeka, Faculty of Civil Engineering, Rijeka, Croatia and University of Zagreb, Faculty of Mining, Geology and Petroleum Engineering, Zagreb, Croatia. pp. 99–106.
- Bernat Gazibara S, Sinčić M, Rossi M, Reichenbach P, Krkač M, Lukačić H, Jagodnik P, Šarić G, Mihalić Arbanas S (2023b) Application of LAND-SUITE for Landslide Susceptibility Modelling Using Different Mapping Units: A Case Study in Croatia. *Progress in Landslide Research and Technology*, Volume 2 Issue 2. Alcántara-Ayala I, Arbanas Ž, Huntley D, Konagai K, Mihalić Arbanas M, Mikoš M, Ramesh MV, Sassa K, Sassa S, Tang H, Tiwari B (eds.). Springer, Cham, Fullerton, CA, USA. (ISBN 978-3-031-44295-7). 503p.
- Breiman L (2001) Random Forests. *Machine Learning* 45:5–32. <https://doi.org/10.1023/A:1010933404324>.
- Catani F, Lagomarsino D, Segoni S, Tofani V (2013) Landslide susceptibility estimation by random forests technique: sensitivity and scaling issues. *Natural Hazards and Earth System Sciences* 13:2815–2831. <https://doi.org/10.5194/nhess-13-2815-2013>.
- Chen W, Xie X, Wang J, Pradhan B, Hong H, Bui DT, Duan Z, Ma J (2017) A comparative study of logistic model tree, random forest, and classification and regression tree models for spatial prediction of landslide susceptibility. *Catena* 151:147–160. <https://doi.org/10.1016/j.catena.2016.11.032>.
- Chung CJF, Fabbri AG (1999) Probabilistic Prediction Models for Landslide Hazard Mapping. *Photogrammetric Engineering and Remote Sensing* 65:1389–1399.
- Chung CJF, Fabbri AG (2003) Validation of Spatial Prediction Models for Landslide Hazard Mapping. *Natural Hazards* 30:451–472. <https://doi.org/10.1023/B:NHAZ.0000007172.62651.2b>.
- Farooq S, Akram MS (2021) Landslide susceptibility mapping using information value method in Jhelum Valley of the Himalayas. *Arabian Journal of Geosciences* 14:824. <https://doi.org/10.1007/s12517-021-07147-7>.
- Fell R, Corominas J, Bonnard C, Cascini L, Leroi E, Savage WZ (2008) Guidelines for landslide susceptibility, hazard and risk zoning for land use planning. *Engineering Geology* 102:85–98. <https://doi.org/10.1016/j.enggeo.2008.03.022>.
- Fu Z, Wang F, Dou J, Nam K, Ma H. (2023) Enhanced Absence Sampling Technique for Data-Driven Landslide Susceptibility Mapping: A Case Study in Songyang County, China. *Remote Sensing* 15, 3345. <https://doi.org/10.3390/rs15133345>.
- Gaidzik K, Ramírez-Herrera MT (2021) The importance of input data on landslide susceptibility mapping. *Scientific Reports* 11:19334. <https://doi.org/10.1038/s41598-021-98830-y>.
- Guzzetti F, Reichenbach P, Cardinali M, Galli M, Ardizzone F (2005) Probabilistic landslide hazard assessment at the basin scale. *Geomorphology* 72, 272–299. <http://dx.doi.org/10.1016/j.geomorph.2005.06.002>.
- Guzzetti F, Mondini AC, Cardinali M, Fiorucci F, Santangelo M, Chang K-T (2012) Landslide inventory maps: New tools for an old problem. *Earth- Science Reviews* 112:42–66. <https://doi.org/10.1016/j.earscirev.2012.02.001>.
- Hemasinghe H, Rangali RSS, Deshapriya NL, Samarakoon L (2018) Landslide susceptibility mapping using logistic regression model (a case study in Badulla District, Sri Lanka). *Procedia Engineering* 212:1046–1053. <https://doi.org/10.1016/j.proeng.2018.01.135>.
- Hussin HY, Zumpano V, Reichenbach P, Sterlacchini S, Micu M, van Westen C, Bălteanu D (2016) Different landslide sampling strategies in a grid-based bi-variate statistical susceptibility model. *Geomorphology*, 253, 508–523. <https://doi.org/10.1016/j.geomorph.2015.10.030>.
- Jacobs L, Kervyn M, Reichenbach P, Rossi M, Marchesini I, Alvioli M, Dewitte O (2020) Regional susceptibility assessments with heterogeneous landslide information: Slope unit- vs. pixel-based approach. *Geomorphology* 356:107084. <https://doi.org/10.1016/j.geomorph.2020.107084>.
- Krkač M, Bernat Gazibara S, Sinčić M, Lukačić H, Mihalić Arbanas S (2022) Landslide inventory mapping based on LiDAR data: A case study from Hrvatsko Zagorje (Croatia) *Proceedings of the 5th regional symposium on landslides in Adriatic-Balkan Region*, 23-26 March 2022. University of Rijeka, Faculty of Civil Engineering, Rijeka, Croatia and University of Zagreb, Faculty of Mining, Geology and Petroleum Engineering, Zagreb, Croatia. pp. 81–86.
- Krkač M, Bernat Gazibara S, Sinčić M, Lukačić H, Šarić G, Mihalić Arbanas S (2023) Impact of input data on the quality of the landslide susceptibility large-scale maps: A case study from NW Croatia. *Progress in Landslide Research and Technology*, Volume 2 Issue 1. Alcántara-Ayala I, Arbanas Ž, Cuomo S, Huntley D., Konagai K, Mihalić Arbanas S, Mikoš M, Sassa K, Tang H, Tiwari B (eds.). Springer, Cham, Fullerton, CA, USA. (ISBN 978-3-031-39011-1). 482p.
- Lucchese LV, de Oliveira GG, Pedrollo OC (2021) Investigation of the influence of nonoccurrence sampling on landslide susceptibility

- assessment using Artificial Neural Networks. *Catena* 198, 105067 <https://doi.org/10.1016/j.catena.2020.105067>.
- Mihalić Arbanas S, Bernat Gazibara S, Krkač M, Sinčić M, Lukačić H, Jagodnik P, Arbanas Ž (2023) Landslide Detection and Spatial Prediction: Application of Data and Information from Landslide Maps. *Progress in Landslide Research and Technology, Volume 1 Issue 2*. Alcántara-Ayala I, Arbanas Ž, Huntley D, Konagai K, Mikoš M, Sassa K, Sassa S, Tang H, Tiwari B (eds.). Springer, Cham, Fullerton, CA, USA. (ISBN 978-3-031-18470-3). 475p.
- Merghadi A, Yunus AP, Dou J, Whiteley J, ThaiPham B, Bui DT, Avtar R, Abderrahmane B (2020) Machine learning methods for landslide susceptibility studies: A comparative overview of algorithm performance. *Earth- Science Reviews* 207:103225. <https://doi.org/10.1016/j.earscirev.2020.103225>.
- Moazzam MFU, Vansarochana A, Boonyanuphap J, Choosumrong S, Rahman G, Djueyep GP (2020) Spatio-statistical comparative approaches for landslide susceptibility modeling: case of Mae Phun, Uttaradit Province, Thailand. *SN Applied Sciences*, 2(3). <https://doi.org/10.1007/s42452-020-2106-8>.
- Razak KA, Straatsma MW, van Westen CJ, Malet JP, de Jong SM (2011) Airborne laser scanning of forested landslides characterization: terrain model quality and visualization. *Geomorphology* 126, 186–200.
- Reichenbach P, Rossi M, Malamud BD, Mihir M, Guzzetti F (2018) A review of statistically-based landslide susceptibility models. *Earth-Science Reviews* 180:60–91. <https://doi.org/10.1016/j.earscirev.2018.03.001>.
- Rossi M, Bornaetxea T, Reichenbach P (2022) LAND-SUITE V1.0: a suite of tools for statistically based landslide susceptibility zonation. *Geoscientific Model Development* 15:5651–5666. <https://doi.org/10.5194/gmd-15-5651-2022>.
- Sandić C, Marjanović M, Abolmasov B, Tošić R (2023) Integrating landslide magnitude in the susceptibility assessment of the City of Dobož, using machine learning and heuristic approach. *Journal of Maps* 19:1. <https://doi.org/10.1080/17445647.2022.2163199>.
- Sinčić M, Bernat Gazibara S, Krkač M, Lukačić H, Mihalić Arbanas S (2022a) The Use of High-Resolution Remote Sensing Data in Preparation of Input Data for Large-Scale Landslide Hazard Assessments. *Land (Basel)* 11:1360. <https://doi.org/10.3390/land11081360>.
- Sinčić M, Bernat Gazibara S, Krkač M, Mihalić Arbanas S (2022b) Landslide susceptibility assessment of the City of Karlovac using the bivariate statistical analysis. *Rudarsko-geološko-naftni zbornik* 37:149–170. <https://doi.org/10.17794/rgn.2022.2.13>.
- Süzen ML, Doyuran V (2004) Data driven bivariate landslide susceptibility assessment using geographical information systems: a method and application to Asarsuyu catchment, Turkey. *Engineering Geology* 71(3-4):303-321 [https://doi.org/10.1016/S0013-7952\(03\)00143-1](https://doi.org/10.1016/S0013-7952(03)00143-1).
- The MathWorks Inc. (2021) *Statistics and Machine Learning Toolbox: 12.1 (R2021)*, Natick, Massachusetts: The MathWorks Inc. <https://www.mathworks.com> [Last accessed: 29.2.2024.].
- Xi C, Han M, Hu X, Liu B, He K, Luo G, Cao X (2002) Effectiveness of Newmark-based sampling strategy for coseismic landslide susceptibility mapping using deep learning, support vector machine, and logistic regression. *Bulletin of Engineering Geology and the Environment* 81, 174. <https://doi.org/10.1007/s10064-022-02664-5>.

Large-scale landslide susceptibility models: Examples and conclusions from the modelling of small and shallow landslides in the continental part of Croatia

Sanja Bernat Gazibara^{(1)*}, Marko Sinčić⁽¹⁾, Mauro Rossi⁽²⁾, Martin Krkač⁽¹⁾, Hrvoje Lukačić⁽¹⁾, Petra Jagodnik⁽³⁾, Snježana Mihalić Arbanas⁽¹⁾

1) University of Zagreb, Faculty of Mining, Geology and Petroleum Engineering, Pierottijeva 6, 10000 Zagreb, Croatia, +38515535760 (sbernat@rgn.unizg.hr)

2) Research Institute for Geo-Hydrological Protection, Italian National Research Council (CNR IRPI), Via della Madonna Alta 126, 06128 Perugia, Italy

3) Faculty of Civil Engineering, University of Rijeka, Radmile Matejčić 3, 51000 Rijeka, Croatia

Abstract Large-scale landslide susceptibility modelling is carried out in the frame of the scientific project *Methodology development for landslide susceptibility assessment for land-use planning based on LiDAR technology* (LandSlidePlan, HRZZ IP-2019-04-9900) on two pilot areas in the City of Zagreb and Hrvatsko Zagorje. The methodology includes defining input data quality, landslide sampling strategies, mapping units, applied statistical method, and zonation method for providing final landslide susceptibility maps. Finally, all landslide susceptibility models were evaluated based on model fitting performance, model prediction performance, and model uncertainty. The purpose of comparing landslide susceptibility models was to define the most suitable methodology for modelling small and shallow landslides in the continental part of Croatia and application in spatial planning systems at a local level. The main results and conclusions were compiled in guidelines for large-scale landslide inventory and susceptibility map production based on high-resolution remote sensing data.

Keywords landslide susceptibility modelling, large-scale, spatial planning system

Introduction

The main motivation to research the large-scale landslide susceptibility modelling for application in spatial planning systems arises from the national landslide risk assessment (Bernat Gazibara et al. 2019), which recognised landslides as a second natural risk in Croatia. The scientific project *Methodology development for landslide susceptibility assessment for land-use planning based on LiDAR technology* (LandSlidePlan, HRZZ IP-2019-04-9900) has three main scientific goals (Bernat Gazibara et al. 2022): (i) to create the optimal digital model of the bare-earth terrain that shows realistic landslide footprints and differences between landslide and non-landslide area that may influence land use; (ii) to create the most reliable

large-scale landslide susceptibility map with the optimal differentiation of landslide-prone and non-susceptible areas using scientific methods customised to specific engineering geological conditions of Croatian environments, and (iii) to create maps depicting information about landslides for the application in land-use planning. The research was based on innovative technologies, limitations related to the availability of spatial data in Croatia (limited amount of geological data), and urgent needs for efficient solutions applicable in the Croatian spatial planning system in line with European and global requirements related to sustainable development, human and environmental protection. This paper presents an overview of the several research papers published in the frame of the LandSlidePlan project. Furthermore, main project results and conclusions regarding input data quality, landslide sampling strategies, mapping units, statistical methods, and zonation for providing accurate and reliable landslide susceptibility maps are given.

Study areas were selected based on similar geological settings and geomorphological conditions but different degrees of urbanisation in the NW part of Croatia (Fig.1): the pilot area (20 km²) in the urbanised part of the Podsljeme area, City of Zagreb and the pilot area (20 km²) in a rural part of Hrvatsko Zagorje. Part of the Podsljeme area of the City of Zagreb was selected as a pilot area because of hilly relief, a high degree of urbanisation, and Neogene and Quaternary deposits extremely susceptible to landslides. The pilot area in Hrvatsko Zagorje is composed of Miocene, Quaternary and Triassic sediments. Landslides in this area mainly occur in weathered clastic rocks and soils of Miocene age. Precipitations and human activity are the primary triggers of landslides in NW Croatia (Bernat et al. 2014). Landslides can be classified as shallow to moderately shallow (1 – 20 m) and small (10¹ – 10³ m²), based on abundant landslide size, which is approx. 500 m².



Figure 1 Podsljeme zone and Hrvatsko Zagorje pilot areas, located in NW Croatia (modified after Bernat Gazibara et al. 2022).

Landslide susceptibility modelling

Input data

Airborne laser scanning (ALS) was undertaken during the leaf-off period in March 2020, resulting in a point cloud for the Hrvatsko Zagorje pilot area with a surface point horizontal accuracy of 3 cm and vertical accuracy of 4 cm, point density of 16.09 pt./m², and average point spacing of 0.28 cm. The bare-earth digital terrain model (DTM) with a 30 cm resolution using the kriging interpolation method was created for visual landslide identification and mapping, while 5 m LiDAR DTM was created for large-scale landslide susceptibility modelling.

The input data for landslide susceptibility assessment (LSA) on a large scale were analysed for the study area in Hrvatsko Zagorje. The result of the visual interpretation of LiDAR DTM morphometric derivatives is the landslide inventory map, which consists of 912 identified and mapped landslides, ranging in size from 3.3 to 13,779 m² and with an average landslide density of 45.1 landslides/km² (Krkač et al. 2022). Sinčić et al. (2022a) compared the geographic and thematic consistency of different geoenvironmental input data sets to address the adequate scale of input data to minimise deviations from actual environmental conditions. The spatial distribution of the classes in landslide conditioning factors was compared using a LiDAR-based landslide inventory map, pointing out the influence of small-scale input data sets on a large-scale LSA. Fig. 2 shows the comparison of slope classes and landslide area distributions for different DTM resolutions available for the study area. Geological data are often available only on a small scale, e.g. in the Republic of Croatia, only The Basic Geological Map on a scale of 1:100,000 is available for most of the territory, which is inadequate for large-scale LSA. Using a combination of geological data from small-scale geological maps to get acquainted with geological settings and terrain information from high-resolution LiDAR data enables distinguishing the geological settings in more detail, improving geological contacts, and aggregating

chronostratigraphic units into engineering formation units, which are more suitable for LSA (Sinčić et al. 2022a). However, the limitations of this approach could be the presence of different geological settings across the study area, in which engineering units cannot be distinguished from the LiDAR DTM derivatives. Sinčić et al. (2022a) concluded that the high-resolution remote sensing data, LiDAR DTM, and orthophoto images are optimal input data sets for large-scale LSA because they enable the following: (i) derivation of geomorphological, geological, hydrological, and anthropogenic input data layers on a large scale, except geological structures and spring data; (ii) verification of input data layers; (iii) derivation of input data layers with the best fit to the actual environmental conditions (spatial accuracy testing); and (iv) efficient derivation of input data layers considering both price and time.

Furthermore, Krkač et al. (2023) compared two different input data sets to derive landslide causal factor maps for landslide susceptibility analysis, i.e. scenarios: (i) Scenario 1 included free-available input data sets with a lower resolution and lower spatial accuracy, such as EU-DEM or Corine Land Cover; and (ii) Scenario 2 included a more detailed input data set, such as high-resolution remote sensing data, i.e. LiDAR point cloud and digital orthophoto imagery in resolution 0.5 m. The landslide data used for susceptibility analysis was LiDAR-based inventory (Krkač et al. 2022). The success and prediction rates for Scenario 1 were approximately 10 % lower than the values for Scenario 2. Moreover, landslide susceptibility maps looked relatively similar based on visual comparison, although the most significant difference between the two scenarios is the percentage of low landslide susceptibility values in valleys. Considering the stated, the landslide susceptibility map based on causal factors derived from high-resolution remote sensing data (Scenario 2) has minor deviations from actual environmental conditions. i.e., the spatial accuracy of the resulting LSA is significantly higher, which is not sufficiently emphasized by the obtained AUC values Krkač et al. (2023).

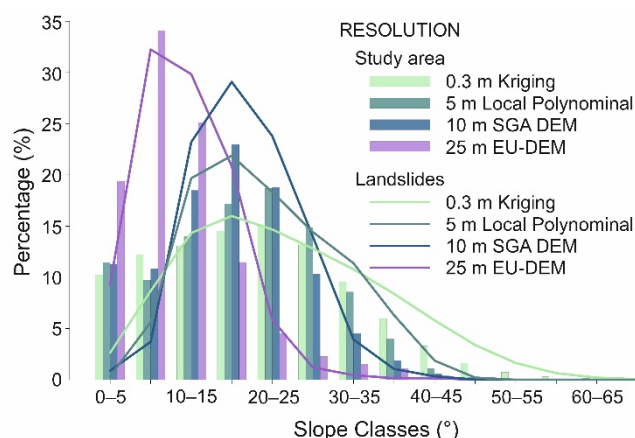


Figure 2 Comparison of slope class area and landslide area distribution on the slope maps derived from 0.3 and 5 m LiDAR DTMs, 10 m DEM, and 25 m EU-DEM (modified after Sinčić et al. 2022a).

Defining the most significant landslide causal factors (LCF) in a study area is one of the most important steps in susceptibility modelling. Bernat Gazibara et al. (2023a) evaluated a large number of geomorphological, geological, hydrological and anthropogenic data as variables for the study area in Hrvatsko Zagorje since general criteria or guidelines for the selection of causal factors for susceptibility modelling are not available. In this work, appropriate LCFs were selected based on the pairwise correlation test and Leave One Out test in LAND-SUITE developed by Rossi et al. (2022). Only six were selected from the 22 original factor maps, considering the lack of variable relevance on the susceptibility model and following the rule "less is more", avoiding over-parameterisation issues. LAND-SUITE proved to be a helpful tool for landslide susceptibility variable analysis and allows the preparation of susceptibility maps of the highest Susceptibility Quality Level, i.e., SQL index, as illustrated in Reichenbach et al. (2018).

Landslide sampling strategy

Bernat Gazibara et al. (2023b) and Sinčić et al. (2024a) analysed different ratios of landslides for model training and validation for the Podsljeme zone pilot area, to provide new insight into the need for detailed landslide mapping for large-scale susceptibility modelling, as well as the impact on the final landslide susceptibility map. The landslide susceptibility analysis consists of ten scenarios that were defined considering the percentage of landslide polygons in the inventory for model training (S100 = 100% of landslides in the LiDAR-based inventory, S90 = 90 % of landslides, S70 = 70% of landslides, etc.), while the rest of the landslides were used for model validation (S90 = 10% of landslides in the LiDAR-based inventory, S70 = 30 % of landslides, etc.). The presented analyses showed that using 70% of inventory landslides for model training (S70) resulted in the model having a training AUC value of 98.1 %. Using half of the landslide inventory for training (S50) keeps the training AUC value higher than 98 %, and the model trained with only 10 % of inventory landslides (S10) resulted in training AUC value higher than 99 %. Using the same 30 % of landslides in the inventory for model validation in scenarios S70, S50, S30, and S10 showed variability of AUC value from 89,4 %, 89 %, 89,2 %, to 87 %. Fig 3. shows the spatial distribution of the absolute difference in probabilistic values of landslide susceptibility models (LSM) regarding scenario S100 and scenarios S90, S70, S50 and S10. Lastly, comparing ten derived susceptibility models, more than 10% of the study area showed a standard deviation of probability values of more than 0.1. The question of minimising the influence of the landslide data sampling on the final large-scale landslide susceptibility zonation maps remains open. However, the research highlights the importance of qualitative assessment, alongside commonly used quantitative metrics, to verify spatial accuracy and to test the applicability of derived LSM in the spatial planning system.

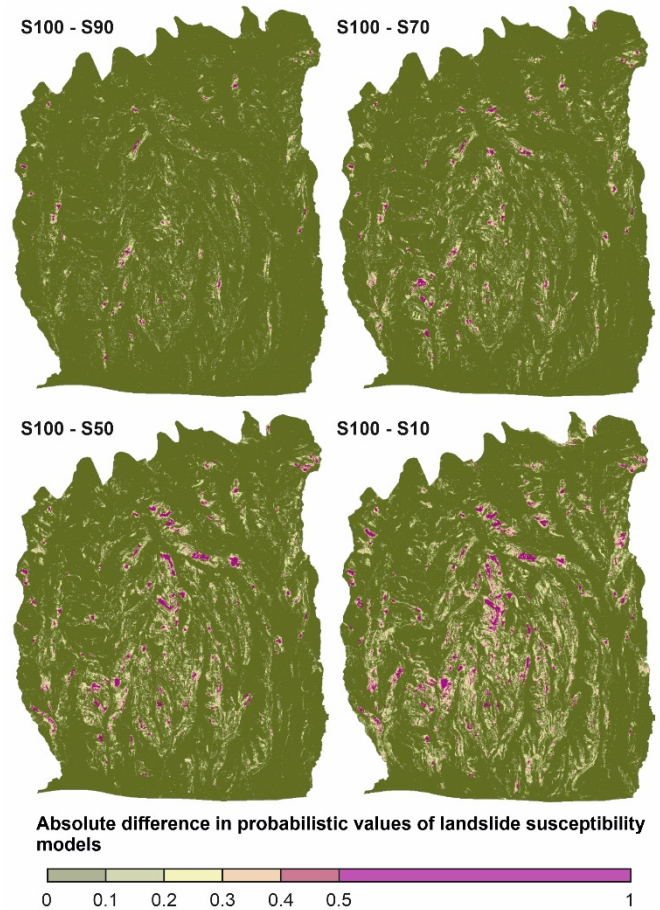


Figure 3 Absolute difference in probabilistic values of landslides susceptibility models regarding scenario S100 (using 100% of landslides in the inventory) and scenarios S90 (using 90 % of landslides), S70, S50 and S10.

Statistical methods

The selection of an appropriate mapping unit and statistical method is a critical phase in landslide susceptibility modelling (Reichenbach et al. 2018). Bernat Gazibara et al. (2023a) considered 5 m x 5 m regular grid cells and slope units (Alvioli et al. 2016) for the Podsljeme pilot area to analyse the effect of different statistical methods on training LSM for application on a local level, i.e. scale 1:5,000. LAND-SUITE was used to prepare landslide susceptibility maps, i.e., four single statistical models (Logistic regression, Linear and Quadratic discriminant analysis, and Neural network analysis) and one combined model for the two mapping units. All model evaluation tests indicate pixel-based models have better model fitting and predictive performance than slope-unit based models, regardless of the statistical method. The probability of landslide occurrence for each of the ten models was classified into five susceptibility classes, based on threshold values 0.2, 0.45, 0.55, 0.8 (Bernat Gazibara et al. 2023a). The pixel and slope unit-based maps displayed differences in the information detail, indicating that pixel-based models are more appropriate for the local-level spatial planning system. However, pixel-based maps require "post-processing" of the susceptibility zones to

produce more clustered and homogeneous information for the final purpose.

Sinčić et al. (2024b) focused their work on the crucial step of classifying continuous landslide conditioning factors for susceptibility modelling in the Podsljeme pilot area by presenting an innovative, comprehensive analysis that resulted in 54 landslide susceptibility models to test 11 classification criteria (scenarios which vary from stretched values, partially stretched classes, heuristic approach, classification based on studentized contrast and landslide presence, and commonly used classification criteria, such as Natural Neighbor, Quantiles and Geometrical intervals) in combination with five statistical methods (Information Value (IV), Logistic Regression (LR), Neural Network (NN), Random Forests (RF) and Support Vector Machine (SVM)). The main conclusions and novelties derived from the comprehensive large-scale landslide susceptibility analysis that Sinčić et al. (2024b) performed are the following: (i) applying input data layers as stretched

rasters and line vectors as buffers with >10 buffer zones prove more reliable simplifies the susceptibility modelling process and provides a uniform solution to preparing LCFs; (ii) optimal method selection remains an open question and generally should be considered regarding the final applicability of the LSA, whereas LR method presents the most stable and representative option, and the RF method offers optimal performance when appropriately applied, achieving far better performance. Fig. 4 shows a close-up view comparison of the landslide susceptibility maps derived using four statistical methods, while input data in all four scenarios are the same. Overall, the SVM method (Fig. 4d) on a close-up view shows minimal pixelization, i.e. depicting zones rather than pixel shaped transfer from class to class. RF method (Fig. 4c) proves its poorest predictive performance, with a substantial amount of visible validation landslides in low or very low susceptibility zones.

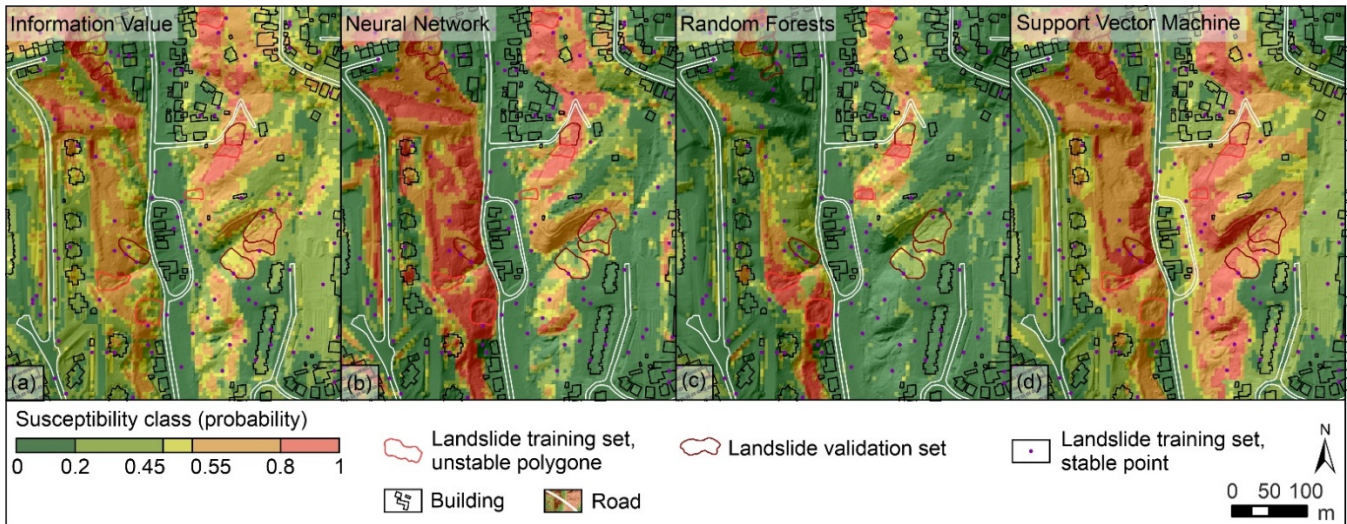


Figure 4 Close-up views of landslide susceptibility maps derived using four statistical methods: (a) Information Value; (b) Neural Network; (c) Random Forests; (d) Support Vector Machine (modified after Sinčić et al. 2024b).

Landslide susceptibility zoning

The landslide susceptibility models obtained through statistical analyses need to be interpreted; that is, a probability classification must be carried out that results in a landslide susceptibility zonation map. By reviewing the world literature, there are no uniform recommendations for landslide susceptibility zonation, and different authors apply different methods. For the application of landslide susceptibility zonation maps in the spatial planning system of the Republic of Croatia, it is recommended to use three zonation classes, i.e. low, medium and high landslide susceptibility zones (Mihalić Arbanas et al. 2023). Threshold values of landslide susceptibility zones are defined by the ROC curve (Fig. 5), i.e., all landslides in the inventory are observed for zonation purposes, and the probabilistic LSM ranging from 0.0 to 1.0 is split into 100 classes with a 0.01 interval to construct the ROC curve.

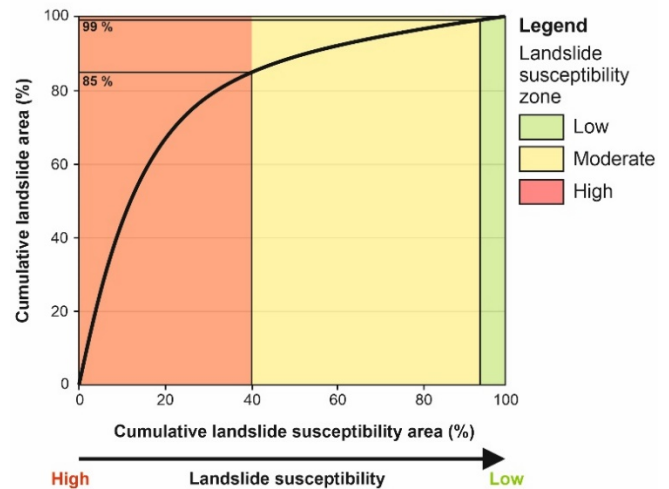


Figure 5 Landslide susceptibility zoning using the ROC curve and threshold values based on cumulative landslide area.

Furthermore, cut-off values for zonation are set to 85% and 99% of cumulative landslide area presence, similar to the approach introduced by Bernat Gazibara, 2019 and applied in Sinčić et al. 2022b and Bernat Gazibara et al. 2023c. As a result, high, medium and low susceptibility zones are defined: (i) low susceptibility zone is defined with only 1 % landslide presence, (ii) medium susceptibility zone is defined with 14 % landslide presence, and (iii) high susceptibility zone is defined with 85 % landslide presence. The proposed zonation method defines distinct landslide density in a particular landslide susceptibility zone and thus enables the regulation of preventative measures for landslide mitigation through the spatial planning system.

After landslide susceptibility zonation, it is necessary to generalize the final map so that the susceptibility zones are relatively homogeneous, which enables simple and unambiguous practical use in the spatial planning system. Generalization involves averaging and filtering the landslide susceptibility zone values obtained for each pixel by applying focal statistics. A close-up view of the susceptibility model, susceptibility zonation map, and a final, generalized landslide susceptibility map is shown in Fig. 6. Generalization of the landslide susceptibility zonation map must preserve the model's spatial accuracy and differences in the susceptibility zone areas should be minimal after processing with focal statistics.

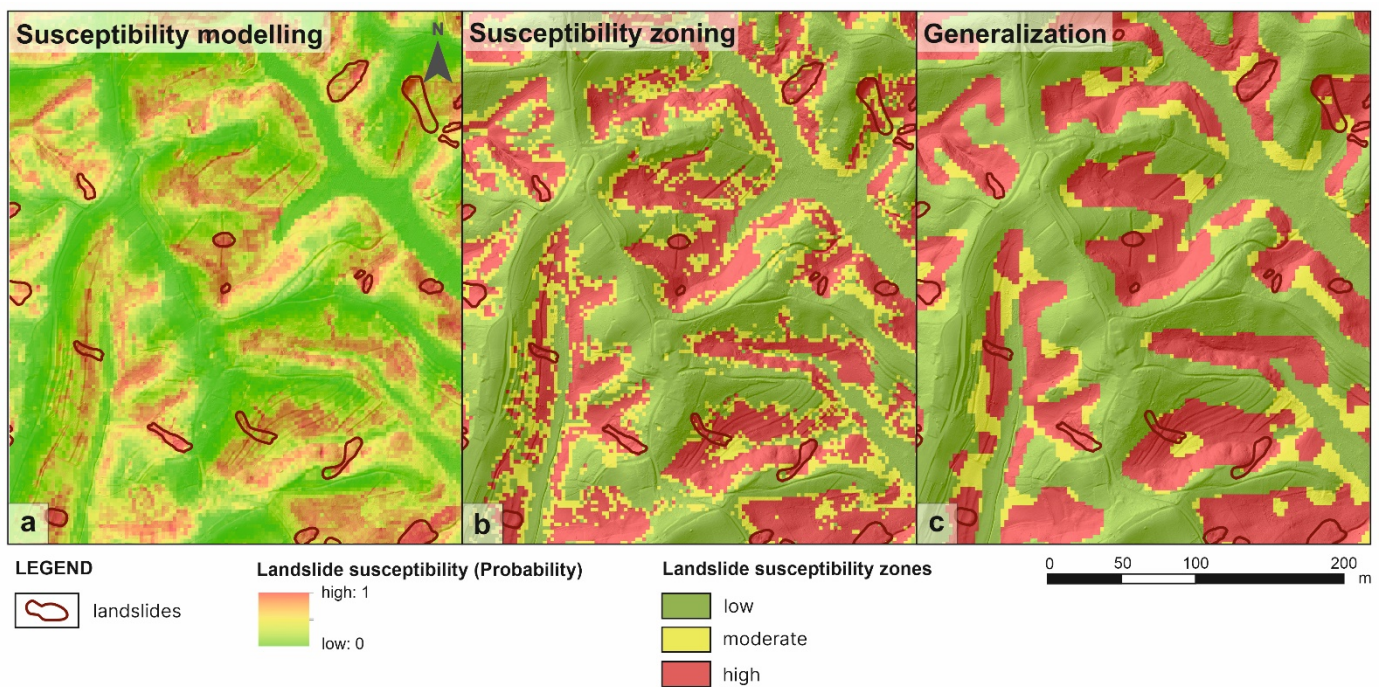


Figure 6 Production of final landslide susceptibility zonation map through three steps: (a) landslide probability after susceptibility modelling; (b) landslide susceptibility map after zonation; (c) final landslide susceptibility map after generalization.

Conclusion

In the framework of the LandSlidePlan project, more than 500 landslide susceptibility models were derived for two pilot areas in NW Croatia regarding differences in resolution and quality of input data, variations of causal factors, geometrical type of LiDAR-based inventory, landslide sampling strategies, mapping units, statistical methods, and zonation methods for providing final landslide susceptibility maps. The main conclusions from the derived comprehensive large-scale landslide susceptibility analysis are:

- (i) relevant and high-resolution input data with sufficient spatial accuracy will result in highly reliable LSM (Krkač et al. 2023) performed by any statistical method or any LCF classification scenario (Sinčić et al. 2024b);
- (ii) landslide sampling significantly influences the spatial accuracy of derived LSM (Bernat Gazibara et al. 2023b, Sinčić et al. 2024a);
- (iii) pixel-based models are more appropriate mapping units for the local-level spatial planning system than slope unit-based models, resulting in more detailed susceptibility information, but also require "post-processing" of the susceptibility zones to produce more clustered and homogeneous information for the final purpose;
- (iv) optimal method selection remains an open question and generally should be considered regarding the final applicability of the LSA, whereas in the study Sinčić et al. 2024b, the LR method presents the most stable and representative option, and the RF method offers optimal performance when appropriately applied, achieving far better performance;
- (v) qualitative assessment, alongside commonly used quantitative metrics, is mandatory to verify spatial accuracy and to test the applicability of derived LSM (Sinčić et al. 2024b).

In landslide science, a large number of published works deal with different aspects of landslide mapping or susceptibility modelling; however, very few of these works focus on the development of landslide susceptibility methodologies that can be applied in spatial planning, construction or civil protection systems. One of the most significant results of the LandSlidePlan project is the guidelines for the compilation and application of large-scale landslide maps in Croatia's spatial planning system (Bernat Gazibara et al. 2023d). Guidelines are designed to introduce future landslide map makers with recommendations based on a review of existing literature and conclusions from scientific research on the LandSlidePlan project. The guidelines contain definitions of basic terms and terminology related to landslides, descriptions of landslide map types and landslide hazard zoning levels, recommendations for creating large-scale landslide inventory and susceptibility zoning maps, and recommendations on the application of landslide maps for

sustainable spatial management, with a focus on spatial planning and construction system.

Acknowledgements

This research has been fully supported by the Croatian Science Foundation under the project methodology development for landslide susceptibility assessment for land use planning based on LiDAR technology, LandSlidePlan (HRZZ IP-2019-04-9900, HRZZ DOK-2020-01-2432). and by Institutional project 311980036 ModKLIZ, co-funded by the Faculty of Mining, Geology and Petroleum Engineering.

References

- Alvioli M, Marchesini I, Reichenbach P, Rossi M, Ardizzone F, Fiorucci F, Guzzetti F (2016) Automatic delineation of geomorphological slope units with r.slopeunits v1.0 and their optimisation for landslide susceptibility modelling. *Geoscientific Model Development* 9:3975–3991. <https://doi.org/10.5194/gmd-9-3975-2016>
- Bernat S, Mihalić Arbanas S, Krkač M (2014a) Inventory of precipitation triggered landslides in the winter of 2013 in Zagreb (Croatia, Europe). *Proceedings of World Landslide Forum 3*, 2-6 June 2014. Springer, Cham. pp. 829-836.
- Bernat Gazibara S (2019) Methodology for landslide mapping using high resolution digital elevation model in the Podsljeme area (City of Zagreb). Doctoral thesis, Faculty of Mining, Geology and Petroleum Engineering, University of Zagreb. (in Croatian)
- Bernat Gazibara S, Cindrić Kalin, K, Erak M, Krkač M, Đomlija P, Arbanas Ž, Mihalić Arbanas S (2019) Landslide hazard analysis in national-scale for landslide risk assessment in Croatia. *Proceedings of the 4th Regional Symposium on Landslides in the Adriatic-Balkan Region*, 23-25 October 2019. Geotechnical Society of Bosnia and Herzegovina, Sarajevo, Bosnia and Herzegovina. pp. 175-182.
- Bernat Gazibara S, Mihalić Arbanas S, Sinčić M, Krkač M, Lukačić H, Jagodnik P, Arbanas Ž (2022) LandSlidePlan -Scientific research project on landslide susceptibility assessment in large scale. *Proceedings of the 5th regional symposium on landslides in Adriatic-Balkan Region*, 23-26 March 2022. University of Rijeka, Faculty of Civil Engineering, Rijeka, Croatia and University of Zagreb, Faculty of Mining, Geology and Petroleum Engineering, Zagreb, Croatia. pp. 99–106.
- Bernat Gazibara S, Sinčić M, Rossi M, Reichenbach P, Krkač M, Lukačić H, Jagodnik P, Šarić G, Mihalić Arbanas S (2023a) Application of LAND-SUITE for Landslide Susceptibility Modelling Using Different Mapping Units: A Case Study in Croatia. *Progress in Landslide Research and Technology*, Volume 2 Issue 2. Alcántara-Ayala I, Arbanas Ž, Huntley D, Konagai K, Mihalić Arbanas M, Mikoš M, Ramesh MV, Sassa K, Sassa S, Tang H, Tiwari B (eds.). Springer, Cham, Fullerton, CA, USA. (ISBN 978-3-031-44295-7). 503p.
- Bernat Gazibara S, Sinčić M, Krkač M, Jagodnik P, Lukačić H, Mihalić Arbanas S (2023b) Influence of the landslide inventory completeness on the accuracy of the landslide susceptibility modelling: A case study from the City of Zagreb (Croatia). *Abstract book of the 6th World Landslide Forum "Landslide science for sustainable development"*, 14-17 November 2023. OIC S.r.l., Firenze, Italy. pp. 644-644.
- Bernat Gazibara S, Sinčić M, Krkač M, Lukačić H, Mihalić Arbanas S (2023c) Landslide susceptibility assessment on a large scale in the Podsljeme area, City of Zagreb (Croatia). *Journal of Maps* 19:1. <https://doi.org/10.1080/17445647.2022.2163197>.

- Bernat Gazibara S, Sinčić M, Krkač M, Jagodnik P, Mihalić Arbanas S (2023d) Guidelines for the development of landslide maps in Croatia. Faculty of Mining, Geology and Petroleum Engineering, University of Zagreb, Zagreb, Croatia, 56p. (in Croatian)
- Krkač M, Bernat Gazibara S, Sinčić M, Lukačić H, Mihalić Arbanas S (2022) Landslide inventory mapping based on LiDAR data: A case study from Hrvatsko Zagorje (Croatia) Proceedings of the 5th regional symposium on landslides in Adriatic-Balkan Region, 23-26 March 2022. University of Rijeka, Faculty of Civil Engineering, Rijeka, Croatia and University of Zagreb, Faculty of Mining, Geology and Petroleum Engineering, Zagreb, Croatia. pp. 81–86.
- Krkač M, Bernat Gazibara S, Sinčić M, Lukačić H, Šarić G, Mihalić Arbanas S (2023) Impact of input data on the quality of the landslide susceptibility large-scale maps: A case study from NW Croatia. *Progress in Landslide Research and Technology*, Volume 2 Issue 1. Alcántara-Ayala I, Arbanas Ž, Cuomo S, Huntley D., Konagai K, Mihalić Arbanas S, Mikoš M, Sassa K, Tang H, Tiwari B (eds). Springer, Cham, Fullerton, CA, USA. (ISBN 978-3-031-39011-1). 482p.
- Mihalić Arbanas S, Bernat Gazibara S, Krkač M, Sinčić M, Lukačić H, Jagodnik P, Arbanas Ž (2023) Landslide Detection and Spatial Prediction: Application of Data and Information from Landslide Maps. *Progress in Landslide Research and Technology*, Volume 1 Issue 2. Alcántara-Ayala I, Arbanas Ž, Huntley D, Konagai K, Mikoš M, Sassa K, Sassa S, Tang H, Tiwari B (eds.). Springer, Cham, Fullerton, CA, USA. (ISBN 978-3-031-18470-3). 475p.
- Reichenbach P, Rossi M, Malamud BD, Mihir M, Guzzetti F (2018) A review of statistically-based landslide susceptibility models. *Earth-Science Reviews* 180:60–91. <https://doi.org/10.1016/j.earscirev.2018.03.001>.
- Rossi M, Bornaetxea T, Reichenbach P (2022) LAND-SUITE V1.0: a suite of tools for statistically based landslide susceptibility zonation. *Geoscientific Model Development* 15:5651–5666. <https://doi.org/10.5194/gmd-15-5651-2022>.
- Sinčić M, Bernat Gazibara S, Krkač M, Lukačić H, Mihalić Arbanas S (2022a) The Use of High-Resolution Remote Sensing Data in Preparation of Input Data for Large-Scale Landslide Hazard Assessments. *Land (Basel)* 11:1360. <https://doi.org/10.3390/land11081360>.
- Sinčić M, Bernat Gazibara S, Krkač M, Mihalić Arbanas S (2022b) Landslide susceptibility assessment of the City of Karlovac using the bivariate statistical analysis. *Rudarsko-geološko-naftni zbornik* 37:149–170. <https://doi.org/10.17794/rgn.2022.2.13>.
- Sinčić M, Bernat Gazibara S, Rossi M, Krkač M, Lukačić H, Mihalić Arbanas A (2024a) Influence of the landslide inventory sampling on the accuracy of the susceptibility modelling using Random Forests: A case study from the NW Croatia. *Proceedings of the 6th regional symposium on landslides in Adriatic – Balkan Region*, 15-18 May 2024. (under review)
- Sinčić M, Bernat Gazibara S, Rossi M, Mihalić Arbanas S (2024b), Comparison of conditioning factors classification criteria in large scale statistically based landslide susceptibility models. *Natural Hazards and Earth System Sciences* (under review). <https://doi.org/10.5194/nhess-2024-29>

Landslide susceptibility assessment using Frequency Ratio model for the Polog region, Macedonia

Natasha Nedelkovska^{(1)*}, Milorad Jovanovski⁽²⁾, Igor Peshevski⁽²⁾, Natasha M. Andreevska⁽²⁾, Gjorgji Gjorgiev⁽²⁾

1) Geohydroconsulting Ltd., Skopje, Manapo 7, n_nedelkovska@hotmail.com

2) Ss. Cyril and Methodius University in Skopje, Faculty of civil engineering, Skopje, blvd. Partizanski odredi 24

Abstract The aim of this study is to assess the landslide susceptibility in the Polog region, which is considered as one of the most landslide prone-areas in Macedonia due to the combination of complex geological setting, an articulate morphology and specific climate conditions. Geographic Information Systems (GIS) and Frequency Ratio (FR) model were implemented in this study to assess the contribution of conditioning factors to landslides, and to produce a landslide susceptibility map of the Polog region. The landslide inventory map for the study area was prepared by applying three approaches: (1) collecting archive landslide data, (2) analysis of DInSAR (Differential Interferometric Synthetic Aperture Radar) indicated zones with registered displacements, and (3) detecting landslides by visual analysis of a digital terrain model (DTM) obtained by LiDAR (Light Detection And Ranging) terrain scanning. Twelve landslide conditioning factors were considered in the landslide susceptibility modeling, which include slope, elevation, aspect, plane curvature, profile curvature, roughness, distance to roads, lithology, distance to faults, rainfalls, distance to rivers and land use/land cover. The relationship between landslides and conditioning factors was statistically calculated with FR analysis. FR values were used to produce the Landslide Susceptibility Index (LSI), based on which the study area was divided into five zones of relative landslide susceptibility, being very low, low, medium, high and very high. The results of the analysis have been validated by estimating the relative density of landslides, that is, calculation of the so-called R-index. The statistical results show that the R-index value increases as the landslide susceptibility level increases from very low to very high, which indicates a high-quality landslide susceptibility map obtained by using the FR model. The results also showed that the FR is simple method for landslide susceptibility assessment since the input, output, and calculation process are readily understood.

Keywords landslide, susceptibility, frequency ratio (FR), inventory, validation, Geographic Information System (GIS)

Introduction

All over the world, people face the challenge of establishing a balance between the risk of natural hazards (geohazards) and the need for space urbanization. Landslides are among the most significant and widespread geohazards, causing enormous social and economic losses worldwide (Herrera et al. 2018). A recent study by Haque et al. (2016) shows that in 27 analyzed European countries, during the 20 years, from 1995 to 2014, 1370 deaths and 784 injuries were recorded within 476 landslides events. As a result of landslides, economic losses were also significant in many of the analyzed European countries.

Every year in Macedonia, various unstable phenomena in the terrain cause significant losses, measured in millions of euros, and unfortunately, a loss of human lives. The history of landslide mapping in Macedonia, is briefly presented in Peshevski et al. 2024 (in print).

Polog region is considered as one of the most landslide prone-areas in Macedonia, comprising almost 2/3 of registered landslides in the country. The first landslide susceptibility study of Polog was done by Peshevski et al. in 2015, and later by Peshevski et al. in 2019. Since landslide susceptibility can change over time due to various factors such as land use changes, climate change, or geological processes, it is important to periodically update the landslide susceptibility maps. In this study landslide susceptibility assessment in Polog region is done, implementing the Geographic Information Systems (GIS) and the Frequency Ratio (FR) model. Delimiting the potential landslide areas through susceptibility assessment, can be used by the decision makers for developing and implementing appropriate landslide mitigation strategies.

Study area

The Polog region is located in the northwestern part of Macedonia (Fig.1) and covers an area of 2416 km². The relief of the study area is complex and diverse. The region consists of the Polog Valley, the mountains of Shar Mountain, Zeden, Suva Gora, Bistra, Mavrovo Plateau, and the valley of the river Radika. In the Polog region geological formations can be found from almost all geological periods, from the Cambrian to the Quaternary

period, with different types of igneous, sedimentary and metamorphic rocks. The region belongs to seismic zones where the maximum expected seismic intensities of 7, 8 and 9 are likely (according to the MSK scale) for return periods of 100 and 500 years. It is characterized by the highest annual rainfall in the country (Ilijovski 2013), from 600 mm/year to more than 1250 mm/year.

In the Polog region, which occupies almost 10% of the territory of Macedonia, the combined presence of a complex geological setting, an articulate morphology, and particular climatic conditions contribute to it being one of the most landslide-prone regions in the country.



Figure 1 Location of Polog region (red outline).

Materials and methods

Landslide inventory

In order to predict the future potential zones for landslide occurrence, it is necessary to know the zones previously affected by landslides. The inventory map is the easiest and most direct method for mapping landslides (Guzzetti et al. 2012). The inventory map is the basis for susceptibility assessment. The landslide inventory map for the study area was prepared by applying three approaches: (1) collecting archive landslide data, (2) detecting landslides by visual analysis of a digital terrain model (DTM) obtained by LiDAR (Light Detection And Ranging) terrain scanning, and (3) analysis of DInSAR (Differential Interferometric Synthetic Aperture Radar) indicated zones with registered displacements.

The process of collecting archive landslide data consisted of several activities (Nedelkovska et al. 2020) and a landslide database of 136 occurrences was established. The number of landslides in the region was thought to be much higher, but they have not been appropriately recorded in the past. Therefore, it was proceeded with upgrading the landslide inventory by detection of landslides using another two methods that were applied for the first time in Macedonia for such purposes.

The first method was use of images acquired by satellite Synthetic Aperture Radar (SAR) sensors and processed using the Differential Interferometry (DInSAR)

technique. Details for application of this remote sensing technology over the Polog region can be found in Jovanovski et al. (2021). By this method, total of 26 already inventoried landslides were found to be moving. Additionally, 38 “hotspots” were identified where a concentration of moving coherent pixels was identified out of the mapped landslides. The indicated 38 zones, jointly with geomorphological/geological criteria and photo-interpretation were exploited to map undetected landslides. The second method was detection of landslides by visual analysis of Digital Terrain Model obtained from data from LiDAR scanning of the terrain. In this way total of 46 new landslides were identified (Nedelkovska 2023).

Landslide causative factors

Landslide susceptibility is the probability of landslide occurrence in a given area based on the terrain conditions (Brabb 1984). Accordingly, to achieve high accuracy of landslide susceptibility models, selecting the landslide causative factors is a very significant step.

The landslide causative factors for the study area are selected based on literature inspection and detailed analysis of regional field conditions. 12 factors were selected, which can be broadly categorized into four groups: topographic (slope, elevation, aspect, plane curvature, profile curvature, roughness, distance to roads), geological (lithology, distance to faults), hydrological (rainfalls, distance to rivers) and land use/cover.

The slope is considered a critical topographic factor that directly influences landslide occurrence. Generally, the slope influences the water infiltration process and stresses distribution, closely related to the slope stability. **The elevation** is a factor used in almost all landslide susceptibility assessment analyses. The elevation is controlled by various geological, geomorphological, and meteorological factors, including lithological units, weathering, wind action, and precipitations (Pourghasemi et al. 2013). **Aspect** refers to slope orientation. This factor affects the exposure to sunlight, wind, and precipitation, which indirectly affect other factors that contribute to landslide occurrence, such as soil moisture, vegetation cover, and soil thickness (Clerici et al. 2006). **Plane curvature** and **profile curvature** are topographic factors that reflect the geometrical characteristics of the slopes (Ohlamacher 2007). Profile curvature affects the driving and resisting stresses within a landslide in the direction of motion. Plane curvature controls the convergence or divergence of landslide material and water in the direction of landslide motion. **Terrain roughness** expressed through a roughness index is an indicator of terrain topography. It refers to the flatness or undulation of the terrain, that is, the variability of the topographic surface of the terrain. **Distance to roads** can be a potential indicator of landslide occurrence. The construction of roads in mountainous areas requires engineering activities such as cutting and excavation. This leads to a change in the initial geological conditions of the terrain, that is, the equilibrium slope state is disturbed, and conditions for

slope instabilities are being created. **Lithology** plays a vital role in landslide occurrence and is a significant internal controlling factor used in all landslide susceptibility analyses performed. Lithological units vary in physical and mechanical characteristics, including type, strength, degree of weathering, fracturing, permeability, etc. **Distance to faults** is an important predisposing factor for landslide susceptibility assessment. Structural discontinuities such as faults lead to joints and fissures in the surrounding rock mass (decreasing the rock strength) and causing instability. **Rainfall** affecting the groundwater level is one of the main landslide-triggering factors. When rainfall exceeds the infiltration capacity of the ground, it becomes saturated, which reduces its strength and makes it susceptible to sliding. Rainfall also affects the erosion process, leading to the slopes' destabilization. **Distance to a river** affects in the way the water erodes and saturates the slope toe and thus adversely affects stability. Therefore this factor is often included in the landslide susceptibility assessment. **Land use/cover** is another of several factors used in almost all landslide susceptibility assessment analyses. This factor is considered dynamic and associated with human activities (Rabby et al. 2022).

These 12 landslide causative factors were generated using Geographical Information System (GIS), so 12 thematic layers (maps) with a 1 m × 1 m spatial resolution pixel size were prepared. Table 1 provides a summary of the factors, the source from which the adopted factors were derived/calculated, the defined classes, and the method according to which the classes were defined.

Landslide susceptibility mapping

Landslide susceptibility (LS) is the measure of how prone an area is to landsliding. It measures the degree to which the terrain may be affected by future instabilities, or in other words, it predicts "where" landslides are likely to occur (Guzzetti 2006). The methods used for LS

assessment have evolved over the years, and can be grouped into two general groups: qualitative and quantitative. More about the LS assessment methods can be found in Reichenbach et al. 2018. Quantitative methods are based on establishing a function between the conditioning factors and the distribution of past landslides. The way the classifier explicitly works is to measure each conditioning factor's contribution to landslides' occurrence based on the spatial correlation between the landslide occurrences and the factors. Past landslides represent dependent variables in these models, while conditioning factors are explanatory/independent variables.

The "Frequency Ratio" method which was proposed by Lee and Talib (2005) is a quantitative method that is used for statistical analysis of landslides. This method is based on the relationship between the distribution of landslides and each predisposing factor (Eq. 1):

$$FR_{ij} = \frac{N_{ij}/N_{total}}{A_{ij}/A_{total}} \quad [1]$$

where: N_{ij} is the number of landslides in the j th class of factor i , N_{total} is the total number of landslides in the study area, A_{ij} is the area of the j th class of factor i , and A_{total} is the total area of the study area. Table 1 shows the results obtained from the analysis.

The "Frequency Ratio" method obeys the principle of conditional probability where the greater the ratio is, the stronger the relationship between landslides and predisposing factor classes, and vice versa. Actually, FR value greater than 1 indicates a strong relationship between landslide occurrence and the factor class, a value less than 1 indicates a weak relationship. The correlation is average if the frequency ratio is 1 (Lee and Sambath 2006).

Table 1 Analysis of the relationship between selected predisposing factors and past landslides using the "frequency ratio" method.

Factor	Class j	Landslides [%]	Class area [%]	FR _{ij}
Slope [°] Source: DTM Class. method: Custom interval	1. < 5	3.31	4.15	0.797
	2. 5 - 10	4.96	8.30	0.597
	3. 10 - 15	9.09	11.96	0.760
	4. 15 - 20	5.79	14.25	0.406
	5. 20 - 25	9.92	15.05	0.659
	6. 25 - 30	15.70	14.68	1.069
	7. 30 - 35	12.40	13.24	0.937
	8. 35 - 40	16.53	9.84	1.680
	9. > 40	22.31	8.54	2.614
Elevation [m] Source: DTM Class. method: Custom interval Natural breaks	1. 447 - 744	20.66	9.45	2.187
	2. 744 - 1031	15.70	11.54	1.361
	3. 1031 - 1292	18.18	13.77	1.320
	4. 1292 - 1544	26.45	15.23	1.736
	5. 1544 - 1786	6.61	15.78	0.419
	6. 1786 - 2029	4.96	12.96	0.383
	7. 2029 - 2272	6.61	12.48	0.530
	8. 2272 - 2749	0.83	8.80	0.094
Aspect	1. Flat (-1)	0.00	0.03	0.000

Factor	Class <i>j</i>	Landslides [%]	Class area [%]	FR _{ji}
Source: DTM Class. method: /	2. North (0 - 22.5; 337.5 - 360)	4.13	9.13	0.453
	3. Northeast (22.5 - 67.5)	9.92	14.44	0.687
	4. East (67.5 - 112.5)	18.18	19.35	0.940
	5. Southeast (112.5 - 157.5)	19.01	21.00	0.905
	6. South (157.5 - 202.5)	34.71	15.85	2.189
	7. Southwest (202.5 - 247.5)	11.57	8.68	1.333
	8. West (247.5 - 292.5)	0.00	5.26	0.000
Plane curvature Source: DTM Class. method: /	9. Northwest (292.5 – 337.5)	2.48	6.27	0.395
	1. Concave	6.61	3.37	1.964
Profile curvature Source: DTM Class. method: /	2. Linear	85.12	93.57	0.910
	3. Convex	8.26	3.06	2.701
Terrain roughness Source: DTM Class. method: Natural breaks	1. Convex	13.22	3.89	3.399
	2. Linear	78.51	92.36	0.850
	3. Concave	8.26	3.75	2.205
	1. 0.1 - 0.389	2.48	2.58	0.962
	2. 0.389 - 0.458	10.74	12.29	0.874
	3. 0.458 - 0.498	38.02	32.75	1.161
Distance to roads [m] Source: DTM Class. method: Natural breaks	4. 0.498 - 0.539	28.10	36.35	0.773
	5. 0.539 - 0.605	18.18	13.25	1.373
	6. 0.605 – 0.9	2.48	2.79	0.889
	1.< 407	83.47	55.81	1.496
	2. 407 - 1118	12.40	19.46	0.637
	3. 1118 - 2058	3.31	10.19	0.325
Lithology Source: Basic geological map 1:100000 Class. method: /	4. 2058 - 3151	0.83	6.72	0.123
	5. 3151 - 4221	0.00	4.69	0.000
	6. 4221 - 6479	0.00	3.14	0.000
	1. Quaternary deposits	9.09	11.83	0.769
	2. Albite chlorite sericite schists	4.13	6.38	0.647
	3. Albite chlorite epidote sericite schists	3.31	3.20	1.033
	4. Gabbro	0.00	0.03	0.000
	5. Granitoid rock masses	16.53	8.89	1.860
	6. Diabases and spilites	0.00	0.39	0.000
	7. Epidote actinolite schists	37.19	35.26	1.055
	8. Carbonate schists	0.00	0.04	0.000
	9. Quartz carbonate sericite schists and phyllites	7.44	9.15	0.813
	10. Quartz-porphry	0.00	0.21	0.000
	11. Quartzite and quartz sandstones	2.48	1.77	1.403
	12. Crystalline limestones with cherts	4.96	8.26	0.600
	13. Marbles and marble limestones	6.61	8.83	0.749
	14. Metasandstones	0.00	0.19	0.000
	15. Serpentinite	0.00	0.10	0.000
	16. Phyllite metamorphosed sandstones & schists	0.00	0.63	0.000
17. Phyllitoid	7.44	4.32	1.722	
18. Harzburgite	0.00	0.01	0.000	
19. Chlorite sericite schists	0.83	0.52	1.600	
Distance to faults [m] Source: Basic geological map 1:100000 Class. method: Natural breaks	1.< 134	42.98	34.23	1.256
	2. 134 - 308	26.45	28.45	0.930
	3. 308 - 513	19.01	18.05	1.053
	4. 513 - 765	5.79	10.58	0.547
	5. 765 - 1097	4.13	5.95	0.694
	6. 1097 - 2012	1.65	2.75	0.600
Rainfalls [mm/year] Source: Rainfalls map 1:100000 Class. method: /	1. 600 – 700	0.00	1.53	0.000
	2. 700 – 800	20.66	19.26	1.073
	3. 800 – 900	20.66	32.14	0.643
	4. 900 – 1050	58.68	47.07	1.247
Distance to rivers [m] Source: DTM Class. method: Natural breaks	1.< 291	31.40	27.91	1.125
	2. 291 - 617	29.75	26.14	1.138
	3. 617 - 964	21.49	20.62	1.042
	4. 964 - 1368	14.88	13.68	1.088

Factor	Class <i>j</i>	Landslides [%]	Class area [%]	FR _{ji}
	5. 1368 - 1906	1.65	8.06	0.205
	6. 1906 - 2859	0.83	3.59	0.230
Land use / land cover Source: CLC2018 Class. method: /	1. Broad-leaved forest	38.84	27.63	1.406
	2. Complex cultivation patterns	4.13	2.60	1.592
	3. Coniferous forest	0.00	1.15	0.000
	4. Discontinuous urban fabric	2.48	2.04	1.214
	5. Land principally occupied by agriculture, with significant areas of natural vegetation	19.83	11.84	1.675
	6. Mixed forest	1.65	4.02	0.411
	7. Moors and heathland	0.83	4.94	0.167
	8. Natural grasslands	15.70	33.35	0.471
	9. Non-irrigated arable land	0.00	0.05	0.000
	10. Pastures	1.65	1.38	1.195
	11. Sparsely vegetated areas	0.00	1.89	0.000
12. Transitional woodland-shrub	14.88	9.11	1.633	

Results and discussion

Once the “frequency ratio” value of each landslide factor's class was found, which represents a weighting coefficient that quantitatively measures the contribution of each value of the factor to the occurrence of landslides, an overlaying of the thematic weight maps is performed in ArcGIS. Summation of each factor’s frequency ratio value in each pixel is done in order to obtain the landslide susceptibility index (LSI). A higher LSI means a higher susceptibility to landsliding. The prepared landslide susceptibility map for the Polog region is presented in Fig. 2. The Natural Breaks (Jenks) classification method was used to classify the landslide susceptibility of the study area into five categories (very low, low, moderate, high, and very high). This method is considered the most appropriate one, because the different classes are generated based on the inherent characteristics of the dataset without any subjective consideration.

The percentage of landslides in each susceptibility class was calculated to check the validity of the final susceptibility map. For this, all the landslides have been overlaid over the landslide susceptibility map. Table 2 presents the obtained results. Namely, the low and very low landslide susceptibility classes occupy 43% of the study area with only 9% of the landslides in these zones. Conversely, the high and very high susceptibility classes occupy 26% of the study area, but all have 52% of the landslides.

Table 2 Results obtained from the landslide susceptibility map.

Landslide susceptibility class	Area [%]	Landslides [%]
Very low	19.0	2.2
Low	23.8	6.5
Medium	31.0	39.1
High	21.1	32.6
Very high	5.1	19.6

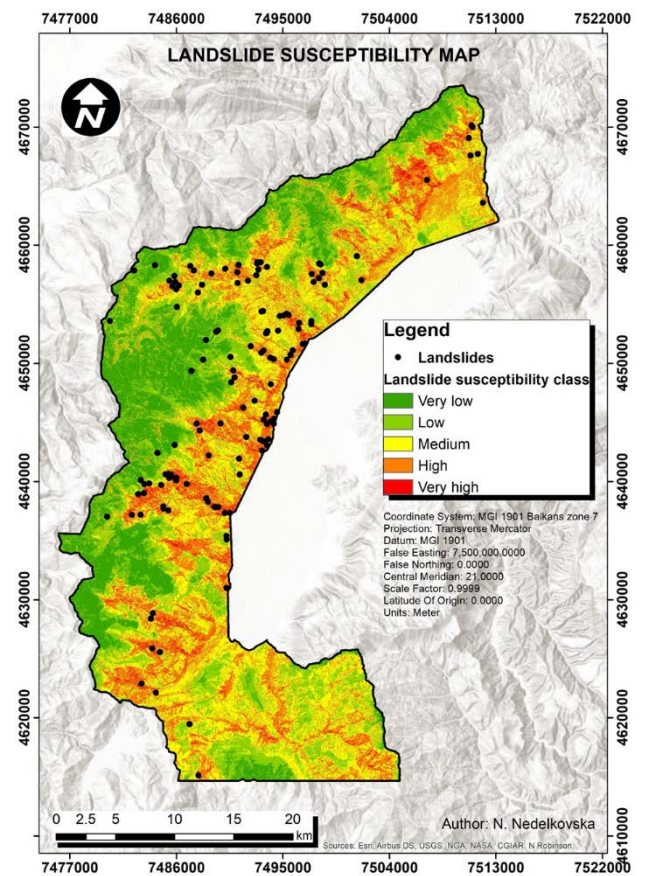


Figure 2 Landslide susceptibility map for the Polog region.

Validation of the landslide susceptibility model is also done by estimating the relative density of landslides by calculation the R-index, using the following equation:

$$R = (n_i/N_i) / \sum(n_i/N_i) \quad [2]$$

where n_i is the number of landslides in each landslide susceptibility class, and N_i is the area of the susceptibility classes. The statistical results show that the R-index value gradually increases as the landslide susceptibility level increases from very low to very high (Tab. 3). Considering this, it can be concluded that the landslide susceptibility map is reasonable and reliable.

Table 3 R-index value per landslide susceptibility class.

Landslide susceptibility class	R-index
Very low	0.114
Low	0.274
Medium	1.260
High	1.547
Very high	3.870

Conclusions

In this study “Frequency ratio” model was used to identify the landslides susceptible areas in the Polog region, Macedonia. Twelve landslide conditioning factors and the landslide inventory map for the study area were used to calculate FR values. Furthermore, the Landslide Susceptibility Index (LSI) was obtained based on which the study area was divided into five zones of relative landslide susceptibility. Validation of the landslide susceptibility map was done by estimating the relative density of landslides through calculation of the statistical R-index value, which gradually increases as the landslide susceptibility level increases from very low to very high.

This case study confirmed that the FR model was found to be simple and effective model for landslide susceptibility assessment of the study area. Its main advantage is the simplicity, i.e. inputs, output, and calculation process are readily understood, and even a large amount of data can be processed quickly, easily and efficiently in GIS environment.

Systematic data collection is crucial in order to make more detailed analyzes related to this topic. This can be achieved by continuous and timely updating of the inventory with new landslides. In such way also a “retrospective validation” of the susceptibility models would be feasible, which implies overlapping the newly inventoried landslides with the susceptibility map, so it can be concluded whether the zones where the new landslides occurred are really zoned as susceptible to landslides.

The final output of landslide susceptibility map can help the decision makers as basic information for district and zonal level of land use planning to formulate and implement proper actions in order to prevent and mitigate the existing landslides occurrence and future once.

References

- Brabb EE, (1984) Innovative approaches to landslide hazard mapping. In: Proc. 4th Int.Symp. Landslides, Toronto: 307–324.
- Clerici A, Perego S, Tellini C, Vescovi P, (2006) A GIS-based automated procedure for landslide susceptibility mapping by the Conditional Analysis method: the Baganza valley case study (Italian Northern Apennines). *Environ Geol* 50:941–961,
- Guzzetti F, Mondini CA, Cardinali M, Fiorucci F, Santangelo M, Chang KT, (2012) Landslide inventory maps: New tools for an old problem. *Earth-Science Reviews* 112: 42-66.
- Haque U, Blum P, Da Silva PF, Andersen P, Pilz J, Chalov RS, Malet JP, Jemec AM, Andres N, Poyiadji E, Lamas CP, Zhang W, Peshevski I, Pétursson GH, Kurt T, Dobrev N, García-Davalillo JC, Halkia M, Ferri S, Gaprindashvili G, Engström J, Keellings D, (2016) Fatal landslides in Europe. *Landslides*: 1–10.
- Herrera G, Mateos RM, García-Davalillo JC, Grandjean G, Poyiadji E, Maftai R, Filipciuc TC, Auflic MJ, Jež J, Podolszki L. (2018) Landslide databases in the Geological Surveys of Europe. *Landslides* 15: 359–379.
- Ilijovski Z, (2013) Methodology for preparation of groundwater vulnerability maps, Doctoral dissertation, Faculty of civil engineering – Skopje.
- Jovanovski M, Peshevski I, Gjorgiev G, Nedelkovska N, Nicodemo G, Reale D, Fornaro G, Peduto D (2021) Landslide characterization in the Polog Region (R.N. Macedonia) by innovative and conventional methods. *Rivista Italiana di Geotecnica*. 4: 7-31.
- Lee S, Talib JA, (2005) Probabilistic landslide susceptibility and factor effect analysis. *Environmental Geology* 47(7), 982-990.
- Lee S, Sambath T, (2006) Landslide susceptibility mapping in the Damrei Romelarea, Cambodia using frequency ratio and logistic regression models. *Environ Geol* 50:847–855.
- Nedelkovska N, (2023) Contemporary methods for detection and characterization of terrain unstable phenomena. Doctoral thesis, University Ss. Cyril and Methodius, Faculty of civil engineering, Skopje.
- Ohlamacher GC, (2007) Plan curvature and landslide probability in regions dominated by earth flows and earth slides. *Eng. Geol.* 91:117–134.
- Peshevski I, (2015) Landslide susceptibility modeling using GIS technology. Doctoral thesis, University Ss. Cyril and Methodius, Faculty of civil engineering, Skopje.
- Peshevski I, Jovanovski M, Abolmasov B, Papić J, Marjanović M, Đurić U, Haque U, Nedelkovska N, (2019) Preliminary regional landslide susceptibility assessment using limited data. *Geologica Croatica* 72(1): 81-92.
- Peshevski I, Jovanovski M, Peduto D, Nedelkovska N, Gjorgiev G, (2024) Landslide mapping and zonation at national, regional and local scale - Recent experiences from Republic of Macedonia. (in print).
- Pourghasemi HR, Moradi HR, Fatemi Aghda SM, (2013) Landslide susceptibility mapping by binary logistic regression, analytical hierarchy process, and statistical index models and assessment of their performances, *Nat. Hazards* 69: 749-779.
- Rabby YW, Li Y, Abedin J, Sabrina S, (2022) Impact of Land Use/Land Cover Change on Landslide Susceptibility in Rangamati Municipality of Rangamati District, Bangladesh. *ISPRS Int. J. Geo-Inf.* 11: 89.
- Reichenbach P, Rossi M, Malamud BD, Mihir M, Guzzetti F, (2018) A review of statistically-based landslide susceptibility models. *EarthSci Rev* 180:60–91.

Žirovac landslide: a case study of the local scale landslide investigation for engineering purposes with its assessment on a regional scale

Davor Marušić

University of Rijeka, Faculty of Civil Engineering, Hydrotechnical and Geotechnical Department, Radmile Matejčić 3, Rijeka, Croatia, e-mail: davor.marusic@uniri.hr

Abstract A detailed analysis of the “Žirovac” landslide on Croatia’s state road section in the village of Žirovac is given in this case study. The landslide was triggered by the Petrinja earthquake in December 2020 and was subject to fast-paced processes of investigation and mitigation. The engineering geological and geotechnical survey including boreholes and geophysical investigations were performed on a large local scale.

The earthquake-induced rotational landslide was observed on the road embankment section, which was reported to be an old landslide, continuously covered by new layers of gravel material. Despite the localized, earthquake-induced landslide, the wider slope area showed significant signs of terrain sliding and/or creeping which could be observed on the existing damaged buildings and shallow constructions.

Performed investigation results indicated the presence of two landsliding mechanisms: (1) The local, rotational landslide of the road embankment induced by the Petrinja earthquake combined with the unfavorable load of the continuously added embankment layers and the underlying material degradation due to groundwater flow; (2) The global, translational creeping landslide of the wider slope area caused by occasional but significant groundwater flow and consequential degradation of the deeper-seated bedrock. The local landslide, as a primary subject of the investigation works performed, was limited to the road embankment section and embankment material. Although 225 m wide, the length of the local landslide was only 20 m, with a sliding surface depth of 2.5 m. The global landslide was reported as an old creeping landslide, causing occasional but continuous damage to the surrounding buildings and infrastructure. According to the investigation works performed, the global landslide was defined as a translational landslide, approximately 300 m wide and 300 m long with its sliding surface formed at a depth of 5-8 m, just above the underlying impermeable cretaceous clays.

Although the investigated local landslide was induced by the Petrinja earthquake, the effect of the global landslide on the local sliding was taken into consideration in the engineering geological report for landslide mitigation purposes. The continuously reported local landslides, before the Petrinja earthquake, were probably induced by the continuous creep of the global landslide.

This case study also observes the imperfections of the fast-paced, local-scale investigations for quick mitigation

purposes regarding the landslide characteristics determination on a regional scale.

Keywords: landslide, earthquake, local scale, engineering

Introduction

The event of the “Petrinja earthquake” occurred on December 29th, 2020, in Sisak-Moslavina County in Croatia (Tomac 2021; Miranda et al. 2021). A 6.4 magnitude earthquake was felt throughout Croatia and large parts of neighboring countries, reportedly affecting and damaging areas within an approximately 50 km radius.

The researched “Žirovac landslide” is situated over 20 km south of the reported earthquake epicenter and was one of the many road section instabilities triggered by the Petrinja earthquake. Although the Petrinja earthquake reportedly triggered the road section landslide, no slope movement around the road embankment followed the event. Regardless, the surrounding slope area showed significant signs of sliding and/or creeping.

Location

The observed instability on a Croatian state road section (state road: DC6, section 004), is situated in the village of Žirovac in the southern part of Sisačko-Moslavačka County. This part of the road section generally extends in the direction west-east and perpendicularly crosses the natural slope, inclined 10-25° towards the south. Within the observed area, the road gradually rises from 330-338 masl. towards the east.

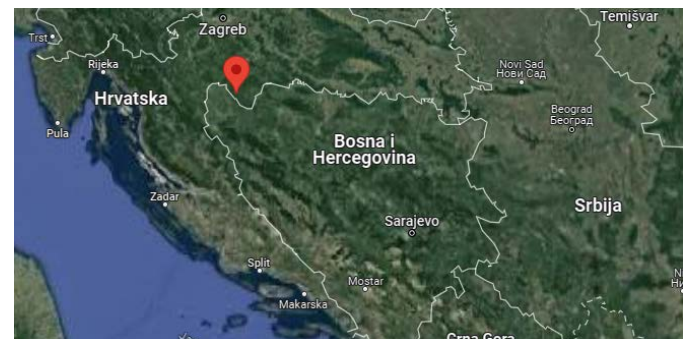


Figure 1. Location of the “Žirovac” landslide on the satellite map; satellite map source (Google)

The left (south) side of the researched road section is made on an embankment, up to 2.5m in height. A relatively shallow embankment is also present in the central part of the right side of the road section. Existing

embankments and shallow cuts had no protection in terms of supporting constructions or other instability mitigation measures as well as no organized drainage system.

Landslide event

The earthquake-induced landslide event encompassed the body of the road in its full width along with the 2.5 m high road embankment. Shortly after the landslide event, to ensure traffic functionality, the unstable part of the landslide was covered with gravel material, forming a relatively denivelated but flat surface road. Such actions consequently covered most of the landslide body and part of the scarp and slip surface, limiting the ability to properly assess the landslide in terms of size.

Disregarding several potholes formed due to the embankment material's internal erosion, the newly formed gravel road section showed no signs of sliding in terms of tension cracks or other significant signs of landsliding. The landslide was evident on a general denivelation of the gravel road section, as well as on the partly covered main scarp which extended along part of the right (north) edge of the road as a shallow, 0.5-1.0 m cut under the natural slope.

According to the local information, the researched road section represents an occasional but persistent landslide, continuously covered with new layers of gravel material.



Figure 2. View towards the west on the unstable road section with the partly covered slide scarp along the northern edge of the road.

Although no instabilities were reported in the nearby vicinity of the earthquake-induced landslide, the surrounding slope area showed significant signs of sliding and/or creeping. Regardless of the absence of newly formed tension cracks or scarps, many irregular forms such as elongated depressions, bulges, and traces of smaller, overgrown secondary scarps perpendicular to the slope decline, characterized the surrounding slope area indicating a continuous sliding/creeping of the wider area.

Most of the abandoned structures and present family houses on the wider slope area showed clear signs of differential subsidence, with many wide diagonal cracks on masonry walls, while almost every shallow construction on the slope (garden fences, paved infrastructure, wooden sheds, etc.) was partially dislocated or leaned.

According to the local information, the wider slope area represents a continuous, slow-moving/creeping landslide with high levels of groundwater during and shortly after the rainy periods.

The global sliding of the wider slope area wasn't initially defined within the scope of the planned research, but it was accounted for in the engineering-geological report to properly assess the engineering-geological characteristics of the unstable slope area and the geotechnical mitigation works needed.



Figure 3. Abandoned and highly damaged masonry building above the unstable road section.



Figure 4. A damaged and leaned wooden shed below the unstable road embankment and an undamaged residential building with completely removed infrastructure.

Methodology

Research works

To better approach and elaborate the given problem, engineering-geological and geotechnical research works (Terraforming Ltd. 2021) performed on the location consisted of:

- Engineering-geological mapping of the area
- Exploratory drilling
- Geophysical Research (seismic refraction)
- Laboratory tests

A more detailed review of the geotechnical research works performed on the location is given in "Tab. 1", while their position concerning the researched landslide is shown in "Fig. 5".

Table 1. Review of geotechnical research works performed on the landslide location.

Geotechnical research works		Qty / Amt (m)
Exploratory drilling (research boreholes)		11 / 79
Standard penetration test (SPT)		35 / 11.7
Geophysical Research (seismic refraction)		1 / 200
Laboratory tests	Atterberg limits	15 / NA
	Particle size distribution	3 / NA
	Unconfined compressive strength of soil	3 / NA
	Shear strength of soil	3 / NA
	Uniaxial compressive strength of rock	1 / NA

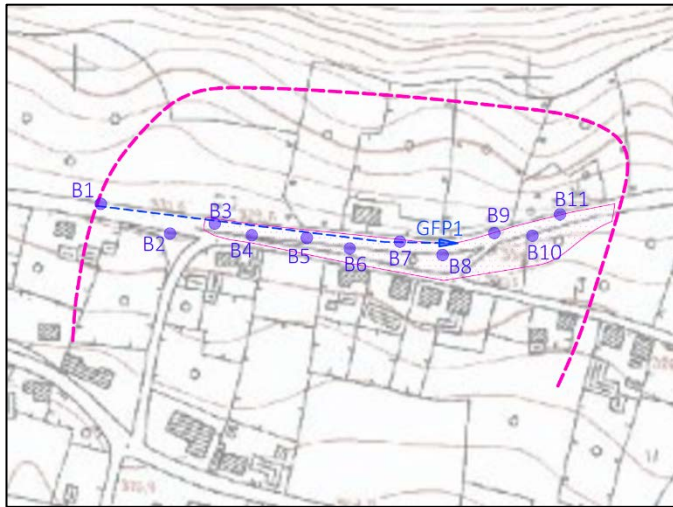


Figure 5. Review of the geotechnical research works performed on the location. Boreholes (purple dots) and geophysics (blue dashed line) within the researched landslides (magenta dashed line); topographic map source (DGU)

Engineering-geological mapping also encompassed the detection and measurement of the evident damages along the researched road section and the wider slope area, the determination of the landslide(s) type and size and the determination of the present instability causes with possible future development and consequences. Within engineering-geological research, the borehole logs determination and correlation with the laboratory test results and the geophysical research were performed. In addition, all the data obtained was cross-referenced with the existing research data of the location and the representative geological profile.

For the geotechnical interpretation of the geological profile, the determined cover and bedrock units were classified according to the governing standards ISO 14688 (EN ISO 14688-1:2002; EN ISO 14688-2:2004) and EN ISO 14689 (EN ISO 14689-1:2003) respectively.

Geological and geotechnical characteristics

Basic structural and geomorphological setting

Based on the existing data, the wider area tectonically represents the broken frontal thrust “Žirovac - D. Stupnica” of the “Inner Dinarides ophiolitic belt” on the “Sana-Una belt” (Šikić 2014; Šikić and Šimunić 2014).

Structurally, it encompasses the frontal thrust of the “Ophiolitic complex of Banija” (K_1 , $\beta\beta$, $J_{2,3}$) within the “Inner Dinarides ophiolitic belt” on the structural unit of “Radašnica” ($T_3^{2,3}$) within the “Sana-Una belt” as shown in “Fig. 6”.

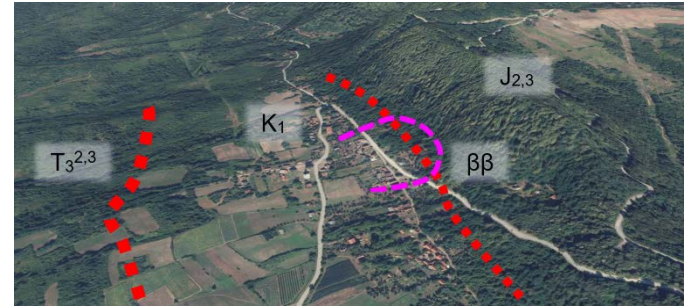


Figure 6. View on the geomorphological characteristics of the wider area with marked location of the global landslide (magenta dashed line) and frontal and secondary thrust (thick and thin red dashed line respectively); satellite map source (Google)

Considering the structural setting of the wider area, the main thrust area is characterized by a very small difference in slope inclination between the neighboring structural units represented with Cretaceous marls and limestones (K_1) and Triassic dolomites ($T_3^{2,3}$), where the dolomites governed area indicate a slight increase in slope steepness towards the south. The significant morphological difference is visible within the structural unit “Ophiolitic complex of Banija”, at the secondary thrust of the metamorphic and Jurassic formations ($\beta\beta$, $J_{2,3}$) on the Cretaceous sedimentary rocks (K_1) where the more resistant, metamorphous, and sedimentary rocks form the hill “Vratnik”, while the weathered marls with limestones form the relatively slightly inclined area of the “Žirovac” village.

Engineering-geological characteristics

Based on the data obtained by geotechnical research works and engineering-geological mapping, the geological and geotechnical characteristics of the governing instabilities were determined.

The determined bedrock is represented by weathered marls with the occurrence of limestones in the central part of the landslide. This geological sequence corresponds well with the existing data which states that the wider area is built on lower-cretaceous marls interbedded with limestone layers (Šikić 2014). Limestones and marls represent the transgressional carbonates of terrestrial origin.

Bedrock layers are continuously covered by the deluvial/eluvial clay (younger) and clayey gravel (older), and the road embankment fill material. The thickness of the cover locally varies from 2.5-6.0 m in the central and eastern parts, with an increase to 7.0-9.5 m in the western part of the road section. This sequence can be observed on borehole cores in “Fig. 7”.

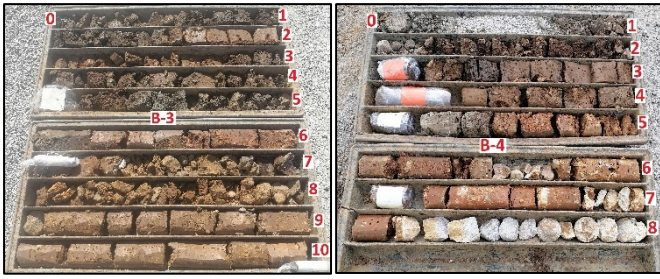


Figure 7. View of the relatively adjacent borehole cores with the cover material overlaying weathered marls at 8.0 m depth (borehole B-3) and limestones at 7.0 m depth (borehole B-4).

A detailed review of the representative engineering-geological units and their characteristics are given in “Tab. 2” through “Tab. 4”.

Table 2. Review of the representative engineering-geological units on the landslide location.

Engineering-geological units		Geotechnical classification	Unit
Cover (Quaternary)	Antropogenic (embankment) fill	clGr, GrP	C1
	Deluvium / eluvium	grsiCIL, grsiCIM	C2
		clGr, Co, Bo	C3
Bedrock (Lower Cretaceous)	Marl	siCIL, siCIM, siCIH	BR1
	Limestone	Limestone	BR2

Table 3. Determined soil units' engineering-geological characteristics.

Unit	Plasticity ¹ /grading ²	Consistency ¹ /density ²	Thickness (m)
C1	poorly ²	loose ²	<2.5
C2	low – medium ¹	stiff – very stiff ¹	1.10 - 6.20
C3	undetermined	medium ²	1.70 – 4.00
BR1	low – high ¹	hard ¹	undetermined
Plasticity/grading (EN ISO 14688-1:2002; EN ISO 14688-2:2004) Consistency/density determined by SPT values (Look 2007)			

Table 4. Determined bedrock (limestone) unit engineering-geological characteristics.

Unit	UCS (Mpa)	RQD (%)	GSI
BR2	123	0-25 (80)	25-30
UCS – Uniaxial Compressive Strength RQD – Rock Quality Designation (Hoek 2007) GSI – Geological Strength Index (Hoek 2007)			

Hydrogeological conditions

Hydrologically, the wider area belongs to the Sava River basin while hydrogeologically, it belongs to the northern part of the so-called “Inner area” with possible local aquifers of intergranular or secondary porosity (Ivković et al. 1983). Surface and groundwater flow is oriented in the direction of the slope decline (south), from the “Vratnik” hill toward the existing creek of “Žirovac”.

In general, the Jurassic, and metamorphic complex of the upslope “Vratnik” hill represents the permeable media

of secondary porosity with dominant groundwater flow. The Cretaceous sedimentary rocks within the researched landslide represent the media of generally low permeability and dominating intergranular porosity, with the possibility of forming local and irregular groundwater paths within the broken limestone layers. Consequently, in the close vicinity of the secondary thrust or at the contact of the metamorphic and Jurassic complex with the Cretaceous layers, temporary springs, and surface drainage paths are registered. Triassic dolomites further to the south also represent the media of low permeability and secondary porosity, maintaining the surface flow of the water (“Žirovac” creek).

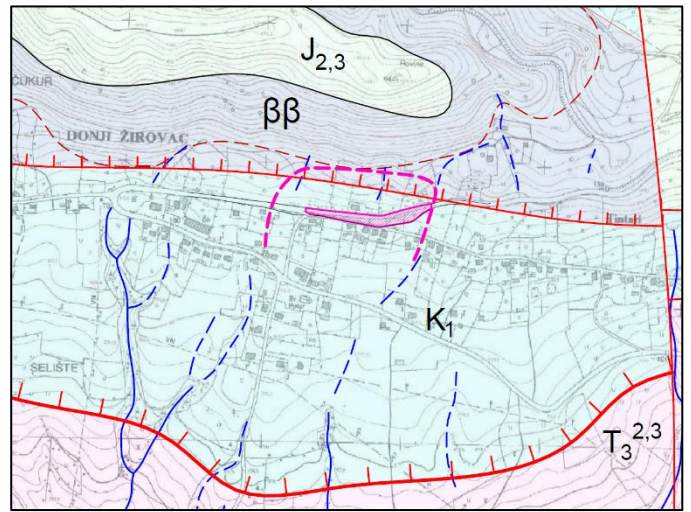


Figure 8. A review of the wider area’s structural setting and representative stratigraphical units with specific hydrogeological characteristics; topographic map source (DGU)

Representative bedrock and cover on the landslide location are characterized by a high variety in permeability, where the gravel-dominated cover and limestone bedrock represent the permeable media, while the clay-based cover and bedrock represent the impermeable media as shown in “Tab. 5”.

Table 5. Porosity and permeability of the representative engineering-geological units on the landslide location.

Unit	Porosity type	Permeability coefficient k (m/s) (Look 2007)
C1	Primary	>10 ⁻⁴
C2		10 ⁻⁵ – 10 ⁻⁷
C3		10 ⁻³ – 10 ⁻⁵
BR1	Secondary	<10 ⁻⁷
BR2		>10 ⁻⁴

Locally, precipitated water is slowly infiltrated in the relatively impermeable natural cover (deluvial-eluvial clay) and tends to accumulate and flow through the permeable embankment material, consequently weakening and eroding the underlying clay material. Groundwater tends to flow through the more permeable layers of cover and bedrock in the direction of the slope decline, also consequently weakening and eroding the bordering clay material.

Groundwater level below the road was determined on the landslide edges at the depths of 3.0-6.5 m with a slight decline towards the west, while at the central part, the groundwater level wasn't reached due to the inadequate boreholes' depth.

Landslide characteristics

The performed engineering-geological and geotechnical research works indicated the presence of two instability mechanisms practically denoted as the local landslide and the global landslide.

Local landslide

The local landslide represents the earthquake-induced landslide of the road embankment in its full width. The road embankment consists of up to 2.5 m thick clayey gravel filling material, overlaying the deluvial-eluvial clay and gravel cover and the deeper bedrock of weathered marls interbedded with limestone layers, situated approximately 2.5-7.0 m below the surface level.

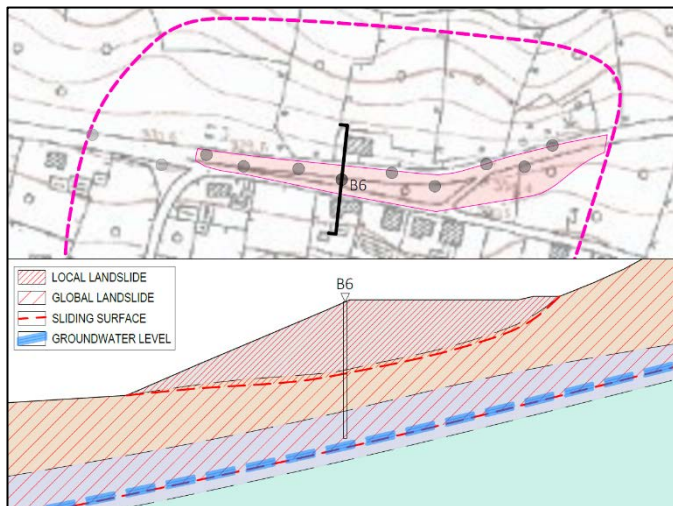


Figure 9. Cross-section of the central part of the “Žirovac landslide” area with the road embankment overlaying the deluvial-eluvial cover (brown), and bedrock of limestones (purple) interbedded within marls (green); topographic map source (DGU)

The earthquake-induced sliding represents the embankment material rotational sliding along the upper cover – deluvial-eluvial clays. Although the sliding material mostly consists of gravel and boulders, the local landslide can be defined as a clay/silt rotational slide, due to the probable failure in the clay cover.

Regardless of the earthquake event, the sliding was also potentiated by the embankment material weight and the sliding surface geotechnical characteristics degradation from groundwater flow. According to the local information, local landslide represents an occasional but persistent landslide, continuously covered with new layers of gravel material.

The Local landslide characteristics are presented in “Tab. 6”.

Table 6. Review of the Local landslide characteristics

Landslide characteristics – Local landslide		
Classification (Hungur et al. 2014)	Clay/silt rotational slide	
Dimensions	Width ≈ 225,0 m Length ≈ 20,0 m Sliding surface depth / Sliding material thickness = 2,5 m	
Activity (Cruden and Varnes 1996)	State	Active
	Distribution	Undetermined
	Style	Complex
Material (Hungur et al. 2014)	C1 – dry gravel C2 – stiff clay	

Global landslide

According to the research data, the global landslide is evaluated as the translational movement of the wider slope area with a sliding depth of 5.0-8.0 m below the road section.

Sliding material consists of both embankment material, and deluvial-eluvial cover, including the permeable limestone layer as an upper bedrock layer. This way the sliding surface of the limestone layer and the overlaying cover material is formed on a contact with weathered impermeable marls.

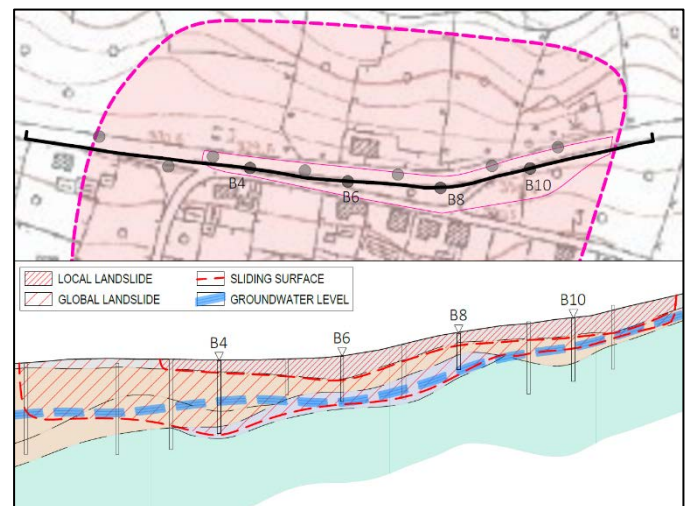


Figure 10. Frontal view of the “Žirovac landslide” along the embankment's southern edge with the surficial road embankment overlaying the deluvial-eluvial cover (brown), and bedrock of limestones (purple) interbedded within marls (green); topographic map source (DGU)

Although such a sliding mechanism could not be confirmed with the limited data acquired for the local landslide mitigation purposes, indications for the global landslide were significant, like the presence of the elongated depressions, bulges, and traces of smaller, overgrown secondary scarps perpendicular to the slope decline as well as the characteristic damages on the present constructions as shown in “Fig. 2” through “Fig. 4”. This was also confirmed by the local information, according to which the wider slope area represents a continuous, slow-moving landslide with high levels of groundwater during and shortly after the rainy periods.

The Global landslide characteristics are presented in “Tab. 7”.

Table 7. Review of the Global landslide characteristics

Landslide characteristics – Global landslide		
Classification (Hungr et al. 2014)		Rock and/or Clay/silt translational slide
Dimensions		Width ≈ 300,0 m Length = ND Sliding surface depth / Sliding material thickness >5 m
Activity (Cruden and Varnes 1996)	State	Active
	Distribution	Undetermined
	Style	Complex
Material (Hungr et al. 2014)		C1 – dry gravel C2 – stiff clay C3 – clayey gravel BR2 – strong rock (limestone)

Concluding remarks

The case study presented here observes the landslide event research for mitigation purposes. Due to the need for immediate mitigation of a state road section, relatively fast-paced geotechnical research works were planned and conducted. Such an approach neglected many of the initial geological aspects of the landslide which could be assessed by detailed analysis of the existing geological data of the wider area and existing topographic data of the area. By conducting previous analysis, geotechnical research works could be performed with a better understanding and focus on the existing problem.

Regarding the presented case study, engineering-geological research was done apart from the geotechnical research works and some of the problems that occurred within the research process are listed below:

- Performed boreholes in the central part of the unstable road section ended in the limestone layer. This is common in practice since the hard bedrock often indicates its continuous occurrence with increasing depth and considering the contracted limitation in total borehole depths, the drilling usually stops within 1 m. However, by assessing the existing geological data of the wider area, it was found that the limestone layers are interbedded within dominant marls, and the boreholes should be performed in a way to validate this since it represents an important factor for the global landslide.
- The researched instability was initially approached and contracted as a local, road section landslide, disregarding the evidence of the global landslide of the wider slope area. This also meant that the geotechnical research works were limited to the local landslide area so that the global landslide characteristics could be evaluated only by a superficial analysis of the existing geological and topographical data.

- The proper research of the global landslide would require additional time and resources that were not covered within the contract scope. Additionally, to prepare all the necessary documentation for the global landslide research, all owners of the affected parcels, including different local and/or state Administrations need to be involved. This often proves to be a long and problematic process, especially in large and inhabited areas.

In conclusion, the imperfections of the fast-paced, local-scale investigations for quick mitigation purposes are evident within this case study, where the global geological, morphological, and hydrogeological conditions were generally neglected within the scope of the geotechnical research works, but relevant regarding the present problem.

References

- Cruden D, Varnes D (1996) Landslide Types and Processes. In: Landslides Investigation and Mitigation, Special Report 247. Transportation Research Board, US National Research Council, Washington DC, p Chapter 3, pp. 36–75
- DGU Geoportal. <https://geoportal.dgu.hr/>. Accessed 6 Feb 2024
- EN ISO 14688-1:2002 Geotechnical Investigation and Testing - Identification and Classification of Soil - Part 1: Identification and Description (ISO 14688-1:2002)
- EN ISO 14688-2:2004 Geotechnical Investigation and Testing - Identification and Classification of Soil - Part 2: Principles for a Classification (ISO 14688-2:2004; EN ISO 14688-2:2004)
- EN ISO 14689-1:2003 Geotechnical Investigation and Testing - Identification and Classification of Rock - Part 1: Identification and Description (ISO 14689-1:2003)
- Google Maps. <https://www.google.com/maps>. Accessed 6 Feb 2024
- Hoek E (2007) Practical Rock Engineering. RocScience
- Hungr O, Leroueil S, Picarelli L (2014) The Varnes classification of landslide types, an update. *Landslides* 11:167–194. <https://doi.org/10.1007/s10346-013-0436-y>
- Ivković A, Šarin A, Komatina M (1983) Tumač za Hidrogeološku Kartu SFR Jugoslavije, 1:500000. Beograd
- Look B (2007) Handbook of geotechnical investigation and design tables. Taylor & Francis, London; New York
- Miranda E, Brzev S, Bijelic N, et al (2021) Petrinja, Croatia December 29, 2020, Mw 6.4 Earthquake Joint Reconnaissance Report (JRR). ETH Zurich
- Šikić K (2014) Republika Hrvatska, Osnovna Geološka Karta, 1:100000, Tumač za List Bosanski Novi, L 33-105. Hrvatski Geološki Institut, Zavod za Geologiju, Zagreb
- Šikić K, Šimunić A (2014) Osnovna Geološka Karta Republike Hrvatske, List Bosanski Novi, L 33-105
- Terraforming Ltd. (2021) Inženjerskogeološki izvještaj za potrebu sanacije klizišta Žirovac na državnoj cesti oznake DC 6, dionica 004 u km 29+000. Terraforming Ltd. Rijeka, Croatia
- Tomac I (2021) Geotechnical Reconnaissance and Engineering Effects of the December 29, 2020, M6.4 Petrinja, Croatia Earthquake, and Associated Seismic Sequence

Investigating the factors governing the damage occurrence on buildings exposed to slow-moving landslide risk

Gianfranco Nicodemo^{(1)*}, Dario Peduto⁽¹⁾, Davide Luongo⁽¹⁾, Settimio Ferlisi⁽¹⁾, Luigi Borrelli⁽²⁾, Diego Reale⁽³⁾, Gianfranco Fornaro⁽³⁾, Giovanni Gullà⁽²⁾

1) Department of Civil Engineering, University of Salerno, Via Giovanni Paolo II, 132, 84084 - Fisciano (SA), Italy
(gnicodemo@unisa.it, dpeduto@unisa.it, dluongo@unisa.it, sferlisi@unisa.it)

2) Research Institute for Geo-Hydrological Protection (IRPI – CNR), National Research Council of Italy, Via Cavour n. 4/6, 87030, Cosenza, Italy (luigi.borrelli@irpi.cnr.it; giovanni.gulla@irpi.cnr.it)

3) Institute for Electromagnetic Sensing of the Environment (IREA – CNR), National Research Council of Italy, Via Diocleziano 328, 80124 Naples, Italy (reale.d@irea.cnr.it; fornaro.g@irea.cnr.it)

Abstract The paper deals with an ongoing research aimed at investigating the relationships between the kinematic features of slow-moving landslides affecting urban areas and the related effects on exposed buildings. These relationships are expressed in terms of changes of damage severity levels over time also considering the factors governing – in different way – the onset and the development of the damage. The building response to slow-moving landslide was analysed by exploring long-term and multi-temporal monitoring/surveying information gathered from conventional and innovative techniques along with background geological, geomorphological and geotechnical data. To this aim, the analysis starts from a well-documented case study in Calabria Region (southern Italy) and then it extends to four other areas in Italian Apennines with similar geological settings, landslide types and built-up features.

The results achieved can help setting up more reliable models for consequence forecasting to be used in quantitative risk analyses.

Keywords slow-moving landslides, building damage, vulnerability, risk.

Introduction

The interaction between slow-moving landslides and human settlements is a remarkable issue for both scientific and technical communities involved in identifying the most suitable strategies for land-use planning and urban management (Ferlisi et al., 2019; Gullà et al., 2021). In the last years, the interest on the topic is increased by the evidence that several urban areas are affected by active landslides involving complex geological formations and moving along shear zones where fine-grained soils prevail. Although the representative velocities of those landslides usually range from extremely slow to slow classes (Cruden and Varnes, 1996), exposed buildings can suffer damages whose severity increases over time as cumulative displacements increase with high socio-economic impacts (Peduto et al., 2018).

To address this issue, empirical procedures implementing data collected by way of in-situ/laboratory tests and monitoring techniques can help in generating tools able to predict the onset and the development of the slow-moving landslide damage to the exposed buildings (Fell et al., 2005, Corominas et al., 2014).

However, to obtain reliable results, a preliminary effort is required in terms of knowledge on the factors governing – in different way – the response of the above buildings to displacement patterns at foundation level such as: *i*) the landslide mechanism, which includes information about the landslide intensity measure (e.g. a representative velocity or differential displacements cumulated in a reference time period), *ii*) the landslide displacement trends and their evolution over time (e.g. weather-induced reactivations and/or accelerations associated with a permanent or episodic activity); *iii*) the characteristics of the involved soils (in terms of both physical and mechanical properties), *iv*) key building characteristics (structural and foundation typology, geometry, state of maintenance); *v*) the suffered (or expected) building damage severity level joint with their vulnerability; *vi*) the position of a given building with respect to the landslide-affected area (i.e. at the head, body or toe).

In this regard, provided that similar geological and geomorphological features as well as landslide types and urban fabric are considered, the analysis of large dataset of multi-source information gathered from in-situ surveys and monitoring data acquired by both conventional (ground-based) and innovative (remote sensing) techniques can help in the activities aimed to investigate the role played by each of the above governing factors. Following this line of thought and with the general intend to go in-depth on all aspects governing the damage occurrence on buildings exposed to slow-moving landslide risk, this research starts from the analysis of a well-documented case study in southern Italy (Lungro village, Calabria region), where the availability of long-term and multi-temporal monitoring/surveying information along with background geological, geomorphological and

geotechnical data, allowed to investigate the relationships between the kinematic features of slow-moving landslides affecting urban areas and the related effects on exposed buildings in terms of changes of damage severity levels over time also considering the building position with respect to the landslide-affected area. Then, the evidences raised from the exploration of the dataset available for Lungro village were jointly analysed with other case studies in the southern Apennine of the Calabria region, wherein a rich sample of slow-moving landslide-induced damage to buildings was collected. The preliminary results provide useful background for activities aimed at generating reliable damage forecasting tools to be used in quantitative risk analyses for built-up environments interacting with slow-moving landslides. These tools can help the decision makers in identifying appropriate structural and/or non-structural measures for risk mitigation.

The case studies

The case studies under consideration are five urban areas (Lungro, Verbicaro, San Mango d'Aquino, Lago and Gimigliano municipalities) located in the southern Italian Apennines (Calabria region, Figure 1), widely affected by slow-moving landslides mainly involving complex-structured and weathered soils. The areas present similar geological and geomorphological features characterized by very steep slopes affected by rotational/translational slides, complex slide/flow and landslide zone where clustering of phenomena is too tight to distinguish different bodies. Urban fabric is composed of masonry objects made up of 2-3 floors with pebbles, or irregular stones on shallow foundations located in the historic centres and reinforced concrete buildings up to 5-6 floors built in the new-developed areas. The best-documented case study is the Lungro village (Fig. 2) for which geological-geomorphological information and geotechnical data with deep and surface displacement monitoring data coming from both conventional (inclinometers and GPS, Fig. 2a) (Gullà et al. 2017; Peduto et al. 2018) and innovative remote sensing (DInSAR) techniques (Peduto et al. 2017), are available. The latter (Fig. 2b) derive from the processing – by way of the SAR tomographic analysis (Fornaro et al., 2009) – of very high-resolution x-band radar images acquired by Cosmo-SkyMed constellation, recently updated within MEFISTO research project to cover a ten-year monitoring interval from May 2011 to September 2021. The comprehensive analysis of the data coming from previous studies carried out in the area through the application of the "aPosIn" procedure (Gullà et al., 2017) - which relies on the combination of geological information, geomorphological criteria and both geotechnical and remote displacement monitoring data This allowed typifying the inventoried slow-moving landslides (Fig. 2a) in six categories (Fig. 2b), differing in geometric and kinematic characteristics, involved soils, and type of movement.



Fig. 1 The analysed case studies: Lungro, Verbicaro, San Mango d'Aquino, Lago and Gimigliano municipalities (southern Italy).

This allowed typifying the inventoried slow-moving landslides in six categories (Fig. 2) of different geometric and kinematic characteristics, soil type, and movement mechanism. A multi-temporal building damage surveys were available on the buildings exposed to landslide risk identified by overlapping the typified slow-moving landslide inventory with the built-up map. During the in-situ surveys, information about the building characteristics in terms of structural and foundation typology, geometry, state of maintenance, the building position with respect to the landslide (at the head, body or toe), the interacting landslide typology and the building damage level (DL) were collected via ad-hoc predisposed building fact-sheets (Ferlisi et al., 2015; Peduto et al., 2017; Nicodemo et al., 2018). The recorded DLs were categorized by adapting the classification system proposed by Burland et al. (1977) on the basis of the visual interpretation of crack patterns exhibited by the building façades considering six categories (Do = negligible; D₁ = very slight; D₂ = slight; D₃ = moderate; D₄ = severe; D₅ = very severe). Figure 3 shows the results of the multi-temporal building damage assessment in Lungro village collected during in-situ surveys in October 2015 (Fig. 3a), June 2019 (Fig. 3b) and October 2022 (Fig. 3c) with two examples of DL evolution over time for both reinforced concrete (Fig. 3d) and masonry (Fig. 3e) buildings. Likewise for Verbicaro, San Mango d'Aquino, Lago and Gimigliano municipalities, remote sensing (DInSAR) displacements data and multi-temporal damage dataset on buildings in slow-moving landslide-affected area are available. The DL and position with respect to the landslide-affected area, collected during in-situ surveys at different time interval, were homogenised using the same ranking scale and damage classification (Burland et al., 1977) adopted for Lungro for the purpose of their cross comparison.

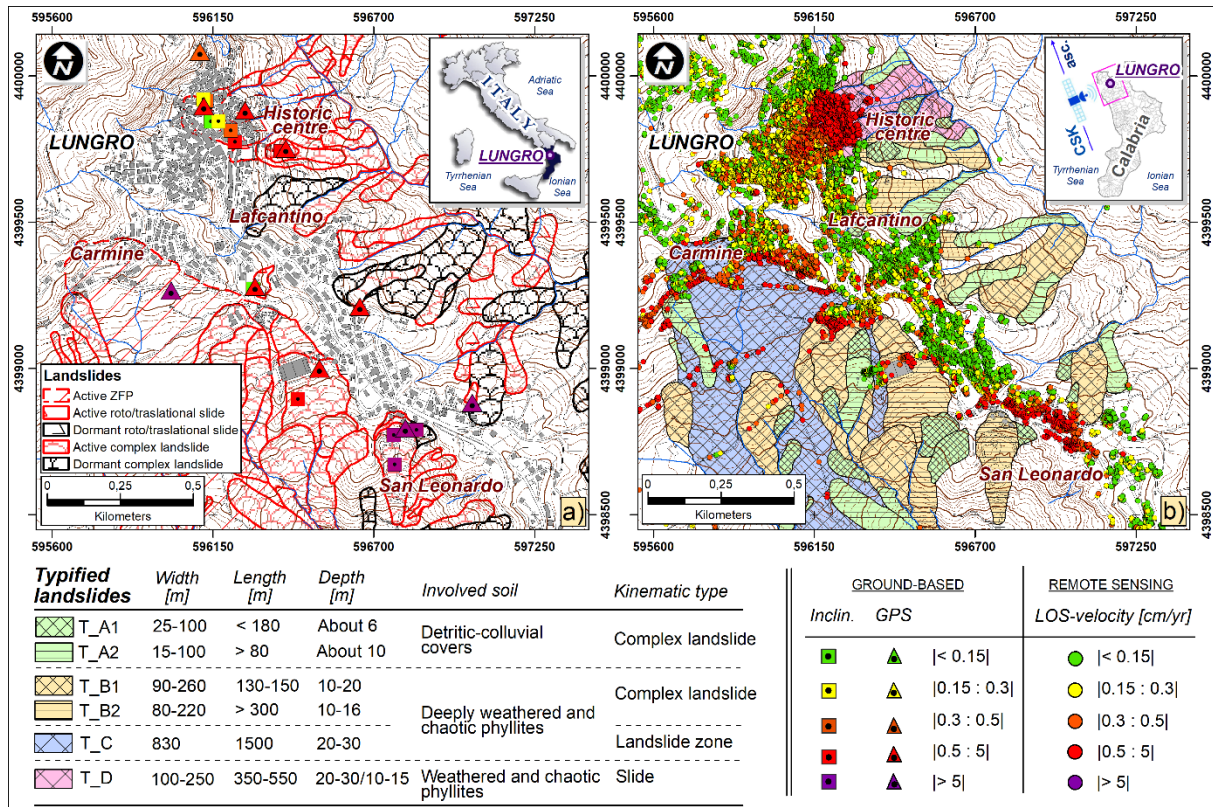


Fig. 2 Lungro village study area: a) landslide inventory map with ground-based (inclinometers and GPS) monitoring network and b) map of typified landslides (from Gullà et al., 2017) with spatial distribution of remote sensing data derived from the DInSAR processing of Cosmo-SkyMed images.

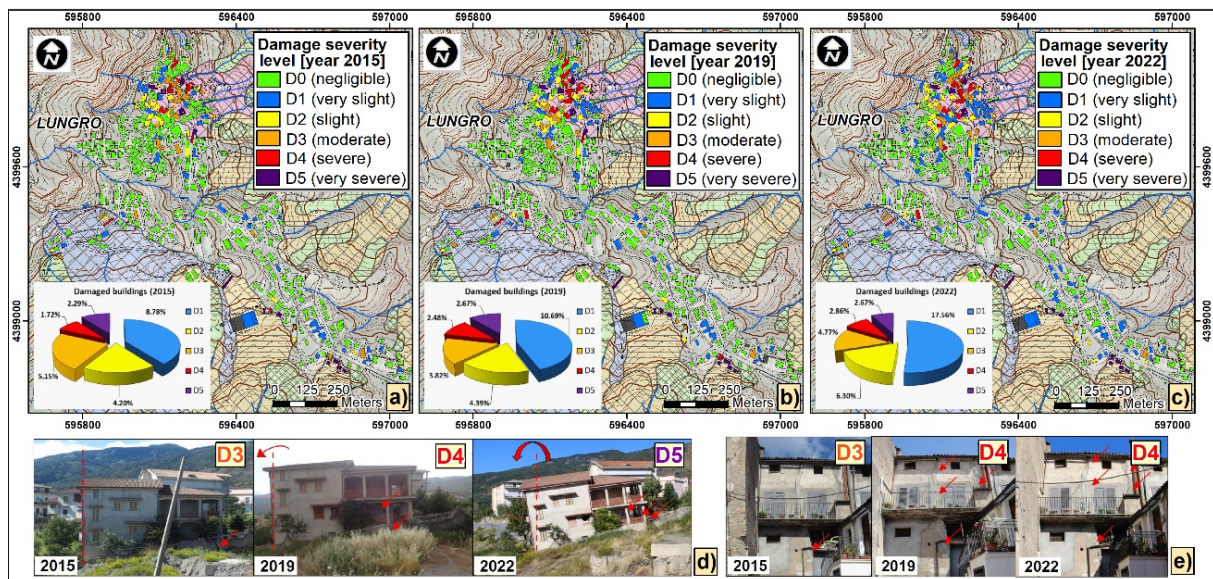


Fig. 3 Multi-temporal damage assessment of buildings in Lungro study area collected during in-situ surveys in a) October 2015, b) June 2019 and c) October 2022 with two examples of damage severity level evolution over time for d) reinforced concrete and e) masonry buildings in slow-moving landslide-affected areas.

Results

As for the Lungro area, the exposed buildings were preliminarily identified by overlaying the topographic map to the landslide inventory map. Out of a total of 470 surveyed buildings, 194 (63 reinforced concrete and 131 masonry buildings) resulted to be located on landslide-affected areas.

Focusing on a sub-sample of 68 masonry buildings composing a homogeneous sample located on landslide-affected areas or close to landslide boundary, a preliminary check of the distribution of damage severity level — ranging from D1 to D5 — was carried out based on the landslide typology and the landslide typified categories (Figure 4).

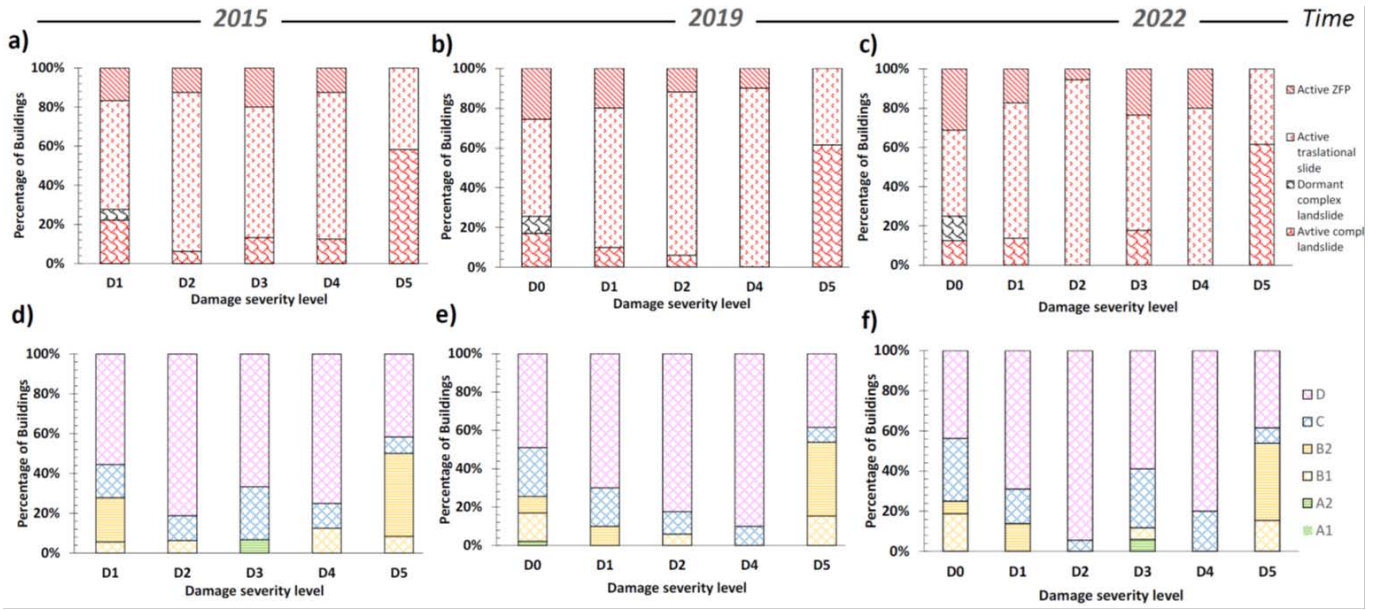


Fig. 4 Distribution of building damage severity level over time recorded in Lungro village in a) 2015, b) 2019 and c) 2022 in-situ damage surveys according to the landslide typology and d) 2015, e) 2019 and f) 2022 according to the landslide typified categories (see Fig. 2 for legend).

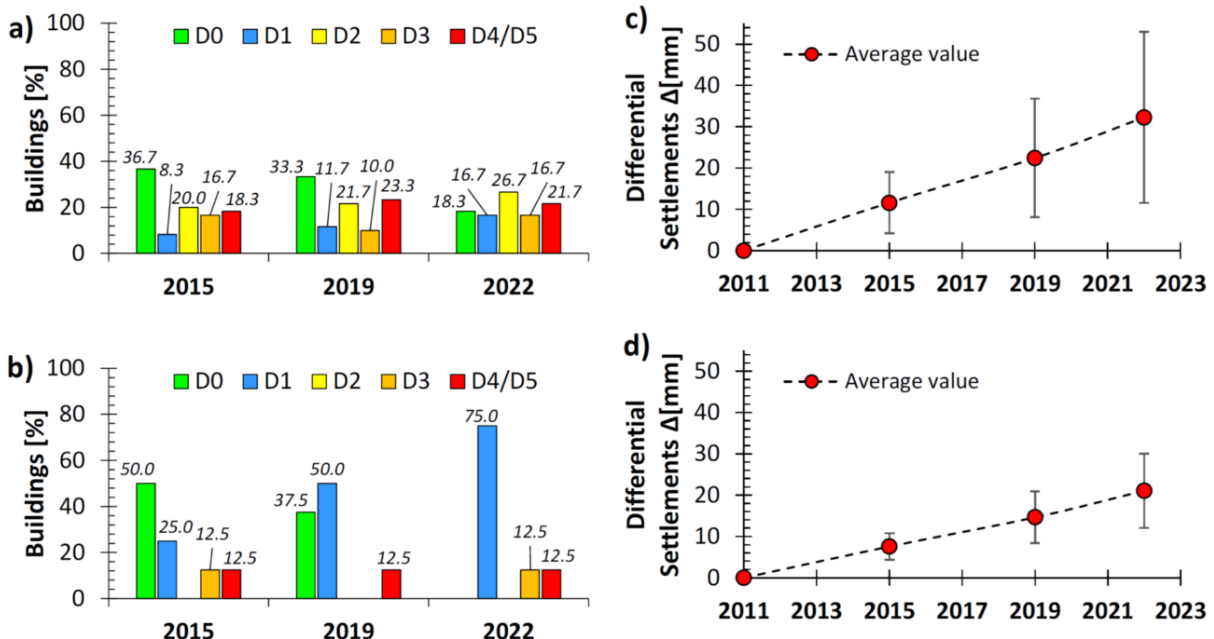


Fig. 5 Multi-temporal damage evolution for masonry buildings in Lungro village located on a) the head or b) the body of a slow-moving landslide and DInSAR-retrieved differential settlement (Δ) trend for buildings located on c) the head or d) the body of slow-moving landslide.

In particular, the analysis of the damage dataset collected in different time intervals (2015, 2019 and 2022) shows that most of the damaged buildings interact with landslide-affected areas mapped as "active" and, as expected, independently of the survey time, those buildings attain damage severity levels that are higher than those located in area mapped as "dormant" landslide. Furthermore, an increasing damage severity level over time is observed for buildings interacting with slow-moving landslides mapped as translational slide.

Referring to the typified landslides, the damage severity level over time seems to keep the same distribution (Figs. 4d, 4e, 4f) with the highest damage severity levels recorded by buildings interacting with the landslides of categories "B2" (medium/large complex landslide involving deeply weathered and chaotic phyllites) and "D" (deep/large translational slide involving weathered and chaotic phyllites) (Fig. 2b).

Additionally, a check of the distribution of damage severity over time was carried out by distinguishing the position of the buildings with respect to the landslide-affected areas (i.e. at the head, Fig. 5a or on the body, Fig. 5b). Figures 5a and 5b highlight that buildings located at the head attain damage severity levels higher than those located on the landslide body. Since damage onset and development relate to the magnitude of building settlements, remote sensing data – previously validated via a cross-comparison with ground-based measurement (Peduto et al., 2021) – were used to derive the differential settlement (Δ) suffered by each building in the different time intervals (i.e. in 2015, 2019 and 2022). First the cumulative settlements were derived by multiplying the average velocity along the vertical direction (i.e. derived from the Line-of-Sight sensor-target direction) for the period of observation of each considered time interval (Peduto et al., 2017). Then, the differential settlement (Δ) value was computed as the maximum difference of the cumulative settlements recorded by the pertaining coherent pixels (Nicodemo et al., 2017).

The above information was merged with the results of the damage surveys (Figs. 5c and 5d) providing a preliminary analysis of the relationship between the differential settlement trend exhibited by the buildings and the recorded damage severity levels according to their position with respect to the landslide-affected areas. Particularly, the average DInSAR-retrieved differential settlement trends for buildings located on the head (Fig. 5c) or on the body (Fig. 5d) of slow-moving landslide show, on average, that buildings located at the head exhibit higher Δ values, which correspond, in turn, to higher building damage severity levels (Fig. 5a and 5b).

In order to better investigate the distributions of building damage severity level over time according to the landslide typology and position within the landslide-affected area, the evidence raised from the Lungro village were merged with the data collected in the Verbicaro, San Mango d'Aquino, Lago and Gimigliano municipalities (Figure 6).

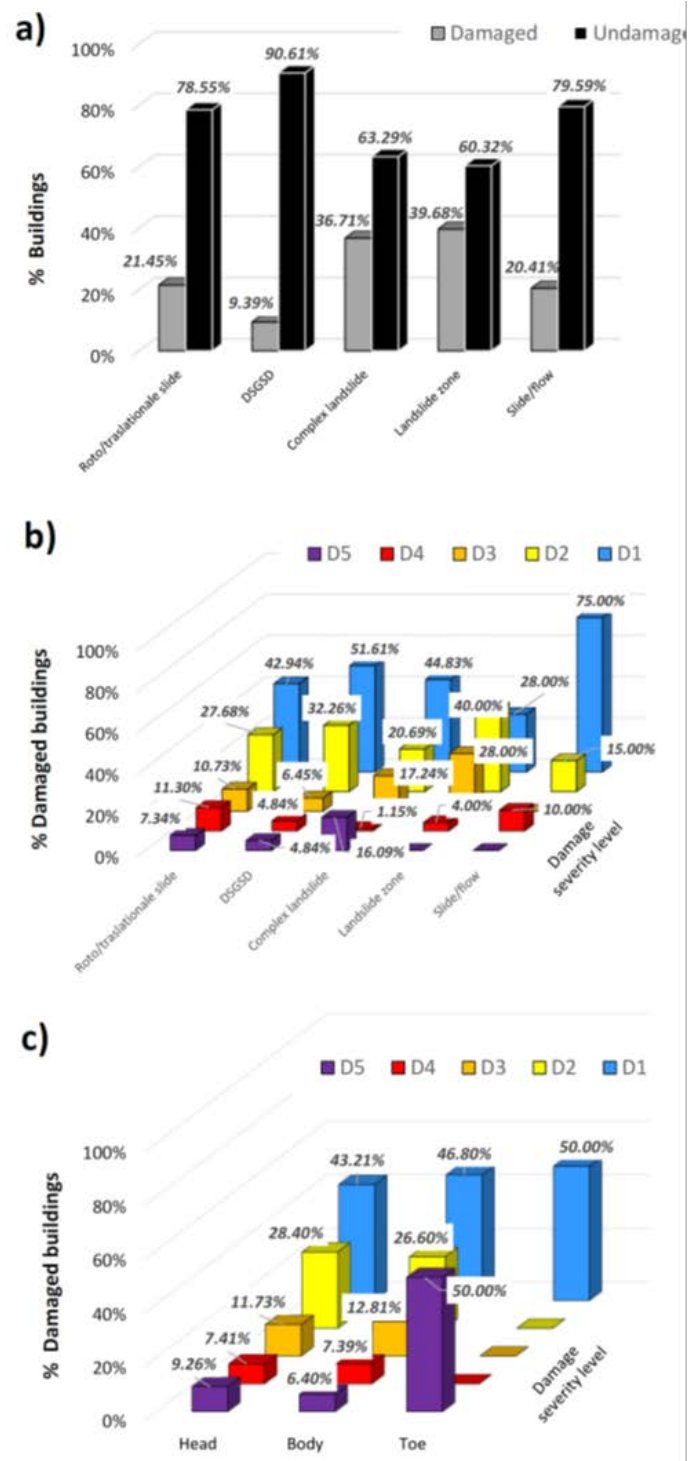


Fig.6 Building damage recorded in slow-moving landslide-affected areas for the five investigated case studies(Lungro, Verbicaro, San Mango d'Aquino, Lago and Gimigliano): a) percentage of damaged and undamaged buildings; b) distribution of the severity level according to the landslide typology; c) distribution of the severity level according to their position with respect to the landslide-affected areas (i.e. head, body and toe).

From the analysis of approximately 1800 buildings it emerges that buildings interacting with landslides classified as roto-translational or complex types (generally shallow) are more susceptible to damage (Fig. 6a) suffering higher severity levels (Fig. 6b). In relation to their position

with respect of the landslide-affected area, higher damage severity levels are recorded for buildings located on the head or on the landslide body (Fig. 6c), although in some cases, high damage severity levels are also collected on buildings located at the toe of the landslide.

Discussion and Conclusions

The presented paper shows that the long-term and multi-source settlement monitoring, jointly with multi-temporal assessment of damage affecting the buildings interacting with slow-moving landslides, provide a useful support in activities aimed at investigating the factors governing the damage occurrence on buildings exposed to landslide risk. Nevertheless, this requires the availability of large dataset in homogeneous geo-lithological contexts with relevant information on slow-moving landslide features (e.g. affected-area, state of activity, shape, etc.), the displacement trends and their evolution over time, the exposed facilities (constituting materials, state of maintenance, position within the landslide-affected area) and their damage severity level (generally associated with the attainment of certain serviceability/ultimate limit states).

The preliminary results obtained highlight that monitoring and survey data derived from technological innovation, if jointly analyzed with background data, can provide useful contribution. Moreover, the in-depth knowledge on the factors governing the onset and development of building damage over time is crucial for a proper definition of reliable damage forecasting tools within slow-moving landslide risk mitigation activities.

Acknowledgements

This research was funded by and carried out in the Italian Space Agency (ASI) contract n. 2021-10-U.o CUP F65F21000630005 MEFISTO—Multi-frequency SAR data processing methods for the hydrogeological instability monitoring.

The activities also fall within the Agreement for scientific cooperation signed by the Italian National Research Council (CNR-IRPI) and the Department of Civil Engineering of the University of Salerno on “*Attività di ricerca mirate ad approfondire le conoscenze sulla tipizzazione di movimenti franosi a cinematica lenta e sulla vulnerabilità di strutture e infrastrutture che con essi interagiscono anche mediante l’impiego di tecniche innovative di monitoraggio satellitare e da terra*” and the related operative Agreement for Research contribution signed by the two institutions on the topic: “*Analisi quantitativa del rischio da frane a cinematica lenta in aree urbane dell’Appennino Meridionale con l’ausilio di modellazione numerica avanzata e dati di monitoraggio satellitare*”.

References

- Burland J B, Broms B B, de Mello V F B (1977) Behaviour of foundations and structures. Proceedings of the 9th International conference on Soil Mechanics and Foundation Engineering, Tokyo. SOA Report, vol. 2, pp. 495–546.
- Corominas J, van Westen C, Frattini P, Cascini L, Malet J-P, Fotopoulou S, Catani F, Van Den Eeckhaut M, Mavrouli O, Agliardi F, Pitilakis K, Winter MG, Pastor M, Ferlisi S, Tofani V, Hervàs J, Smith JT (2014) Recommendations for the quantitative analysis of landslide risk. *Bulletin of Engineering Geology and the Environment*, 73(2):209–263.
- Cruden DM, Varnes DJ (1996) Landslide types and processes. In: Turner AK, Schuster RL (eds), *Landslides investigation and mitigation*. Transportation research board, US National Research Council, Washington DC, Special Report 247, Chapter 3, pp. 36–75.
- Fell R, Ho KKS, Lacasse S, Leroi E (2005) A framework for landslide risk assessment and management. In: Hungr O, Fell R, Couture R, Eberhardt E (eds) *Landslide risk management*. Taylor and Francis, London, pp. 3–26.
- Ferlisi S, Gullà G, Nicodemo G, Peduto D (2019) A multi-scale methodological approach for slow-moving landslide risk mitigation in urban areas, southern Italy. *Euro-Mediterranean Journal for Environmental Integration*, 4:20.
- Ferlisi S, Peduto D, Gullà G, Nicodemo G, Borrelli L, Fornaro G (2015) The use of DInSAR data for the analysis of building damage induced by slow-moving landslides. *Engineering Geology for Society and Territory - Landslide Processes*, © Springer International Publishing - Vol. 2. pp. 1835–1839.
- Fornaro G, Pauciuolo A, Serafino F (2009) Deformation monitoring over large areas with multipass differential SAR interferometry: A new approach based on the use of spatial differences. *International Journal of Remote Sensing*, 30(6):1455–1478.
- Gullà G, Nicodemo G, Ferlisi S, Borrelli L, Peduto D (2021) Small-scale analysis to rank municipalities requiring slow-moving landslide risk mitigation measures: the case study of the Calabria region (southern Italy). *Geoenvironmental Disasters* (2021) 8:31.
- Gullà G, Peduto D, Borrelli L, Antronico L, Fornaro G (2017) Geometric and kinematic characterization of landslides affecting urban areas: the Lungro case study (Calabria, southern Italy). *Landslides*. 14(1):171–188.
- Nicodemo G, Peduto D, Ferlisi S, Gullà G, Borrelli L, Fornaro G, Reale D (2017) Analysis of building vulnerability to slow-moving landslides via A-DInSAR and damage survey data. In: Mikos M, Tiwari B, Yin Y, Sassa K (eds) *Advancing culture of living with landslides, proceedings of the 4th world landslide forum— WLF 2017*, Ljubljana, Slovenia, May 29–June 02, 2017, vol 2. © 2017 Springer International Publishing AG 2017, Cham, pp. 889–907.
- Nicodemo G, Peduto D, Ferlisi S, Gullà G, Reale D, Fornaro G (2018) DInSAR data integration in vulnerability analysis of buildings exposed to slow-moving landslides. In: *Proceedings of IEEE International Geoscience and Remote Sensing Symposium (IGARSS 2018)*, Valencia (Spain), 22–27 July, 2018, pp. 6111–6114.
- Peduto D, Ferlisi S, Nicodemo G, Reale D, Gullà G (2017) Empirical fragility and vulnerability curves for buildings exposed to slow-moving landslides at medium and large scales. *Landslides*. 14(6):1993–2007.
- Peduto D, Nicodemo G, Caraffa M, Gullà G (2018) Quantitative analysis of consequences induced by slow-moving landslides to masonry buildings: a case study. *Landslides*. 15(10):2017–2030.
- Peduto D, Santoro M, Aceto L, Borrelli L, Gullà G (2021) Full integration of geomorphological, geotechnical, A-DInSAR and damage data for detailed geometric-kinematic features of a slow-moving landslide in urban area. *Landslides*, 18:807–825.

Harmonized approach for earthquake - induced landslide susceptibility and risk assessment in Vodno urban area

Done Nikolovski^{(1)*}, Radmila Salic Makreska⁽²⁾, Kemal Edip⁽²⁾, Julijana Bojadjieva⁽²⁾

1) International Balkan University, Makedonsko-Kosovska Brigada bb. 1000, Skopje, R. Macedonia, +389 71 248 604

(done.nikolovski@gmail.com)

2) University Ss. Cyril and Methodius, Institute of Earthquake Engineering and Engineering Seismology, Todor Aleksandrov 165, Skopje, R. Macedonia

Abstract During the last 20-25 years Skopje, and more specifically Vodno mountain, has been exposed to intense urbanisation, population growth, followed by intense anthropogenic processes such as application of structural loads, vegetation cuts and excavations, which have significantly changed the initial conditions of the terrain. These factors, along with the continual changes and degradation of the terrain, have provoked numerous instabilities in the area, and thus raised great concern and interest among the media and the scientific community, which work in the field of landslide hazard and risk assessment. As well, it should be emphasised that this area contains critical infrastructure, such as hospitals, schools, kindergartens, police station, roads etc., as well as around eleven international embassies and residences, which accentuates the problem furthermore.

In this paper, we provide a harmonised approach for earthquake induced landslide susceptibility in this urban area, through the infinite slope limit equilibrium method. For the analysis we used several datasets such as geomorphological (DEM raster file), detailed plan of the buildings and loads, geological and finally seismological datasets. The results obtained are shown accordingly in QGIS open-source software for spatial analysis. It has been proven that the influence from the constructions with different loads and typology, is of great importance for the analysis of the stability and the risk evaluation as a result. This approach proves the combined effect of anthropogenic influences on the terrain through the non-controlled urbanisation process, on the stability of the Vodno urban area under expected seismic scenario. Furthermore, the paper provides directions for reduction of the vulnerability of the people in the aforementioned area, through the process of the future spatial planning in synergy with scientific approach and possible construction measures.

Keywords earthquake - induced landslides, landslide risk, QGIS

Introduction

According to some sources (Vale C, 2019), during the 20-th century, nearly 80 earthquakes have triggered between 100.000 - 1.000.000 movements of the earth masses, which

has resulted in large material, as well as loss of several thousand human lives. Moreover, about past major landslides (period between 1900-2020) across the World, it can be emphasised that, around 50% of the total death toll is from landslides triggered by earthquakes. On another hand, the landslides triggered by rainfall are responsible for about 15% of the total casualties, even though they are 2,5 times more frequent than the ones triggered by earthquakes (Fig. 1). Another interesting insight from the analysed data of landslides is that, in time the number of casualties from rainfall-induced landslides is slightly decreasing, which is not the case with the ones triggered by an earthquake. Having in mind this, earthquakes are considered among the most significant natural trigger for landslides, due to the fact that they can't be predicted and their influence on the slope stability might be disastrous.

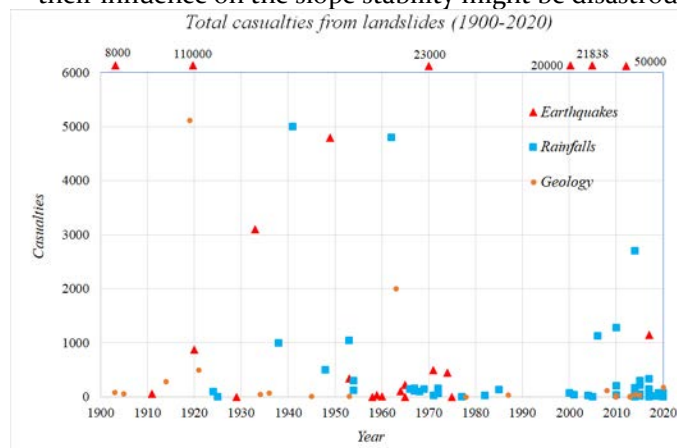


Figure 1 Human loss from landslides 1900–2020 (D. Nikolovski 2021)

The Republic of North Macedonia (25,713 km²) is a country with a hilly-mountainous morphology. Namely, almost 2% of the territory is covered by water bodies, about 19% are plains and valleys, while the largest part of about 79% are hills and mountains (Milevski 2018), which is a great indicator for the potential of the terrain towards geo-hazards in general. In addition, the country and especially its capital Skopje, has been and unfortunately still is, threatened by many hazards such as: earthquakes, landslides, floods, air pollution, etc. The main aim of this study is to produce a landslide hazard and risk assessment of the Vodno urbanised area, due to earthquake event with a return period of 475 years, for the first time in recent

history, . This initiative is in context to reduce the risk from this type of hazard as much as possible, through constructive and non-constructive measures, as well as to adapt and be prepared for both the expected and possible earthquake induced disasters.

Case study and parameters definition

Vodno mountain stretches in an east-west direction for about 12 km, where the highest point is Krstovar peak which is at around 1066 metres ASL. The natural slope of the terrain in the Vodno suburb is at around 10 – 20°, while in the upper zones the terrain is steeper with inclinations >25°. The mountain is surrounded in all directions with urban areas of approximately 4481,0 ha. The most densely populated area is Vodno settlement, which is part of

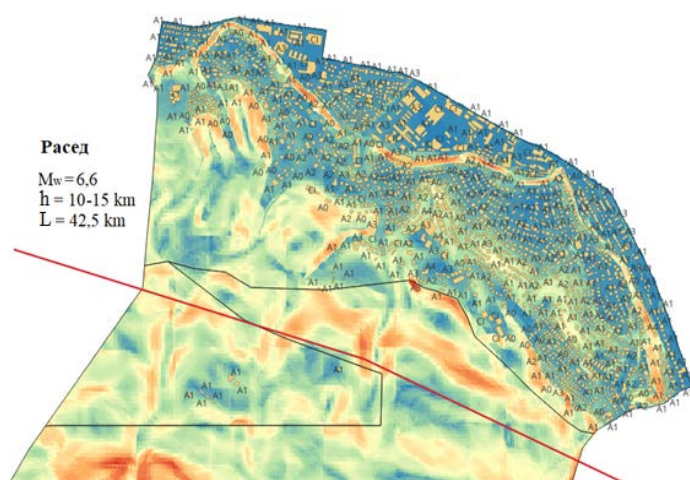
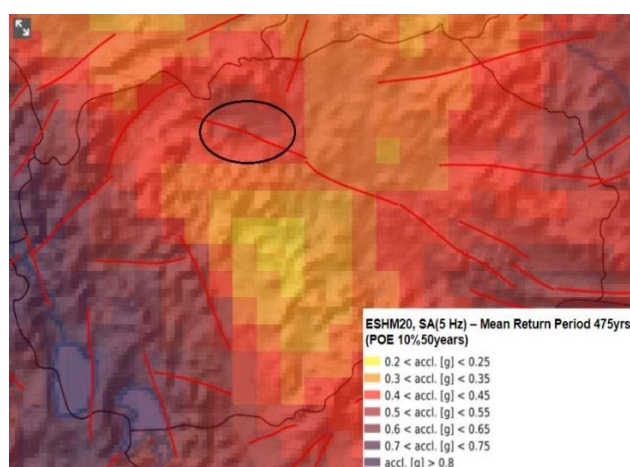


Figure 2 Digital elevation model (DEM), fault line and PGA for return period of 475 years for the study area

Related to the parameters, the identification of the slope angles (α) and heights, are derived from a detailed digital elevation model of the terrain (DEM), of 5 x 5 m spatial resolution. The lithology of the region has been investigated in the past, (Geologic Map - Skopje K 34 – 79), through detailed engineering-geologic mapping of the terrain. Furthermore, in a more detailed manner, the terrain properties have been explored during the urbanisation purposes in the last two decades, through geophysical soundings, as well as direct investigation methods (boreholes, CPT and SPT tests). The terrain investigations have shown rather complex and heterogeneous lithology of the terrain. It's composed of Pliocene clays (*Pl*) in the shallow zones, which overlay older Miocene claystone and marlstone sediments (*M₃*) with thickness of around 300 m., these materials are used as foundation materials below the structures in the area, and they can be treated as quasi-homogeneous zone.

The earthquake magnitude (M_w) as well as the location and type of fault structures that are near the region, is defined according to the probability of seismic hazard from the European-Mediterranean seismic hazard model (ESHM-20). This model incorporates a harmonised approach to earthquake records, tectonic zoning, a list of

Centar municipality. This is an area of around 1,59 km², and the population density is approx. 2498 people/km², with constantly increasing population . Some official stats provide the information that the number of households in the area has increased for around 10,0%, while the number of apartments for around 30,4% in the time span of just 20 years. Interestingly, according to the official statistics, around 66% of the population in this area are inactive and older people, which according to latest research (UN Office for Disaster Risk Reduction) has proven that are more vulnerable and experience more casualties in case of natural disasters. It's also important to emphasise that the Vodno area contains facilities, which are considered as critical infrastructure, such as 2 hospitals, 3 schools, 3 kindergartens, 1 police station, roads etc., as well as around eleven international embassies and residences.



active fault zones and information on the geological structure of the terrain, types of ground motion, etc. The results for magnitudes and fault zones, with its geometric and topological parameters are derived for the region AL-MK-BG, from the Share SHEEC 1900-2006 data file, which is aligned based on data from more than 13600 earthquakes., a seismic scenario is defined with a return period of 475 years, which is considered the age of exploitation of the objects of the analysed region. The values of maximum ground acceleration are defined by the same hazard model (EFEHR | Hazard Maps), where for the location for a period of 475 years, a value of PGA = 0.40 is obtained.

The calculated arias Intensity (I_a) is a function of the depth and distance of will be defined for the location of Vodno, from the database of known fault lines, that are in the Skopje Depression (Fig 2). In the literature on the European seismic hazard model ESHM-20, it can be found one active normal fault structure, which is at a depth of between $h=10-15$ km, length of 42,5 km and is with expected magnitude $M_w=6,6$. The distance of the fault from is 800 - 1000 m from the centre of gravity of the area analysed in this research paper. Furthermore, to define the arias intensity, the spatial parameters of this fault will

be taken, and according to the method of *Wilson and Keefer 1985*:

$$\log_{10} I_a = -4,1 + M_w - 2\log_{10} (d^2+h^2)^{0,5} - 0,5P \quad [1]$$

Where:

- I_a arias intensity (m/s)
- M_w magnitude
- d shortest distance from the hypocentre to the fault
- h depth of earthquake occurrence (km)
- P probability

Above mentioned parameters are going to be used in further regional analysis of earthquake – induced sliding of Vodno.

Earthquake-induced landslide hazard and risk assessment

In the last two-to-three decades, GIS has been recognized among the scientific community as a powerful set of tools for collecting, storing, analysing, and displaying spatial data, for different purposes. Mostly due to the time-consuming and local based approach of the FEM analysis, it is considered that this type of approach, through the Geographical Information System, may be more efficient in the landslide hazard assessment, by application on a whole variety of spatial data and variables. Hereby, in the research paper, the landslide susceptibility as well as the risk analysis are going to be analysed through the open source QGIS platform, which is a Geographical Information System for spatial and more efficient hazard assessment. The most common method used in practice, and which will be applied in the paper, is the so-called mechanical

model of a “rigid block”, which in the first stage analyses the stability of slopes in seismic conditions, so that the pseudo-static factor of safety is calculated (FS). In addition to this, the critical horizontal acceleration (a_y)

and then the total displacements of the soil block (U) based on deterministic methods are going to be defined.

$$FS = \frac{c' + (\gamma H \cos^2 \alpha - \gamma H k \cos \alpha \sin \alpha - \gamma_w h_w \cos^2 \alpha) \tan \phi'}{\gamma H \sin \alpha \cos \alpha + \gamma H k \cos^2 \alpha} \quad [2]$$

As it was explained before, landslides are in function of wide variety of natural and anthropogenic variables, while in this study, the landslide susceptibility in function of five (5) predisposing factors: lithological composition of the region, slope angle (α), height, seismicity of the region and finally the type, position and loads from the structures (1860 buildings) in the urban area of Vodno. Previously, it was explained how all the variables needed for the analyses have been defined, while there has always been discussion regarding the height of the sliding plane (H) in relation to the slope of the terrain. To reduce the possibility of subjective error in the analyses, previous experience of landslides caused by earthquakes was consulted. Thus, it is quite interesting that based on a statistical analysis of a large number of landslides (144) caused by earthquakes in El Salvador, it was concluded that 76% of the earthquake-induced landslides have a sliding depth of about 2-6 m, while only 15% of the landslides have a slip plane at a depth >20 m. Based on this fact, in the research paper, the slip plane will be assumed at a depth of $H=5$ m below the ground surface, parallel to the slope. The anthropogenic influence from the residential buildings is added through the change/increase of the height of the lamella (H'), depending on the calculated contact stresses that they transfer in the base. The analysed region is divided into a net of square segments with dimensions 50 x 50 m, and all of the variables and assessments about the output results are done for such raster as it is shown on figure 3 below.

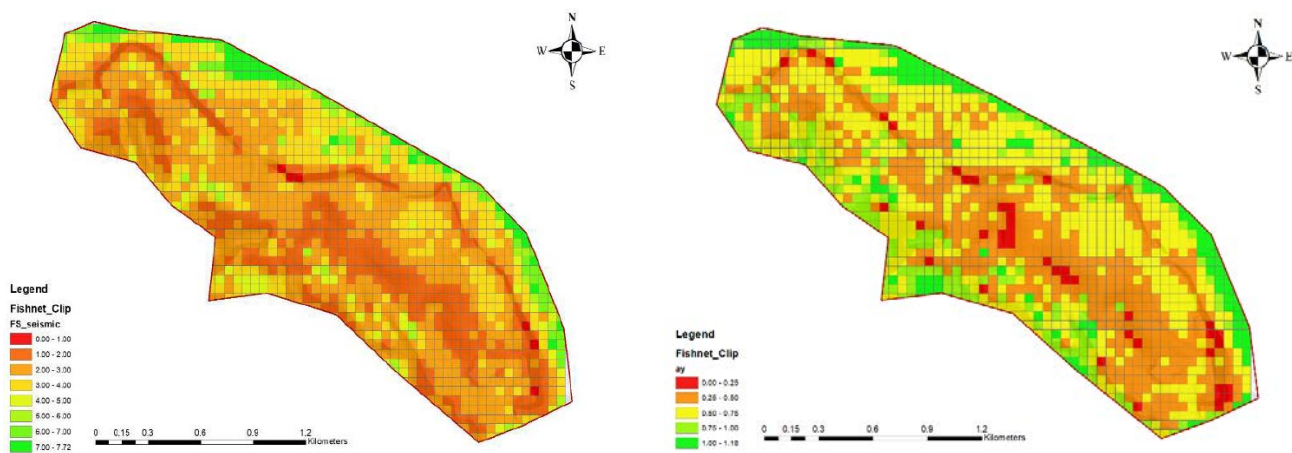


Figure 3 Factor of safety and critical acceleration (a_y) of the Vodno urbanised area due to earthquake

On the given figure, we can see the results about the pseudo-static stability of the urbanised region, where we can draw important conclusions. Firstly, it's essentially important to underline that the zones which fall in the area of $FS < 1$, correspond in large extent to the situation on the field; the locations found as critical through the

spatial QGIS analysis, correspond to some of the instabilities that were already registered. Furthermore in this context, it is evident that the zone which has been with significantly steeper incline, in the toe of the slope of the mountain is more susceptible towards instability, where the factor of safety reaches on some positions even

below 1,0. Furthermore, the urbanised region, the factor of safety is between 1,0-2,0, while interestingly, for the same inclination of the terrain and same lithological conditions, but without structural loads, the stability is significantly higher-reaching values of $FS=3,0-4,0$. This is surely, great indicator, about the influence on the loads and density of the structures on the terrain stability in earthquake conditions. According to the pseudo-static stability of the terrain, we are about to calculate the dynamic resistance of the earth mass. This parameter known as dynamic resistance (k_y), is a value necessary for the movement of a potentially unstable soil mass. This coefficient practically represents the overall dynamic resistance of the geological environment, but in this study also by considering the loads from the structures in the urban area. Hereby, we are going to use the theory of *Newmark* (1965). Finally, after all the necessary parameters are defined, we can calculate the earthquake - induced sliding displacements (U), which are necessary to assess the seismic performance of slopes and risk analysis. These displacements represent the cumulative, downslope movement of a rigid sliding block, due to earthquake shaking. In this research paper, we are going to use, the formula derived from *Jibson and Keefer* 1993, which represents classic regression formula, based on large data on measured displacements, provoked by earthquakes in California – USA:

$$\log U = 1,521 \log I_a - 1,993 \log a_c - 1,546 \quad [3]$$

While the sliding block model is a simplified representation of the field conditions, the displacements

predicted from this approach, have been shown to be useful to define so-called hazard maps. Here, it is necessary to emphasise that from a theoretical point of view, an effort has been made to define the displacements of the slopes as precisely as possible under the conditions of an earthquake with a probability of occurrence of 475 years, through the so-called limit equilibrium methods. However, since in this type of regional analyses, we have more natural variables, both in time and in space, we can't determine with certainty whether the specific/calculated ground displacements would occur under certain conditions. However, the relative difference in field behaviour exists, depending on the variables that are assigned in each cell in the analysis. This concept is explained in detail in the paper by *Jibson et. al.* 2000, where it is emphasised that the predicted displacements according to the analytical method of a rigid block should be understood as an index that would correlate with the behaviour of the terrain in certain conditions, and not a "real" displacement that we should expect. Thus, for this reason, when evaluating the degree of hazard, the slope behaviour index will be used, which is defined in the following limits 0 - 25 cm - low hazard (green), further 25 - 50 cm - medium hazard (yellow) and >50 cm - high hazard (red colour), as adopted in *J. Bojadjieva et al* (2017). In the following steps, after the hazard identification and assessment, depending on the elements at risk and exposure, for which we have detailed spatial and numerical data, we can conclude the landslide risk analysis.

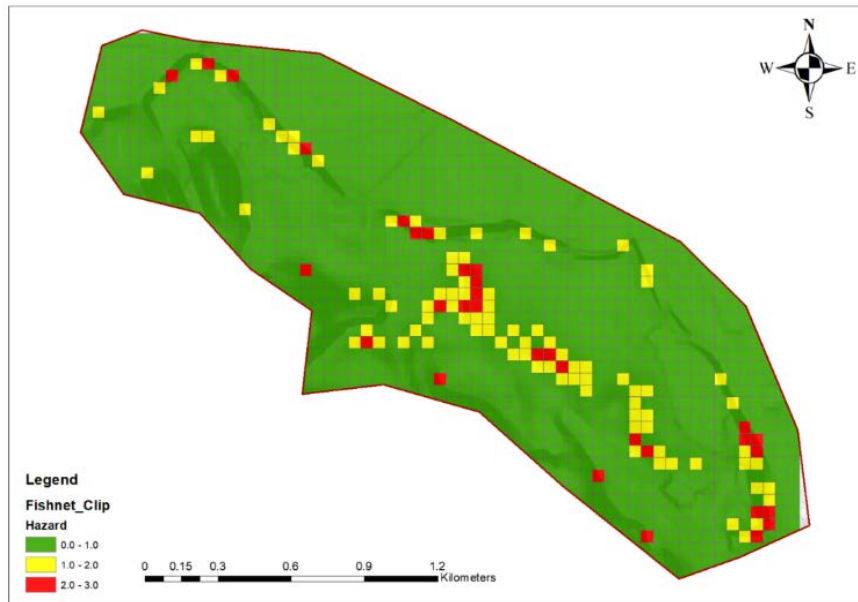


Figure 4 Risk map from earthquake-induced landslide for urbanised Vodno study area

From the obtained results, the distinction in risk is evident, where in the urbanised part, especially the one where we have significantly higher buildings, the risk is significantly increased. From the output results we can conclude that about 15,7 ha fall into a high-risk zone, while 36,4 ha are in a medium-high risk zone. Of these, 728 m², and 2806 m², are critical infrastructure facilities affected by high and medium-high risk accordingly.

Such maps are typically intended for use in disaster planning and for incorporation in decision support systems. But in cases when we already have developed urban area, they can be also used as a great resource in the allocation and design of remediation measures in the zone of high risks.

Conclusions

The paper has presented a harmonised approach for earthquake – induced landslide hazard and risk evaluation, for urbanised slopes, according to a deterministic approach, by the infinite slope theory.

The most significant contribution of this research paper is the quantification of the anthropogenic impact of the structures in the assessment of the risk of landslides under dynamic conditions. Thus, it has been proven that under construction conditions of relatively high buildings of >6 floors, under the influence of an earthquake with a return period of 50 years, the risk of landslides increases by significant 52-60%. While, in conditions where we have low-rise structures of type A₀, A₁, A₂, the risk increases insignificantly, by 3-4%, which in fact is related to the excess earthquake force and not the structural loads necessarily. Thus, we can easily see what the impact of urbanisation on the terrain is, on its general stability, under some earthquake scenario.

Considering the fact taken from the State Statistics Office of North Macedonia, that mainly inactive population of about 66%, means high exposure, but also vulnerability in the area. This fact provides forecast estimates for the affected population, in the high-risk zone, range between 2900 - 3400 people. Although, in the area of mid-risk the numbers are significantly higher. Here, worth mentioning is that in this paper, we have analysed only the cells that are affected, and no kinematic type of failure - interaction scenario was considered. The area around those zones should be investigated in further detailed manner. In case that those detailed analysis, confirm this unfavourable scenario, some remediation measures must be designed to reduce the risk as low as reasonably possible (ALARP).

Through the methodology proposed in this research paper, it is possible to generate earthquake induced landslide hazard maps, and in other similar regions because it relies on analytical methods and not on rough regionalization and "experience". In this way, it is possible to identify different zones that in the urbanisation phase in the future will make appropriate spatial planning, and to propose the type of buildings that can be built depending on a series of parameters. On the other hand,

in conditions where the region is already affected by uncontrolled urbanisation, this type of analysis can be used to reduce the risk through the so-called constructive measures, up to some level of acceptable risk. Furthermore, such analyses aim to identify potential hotspots in a wider region, but for a more detailed analysis of the time, mechanism as well as the conditions of occurrence of landslides, it is necessary to conduct FEM analyses. By this approach, through precise geometry and appropriate material laws for the behaviour of materials, an assessment of the nonlinear and dynamic response of the environment will be made, which will certainly be a significantly longer process. For this reason, we consider it as necessary to analyse the problem multi-disciplinary through the synergy of these two different methodologies.

References

- D. Nikolovski, (2021) "1st Doctoral Seminar, UKIM"
- D. K. Keefer, (1984) "Landslides Caused by Earthquakes". Geological Society of America Bulletin, Vol. 95: pp. 406-421.
- D. N. Moses, (2019) "Landslides Mapping and Susceptibility Analysis Using RS and QGIS Techniques in Chiweta Area, Northern Malawi". Journal of Environmental Hazards vol 2: pp. 1-5
- Danciu L., Nandan S., Reyes C., Basili R., Weatherill G., Beauval C., Rovida A., Vilanova S., Sesetyan K., Bard P-Y., Cotton F., Wiemer S., Giardini D. (2021) - The 2020 update of the European Seismic Hazard Model: Model Overview. EFEHR Technical Report 001, v1.0.0, <https://doi.org/10.12686/a15>
- State Statistics Office of North Macedonia, last access: (01.2024) <https://www.stat.gov.mk/>
- Fell, R., Corominas, J., Bonnard, C., Cascini, L., Leroi, E., & Savage, W. Z. (2008). "Guidelines for landslide susceptibility, hazard and risk zoning for land use planning. Engineering Geology, 102": pp. 75–125.
- J. Bojadjieva, V. Sheshov, C. Bonnard, (2017). "Hazard and risk assessment of earthquake-induced landslides—case study" Landslides: pp. 161-171.
- J. D. Bray, (2007) "Simplified seismic slope displacement procedures" Chapter 14, Earthquake Geotechnical Engineering - Springer, pp 327-351.
- M. Jovanovski, I. Peshevski, V. Gruevska, N. Nedelkovska, N. Malijanska Andreevska, (2023). "Gis-based approach in preparation of geotechnical maps for planning of Skopje city development by applying polynomial interpolation method".
- N. Klimis, K. Papatheodorou, P. Moutsokapas, B. Margaritis, (2013). "Landslide hazard assessment using gis: evaluation of methodologies under static and seismic conditions" ICEGE Istanbul 2013: pp 1.1.
- QGIS User Guide (2024).
- S. D. Fotopoulou, K. D. Pitilakis (2015). Predictive relationships for seismically induced slope displacements using numerical analysis results. Springer: pp 1-32.
- T. Mersha, M. Meten, (2020). "GIS-based landslide susceptibility mapping and assessment using bivariate statistical methods in Simada area, northwestern Ethiopia", Geoenvironmental Disasters- Springer: pp 1-22.
- UN Office for Disaster Risk Reduction, (2015). "Sendai Framework for Disaster Risk Reduction".
- Vale C, (2019) "The CRED presents the bill: the socio-economic cost of natural hazards"

Preliminary landslide hazard map of Serbia

Miloš Marjanović⁽¹⁾, Olivera Kitanović⁽¹⁾, Saša Todorović⁽²⁾

1) University of Belgrade, Faculty of Mining and Geology, Djusina 7, Belgrade, milos.marjanovic@rgf.bg.ac.rs

2) Geological Survey of Serbia, Rovinjska 12, Belgrade, Serbia

Abstract In this work a preliminary landslide hazard map of Serbia is presented as an output of a work group assignment in 2018. Simple multi-criteria approach based on experts' opinion is implemented over a set of data which are mostly publicly available. Input data included: Digital Terrain Model (and its derivatives) at 30 m resolution; Engineering geological map of Serbia at 1:300 000 scale (and its derivatives); Hydrometeorological dataset (and its derivatives); depth to bedrock model at 250 m resolution. There were seven conditioning factors which were derived from these input raster datasets. In addition, available landslide inventory on the national level was used to validate the model. The methodology first involved creating a questionnaire for domestic practitioners in the field of engineering geological mapping, to determine the sub-setting of conditioning factors into classes and individual weights of each conditioning factor in accordance with their influence on landslides. The weights were normalized in 0-100% range and then used as raster multipliers for each reclassified conditioning factor. After their multiplication and addition in GIS environment a landslide hazard model was created. Result suggests that very high and high hazard class occupy about 12% and 28% of the territory, respectively. Administratively and spatially, the SW and W Serbia are the most affected. Validation suggests that very high and high hazard classes were confirmed in 46% of the inventory, moderate class has 31.5%, whereas remaining 22.5% can be considered as false negatives, leaving room for further improvements of this preliminary map version of the map.

Keywords landslide hazard, Serbia, multi-criteria analysis

Introduction

Landslide hazard mapping is becoming essential tool in planning and design worldwide (Mateos et al., 2020). It can be established at different levels or scales, ranging from global and continental, to national, regional, and site-specific. Naturally, the applied methodology varies accordingly, while also depending on the input data availability (Fell et al., 2008). In the case of Serbia, there were individual attempts to deal with the landslide susceptibility and hazard at different scales (Abolmasov et al., 2017b; Dragičević et al., 2012; Krušić et al., 2017; Marjanović et al. 2013; Tešić et al. 2020), but the matter was also recognized by authorities and there is a strong initiative to involve it in legislation. According to the

current Law on mining and geological explorations (RS Official Gazette No. 40/2021), together with engineering geological mapping the duty to develop and update landslide hazard map of Serbia is entrusted to Geological Survey of Serbia (GSS). Under assignment of the Ministry of interior and Ministry of Mining and Energy, a Work Group involving esteemed landslide experts, steered by the GSS was assembled in 2018 with a task to develop *inter alia* a preliminary landslide hazard map on national level. This is the first map of such kind developed for the entire territory and the first one to be a joint venture of all respective landslide experts from their respective institutions, such as GSS, Faculty of Mining and Geology University of Belgrade, Highway institute Belgrade, Institute of Transportation "CIP", Institute "Jaroslav Černi", Ministry of interior Emergency Sector, and Ministry of Mining and Energy Geological investigations Department. One of the motifs for assembling such a group was the massive 2014 landsliding (Abolmasov et al, 2017ac), and constant urge to mainstream the landslide hazard issues, ever since. As indicated, the landslide hazard mapping was attempted in numerous occasions in Serbia, through different research and commercial projects. As they were mostly concentrated on local to regional level, an attempt to deliver national scale landslide hazard model is a pioneering one in Serbia. Practice and experience from these earlier projects were implemented in the national level case. The modelling was done in 2018-2019 by compiling the best international and domestic practices in large-scale studies (Abolmasov et al., 2017a). It is also important to mention that term landslide is herein considered in its widest form (Hungr et al., 2014) and includes various typology of mechanisms and materials, but primarily earth slides, and subordinately debris flows, while other types have not been considered.

Methodology

The applied methodology can be split into three sections: input data acquisition and processing; multi-criteria modelling; and validation (Fig. 1).

Input data preparation

Data repository included data on conditioning factors, i.e., factors that in combination outline zones that are likely to host landslides; triggering factors, i.e., factors that directly initiate landslide activation both spatially and temporally; and landslide inventory used for model validation.

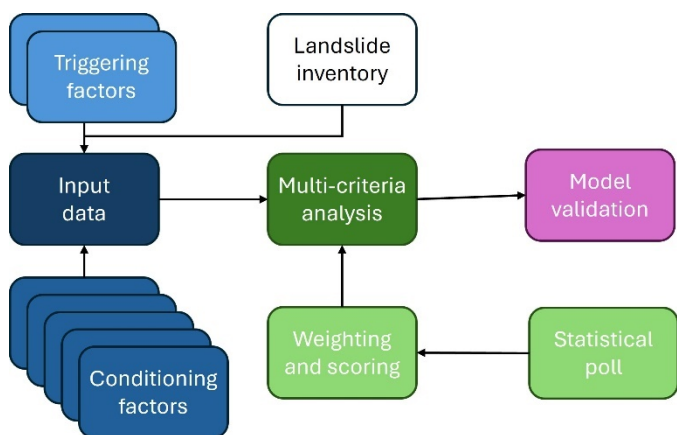


Figure 1 Methodology workflow.

A common set of conditioning factors (Tab. 1) that influence landsliding at large scales was used: Slope angle S ; Lithology L (complexes of same engineering-geological features); Distance to structure D_2S ; Distance to river D_2R ; and Depth to bedrock D_2B . Sloping indicates areas that are prone to instabilities, but not in linear fashion (steeper the slope higher the probability of landsliding), as steep angles in good rocks are not necessarily indicative of landslides, whereas gentle slopes in poor rocks can be. Therefore, lithology is another factor that can well control such combinations with slope angle. Rivers and linear structures, such as faults and joints are also commonly considered as weakened zones where weathering is intensive, groundwater is present and rock strength is weakened, therefore providing suitable conditions for instabilities. Areas closer to such lineaments are more likely to host landslides than those further away. All numerical conditioning factors (S , D_2S , D_2R , and D_2B) were split into five classes using quantile interval splitting, to ensure them being spatially equally distributed. Nominal factor (L) was aggregated to a reasonable number of classes, whereby engineering-geological units with similar characteristics were generalized (Tab. 2). Subsequently these all classes in all rasters were assigned a score 1-5, wherein 1 depicts the least influence (e.g., flat slopes, good rock, areas away from lineaments and with shallow bedrock) and 5 depicts the most influence on the landsliding process (steep slopes, poor rock, areas close to rivers and faults with deep bedrock).

Table 1 Landslide conditioning and triggering factors.

Conditioning factor name and symbol	Data source	Scale/ resolution
Slope angle S	www.usgs.gov	30 m
Lithology L	https://geoliss.mre.gov.rs	1:300k
Distance to structure D_2S	https://geoliss.mre.gov.rs	1:300k
Distance to river D_2R	www.usgs.gov	30 m
Depth to bedrock D_2B	https://soilgrid.org	250 m
Triggering factor name and symbol	Data source	Scale/ resolution
Long-term rain LTR	https://hidmet.gov.rs	NA
Short-term rain STR	https://hidmet.gov.rs	NA

The most common landslide triggering factor in these latitudes and climate is rainfall. Its spatial pattern delineates the areas that are more prone to instabilities, while their temporal frequency additionally impacts their probability of occurrence in time (e.g., annually). To match those two aspects the following rainfall triggering factors were defined: long-term rainfall LTR pattern, interpolated by using average annual sums over the baseline period 1991-2010; and short-term intensive rainfall STR interpolated as the number of days with rainfall exceedance of 10 mm. All interpolations were performed by using a national hydro-meteorological rain gauge network (29 stations) and resampled to 30 m resolution (<https://www.hidmet.gov.rs/>). Similarly to conditioning factors, these two rasters were split into equally distributed classes.

Table 2 Lithological units scoring (nominal input data type).

L unit name	Score	Weight (%)
Igneous hard rock complex	0.5	20
Loess	1	
Alluvial sediments	1,5	
High-grade metamorphic rock	2	
Meta-clastic sediments	2.5	
Carbonate rock	3	
Marls and pyroclastic rock	3.5	
Flysch complex	4	
Low-grade metamorphic rock	4.5	
Ophiolitic mélange and clayey complex	5	

Landslide inventorying is a long-term project conducted continuously by GSS since 2007 in parallel to engineering geological mapping. So far, 67% of the territory is covered (Đokanović, 2023) and contains over 6,000 of landslide events at point level, with assigned location, date of recording, activity status and confidence level. Out of these, only the events occurring within the meteorological baseline (1991-2010) were used (2010-2018 were excluded to be consistent with the triggering data), and only active events (at the time of recording) that suggests a confident registration. In effect, a final set with 3265 landslides was used for model validation.

Multi-criteria analysis

To ensure that these datasets are used in comprehension with domestic practice, a questionnaire for assigning 1-5 scores for each factors class and overall factors weight 0-100% were created and poll was conducted within the Work Group but also including the external colleagues. After statistical analysis, i.e., by majority of votes, the final scores and weights were assigned (Tab. 3). These were used in a GIS environment as follows:

- a) scores were used to reclassify original rasters using 1-5 values span;
- b) weights W were used in multi-criteria analysis as multipliers of each i^{th} reclassified raster (Eq.1);
- c) weighted rasters were summed up (Eq.1)
 - o conditioning factors CF subtotal;

- o landslide hazard H calculation as a sum of the CF subtotal and the triggering factor TF subtotal;
- d) resulting sum was normalized to 0-1 relative probability range;
- e) the final hazard model was split into five classes, from very low to very high using the natural break interval (Tab. 6).

$$H = \sum_{i=1}^5 W_i \cdot CF_i + \sum_{i=1}^2 W_i \cdot TF_i = (0.2L + 0.18S + 0.16D2B + 0.12D2S + 0.1D2R) + (0.14STR + 0.1LTR) \quad [1]$$

Such grouping would be in line with a general theory that landslide susceptibility should consider static data while landslide hazard component should add dynamic data upon that static set (Fell et al., 2008).

Table 3 Nominal factors interval scoring and factor weights.

S intervals (°)	Score	Weight (%)
<3	1	18
3-6	2	
6-10	4	
10-17	5	
>17	3	
D2S intervals (m)	Score	Weight (%)
<5	5	12
5-10	4	
10-30	3	
30-100	2	
>100	1	
D2R intervals (m)	Score	Weight (%)
<50	5	10
50-100	4	
100-500	3	
500-1000	2	
>1000	1	
D2B intervals (m)	Score	Weight (%)
<0.5	1	16
0.5-2	2	
2-5	3	
5-10	4	
>10	5	
LTR intervals (mm)	Score	Weight (%)
<500	1	10
500-750	2	
750-900	3	
900-1000	4	
>1000	5	
STR intervals (days)	Score	Weight (%)
<5	1	14
5-10	2	
10-30	3	
30-80	4	
>80	5	

Validation

A simple validation principle was applied – landslide points were plotted against the corresponding pixel values of the final hazard model, thereby revealing a distribution of true positives (which can be considered as all points correctly classified as high or very high hazard), idle (all points classified as moderate) and false negatives (all points misclassified as low or very low hazard). In addition, Mean Squared Error (Eq. 2) was calculated for relative probability $p(H)$ values (generated under step d) in respect to landslide instances ($p=1$).

$$MSE = \frac{1}{n} \sum_{i=1}^n [p(H) - 1]^2 \quad [2]$$

Results and discussion

The preliminary landslide hazard map of Serbia was generated by using scoring and weighting based on domestic experts' opinions. Arguably, another group of experts might have come up with a different map, while using other inputs or weighting them differently. However, local knowledge is a heuristic component that is essential herein, and it is incorporated in the model indirectly, by accounting for experts' experience with landslides in various parts of Serbia, and their knowledge what conditions and what triggers landslides.

Final model class distribution is visually appealing (Fig. 2). Expectedly, hilly areas, long and steep valleys, and basins are characterized as high or very high hazard zones. Normalized probability threshold $p(H)$ on annual level and class size s (in %) is matched against the hazard class:

- very low hazard, $p(H) < 0.36$, $s = 12.8\%$;
- low hazard, $0.37 < p(H) < 0.46$, $s = 23.4\%$;
- moderate hazard, $0.47 < p(H) < 0.56$, $s = 28.2\%$;
- high hazard, $0.57 < p(H) < 0.66$, $s = 23.6\%$;
- very high hazard, $p(H) > 0.67$, $s = 11.9\%$.

This formally means that all high and very high hazard zones can host landslides every second year within their premisses. Although temporal probability is included through LTR and STR it is fair to note that this is only a relative annual estimate, since the frequency information is deducted, and not actually calculated. Very low and very high classes are least widespread, while all other classes are balanced in size. Administratively, the Western and SW parts of Serbia are most affected (Fig. 3), while the national road network is showing highly affected stretches along important corridors (Fig. 3). About 8% of the roads is under very high annual hazard probability, while almost 30% is under very high and high hazard combined.

The numerical validation (Fig. 2) suggests that distribution is right skewed which is encouraging outcome. Most of the actual landslides are classified as high or very high hazard (46%), while moderate class covers about 31.5%. Inconveniently, some landslides (3.5%) are misclassified as very low hazard, as well as low hazard (19%). The MSE is relatively low, equalling 0.06 (its root is about 0.25), although it has been tested only against the existing landslide cases, which have probability of 1.

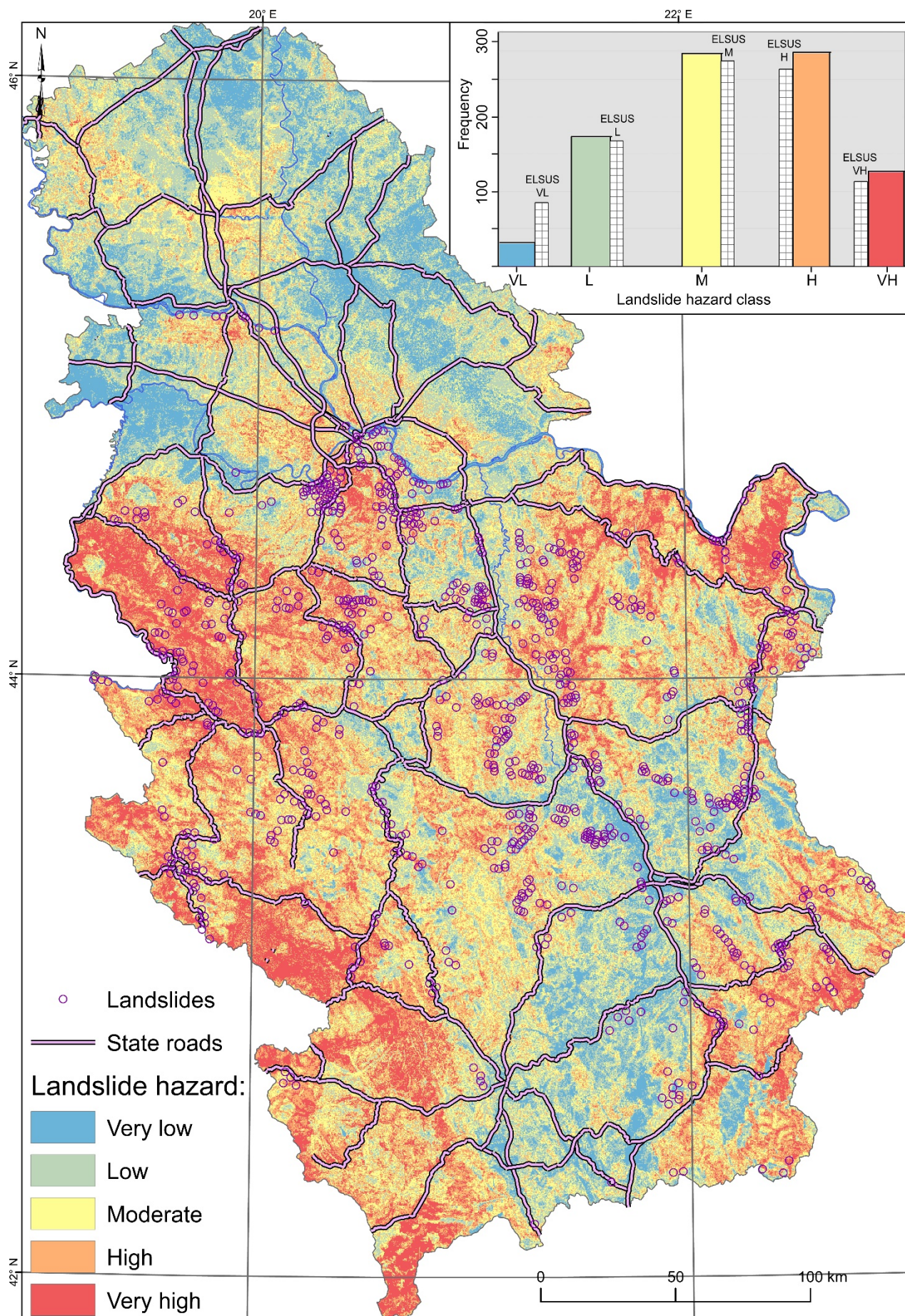


Figure 3 Preliminary landslide hazard map of Serbia with validation histogram in the upper right.

When compared against even higher-level (open) map of continental scale, ELSUS₂ (Wilde et al., 2018), which has coarser (200 m) resolution, but is based on similar multi-criteria methodology, the preliminary map brings some improvements, and should be preferred over ELSUS₂ output. In particular, the false negative rate is higher in the ELSUS₂, while all other classes have similar distribution (Fig. 2). False negatives are the most severe type of errors in landslide assessment, as they suggest landslide-safe area at location which is an actual landslide. In addition, MSE of the ELSUS₂ model is considerably higher (0.18) than in the case of the preliminary national model.

The Preliminary landslide hazard map of Serbia is for now published as a static document in PDF format on the GSS web page https://gzs.gov.rs/doc/portali/inz-geomehanika/2_Karta%20Hazarda%20od%20klizista.pdf, but it is in plan to create a web service on the Ministry of Mining and Energy portal, i.e., Geological Information System of Serbia (<https://geoliss.mre.gov.rs/>) as an interactive map.

Conclusions

In this pioneering work, it has been shown that a proper landslide hazard assessment at national level requires an institutional support and guidance regarding both, connecting the group of most relevant experts in the field and providing the necessary data. Legislation could be directed further to bylaws and rulebooks which will more closely define standards of developing landslide hazard maps at national or regional scales.

Although encouraging, results leave room for further improvements by introducing other potentially relevant inputs for condition factors, such as land use or other DTM derivatives. Strategies for class intervals selection and scoring can also be based on data approach (statistical assessment, calibration with independent inventory subset, etc.) instead of expert-driven one, or perhaps their combination. Also, triggering factors can be improved by using advanced climate indices or even climate change projections to ensure the applicability of the hazard map beyond the climatic baseline.

The applicability of such output can be versatile, but primarily oriented towards general levels of planning and design. It can be also used for upscaling for wider regions analysis (e.g., the Western Balkan Region), which is common investment framework (especially in climate change context) and will require such kind of inputs for further developments or reconstruction, mitigation etc. It is not suitable to be used at municipal or more detailed levels, due to its input data which are too coarse, and landslide inventory which is point based (at municipal level or finer, polygon based is more appropriate).

Finally, it is important to note that landslide hazard map is a dynamic one in nature, and it can vary considerably. One reason is the dynamic nature of the landslide inventory itself, so that in case of data-driven

approach it can change as new locations are reported. It can especially vary if climate-change projections are introduced for specific time splits in the future. Therefore, it can be fix-termed to a span ranging from anything between several years to a decade. It is well matching period with its potential application in spatial planning at national or regional levels, because these plans also expire after five years or more. New version of the national landslide hazard map is already in progress.

References

- Abolmasov B, Damjanović D, Marjanović M, Stanković R, Nikolić V, Nedeljković S, Petrović Ž (2017) Project BEWARE—landslide post-disaster relief activities for local communities in Serbia. In *Advancing Culture of Living with Landslides: Volume 3* (pp. 413-422). Mikoš, Arbanas, Yin, Sassa (eds). Springer International Publishing. (ISBN 978-3-319-53500-5).
- Abolmasov B, Krušić J, Andrejev K, Marjanović M, Stanković R, Đurić U (2017). Application of AHP and WoE methods for landslide susceptibility assessment on Krupanj municipality. *Izgradnja*. 7(10):239-46.
- Abolmasov B, Marjanović M, Đurić U, Krušić J, Andrejev K (2017) Massive landsliding in Serbia following cyclone Tamara in May 2014 (IPL-210). In *Advancing Culture of Living with Landslides: Volume 1 ISDR-ICL Sendai Partnerships 2015-2025* (pp. 473-484). Sassa, Mikoš, Yin (eds). Springer International Publishing. (ISBN 978-3-319-53500-5).
- Đokanović S (2023) Basic engineering geological map of Serbia project achievement. *Tehnika*. 78(6): 673-678.
- Dragičević S, Carević I, Kostadinov S, Novković I, Abolmasov B, Milojković B, Simić D (2012) Landslide susceptibility zonation in the Kolubara river basin (western Serbia) - analysis of input data. *Carpathian journal of earth and environmental sciences*. 7(2): 37-47.
- Fell R, Corominas J, Bonnard C, Cascini L, Leroi E, Savage W Z (2008) Guidelines for landslide susceptibility, hazard and risk zoning for land use planning. *Engineering geology*. 102(3-4): 85-98.
- Hungr O, Leroueil S, Picarelli L (2014) The Varnes classification of landslide types, an update. *Landslides*. 11: 167-194.
- Krušić J, Marjanović M, Samardžić-Petrović M, Abolmasov B, Andrejev K, Miladinović A (2017) Comparison of expert, deterministic and Machine Learning approach for landslide susceptibility assessment in Ljubovija Municipality, Serbia. *Geofizika*. 34(2): 251-273.
- Marjanović M, Abolmasov B, Đurić U, Bogdanović S (2013) Impact of geo-environmental factors on landslide susceptibility using an AHP method: A case study of Fruška Gora Mt., Serbia. *Geološki anali Balkanskoga poluostrva*. 74(1): 91-100.
- Mateos R M, López-Vinielles J, Poyiadji E, Tsagkas D, Sheehy M, Hadjicharalambous K, Liscák P, Podolski L, Laskowicz I, Iadanza C, Gauert C, Todorović S, Jemec Auflič M, Maftai R, Hermanns R L, Kociu A, Sandić C, Mauter R, Sarro R, Béjar M, Herrera G (2020) Integration of landslide hazard into urban planning across Europe. *Landscape and urban planning*. 196: 103740.
- Tešić D, Đorđević J, Hölbling D, Đorđević T, Blagojević D, Tomić N, Lukić A (2020) Landslide susceptibility mapping using AHP and GIS weighted overlay method: a case study from Ljig, Serbia. *Serbian Journal of Geosciences*. 6(1): 9-21.
- Wilde M, Günther A, Reichenbach P, Malet J P, Hervás J (2018) Pan-European landslide susceptibility mapping: ELSUS Version 2. *Journal of maps*. 14(2): 97-104.

Assessment of risk scenarios to support landslide studies

Giovanna Capparelli^{(1)*}, Pasquale Versace⁽¹⁾, Danilo Spina⁽¹⁾

1) University of Calabria, Department of Computer Engineering, Modeling, Electronics and Systems (DIMES), Ponte Pietro Bucci, cubo 41/B – 87036 Rende, Italy

Abstract The definition of risk scenarios that are as reliable and detailed as possible is a primary objective to increase the effectiveness of civil protection actions in the alert phases, together with adequate self-protection actions. In the workflow that characterizes integrated emergency management systems, risk scenarios are an essential element for connecting the information coming from the early warning systems and the actions at responding to the need of safeguard human life. Nowadays, the availability of high-resolution terrain data allows access to an almost precise knowledge of the territory, forgetting purely topographical approaches whose application over a vast domain has proven impractical or misleading. This translates into new potential in the definition of event scenarios and risk scenarios. In reality, alongside highly advanced pre-announcement and monitoring systems, there are often barely outlined event scenarios and mostly qualitative risk scenarios, and therefore lacking the effectiveness they should and could have. To achieve a level of detail that effectively supports the activities in the intervention phase, it is necessary to aim, even more decisively, towards a quantitative analysis of the risk deriving from hydrogeological phenomena. Event scenarios, as is known, describe the phenomena that can occur, quantitatively define their magnitude, locate the vulnerable areas, i.e. those that can be affected by the event. Landslide phenomena, for example, are distinguished by kinematics, the type and size of the material involved, the speed of movement, the impact energy.

The risk scenarios, therefore, describe the foreseeable effects of the events identified and described by the event scenarios on the exposed elements. In general, in risk analysis, vulnerability is considered invariant or, in any case, is only assessed quickly, whereas it is almost always decisive in defining the level of risk to which a vulnerable area is subject.

In this work we propose a simplified vulnerability assessment method for people exposed to fast moving landslides. The procedure is very flexible because it can be developed at different levels of detail and at different spatial scales depending on the size of the objects involved. The proposed approach has some similarities with other methods used in the vulnerability assessment to other natural risks, as earthquake and floods and, therefore, it can be adopted for multi-risk analyses. Referring to a case study, it shows the advantages and

potential of the approach for a high-resolution landscape mapping at reach scale to support landslides studies.

Keywords risk assessment, vulnerability index, integrated approach, non-structural measures

Introduction

Risk scenarios describe the foreseeable effects of events identified and outlined by event scenarios on exposed elements. Various models for the quantitative assessment of risk have been proposed in the literature. Generally, the factors determining risk depend on the severity of the phenomenon (magnitude), the extent of exposed elements, and their ability to withstand the event (vulnerability). A key element is the definition of vulnerability to natural risks, expressed on a scale from 0 (no damage) to 1 (total loss). In technical literature, the concept has many connotations depending on the research perspective (Dow, 1992; Cutter, 1996). There are three fundamental principles in vulnerability research: "Vulnerability as hazard exposure" - the identification of conditions that make people or places vulnerable to extreme natural events (Burton, Kates, and White, 1993; Anderson, 2000); "Vulnerability as social response" - the assumption that vulnerability is a social condition, measuring social resistance to events, resilience, and recovery (Blaikie et al., 1994); "Vulnerability of places" - the integration of exposure and social resilience with a specific focus on particular places or regions (Kasperson and Turner, 1995).

Similarly, it has been widely recognized that vulnerability can have three dimensions. Economic, referring to potential economic damage as a risk to production, distribution, and consumption (Comfort et al., 1999). Social vulnerability recognizes the vulnerability of individuals, emphasizing their coping ability. Social vulnerability is related to various characteristics of human beings (Blaikie et al., 1994). The ecological dimension of vulnerability acknowledges ecosystem or environmental fragility. According to Williams & Kaputcka (2000), vulnerability can be seen as the "inability of an ecosystem to tolerate stress factors over time and space," emphasizing the importance of understanding how different types of natural environments cope or adapt differently. Cutter et al. (2000) has integrated various elements contributing to the overall vulnerability of places, referred to as the "Hazard of place model of Vulnerability."

The new definition of vulnerability, apart from minor oscillations as indicated, remains fundamentally unchanged at the United Nations until the most recent formulation (UNISDR, 2016), where it is clearly emphasized that vulnerability is a context and a factor that, in relation to hazards, contributes to risk. To cite a few, vulnerability represents: "Conditions determined by physical, social, economic, and environmental factors or processes that increase the community's susceptibility to the impact of hazards (UNISDR, 2005)"; "The characteristics and circumstances of a community that make it susceptible to the damaging effects of a hazard (UNISDR, 2009)." The ability to measure vulnerability is an essential prerequisite for reducing the risk of disasters and for adaptation strategies, but it requires the capacity to identify and better understand the various vulnerabilities that largely determine the risk.

The complexity of the vulnerability concept itself requires the reduction of potentially collected data to a series of important indicators and criteria that facilitate the estimation of vulnerability. The World Conference on Disaster Reduction (WCDR) held in Kobe, Japan, in 2005, emphasized the need to develop vulnerability indicators. The final document of the WCDR, the Hyogo Framework for Action 2005–2015 (UN, 2005), emphasizes that it is important to: "develop systems of disaster risk and vulnerability indicators at the national and sub-national levels that allow decision-makers to assess the impact of disasters on social, economic, and environmental conditions and to disseminate the results to decision-makers, the public, and the at-risk population" (UN, 2005, p. 9).

The following describes the methodological criteria for the quantitative identification of risk scenarios, considering people as the sole element at risk. From an existing literature analysis, the main factors contributing to the vulnerability of individuals and the methods used for quantitative assessment have been identified.

From the analysis of the developed survey, a procedure called EVIL (Evaluation of Vulnerability to Inundations and Landslides) has been defined, which was applied to a case study "Frana di Gimigliano," producing the vulnerability map and the risk scenarios map. The following provides a detailed description of the EVIL procedure, in its version dedicated to landslide phenomena, and the application to the Gimigliano case study.

Description of the EVIL method for landslide risk assessment

Object Identification

The object is defined as the minimum territorial element of reference: for it, intrinsic characteristics (position, geometric features, conditions of occupants, etc.) and contextual conditions (event characteristics, environmental conditions, etc.) are considered constant.

The level of detail intended in the analysis influences the choice of objects for which to define the risk index and the attributes that will be used for its estimation. With fixed times and available resources, the smaller the scale of the investigation, the larger the size of the objects considered, and the lower the level of detail of the result. Conversely, the larger the scale of the investigation, the smaller the size of the identified objects, and the greater the achievable level of detail. Developing at the maximum expected level of detail, the objects considered as the minimum unit of reference can belong to one of the following categories: Buildings (residential, productive, commercial, directional/tertiary, tourist/receptive, services, etc.); Short stretches of roads and railway network (highways, main rural roads, secondary rural roads, urban arterial roads, neighborhood urban roads, and local roads); Individual portions of open spaces (paved areas in general, including sidewalks, parking lots, courtyards; urban green areas and agricultural green areas, pastures, wooded areas, uncultivated areas, etc.).

Estimation of Vulnerability Index

The Vulnerability Index (IVI), expressed for each of the objects into which the territory is divided, is assessed using several factors, F_i ($i= 1, 2, \dots, m$), which indicate the main elements contributing to determining the vulnerability of an individual object. In the EVIL procedure for landslides, m is assumed to be 4. Its value is given by:

$$IVI = \sum_i F_i W_i \quad [1]$$

Where W_i is the weight of factor F_i and is between 0 and 1. It must also be:

$$\sum_i W_i = 1 \quad [2]$$

For the estimation of F_i , certain attributes A_{ij} ($j= 1, \dots, n_i$) are used to characterize it. The value of F_i is given by:

$$F_i = \sum_j V(A_{ij})w_{ij} \quad [3]$$

Where $V(A_{ij})$ is the value of attribute A_{ij} , which is between 0 and 1, w_{ij} is the weight of attribute A_{ij} , and it can also take values between 0 and 1. Additionally, it must be:

$$\sum_j w_{ij} = 1 \quad [4]$$

Therefore, both F_i and IVI are bounded between 0 and 1. For the estimation of $V(A_{ij})$, EVIL uses the following criteria: $V(A_{ij})$ is a discrete variable that can take only a limited number of values predetermined by the class to which the attribute belongs; the assignment of an attribute to a class is based on indicators that can be numerical when there is a procedure to measure them or descriptive when there are no concrete procedures applicable for their measurement. In the case of numerical indicators, a rule is

defined for each attribute that allows, based on the values assumed by the indicators, to assign A_{ij} to a class and consequently assign the corresponding value to $V(A_{ij})$ for that class. In the case of descriptive indicators, each class is characterized by a concise description that uniquely places the analyzed indicator in a specific class and assigns the attribute the corresponding value.

If an object is affected by multiple phenomena, this calculation must be repeated for each potentially harmful phenomenon to the occupants of that object. The vulnerability of the object, in this case, will be the maximum calculated vulnerability. The factors, attributes, indicators, and assignment criteria that characterize the EVIL method for landslides are listed below.

The four considered factors are: F1: Event characteristics, F2: Characteristics of people, F3: Position, and F4: Possibility of escape and rescue.

For each category of objects (buildings, roads and railway network, open spaces), these factors do not change even though their weights may differ. However, within each category of objects, the attributes that define these factors are slightly different. The weights assigned to the various factors are reported in Tab. 1

Table 1 List of factors and their respective weights.

Fattore F_i		Valore peso W_i
Event characteristics	F1	0,35
Characteristics of people	F2	0,2
Position	F3	0,35
Possibility of escape and rescue	F4	0,1

Estimation of the Crowding Index

The estimation of the crowding index assumes that the population affected by landslide events is the one present in the at-risk areas at the time of the event and is referred to as PP (present population). PP is divided into two components: RP (resident population present) and NRP (non-resident population present). Documents provided by ISTAT (ISTAT, is the National Institute of Statistics and is a public research body. It has been present in the country since 1926 and is the main producer of official statistics to support citizens and public decision-makers), allow for the estimation of PR (resident population) broken down and divided at the level of census sections. From this, RP and NRP can be estimated:

$$\begin{cases} RP = \alpha PR \quad (0 \leq \alpha \leq 1) \\ NRP = \beta PR \quad (\beta \geq 0) \end{cases}$$

Therefore:

$$PP = (\alpha + \beta) PR$$

Usually, $\alpha=1$ and $\beta=0$, so $PP=PR$. However, in some cases, PP and PR can be different, for example, in summer in large cities, $PP < PR$, in tourist areas $PP > PR$.

At the time of the event, PP can be in buildings (PPE), on the streets (PPS), in open areas (PPA), or in other

spaces different from the previous ones (special categories: railway, hospitals, schools, barracks). For example, people (PPF) on trains in the vulnerable area and at the station can be considered. PPE, PPS, PPA are usually expressed as fractions of PP; PPF is expressed as the number of people. The distribution of the population can take different configurations depending on the period in which the event occurs, for example:

A. Average daytime configuration, in which a substantial part of the population is expected to be inside a building (home, workplace, commercial activity, school, etc.). The remaining part will be distributed outside a building, moving between various buildings by car, train, or on foot. B. Nighttime configuration, in which a majority percentage of the population (compared to configuration A) will be inside their homes, and only a small fraction will be outside. C. Special event configuration, in which a representative configuration of presence in the area is proposed, including the resident population PR, the population on the railway network PPF, and also non-resident people PNR (this extraordinary presence may be due to events, attractions, tourism, etc.).

Calculation of the Risk Index

The calculation of the risk index divides the Vulnerability Index (IVI) into three classes:

- V_1 (Moderate Vulnerability): per $0 < IVI \leq 0.5$
- V_2 (Medium Vulnerability): per $0.5 < IVI \leq 0.75$
- V_3 (High Vulnerability): per $0.75 < IVI \leq 1$

The number of occupants for each object has been discretized as follows:

- IF1 – Modest Crowding: 0 – 5 people
- IF2 – Medium Crowding: 5 – 10 people
- IF3 – High Crowding: 10 – 15 people
- IF4 – Very High Crowding: >15 people

The vulnerability and crowding classes have been set considering the values found for different objects in the specific case, providing a sufficient representation of the various classes. Once the three vulnerability classes and the four crowding classes are defined, the Risk Index for People's Safety (IRIP) is calculated using the following matrix (Fig. 1):

	V1	V2	V3
IF1	IRIP1	IRIP1	IRIP2
IF2	IRIP1	IRIP2	IRIP3
IF3	IRIP2	IRIP3	IRIP4
IF4	IRIP3	IRIP4	IRIP4

Figure 1 Index Risk Matrix for People's Safety (IRIP)

Application

Identification of risk scenario for the study case.

The procedure was applied for the landslides occurred in Gimigliano village, in Calabria region, South of Italy (Fig. 2). The resident population amounts to 3035 inhabitants as of January 1, 2022 (source: ISTAT), with 1682 residing in the central area, while the remaining residents are distributed among the near zones. From a morphological perspective, the municipality has a predominantly hilly terrain (about 40%) and mountainous terrain (about 60%).

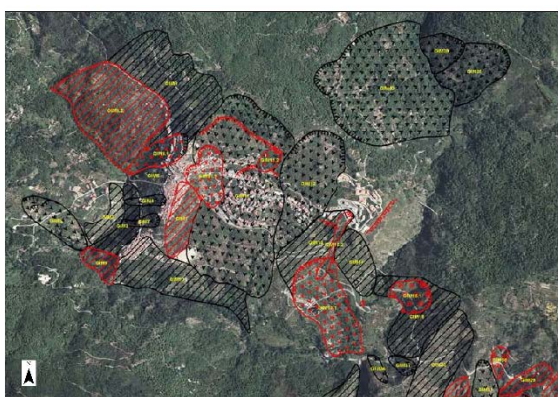


Figure 2: Inventory map of unstable inhabited centers, Municipality of Gimigliano - Calabria Region - Italy. Source: Extract basin plan for the iderogological structure (Legislative Decree 180/98) - Regional Basin Authority - Department of Public Works and Water

The entire territory of Gimigliano is affected by numerous landslide phenomena, characterized not only by different mechanisms but also by different states, distributions, and styles of activity. This is a consequence of an extremely complex geological framework involving lithological units that have undergone various deformation phases.

Among all instability phenomena affecting the territory, the attention has been focused on the landslide, which involves the recently developed inhabited center. A detailed geomorphological study (MUTO, 2012b) revealed a highly complex situation, characterized by the presence of minor landslide movements that overlap and, in the central part, cover the main landslide. Some of these phenomena are characterized by a complex and sometimes composite kinematic style.

The main landslide extends for a width of about 800 meters and a length of about 1,300 meters, ranging between elevations of 820m and 420m. It features a pronounced main scarp, a well-defined right flank, and a less evident left flank, partly overlapped or covered by other landslide phenomena.

The mid-upper portion of the slope is affected by minor landslides showing translational sliding kinematics and, in some cases, rotational components. Other landslide phenomena exhibit complex kinematics. The

estimated depth is greater than 20 meters in the central part, showing signs of slow activity and deformation.

The movement is active with speeds falling within slow movements. The depth data, although the landslide body consists of a heterogeneous mass, indicate the existence of a single sliding surface for the main Gimigliano landslide. Almost the entire inhabited center is affected by this complex and articulated system of landslide phenomena, showing more or less evident signs on structures.

For developing the analysis of the degree of vulnerability and risk in the territory, a deep-seated phenomenon has been considered as a large unitary accumulation with a single sliding surface set at a depth of over 50 m. It exhibits characteristics of rock sliding, with a constant activity distribution; five superficial phenomena; two fast superficial flows; a phenomenon identified as rock collapse and/or debris avalanches.

For the application of the method, after identifying and selecting the phenomena to be addressed, their intensity was evaluated—their capacity to cause damage to property and people—through a geomorphological approach (PON LEWIS). Each phenomenon was characterized with the attributes listed in Tab. 2.

Table 2 Attributes necessary for estimating the intensity of landslide phenomena

Field	Content
Code	Progressive numeric unique identifier of the event
Typology	Indication of the type of landslide movement
Activity	Indication of the landslide activity status
Area	Surface affected by the instability expressed in m2
Depth	Estimation of the thickness of the displaced mass
Volume	Estimation of the volume of material involved in the movement
Crown	Crown length
Landslide face	Length of the landslide front
Intensity	Estimation of landslide intensity
Speed	Estimation of landslide speed
Frequency	Estimate of the probable frequency of the landslide

Once the phenomena have been characterized, the geometric severity index is estimated. For lateral spreading, debris flows and/or earth flows, complex landslides, and rock slides, the geometric severity index is estimated based on the landslide surface area (SUP), crown length (COR), landslide front length (FRO), thickness (SPE), and the volume of material involved in the movement (VOL). For rockfalls and/or topples, the dimensions of the fallen or potentially mobilizable blocks are evaluated (DIM).

After determining and classifying the parameters, the geometric severity index is assessed for each landslide by intersecting the five parameters (SUP+COR+FRO+SPE+VOL). The geometric severity index is divided into five classes ranging from very low to very high. The intensity of a landslide defines the impact

of the event on the territory, categorizing it into three intensity classes (low, medium, and high).

For landslides *latu sensu*, the intensity (INF) is evaluated by combining the geometric severity index (ISG) with the speed of the mapped landslide phenomena. In the case of rockfalls and/or topples, for the intensity estimate (INR), the combination of the dimensions of the fallen blocks with the speed is carried out.

The proposed scheme has been applied to individual identified phenomena, which have been considered as possible scenarios. Material involved, type of movement, activity status, surface area, maximum depth of the sliding surface, crown length, and front length were evaluated. The estimation of landslide volume was performed using geological cross-sections of individual landslide bodies. The speed of deep landslides and superficial landslides was derived by assessing the results of inclinometer readings, surface topographic monitoring, and data from satellite interferometry. For rockfalls/debris avalanches and fast superficial flows, the classification of CRUDEN & VARNES (1996) was used.

Once the individual attributes were evaluated and classified, it was possible to calculate the geometric severity index (ISG) first and then the intensity (INF/INR) of the phenomena.

Identification of the Objects

The identified objects belong to one of the following categories: buildings, roads/railway network, and open spaces. For this case study, the objects have been primarily identified based on cartographic data, using information represented on the map at a scale of 1:5000 (CTR).

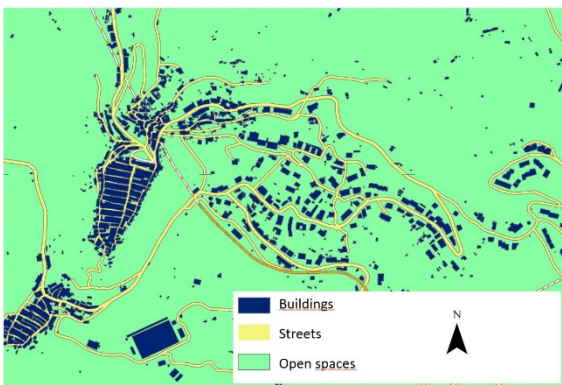


Figure 3 – objects identified in the study area, grouped by category.

Assessment of Vulnerability Index

The Vulnerability Index (IVI) was assessed using the factors (Fi) outlined in the EVIL procedure. For each object category (buildings, roads/railway network, open spaces),

the following factors were considered: F1 Event Characteristics, F2 People Characteristics, F3 Location, and F4 Escape and Rescue Possibility.

The vulnerability index was calculated for buildings using the attribute values listed below. Additionally, this calculation was repeated for various identified landslide phenomena.

The IVI is calculated by applying the procedure described above, summarized by the mathematical expression number 1. Below are the attributes used for each factor (Tab. 3).

Table 3 Attributes used for the estimation of the four factors.

Fattore	Attributo
F1 - Event characteristics	Intensity of the event
F2 - Characteristics of people Position	Age
	Physical conditions
F3 - Possibility of escape and rescue Event characteristics	Relative position
	Degree of protection
F4 - Characteristics of people	Length of the escape route
	Extension of the area involved
	Effectiveness of the warning system

After calculating the IVI value for each object and for each phenomenon included in the reference event scenarios, each object was assigned the maximum vulnerability value obtained. An example of the spatial distribution of the vulnerability index for the buildings category is shown in Fig. 4.

Estimation of Crowding Index

The crowding index (IF) was calculated as explained, particularly for risk calculation, considering the average daytime crowding configuration A as an example. In this configuration, the total population present coincides with both the resident population (PR) and the population on the railway network (PPF). In this setup, a significant portion of the population is expected to be inside a building (home, workplace, commercial activity, school, etc.). The remaining part will be distributed outside a building, moving between various buildings by car, train, or on foot. The distribution of the crowding index (IF) for the buildings category is shown in Fig. 4.

Risk Index Estimation

Once the three vulnerability classes and four crowding classes were defined, the risk index for people's safety (IRIP) was calculated. Fig. 4 illustrates the distribution of the risk index for the buildings category..

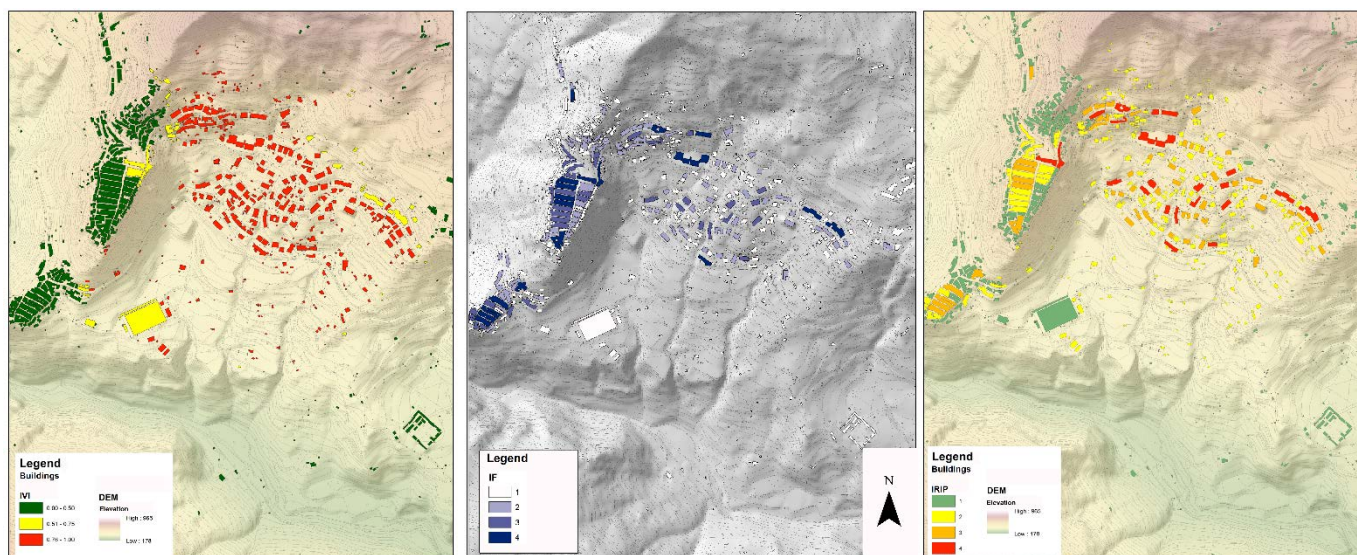


Figure 4 distribution of the vulnerability index (maximum), the IF crowding index and the risk index for the safety of people (IRIP) for the "buildings" object category”

Conclusion

Risk scenarios are strongly connected to the level of detail in the event scenarios. Moreover, for the estimation of various indicators contributing to the cascading assessment of attributes and their related factors, different types of data can be utilized. In some cases, this involves simply consulting existing databases (ISTAT), in others, it requires the development of activities for consulting and interpreting existing documents (thematic cartography, technical documents), and in still others, it involves the development of targeted investigations and studies (specific surveys and studies). Therefore, where detailed information is available, the EVIL procedure can be applied for the construction of the corresponding risk scenario. The procedure described is a preliminary application for the construction of risk scenarios. This procedure, or rather, the EVIL method, as described, is subjected of further future developments. Even the logical framework for assessing the vulnerability index is largely similar, the update involves some of the indicators incorporated into the methodology with the aim of using indicators based on an objective and scientifically grounded assessment.

Acknowledgements.

These are a preliminary results of long work into research carried out with great dedication by the late Prof. Emeritus Pasquale Versace, to whom we would like to extend our heartfelt thanks for the path taken so far.

References

- Anderson, M. B. (2000). Vulnerability to Disaster and Sustainable Development: A General Framework for Assessing Vulnerability. Pp. 11–25 in R. Pielke, Jr. and R. Pielke Sr., eds. *Storms* (Vol. 1). London: Routledge
- Blaikie, P., T. Cannon, I. Davis, and B. Wisner. (1994). *At Risk: Natural Hazards, People's Vulnerability, and Disasters*. London: Routledge
- Burton, I., R. W. Kates, and G. F. White. (1993). *The Environment as Hazard* (2nd ed.). New York: Guildford
- Cutter, S. L. (1996). Vulnerability to Environmental Hazards. *Progress in Human Geography* 20(4), 529–39
- Dow, K. (1992). Exploring Differences in Our Common Future(s): The Meaning of Vulnerability to Global Environmental Change. *Geoforum* 23(3), 417–36
- ISTAT. <https://www.istat.it/it/censimenti/popolazione-e-abitazioni>
- ISTAT. [https://www.istat.it/it/benessere-e-sostenibilit%C3%A0/la-misurazione-del-benessere-\(bes\)/il-rapporto-istat-sul-bes](https://www.istat.it/it/benessere-e-sostenibilit%C3%A0/la-misurazione-del-benessere-(bes)/il-rapporto-istat-sul-bes)
- Landslides Types and Processes. Cruden D.M., Varnes D. J. (1996) *Landslides: Investigation and Mitigation*. Transportation Research Board Special Report 247. Turner A.K. & Schuster R.L.(Eds.). National Academy Press, WA, 36-75
- MUTO F. (2012b) - “Studi ed indagini geologiche, geotecniche, idrologiche ed idrauliche nel Comune di Gimigliano” - Codice Intervento CZ/3862/1/008 - A-G4 - Indagine Geomorfologica.
- MUTO F. (2015) – “PON LEWIS, Deliverable WP 1.1– Linee guida per l’identificazione di scenari di rischio/Parte seconda”. Resp. Scientifico Prof. Pasquale Versace
- R. E. Kasperson, and B. L. Turner, eds. (1995). *Regions at Risk: Comparisons of Threatened Environments*. Tokyo: United Nations University Press
- UN/ISDR (International Strategy for Disaster Reduction) (2004) *Living with Risk: A Global Review of Disaster Reduction Initiatives*, Geneva: UN Publications

Regional landslide susceptibility assessment: case studies from Greece

Katerina Kavoura⁽¹⁾, Natalia Spanou^{(1)*}, Emmanuel Apostolidis⁽¹⁾, Panagiota Kokkali⁽¹⁾

1) Hellenic Survey of Geology and Mineral Exploration (HSGME), Greece, (spanou@igme.gr)

Abstract In this study, regional-scale landslide susceptibility mapping was conducted for two well-known landslide-prone regions in Greece, employing both qualitative and quantitative methods. The geological settings, particularly the variety of geological units, was the key difference between these areas. The Analytic Hierarchy Process (AHP) and Frequency Ratio (FR) methods were employed in both cases for six common-used predisposing factors (lithology, slope, land use, distance from faults, distance from hydrographic network and road density). The Landslide Susceptibility Index (LSI) was used for mapping landslide susceptibility level, with validation performed via ROC curves. Thus, the output maps generated by this procedure were verified by comparison with known landslides not used for training the models (prediction rates) or known landslides with an equal number random set of points free of landslides (success rates). The primary aim of this work was to evaluate the importance of conditioning factors in predicting landslide occurrences using the mentioned models. According to the results, in both areas the importance of different predisposing factors seems to vary in shaping the landslide susceptibility level. This research recognizes the critical role played by scale for landslide susceptibility modelling. Therefore, part of the aim of this work is to discuss the minimum, yet sufficient data required to develop more versatile, generalized regional susceptibility models (medium scale), that can then be used as indicators for national scale (small scale) analysis and in the exploitation of research results by local stakeholders and Civil Protection authorities.

Keywords landslide inventory, susceptibility assessment, Greece, LSI, ROC curves

Introduction

Landslide susceptibility assessment is a key component of landslide hazard and risk management, which can help civil protection authorities to establish specific landslide hazard reduction programs and strategies. Over the last three decades many researchers around the world have applied plenty of qualitative or quantitative approaches for landslide susceptibility evaluation. Regional scale landslide susceptibility maps (<1:50000) portrays areas with different levels of threat to failure. This information can be used to establish land use plans, development activities and patterns of building regulations (SafeLand 2010). Landslide susceptibility mapping relies on a rather complex knowledge of slope movements and their

controlling factors. The reliability of landslide susceptibility maps mainly depends on the amount and quality of available data, the working scale, and the selection of the appropriate methodology of analysis and modeling (Baeza and Corominas 2001).

Due to the variety of information and the abundance of data provided, some interesting outcomes were reached, concerning the characteristics of the landslides, after applying simple statistical analysis.

Study areas

Corfu island

The island of Corfu in the Ionian Sea, covering an area of about 590 km². The morphological relief of the island is more pronounced in the northern part due to its geological and tectonic structure. Concerning the geology, formations from the Ionian geotectonic zone (mainly limestone), as well as Neogene and Quaternary formations, contribute to the geological structure of Corfu. The geological structure is characterized by intense folded structures, reverse faults, large transverse ruptures with a significant horizontal component, and phenomena of uplifting movements. These geotechnical conditions have increased the susceptibility to landslides, with specific types including rotational landslides, rockfalls, and land subsidence.

Landslide phenomena in Corfu mainly occur in Neogene sediments, accounting for over 65% of the occurrences.

Evritania region

Evritania region is situated in central Greece, encompassing the southern region of the Pindos Mountain range, with an area spanning 1870 km². The area's tectonic activity is notable, primarily attributed to the presence of the Pindos Mountain range, characterized by extensive folds and successive thrusts. This tectonic activity, coupled with neotectonic processes and lithological factors, has contributed to the development of an intense relief and a complex hydrological network.

The geological structure of the region is predominantly composed of formations from the Olonos-Pindos geotectonic zone, along with Quaternary formations. Landslide occurrences are predominantly associated with flysch formation and they are mostly in the completely weathered zone.

Methods

The adopted methodology consists of four stages. In particular, the first stage gathers predisposing factors, usually used to literature, which deals with landslides activation. In addition, the appropriate landslide inventories were prepared for each study area. Next, the landslide susceptibility assessment was carried out with AHP both FR methods. The overall susceptibility of an area was determined by synthesizing all the factors using an algebraic approach, resulting in a Landslide Susceptibility Index (LSI) used to map the level of landslide susceptibility. Finally, the validation and the evaluation of results achieved in the previous stage was conducted by ROC curves.

AHP method

The application of the Analytical Hierarchy Process (AHP) method, developed by Saaty (1977), has been used by many authors worldwide, as a multi-criteria decision-making method. It involves making binary comparisons of factors within a complex problem.

After constructing a hierarchical representation of the problem, the next steps involve pairwise comparisons of factors and subfactors using a nine-point scale in a matrix table. The scale values range from 1 (equal importance) to 9 (extremely stronger importance), with intermediate values such as 2, 4, 6, and 8 indicating intermediate levels of importance (Saaty, 1977). Each factor is assessed in relation to every other factor using

values from 1/9 to 9. Subsequently, the relative weights for each factor and subfactor in the decision hierarchy are estimated.

The consistency ratio (CR) is then calculated to validate the AHP results and prevent arbitrary choices in the matrix. The CR is considered valid if it is equal to or less than 0.1 (10%) (Saaty, 1978). The equation for calculating the consistency ratio is:

$$CR = (CI/RI) * 100 \quad [1]$$

where RI is the random consistency index and CI is the average consistency index calculated as:

$$CI = (\lambda_{max} - n) / (n - 1) \quad [2]$$

where λ_{max} is the maximum eigenvalue of the comparison matrix, and n is the number of factors.

FR method

The Frequency Ratio (FR) model, as a statistical approach, based on the analysis between distribution of landslides and each landslide-related factor, to reveal the correlation between landslide locations and the factors in a specific area (Lee and Pradhan 2007). Therefore, the frequency ratios of each factor class were calculated from their relationship with landslide events. According to the method, the number of landslides in each class is evaluated and the frequency ratio for each factor class is found by dividing the landslide ratio by the area ratio (Lee and Talib 2005). If the ratio (FR) is greater than 1, then the relationship between a landslide and the factor's class is strong while if ratio is less than 1, the relationship is weak.

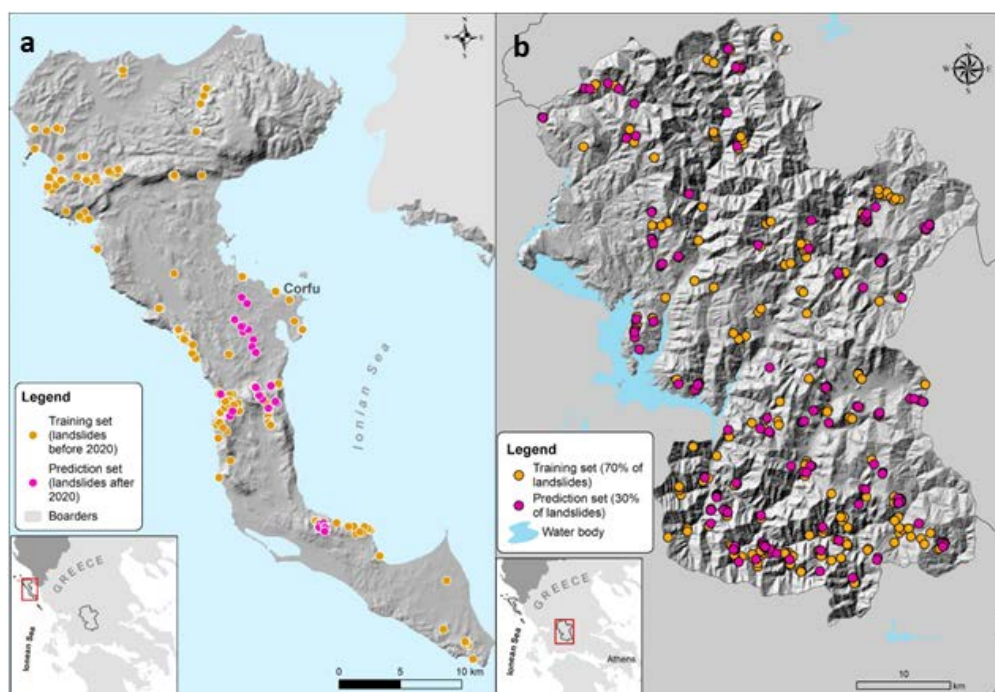


Figure 1 Landslide inventory maps of a) Corfu island and b) Evritania region.

Input data

Six commonly used predisposing factors were chosen reflecting general natural settings in the study areas. Initial

landslide predisposing factors considered were as follows: (a) Lithology is based on the engineering geological mapping scale of 1:50000, (b) Slope is calculated from the DEM of Greek Cadastral with a pixel size of 50 m, (c) Land use is at an original scale of 1:100000 provided by Land

Corine 2018, (d) road density map (km/km²) based on Open Street Map road network, (e) distance from faults in meters, as they have mapped on the relevant 1:50000 Hellenic Survey of Geology and Mineral Exploration (HSGME) geological map sheets of these areas and (f) distance from hydrographic network in meters. Therefore, all the thematic layers for each area, Corfu island and Evritania region, were prepared in 1:50000 scale.

Landslide inventory

Using the National Database of Landslides provided by HSGME and conducting extensive field surveys, ensured the accuracy of landslide spatial distribution and captured their distinctive features. More precisely, in Corfu island 203 landslides are recorded since 1959 while in Evritania region 483 since 1963. However, a second inventory independent of the main one was mandatory to be generated, under the purpose of verification. Here, the secondary landslide inventories were drawn up as proposed by Remondo et al. (2003). Thus, at Evritania region the initial inventory was randomly split into two groups, one for the susceptibility analysis (70% of the total) and one for validation (30% of the total). In the case of Corfu island, the analysis was made using landslides

activated in a certain period (before 2020), and validation was performed by means of landslides that occurred in a different period (after 2020) (Figure 1).

Results

Utilizing AHP in both areas, the calculation commenced with pairwise comparisons of all possible pairs of factors in a matrix based on expert knowledge. Subsequently, values and weights were determined, and in the final step, the consistency index (CI) and consistency ratio (CR) were calculated. Based on the results of the hierarchy process analysis (Table 1), the landslide susceptibility map for each area using AHP model was constructed using the following equations (Figure 2a and Figure 3a):

$$LSI_{Corfu} = 0.037 * Landuse + 0.328 * Lithology + 0.303 * Slope + 0.089 * Road\ density + 0.095 * Distance\ from\ rivers + 0.148 * Distance\ from\ faults \quad [3]$$

$$LSI_{Evritania} = 0.045 * Landuse + 0.271 * Lithology + 0.353 * Slope + 0.085 * Road\ density + 0.098 * Distance\ from\ rivers + 0.147 * Distance\ from\ faults \quad [4]$$

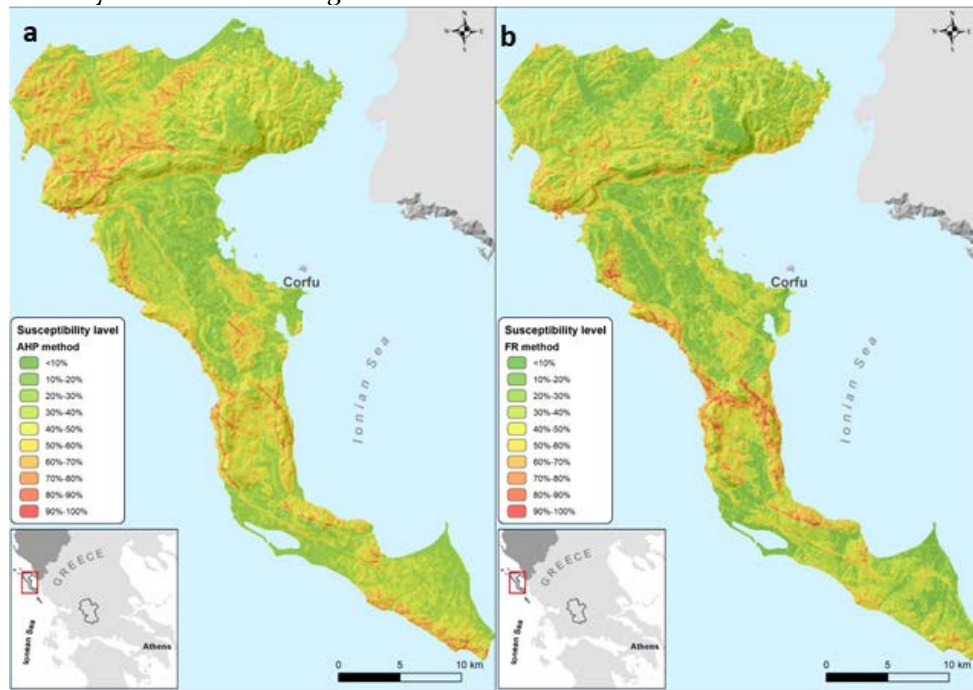


Figure 2 Landslide susceptibility map of Corfu island a) AHP method and b) FR method

Table 1: Relative weights from pairwise comparison with AHP method in both areas.

Factors	Weights	
	Corfu	Evritania
Slope	0.303	0.353
Lithology	0.328	0.271
Land use	0.037	0.045
Road density	0.089	0.085
Distance from faults	0.148	0.147
Distance from rivers	0.095	0.098

For Corfu, the CR was found to be 0.056, while for Evritania, it was 0.034. For both cases, CR values are considered valid as they are less than 0.1. Therefore, the weights determined through the AHP are accepted for use in landslide susceptibility mapping.

It is noted that, at Corfu island LSI_{AHP} ranges between 0.04 to 0.32 and for Evritania region LSI_{AHP} takes values between 0.06 to 0.34.

To simplify the legibility and the comparison between the landslide susceptibility maps, the LSI range was subdivided into susceptibility zones of 10%. The lower the percentage the lower the susceptibility level.

In contrast to AHP method, FR method requires a training data set to compute the weights for each factor and its classes. Training sets as well as test sets were generated as described above. The FR model was applied to define weights for each factor, using the ratio of the percentage of landslides in a class of the selected factor to the percentage of the area of this class in the study area.

Finally, the Landslide Susceptibility Index was used for landslide susceptibility mapping based on the weights were derived from the bivariate statistical analysis (Figure 2b and Figure 3b). Here, the LSI_{FR} for Corfu island ranges between 1.7 to 16.2 while in Evritania region between 2.2 to 18.

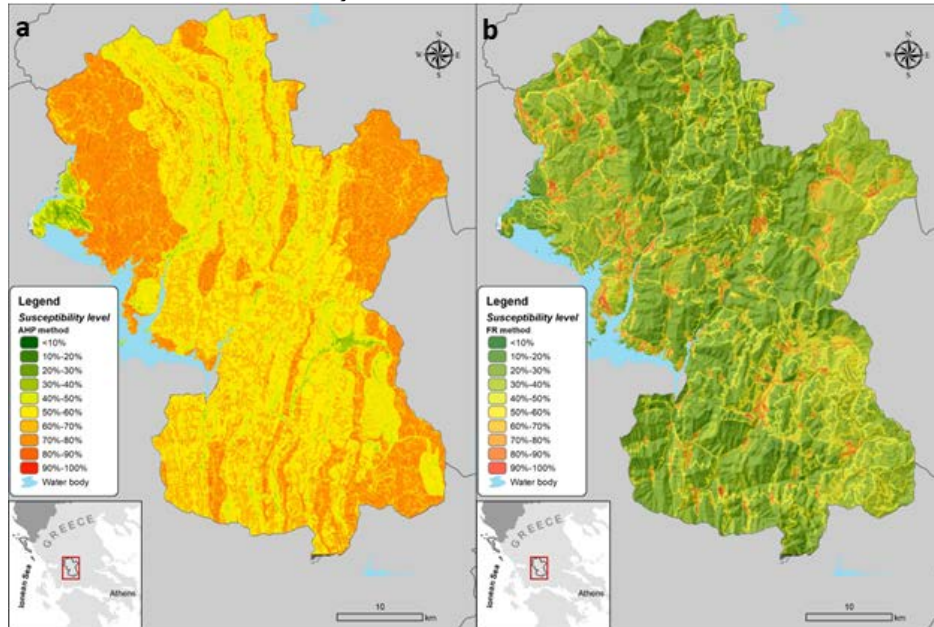


Figure 3 Landslide susceptibility map of Evritania region a) AHP method and b) FR method

Model validation and evaluation

An important stage on landslide susceptibility assesmenet is to evaluate the effectiveness of the produced landslide susceptibility map. For this purpose, receiver operating characteristic (ROC) curves are used, firstly for checking the reliability of the proposed model (success rate curves) as well as to check the ability of the model to pinpoint landslide-prone areas (prediction rate curves).

The accuracy of the model is checked for each area, using the the training set and an equal number random set of points free of landslides. This was repeated for the validation set of landslides in order to find if these independent landslide occurrences were correctly adapted in different susceptible areas.

Based on these, comparing the methods, the landslide susceptibility maps of Corfu island gives $AUC=0.737$, $std=0.026$ for AHP method and $AUC=0.893$, $std=0.017$ for FR method (Figure 4a). Interestingly, the prediction rate for FR method is characterized by $AUC=0.906$ while for AHP method the results are similar as before with $AUC=0.706$ (Figure 4b).

In Evritania region, the success rate results showed that the AUC was 0,499 ($std=0.023$) for AHP method and 0,872 ($std=0,014$) for FR method (Figure 5a). Furthermore, the prediction rate results were 0.429 and 0.874 respectively (Figure 5b).

Discussion

The landslide susceptibility analysis at the regional level defines areas with high susceptibility and allows the focus for a detailed local research and urban and regulation plans for areas of interest.

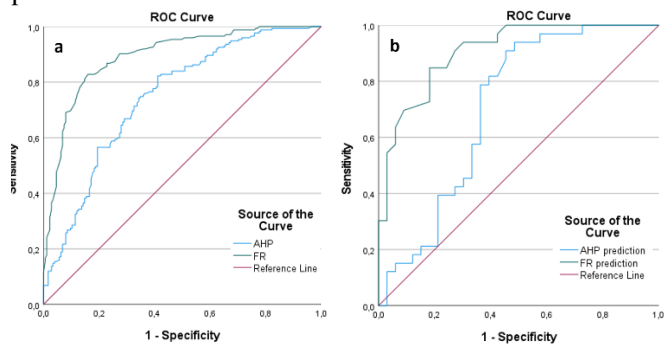


Figure 4 ROC curves for Corfu Island a) Success rate b) Prediction rate

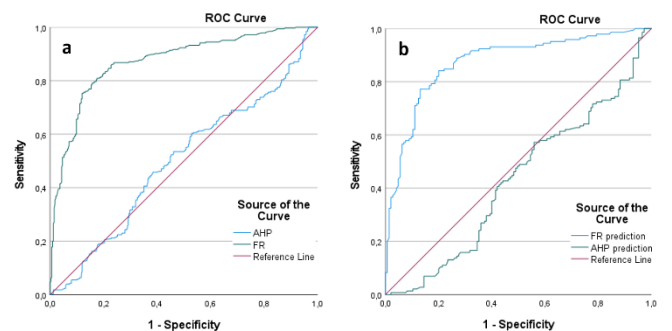


Figure 5 ROC curves for Evritania region a) Success rate b) Prediction rate

According to the ROC analysis, it is seen that both the success rate and prediction rate curve show almost similar result in any case. However, FR model seems to have better performance than AHP model. A comparison of the two susceptibility maps of Corfu island reveals that both highlight the most susceptible areas such as the central and the western part of the island, where annually suffer by landslides. On the other hand, landslide susceptibility analysis with AHP and FR methods in Evritania region differs a lot. Comparing the relevant ROC curves, the AHP method with $AUC < 0.7$ is not able to sufficiently determine susceptibility levels. However, the FR model showed reasonably good accuracy in predicting the landslide susceptibility of the road section and the settlements. Nevertheless, in Evritania region the results are vague has to do maybe with the fact that, a) the majority of landslides in database are recorded along the road and into settlements, b) large mountainous areas into the region is difficult to access and c) the experts were based mainly on an geological point of view to suggest the factors weights.

Acknowledgements

This study was conducted in the framework of the Operational Program entitled "Competitiveness, Entrepreneurship and Innovation (2015-2020), Project «Studies and researches support to the energy sector, industry and entrepreneurship», Sub-Project «Susceptibility assessment of landslides in the Greek territory - Volcanic study and risk assessment», financed by the European Regional Development Fund.

References

- Baeza C, Corominas J (2001) Assessment of shallow landslide susceptibility by means of multivariate statistical techniques. *Earth Surface Processes and Landforms*, 26 (12):1251-1263. DOI: 10.1002/esp.263
- Lee S, Pradhan B (2007) Landslide hazard mapping at Selangor, Malaysia using frequency ratio and logistic regression models. *Landslides*, 4 (1):33-41. DOI: 10.1007/s10346-006-0047-y
- Lee S, Talib A T (2005) Probabilistic landslide susceptibility and factor effect analysis. *Env Geol* 47:982-990. DOI: 10.1007/s00254-005-1228-z
- Ntelis, G., Maria, S. and Efthymios, L. (2019) Landslide Susceptibility Estimation Using GIS. *Evritania Prefecture: A Case Study in Greece. Journal of Geoscience and Environment Protection*, 7, 206-220. doi: 10.4236/gep.2019.78015.
- Remondo J, González A, Díaz de Terán J.R., Cendrero A, Fabbri A, Chung C.-J.F (2003) Validation of landslide susceptibility maps; examples and applications from a case study in northern Spain. *Natural Hazards*, 30 (3): 437-449. DOI: 10.1023/B:NHAZ.0000007201.80743.fc
- Saaty, T. (1977) A Scaling Method for Priorities in Hierarchical Structures, *Journal of Mathematical Psychology*. Vol. 15,234-281.
- Saaty, T. (1978) Modeling Unstructured Decision Problems-The Theory of Analytical Hierarchies *Mathematics and Computers in Simulation*. XX:147- 158.
- Safeland (2010) Work Package D2.1- Harmonisation and development of procedures for quantifying landslide hazard.

Landslide events in Slovenia 2023: causes and consequences

Mateja Jemec Auflič^{(1)*}, Jernej Jež⁽¹⁾, Ela Šegina⁽¹⁾, Tina Peternel⁽¹⁾, Andrej Novak⁽¹⁾, Špela Kumelj⁽¹⁾, Domen Turk⁽¹⁾

1) Geological Survey of Slovenia, Dimičeva ulica 14, 1000 Ljubljana, mateja.jemec-auflic@geo-zs.si

Abstract Between August 3 and 6, 2023, Slovenia was hit by a natural disaster of national scale. Extreme rainfall with a return period of up to 250 years led to flooding and triggered several thousand landslides. Most landslides were recorded in the area north of Kamnik, in the area of Zgornja Savinjska dolina and in the wider Koroška region between Črna na Koroškem and Dravograd, as well as in the area of Poljanska dolina. At the Geological Survey of Slovenia (GeoZS), field data on landslides and related phenomena were mainly collected during intervention visits, which we carried out in coordination with the civil protection headquarters. Due to the large amounts of water, the landslides mostly turned into mud or debris flows, with material deposited on the foothills some 10, 50, 100, sometimes even more than 100 meters away from their original location. We estimate that around 10,000 slope mass movements were triggered during the event, with extremely high densities in some areas.

Keywords landslides, slope mass movements, extreme rainfall event, Slovenia

Introduction

Due to geological structures, relief and climatic conditions, Slovenia is very susceptible to the occurrence of various types of landslides. The most common of these are shallow landslides, which are usually triggered by rainfall. The scale and magnitude of the landslides are of a magnitude that has never been observed in the history of the Geological Survey of Slovenia. At the time of the event, we identified a number of landslides, the extent of the events and the causes of creep during the intervention visits and assessed the possibilities of further movements and provided for possible temporary intervention reinforcements. During the intervention visits, we determined the type of slope mass movements, the extent of the events and the causes of creep, as well as assessing the potential for further movements and planning possible temporary intervention measures. In most cases, the rock surface is covered by clastic sediments of varying thickness. In Koroška, weathering of metamorphic and magmatic rock can also be observed. Less frequent were wedge-shaped rockslides, where material slide along deep structural discontinuities in the slope. In some exceptional cases, landslides occurred for very unusual geological grounds, where they would not otherwise be expected. To assess the damage caused by the landslide in August, we

also prepared expert bases on the basis of which we estimated that around 10,000 landslides occurred during this period. The recent disaster, which caused enormous damage and also fatalities (Fig. 1), is clear proof that Slovenia is highly susceptible to landslides. This undoubtedly underlines the need for the inclusion and implementation of preventive measures to cope with natural disasters.

In order to coordinate flood recovery as efficiently as possible, a Flood Recovery Coordination Working Group was established in August 2023, as well as the Post-Flood and Landslide Reconstruction Office. Technical offices are being established to speed up the implementation of recovery and to ensure coordinated implementation between the different bodies responsible for the various measures. The Reconstruction Council advises the Government on the formulation of disaster recovery measures and the development of disaster resilience.

This paper examines the rainfall conditions during the event and the nature of the slope mass movements.

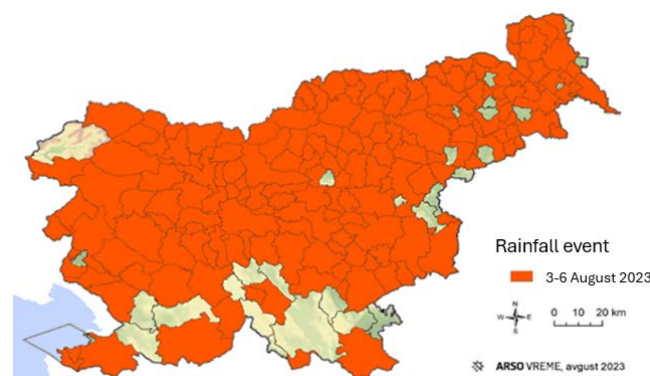


Figure 1 Municipalities that reported damage after flood event (181 out of 212 municipalities).

What causes landslides?

Extreme rainfall

The natural disaster that occurred in August 2023 was a consequence of a set of meteorological circumstances. Conditions typical of winter or autumn time occurred in the mid-summer when, in addition, the Mediterranean Sea was extremely warm, affecting the amount of water vapour in the air and thus the amount of precipitation. Already in July 2023, the amount of precipitation was at

least 100 % exceeding the long-term average in the entire country. Such conditions resulted in extremely high soil saturation.

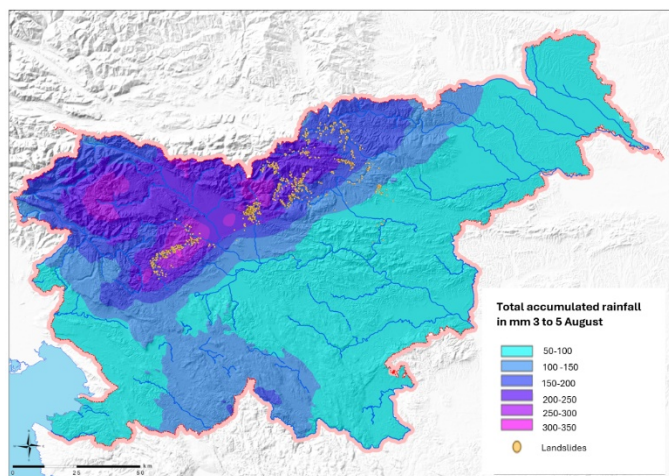


Figure 2 Total accumulated rainfall during rainfall event from 3 to 5 August 2023. Location of mapped landslides from orthophoto images (DOF).



Figure 3 A-The extent of available DOF data. B- Visual digitization of landslides from DOF.

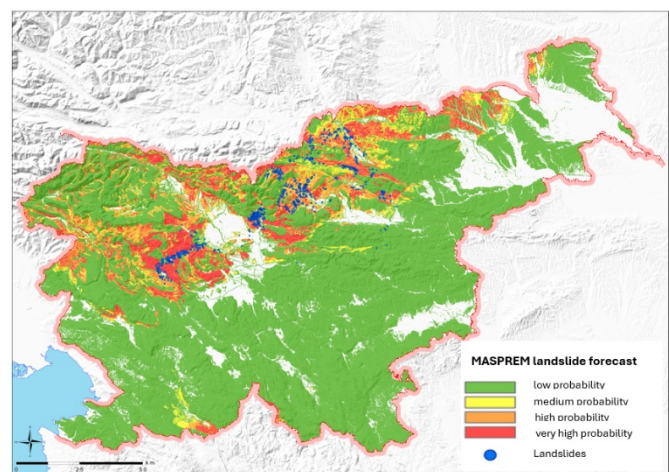


Figure 4 National landslide forecast system with total event accumulated rainfall.

On the days between August 3 and 6 at some measuring points, the monthly average amount of precipitation fell within a few hours. On August 4, the record values of daily precipitation were measured at several measuring stations. The estimated return period of extreme rainfall was 250 years or even more (Slovenian Environmental Agency 2023). High soil saturation as a result of a high amount of

precipitation in July in combination with intense precipitations at the beginning of August induced massive disruptions in slope stability across the entire territory of Slovenia.

The actual conditions in a limited area are to be captured by the accessible method (remote sensing, field inspection etc.). In our case, in the most affected parts of the country, interventive aerial photography was performed right after the event on 7 and 8 August 2023. Systematic landslide digitization was carried out on a part of a photographed area. Digitization of landslides from DOF was performed using the method of manual visual interpretation (Scaioni et al. 2014). A total of 2142 landslides have been evidenced on 1620 km² (Fig 3 A, B).

In order to estimate the total landslide damage on the national scale we used landslide forecasting system (Jemec Auflič et al. 2016; Peternel et al. 2022) that integrates environmental (geologic, geomorphologic and hydrologic) and weather conditions on a national level. The classes has been recalculated for the total amount of precipitation received between August 3 and August 5, 2023. The resulting area was classified into four classes of landslide vulnerability: small, medium, high and very high susceptible to landslides based on the rainfall received between 3 and 5 August. A total area is attributed to each susceptibility class (Fig 4).

Most landslides were recorded in the area north of Kamnik, in the area of Zgornja Savinjska dolina and in the wider region of Koroška, between Črna na Koroškem and Dravograd, as well as in the area of Poljanska dolina. The Geological Survey of Slovenia collected field data on landslides and related phenomena mainly during intervention visits, which we carried out in coordination with the Civil Protection Headquarters. During the intervention visits, we determined the type of slope mass movements, the extent of the events and the causes of the creep processes, assessed the potential for further movements and planned possible first and temporary intervention measures.

Consequences of landslides

We estimate that up to 10,000 slope mass movements were triggered in Slovenia during the event, with exceptionally high densities in some areas. (Fig. 5). The affected areas of the individual landslides, i.e. the areas of material deposition, show that these was extreme event that differ from the previously known landslide phenomena in these areas. In very few cases was the landslide deposited in the immediate vicinity of the source areas (Fig. 5). Due to the large amounts of water, the landslides often mobilised into mud or debris flows (Fig. 6), whose material was deposited on the foothills 10, 50, 100, sometimes even more than 100 meters away from their original location. As a result, facilities and infrastructure were also affected and threatened, sometimes far from the primary areas of origin of the phenomena (Fig. 6 A and B).

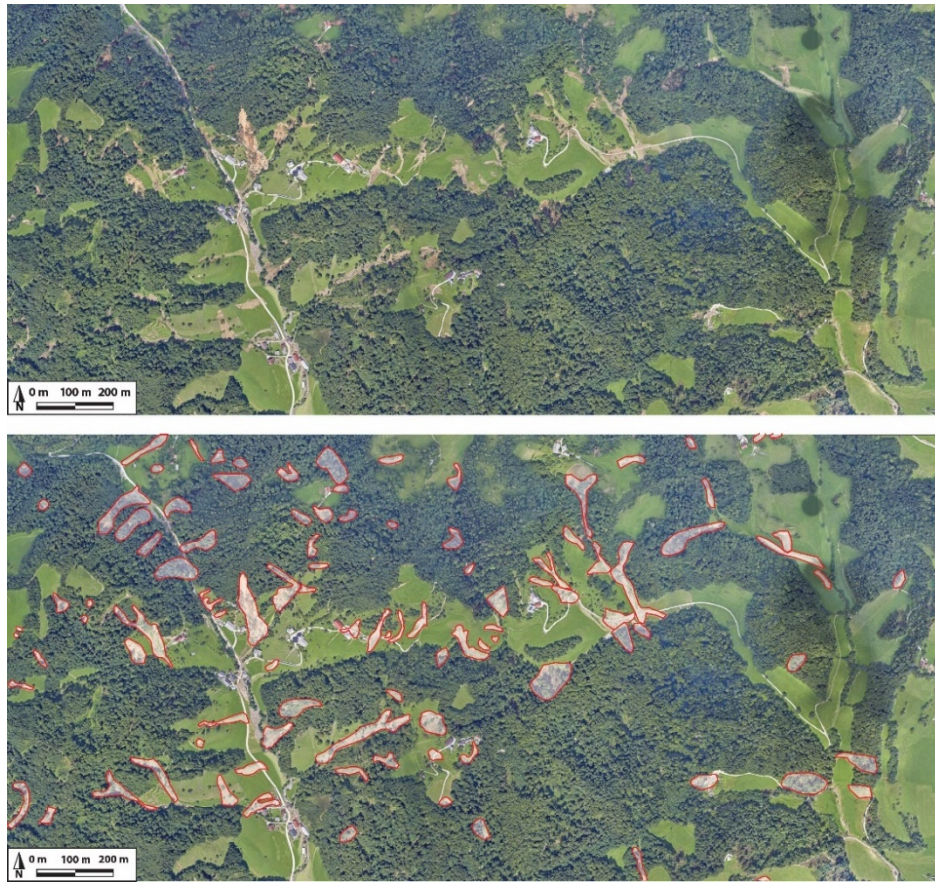


Figure 5 Comparison of a section from a digital orthophoto image of the area of Lanišče in the municipality of Kamnik, where the area consists of Oligocene clastic rocks. Over 50 landslides can be counted on an area of about 1 km² (polygons outlined in red), most of which have turned into mud or debris flows. As a result, their area of influence and thus the damage was much greater.



Figure 6 Examples of slope mass movements. A) Landslide that has mobilised into a debris flow, consisting of sand, gravel and several boulders with a size of several m². B) At the bottom of the valley, the debris flow has partially covered the stream bed. C) An example of a landslide that has mobilised into a mudslide of sand, silt and clay. D) An example of a water-saturated slide with roots and trees that led to the complete destruction of a house. The landslide occurred on a limestone base, which is unusual for landslides to occur.

In most cases, the weathered soils are covered by clastic sediments of varying thickness. In Koroška region there is also weathering of metamorphic and magmatic rocks. Less frequent were cases of wedge-shaped rockfalls, where material slid along deep structural discontinuities in the slope. In some exceptional cases, landslides occurred on very unusual geologic units where they would not otherwise be expected, such as steep limestone and dolomite slopes. In these cases it was a shallow landslide with roots and trees, indicating that there was an exceptional amount of water liquefying the soil (Fig. 6 C).

Landslides vary greatly in size, ranging from shallow deposits of a few meters (up to 1000 m²) to large-scale landslides that mobilized tens of thousands of m³ of material. In addition to the classic landslides, rockfalls, mudflows and debris flows, various hyper-concentrated flows (a mixture of water, rock, soil and sediments of different grain sizes) were also important processes during the rainfall event. These formed along torrential ravines with a carbonate background and high energy potential. In these cases, the water in the hinterland eroded large quantities of carbonate aggregates and carried them into the valleys in the form of grain streams or debris floods along the river beds. In such cases, over 100,000 m³ of material could be transported in places. The material was mostly deposited on alluvial fans or in river valleys, where it blocked the path of larger watercourses. But various other types of slope movements also brought material directly into the watercourses, causing the water to gain a lot of erosive power and destroy buildings and infrastructure downstream.

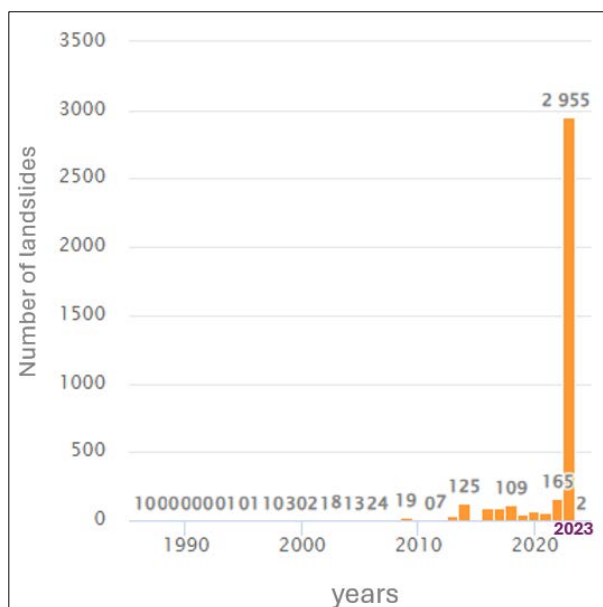


Figure 7 Recorded landslides in the e-Plaz application for landslide collection after rainfall event in August 2023.

These landslides have reduced the stability of the banks and as a result, many areas are prone to the reactivation of existing or the formation of new ones. All these areas must be carefully monitored until remediation is complete, especially during periods of heavy rainfall.

The lateral mass movements also had a significant impact on watercourses by introducing a greater amount of sediment into the riverbeds, streams and torrents. Larger quantities of material remained in the riverbeds after collection, which present a risk for triggering bedload and hyper-concentrated flows during heavy rainfall. At the end of February 2024 the landslide database contained 2955 landslide events reported in municipalities after flood event in August 2023. Even this inventory does not reflect the full number of landslides, as municipalities are still entering landslides into the database.

Conclusions

The heavy rainfall in August 2023 triggered a large number of different slope mass movements, with a large proportion of the slopes and landslides becoming mudflows and mudslides. The formation of debris flows and mudflows increased the extent of the affected areas as well as the damage to buildings and infrastructure. At the same time, the movements took place on an unusual geological base (limestones and dolomites) where they would not otherwise be expected. The lateral mass movements brought large amounts of material into the river, stream and torrent beds, increasing the erosive force of the water and destroying buildings and infrastructure downstream. The material remained in the riverbeds in many places. In the event of further heavy rainfall, the locations of slope movements and riverbeds with large amounts of sediment must be carefully monitored, as there is a risk of new events being triggered. A systematic inventory of the locations and extent of landslides was not carried out after the accident, so data on the resulting phenomena is still being collected, mainly via the e-Plaz system.

Acknowledgement

The authors would like to thank the Slovenian government for providing orthophotos, Civil protection administration office and the Landslide Reconstruction Office for making field visits possible.

References

- ARSO, 2023. Hidrometeorološko poročilo Nalivi in obilne padavine od 3. do 6. avgusta (2023) Ljubljana. Hydrometeorological report Rain and abundant precipitation from 3 to 6 August 2023.
- Jemec Auflič, M., Šinigoj, J., Krivic, M., Podboj, M., Peternel, T., Komac, M. (2016) Landslide prediction system for rainfall induced landslides in Slovenia (Masprem). *Geologija* 59: 259-271. <https://doi.org/10.5474/geologija.2016.016>.
- Peternel, T., Šinigoj, J., Jemec Auflič, M., Kumelj, Š., Krivic, M. (2022) MASPREM - Slovenian landslide forecasting and warning system. In: PERANIĆ, Josip (eds.), et al. *Landslide modelling & applications : proceedings of the 5th Regional Symposium on Landslides in the Adriatic-Balkan Region : [23-26 March 2022, Rijeka]*. Rijeka: Faculty of Civil Engineering, University of Rijeka; Zagreb.
- Scaioni, M., Longoni, L., Melillo, V., Papini, M. (2014) Remote Sensing for Landslide Investigations: An Overview of Recent Achievements and Perspectives. *Remote Sensing* 6: 9600-9652.

Landslide impact on road infrastructure in the Western Balkans

Miloš Marjanović^{(1)*}, Ivana Stevanović⁽²⁾, Danijel Vučković⁽³⁾, Aleksandar Bajović⁽²⁾, Nedim Begović⁽⁴⁾, Nerejda Hoxha⁽⁴⁾

1) University of Belgrade, Faculty of Mining and Geology, Djusina 7, Belgrade, Serbia, milos.marjanovic@rgf.bg.ac.rs

2) Arup d.o.o. Beograd, Kneginje Zorke 77, Belgrade, Serbia

3) Etecon d.o.o., Tabanovačka 27, Belgrade, Serbia

4) Transport Community Permanent Secretariat, Masarikova 5, Belgrade, Serbia

Abstract Landslides stand among the most common road-related disruptions throughout the Western Balkans Region, especially in the last couple of decades that have been witnessing severe weather anomalies, likely related to climate change. It is therefore inferred that landslides will become even more prominent in near future. Their assessment is, therefore, crucial for all further road planning, design, and management entailed. By fitting into EU frameworks, the Western Balkan countries are lately taking actions to pinpoint landslide and otherwise hotspot areas along the road networks and prioritize future investments accordingly. Herein, an example of landslide assessment along the road network and its impact is presented, with an adjusted methodology for large-scale frameworks, such as Western Balkans. The results show that roads are significantly affected by landslides in the Region to a level that it is difficult to discern areas of higher priority, thereby highlighting the need for developing sophisticated methodologies for their impact assessment. Landslides are confirmed as one of the topmost natural hazard types that cause road network disruption. When it comes to climate change, anticipated for the near and far future, it has been indicated that there are zones where the landslide hazard and their impact are expected to increase locally, but also zones where it will stagnate or drop. It has been demonstrated that such large-scale assessment can be very useful for public enterprises and governmental entities in their further decision-making and financing the road network maintenance, reconstruction, and extension.

Keywords landslide hazard, road network, climate change, the Western Balkans

Introduction

Resilience to climate-related natural hazards which are affecting road networks are emphasized in many agendas (Global Agenda 2030, EU Green Deal) linked to the Western Balkans Region (Albania, Bosnia and Herzegovina, Kosovo^{*1}, North Macedonia, Montenegro, and Serbia). To ensure that future investments are wisely

spent, various frameworks and action plans, targeted at engaging road sector governmental and public enterprise entities, are launched and all include improving climate resilience strategies (Corporate Authors, 2021). Such is the case with Trans-European Transport Network (TEN-T), which includes 5,287 km of roads (existing and planned) throughout the Western Balkan Region (Fig. 1).

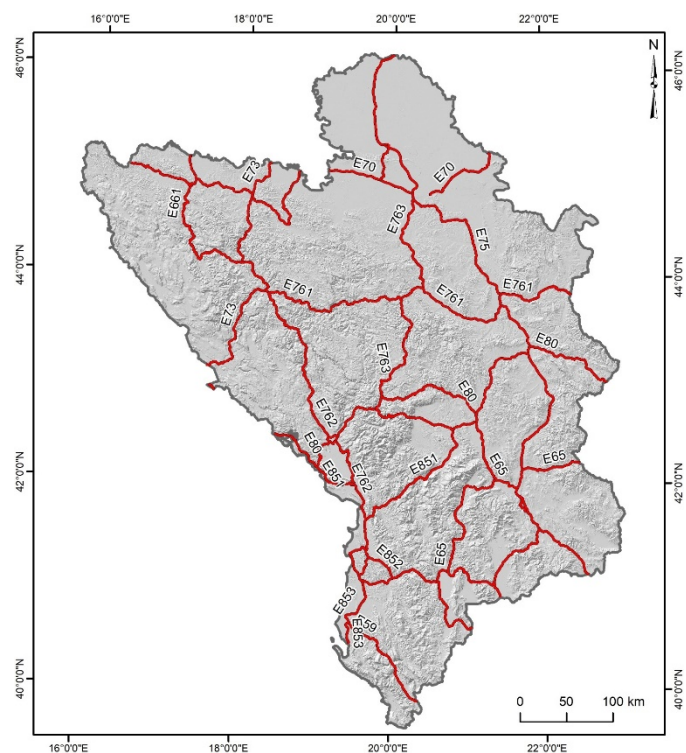


Figure 1. Indicative TEN-T core and comprehensive road network of the target Western Balkans area for 2050.

Among the natural phenomena that are recognized as climate-sensitive, landslide stand hand-in-hand with floods as the most damaging to road and railway networks in this area (Delforge et al, 2023, Marjanović et al, 2019). Other natural hazard types (sea surge, wildfire, snowdrift, drought) are not as damaging and more localized (e.g. to coastal areas, or high mountains). It is also important to note that the landslides are herein defined according to the internationally adopted classification (Hungar et al.

¹ In line with UNSCR 1244 (1999) and the ICJ Opinion on the Kosovo status.

2014), and include various types of mass movements, such as rockfalls, debris-flows, slumps etc. Hence, there are zones highly susceptible to landslides throughout the Region and zones which are landslide-free. Road networks cross-areas with landslide susceptible zones and it is a principal step to determine these stretches of the road network and define to which extent are they affected, and ultimately pick the most vulnerable hotspots.

The principal idea of this work was implemented in the project *Improving climate resilience and adaptation measures in the indicative extension of TEN-T road and rail networks in Western Balkans*, executed by Arup d.o.o. Beograd in 2023 (Transport Community, 2023). This work briefly overviews only the landslide hazard and only mid-term time split of 2050, although other hazard types and other time splits are included in the original project.

Methodology

Techniques available for landslide susceptibility assessment at regional scales are becoming countless (Pourghasemi et al. 2018), ranging from simple heuristics to statistical, deterministic and machine learning-based approaches. Regardless of the technique, determining the zones susceptible to landslides (spatial probability), and then highlighting those where landslide events are repetitive, i.e. hazardous (spatio-temporal probability), it requires two types of input data (Tab. 1):

- static morphological, geological, geotechnical and environmental features for determining where their combination is likely to cause landslides;
- dynamic triggering feature (rainfall, earthquake or other data) which changes over time;

In addition, a landslide inventory is needed to provide existing cases of landslide events during model calibration, as well as to validate its accuracy afterwards. Throughout the Western Balkans, there are differences regarding the data enlisted above. These data are prone to the level of detail and quality differences, which makes it unfeasible to generate a landslide hazard map of the entire Region by integrating the national level data. Such patchwork would cause inaccuracy of comparison of one part of the Region against another. Since consistency is essential in deciding which landslide hotspots are priorities, a downscaling approach is proposed instead.

Table 1 List of used datasets.

Dataset	Source	Resolution
Digital Ter. Model (DTM)	SRTM https://earthexplorer.usgs.gov/	30 m
Landslide suscept. map	EUROPEAN COMMISSION JRC ESDAC https://esdac.jrc.ec.europa.eu/	200 m
Precipitation RCP4.5 map	Climate Change Centre Austria https://data.ccca.ac.at/	1 km
Landslide inventory	Western Balkan stakeholders (national public road enterprises)	NA
TEN-T road network	TCT https://todis.transport-community.org/TODIS-APP/	NA

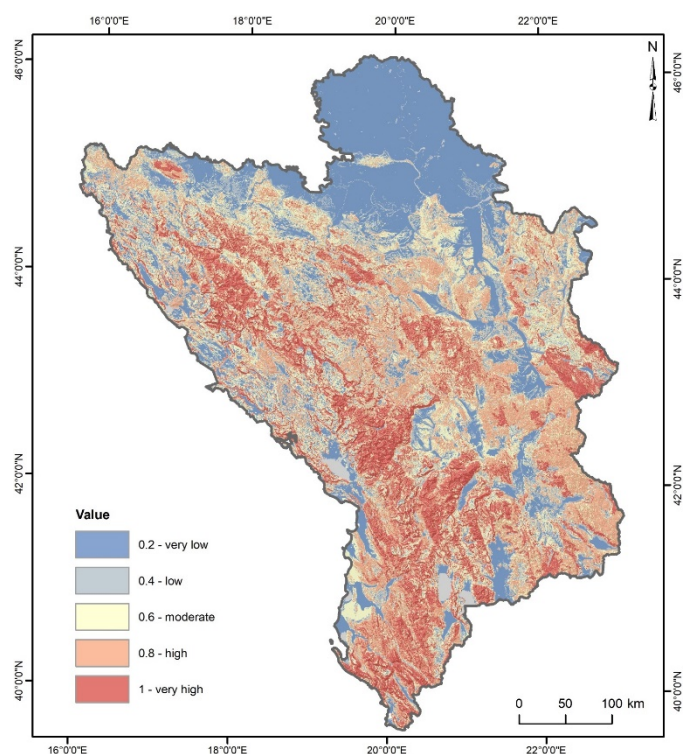


Figure 2. ELSUS2 landslide susceptibility map of the Western Balkans (source: <https://esdac.jrc.ec.europa.eu/>).

Downscaling the landslide data

Although coarser in resolution and more general in methodology, large-scale landslide susceptibility models provide the consistency needed for this task. The zones that are classified into five intervals, ranging from very low to very high landslide susceptibility are modelled (ELSUS2) for the entire Europe at 200 m resolution (Wilde et al, 2018). When downscaled to the extent of the Western Balkan, reclassified to 0-1 scale of values, and resampled to 30 m resolution using spline interpolation (Fig. 2) the ELSUS 2 model becomes a foreground for further modelling.

Downscaling the rainfall data

Rainfall data, especially those acquired from satellites such as TRMM mission and its successors, even more gravely suffer from coarse resolution (e.g., 1 km or larger pixel size). Their downscaling from to finer pixels is more complex interpolation problem, which requires not only adjacent pixels, but also time series analysis, as it is a dynamic dataset. Due to a vast database with countless climate indices provided especially for the Western Balkans, alongside with the spatio-temporal interpolation tools (in particular patch resampling), the precipitation data for RCP4.5 climate scenario is obtained and processed for 2050 time split, using the ClimaProof project tools (Tab. 1). Once downscaled, from 11 km to 30 m resolution (which now matches downscaled landslide susceptibility map), the precipitation map was normalized to 0-1 range to depict the relative distribution of rainfall throughout the area (Fig. 3).

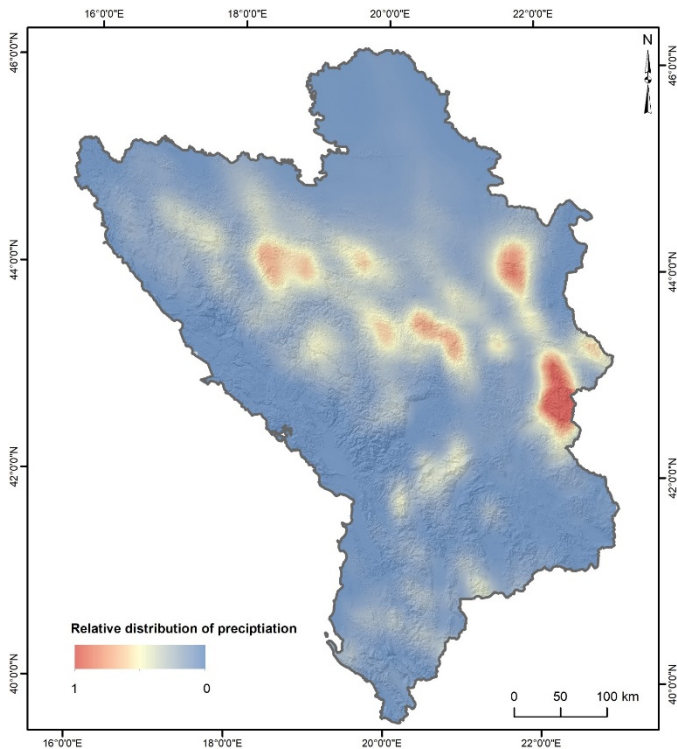


Figure 3. The downscaled original precipitation model (labelled pr_MPI-M-MPI-ESM-LR_rcp45_r11ip1_SMHI-RCA4_v1a_2011-2100) for 2050 time split (source: <https://data.ccca.ac.at/>).

Landslide hazard map

It was further required to append dynamic trigger data, in this case rainfall, which would reflect not only the local anomalies in rainfall in the past, but also rainfall distribution in the future for 2050 time split (under RCP4.5 scenario). This is performed by multiplying the landslide susceptibility and rainfall map (now both downscaled), thereby highlighting the zones where the landslides are likely to occur, and occur more frequently than in other areas (Fig. 4).

The validity of this map was checked using a limited landslide inventory obtained from regional stakeholders in charge of the road sector in the Western Balkans (Tab. 1).

Road network exposure

Road network elements of the TEN-T network are introduced as vectors represented by links and nodes. Given a large extent of the network (some links are tens and hundreds of km long while others are very short), a version of the network vector wherein all links are segmented into 1 km sub-links is also introduced. The latter version turned out to be more useful for network exposure assessment. When overlapping the previously created landslide hazard map, the road segments (links and sub-links) collect the pixels encountered along their extent and sum their relative hazard values. These sums are subsequently normalized into 0-1 range by using the network maxima and minima of the landslide hazard sums. In this way, two distant parts of the network can have equal criteria when compared to which one is more affected.

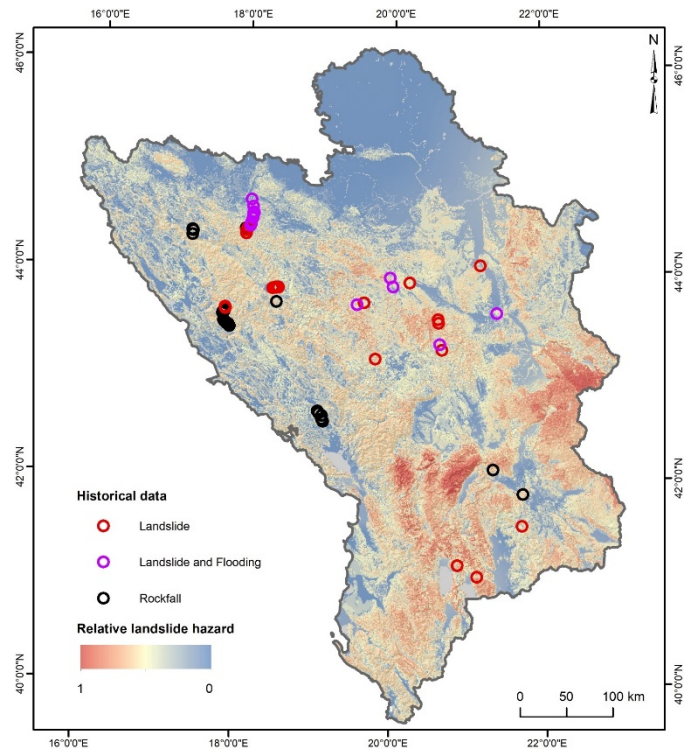


Figure 4. Landslide hazard map of the Western Balkans for the 2050 against the landslide inventory and alike mass movements.

Outputs

The 2050 time split of landslide hazard, anticipated by means of moderate RCP4.5 scenario (suggesting that greenhouse gas emissions will remain the same or slightly decrease by then) is translated from previously outlined very high to very low hazard zones to road vectors.

The link exposure (Fig. 5) suggests that the most affected are the ones in the hilly areas and along large river valleys or coastlines, e.g., in mountainous regions in western Serbia, central Albania, central Montenegro and central Bosnia and Herzegovina. Exposure to landslides might be even reduced in the future (due to a general decrease in precipitation and an increase in temperature) when the links are observed in general. However, local climate change effects (more extreme rainfalls with higher intensity and concentrated frequency) are better depicted in the case of sub-link exposure to landslides (Fig. 6). Sub-links are more prone to localized effects, but the patterns are clear (mountainous and remote areas are most prone). It is also apparent that much greater extents of the network is categorized as potentially highly impacted in the case of links (e.g., all red links), whereas sub-link analysis provides a more realistic output. The very high exposure class is identified to a total of 1005 km (or ~20% of the network) along the links while 763 km (or 15% of the network) along the sub-links.

It is further possible to extract a desired number of all links or sub-links, per entire network or per country etc. Making comparisons is thereby enabled as well as prioritization of the hotspots (identified spatially and by ID) which require more attention than the others (Tab. 2).

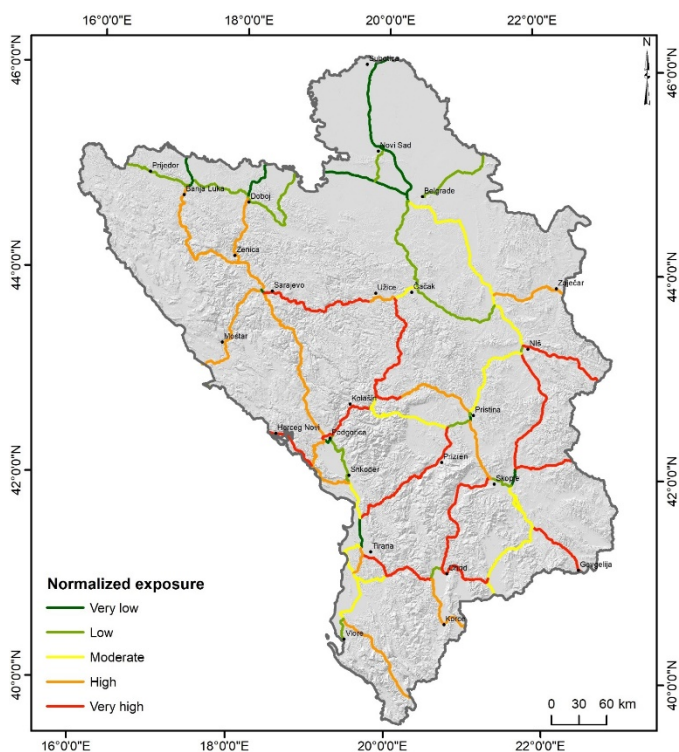


Figure 5. The spatial extent of the road link exposure to landslide hazard for 2050 time split.

Based on their length, the identified type of hazard (landslides) and other features it is possible to direct design measures for their efficient remediation or prevention. Landslide impact is herein directly reflected through the relative hazard value, whereas one can argue that road features are also important when calculating the total risk and its impact. These aspects are elaborated in detail in the project and continued through the Criticality Assessment, but herein, omitted due to simplicity.

Table 2 Top ten links and their hazard exposure score.

Link ID	Length (km)	Route	Hazard score	Rank
243	25.86	E65	1.00	1
177	27.58	E80	0.90	2
4791	41.54		0.86	3
276	21.69		0.75	4
174	18.68	E80	0.75	5
109	38.26	E763	0.70	6
114	31.24	E763	0.69	7
5589	10.61		0.66	8
1948	11.43		0.64	9
4777	22.72	E65	0.62	10

Conclusions

The proposed methodology benefits over the official EU Guidance in several aspects (Corporate Authors, 2021). Although it is successful in labelling high and low vulnerable (exposed) parts of the road network, it fails to establish a comparative ranking among them and therefore disables prioritisation as an important step in road management. The sub-link analysis level allows for a more

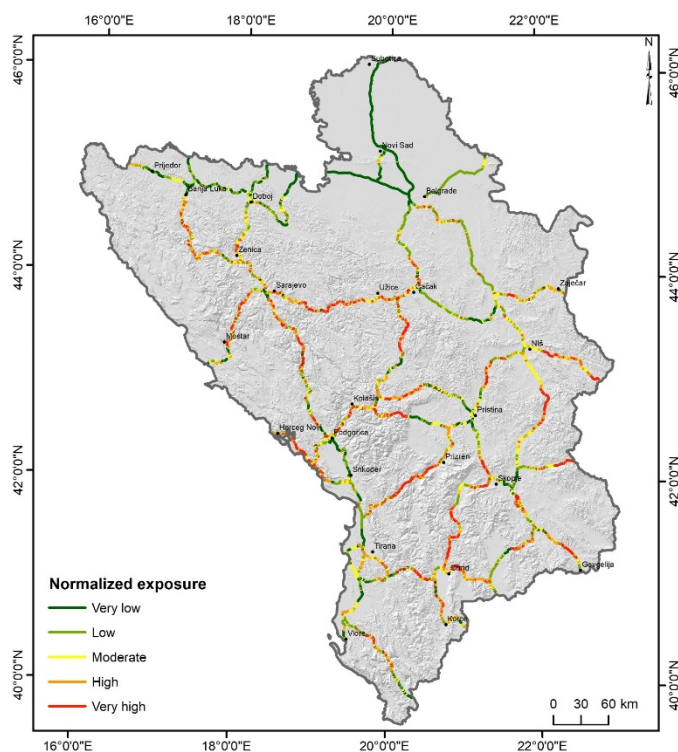


Figure 6. The spatial extent of the road sub-link exposure to landslide hazard for 2050 time split

detailed analysis and seem more realistic. Naturally, this level can have a significant mismatch with the concrete cases from the field and should be used for general planning purposes. This approach is also convenient for comparison among different time splits which might confirm or disproof specific link's priority over time.

References

Corporate Authors (2021) Commission Notice - Technical guidance on the climate proofing of infrastructure in the period 2021-2027. Official Journal. C(373): 92 p. URL: [https://eur-lex.europa.eu/legal-content/EN/TXT/?uri=CELEX:52021XC0916\(03\)](https://eur-lex.europa.eu/legal-content/EN/TXT/?uri=CELEX:52021XC0916(03))

Delforge D, Wathelet V, Below R, Sofia CL, Tonnelier M, van Loenhout J, Speybroeck N (2023) EM-DAT: the Emergency Events Database. Research Square. URL: <https://doi.org/10.21203/rs.3.rs-3807553/v1> [Last accessed: 1.3.2024].

Hungr O, Leroueil S, Picarelli L (2014) The Varnes classification of landslide types, an update. *Landslides*. 11: 167-194.

Marjanović M, Abolmasov B, Milenković S, Đurić U, Krušić J, Samardžić-Petrović M (2019) Multihazard exposure assessment on the Valjevo City road network. In Pourghasemi & Rossi (eds.) *Spatial Modeling in GIS and R for Earth and Environmental Sciences*. Elsevier. pp. 671-688

Pourghasemi H R, Teimoori Yansari Z, Panagos P, Pradhan B (2018) Analysis and evaluation of landslide susceptibility: a review on articles published during 2005–2016 (periods of 2005–2012 and 2013–2016). *Arabian Journal of Geosciences*. 11:1-12.

Wilde M, Günther A, Reichenbach P, Malet J P, Hervás J (2018) Pan-European landslide susceptibility mapping: ELSUS Version 2. *Journal of maps*. 14(2): 97-104.

Transport Community (2023) URL: <https://www.transport-community.org/reports/improving-climate-resilience-and-adaptation-measures-in-the-indicative-extension-of-ten-t-road-and-rail-networks-in-western-balkans/> [Last accessed: 1.3.2024].

Alpine rock slope failures, rockfalls and debris flows in a changing climate and their anticipation

Michael Krautblatter

Chair of Landslide Research, Technical University of Munich, Germany (m.krautblatter@tum.de)

Introduction

Climate change effects on rock slope failures, rockfalls and debris flows have been commonly postulated but there is still restricted evidence on the processual coupling. Climate warming in mountains occurs ca. 2 times faster than in lowlands and affects temperature patterns, precipitations patterns, snow cover and duration, permafrost and glacier retreat. This directly conditions weathering rates, hydro- and cryostatic forcing as well as rock-ice mechanical destabilization and glacial unloading/debutressing. Indirect effects include enhanced river incision rates, altered vegetation dynamics and release of organic acids, altered hydrological pathways and conditions etc. This talk reports contributes to the understanding of processual couplings of rock slope failures, rockfalls and debris flows to climate change effects and shows future chances for their anticipation.

Permafrost-affected rock slope failures

In a benchmark mechanical concept [Krautblatter et al., 2013], we developed a model that relates the destabilisation of thawing permafrost rock slopes to temperature-related effects on both, rock- and ice-mechanics; and laboratory testing of key assumptions has been performed. The destabilisation of permafrost rocks had before been purely attributed to changes in ice-mechanical properties. The effect of thawing on mechanical properties of bedrock and its mechanical relevance for friction and brittle fracture propagation had not been considered yet. This effect is significant since compressive and tensile strength as well as fracture toughness of intact rock are reduced by up to 50 % and

more when intact rock thaws. Based on literature and experiments, a modified Mohr-Coulomb failure criterion has been developed for an ice-filled rock fracture that takes into account (i) fracturing of cohesive rock bridges, (ii) friction of rough fracture surfaces, (iii) ductile creep of ice and (iv) a representation of rock-ice interfaces. The model implies that warming-related changes in rock-mechanical properties may significantly influence early stages of the destabilisation and also explains high-magnitude failures in permafrost rock slopes irrespective of the presence of ice in fractures. Only after the deformation accelerates to a certain velocity level, where significant strain is applied to ice-filled fractures, ice-mechanical properties outbalance the importance of rock-mechanical components. Rock-mechanical properties become more important for higher normal stress, i.e. higher magnitudes of rock slope failure.

The applicability of the model has been proven and developed in field, lab and modelling studies. In the laboratory, we measured p-wave velocities of 22 decimetre-large low porosity metamorphic, magmatic and sedimentary rock samples from permafrost sites with a natural texture (>100 micro-fissures) in 0.3 C increments close to the freezing point to prove significant changes in elastic properties in unfreezing rocks and developed a modified Timur's two phase-equation implementing changes in matrix velocity in freezing low porosity bedrock [Draebing and Krautblatter, 2012; Krautblatter and Draebing, 2014]. Fatigue, critical and subcritical fracture propagation under relevant conditions were assessed [Jia et al., 2017; Jia et al., 2015; Voigtländer et al., 2018].

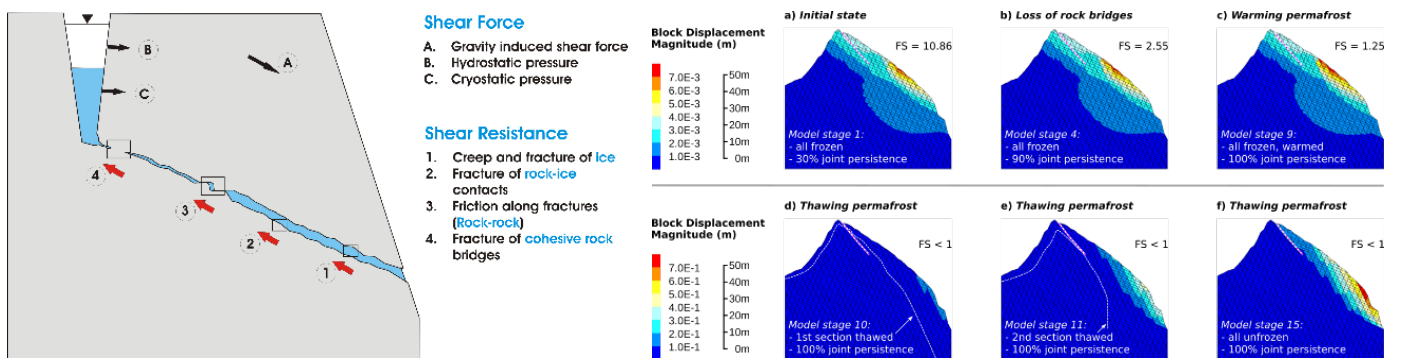


Fig. 1: Components of the Rock-Ice Mechanical model (left) and its implementation into a UDEC model from an instable rock mass at the Zugspitze (right).

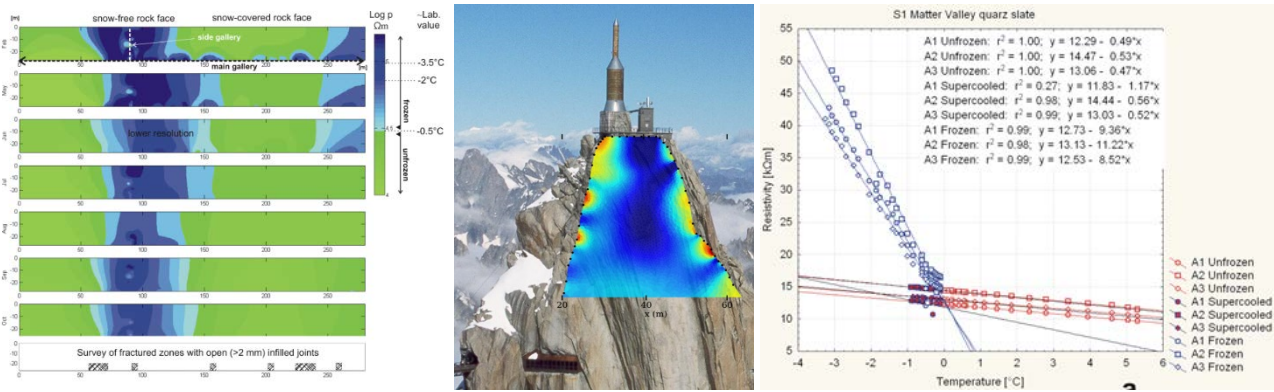


Fig. 2: Monthly distribution of frozen rock at the Zugspitze derived from ERT (left), ERT under the summit of the Aiguille du Midi showing the frozen part in blue/turquoise (mid) and lab-calibration of electrical resistivities with frozen/unfrozen rock temperature for and water-saturated quartz slate (right).

We performed experiments for the least known mechanical component, the rock ice-interfaces under relevant permafrost stress and temperature conditions, yielding a novel, temperature-dependent Mohr-Coulomb failure criterion for rock-ice interfaces [Mamot et al., 2019]. Summarising these findings, we could develop the 1st mechanical model that can anticipate the mechanical destabilisation of warming permafrost rocks [Mamot et al., 2021]. This article also generalises the susceptibility of permafrost rock walls according to lithology, fracture orientation and steepness – a starting point for generalising the susceptibility of permafrost rock walls to future failure.

Quantitative geophysics to constrain state of permafrost and mechanical degradation of rock slopes

The application of near surface geophysics in permafrost-affected loose material with significant ice content became popular subsequent to 2000. However, bedrock was not commonly tested since resistivity and p-wave velocity gradients for frozen bedrock were believed to be too small for reliable detection. In an extensive field monitoring program 2005-2007 in a permafrost affected rock ridge

(Matter Valley), we could demonstrate for the 1st time that Electrical resistivity tomography (ERT) is capable of detecting and monitoring permafrost extend in bedrock, i.e. rock slopes [Krautblatter and Hauck, 2007]. Performing laboratory test on the electrical resistivity of fully water-saturated frozen rock specimen with different lithologies, we derived a bilinear temperature-resistivity relationship for unfrozen and frozen bedrock with average gradients of $2.9(\pm 0.3) \text{ } \%/^{\circ}\text{C}$ (unfrozen, known before) and a tenfold $29.8 \pm 10.6 \text{ } \%/^{\circ}\text{C}$ frozen gradient [Krautblatter, 2009]. Using accurate laboratory-calibration, we could publish a quantitative temperature-calibrated ERT time series of permafrost bedrock along a gallery at the Zugspitze (see above) [Krautblatter et al., 2010]. P-wave velocities of 22 decimetre-large low porosity metamorphic, magmatic and sedimentary rock samples show significant changes in p-wave velocity and developed a modified Timur's two phase-equation implementing changes in matrix velocity in freezing low porosity bedrock [Draebing and Krautblatter, 2012]. Refraction seismic tomography can equally be applied for permafrost monitoring in frozen bedrock [Krautblatter and Draebing, 2014].

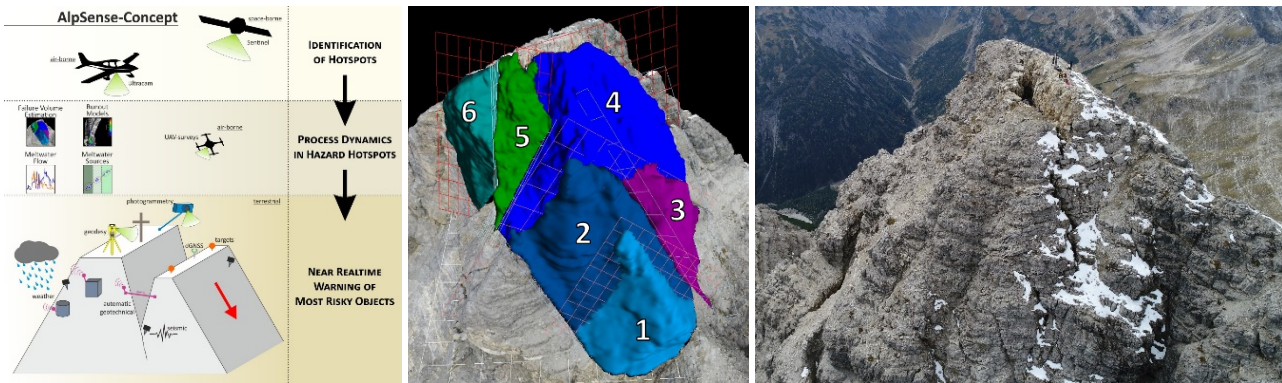


Fig. 3: Early warning strategy at the Hochvogel (D/A, left), potential compartments of future failures comprising altogether 260000 m³ (mid) and the Hochvogel with the visible decameter deep crack (right, persons for scale)



Fig. 4: Debris flow layers in a short core from the Plansee (left), the drill rig (mid) and lake bathymetry showing underwater debris flow deposits (right).

These methods and especially temperature-calibrated ERT have since been successfully adopted for applications ranging from extreme Alpine rock slopes to Arctic environments [Magnin et al., 2015; Siewert et al., 2012]. T-calibrated ERT has also been modified for the applied usage in early warning systems for alpine cable cars [Keuschnig et al., 2016].

A 900-day freezing laboratory study in Sussex, UK, shows that temperature-resistivity behavior over 25 subsequent freezing cycles in 6 highly-equipped large rock samples with galvanic and capacitive EIT monitoring [Murton et al., 2016]. Recently, we have further developed this method to 4D-applications of quantitative bedrock permafrost monitoring over a decade; the 1st method that can measure volumetric permafrost loss in rock slopes [Scandroglia et al., 2021].

Anticipating and modelling rock slope failure and hazardous landslides (in a changing climate)

In 2007, we developed a suggestion for a universal model for rockfall activity and rock wall retreat based on geological, geotechnical and ambient parameters [Krautblatter and Dikau, 2007]. Based on direct measurement of 140 t of rockfall deposition, we suggested a nonlinear rainfall intensity – rockfall model spanning 6 magnitudes of rockfall intensity [Krautblatter and Moser, 2009]. This was complemented with an assessment of the proportional contribution of different magnitudes of rockfalls and rock slope failure [Krautblatter et al., 2012].

The rock-ice mechanical model that explains the weakening of rock slopes in degrading permafrost due to rock and ice mechanics, the mechanics at the rock-ice interface and hydrostatic and cryostatic pressures [Krautblatter et al., 2013] was conceptually combined with the effects of stress changes in deglaciating valleys [Krautblatter and Leith, 2015] and nonlinear spatial and

temporal effects [Krautblatter and Moore, 2014]. Further studies added relevant mechanical understanding of path-dependent fracture propagation [Jia et al., 2017], subcritical fracture propagation [Voigtländer et al., 2018], stress corrosion [Voigtländer et al., 2020] and the efficacy of frost weathering [Draebing and Krautblatter, 2019]. A validation of long-term effects has recently been published in a multiyear observation by a co-supervised PhD of rockfall activity in deglaciating cirques [Hartmeyer et al., 2020]. Enhanced mechanical understanding was transformed into multi-phase models of rock-ice avalanches [Pudasaini and Krautblatter, 2014], a cyclic fatigue model [Jia et al., 2015], lahar models for glacier-capped volcanoes [Frimberger et al., 2021], a comprehensive model for permafrost rock slope destabilisation [Mamot et al., 2021] and erosive landslide mobility [Pudasaini and Krautblatter, accepted].

A systematic assessment of the kinematic forecasting potential of well-documented rock slope failures has been undertaken by Saettele et al. [2016]. Since 2018 we instrumented 5 alpine sites in the projects AlpSenseBench and AlpSenseRely to develop cutting edge landslide prediction at instrumented benchmark sites with latest satellite-based, air-based, geotechnical and geophysical instrumentation. Hereby we hypothesize that electric, seismic, acoustic and gravimetric geophysical signals [Dietze et al., 2021] can support anticipation of future failures prior to kinematic signals and enlarge the forecasting window [Hermlle et al., 2021; Leinauer et al., 2023].

Debris flows in a changing climate and environment

Aerial photography and geophysical analysis of Lateglacial/Holocene debris cone volumes since 1947 at the Plansee (A) indicates that debris flow activity since the 1980s has increased 3 times in comparison to the 3 decades

before and 2 times in comparison to the entire Lateglacial/Holocene debris cone deposition rate [Dietrich and Krautblatter, 2017; 2019]. Comparing recent debris flow rates to a 4000 year record of lake sediments in the Plansee, yielded evidence that debris flow activity in the last hundred years is >10 times higher than in the 4000 years before [Kiefer et al., 2021]. This coincides with evidence from the Reintal (D) where debris flow rates in the 20th/21st century were >5 times higher than in the 19th century [Sass et al., 2007]. Recent debris flow rates are seemingly increasing in many Alpine Environments worldwide and can feature massive sediment redistribution rates in high alpine catchments often modifying stream bed heights by several meters [Barbosa et al., 2024]. Such hyperconcentrated flows can be massively erosive even in bedrock channels and pose massive threat in environments that have not before experienced debris/hyperconcentrated flow activity [Stammberger et al., 2024].

References

- Barbosa, N., J. Leinauer, J. Jubanski, M. Dietze, U. Münzer, F. Siegert, and M. Krautblatter (2024), Massive sediment pulses triggered by a multi-stage 130m³ alpine cliff fall (Hochvogel, DE-AT), *Earth Surface Dynamics*, 12(1), 249-269, doi:10.5194/esurf-12-249-2024.
- Dietrich, A., and M. Krautblatter (2017), Evidence for enhanced debris-flow activity in the Northern Calcareous Alps since the 1980s (Plansee, Austria), *Geomorphology*, 287, 144-158, doi:10.1016/j.geomorph.2016.01.013.
- Dietrich, A., and M. Krautblatter (2019), Deciphering controls for debris-flow erosion derived from a LiDAR-recorded extreme event and a calibrated numerical model (Roßbichelbach, Germany), *Earth Surface Processes and Landforms*, 44(6), 1346-1361, doi:10.1002/esp.4578.
- Dietze, M., M. Krautblatter, L. Illien, and N. Hovius (2021), Seismic constraints on rock damaging related to a failing mountain peak: the Hochvogel, Allgäu, *Earth Surface Processes and Landforms*, 46(2), 417-429, doi:10.1002/esp.5034.
- Draebing, D., and M. Krautblatter (2012), P-wave velocity changes in freezing hard low-porosity rocks: a laboratory-based time-average model, *Cryosphere*, 6(5), 1163-1174, doi:10.5194/tc-6-1163-2012.
- Draebing, D., and M. Krautblatter (2019), The Efficacy of Frost Weathering Processes in Alpine Rockwalls, *Geophysical Research Letters*, 46(12), 6516-6524, doi:10.1029/2019GL081981.
- Frimberger, T., S. D. Andrade, S. Weber, and M. Krautblatter (2021), Modelling future lahars controlled by different volcanic eruption scenarios at Cotopaxi (Ecuador) calibrated with the massively destructive 1877 lahar, *Earth Surface Processes and Landforms*, 46(3), 680-700, doi:10.1002/esp.5056.
- Hartmeyer, I., R. Delleske, M. Keuschnig, M. Krautblatter, A. Lang, J. Christoph Otto, and L. Schrott (2020), Current glacier recession causes significant rockfall increase: The immediate paraglacial response of deglaciating cirque walls, *Earth Surface Dynamics*, 8(3), 729-751, doi:10.5194/esurf-8-729-2020.
- Hermle, D., M. Keuschnig, I. Hartmeyer, R. Delleske, and M. Krautblatter (2021), Timely prediction potential of landslide early warning systems with multispectral remote sensing: A conceptual approach tested in the Sattelkar, Austria, *Natural Hazards and Earth System Sciences*, 21(9), 2753-2772, doi:10.5194/nhess-21-2753-2021.
- Jia, H., K. Leith, and M. Krautblatter (2017), Path-Dependent Frost-Wedging Experiments in Fractured, Low-Permeability Granite, *Permafrost and Periglacial Processes*, 28(4), 698-709, doi:10.1002/ppp.1950.
- Jia, H., W. Xiang, and M. Krautblatter (2015), Quantifying rock fatigue and decreasing compressive and tensile strength after repeated freeze-thaw cycles, *Permafrost and Perigl. Process.*, doi:10.1002/ppp.1857.
- Keuschnig, M., M. Krautblatter, I. Hartmeyer, C. Fuss, and L. Schrott (2016), Automated Electrical Resistivity Tomography Testing for Early Warning in Unstable Permafrost Rock Walls Around Alpine Infrastructure, *Permafrost and periglacial processes*, n/a-n/a, doi:10.1002/ppp.1916.
- Kiefer, C., P. Oswald, J. Moernaut, S. C. Fabbri, C. Mayr, M. Strasser, and M. Krautblatter (2021), A 4000-year debris flow record based on amphibious investigations of fan delta activity in Plansee (Austria, Eastern Alps), *Earth Surface Dynamics*, 9(6), 1481-1503, doi:10.5194/esurf-9-1481-2021.
- Krautblatter, M. (2009), Detection and quantification of permafrost change in alpine rock walls and implications for rock instability, Ph.D. thesis, Univ. of Bonn., Bonn.
- Krautblatter, M., and R. Dikau (2007), Towards a uniform concept for the comparison and extrapolation of rockwall retreat and rockfall supply, *Geografiska Annaler*, 89 A(1), 21-40.
- Krautblatter, M., and D. Draebing (2014), Pseudo 3-D P wave refraction seismic monitoring of permafrost in steep unstable bedrock, *Journal of Geophysical Research-Earth Surface*, 119(2), 287-299, doi:10.1002/2012jf002638.
- Krautblatter, M., D. Funk, and F. Guenzel (2013), Why permafrost rocks become unstable: a rock-ice-mechanical model in time and space, *Earth Surf. Process. Landforms*, 38(8), 876-887, doi:10.1002/esp.3374.
- Krautblatter, M., and C. Hauck (2007), Electrical resistivity tomography monitoring of permafrost in solid rock walls, *Journal of Geophysical Research - Earth Surface*, 112(F2), F02S20, doi:10.1029/2006JF000546.
- Krautblatter, M., and K. Leith (2015), Glacier- and permafrost-related slope instabilities, in *THE HIGH-MOUNTAIN CRYOSPHERE: Environmental Changes and Human Risks*, edited by C. Huggel, M. Carey, J. J. Clague and A. Kääb, pp. 147-165, Cambridge University Press, Cambridge.
- Krautblatter, M., and J. R. Moore (2014), Rock slope instability and erosion: toward improved process understanding, *Earth Surface Processes and Landforms*, 39(9), 1273-1278, doi:10.1002/esp.3578.
- Krautblatter, M., and M. Moser (2009), A nonlinear model coupling rockfall and rainfall intensity based on a four year measurement in a high Alpine rock wall (Reintal, German Alps), *Natural Hazards and Earth System Science*, 9, 1425-1432.
- Krautblatter, M., M. Moser, L. Schrott, J. Wolf, and D. Morche (2012), Significance of rockfall magnitude and carbonate dissolution for rock slope erosion and geomorphic work on Alpine limestone cliffs (Reintal, German Alps), *Geomorphology*, 167, 21-34, doi:10.1016/j.geomorph.2012.04.007.
- Krautblatter, M., S. Verleysdonk, A. Flores-Orozco, and A. Kemna (2010), Temperature-calibrated imaging of seasonal changes in permafrost rock walls by quantitative electrical resistivity tomography (Zugspitze, German/Austrian Alps), *Journal of Geophysical Research-Earth Surface*, 115, F02003, doi:10.1029/2008JF001209.
- Leinauer, J., S. Weber, A. Cicoira, J. Beutel, and M. Krautblatter (2023), An approach for prospective forecasting of rock slope failure time, *Communications Earth and Environment*, 4(1), doi:10.1038/s43247-023-00909-z.

- Magnin, F., M. Krautblatter, P. Deline, L. Ravel, E. Malet, and A. Bevington (2015), Determination of warm, sensitive permafrost areas in near-vertical rockwalls and evaluation of distributed models by electrical resistivity tomography, *Journal of Geophysical Research-Earth Surface*, 120(5), 745-762.
- Mamot, P., S. Weber, S. Eppinger, and M. Krautblatter (2021), Stability assessment of degrading permafrost rock slopes based on a coupled thermo-mechanical model, *Earth Surf. Dynam.*, 2020, 1-45, doi:10.5194/esurf-2020-70.
- Mamot, P., S. Weber, T. Schröder, and M. Krautblatter (2019), A temperature- and stress-controlled failure criterion for ice-filled permafrost rock joints, *The Cryosphere*.
- Murton, J., O. Kuras, M. Krautblatter, T. Cane, D. Tschofen, S. Uhlemann, S. Schober, and P. Watson (2016), Monitoring rock freezing and thawing by novel geoelectrical and acoustic techniques, *Journal of Geophysical Research – Earth Surface*.
- Pudasaini, S. P., and M. Krautblatter (2014), A two-phase mechanical model for rock-ice avalanches, *Journal of Geophysical Research F: Earth Surface*, 119(10), 2272-2290, doi:10.1002/2014JF003183.
- Pudasaini, S. P., and M. Krautblatter (accepted), The Mechanics of Landslide Mobility with Erosion, *Nature Communications*.
- Sass, O., M. Krautblatter, and D. Morche (2007), Rapid lake infill following major rockfall (bergsturz) events revealed by ground-penetrating radar (GPR) measurements, Reintal, German Alps, Holocene, 17(7), 965-976, doi:10.1177/0959683607082412.
- Sättele, M., M. Krautblatter, M. Bründl, and D. Straub (2016), Forecasting rock slope failure: how reliable and effective are warning systems?, *Landslides*, 13(4), 737-750, doi:10.1007/s10346-015-0605-2.
- Scandroglio, R., D. Draebing, M. Offer, and M. Krautblatter (2021), 4D quantification of alpine permafrost degradation in steep rock walls using a laboratory-calibrated electrical resistivity tomography approach, *Near Surface Geophysics*, 19(2), 241-260, doi:10.1002/nsg.12149.
- Siewert, M. B., M. Krautblatter, H. H. Christiansen, and M. Eckerstorfer (2012), Arctic rockwall retreat rates estimated using laboratory-calibrated ERT measurements of talus cones in Longyearfjorden, Svalbard, *Earth Surface Processes and Landforms*, 37(14), 1542-1555, doi:10.1002/esp.3297.
- Stammberger, V., B. Jacobs, and M. Krautblatter (2024), Hyperconcentrated flows shape bedrock channels, *Communications Earth and Environment*, 5(1), doi:10.1038/s43247-024-01353-3.
- Voigtländer, A., K. Leith, and M. Krautblatter (2018), Subcritical Crack Growth and Progressive Failure in Carrara Marble Under Wet and Dry Conditions, *Journal of Geophysical Research: Solid Earth*, 123(5), 3780-3798, doi:10.1029/2017JB014956.
- Voigtländer, A., K. Leith, J. M. Walter, and M. Krautblatter (2020), Constraining Internal States in Progressive Rock Failure of Carrara Marble by Measuring Residual Strains With Neutron Diffraction, *Journal of Geophysical Research: Solid Earth*, 125(6), doi:10.1029/2020JB019917.

Rapid 3D rockfall susceptibility assessment of the Orašac rock slope, Croatia

Hrvoje Lukačić⁽¹⁾, Josip Katić⁽¹⁾, Sanja Bernat Gazibara⁽¹⁾, Snježana Mihalić Arbanas⁽¹⁾, Martin Krkač^{(1)*}

1) University of Zagreb, Faculty of Mining, Geology and Petroleum Engineering, Pierottijeva 6, 10000 Zagreb, Croatia (mkrkac@rgn.hr)

Abstract This paper presents a rockfall susceptibility assessment on a detailed (cliff) scale, by using the data from the high-resolution 3D point cloud obtained by unmanned aerial vehicle (UAV) digital photogrammetry. The studied limestone rock slope is located in Dubrovnik-Neretva County, south Croatia. Discontinuity orientations, required for 3D rockfall susceptibility assessment, were manually mapped, using the structural geology toolbox Compass, integrated within CloudCompare v2.12, providing information about the number and orientation of individual discontinuity planes, the number of discontinuity sets and weighted density concentrations associated with certain discontinuity set. Based on the acquired input data, a 3D rockfall susceptibility assessment was done for planar failure, wedge failure, and flexural toppling failure. Rockfall susceptibility assessment consisted of performing spatial kinematic analysis for normal and overhanging slopes based on the Markland test and highlighting points in the 3D point cloud susceptible to certain types of failure. Based on discontinuity orientations and orientations of the points in the point cloud, the Kinematic Hazard Index was calculated for every point in the 3D point cloud, and potential rockfall source areas were highlighted. The Kinematic Hazard Index was calculated by in-house MATLAB code which enables rapid 3D rockfall susceptibility assessment considering complex slope topology in both normal and overhanging areas of the studied rock slope.

Keywords rockfall susceptibility assessment, 3D point cloud, discontinuity mapping, UAV

Introduction

Rockfall hazard and risk assessment is a crucial part of responsible spatial planning and construction in rock masses due to the sudden occurrence and unpredictable nature of rockfall events (Evans and Hungr 1993). Due to that reason, numerous research exists regarding to rockfall susceptibility, hazard and risk assessment, in both, regional (e.g. Loye et al. 2009; Rossi et al. 2021) and detailed (cliff size) scales (e.g. Gigli et al. 2012; Matasci et al. 2017; Menegoni et al. 2021). In recent years, a rockfall susceptibility analysis has often been performed on the data obtained from remote sensing methods (Matasci et al. 2017, Farmakis et al. 2020, 2023). The most widely used remote sensing methods for obtaining data for susceptibility analysis on a detailed scale are terrestrial

laser scanning and digital photogrammetry (Menegoni et al. 2019, Fanti et al. 2013). LiDAR (Light Detection and Ranging) is a fully automated remote sensing technology that uses light beams to acquire data about slope topology (Wehr & Lohr 1999), while digital photogrammetry uses images captured with a high-resolution camera with appropriate overlap (Luhmann et al. 2014). From both techniques, it is possible to generate high-resolution 3D point clouds of vertical rock slopes.

Based on the acquired point cloud data, engineering geological mapping can be done by applying manual and semi-automated mapping techniques for obtaining discontinuity orientation, spacing, and persistence data (Battulwar et al. 2021). Applying such methods enables the collection of large amounts of discontinuity data compared to traditional field surveys. A large amount of collected discontinuity data, predominantly orientation, in combination with precise data about slope morphology, enables research to perform spatial kinematic analysis for assessing the potential of a rock slope for the occurrence of different types of failure. By performing the spatial kinematic analysis, it is possible to overcome some of the drawbacks of conventional stereonet-based analysis, like (1) uniform slope angle, (2) assumption of tightly clustered discontinuity data, (3) even spatial distribution of discontinuity planes and (4) unbiased representation of discontinuity sets (Admassu et al. 2013).

This study aims to demonstrate how the combination of engineering geological mapping using remote sensing techniques, with the help of MATLAB (MathWorks 2023) computing, can be used for producing reliable cliff scale rockfall susceptibility maps for rapid susceptibility assessment. Discontinuity planes are mapped manually using the open-source software CloudCompare (CloudCompare 2021) on a 3D point cloud, derived from Unmanned Aerial Vehicle (UAV) digital photogrammetry. The rockfall susceptibility is assessed by applying the Kinematic Hazard Index proposed by Casagli & Pini (1993).

Study area

The investigated rock slope is located on the state road DC8 (Trsteno-Orašac) in Dubrovnik-Neretva County, south Croatia. The vertical rock slope has a total length of approximately 35 meters and a maximum height of 12.30 meters. Analysed slope, with its concave shape, generally strikes NW-SE, and it is located on the hillslope dipping

towards SW. The majority of the rock slope has an angle greater than 70° with an average value of 75° . The height of the studied slope ranges from four to approximately 12 meters.

The rock slope area is located near the geological contact between Paleogene, Cretaceous and Triassic deposits. According to the Basic Geological Map of Croatia (Geological survey Sarajevo 1967) and the results of field mapping, it was determined that the rock slope is composed of Paleogene alveolinic-numulitic limestones. The limestone rock is moderately strong to strong with uniaxial compression strength around 80 MPa and grey to light grey in colour. Based on the results of the engineering geological mapping, four engineering geological zones can be distinguished based on the local average slope orientation, degrees of fracturing, and weathering conditions.

Methodology

UAV data acquisition and processing

The UAV survey was undertaken in March 2023 using DJI Phantom 4 Pro V2.0. The survey was done using a manual flight mission with an average front and side overlap of 70-80% at approximately 6 meters of horizontal camera-outcrop distance. A manual flight mission was applied for collecting data for both orthophoto images as well as 3D point cloud creation. The photogrammetric survey resulted in collecting a total of 475 images in JPEG format. Images were taken by a 20-megapixel resolution on-board camera equipped with 1.1-inch CMOS sensor. All collected images were directly georeferenced using an integrated Global Navigation Satellite System (GNSS). Details of the UAV system used for this study and survey characteristics are reported in Table 1, while generated 3D point cloud is presented in Fig. 1.

High-resolution images were processed by means of the Structure from Motion (SfM) technique using Agisoft Metashape Professional software (Agisoft 2020). The final point cloud (Fig. 1) has approximately 220 million points in the .xyz file with an average point density of 271 470 points/m². As a postprocessing step, vegetation was removed using the CANUPO plugin for CloudCompare (Brodu and Lague 2012), and only points corresponding to the rock slope were filtered. After removing vegetation, approximately 43% of points remained in the point cloud, representing only the rock slope.

Table 1 Details of the UAV system and photogrammetric survey.

UAV SYSTEM	
UAV device	DJI Phantom 4 Pro V2.0
Maximum weight	1375 g
Gimbal stabilisation	3-axis
Satellite positioning system	GPS/GNSS
ON-BOARD CAMERA PARAMETERS	
Lens	8,8 mm/24 mm, f/2,8-f/11
Sensor	CMOS, 1"
FOV	85°
Photo resolution	5472 x 3078
SURVEY DETAILS	
Flight mode	Manual
Coverage area (m ²)	3536
Frontal distance from the slope (m)	6
Number of photos	475
Photos overlap (%)	70 - 80
Frame shooting interval (s)	2

Engineering geological mapping

Engineering geological mapping was performed on homogeneous engineering geological zones on the 3D point cloud model. The investigated rock slope was divided into four homogeneous engineering geological zones based on the local average slope orientation, degrees of fracturing, and weathering conditions. For each zone, structural analysis was performed. High-resolution 3D point cloud data was used to manually measure individual discontinuity orientations using the Compass tool (Thiele et al. 2017), a plugin implemented into CloudCompare v2.12 software.

When collecting discontinuity orientation data, it is necessary to detect individual discontinuity surfaces and, by using the function Plane tool, select the radius within which all points are used to calculate the orientation of the best-fit plane using the least-squares method. The number of performed measurements depended on the fracturing conditions in each engineering geological zone, varying from 24 up to 174 measurements per zone. Measured discontinuity planes were grouped into individual discontinuity sets using the Fuzzy Cluster methodology implemented into Dips 7.0 software by RocScience (RocScience 2022). Mean discontinuity set orientations were compared with the data from the field mapping to check the quality of remote sensing data.

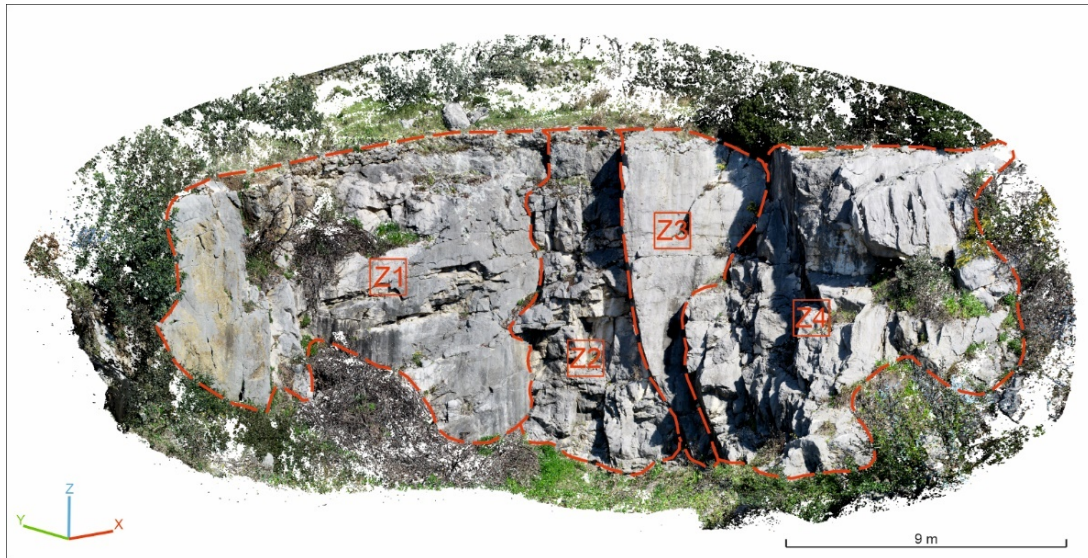


Figure 1 3D point cloud representing the rock slope with highlighted (in red) four engineering geological zones.

3D rockfall susceptibility assessment

The 3D kinematic analysis was executed to identify the potential rockfall source areas in normal dipping and overhanging slopes based on the high-resolution 3D point cloud data. Analysis was done for planar, wedge, and flexural toppling failure by applying conditions proposed by Gigli et al. (2022). The analysis made it possible to highlight points in the 3D point cloud on locations that are prone to certain types of failure. Input parameters for the 3D kinematic analysis included raw 3D point cloud data of the rock slope, orientations of the mapped discontinuity planes in the form of dip and dip direction, and average value of friction angle of 30° obtained from Vallejo and Ferrer (2011).

Based on the performed kinematic analysis for each point in the 3D point cloud, rockfall susceptibility was assessed by calculating the Kinematic Hazard Index (Casagli & Pini 1993). The KHI is calculated for each point in the 3D point cloud by calculating the percentage of discontinuity poles and discontinuity intersections that satisfy geometrical conditions for certain types of failure according to the following equations:

$$KHI_{PF} = \frac{N_{PF}}{N} (\%) \quad [1]$$

$$KHI_{WF} = \frac{I_{WF}}{I} (\%) \quad [2]$$

$$KHI_{FTF} = \frac{N_{FTF}}{N} (\%) \quad [3]$$

where KHI_{PF} , KHI_{WF} , and KHI_{FTF} represent calculated Kinematic Hazard Index (KHI) values for planar, wedge, and flexural toppling failures, respectively. N_{PF} and N_{FTF} denote the number of discontinuity planes meeting geometric criteria for planar and flexural toppling failures,

while I_{WF} indicates the number of discontinuity intersections satisfying geometric conditions for wedge failure. N and I stand for the total number of mapped discontinuity planes and discontinuity intersections.

Results

Engineering geological mapping using 3D point cloud data resulted in the recognition of 373 individual discontinuity planes grouped into five discontinuity sets, four fracture sets (JS-1 – JS-4) and a bedding plane (JS-0) as presented in Fig. 2. Discontinuities were grouped using the Fuzzy cluster approach based on the provided discontinuity orientation data, with number of input data ranging from 24 in Z-3 up to 174 in Z-4. Based on cluster analysis, mean discontinuity set orientations were determined (Table 2).

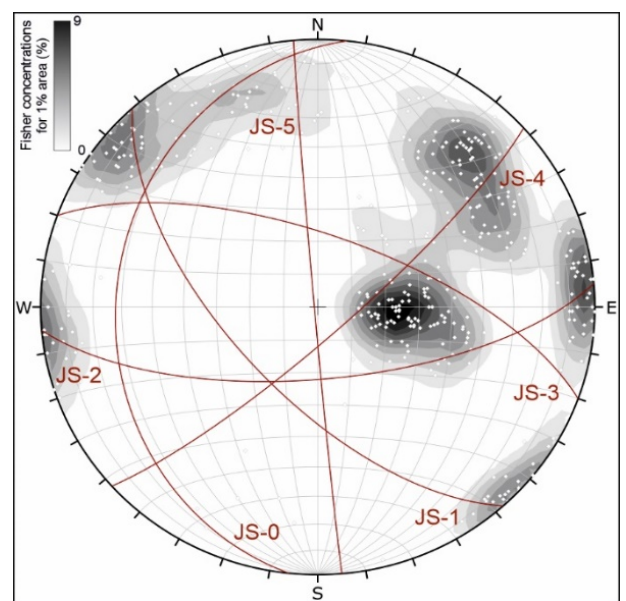


Figure 2 Stereographic projection (lower hemisphere and equal area) of the discontinuities for the study area.

Table 2 Discontinuity set orientations extracted by manual mapping in CloudCompare.

Discontinuity set ID	Slope Orientation	Zone ID
JS-0	266/29	Z1, Z2, Z3, Z4
JS-1	228/64	Z1, Z2, Z3, Z4
JS-2	170/70	Z1, Z2
JS-3	20/68	Z1
JS-4	135/82	Z2, Z3, Z4
JS-5	265/88	Z2, Z4

Results of engineering geological mapping of discontinuities were used as input data for 3D rockfall susceptibility assessment using in-house MATLAB code. Rockfall susceptibility, i.e. KHI values were assessed for planar, wedge, and flexural toppling failure. The generated rockfall susceptibility maps are presented in Fig. 3. From the maps, it is visible that the highest maximal values of

KHI are observed for wedge failure (92.5%), while the lowest maximal KHI values are observed for flexural toppling failure (18%). The maximal KHI value for the planar failure mechanism is 47%.

Analysing the spatial distribution of calculated KHI values for three failure mechanisms, it is evident that flexural toppling mechanics represent an insignificant possibility of occurrence, while possible rockfalls occur due to wedge and planar failure mechanisms. Planar and wedge failure mechanisms occur at similar locations, with the most highlighted hotspot in the upper part of the engineering geological zone Z4.

Upon inspecting the 3D point cloud, it is visible that this hotspot area was previously affected by rockfall activity in its overhanging part, as shown in Fig.4. Furthermore, the majority of the potential rockfall sources are located in the overhanging areas of the rock mass.

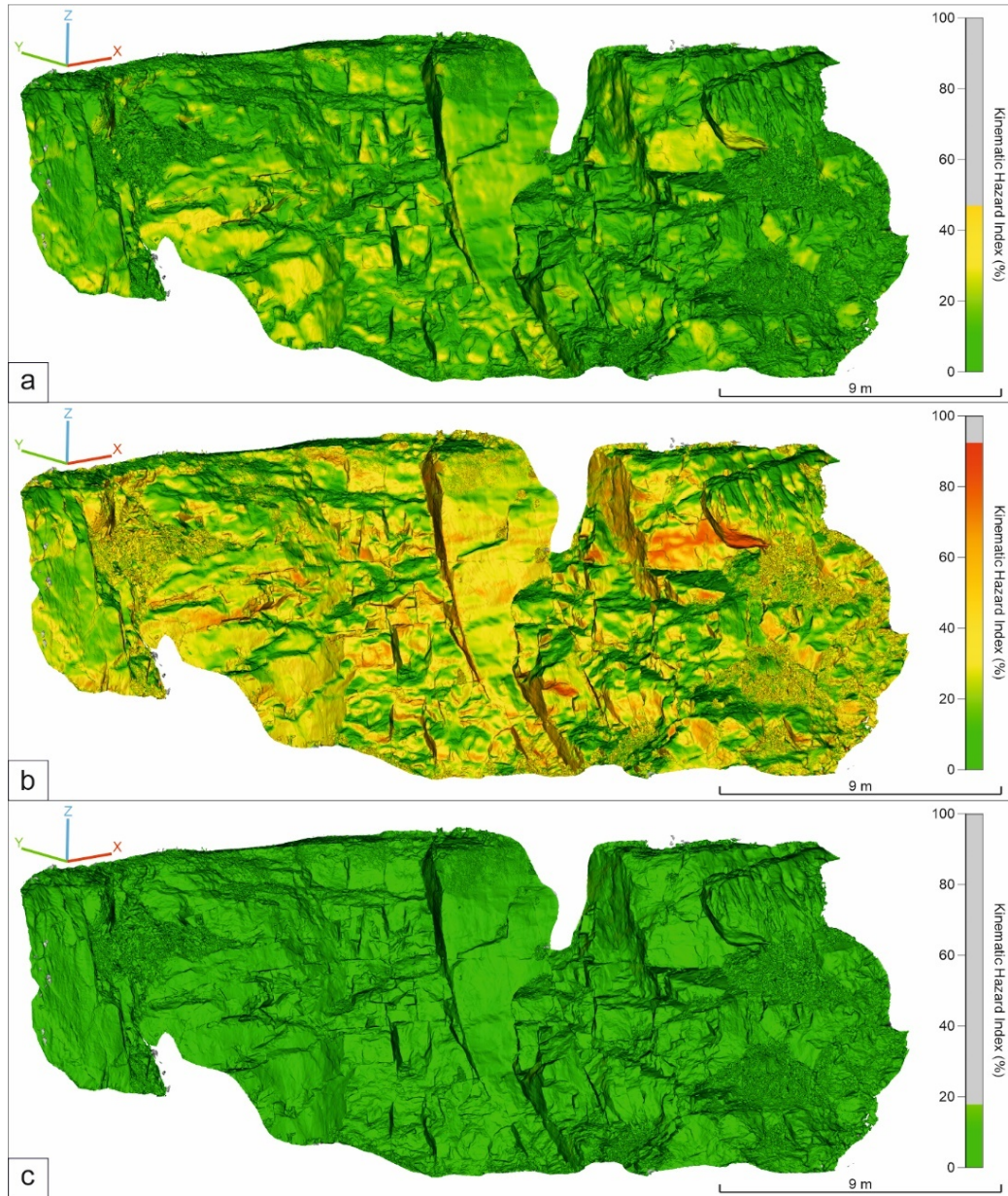


Figure 3 3D rockfall susceptibility maps produced for: a) planar failure, b) wedge failure, and c) flexural toppling failure.

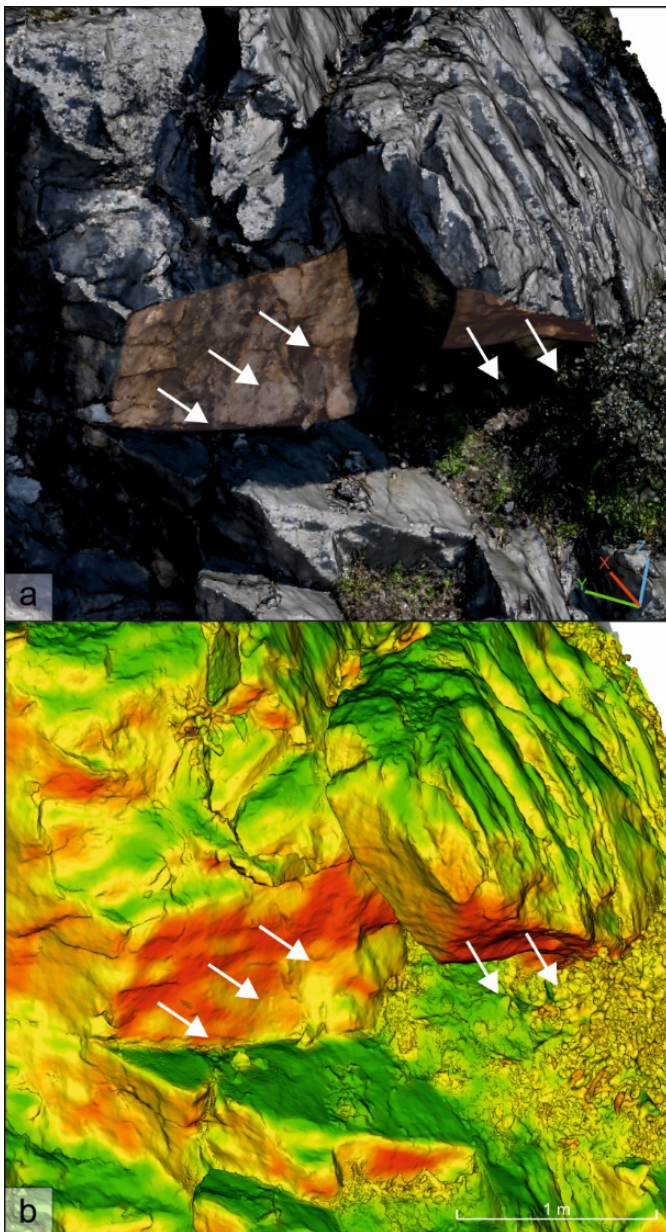


Figure 4 Close-up view on the portion of the rock slope affected by rockfall: a) Digital Outcrop Model and b) rockfall susceptibility map for wedge failure.

Discussion and conclusions

This study demonstrates the application of rapid rockfall susceptibility assessment at a detailed scale utilizing high-resolution 3D point cloud data. High-resolution 3D point cloud used for this study was obtained through UAV digital photogrammetry by applying SfM methodology.

Engineering geological mapping of discontinuity orientations, as input data from rockfall susceptibility assessment, was done on a point cloud with an average point density of 271 470 points/m². Mapping was performed manually using the Compass tool integrated within CloudCompare v2.12. Engineering geological mapping resulted in identifying 373 individual

discontinuity planes grouped into five sets across four engineering geological zones. The acquired discontinuity orientation data were then used to conduct a comprehensive 3D rockfall susceptibility assessment by analysing three types of failure (planar, wedge, and flexural toppling).

The 3D rockfall susceptibility assessment involved spatial kinematic analysis for normal and overhanging slopes, considering complex slope topology, the data available for high-resolution 3D point cloud. The Kinematic Hazard Index (KHI) was calculated for each point of the point cloud, highlighting potential rockfall source areas. The rockfall susceptibility maps reveal that the highest KHI values are associated with a wedge failure, reaching 92.5%, whereas the lowest maximal values are associated with a flexural toppling failure, up to 18%. The planar failure mechanism exhibits maximum values of up to 47%. The spatial distribution of rockfall sources (maximal KHI values), for all types of failure, are located on the overhanging parts of the rock slope.

The results of the study indicated that the proposed approach, based on high-resolution 3D point cloud data, is useful for rapidly assessing rockfall susceptibility. The proposed approach enables insights into planar, wedge, and flexural toppling failure mechanisms, and highlights locations of the rock slope that may become unstable, providing valuable data for characterizing and mitigating rockfall hazards and for emergency measures.

References

- Admassu Y, Shakoor A (2013) DIPANALYST: A computer program for quantitative kinematic analysis of rock slope failures. *Comput Geosci.* 54:196–202. <https://doi.org/10.1016/j.cageo.2012.11.018>.
- Agisoft. General Image Capture Tips (2020) Available online: <https://www.agisoft.com/> [Last accessed: 10 November 2023].
- Battulwar R, Zare-Naghadehi M, Emami E, Sattarvand J (2021) A state-of-the-art review of automated extraction of rock mass discontinuity characteristics using three-dimensional surface models. *Journal of Rock Mechanics and Geotechnical Engineering* 13:920–936. <https://doi.org/10.1016/j.jrmge.2021.01.008>.
- Brodu N, Lague D (2012) 3D terrestrial lidar data classification of complex natural scenes using a multi-scale dimensionality criterion: Applications in geomorphology. *ISPRS Journal of Photogrammetry and Remote Sensing* 68:121–134. <https://doi.org/10.1016/j.isprsjprs.2012.01.006>.
- Casagli N, Pini N (1993) Analisi cinematica della stabilità di versanti naturali e fronti di scavo in roccia. *Geol Appl Idrogeo* 28:223–232.
- Evans SG, Hungr O (1993) The assessment of rockfall hazard at the base of talus slopes. *Canadian Geotechnical Journal* 30:620–636. <https://doi.org/10.1139/t93-054>.
- Fanti R, Gigli G, Lombardi L, Tapete D, Canuti P (2013) Terrestrial laser scanning for rockfall stability analysis in the cultural heritage site of Pitigliano (Italy). *Landslides* 10:409–420. <https://doi.org/10.1007/s10346-012-0329-5>
- Farmakis I, Hutchinson DJ, Vlachopoulos N, Westoby M, Lim M (2023) Slope-Scale rockfall susceptibility modeling as a 3D computer

- vision problem. *Remote Sens (Basel)* 15:2712. <https://doi.org/10.3390/rs15112712>
- Farmakis I, Marinos V, Papathanassiou G, Karantanellis E (2020) Automated 3D jointed rock mass structural analysis and characterization using LiDAR terrestrial laser scanner for rockfall susceptibility assessment: Perissa Area Case (Santorini). *Geotechnical and Geological Engineering* 38:3007–3024. <https://doi.org/10.1007/s10706-020-01203-x>
- Geological survey Sarajevo Sarajevo (1967) Basic Geological Map, scale 1:100 000, Trebinje sheet.
- Gigli G, Frodella W, Mugnai F, Tapete D, Cigna F, Fanti R, Inrieri E, Lombardi L (2012) Instability mechanisms affecting cultural heritage sites in the Maltese Archipelago. *Natural Hazards and Earth System Sciences* 12:1883–1903. <https://doi.org/10.5194/nhess-12-1883-2012>.
- Gigli G, Lombardi L, Carlà T, Beni T, Casagli N (2022) A method for full three-dimensional kinematic analysis of steep rock walls based on high-resolution point cloud data. *International Journal of Rock Mechanics and Mining Sciences* 157:105178. <https://doi.org/10.1016/j.ijrmms.2022.105178>.
- Gonzalez de Vallejo L, Ferrer M (2011) *Geological Engineering*. CRC Press. 700p.
- Loye A, Jaboyedoff M, Pedrazzini A (2009) Identification of potential rockfall source areas at a regional scale using a DEM-based geomorphometric analysis. *Natural Hazards and Earth System Sciences* 9:1643–1653. <https://doi.org/10.5194/nhess-9-1643-2009>.
- Luhmann T, Robson S, Kyle S, Boehm J (2019) Closer-range photogrammetry and 3D imaging. De Gruyter.
- Matasci B, Stock GM, Jaboyedoff M, Carrea D, Collins BD, Guérin A, Matasci G, Ravelin L (2017) Assessing rockfall susceptibility in steep and overhanging slopes using three-dimensional analysis of failure mechanisms. *Landslides* 15:859–878. <https://doi.org/10.1007/s10346-017-0911-y>.
- Mauro Rossi Paola Reichenbach Rosa María Mateos RS (2021) Probabilistic identification of rockfall source areas at regional scale in El Hierro (Canary Islands, Spain). *Geomorphology* 281.
- MathWorks Inc (2023) Available online: <https://www.mathworks.com> [Last accessed: 8 October 2023].
- Menegoni N, Giordan D, Perotti C (2021) An open-source algorithm for 3D rock slope kinematic analysis (ROKA). *Applied Sciences* 11:1698. <https://doi.org/10.3390/app11041698>.
- Rocscience (2022) Available online: <https://www.rocscience.com/software/dips> [Last accessed: 3 November 2023].
- Thiele ST, Grose L, Samsu A, Micklethwaite S, Vollgger SA, Cruden AR (2017) Rapid, semi-automatic fracture and contact mapping for point clouds, images and geophysical data. *Solid Earth* 8:1241–1253. <https://doi.org/10.5194/se-8-1241-2017>.
- Wehr A, Lohr U (1999) Airborne laser scanning—an introduction and overview. *ISPRS Journal of Photogrammetry and Remote Sensing* 54:68–82. [https://doi.org/10.1016/S0924-2716\(99\)00011-8](https://doi.org/10.1016/S0924-2716(99)00011-8)

Fines content influence on the dynamic slope behavior in small-scale physical models

Vedran Jagodnik^{(1,2)*}, Davor Marušić⁽¹⁾, Željko Arbanas⁽¹⁾, Nina Čeh⁽¹⁾, Josip Peranić⁽¹⁾, Martina Vivoda Prodan⁽¹⁾

1) University of Rijeka, Faculty of Civil Engineering, Radmile Matejčić 3, Rijeka, Croatia, +38551265941
(vedran.jagodnik@gradri.uniri.hr)

2) Center for Artificial Intelligence and Cybersecurity, University of Rijeka, Radmile Matejčić 2, Rijeka, Croatia

Abstract Small-scale physical models have already been used for some time to simulate the natural slope behaviour subjected to static and dynamic loading. This research presents the results of small-scale physical slope models with a 40° slope inclination that were made by using pure sand specimens and two artificial mixtures of sand and kaolinite powder with different mass ratios. Physical models were saturated and subjected to dynamic loading to simulate the behaviour of slopes that can form shallow landslides. The shaking table was used to apply the dynamic loading, using a loading frequency of 5.5 Hz and a horizontal displacement amplitude of 0.2 cm. Using two high-speed cameras, the model's surface displacements were measured. Accelerometers were placed inside the slope body to measure the acceleration response during dynamic loading. Performed simulations showed the significance of fines content on the dynamic slope behaviour. Unlike the models made with pure sand, slopes with mixtures of sand and kaolinite powder were able to withstand a larger number of loading cycles without any amplification recorded during cyclic loading. The crown and the foot of the slope have proven to be the most critical parts in small-scale models. The presented results are focused on the loading time necessary for the first crack to open on a small-scale slope model. Cracks on the slope's surface formed during the dynamic loading can infiltrate additional water, ensuring locally higher slope saturation resulting in soil softening and additional strength degradation. The influence of fines content on the response of the small-scale slope model was presented simply by comparing the time of the crack appearance. The results show that the slope made from pure sand was the most critical one out of three tested materials.

Keywords landslide, small-scale model, dynamic soil behaviour, sand-clay mixtures

Introduction

Two primary factors responsible for the initiation of landslides are precipitation and seismic activity. If heavy rainfall is closely followed by an earthquake, a catastrophic event may occur (e.g., Popescu 2002; Chen et al. 2012; Wu et al. 2015). The seismic shaking induces shear strain in the

soil, resulting in the degradation of its structural integrity and subsequent collapse. Slopes that are susceptible to shallow landslides are particularly influenced by both earthquakes and rainfall (Gabet and Mudd 2006; Yang and Luo 2015). As defined by the ICL (Icl 2016), shallow landslides are typically characterized by a depth of approximately five meters.

Both basic and sophisticated physical models were studied to better understand the process and behaviour of slopes. For the past thirty years, researchers have focused on the initiation, accumulation, and mechanism of landslides that are caused by water seeping into a slope (Spence and Guymer 1997; Wang and Sassa 2001; Okura et al. 2002; Rahardjo et al. 2002; Kim et al. 2004; Moriwaki et al. 2004; Ochiai et al. 2004; Orense et al. 2004; Pajalić et al. 2021). Additionally, research is carried out on small-scale models under dynamic loads (Ichii and Ohmi 2004; Cao et al. 2019) with a focus on examining the slope behaviour under different dynamic loading scenarios.

Landslide modelling requires the application of similarity laws to accurately simulate the behaviour of landslides. These laws ensure that the model experiments represent the prototype conditions as accurately as possible. The similarity laws include geometric, kinematic and dynamic similarity simultaneously (You et al. 2012; Lai et al. 2013; Pajalić 2024). The complexity of the similarity laws can be depicted in Figure 1. In the case of earthquake-induced landslides, seismic parameters, topography and landform features, and engineering properties of soil are considered the main factors affecting landslide dynamics (Stark and Hovius 2001). The choice of similar materials and mix proportions is also important in landslide model tests (Baronin 1992).

The scaling principles for modelling a large-scale prototype subjected to an earthquake were described simply by Iai et al. in 2005. The shear modulus at small deformation ($\leq 10^{-6}$) is assumed to be proportional to the square root of confining pressure. This results in Type II relations, which are frequently applied to models that employ sand that is identically dense like the material in the prototype (Iai et al. 2005).

The relationship between dynamic loads and other potential mechanisms leading to failure can be defined and described using the dynamic characteristics of soil. An

earthquake causes cyclic loading of the soil. Different amplitudes and frequency of cyclic shear stresses are applied to the soil, which can cause both temporary and permanent deformations (Pecker 2008).

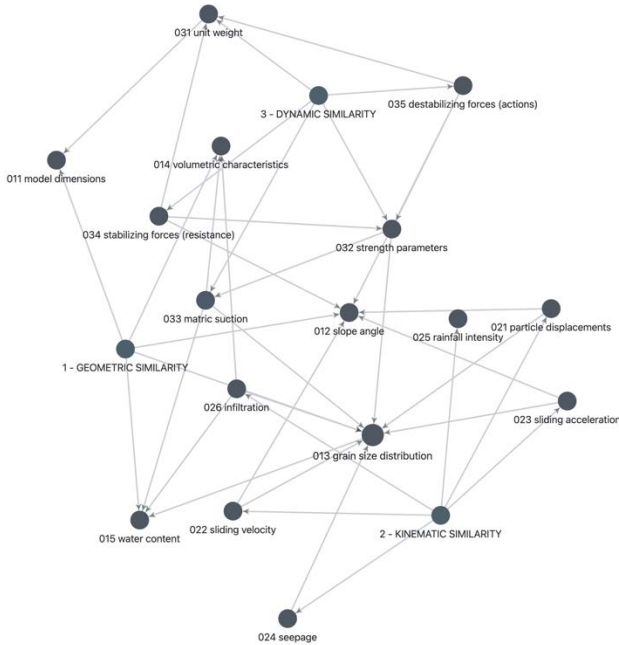


Figure 1 Complexity of similarity law interactions

The results in this paper are the outcome of a four-year research project titled “Physical modelling of landslide remediation constructions behaviour under static and seismic actions” that was funded by the Croatian National Science Foundation. An example of a small-scale slope made from different material is examined on the dynamic loading. A scaling factor of 40 was applied following the property scaling defined by (Iai et al. 2005). The motivation behind this research was to examine the mechanics of shallow landslides in a small-scale model under dynamic excitation and to examine the influence of remediation measures on the small-scale slope behaviour under dynamic excitation.

Methodology

Model setup

The tests were performed in fine-grained sand called Drava sand (0–1.0 mm) and the mixtures of Drava sand and kaolin powder in 10% and 15% mass ratio. Material made purely out of Drava sand has been assigned with the ID “SK0”, while the material with 10% and 15% of kaolin powder have been assigned with the IDs’ “SK10” and “SK15”, respectively. The grain size distribution of sand used is presented in Figure 2. The physical properties of the selected materials are presented with Tab. 1. The small-scale slope model was scaled according to the scaling laws defined by Iai et al. 2005). In this case, scaling factors for 1g conditions were used and summarised in Tab.

2. The width of the model box is 50 cm. The length of the model is around 90cm. The slope angle, which was constant throughout all three tests, was 40°. This assured the critical acceleration to be smaller than the slope angle.

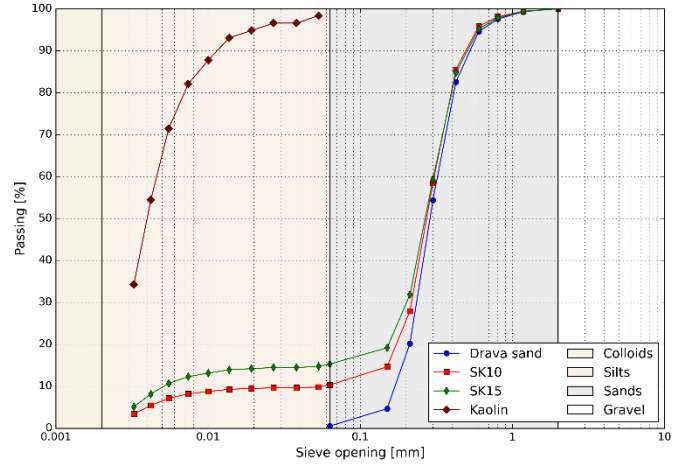


Figure 2 Sieve analysis of basic material and its mixtures

Table 1 Physical properties of testing materials

Physical property	Symbol	SK0	SK10	SK15
Specific gravity	G_s [-]	2.7	2.69	2.67
Particle size	D_{10} [mm]	0.183	0.054	0.0045
	D_{30} [mm]	0.237	0.219	0.206
	D_{60} [mm]	0.32	0.307	0.303
Coefficient of uniformity	C_u [-]	1.749	5.685	-
Coefficient of curvature	C_c [-]	0.959	2.893	-
Minimum void ratio	e_{min} [-]	0.641	0.647	0.544
Maximum void ratio	e_{max} [-]	0.911	1.121	1.43
Initial relative density	$D_{r,i}$ [%]	50	50	75

Table 2 Scaled properties based on the similarity laws

Property	Scaling factor, Type II	Value
Length	μ	40
Time	$\mu^{0.75}$	15.91
Frequency	$\mu^{-0.75}$	0.0635
Stress	$\mu^{0.5}$	6.32
Displacement	$\mu^{1.5}$	252.98
Acceleration	1	1

Material was built in a small-scale frame made of aluminium and plexiglass applying the undercompaction method proposed by Ladd (1978). The height of each layer was calculated based on the considered layer undercompaction, as stated in the equation (1).

$$U_n = U_{n,i} - \left[\frac{(U_{n,i} - U_{n,t})}{n_t - 1} \cdot (n - 1) \right] \quad [1]$$

where: U_n is an undercompaction of a layer being considered, $U(n,i)$ is the chosen value of percent of undercompaction of the first layer, n is the number of layer being considered and n_t is the total number of layers.

Measuring equipment

Several different measuring techniques were used and applied. Two governing measuring equipment were: (i) surface marker points for monitoring the displacement using a pair of high-speed cameras and (ii) accelerometers. The type of accelerometers used are presented in Figure 3. The Seika BDK₃ accelerometer is an analogue measuring instrument designed to measure acceleration within a range of $\pm 3g$. It operates within a frequency range of 1 to 300 Hz, and its sensitivity is 150 mg/V when subjected to a 5V excitation. The position of accelerometers inside the model itself is presented in Figure 4.

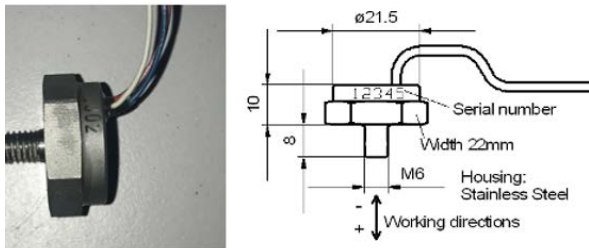


Figure 3 Seika BDK₃ accelerometer used for monitoring accelerations inside small-scale model

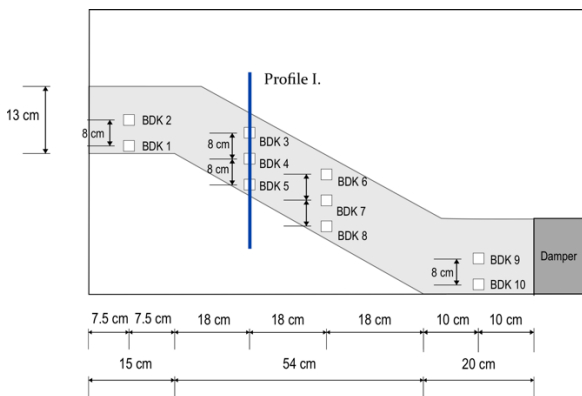


Figure 4 Positions of the measuring equipment inside the small-scale slope model

GOM Aramis 4M system of high-speed cameras is used, with each camera’s resolution of 2400x1728 pixels. Each measurement is conducted with 100 fps and post-processed using digital image correlation.

Shake table system

The Quanser STI-III seismic platform is a versatile biaxial shake table system, with 120 kg mass capacity. It can reproduce ground motions to examine shaking responses of subjected materials and/or constructions. With a travel range of ± 10.8 cm in both the x and y directions, this

system allows for comprehensive testing under various seismic scenarios. Its operational bandwidth is 10 Hz, making it a reliable tool for earthquake engineering research. The biaxial design enhances its capability to replicate complex seismic motions, providing valuable insights into the performance of subjected structures in multidirectional forces. Figure 5 presents the small-scale slope model positioned on the shaking table.

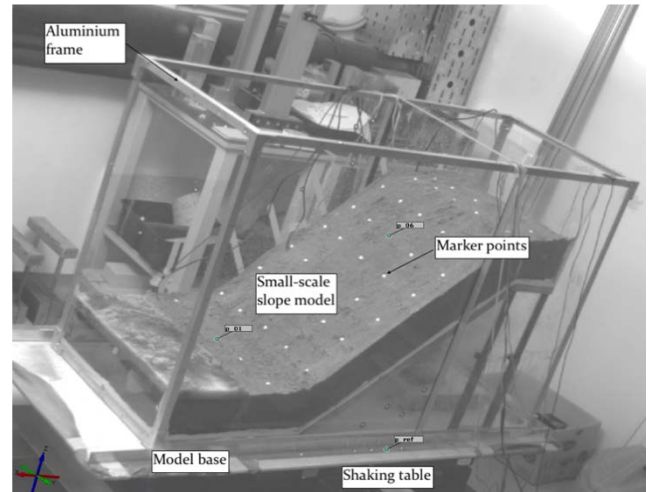


Figure 5 High-speed camera photo before the test initiation

Results

The results of dynamic test on small-scale models made from different types of material are presented in the following section. Acceleration measured using Seika BDK₃ accelerometers in combination with high-speed cameras were used to determine the time needed for first crack to appear during dynamic loading.

Model slopes are loaded with sinusoidal dynamic loading like the one presented on Figure 6. The amplitude of dynamic loading was 0.2cm and the frequency was gradually increased from 0Hz to 5.5Hz in 10 seconds, and decreased in the last 10 seconds. The loading lasted for 60 seconds.

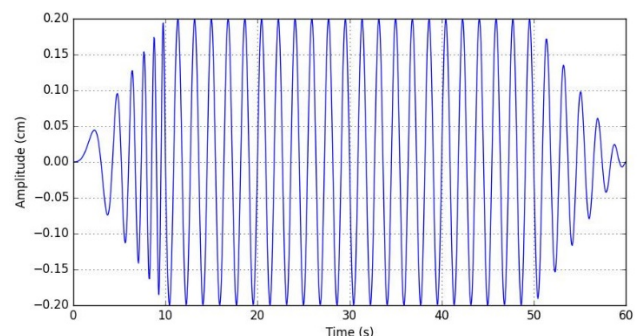


Figure 6 The shape of dynamic loading applied with shaking table

The time of the first crack appearance is marked with the dashed red line, as presented in Figure 7.

Results of a dynamic test on pure sand (SK0)

A small-scale slope model made of pure sand withstood a load of about 35 seconds before the first crack appeared. The acceleration plots of the BDK3 and BDK4 accelerometers placed inside the model are shown in Figure 7(a). The maximum acceleration measured by the BDK3 accelerometer (Figure 4) at the top of the slope model is 0.25g.

Results of a dynamic test on sand mixed with 10% of kaolin (SK10)

The acceleration plots of the BDK3 and BDK4 accelerometers placed in a small-scale slope model made of sand mixed with 10% kaolin are shown in Figure 7(b). The model withstood approximately 55 seconds of loading before the first crack appeared. Figure 7(b) shows that the

accelerations decrease again after about 65 seconds of testing. This time corresponds to a further opening of the tension crack, which occurred for the first time in the 55th second of a test. The maximum acceleration measured with the accelerometer BDK3 (Figure 4) at the top of the slope model is 0.35 g.

Results of a dynamic test on sand mixed with 15% of kaolin (SK15)

The physical model of a small-scale slope model made of sand mixed with 15% kaolin has shown that it can withstand a dynamic load of about 40 seconds. At $t=40s$ the first crack appeared. The acceleration diagrams of BDK3 and BDK4 are shown in Figure 7(c). The maximum acceleration measured by the accelerometer BDK3 (Figure 4) at the top of the slope model is 0.45g.

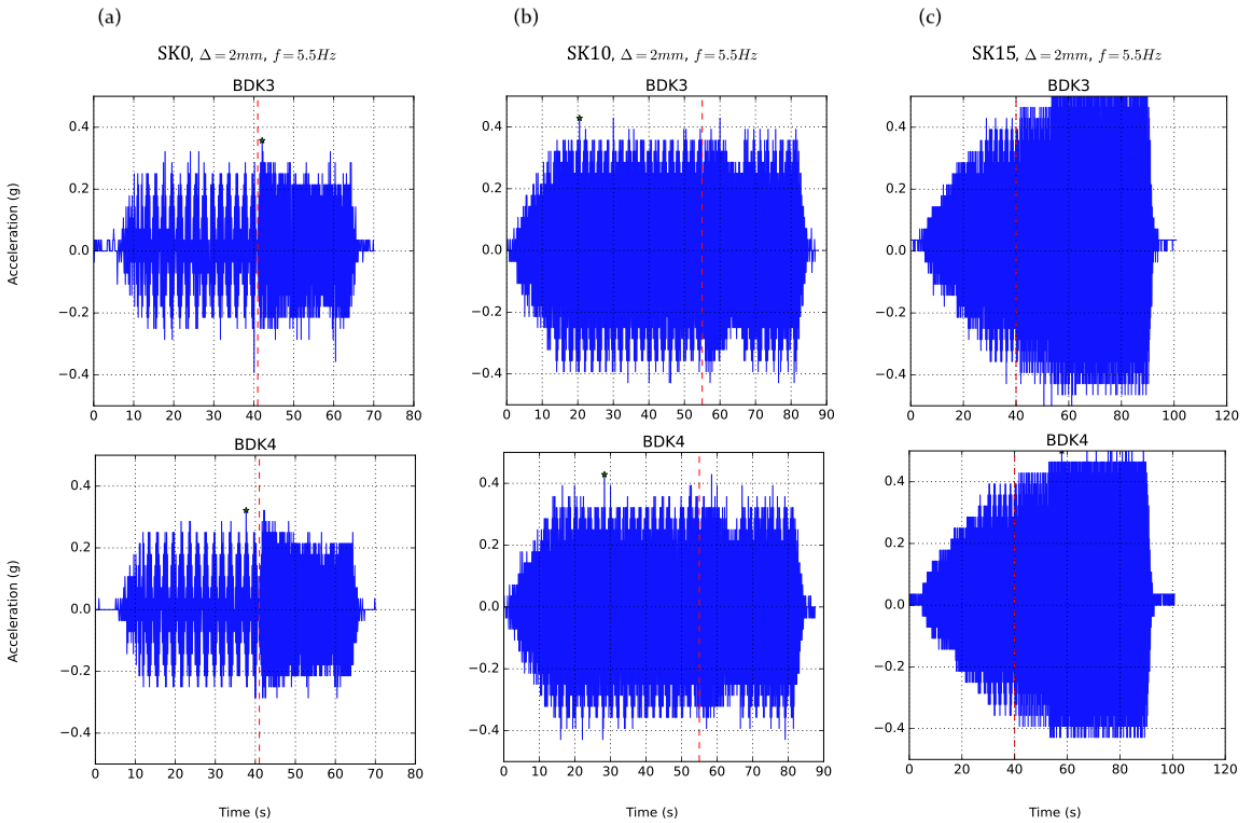


Figure 7 Accelerations of small-scale model made from pure sand

Analysis of performed test

Based on the results of dynamic test on a small-scaled slopes made from different materials, time necessary for a first crack to appear was detected. The values are summarised in Tab 3. The recorded times are normalized with respect to the time corresponding with the results of a model made form pure sand ($t_{crack,SK0} = 35s$) using the equation (2):

$$T_N = \frac{t_{crack,ID}}{t_{crack,SK0}} \quad [2]$$

The plot of normalized time failure and percent of fines are presented with the Figure 8.

Table 3 Scaled properties based on the similarity laws

Model material, ID	Time of first crack, $t_{crack,ID}$ (s)	% of material <63 μ m	% of material <2 μ m	Normalized time of first crack, T_N (-)
Pure sand (SK0)	35	<1	0	1.00
Sand with 10% of kaolin (SK10)	55	10	≈3.5	1.57
Sand with 15% of kaolin (SK15)	40	15	≈5	1.14

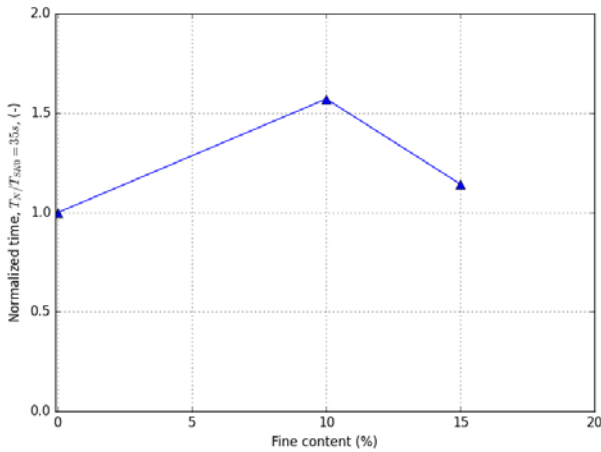


Figure 8 Normalized time failure with respect to fines content

Discussion

The influence of fines content on cyclic soil behaviour can simply be characterised with the cyclic shear strain threshold for pore water pressure generation, degradation, etc. (Vucetic 1994; Mortezaie and Vucetic 2016; Ichii and Mikami 2018). This is consistent if the response of materials with the ID’s “SKo” and “SK1o” are compared. Since mixture “SK1o” has a plasticity index, the cyclic threshold is larger than in ”SKo”. This led to the time of the first crack appearance 36% greater than for slope made of “SKo”. By further increasing the fines content, the plastic index should be larger, thus the threshold should be larger for “SK15” compared to “SK1o”, making the material subjectable to a larger number of cycles. If the times of first crack appearance in “SKo” and “SK15” are compared, the material “SK15” can be subjected to dynamic loading for 12% longer. But, if the materials “SK1o” and “SK15” are compared, “SK15” can be subjected to dynamic loading 27% less. This is due to inter-grain connections and the formation of metastable soil, in combination with the presence of low confining pressure.

Conclusions

In conclusion, this comprehensive study provides valuable insights into critical small-scale slope behaviour, subjected to dynamic loading. The inter-grain connections and interactions emerge as a significant element, influencing the overall performance of the soil matrix. Significantly, the identification of pore water pressure thresholds and fines content thresholds contributes to the understanding

of small-scale slope behaviour. The role of overburden stress under ig conditions significantly impacts soil behaviour, from which slope models were made. Further analysis will be made to examine the inter-grain interaction and behaviour at low confining stresses under static and dynamic loading for both artificial and natural soil mixtures.

Acknowledgements

Physical modelling of landslide remediation constructions behaviour under static and seismic actions (ModLandRemSS, IP-2018-01-1503) funded by Croatian Science Foundation
 “Laboratory Research of Static and Cyclic Behavior at Landslide Activation” (uniri-tehnic-18-113) funded by the University of Rijeka, Croatia

References

Baronin V V. (1992) Modeling of landslide-generated surges. *Hydrotechnical Construction* 26:280–285. <https://doi.org/10.1007/BF01545039>

Cao L, Zhang J, Wang Z, et al (2019) Dynamic response and dynamic failure mode of the slope subjected to earthquake and rainfall. *Landslides* 16:1467–1482. <https://doi.org/10.1007/s10346-019-01179-7>

Chen XL, Zhou Q, Ran H, Dong R (2012) Earthquake-triggered landslides in southwest China. *Natural Hazards and Earth System Sciences* 12:351–363. <https://doi.org/10.5194/nhess-12-351-2012>

Gabet EJ, Mudd SM (2006) The mobilization of debris flows from shallow landslides. *Geomorphology* 74:207–218. <https://doi.org/10.1016/j.geomorph.2005.08.013>

Iai S, Tobita T, Nakahara T (2005) Generalised scaling relations for dynamic centrifuge tests. *Geotechnique* 55:355–362. <https://doi.org/10.1680/geot.2005.55.5.355>

Ichii K, Ohmi H (2004) Slope stability of cohesionless material under large seismic shakings. In: 11th international conference on soil dynamics and earthquake engineering and the 3rd international conference on earthquake geotechnical engineering proceedings. pp 388–395

Icl (2016) Instruction for World Reports on Landslides

Kim J, Jeong S, Park S, Sharma J (2004) Influence of rainfall-induced wetting on the stability of slopes in weathered soils. *Eng Geol* 75:251–262. <https://doi.org/https://doi.org/10.1016/j.enggeo.2004.06.017>

Ladd R (1978) Preparing Test Specimens Using Undercompaction. *Geotechnical Testing Journal* 1:16–23. <https://doi.org/10.1520/GTJ10364J>

Lai CJ, Zhu YP, Wang CQ, Ma TZ (2013) Theory Study on Similitude Design of Shaking Table Tests of Earthquake-Induced Landslide. *Applied Mechanics and Materials* 353–356:2294–2300. <https://doi.org/10.4028/www.scientific.net/AMM.353-356.2294>

- Moriwaki H, Inokuchi T, Hattanji T, et al (2004) Failure processes in a full-scale landslide experiment using a rainfall simulator. *Landslides* 1:277–288. <https://doi.org/10.1007/s10346-004-0034-0>
- Ochiai H, Okada Y, Furuya G, et al (2004) A fluidized landslide on a natural slope by artificial rainfall. *Landslides* 1:211–219. <https://doi.org/10.1007/s10346-004-0030-4>
- Okura Y, Kitahara H, Ochiai H, et al (2002) Landslide fluidization process by flume experiments. *Eng Geol* 66:65–78. [https://doi.org/10.1016/s0013-7952\(02\)00032-7](https://doi.org/10.1016/s0013-7952(02)00032-7)
- Orense RP, Shimoma S, Maeda K, Towhata I (2004) Instrumented Model Slope Failure due to Water Seepage. *Journal of Natural Disaster Science* 26:15–26. <https://doi.org/10.2328/jnds.26.15>
- Pajalić S (2024) Contribution to the development of similarity laws in small-scale landslide physical models (in preparation). PhD Thesis, University of Rijeka, Faculty of Civil Engineering
- Pajalić S, Peranić J, Maksimović S, et al (2021) Monitoring and data analysis in small-scale landslide physical model. *Applied Sciences (Switzerland)* 11:. <https://doi.org/10.3390/app11115040>
- Pecker A (2008) Advanced earthquake engineering analysis. In: CISM International Centre for Mechanical Sciences, Courses and Lectures. SpringerWienNewYork, pp 1–13
- Popescu ME (2002) Landslide causal factors and landslide remedial options. In: 3rd International Conference on Landslides, Slope Stability and Safety of Infra-Structures. pp 61–81
- Rahardjo H, Leong EC, Rezaur RB (2002) Studies of rainfall-induced slope failures. pp 15–29
- Spence KJ, Guymer I (1997) Small-scale laboratory flowslides. *Géotechnique* 47:915–932. <https://doi.org/10.1680/geot.1997.47.5.915>
- Stark CP, Hovius N (2001) The characterization of landslide size distributions. *Geophys Res Lett* 28:1091–1094. <https://doi.org/10.1029/2000GL008527>
- Wang G, Sassa K (2001) Factors affecting rainfall-induced flowslides in laboratory flume tests. *Géotechnique* 51:587–599. <https://doi.org/10.1680/geot.2001.51.7.587>
- Wu LZ, Huang RQ, Xu Q, et al (2015) Analysis of physical testing of rainfall-induced soil slope failures. *Environ Earth Sci* 73:8519–8531. <https://doi.org/10.1007/s12665-014-4009-8>
- Yang J, Luo XD (2015) Exploring the relationship between critical state and particle shape for granular materials. *J Mech Phys Solids* 84:196–213. <https://doi.org/10.1016/j.jmps.2015.08.001>
- You Y, Liu J, Chen X (2012) Study on Similarity Laws of Model Experiments of Debris Flow Channels. In: 2012 2nd International Conference on Remote Sensing, Environment and Transportation Engineering. IEEE, pp 1–5

Influence of precipitation and soil conditions on the Krbavčići Landslide reactivation (Istria Peninsula, Croatia)

Martina Vivoda Prodan^{(1)*}, Josip Peranić⁽¹⁾, Vedran Jagodnik⁽¹⁾, Hendy Setiawan⁽²⁾, Željko Arbanas⁽¹⁾

1) Faculty of Civil Engineering, University of Rijeka, Radmile Matejčić 3, 51 000 Rijeka, Croatia (martina.vivoda@gradri.uniri.hr)

2) Universitas Gadjah Mada, Faculty of Engineering, Department of Geological Engineering, Yogyakarta, Indonesia

Abstract The Krbavčići landslide occurred at the end of January 1979 near the City of Buzet, Croatia, after prolonged heavy rainfall. The landslide damaged the local road and the retaining wall at the landslide foot, and a new stable landslide position was taken after major sliding. The Krbavčići landslide is located in an area built of flysch rock mass, which is susceptible to sliding and where many different types of mass movements have been recorded in the past. The determined dimensions of the landslide are 370 m in length, 30 m in width in the upper part and 150 m in the lower part, with an estimated landslide volume of $3 \times 10^5 \text{ m}^3$. The field investigation indicated that the sliding surface is located within the weathered bedrock zone at the contact between the weathered and fresh flysch rock mass at the depth of 13 m. Weathering of the flysch rock mass changes the geotechnical properties and shear strength, and potentially unstable deposits are formed. This paper presents the available information about the Krbavčići landslide occurrence, precipitation conditions for landslide reactivation, and laboratory testing of flysch deposit samples from the landslide body. Among the basic laboratory tests, ring shear test on the disturbed samples from the landslide body will be performed to determine the residual shear strength. Due to the specific shape of soil samples, the ring shear apparatus is commonly used to test disturbed soil samples. Therefore, a new sampling cutter was designed and a procedure developed to enable the collection, installation, and testing of the undisturbed soil samples. The precipitation and soil conditions that lead to the reactivation of the Krbavčići landslide are analysed and discussed.

Keywords landslide, precipitation, ring shear apparatus, sample cutter

Introduction

Climate change affects the stability of natural and engineered slopes and has consequences on landslides and similar phenomena. Landslides are mainly triggered by rainfalls and earthquakes. Rainfall-triggered shallow and deep landslides in flysch deposits are a common natural hazard on the Istria Peninsula and in the Rječina River Valley in Croatia. The Krbavčići landslide is located on the Istria Peninsula in an area built of flysch rock mass that are susceptible to sliding and where many different types of mass movements have been recorded in the past. The

Krbavčići landslide occurred on 31st January 1979 after prolonged heavy rainfall (Vivoda Prodan & Arbanas, 2020). The landslide damaged the local Buzet–railway station road and the retaining wall at the foot of the landslide, and after major sliding a new stable landslide position was taken. Based on the field investigations, the dimensions of the landslide were determined: 370 m in length, 30 m in width in the upper part and 150 m in the lower part, the depth of the sliding surface is 13 m at the contact between the weathered and fresh flysch rock mass (WP/WLI & Glossary, 1993). According to Skempton & Hutchinson, 1969, it is classified as a translational landslide, and as a rock planar slide according to Hungr et al., 2014, while according to Cruden & Varnes, 1996 the style was moderately moving. The landslide is now dormant as no movement was visible on the local road or the remains of the retaining wall after the initial sliding.

The assessment of landslide stability requires the determination of the geotechnical properties of the material, which usually requires the use of various laboratory devices. This paper describes the laboratory testing of flysch deposit samples from the Krbavčići landslide body (Figure 1) to obtain data of their geotechnical properties. Details of the testing methodology used are described in the following sections. Shear strength is an important parameter for estimating slope stability and dynamics during mass movements and generally depends on the shear rate and drainage conditions in a slope. A better understanding of soil behaviour during the initiation and propagation phase of a landslide using ring shear apparatus is very important. Ring shear tests (RST) have been used to investigate residual strength properties and analyse geological hazards (Liao et al., 2011; Lin et al., 2018; Li et al., 2022; Sassa et al., 2004; Setiawan et al., 2016; Tika & Hutchinson, 1999; Tiwari & Marui, 2004; Wang et al., 2002). In addition, a dynamic RST with possibility to apply seismic loads has been developed to investigate the sliding mechanisms of earthquake triggered slopes (Liao et al., 2011; Sassa et al., 2010, 2014; Setiawan et al., 2016). Although extensive research has been conducted on coarse-grained soils, less work has been conducted on clay-like soil materials (Carrubba & Colonna, 2006; Duong et al., 2018; Tiwari & Marui, 2005). RSTs that enable the measurement of pore water pressure (PWP) are quite rare and only performed by a few authors (Lin et al., 2018; Sassa et al., 2004). Rate effects on residual strength play an important

role in predicting and evaluating the behaviour of reactivated landslides. Although the rate dependence of residual strength has been extensively studied, there is a lack of consistency in test results (Li et al., 2022). RSTs on undisturbed samples are rare (Jeong, 2022; Tiwari et al., 2005), and not clearly investigated. The investigation of the weathering influence on the residual strength of the flysch rock mass on remoulded samples for Valići and Krbavčići landslide reactivation analysis was performed in the RSA (Vivoda Prodan et al., 2016; Vivoda Prodan & Arbanas, 2017, 2020).

The Ring shear apparatus (RSA) ICL-1 in the Geotechnical Laboratory of the Faculty of Civil Engineering, University of Rijeka was obtained as a part of the Croatian-Japanese project „Risk identification and land-use planning for disaster mitigation of landslides and floods in Croatia“. The main advantages of the RSA are the possibility of testing under high normal stress (up to 1 MPa) and high PWP (up to 1 MPa) (Oštrić et al., 2014; Sassa et al., 2004). For this reason, it is most often used to investigate deep-seated, rapid landslides. So far, the device has been used to investigate the shear strength properties of remoulded soil samples originating from flysch rock mass by performing strain-controlled tests under drained and undrained conditions, and PWP controlled tests under static conditions, which are crucial for investigation of landslide reactivation (Vivoda Prodan, 2016; Vivoda Prodan & Arbanas, 2017, 2020). RSTs under dynamic conditions in the described device have not yet been performed. Due to the specific shape of soil samples, RSA is commonly used for testing of remoulded soil samples. A sample cutter was developed that enables collection, installation and testing of undisturbed soil samples.

Numerical 2D slope stability and 3D landslide simulations were performed by Vivoda Prodan & Arbanas, 2020, based on the input parameters obtained by ring shear and direct shear tests on disturbed siltstone samples from flysch rock mass of different weathering grades from nearby location. Further research is needed to provide relevant soil properties from landslide location for the validation and calibration of landslide numerical models.

Defining the duration of the precipitation during which cumulative precipitation should be considered is essential for predicting the landslide occurrence. Arbanas et al., 2014; Dugonjić Jovančević & Arbanas, 2012 have shown that the cumulative twelve-month values as well as the maximum monthly, weekly or daily precipitation preceding the landslide have no significant influence on the triggering of a landslide initiation in the North Istria. Their analyses show that the precipitation from approximately three months before a landslide initiation has the primary influence on the rising infiltration and ground water level as the main triggering factor for the activation of landslides on flysch slopes in North Istria. In the last 10 years, many shallow landslides triggered by short intensity rainfalls have occurred on flysch slopes in the North Istria and they were. Prolonged rainfall events are critical for triggering deep-seated landslides, while

short and intense rainfall events play a greater role in triggering shallow landslides and erosion process.

This paper describes the performance of laboratory tests on flysch deposit samples to determine basic physical properties and to investigate shear strength and pore water pressure conditions during shear deformation on disturbed samples using RSA, as well as the development of a procedure for installing and testing undisturbed soil samples using RSA. The results of the precipitation analysis and laboratory tests would provide a better insight into the soil properties, which will be valuable input data for conducting numerical analysis of slope stability and landslide propagation in such materials. The results obtained will be valuable for future research as they will provide insights into the response of the soil under different shear conditions as well as input parameters for different numerical models.



Figure 1 Krbavčići landslide on a detailed orthophoto map from 2016 with sampling location and landslide boundary ($Q_{(br,dl)}$ -cover deposits, ${}^3(2)E_2$ -marl and siltstone outcrops, $P_{c,E}$ -limestone).

Precipitation conditions

Based on the precipitation data for the last 57 years (from 1966 to 2022) obtained from the Lupoglav rain gauge (390 m a.s.l.), about 10 km from the Krbavčići landslide, the daily and monthly precipitation amounts were observed.

The crucial cumulative three-month precipitation amount that triggered the Krbavčići landslide on 31st January 1979, was 509.2 mm. The amount of precipitation in January 1979 reached 327.2 mm, which was almost three times higher than the average amount of precipitation in January in the period 1966-2022. Figure 2 shows that all monthly precipitation within one year before the Krbavčići landslide occurrence was above the average monthly precipitation value, with the exception of the months of September and November 1978: the wet and dry period before the landslide occurrence was rainy with amounts above the average values.

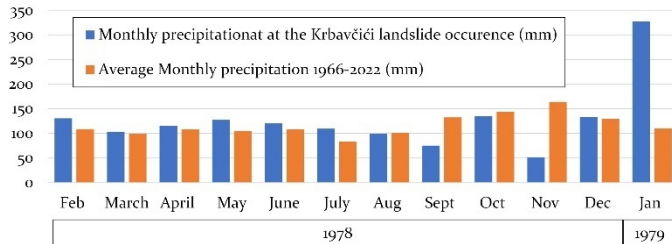


Figure 2 Monthly precipitation within a year before the Krbavčići landslide occurrence.

Laboratory testing

Soil properties

Disturbed and undisturbed residual soil samples originating from flysch rock mass were taken from the sample pit in the central part of the Krbavčići landslide (Figure 1). Sampling was carried out from the surface at a depth of 0.5 m. A series of tests were performed to determine the basic physical properties of the soil samples: specific gravity of soil solids (ASTM D854-14, 2014), saturated unit weight, particle size distribution (ASTM D422-63, 2007), liquid limit (*LL*), plastic limit (*PL*), plasticity index (*PI*) (ASTM D4318-10e1, 2010), classification of the material according to the USCS (ASTM D2487-17e1, 2020) and saturated coefficient of permeability using the falling head method (ASTM D5084-03, 2010). In addition to determining the basic physical properties, disturbed and undisturbed samples were taken to investigate the shear strength in the RSA.

Sample cutter design

Due to the specific shape of soil samples, RSA is commonly used to test remoulded soil samples. Here is described the development of a sample cutter (Figure 3) that makes it possible for the first time to obtain and analyse undisturbed samples of residual soil from a flysch rock mass from landslides which occur frequently on the Istria Peninsula and in other areas prone to sliding.

The sample cutter was designed together with the extruder in January 2024. The sample extruder was printed using a 3D printer with PLA material in the Hydrotechnical Laboratory of the Faculty of Civil Engineering, University of Rijeka. The two rings are

connected with a threaded rod and M5 nuts (Figure 3b). Sampling was carried out from the surface at a depth of 0.5 m using a newly developed sample cutter for ring shear tests (Figure 3a). After the cutter was pushed into the soil, it was excavated and sealed to prevent evaporation, and the sample was prepared (Figure 3c) and extruded into the ring shear box in the Geotechnical laboratory (Figure 4).

Ring shear testing procedure

An important advantage of the RSA is possibility of measuring PWP conditions at the shear surface during shearing, obtaining both peak and residual stress envelopes through infinite deformation under static (rainfall) and dynamic (earthquake) loading.

Disturbed residual soil samples were fully saturated with deaired distilled water and tested in the RSA. The ring shear box was first filled with CO₂ and de-aired distilled water and then with the saturated sample. After checking the sample saturation and consolidation under normal effective stresses of 235 kPa, the sample was sheared under a constant shear rate of 0.01 cm/s in undrained conditions until a steady state was reached. The procedure for installing and testing undisturbed residual soil samples from a flysch rock mass is currently being developed. For both types of sampling, basic parameters (peak and residual friction angle and cohesion) as well as the steady-state normal and shear stresses can be determined.

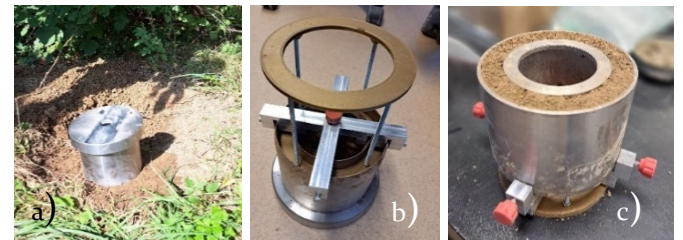


Figure 3 Collection of near-surface soil samples with the newly developed equipment for undisturbed soil sampling for RST: a) sampling in the field; b) sampling extruder; c) preparation of the sample surface.

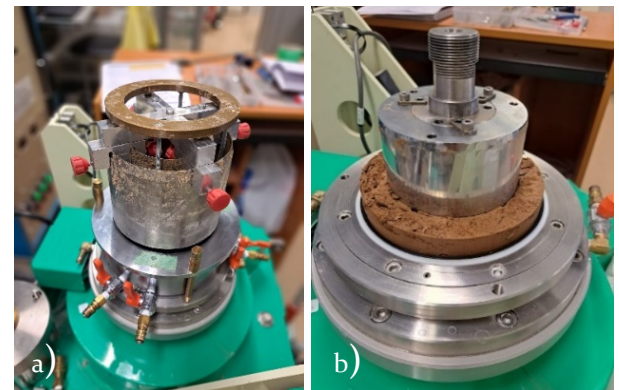


Figure 4 Installing undisturbed sample in the ring shear box: a) during extruding procedure; b) at the beginning of RST.

Results

The silt and clay content of the residual soil originating from the flysch rock mass were 40% (Figure 5), The sample had a liquid limit of 39% and a plastic limit of 20%, while

the plasticity index was 19%. The sample was classified as clay of low plasticity (CL) in the plasticity chart according to USCS soil classification (ASTM D2487-17e1, 2020). The specific gravity value was 2.7. The determined value of the saturated coefficient of permeability was 1.12×10^{-4} cm/s. Table 1 gives an overview of the test results with the basic physical properties of the sample.

The residual shear strength was determined based on the RST. Figure 6a presents changes in shear stress, total and effective normal stress and pore water pressure in time during shearing with shear rate control while Figure 6b shows a normal/shear stress diagram for the disturbed sample from the Krbavčići landslide. In Figure 6b, the green line represents the effective stress path, the purple line is the total stress path. When the effective stress path reached the failure line, it started to decrease due to pore water pressure generation along the failure line until the steady-state shear resistance was reached. The total shear resistance measured during the sample shearing, was additionally reduced by the value of rubber friction (12.6 kPa) to obtain the actual value of the shear resistance of a tested sample. The graph on Figure 6b shows that the residual friction angle was 19.3° , the residual cohesion was 18.4 kPa and the steady-state shear resistance was 39.4 kPa.

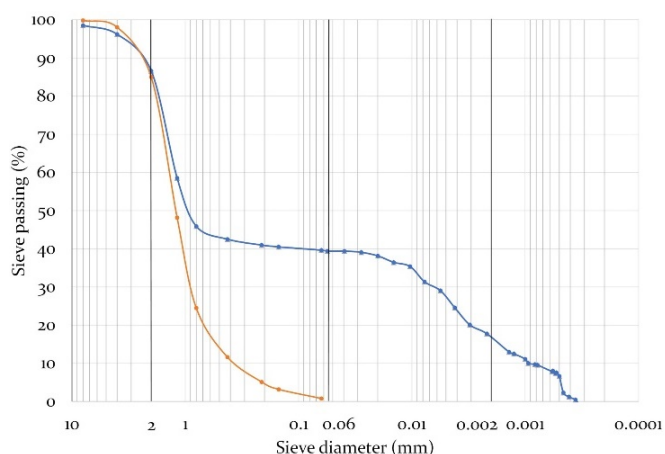


Figure 5 Grain size distribution curve of sample from Krbavčići landslide based on the dry sieving (orange line) and wet sieving + hydrometer test (blue line).

Table 1 Basic physical properties of the tested sample from the Krbavčići landslide.

Parameter	Symbol	Unit	Value
Specific gravity	G_s	(-)	2.7
Liquid limit	LL	(%)	39
Plastic limit	PL	(%)	20
Plasticity index	PI	(%)	19
Effective particle size			
	D_{10}	(mm)	0.001
	D_{60}	(mm)	1.2
Coefficient of permeability	k_s	(m/s)	1.12×10^{-6}

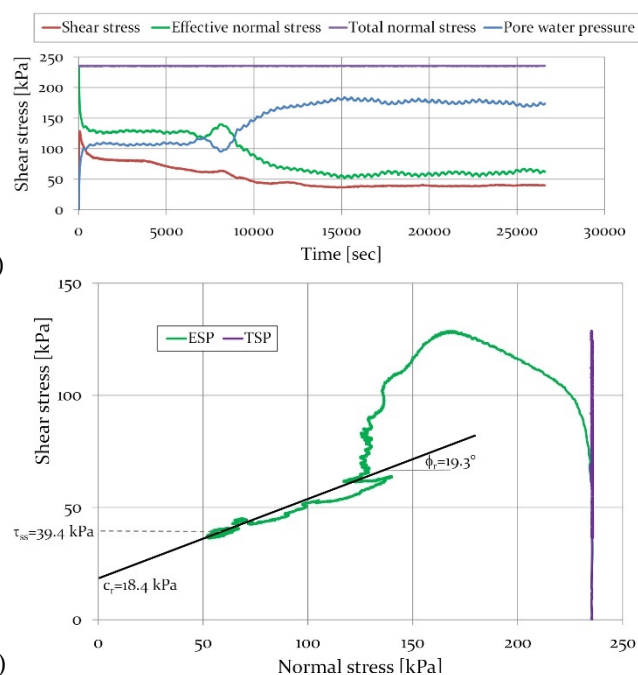


Figure 6 Undrained shear rate control test: a time series data, b stress path (green-effective stress path ESP, purple-total stress path TSP).

Summary and conclusions

In 2012, a high stress undrained ring shear apparatus, ICL-1, has been developed for the landslide research, and donated by the Japanese government for landslide analysis in Croatia. This RSA is suitable for undrained shear tests under all types of loading and enables the observation of the undrained shear behaviour of soils at high stresses up to 1 MPa at high speed movements with unlimited shear displacement.

The samples of residual soil from flysch rock mass taken from the Krbavčići landslide were tested. This paper presents experimental results of undrained speed control test until steady state condition is reached on the disturbed samples. From this test, the basic material properties, the residual friction angle, the residual cohesion and the steady state shear resistance were obtained. A newly developed sample cutter and a subsequent sample extruder will enable to obtain and test undisturbed samples in the ring shear apparatus. The results obtained on the disturbed samples must be compared with the results obtained on the undisturbed samples in the ring shear apparatus and also with the test results of other devices and further investigations are required. It should also be noted that in addition to the strength properties of the soil, other factors such as the hydraulic conductivity, the slope terrain and the initial moisture condition of the soil can also influence the triggering of landslides. The slopes in the Krbavčići area lie under deep deposits of flysch residual soils with intermediate permeability. Prolonged and low-intensity precipitation could lead to a relatively large amount of infiltration and eventually cause the slope more susceptible to failure.

The developed sample cutter is a new practical tool for research of undisturbed soil samples taken near the ground surface with the ring shear apparatus and for the subsequent research of landslides in Croatia. The future laboratory results and precipitation analysis will serve as a basis for the numerical simulation of the selected Krbavčići landslide and the analysis of a possible reactivation of the landslide in the surrounding area.

Acknowledgements

This research was funded by the University of Rijeka under the project ZIP-UNIRI-1500-1-22 and partially supported by the project uniri-mladi-tehnic-22-62. This paper has been supported by the International Consortium on Landslides under the IPL-256 project. Rainfall data received from Croatian Meteorological and Hydrological Service are also gratefully acknowledged. The authors would like to thank Duje Kalajžić for the construction of sample extruder. These supports are gratefully acknowledged.

References

- Arbanas, Ž., Jovančević, S. D., Vivoda, M., & Arbanas, S. M. (2014). Study of Landslides in Flysch Deposits of North Istria, Croatia: Landslide Data Collection and Recent Landslide Occurrences. In K. Sassa, P. Canuti, & Y. Yin (Eds.), *Landslide Science for a Safer Geoenvironment* (pp. 89–94). Springer International Publishing.
- ASTM D422-63. (2007). Standard Test Method for Particle-Size Analysis of Soils.
- ASTM D4318-10e1. (2010). Standard Test Methods for Liquid Limit, Plastic Limit, and Plasticity Index of Soils.
- ASTM D854-14. (2014). Standard Test Methods for Specific Gravity of Soil Solids by Water Pycnometer.
- ASTM D2487-17e1. (2020). Standard Practice for Classification of Soils for Engineering Purposes (Unified Soil Classification System).
- ASTM D5084-03. (2010). Standard Test Methods for Measurement of Hydraulic Conductivity of Saturated Porous Materials Using a Flexible Wall Permeameter.
- Carrubba, P., & Colonna, P. (2006). Monotonic fast residual strength of clay soils.
- Cruden, D. M., & Varnes, D. J. (1996). *Landslide Type and Processes. Landslides: Investigation and Mitigation*. In A. K. Turner & R. L. Schuster (Eds.), Special report 247 (pp. 36–75).
- Dugonjić Jovančević, S., & Arbanas, Ž. (2012). Recent landslides on the Istrian Peninsula, Croatia. *Natural Hazards*, 62(3), 1323–1338. <https://doi.org/10.1007/s11069-012-0150-4>
- Duong, N. T., Suzuki, M., & Van Hai, N. (2018). Rate and acceleration effects on residual strength of kaolin and kaolin–bentonite mixtures in ring shearing. *Soils and Foundations*, 58(5), 1153–1172. <https://doi.org/https://doi.org/10.1016/j.sandf.2018.05.011>
- Hungr, O., Leroueil, S., & Picarelli, L. (2014). The Varnes classification of landslide types, an update. *Landslides*, 11(2), 167–194. <https://doi.org/10.1007/s10346-013-0436-y>
- Jeong, S. W. (2022). Determining the Shear Resistance in Landslides with Respect to Shear Displacement and Shearing Time in Drainage-Controlled Ring Shear Tests. *Applied Sciences (Switzerland)*, 12(11). <https://doi.org/10.3390/app12115295>
- Liao, C.-J., Lee, D.-H., Wu, J.-H., & Lai, C.-Z. (2011). A new ring-shear device for testing rocks under high normal stress and dynamic conditions. *Engineering Geology*, 122(1), 93–105. <https://doi.org/https://doi.org/10.1016/j.enggeo.2011.03.018>
- Lin, H.-M., Wu, J.-H., & Sunarya, E. (2018). Consolidated and Undrained Ring Shear Tests on the Sliding Surface of the Hsien-dushan Landslide in Taiwan. *Geofluids*, 2018, 9410890. <https://doi.org/10.1155/2018/9410890>
- Li, W., Xu, G., & Yu, Z. (2022). Analysis of Failure Behavior Based on the Ring Shear Test in a Bedding Rock Landslide of the Three Gorges Reservoir. *Frontiers in Earth Science*, 10. <https://doi.org/10.3389/feart.2022.885152>
- Oštrić, M., Sassa, K., Ljutić, K., Vivoda, M., He, B., & Takara, K. (2014). Manual of transportable ring shear apparatus, ICL- 1. Proceedings of 1st Regional Symposium on Landslides in the Adriatic-Balkan Region “Landslide and Flood Hazard Assessment,” 1–4.
- Sassa, K., Dang, K., He, B., Takara, K., Inoue, K., & Nagai, O. (2014). A new high-stress undrained ring-shear apparatus and its application to the 1792 Unzen–Mayuyama megaslide in Japan. *Landslides*, 11(5), 827–842. <https://doi.org/10.1007/s10346-014-0501-1>
- Sassa, K., Fukuoka, H., Wang, G., & Ishikawa, N. (2004). Undrained dynamic-loading ring-shear apparatus and its application to landslide dynamics. *Landslides*, 1(1), 7–19. <https://doi.org/10.1007/s10346-003-0004-y>
- Sassa, K., Nagai, O., Solidum, R., Yamazaki, Y., & Ohta, H. (2010). An integrated model simulating the initiation and motion of earthquake and rain induced rapid landslides and its application to the 2006 Leyte landslide. *Landslides*, 7, 219–236.
- Setiawan, H., Sassa, K., Takara, K., Miyagi, T., & Fukuoka, H. (2016). Initial Pore Pressure Ratio in the Earthquake Triggered Large-scale Landslide near Aratozawa Dam in Miyagi Prefecture, Japan. *Procedia Earth and Planetary Science*, 16, 61–70. <https://doi.org/https://doi.org/10.1016/j.proeps.2016.10.007>
- Skempton, A. W., & Hutchinson, J. N. (1969). Stability of natural slopes and embankment foundations. Proceedings of 7th International Conference on Soil Mechanics and Foundation Engineering, 291–340.
- Tika, Th. E., & Hutchinson, J. N. (1999). Ring shear tests on soil from the Vaiont landslide slip surface. *Géotechnique*, 49(1), 59–74. <https://doi.org/10.1680/geot.1999.49.1.59>
- Tiwari, B., Brandon, T. L., Marui, H., & Tuladhar, G. R. (2005). Comparison of Residual Shear Strengths from Back Analysis and Ring Shear Tests on Undisturbed and Remolded Specimens. *Journal of Geotechnical and Geoenvironmental Engineering*, 131(9), 1071–1079. [https://doi.org/10.1061/\(ASCE\)1090-0241\(2005\)131:9\(1071\)](https://doi.org/10.1061/(ASCE)1090-0241(2005)131:9(1071))
- Tiwari, B., & Marui, H. (2004). Objective Oriented Multistage Ring Shear Test for Shear Strength of Landslide Soil. *Journal of Geotechnical and Geoenvironmental Engineering*, 130(2), 217–222. [https://doi.org/10.1061/\(ASCE\)1090-0241\(2004\)130:2\(217\)](https://doi.org/10.1061/(ASCE)1090-0241(2004)130:2(217))
- Tiwari, B., & Marui, H. (2005). A New Method for the Correlation of Residual Shear Strength of the Soil with Mineralogical Composition. *Journal of Geotechnical and Geoenvironmental Engineering*, 131(9), 1139–1150. [https://doi.org/10.1061/\(ASCE\)1090-0241\(2005\)131:9\(1139\)](https://doi.org/10.1061/(ASCE)1090-0241(2005)131:9(1139))
- Vivoda Prodan, M. (2016). The influence of weathering process on residual shear strength of fine grained lithological flysch components [Dissertation]. Dissertation, University of Rijeka (in Croatian).
- Vivoda Prodan, M., & Arbanas, Ž. (2017). Parametric Analysis of Weathering Effect on Possible Reactivation of the Valići Landslide, Croatia BT - Advancing Culture of Living with Landslides (M. Mikos, B. Tiwari, Y. Yin, & K. Sassa, Eds.; pp. 621–631). Springer International Publishing.
- Vivoda Prodan, M., & Arbanas, Ž. (2020). Analysis of the Possible Reactivation of the Krbavčići Landslide in Northern Istria, Croatia.

In Geosciences (Vol. 10, Issue 8).
<https://doi.org/10.3390/geosciences10080294>

Vivoda Prodan, M., Mileusnić, M., Mihalić Arbanas, S., & Arbanas, Ž. (2016). Influence of weathering processes on the shear strength of siltstones from a flysch rock mass along the North Croatian Adriatic Coast. *Bulletin of Engineering Geology and the Environment*, in press.

Wang, F. W., Sassa, K., & Wang, G. (2002). Mechanism of a long-runout landslide triggered by the August 1998 heavy rainfall in Fukushima Prefecture, Japan. *Engineering Geology*, 63(1), 169–185. [https://doi.org/https://doi.org/10.1016/S0013-7952\(01\)00080-1](https://doi.org/https://doi.org/10.1016/S0013-7952(01)00080-1)

WP/WLI, I. G. S. U. W. P. on W. a, & Glossary, M.-L. L. (1993). *A multi-lingual landslide glossary*. Bitech Publishers

Debris-flow Susceptibility Assessment in Flow-R: Ribnica River Case Study

Ksenija Micić^{(1,2)*}, Miloš Marjanović⁽²⁾, Biljana Abolmasov⁽²⁾

1) University of Belgrade, Faculty of Civil Engineering, Chair of Geotechnical Engineering, Belgrade, Bulevar Kralja Aleksandra 73, Serbia, +381 11 3218-587 (kmicic@grf.bg.ac.rs)

2) University of Belgrade, Faculty of Mining and Geology, Belgrade, Đušina 7, Serbia

Abstract Debris flows are among the most dangerous erosional geohazards due to the fast rate of movement and long runout zones. Even though the initiation can be triggered in mountainous areas, inhabited and with steep slopes, their propagation and deposition can endanger not only buildings and infrastructure in the urbanized areas, but also threaten human lives. As these initiation areas usually represent unattainable terrains with rapid vegetation cover development, field observations and aerial photo analysis become high-demanding tasks. Consequently, medium-to-regional scale susceptibility assessments are increasing in interest. They allow for efficient and effective identification of the most endangered zones and can be used to propose where further detailed studies should take place. In those terms, since it can be challenging to obtain enough data for larger regions, empirical models with low data requirements represent an adequate solution to the susceptibility modelling problem. In this paper, a medium-scale debris flow susceptibility assessment has been carried out along the Ribnica River in western Serbia. Both the source areas and the propagation extent have been identified with the Flow-R empirical model based on simple probabilistic and energy calculations. The key input data used to investigate debris flow susceptibility in the study area was 10 m resolution DEM. The combination of DEM, its associated morphological derivatives, landuse and lithology datasets, with Holmgren's modified propagation algorithm and the angle of reach, allowed for the 1:25000 susceptibility assessment. The results are reasonable and can be of great use for determining the areas that need to be prioritized for further detailed studies.

Keywords debris flow, Flow-R, susceptibility assessment, empirical model

Introduction

Debris flows are gravity-driven masses of poorly sorted water-saturated sediment surged down the slopes, with an unsteady and nonuniform flow. Interaction of solid and fluid forces in debris flows is not only a distinguishing factor in relation to other phenomena such as rock avalanches and sediment-laden water floods, but also a leading factor of their unique destructive power. They

usually occur with little or no warning, because of slope failure in continental and seafloor environments, sometimes exerting enormous loads on objects they encounter. Similar to water floods, their fluid-phase provides them with enough energy to travel long distances in channels with modest slopes, to inundate vast areas, damage structures and endanger humans (Iverson, 1997).

Considering the material and human consequences debris flows can have, it is of great importance to conduct hazard assessment for management and reduction of the risk posed by this geohazard. However, detailed studies require numerical modelling and comprehensive field work to determine the hazard in the debris flow deposition areas (e.g., Medina et al., 2008). Difficulties in mechanical debris flow modelling and hazard assessment are a result of a very complex nature of the phenomenon, the variability of controlling factors and the uncertainty of modelling parameters (Iverson, 1997; He et al., 2003). Since it is cost and time-consuming to acquire physical parameters necessary for deterministic debris flow modelling in regional scale (Carrara et al., 2008), the modelling approach must be as simple as possible with minimum data requirements. Such characteristics seem to be best acknowledged by spatially distributed region-scale models based on empirical approaches (Rickenmann, 1999). Empirical methods seem to be the most transferable to any site because of the degree of generalisation from the data on which they were created. One of those is introduced by Horton et al. (2013) through a Flow-R model (Flow path assessment of gravitational hazards at a regional scale). "The model allows for automatic source area delineation, given user criteria, and for the assessment of the propagation extent based on various spreading algorithms and simple frictional laws. The choices of the datasets and the algorithms are open to the user, which makes it compliant for various applications and dataset availability. Amongst the possible datasets, the DEM is the only one that is really needed for both the source area delineation and the propagation assessment, with its quality being of major importance for the results accuracy" (Horton et al., 2013). The Flow-R model has been successfully applied to different case studies for which regional susceptibility maps have been generated (e.g., Horton et al., 2008; Baumann et al., 2011; Kappes et al., 2011;

Jaboyedoff et al., 2012; Fischer et al., 2012; Pastorello et al., 2017). So, the starting point of the debris flow hazard assessment at regional scale is the identification of the debris flow-prone areas, which is known as susceptibility assessment (Guzzetti et al. 2005). Two main steps in debris flow susceptibility analysis are the identification of the potential source areas and the estimation of the runout. Methods used in those purposes vary in approaches they use and data they require. For the source-area identification there are statistical methods, linking a variety of environmental factors to an inventory of past events (van Westen et al., 2006), empirical methods that analyse the environmental parameters on the experience-base (Horton et al., 2008) and physical methods that couple hydraulic models with the calculation of safety factor (Carrara et al., 2008). For the runout computation, empirical relationships are the primary approach in use, which is based on the so-called angle of reach (Corominas, 1996). Many authors express this angle as a function of the debris flow volume (Corominas, 1996; Rickenmann, 1999; Iverson, 1998).

This paper presents an application of the regional-scale Flow-R empirical model for debris flow susceptibility assessment along the Ribnica River situated in mountainous area of the Zlatibor region in western Serbia. Through modelling with Flow-R, a first overview of the debris flow susceptibility of the study area has been conducted even without the records of the past events and numerous environmental data for the calibration. The main objective of this paper was to acquire preliminary information on hazard-prone areas along the Ribnica River which could be used as a base for future investigations and detailed studies on hazard and risk assessment.

Study Area

Geographical characteristics

Study area is located in the western-southwestern part of the Republic of Serbia, in the municipality of Čajetina. It extends between 43° 42' N and 43° 40' N and between 19° 37' E and 19° 34' E and covers the area of approximately 12 km² (Fig. 1, left). The territory of the municipality, including the study area, belongs to the Zlatibor district, dominated by the Zlatibor mountain. This entire domain is mountainous with its elevations ranging from 650 to 1100 m. It's characterized by a well-

developed hydrological network consisting of several rivers and streams, with the most important ones being the Rzav Rivers and Ribnica hydro-accumulation. The climate of this area is dominantly humid continental with the annual precipitation average of 990 mm.

The most dominant entity of the study area is Ribnica River, the main branch of Crni Rzav River. The hazard-prone areas, common in the study area, are mainly determined by the Ribnica River flow and numerous gullies along the river.

From the geomorphological point of view, the territory of the study area belongs to Zlatibor plateau and is characterized by an elevation minimum of 606 m and a maximum of 1222 m (see Fig. 1, left). Most of the study area territory has slopes higher than 20°, especially in the parts along the Ribnica River with maximum value of 67°.

Geological setting

Study area consists of Jurassic rocks (Fig. 1, right) whose distribution is mainly associated with the Zlatibor ultramafic massif and its edges, which extend from Tara Mountain to Rzav Rivers

There are different understandings about the tectonic position, the way of appearance, the structural form, and the age of the Zlatibor massif. It is located in the central part of the Dinaridic ophiolite belt, tectonically representing a slice that rests against sedimentary rocks with high-angle contact. Ultramafic rocks composing the massif are intensively fractured and serpentinized at the base of the thrust slice, and they are weathered and cut by magnesite veins in the upper part of the massif. According to Mojsilović et al. (1971), the Zlatibor massif is predominantly of harzburgite character. In addition to the harzburgites, lertzolites, dunites and from them formed serpentinites were distinguished. All the primary rocks represent the differentiations of the harzburgite magma. Differentiation of study area's harzburgites was based on the petrological investigations, due to them macroscopically not differing from the other peridotite rocks. Serpentinites, which make up the edges of the massif, are of harzburgite and dunite character. From the lithological point of view, the study area could represent a mass movement-prone area because western-Serbia peridotite rocks are generally very jointed and prone to the weathering processes.

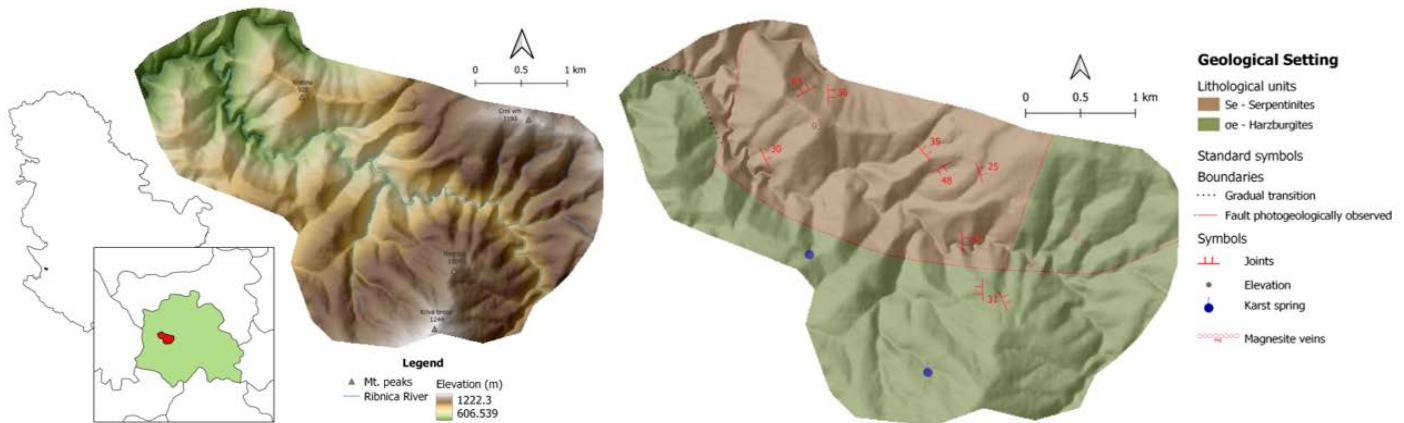


Figure 1 Study area. Its position and elevation - left. Its geological setting - right

Materials and Methods

Debris-flow modelling in Flow-R

Flow-R is an empirical debris flow susceptibility model, developed under Matlab®, with a clear and user-friendly interface. It allows for the simulation and hazard assessment at a regional scale for different types of natural hazards such as debris flows, snow avalanches and rockfalls. Trough modelling with Flow-R, regional debris flow susceptibility maps can be generated with low-data requirements and satisfying accuracy, at the same time.

The This GIS-based susceptibility tool processes the input data in order: 1) to delineate the potential source areas by means of morphological and user-defined criteria, and 2) to compute the propagation of the debris flow on the basis of the frictional laws and flow direction algorithms (Horton et al., 2013). Important to emphasize, such regional-scale computation processes cannot take the debris flow volume or mass into account.

The computational phase number 1 – source area identification consists of an index-based approach in which multiple spatial data is incorporated, such as Digital Elevation Model (DEM), slope gradient, flow accumulation, lithology etc. Importation of the entering datasets requires the definition of the computation criteria or thresholds for each one of them. The source area assessment consists of classifying the input datasets grid cells as either favourable, excluded or ignored, if the initiation is possible, unlikely or no decision can be made, respectively. A grid cell can be marked as potential source area if it has been selected as favourable at least once, and never excluded.

The computational phase number 2 – assessment of the propagation is based on the spreading algorithms which control the path of the debris flow, and the friction laws which determine the runout distance. Even though there are several different direction algorithms to choose from, Horton et al. (2013) recommend the application of Holmgren’s or Holmgren’s modified version, since it allows reproducing most of the other algorithms and parametrizing the spreading. Runout distance can be assessed by implementing one of the two available algorithms: the friction model from Perla et al. (1980) –

originally developed for avalanches, that calculates the runout distance as a function of the coefficient of friction μ and the mass-to-drag-ratio ω , and the simplified friction-limited model (SFLM) characterized by a minimum travel angle.

Input datasets

According to Takahashi (1981) and Rickenmann and Zimmermann (1993), three critical factors for debris flow initiation are: terrain slope, water input, and sediment availability. While the first two factors refer to the general disposition, the water input plays a role of a triggering factor.

To represent these critical factors in the source area assessment, the following datasets have been imported to the Flow-R – all with the same resolution (10 m), coordinates and in ASCII format:

- Digital elevation model, as the only essential data to model the debris flow susceptibility;
- Slope gradient and plan curvature, to take into account the slope shape influence;
- Flow accumulation, to take into account the water input related to the upslope contributing area;
- Lithology, to take into account the debris production related to the material characteristics;
- Land use – vegetation classification, to take into account the forested areas.

Digital elevation model (DEM) with a resolution of 10 m, smoothed and filled, has been used to assess the debris flow susceptibility of the study area. This elevation raster has also been used to derivate the other morphological and hydraulic input datasets - slope gradient, plan curvature and flow accumulation. According to many studies (e.g., Zhang and Montgomery, 1994; Quinn et al., 1995; Horton et al., 2013) 10 m grid size represents an adequate resolution for simulating different geomorphic and hydrological processes, without missing some significant areas (finer resolution), or enlarging the extents (lower resolution).

An orthophoto image has been used to generate the vegetation classification needed to represent the land use, or to be more precise, to include the forested areas in the source assessment procedure. The vegetation cover has

been segmented by a vegetation index generated from red, green and blue band of the orthophoto image (eq. 1):

$$I = \frac{Red+Blue}{Green} \quad [1]$$

where I represents the vegetation index, and Red , $Green$ and $Blue$ are the orthophoto image's bands.

Lithology data has been extracted from the Geological Map of the Republic of Serbia (1:100 000), by digitising it for the study area's extent, and converting it into a raster file with 10 m resolution. Both serpentinites and harzburgites have been included in the modelling process.

Simulation parameters

For the source area delineation, the model elaborates the input datasets using different threshold values and classifies every grid cell as explained above. Considering the fact that most debris flows occur in terrains with a slope gradient higher than 15° (Rickenmann and Zimmermann, 1993; Takahashi, 1981; Bathurst et al. 1997), this value has been taken as the lower initiation threshold. Since the plan curvature can contribute to localizing hollows, gullies and channels, by its negative values indicating a concave morphology (Carrara et al. 2008), for the triggering value $-2/100 \text{ m}^{-1}$ has been chosen. Horton et al. (2013) recommend this value as an optimum for the 10 m resolution DEM (for western Switzerland). For defining the flow accumulation threshold, based on the relationship between the upslope contributing area and the terrain slope, Horton et al. (2008) suggest two curves, combining the work of Rickenmann and Zimmermann (1993) and of Heinimann (1998) – one for the extreme and one for the rare events, respectively. For the computation process in this paper the 'extreme events' equation has been applied:

$$\begin{cases} \tan\beta_{thresh} = 0.31S_{uca}^{-0.15} & \text{if } S_{uca} < 2.5 \text{ km}^2 \\ \tan\beta_{thresh} = 0.26 & \text{if } S_{uca} \geq 2.5 \text{ km}^2 \end{cases} \quad [2]$$

where $\tan\beta_{thresh}$ is the slope threshold, and S_{uca} the surface of the upslope contributing area.

Probabilistic energy-based propagation calculation, for the previously delineated source areas, uses a variety of flow direction algorithms, depending on user's needs and preferences. Developed and recommended by Horton et al. (2013), modified Holmgren's (1994) multiple flow direction method has been used for the debris flow spreading assessment in this paper. It is expressed by the equation 3:

$$p_i^{fd} = \frac{(\tan\beta_i)^x}{\sum_{j=1}^8 (\tan\beta_j)^x} \forall \begin{cases} \tan\beta > 0 \\ x \in [1; +\infty[\end{cases} \quad [3]$$

Where i, j are the flow directions, p_i^{fd} the susceptibility proportion in direction i , $\tan\beta_i$ the slope gradient between the central cell and the cell in direction i , and x the variable exponent. For $x = 1$ the spreading simulates the multiple flow direction by Quinn et al. (1991), whereas for when x increases in its value, the divergence is reduced up to resulting into the single direction for $x \rightarrow \infty$ (O'Callaghan and Mark 1984). Horton

et al. (2013) introduced the dh variable which enables the central cell of the computational window (3x3 matrix) to be risen up to 70 m, and to allow for the flow to be guided by the general topography. The authors suggest that a 10 m resolution DEM is not very sensitive to the dh parameter and recommend the usage of exponents in range from 4 to 6. Following the stated above, the dh variable has been set to 1 m, whereas for the x exponent the value of 4 has been used. An additional parameter being considered in the computation is the persistence function (inertial parameter), that represents the change of the flow direction angle between the two consecutive cells. The one implemented in this paper is the Gamma (2000) function.

The runout distance computation doesn't take into account a source mass, so it is based on a simple energetic balance between a cell and the next one, represented by the equation 4:

$$E_{kin}^i = E_{kin}^0 + \Delta E_{pot}^i - E_f^i, \quad [4]$$

where E_{kin}^i is the kinetic energy of the cell in direction i , E_{kin}^0 is the kinetic energy of the central cell, ΔE_{pot}^i is the change in potential energy to the cell in direction i , and E_f^i is the energy lost in friction to the cell in direction i .

There are two frictional models available for use: Perla et al. (1980) and the simplified Friction Limited Model (SFLM). SFLM is based on the maximum possible runout distance, which is characterized by a minimum travel angle, also named the angle of reach (Corominas, 1996). It is the angle of the line that connects the source area to the most distant point reached by the debris flow. For this paper's purpose, the angle of reach has been set to 11°, and to ensure there are no improbable runout distances produced, the velocity limit has been set to 15 m/s.

Threshold values implemented in the source area delineation and propagation assessment for the Ribnica study area are summarized in Tab. 1.

Table 1 Flow-R modelling parameters for the study area

Source area delineation	
imported dataset	criteria
Digital elevation model	above 600 m
Slope gradient	above 15°
Flow accumulation	extreme events for 10m DEM
Plan curvature	-2/100m ⁻¹
Land use	default
Lithology	default
Propagation assessment	
algorithm / function	criteria
Holmgren (1994) modified	dh=01m; exp=04
Inertial parameter	Gamma (2000)
SFLM (travel angle)	11°
Velocity	15 m/s

Results

Simple, yet effective empirical medium to regional scale debris flow model Flow-R allowed for the delineation of debris flow source areas and estimation of propagation extent in medium scale of 1:25000 for Ribnica study area.

Despite the fact that the model essentially only requires the digital elevation model as input data, morphological, vegetational and lithological characteristics have also been taken into account for this study case.

Source areas have dominantly been identified in two main parts of the study area, as shown in Fig. 2. Majority of them is located along Ribnica River, in central to eastern parts of the study area, characterized by elevations ranging from 850 to 1000 m, mostly at north-facing slopes with angles of inclination ranging from 30 to 40°. Other source area cluster is located in NW part of the study area. It is characterized by the lowest elevations of the study area, ranging from 620 to 700 m, mostly north-facing slopes with angles of inclination ranging from 20 to 40°. Through visual orthophoto image interpretation, Flow-R delineated

source areas have been found to be reasonably outlined, with majority of them being placed in river gullies at high elevations, as expected.

As it comes to assessing the spreading of debris flow material, modified Holmgren’s algorithm in combination with SFL model and velocity limitations allowed the calculation from all the determined source areas. The results are shown in Fig. 3 and represent rational outcomes in regard to estimated size of runout zones.

Since there is no inventory map to be taken into account for the validation process, the results can be observed as a preliminary debris flow spatial prediction of sufficient accuracy.

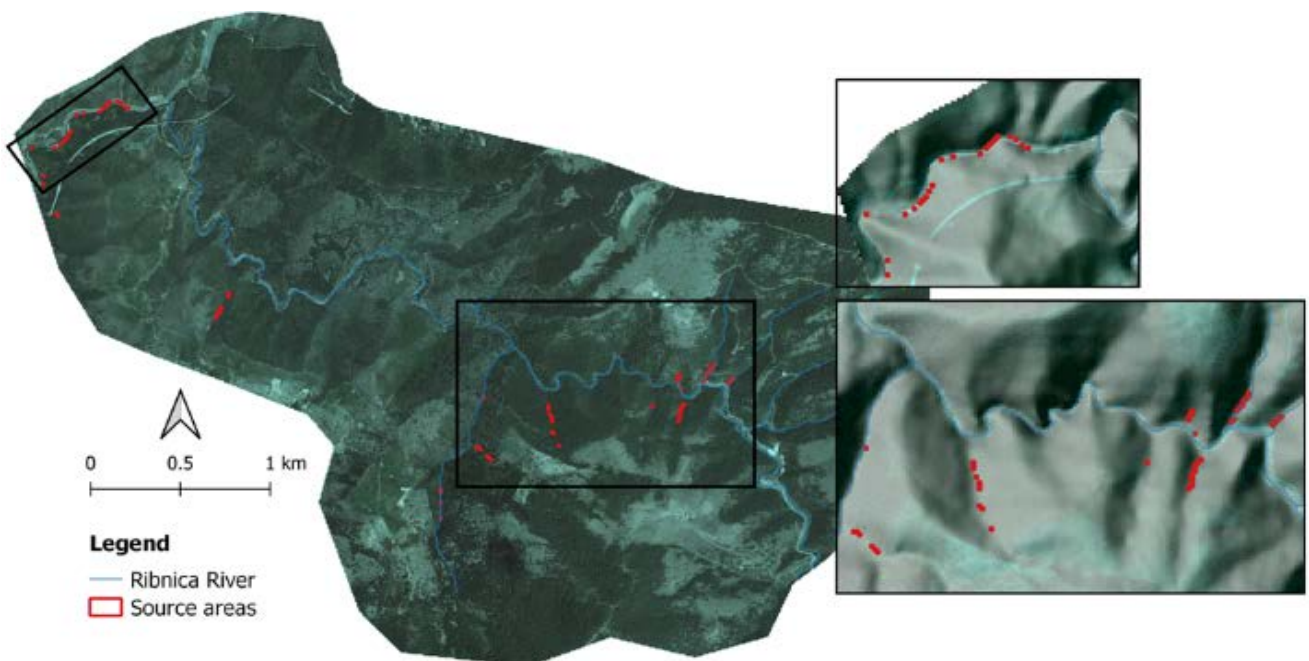


Figure 2 Delineated source areas with amplifications of two major cluster zone

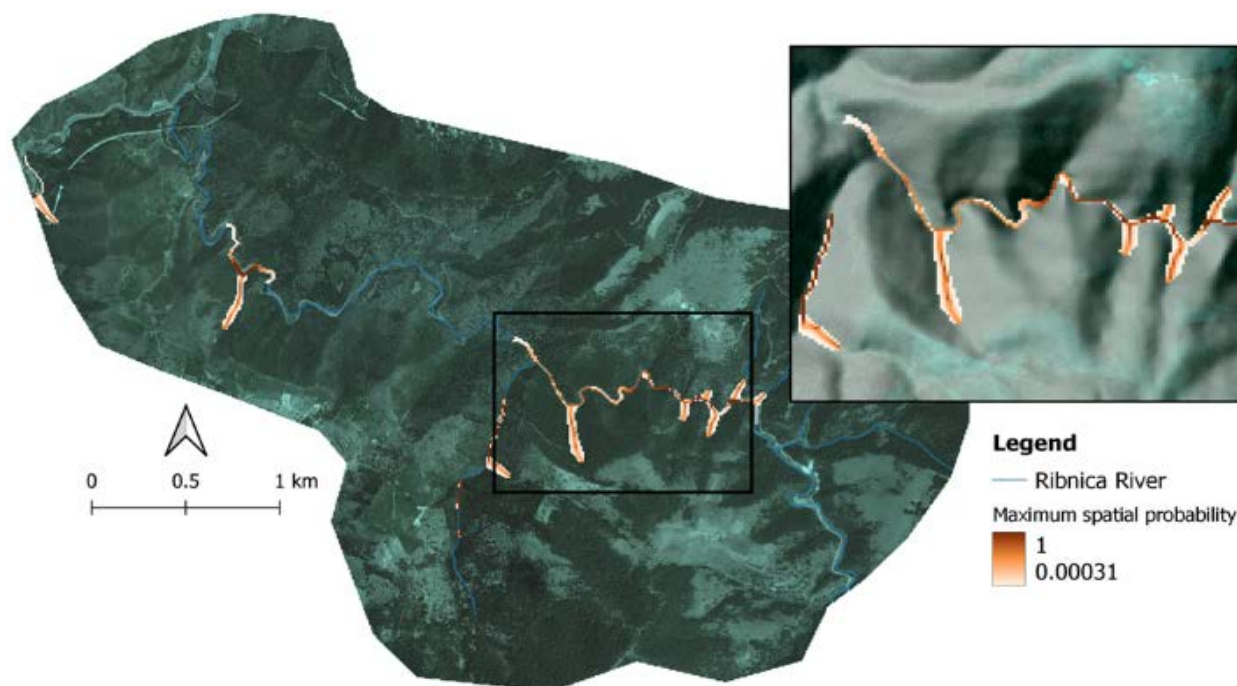


Figure 3 Calculated propagation extent with amplified debris flow prone zones in eastern parts of the study area

Conclusion

Susceptibility assessment, through an empirically distributed approach implemented within the Flow-R modelling framework, seems to be an appropriate first step in hazard and risk analysis. Even though Flow-R cannot integrate local controlling factors and actual behaviours, it is still characterized by many advantages in hazard susceptibility assessment. It enables the user to conduct a regional to medium scale analysis with minimum input data requirements and short computation time, by adapting the functions and algorithms to the needs of the case study. Also, as a topography-based model, it results in propagation areas larger than observed in the field, which allows for more precaution.

This study represents the first debris flow susceptibility assessment along the Ribnica River in western Serbia. Unlike most of the similar analysis in Flow-R, for Ribnica study case there hasn't been an inventory map to take into account for validation of the generated results. This lack shouldn't seem to be an issue in assessing the debris flow susceptibility of the study area, because the key objective of this paper was to delineate the possible hazard prone zones. Generated results should be considered as a first phase of the hazard analysis in the study area that provides information on where field investigations should be conducted in the future. They should be used as a base for the next phase, which should consist of detailed studies needed to be performed in order to propose adequate mitigation measures.

The combination of available input datasets and chosen algorithms for debris flow susceptibility modelling in the study area has shown realistic results. Delineated source areas and propagation extents are in good

agreement with expected outcomes based on study area's morphological features and the orthophoto visual evaluation. Most of them are found to be located along the Ribnica river in the eastern part of the study area, which is characterized by the highest elevations and slopes between 30 and 40°.

For the future work, it would be of great interest to perform detailed studies on the hazard assessment in the study area, conduct field investigations, and compare the results and conclusions with modelling results generated with limited input data.

References

- Baumann, V., Wick, E., Horton, P., and Jaboyedoff, M (2021) Debris flow susceptibility mapping at a regional scale along the National Road N7, Argentina. Proceedings of the 14th Pan-American Conference on Soil Mechanics and Geotechnical Engineering, 2–6 October 2011. Toronto, Ontario, Canada.
- Bathurst, J., Burton, A., and Ward, T (1997) Debris flow runout and landslide sediment delivery model tests. *J. Hydraul. Eng.-ASCE*, 123, 410–419.
- Carrara, A., Crosta, G., and Frattini, P (2008) Comparing models of debris-flow susceptibility in the alpine environment. *Geomorphology*, 94, 353–378.
- Corominas, J (1996) The angle of reach as a mobility index for small and large landslides. *Can. Geotech. J.* 33, 260–271.
- Fischer, L., Rubensdotter, L., Sletten, K., Stalsberg, K., Melchiorre, C., Horton, P., and Jaboyedoff, M (2012) Debris flow modeling for susceptibility mapping at regional to national scale in Norway. Proceedings of the 11th International and 2nd North American Symposium on Landslides, 3–8 June 2012, Banff, Alberta, Canada.
- Gamma P (2000) Dfwalk - Ein Murgang Simulationsprogramm zur Gefahrenzonierung, Rapport final. Geographisches Institut der Universität, Bern, Switzerland. pp 158 (A debris flow simulation program for hazard zonation). (In German)
- He, Y. P., Xie, H., Cui, P., Wei, F. Q., Zhong, D. L., and Gardner, J. S (2003) GIS-based hazard mapping and zonation of debris flows in Xiaojiang Basin, southwestern China. *Environ. Geol.*, 45, 286–293.
- Heinimann H (1998) Methoden zur Analyse und Bewertung von Naturgefahren. Bundesamt für Umwelt, Wald und Landschaft (BUWAL), Vol. 85. Bern, Switzerland, pp. 247. (Methods for the analysis and assessment of natural hazards). (In German)
- Holmgren, P (1994) Multiple flow direction algorithms for runoff modelling in grid based elevation models: An empirical evaluation. *Hydrol. Process.*, 8, 327–334.
- Horton, P., Jaboyedoff, M., Rudaz, B., Zimmermann, M (2013) Flow-R, a model for susceptibility mapping of debris flows and other gravitational hazards at a regional scale. *Natural Hazards and Earth System Sciences* 13 (4), 869–885.
- Horton, P., Jaboyedoff, M., and Bardou, E (2008) Debris flow susceptibility mapping at a regional scale. In Proceedings of the 4th Canadian Conference on Geohazards, 20–24 May 2008, 339–406.
- Iverson, R. M., Schilling, S. P., and Vallance, J. W (1998) Objective delineation of lahar-inundation hazard zones. *Geol. Soc. Am. Bull.*, 110, 972–984.
- Iverson, R. M (1997) The physics of debris flows, *Rev. Geophys.*, 35, 245–296.
- Jaboyedoff, M., Choffet, Ch., Derron, M.-H., Horton, P., Loye, A., Longchamp, C., Mazotti, B., Michoud, C., and Pedrazzini, A (2012) Preliminary Slope Mass Movements Susceptibility Mapping Using DEM and LiDAR DEM. In: *Terrigenous Mass Movements: Detection, Modelling, Early Warning and Mitigation Using Geoinformation Technology*, 109–170.
- Kappes, M. S., Malet, J.-P., Remaitre, A., Horton, P., Jaboyedoff, M., and Bell, R (2011) Assessment of debris-flow susceptibility at medium-scale in the Barcelonnette Basin. *Nat. Hazards Earth Syst. Sci.*, 11, 627–641.
- Medina, V., Hürlimann, M., Bateman, A (2008) Application of FLATModel, a 2D finite volume code, to debris flows in the northeastern part of the Iberian Peninsula. *Landslides* 5:127–142.
- Mojsilović, S., Baklajić, D., Đoković, I., Avramović, V (1971) Tumač Osnovne Geološke Karte SFRJ za list Titovo Užice K34-4. Zavod za geološka i geofizička istraživanja, Beograd.
- O’Callaghan, JF., Mark, DM (1984) The extraction of drainage networks from digital elevation data. *Computer Vision, Graphics, and Image Processing* 27 (3): 247.
- Pastorello, R., Michelini, T., and D’agostino V (2017) On the criteria to create a susceptibility map to debris flow at a regional scale using Flow-R. *Journal of Mountain Science* 14(4).
- Perla, R., Cheng, T.T., McClung, D.M (1980) A two-parameter model of snow-avalanche motion. *Journal of Glaciology* 26 (94): 197–207.
- Quinn, P., Beven, K., and Lamb, R (1995) The in ($a/\tan\beta$) index: How to calculate it and how to use it within the topmodel framework. *Hydrol. Process.*, 9, 161–182.
- Quinn, P., Beven, K., Chevallier, P (1991) The prediction of hillslope flow paths for distributed hydrological modelling using digital terrain models. *Hydrological Processes* 5 (1): 59–79.
- Rickenmann, D (1999) Empirical relationships for debris flows. *Nat. Hazards*, 19, 47–77.
- Rickenmann, D. and Zimmermann, M (1993) The 1987 debris flows in Switzerland: documentation and analysis. *Geomorphology*, 8, 175–189.
- Takahashi, T (1981) Estimation of potential debris flows and their hazardous zones: Soft countermeasures for a disaster. *Journal of Natural Disaster Science*, 3, 57–89.
- van Westen, C. J., van Asch, T. W. J., and Soeters, R (2006) Landslide hazard and risk zonation – why is it so difficult?. *B. Eng. Geol. Environ.*, 65.
- Zhang, W. and Montgomery, D (1994) Digital elevation model grid size, landscape representation, and hydrologic simulations. *Water Resour. Res.*, 30, 1019–1028.
- Guzzetti, F., Reichenbach, P., Cardinali, M., Galli, M., Ardizzone, F (2005) Probabilistic landslide hazard assessment at the basin scale. *Geomorphology* 72:272–299.

Optimization of pipeline design solutions for slope stability in Sakhalin region, Russia

Michael Naumov⁽¹⁾, Denis Gorobtsov⁽¹⁾, Daria Shubina^{(1,2)*}

1) Russian State University for Geological Prospecting, Moscow, Mikluho-Maklaya st., 23, Russia, +7910 452 36 03 (shubinadd@mgri.ru)

2) LLC "Avtodor Engineering", Moscow, Strastnoy blvd., 9, Russia.

Abstract The article discusses the optimization of design solutions for stabilizing landslide prone slopes on the main pipeline route on the Sakhalin Island, Russia. The calculations of slope stability for various areas located in difficult engineering and geological conditions reveal the possibility of significantly reducing the length of bored piles.

Keywords: pipelines on landslide prone slopes, safety factor, sensitivity analysis, retaining wall, landslide protection measures.

The territory description

In terms of geological structure, Sakhalin Island and the adjacent waters of the Japan Sea and the Okhotsk Sea are part of a transitional zone from the continent to the ocean and belong to the northwest segment of the Pacific mobile belt. The island's territory is part of the Hokkaido-Sakhalin geosyncline fold system. The pipeline route passes through a hilly, dissected area, composed of Cretaceous and Neogene deposits (fig. 1, 2), represented by siltstones, mudstones and sandstones. The area can be characterized by active tectonics: presence of faults, intrusions (neogene diorites and quartz diorites), and high seismicity.

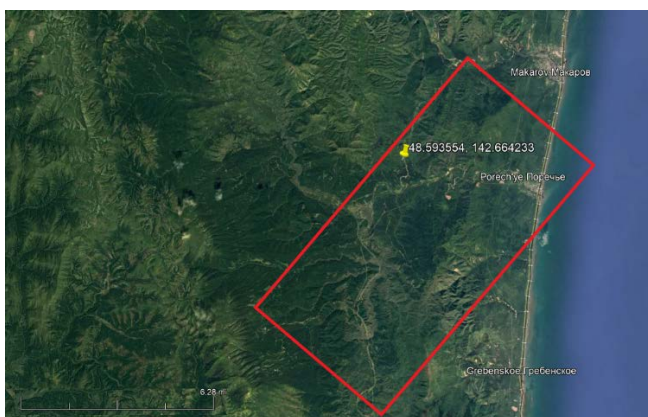


Figure 1 Study area location

The slope heights along the route varies from 15 to 25 meters, with average angles of 25-35°. Field observations on the route reveals the signs of landslides on the slopes and the threat of the existing pipeline destruction.

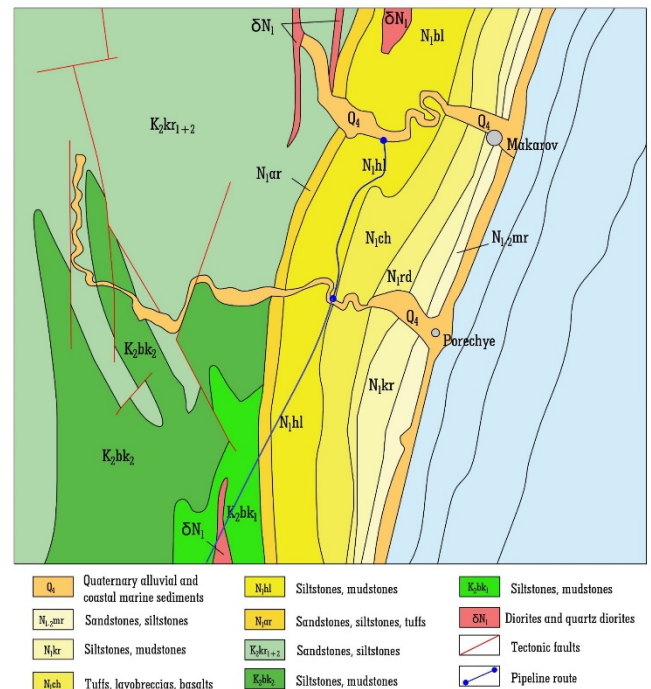


Figure 2 Geological map of the area of 1:200 000 scale.

The geological structure of the studied sections includes: artificial deposits represented by clayey deposits ranging from semi-solid to solid consistency (layer t1); modern eluvial and colluvial-deluvial deposits represented by clayey sandy and gravelly deposits ranging from semi-solid to solid consistency (layers 50, 51, 51a, 51b); deposits of Bykovskaya formation (K_2bk_2) of Santonian-Campanian stages represented by weakly fissured argillites (IGE 30).

Groundwater is prevalent in fissured siltstones of Cretaceous age and is located at depths ranging from 5 to 20 meters. They have sporadic distribution in coluvial-deluvial and eluvial clayey deposits and have not been encountered in the studied areas.

One of the most dangerous geological processes closely related to tectonic structure is seismic activity in the area. According to Russian codes of practice the seismicity of the area is rated 8 points on the MSK64 scale on map A (10%-possibility in 500-years' time period) and 9 points on map B (5%-possibility in 1000-years' time period).

The main factors contributing to the development of landslide processes and determining the slope stability in

some chosen sections are seismic effects, as well as actively occurring erosion processes (fig. 3).



Figure 3 Landslides and erosion processes on the pipeline route.

To prevent further development of landslide processes, a project was developed for the construction of a deep-seated retaining wall in the form of a single-row pile embankment with a wall on the embankment.

The goal of the research work was to develop recommendations for adjusting the design solutions for landslide protection structures to optimize the overall project cost.

Used calculation method

Currently, there are many methods for calculating slope stability. The type of landslide process and the mechanism of possible displacement primarily determine the choice of specific methods.

In the calculations we use the limit equilibrium method, represented by the Morgenstern-Price method, the simplified Bishop method, and the generalized Janbu method. The Bishop and Morgenstern-Price methods are considered accepted methods for slope stability calculations according to Russian regulatory documents (section 4.2.11 of SP 11-105-97, Part II)

Seismic effects, when assessing the stability of landslide-prone slopes, can be considered by the pseudo-static analysis.

In this approach introducing an additional force models the earthquake effect. The force F is determined as follows:

$$F = \frac{aW}{g} - kW, \quad [1]$$

where a – is horizontal seismic acceleration; g – gravitational acceleration, W – the weight of the block; k – seismicity coefficient.

When calculating the stability of a slope to justify landslide protection structures, in accordance with the recommendations of regulatory documents the seismic acceleration value was taken with $K_1=0.5$. Thus, the calculated seismic coefficient for period of 500 years is 0.2.

Normative safety factor should be calculated by the formula:

$$[Fs] = \frac{\gamma_n \psi}{\gamma_d}, \quad [2]$$

where $\gamma_n=1.21$ is the reliability coefficient for the responsibility of the pipeline;

ψ – load combination factor = 0.90 – for a special combination of loads, consisting of permanent, long-term, short-term and one of the special loads (seismicity).

γ_d – coefficient of operating conditions of the pipeline system = 0.99.

The value of the standard stability coefficient is:

For the main load combination:

$$[Fs] = \frac{1,21 \times 1}{0,99} = 1,22 \quad [3]$$

For the special load combination:

$$[Fs] = \frac{1,21 \times 0,90}{0,99} = 1,1 \quad [4]$$

Construction of a geomechanical model and calculation methods

The design solution involves the placement of a deep foundation retaining wall in the form of a single-row pile raft with a wall on the raft. The piles are designed with a diameter of 630 mm, a length of 17.5 m, and a spacing of 1.6 m on axes (fig. 4). Driven piles were taken into account in the calculations using specialized software support tools (Pile/Micro Pile) in the Rocscience complex. The piles are designed for a shear strength of 200 kN, and the pile driving spacing of 1.6 m is also considered. The retaining wall with the raft was accounted for by adding a new material to the model - reinforced concrete, its characteristics are specified in Table 1.

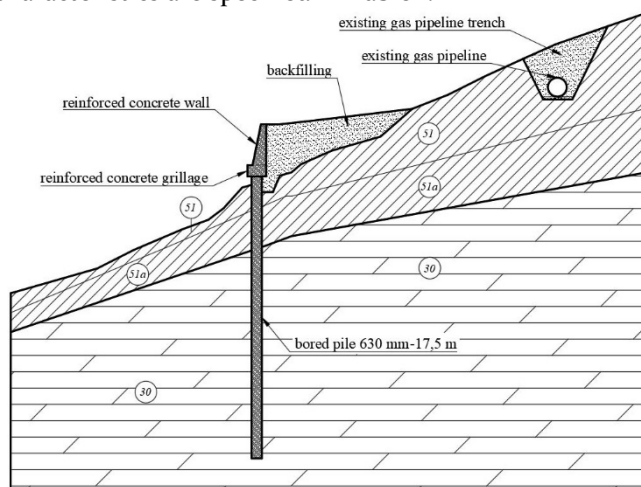


Figure 4 The scheme of retaining wall construction.

Calculations for the selected profiles were carried out for two scenarios:

- 1) slope stability calculation considering the adopted design solutions (without seismic effects);
- 2) calculation of the predicted stability considering the adopted design solutions and a special combination of loads (considering seismic effects). The adopted horizontal seismic coefficient = 0.2.

The model takes into account the groundwater level obtained from engineering-geological surveys.

The physical-mechanical properties of the soils used are provided in Table 1.

Table 1. Used properties of soils and concrete.

Layer	Color in model	Unit weight (kN/m ³)	Strength criterion	Cohesion (kPa)	Int. friction angle(degrees)
t1	Yellow	19.6	Mohr-Coulomb	41.6	22.7
50	Cyan	18.8	Mohr-Coulomb	57	18
51	Orange	19.4	Mohr-Coulomb	24	26
51a	Red-Orange	19.6	Mohr-Coulomb	35.3	21.6
30	Blue	21.4	Mohr-Coulomb	30.5	63
concrete	Grey	25	Mohr-Coulomb	250	55

The results of modelling are on figures 5 and 6. After performing the standard slope stability analysis, stability calculations were carried out with various pile lengths - from 2.5 m to the design length. The dependence

of the safety factor on pile length is on the plots (fig. 8, 9). The article presents an example of stability calculation for one analyzed section, with results for other calculated sections summarized in the conclusion.

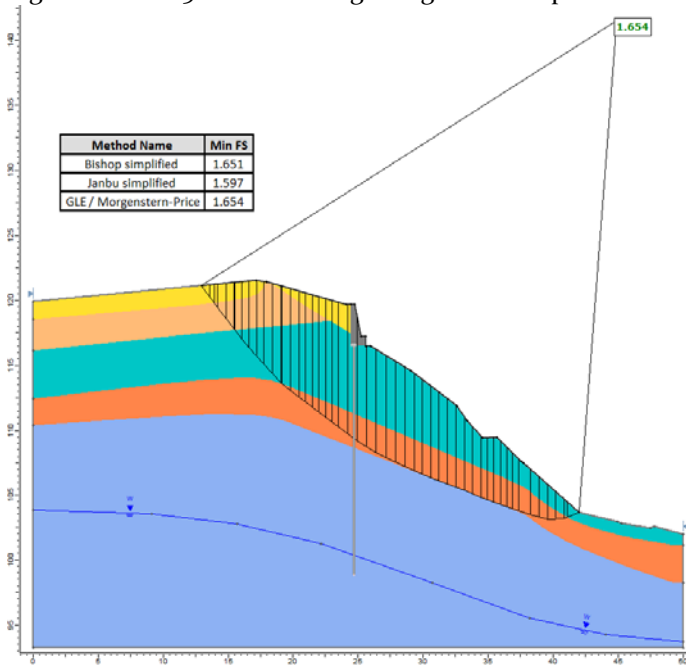


Figure 5 Modeling results without considering of seismic effects.

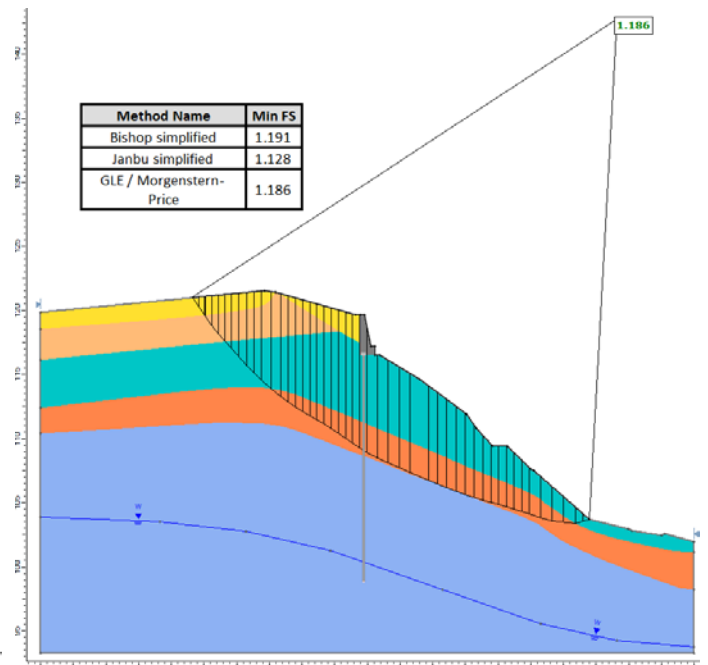


Figure 6 Sliding surface considering of seismic effects.

Calculation results

According to the calculation results, the analyzed slope with the preliminary protection measures decisions is in a stable state, both considering seismic effects and without them.

Additionally, a sensitivity plot of the safety factor (Fs) to the shear strength of the pile is shown on figure 7 considering seismic effects (in the worst-case scenario). It is worth noting that safety factor significantly decreases with increasing seismic effects.

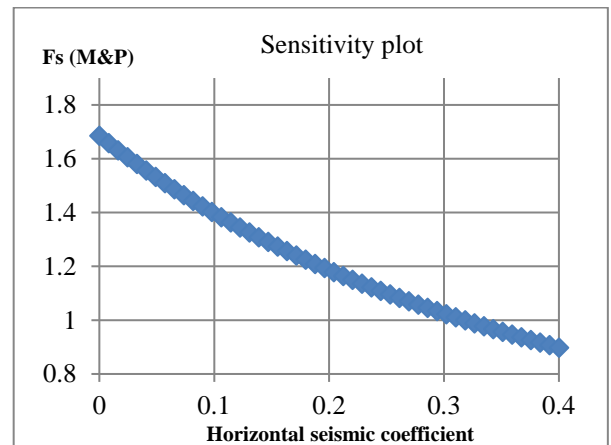


Figure 7 Safety factor dependence on seismic effects.

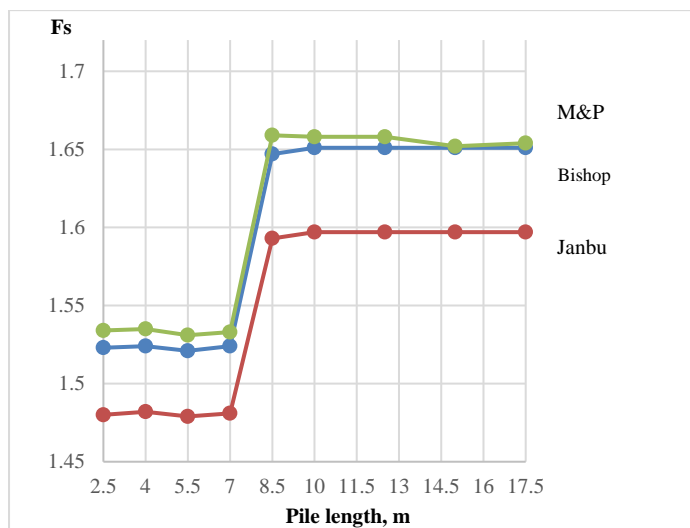


Figure 8 Safety factor on pile length dependence plot (not considering seismic effect)

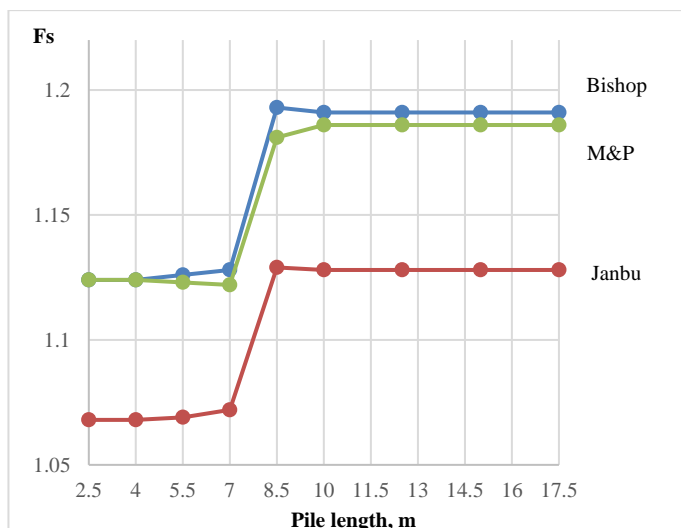


Figure 9 Safety factor on pile length dependence plot (considering seismic effect)

From the graphs, it can be seen that for pile depths up to 7 meters, the stability coefficient is below the normative value (Yanbu method), but in the range of 7-8.5 meters, there is a sharp increase in the stability coefficient. Beyond that, the coefficient remains within a consistent range.

Conclusion

The calculations analysis allows us to conclude that on one of the sections of the pipeline route considered, the designed length of piles can be reduced to 10-11 meters. Embedding piles into the underlying mudstones by an additional 2 meters is presumed to provide a sufficient margin for safe operation.

Using the method mentioned above, calculations were also performed for six other sections located along the pipeline route. Similar conclusions were drawn regarding the possibility of reducing the designed pile length while maintaining the safety of the structure's operation. Considering the piles embedding for 2 more meters, the pile length on the considered sections can range from 9 to 12.5 meters, which is significantly less than the designed pile length of 17 meters.

It is worth noting that an increase in the seismic coefficient entails a sharp drop in the stability coefficient. To ensure greater reliability of calculations, data on seismic microzoning of the study area is required.

The calculations performed justify the safety of the landslide protection structures with a possible reduction in the length of the piles, which will significantly reduce the cost of design work.

References

- SP 11-105-97 Engineering-geological surveys for construction. Part II. Rules for carrying out work in areas of development of hazardous geological and engineering-geological processes (in Russian).
- SP 36.13330.2012 Main pipelines (in Russian).
- SP 14.13330.2018. Construction in seismic areas (in Russian).
- SP 116.13330.2012 Engineering protection of territories, buildings and structures from hazardous geological processes (in Russian).

Assessment of landslide stability of ground cuts in Permian sediments of the Urzhum stage in the territory of the Volga uplands (Russia)

Fedor Bufeev^{(1)*}, Airat Latypov⁽²⁾, Anastasiya Garaeva⁽²⁾, Kirill Gudoshnikov⁽³⁾, Albert Korolev⁽²⁾

1) Sergeev Institute of Environmental Geoscience RAS (IEG RAS), Laboratory of Soil Science and Soil Mechanics, Moscow, Ulanskiy lane 13 bldg 2, PO box 145 (direct@geoenv.ru)

2) Kazan Federal University, Department of General Geology and Hydrogeology, Kazan, 18 Kremlyovskaya Street

3) Sergo Ordzhonikidze Russian State University for Geological Prospecting, Moscow, 23, Miklouho-Maclay Street.

Abstract The article discusses the problem of landslide processes activation during the construction of highways on the Volga upland territory in the central part of the East European platform. Currently, this territory is actively developing and requires the construction of a significant number of highways, including high-speed ones. At the same time, the roads geometry requires excavating deep roadway recesses in the existing terrain. This has provoked landslides activation in some areas, the scale of some of them can be classified as catastrophic.

Keywords: Landslide hazard assessment, East European platform, Permian deposits, Numerical stability calculation

The territory description

In recent decades, beginning in the 1990s, the Central Russian region has experienced remarkable development. Urban agglomerations have expanded, agro-industrial complexes have been established, and new cities have emerged as vital industrial and economic hubs. Such growth necessitates the establishment of more efficient logistics systems to manage transportation networks. Among these corridors are the M-7 and M-12 federal highways, currently under construction, which will connect to Moscow. These highways encompass extensive engineering structures within the road infrastructure, traversing diverse geomorphological landscapes often characterized by significant differences in elevation. The need to level the Earth's surface often requires extensive excavation work, particularly in areas with steep terrain. In such cases, disregarding the long-standing engineering-geological conditions of the terrain can lead to the activation of adverse geodynamic processes, such as landslides, rockfalls and erosion. This article explores the characteristics of landslide development within the sedimentary complex of the Middle Permian system along the embankments of the high-speed road excavation on the highway M-12, traversing the northeastern part of the Volga Upland.

Considering that the formation of engineering-geological conditions is influenced by both internal and external factors, the stages of Volga Upland geological evolution should be briefly examined. The starting point will be the period of formation Urzhum stage deposits, which compose the upper part of the geological section and serve as the foundation for road construction. In the area under consideration during the Urzhum Age, sediments of a continental variegated carbonate-terrigenous formation were deposited. Within the formation

sections, there are cyclic alternations of light gray dolomites, greenish-gray and red dolomite marls, red-brown clays, greenish-gray sandstones, and dark gray limestones. The accumulation of the variegated formation occurred in a single, very large basin (lake), which in terms of its size could be referred to as a sea. Hydrochemically the sedimentation basin exhibited an unstable regime; periods of salinization were interspersed with periods of desalination. This resulted in repeated alternations of carbonate and carbonate-clayey rock layers with clays and layers of clayey-sandy sediments.

A vast shallow reservoir with a leveled, gently sloping bottom contributed to the formation of layers with horizontally occurring deposits, which can be traced for hundreds of kilometers. Towards the end of the Urzhum age, significant quantities of coarse clastic material began to enter the territory from the Middle Urals. This influx of terrigenous components led to the gradual shallowing of Lake Urzhum and the formation of an accumulative alluvial plain in its place. Meandering rivers carved water-erosive paleovalleys filled with sandy material, around which swampy lowlands developed. The transition from an arid climate to a colder and more humid one at the end of the Urzhumian era facilitated the growth of shrub vegetation and the colonization of the territory by terrestrial vertebrates.

In the Mesozoic era, a restructuring of the structural plan of the territory commenced due to the emergence of ramparts within the Vyatka ridges system. During the Jurassic period, uneven amplitude uplift of the crystalline basement blocks resulted in uplift and folding deformations of sedimentary cover rocks, including those from the Urzhum age, forming the foundation of the Volga Upland. Presently, the Volga Upland comprises several gentle anticlinal folds alternating with gentle synclinal troughs. Alongside wide arched uplifts, various local tectonic disturbances in the form of intersecting regional faults further complicate the tectonic landscape.

As per the layout, the M-12 highway's bridge section across the Volga River must traverse the domed part of the Oktyabrskiy uplift.

The height difference from the highest hypsometric point on the hill (175 m) to the Volga River's waterline (53 m) totals approximately 122 m. Following excavation work during site preparation for construction, an extensive road excavation with a depth of about 80 m and a width of up to 20 m was constructed. To facilitate excavation, the road excavation slopes were terraced, with terrace ledge heights around 6.0 m and platform widths about 3.5 m. Given that the excavation slopes primarily consist of rocky soils, the slope angles of the ledges ranged between 80-90 degrees.

Exposed soil massif sections reveal a layered occurrence of rocks. In the lower part, interlayers of light gray dolomites alternate with greenish-gray and red-pink dolomite marls, red-brown mudstone-like clays, and occasional greenish-gray sandstones. Layer thicknesses range from 0.5-2.5 m. Notably, dolomite marls in some areas feature thin (up to 5.0 cm) layers of greenish-gray and black wet clay due to organic matter enrichment. These clay layers often act as waterproof barriers against infiltration water from atmospheric precipitation. Moistened clay exhibits a viscous-plastic state, allowing deformation without loss of layer continuity. Higher up the section, greenish-gray sandstone interlayers appear among dolomite marls and mudstone-like clays. Generally, dolomite layer proportions decrease from bottom to top along the section, while clayey-sandy rock proportions increase. Sedimentary rocks from the Urzhum stage feature horizontal, inclined, and vertical cracks, with block structures predominant in dolomites and dolomite marls, and fragmented structures in mudstone-like clays

Sharp-edged fragments of dense clayey rocks and blocks of carbonate and carbonate-clayey rocks are separated by extended shiny cracks. Consequently, the soil massif is classified as medium-fractured in areas with dolomites and dolomite marls and as collapsible in areas with dense mudstone-like clays. Large-scale technogenic exposures enable the observation of Urzhum carbonate-clayey sedimentary complex rock occurrence features not only vertically but also laterally. A folded depression of Urzhum stage rock layers from east to west is observed between the villages of Grebeni and Sviyag, following the Volga River's right bank.

The most elevated anticlinal structure corresponds to the dome part of the Oktyabrsky uplift, featuring a gentle fold about 1.5 km wide and an amplitude of around 8.0 m. This fold abruptly terminates on the eastern side with the Volga River valley, while smoothly transitioning into a synclinal fold on the western side. The synclinal fold is approximately 1.0 km wide with an amplitude of about 6.0 m, gradually transforming into another gentle anticlinal fold about 1.0 km wide, with an amplitude of 5.0-6.0 m on the western side. All folds exhibit straight vertical axial planes, symmetrical, lock-shaped configurations, with wing incidence angles not exceeding 15 degrees. Along the folds complicating the western slope of the Oktyabrsky uplift, a gradual decrease in plicative disturbances in the western direction is observed. This nature of folded deformations of sedimentary rocks arises from the vertical movement vector of crystalline foundation blocks along moving faults.

Sedimentary rocks above the basement blocks with the greatest uplift intensity form gentle anticlinal folds, while those with the least intensity form synclinal folds. By the time of tectonic activation, sedimentary rocks from the Urzhum stage had already acquired rigid structural connections of the crystallization type. Consequently, layer bending was accompanied by disjunctive disturbances. Sections distinctly reveal wing bends complicated by parallel cracks, along which sedimentary layers experienced stepwise displacement from east to west, with displacement amplitudes reaching up to 0.5 m. Some areas of the folds exhibit graben-like structures.

In hydrogeological terms, the soil massif traversed by the M-12 highway excavation locally contains aquifers. The primary aquifers are confined to layers of sandstones, fractured dolomite marls, and argillite-like clays, beneath which lie layers of viscous-plastic greenish-gray clays enriched in organic matter.

These aquifers contain free-flowing, infiltration-origin, fresh waters with a hydrocarbonate-calcium-magnesium composition. Their levels in aquifers are influenced by seasonal fluctuations. Hydrodynamic connection between the underlying and overlying aquifers is evident in sections. Groundwater flows downward can be traced to the river level of the Volga, indicating that the entire fractured soil mass functions as a single transit zone for the infiltration of atmospheric precipitation.

Construction of a geomechanical model and calculation methods

One of the primary stages in conducting slope stability quantitative assessment involves schematization during the construction of mathematical models. This schematization can be broadly categorized as either generalized or specialized. Generalized schematization simplifies a complex real-world object into a conceptual model, bounded by the constraints of scientific knowledge and information security achieved during geotechnical work. In contrast, specialized schematization simplifies the conceptual model into a specialized (geomechanical) scheme tailored to the specific task at hand, aiming to maintain adequacy while providing detailed descriptions of the real-world object. The objective of specialized schematization is to achieve maximum simplification with minimal loss of adequacy.

The implementation of specialized schematization involves several interrelated stages, including schematization of the slope massif structure and soil properties and their distribution within the studied massif. During engineering surveys in the study area, more than 20 engineering-geological elements were identified. Twelve engineering geological sections were constructed within the excavation area, forming the basis for 12 geomechanical models. Stability calculations for the excavation sides indicated stability coefficient values of at least 1.41, suggesting a significant stability margin for the design.

However, during the road construction stage from April to October 2022, five landslides of various sizes occurred for unknown reasons. The largest of these had lengths of up to 100 m and heights of up to 30.0 m (see fig.1). To assess the situation after excavation opening, K(P)FU employees conducted fieldwork on its sides, including layer-by-layer examination and description of rocks, recording of identified cracks' characteristics, and selection of monoliths. Based on these results, large-scale (1:500) zoning maps were compiled to depict the degree of danger of geological and engineering-geological processes, along with a special map of engineering-geological conditions.



Figure 1 Sliding landslide at the construction site of the M-12 highway.

Based on the analysis of the work results, the primary conclusion drawn was that the initiation of landslide processes stemmed from the removal of weathered sandstone materials through suffusion during groundwater unloading into the excavation. The exposure of sandstones to the surface, resulting from excavation, intensified weathering processes.

Concurrently with the increase in soil removal due to suffusion, extensive separation cracks began forming on the upper terraces of the southern slope of the road excavation. These cracks gradually widened, separating large rock blocks from the main soil mass. The development of radial sidewall crack systems is attributed to the absence of supporting forces from the open space of the mine workings, capable of counterbalancing surrounding pressure.

Avulsion cracks, intersecting all horizontal sedimentary rock layers in the massif, determined the subsequent mechanism of landslide displacement. Vertical fissure channels, intersecting aquiferous sandstones and fractured dolomite marls, act as pathways for downward groundwater migration, leading to increased rock moisture and reduced stability within the soil massif.

The separated soil mass, which retains some cohesion in the form of fallout blocks, exerts pressure on the underlying rocks of the slope. This additional load triggers detachment cracks further down the slope, affecting rocks on the lower terraces.

Upon surpassing a certain rock strength limit in the probabilistic slope collapse prism, an avalanche-like destruction of the undermined soil mass occurs in a localized area.

Landslide bodies exhibit a complex structure, consisting of multiple terraced steps formed by stacked large block heaps. Aquiferous sandstone layers at the base of the slopes serve as the foundation for landslide displacement.

Utilizing Rocscience software products, stability calculations of the excavation sides were conducted using updated data.

The simulation results, without considering the suffusion process development resulted in the safety factor values exceeding 1.3. However, accounting for the formation of suffusion cavities within water-saturated sandstone interlayers at sites of groundwater discharge resulted in safety factor values lower than 1 (refer to Fig. 2).

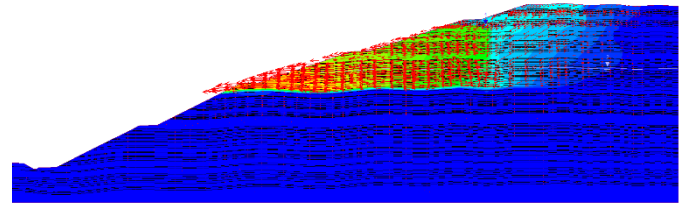


Figure 2 Slope stability modeling results.

Conclusion

Hence, in challenging natural environments, particularly when designing critical engineering structures, it is crucial to accurately evaluate changes in natural conditions during construction and operation. This includes recognizing potential and not always apparent interactions of engineering-geological processes, which could result in significant social and economic consequences.

References

- SP 11-105-97 Engineering-geological surveys for construction. Part II. Rules for carrying out work in areas of development of hazardous geological and engineering-geological processes (in Russian).
- SP 36.13330.2012 Main pipelines (in Russian).
- SP 14.13330.2018. Construction in seismic areas (in Russian).
- SP 116.13330.2012 Engineering protection of territories, buildings and structures from hazardous geological processes (in Russian).

Temperature and rate effects on the residual shear strength of clays: a state of the art

Gianvito Scaringi^{(1)*} and Marco Loche^{(1)*}

1) Institute of Hydrogeology, Engineering Geology and Applied Geophysics, Faculty of Science, Charles University, Albertov 6, 128 00 Prague, Czech Republic (gianvito.scaringi@natur.cuni.cz)

Abstract The temperature within a landslide's shear zone can undergo changes due to internal processes such as frictional heating and chemical reactions – the magnitude of which can be particularly relevant during fast runoff phases in large landslides. Alterations in boundary conditions, including heat transfer from the bedrock or ground surface, but also groundwater flows and changes in vegetation cover can contribute to these temperature variations, over timeframes especially relevant to shallow, slow-moving landslides. The hydro-mechanical properties of soils, particularly those rich in clay minerals, exhibit dependency on temperature. Studies indicate that the residual shear strength, a crucial parameter in reactivated landslides, can vary significantly within typical temperature ranges in landslide shear zones in temperate climates. The literature also highlights the influence of the rate of shearing on the shear strength parameters of soils, including the residual shear strength, with the soil's mineral composition controlling rate strengthening and weakening behaviours in slow to rapid landslides. This contribution summarises the state of knowledge and presents recent findings from ring-shear experiments which indicate the coupled nature of temperature- and rate-dependence of the residual shear strength, which may play a substantial role especially in shallow clay landslides. This influence is particularly noteworthy in the context of climate change, emphasizing the need for explicit consideration in modeling efforts.

Keywords residual shear strength, rate effect, temperature effect, thermo-mechanical coupling, clay, landslide

Introduction

Climate change is a multifaceted and profoundly disruptive phenomenon. It is imperative to comprehend the physical processes driving these disruptions, manifested in various ways such as natural disasters, in order to mitigate the impacts of climatic changes at both local and global levels. Landslides frequently play a crucial role in natural disaster chains and are significantly influenced by the effects of climate change (Gariano and Guzzetti, 2016).

Slope stability is typically explained through mechanical equilibrium and hydraulic flow equations.

Models can effectively consider disturbances caused by seismic activity, earthworks, variations in moisture content, and fluid pressure. Soils rich in clay are particularly prone to slope instability due to their low frictional resistance and increased interaction with water. Under compression and shearing, these soils deform easily, resulting in smooth surfaces that facilitate preferential sliding with minimal resistance.

The notion of residual shear strength originated from the experimental studies of Tiedemann, Haefeli, and Hvorslev in the 1930s, and MacNeil Turnbull in the 1950s. However, it was Skempton who synthesized these findings in his Rankine Lecture (Skempton, 1964).

Effect of temperature on the hydro-mechanical behaviour of clays

Clay soils exhibit sensitivity to temperature changes, with their hydro-mechanical properties significantly influenced by temperature (Scaringi and Loche, 2022). Beyond the effects of water phase changes on volume, stiffness, and hydraulic conductivity, this thermal sensitivity is noteworthy even within the temperature range of liquid water under atmospheric pressure. While research on thermo-hydro-mechanical coupling in clays dates back to the 1960s (e.g., Mitchell, 1969), its early findings did not impact norms and engineering practices. Recent developments in energy geotechnics and studies on engineered clay barriers (ECBs) for geological repositories of spent nuclear fuel have brought attention to thermal effects in geomaterials.

It is now recognized that temperature changes can influence internal stresses and water pressures, initiating flows and strains through intricate, coupled mechanisms. The expansion differences between water and clay minerals upon heating result in changes in water pressure. As temperature increases, physico-chemical interaction interparticle forces alter, with water becoming less viscous and more electrically conductive, and clay surfaces losing their capacity to retain water. Heating-cooling cycles in soft soil may lead to stiffening and, unexpectedly, net shrinkage (Tang et al., 2008), while the reverse is true in overconsolidated soil.

The influence of temperature on shear strength is not critical in domains experiencing small strains, such as in

the ECB problem, leading to limited research in this area (Scaringi and Loche, 2022; Loche et al., 2021, 2022). Whether shear strength increases or decreases with temperature depends on soil nature and structure, shaped by its stress-strain-thermal history. Residual shear strength (τ_r), commonly found in landslide shear zones after large strains, remains unaffected by soil history, making the evaluation of its thermal sensitivity more straightforward. However, there is a scarcity of literature on such assessments. In a notable study, the remobilization of clay landslides was attributed to cooling-induced soil weakening (Shibasaki et al., 2017), supported by experiments emphasizing the significance of shearing rate and suggesting distinct effects in slow and fast movements, an area largely unexplored to date.

Temperature – shear-rate coupling

The phenomenon of velocity-weakening has been a focal point in the study of long-runout landslides (especially large rock avalanches), as elucidated by Scaringi et al. (2018). Various mechanisms have been proposed to account for this phenomenon, with most emphasizing the dissipation of frictional heat in the shear zone, where elevated temperatures may be reached. In the realm of slow-moving landslides, the role of frictional heating is minimal, given that heat conduction and convection effectively curtail temperature growth. Consequently, processes dependent on temperature are not typically anticipated in such scenarios.

Nevertheless, factors influencing temperature variation exist, both internal and external. Internally, this can involve endothermic or exothermic chemical and biological processes. Externally, linked to changing boundary conditions, both direct and coupled flows contribute to heat transfer. For example, groundwater flow not only influences pore water pressures but also impacts the thermal energy balance. Despite the plethora of processes potentially altering temperature patterns within the ground and thereby affecting hydraulic and mechanical properties, little attention has been devoted to incorporating these considerations explicitly in landslide studies and most geotechnical problems (Scaringi and Loche, 2022).

Concerning the shearing behavior, the outcomes of shear experiments across a wide spectrum of normal stresses (typical of shallow to deep-seated landslides), shear rates (typical of extremely slow to rapid landslides), experimental setups, and soil compositions are often intricate and occasionally challenging to interpret comprehensively (Scaringi et al., 2018a; Scaringi and Di Maio, 2016). The introduction of temperature adds an additional layer of complexity to the interpretation of these experiments. In a recent review, we underscored the existence of a diverse literature on temperature effects in geomaterials, albeit lacking systematicity and clear field evidence (Scaringi and Loche, 2022).

Modelling thermo-hydro-mechanical behaviour

Traditional slope stability models typically consider only hydro-mechanical coupling, neglecting thermal effects. However, more advanced model formulations, initially developed for other applications like engineered clay barriers modeling, explicitly incorporate thermo-hydro-mechanical processes (Mašín, 2017). Despite their potential, these models have not yet been adapted or further developed for landslide applications. Their usage remains confined to small-scale domains due, in part, to computational complexities.

In the absence of a modeling tool and comprehensive understanding of thermal sensitivity, one might assume that anticipated changes in slope stability in temperate regions under climate change primarily result from altered hydrological inputs. This perception is somewhat justified by the soil's heterogeneity acting as a "dampening role" and temperature fluctuations diminishing at greater depths. However, a thorough examination of the literature (Scaringi and Loche, 2022) reveals that recent studies tend to consider thermal effects as negligible, dismissing the need for investigation. Similar qualitative conclusions can be found in various studies (e.g., Cekerevac and Laloui, 2004). Yet, a quantitative argument either supporting or neglecting the temperature-shear strength dependence systematically, especially in specific conditions like clay-rich formations, pre-existing landslide bodies, or shallow movements, is currently lacking.

Results of recent research and perspectives

In our current research (e.g., Loche and Scaringi, 2023), our goal is to evaluate, quantitatively, the role of changes in temperature in the kinematics of landslides in clay soils. In particular, we are interested in changes in the available (or mobilised) shear resistance in basal shear zones, especially in landslide bodies for which changes in the top boundary condition (ground-atmosphere interaction) produce a measurable effect over a seasonal timescale. In a numerical simulation, we indeed reproduced the seasonal changes in in temperature in shallow landslide bodies (Fig. 1).

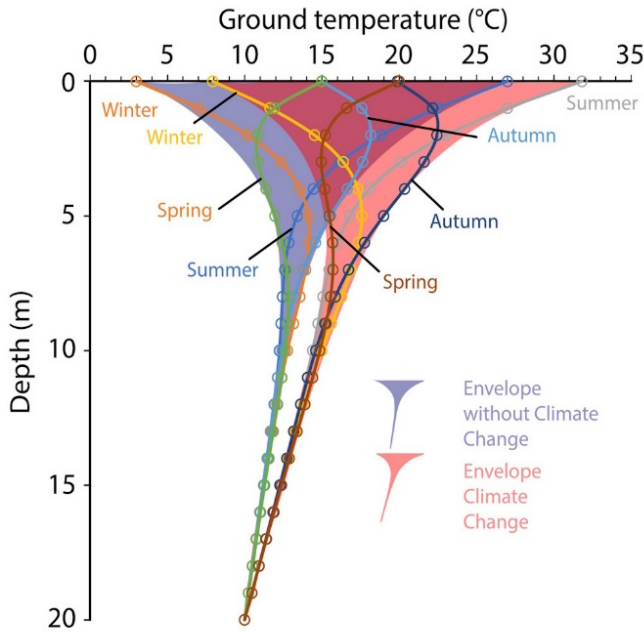


Figure 1 Depth profiles of ground temperature: seasonal variations in a hypothetical baseline case (“no climate change”) and after 5°C of warming (“climate change”). Modified from Loche and Scaringi (2023).

Adopting a simplified geometry and considering a homogeneous and saturated soil featuring a groundwater flow parallel to the slope direction, we investigated in a virtual experiment the seasonal and long-term temperature changes in landslide shear zones and how these can affect slope stability via thermo-mechanical coupling with respect to a single soil parameter: the residual shear strength.

In order to quantify this coupling, we performed ring-shear experiments on saturated samples of pure clays (commercial Ca-Mg-bentonite and kaolin) while controlling both the temperature and rate of shearing. During the experiments, after attaining the residual shear condition, we increased the temperature of the water bath (from 20 °C to 50 °C) and kept it elevated for hours to days before restoring room temperature conditions (Fig. 2). During slow shearing (0.018 mm/min), we typically observed a “positive temperature effect” – that is, an increase in shear strength with temperature – when testing bentonite samples under various normal stresses (Fig. 2a). Conversely, kaolin samples did not exhibit any temperature effect or even showed some weakening (“negative temperature effect”) under the same test conditions (Fig. 2b).

Interestingly, we observed that the effect of temperature depends in the rate of shearing. In other words, temperature and shear rate effects are somewhat coupled, implying that they should be investigated jointly and that they may be caused by the same or by coupled physico-chemical mechanisms at the micro-scale. As an example, Fig. 3 shows the residual failure envelopes for the Ca-Mg-bentonite at 20 °C and 50 °C, sheared at 0.018 mm/min and 0.5 mm/min. Notably, the positive

temperature effect is evident at 0.018 mm/min (Fig. 3a) while is absent at 0.5 mm/min (Fig. 3b). This possibly relates to a transition from laminar shearing to transitional or turbulent shearing, which has also been shown to affect the shear rate effect (Tika et al., 1996; Duque et al., 2023).

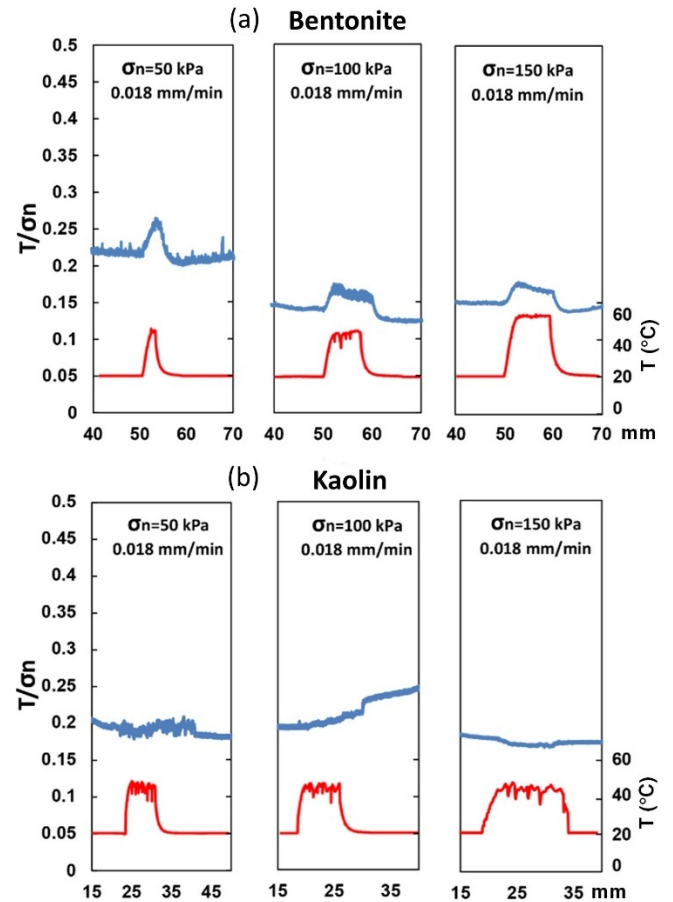


Figure 2 Results of ring-shear tests on (a) bentonite and (b) kaolin: the tests were performed under normal stresses (σ_n) of 50, 100, and 150 kPa and a shear rate of 0.018 mm/min. Modified from Loche and Scaringi (2023).

Overall, our experiments revealed changes in residual shear strength by up to 1.5%/°C, with the sign of the effect depending on both the mineral composition of the clay and the rate of shearing.

By incorporating this temperature effect into a slope stability analysis (Loche and Scaringi, 2023) while also considering seasonal and long-term temperature changes in the underground, we evaluated, for instance, that a smectite-rich landslide body with a curvilinear slip surface down to a depth of ~6 m would experience seasonal changes in the global factor of safety by around 20% solely due to the temperature-dependency of the residual shear strength. Notably, by also accounting for long-term warming (e.g., surface warming by up to +5 °C over decades) we quantified an additional variation by ~7% (Table 1).

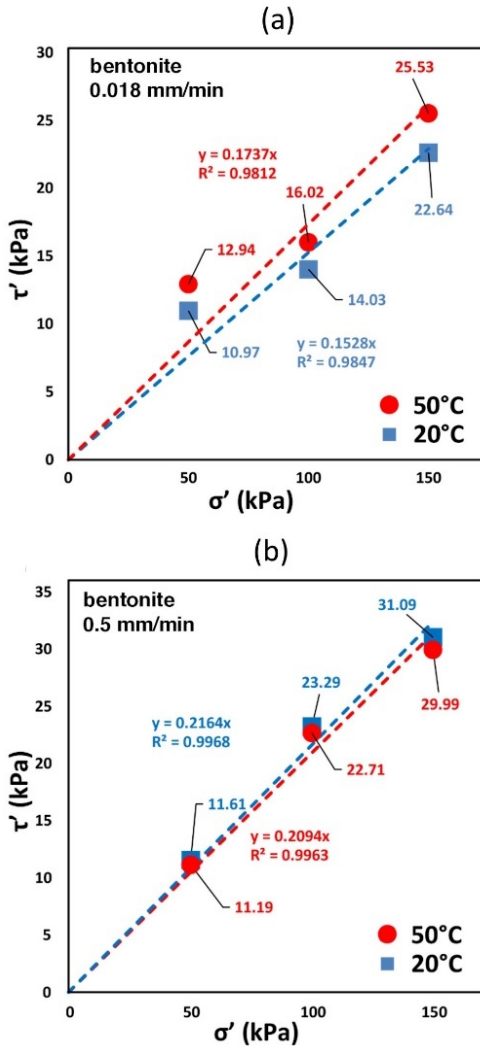


Figure 3 Residual shear strength envelope for bentonite at (a) 0.018 mm/min and (b) 0.5 mm/min: an increase in temperature from 20°C to 50°C caused an increase in friction coefficient from ca. 0.15 to ca. 0.17 (+13%) at 0.018 mm/min but a decrease from ca. 0.22 to ca. 0.21 (-3%) at 0.5 mm/min. Modified from Loche and Scaringi (2023).

Table 1 Example of global factor of safety (FS) for a 6 m deep curvilinear slope failure in smectitic clay (reactivated landslide) according to seasons in the numerical experiments by Loche and Scaringi (2023).

Season	FS in current climate	FS after +5 °C warming
Spring	1.22	1.14
Summer	1.08	1.00
Autumn	1.11	1.02
Winter	1.27	1.18

In our study, we explored a simplified numerical scenario in which no other couplings were introduced – such as dependencies of water retention behaviour and hydraulic conductivity on temperature – and did not consider that, under global warming, atmosphere-ground interaction is affected in a non-straightforward manner by changes in precipitation patterns and (where applicable)

vegetation cover. Also, the sensitivity of the residual shear strength on temperature evaluated in our experiments should be considered as an upper limit because natural soils are mineral mixtures in which the components may respond to changes in temperature in opposite ways and specific responses may even emerge from the mineral combinations. In fact, we suggest that experiments on natural soils should be conducted systematically and enhancements in thermo-hydro-mechanically coupled modelling capabilities should be prioritized. Nevertheless, we can still conclude that, by overlooking the dependency of soil properties and behaviours on temperature altogether, errors and misestimations could occur at any scale, from laboratory determinations to slope stability assessments and regional analyses and predictions of landslide patterns and trends, their hazard, and risk.

Acknowledgements

The authors acknowledge financial support from the Czech Science Foundation (GAČR grant No. 24-12316S).

References

Cekerevac C, Laloui L (2004) Experimental study of thermal effects on the mechanical behaviour of a clay. *Int J Numer Anal Methods Geomech* 28, 209–228.

Duque J, Loche M, Scaringi G (2023) Rate-dependency of residual shear strength of soils: implications for landslide evolution. *Géotechnique Letters* 13(2), 1–16.

Gariano SL, Guzzetti F (2016) Landslides in a changing climate. *Earth-Sci Rev* 162, 227–252.

Loche M, Scaringi G (2023) Temperature and shear-rate effects in two pure clays: Possible implications for clay landslides. *Results in Engineering* 20, 101647.

Loche M, Scaringi G, Blahůt J, Melis MT, Funedda A, Da Pelo S, Erbi I, Deiana G, Meloni MA, Cocco F (2021) An Infrared Thermography Approach to Evaluate the Strength of a Rock Cliff. *Remote Sens* 13, 1265.

Loche M, Scaringi G, Yunus AP, Catani F, Tanyaş H, Frodella W, Fan X, Lombardo L (2022) Surface temperature controls the pattern of post-earthquake landslide activity. *Sci Rep* 12, 988.

Mašín D (2017) Coupled thermohydro-mechanical double-structure model for expansive soils. *J Eng Mech* 143, 04017067.

Mitchell JK (1969) Temperature effects on the engineering properties and behavior of soil. In: *Effects of Temperature and Heat on Engineering Behavior of Soils*, Special Report 103, Highway Res Board Washington DC, pp. 9–27.

Kurylyk BL, MacQuarrie KTB (2014) A new analytical solution for assessing climate change impacts on subsurface temperature. *Hydrol Process* 28, 3161–3172.

Scaringi G, Di Maio C (2016) Influence of Displacement Rate on Residual Shear Strength of Clays. *Procedia Earth Planet Sci* 16, 137–145.

Scaringi G, Hu W, Xu Q (2018a) Discussion on: “Experimental study of residual strength and the index of shear strength characteristics of clay soil” [Eng. Geo. 233:183–190]. *Eng Geol* 242, 218–221.

Scaringi G, Hu W, Xu Q, Huang R (2018b) Shear-Rate-Dependent Behavior of Clayey Bimaterial Interfaces at Landslide Stress Levels. *Geophys Res Lett* 45, 766–777.

Scaringi G, Loche M (2022) A thermo-hydro-mechanical approach to soil slope stability under climate change. *Geomorphology* 401, 108108.

- Shibasaki T, Matsuura S, Hasegawa Y (2017) Temperature-dependent residual shear strength characteristics of smectite-bearing landslide soils: Temperature-Dependent Residual Strength. *J Geophys Res Solid Earth* 122, 1449–1469.
- Skempton AW (1964) Long-term stability of clay slopes. *Géotechnique* 14(2), 77-102.
- Tang AM, Cui YJ, Barnel N (2008) Thermo-mechanical behaviour of a compacted swelling clay. *Géotechnique* 58, 45–54.
- Tika TE, Vaughan PR, Lemos LJJ (1996) Fast shearing of pre-existing shear zones in soil. *Géotechnique* 46, 197–233.

Landslide information for land management and planning: Examples from Italy and Croatia

Paola Reichenbach^{(1)*}, Snjezana Mihalić Arbanas⁽²⁾, Mauro Rossi⁽¹⁾, Sanja Bernat Gazibara⁽²⁾

1) Istituto di Ricerca per la Protezione Idrogeologica, CNR, Perugia (Italy), Via della Madonna Alta 126, paola.reichenbach@irpi.cnr.it

2) University of Zagreb, Faculty of Mining, Geology and Petroleum Engineering, Zagreb (Croatia), Pierottijeva 6, snjezana.mihalic@unizg.rgn.hr

3) Istituto di Ricerca per la Protezione Idrogeologica, CNR, Perugia (Italy), Via della Madonna Alta 126, mauro.rossi@irpi.cnr.it

4) University of Zagreb, Faculty of Mining, Geology and Petroleum Engineering, Zagreb (Croatia), Pierottijeva 6, sanja.bernat@unizg.rgn.hr

Abstract Landslide information and derived mapping products are relevant tools to support local authorities in land use management and planning. Landslide inventory maps are the basis to evaluate landslide susceptibility, hazard, and risk at different scales. Accurate landslide mapping and geotechnical characterisations can be of paramount importance for the comprehension and set-up of landslide forecast models. In addition, information on landslide spatial occurrence (i.e., susceptibility) is fundamental to evaluate the instability of the territory and can be a relevant component of early warning systems, which focuses on the forecast of multiple or populations of landslides over large areas based on the monitoring of a potential landslide trigger (e.g., rainfall). The article presents different landslide maps produced at different scales for scientific, technical, or institutional purposes in Croatia and Italy. The maps at national, regional and local scales can be relevant tools and scientific support for land management and planning.

Keywords Landslide maps, Croatia, Italy, land management and planning

Introduction

Landslides are widespread phenomena that cause casualties and extensive damage worldwide. Landslides can be caused by different triggers, including rainfall, earthquakes, rapid snowmelt, and human activities. The approach of avoiding landslide-prone areas is rarely feasible, and it is neither possible nor desirable to proscribe development in all landslide-prone areas. The challenging task is to choose and apply, implement and finance the most effective mitigation approaches. For this, it is necessary to have information on landslides spatial occurrences in the form of landslide inventory and susceptibility maps. Significant reductions in potential losses and damages can be achieved by combining landslide hazard mitigation measures through spatial planning with emergency management measures.

In Italy, intense or prolonged rainfall is the primary trigger of landslides. Damaging failures occur every year in

this country, where they have caused more than 6 300 casualties in the 60-year period, 1950–2009 (Salvati et al., 2010). Consequently, research to determine the amount of rainfall necessary to trigger landslides is of scientific and social interest. In Italy, there are several examples of landslide maps prepared at different scales: (i) the IFFI catalogue compiled at a national level, by the Italian Institute for Environmental Protection and Research for the entire Italian territory; (ii) a mosaic of landslide hazard maps, originally prepared by the regional administrations following national criteria. As an example of the use of landslide maps, the prototype SANF system (Sistema per l'Allertamento Nazionale da Frana), developed by CNR IRPI for the Italian Civil Protection Department, forecasts the possible occurrence of landslides by comparing rainfall measurements and forecasts with rainfall thresholds for the possible occurrence of failures.

In Croatia, despite the long tradition of landslide mapping in Zagreb city (1950–today), there is a lack of suitable, officially accepted landslide maps, which is the main problem with the current landslide risk management practices at all levels, from national to local (Mihalić Arbanas et al., 2016). Since landslides are widespread in different parts of Croatia, and thus the risk of possible accidents and catastrophic consequences, it is necessary to establish a systematic of landslide maps to mitigate landslide hazards and risks. Important results were achieved in the framework of two scientific projects (2020–2023) that provided prototypes of different types of landslide maps for land management and planning at all levels (Mihalic Arbanas et al., 2023; Bernat Gazibara et al., 2023). Besides mapping methodologies, the research projects were also focused on multiple aspects related to map uses and were conducted together with spatial planners, developers and administrations at all levels in the Republic of Croatia.

The aim of this paper is to describe two approaches and experiences of multi-level landslide mapping: the Croatian derived from national scientific projects and the Italian from current practices and trends. The first part presents all landslide maps required by potential users

dealing with the creation and implementation of spatial and urban plans in Croatia. The second part illustrates different landslide maps produced in Italy at different scales for scientific, technical, or institutional purposes.

Landslide maps in Croatia

Background

In Croatia in the past decade, various types of landslide mapping and modelling have been applied for the purpose of land management and planning. Several recent examples of inventory maps were prepared at large scale (1:2 000) using visual interpretation of LiDAR DTM (Digital Terrain Model) morphometric derivatives. The EU-funded project PRI-MJER (<https://pri-mjer.hr/>) explored the optimal landslide inventory required at the municipal level. Large-scale landslide susceptibility zonations were derived using statistically based methods in the framework of the scientific research project LandSlidePlan (<https://landslideplan.eu/>), funded by the Croatian Scientific Foundation. To ensure a rational approach to landslide mapping in the entire Croatian territory, a prototype of a landslide susceptibility map was produced at a medium scale (1:25 000) with areas classified into three levels (Fig. 1a).

Large-scale inventory maps

The large-scale inventory maps for different study areas were compiled in the period 2017-2023 (Đomlija, 2018; Bernat, 2019; Jagodnik et al., 2023; Krkač et al., 2022; Bernat Gazibara & Mihalić Arbanas, 2023). Identification and mapping of landslides was carried out for six study areas (total area of about 194 km²) by visual interpretation of morphometric maps derived from LiDAR DMT of 0.3 - 1-m resolution (Airborne LiDAR Scanning in the periods 2012-2020). The results are representative landslide inventories containing precise and reliable landslide contours on a detailed scale for the entire study area, including densely vegetated areas. Landslide inventory maps on a 1:2,000 scale can be used to prepare maps of special restrictions

for the development and implementation of spatial plans, but they are also input data for landslide susceptibility evaluation, as well as hazard and risk assessments.

Table 1 shows a summary of information about landslide types and dimensions derived from the inventory maps. Landslide area statistics performed for study areas in different geomorphological environments in Croatia provided useful information on the number and dimensions of the phenomenon. For example, the landslide density in Zagreb is 33.3 landslides/km², but the total area is only 0.5 km² or 2.43% of the area because the phenomena are small and shallow. Figure 1c presents an example of information derived from the landslide inventory map showing the spatial distribution of all historical landslides in Zagreb hills (Pannonian Basin).

Large-scale landslide susceptibility maps

Landslide susceptibility assessment was performed to produce zoning maps on 1:5,000 scale for six study areas (total area of about 194 km²) using LIDAR-derived landslide inventories. The assessment was performed by statistical analysis of random forests using relevant factor maps belonging to morphological, geological, hydrological, and anthropogenic conditions. The research was also focused on the influence of different modelling methods, cartographic units and graphical representations of landslides used in analyses (Bernat Gazibara et al., 2023). The optimal results were derived using a regular grid of 5x5 m and 50 % of randomly selected landslide polygons.

Figure 1d shows examples of landslide information from the landslide susceptibility map of the study area in Zagreb: 45.9 % of low susceptibility zone (9,7 km²), 39.3 % of medium susceptibility zone (8.3 km²), 14.7 % of high susceptibility zone (3.1 km²). Unlike the Pannonian basin environments, the spatial distribution of susceptibility zones in flysch areas in the Dinarides and Adriatic Plate (Istrian Peninsula) is strongly related to erosion phenomena and deep fossil landslides.

Table 1 Information on landslide type and dimension derived from inventory maps

Study area	Landslide types	Total number of landslides	Landslide density (number per km ²)	Landslide area (m ²)				
				Min.	Max.	Mean	Median	St. dev.
Hrvatsko Zagorje (20 km ²)	Soil slide, soil flow	912	45	3	13,778	448	173	879
Podsljeme Hills (20 km ²)	Soil slide	702	33	43	8,064	730	427	942
Karlovac (50 km ²)	Soil slide	1,069	21	13	8950	224	131	420
Vinodol Valley (20 km ²)	Soil slide, soil slide-debris flow	627	31	65	49,462	2337	1218	4498
Rječina River Valley (19 km ²)	Soil slide, soil slide-debris flow	1300	68	14	78,364	720	179	3122
Buzet (20 km ²)	Soil slide, soil slide-debris flow	1,782	89	-	-	-	-	-

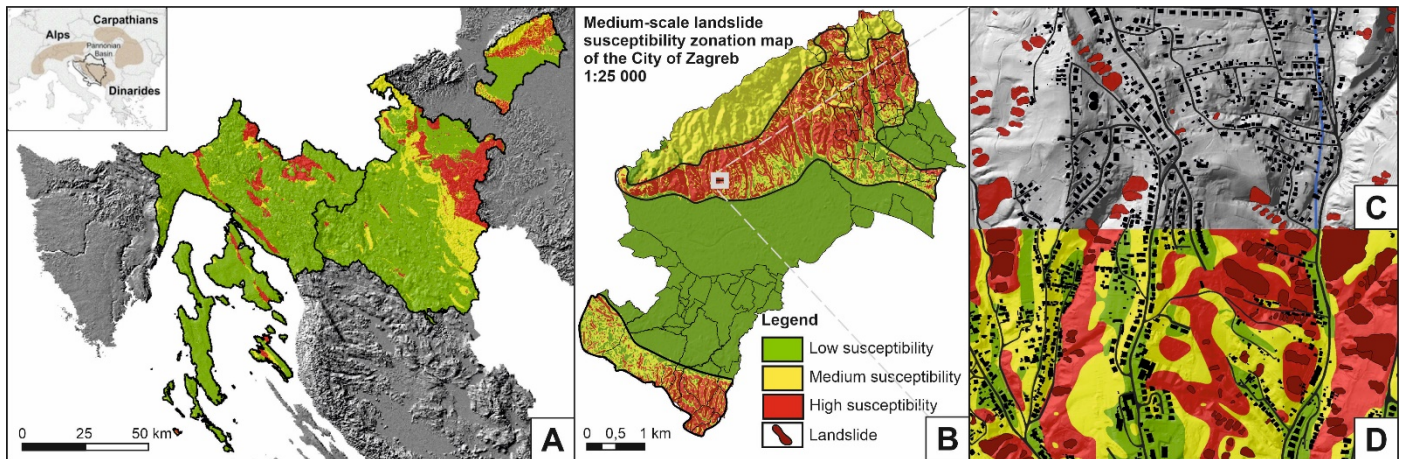


Figure 1 Examples of landslide maps in Croatia: (a) regional level mosaic susceptibility map; (b) susceptibility map of the City of Zagreb (regional level, County status) at 1:25,000 scale; (c) local level susceptibility map at 1:5,000 scale; (d) local level inventory map at 1:2,000 scale.

Medium-scale landslide susceptibility maps

Another important piece of information for land management and planning is the susceptibility map at 1:25,000 scale that subdivides the territory into three zones according to the probability of landslide occurrence across three counties (Fig 1a). Spatial probability is estimated using a Fuzzy heuristic approach because of the lack of representative landslide inventory (Bernat Gazibara et al., 2023). Verification performed by incomplete landslide inventory (about 2,000 phenomena) showed satisfactory prediction results for regional scale landslide modelling (86 % of mapped landslides fall in high and very high susceptibility zones in Karlovac County and 89 % in Primorje-Gorski Kotar County).

The medium-scale susceptibility map shows the proportion of the area potentially prone to landslides for counties. For example, approx. 12% of the Primorje-Gorski Kotar County, approx. 32% of the Karlovac County and approx. 48 % of the City of Zagreb belongs to zones of medium and high susceptibility. Due to the lower precision of susceptibility assessment, the information provided by this map is recommended for use in spatial planning to identify where a more detailed susceptibility assessment is needed. Fig. 1b shows an example of how to outline areas where susceptibility mapping on a large scale is necessary for the City of Zagreb based on medium-scale zonation.

Landslide maps in Italy

Background

In Italy in the past decades, various types of landslide mapping and modelling have been produced at different scales for scientific, technical, or institutional purposes. For the entire national territory, institutional landslide maps have been mosaicked by the Italian Institute for Environmental Protection and Research (ISPRA) and the Basin Authorities (AdB, now organized into Hydrographic Districts), starting from cartographic products realized by Regions and the Autonomous Provinces. Recently, ISPRA has implemented IdroGEO, a national web platform, that

allows the navigation, social sharing and download of data, maps, reports of the Italian landslide inventory, national hazard maps, and risk indicators (Iadanza et al., 2021).

The IFFI landslide inventory map

The most detailed landslide inventory map for the entire Italian territory (IFFI), was harmonized by ISPRA in the framework of a dedicated project (www.progettoiffi.isprambiente.it; <https://idrogeo.isprambiente.it/app/>). The IFFI map (Fig. 2) was realized by Regions and Autonomous Provinces following standardized and shared methods (Trigila et al., 2007) and includes 620,808 landslides, affecting an area of approximately 23,700 km²,

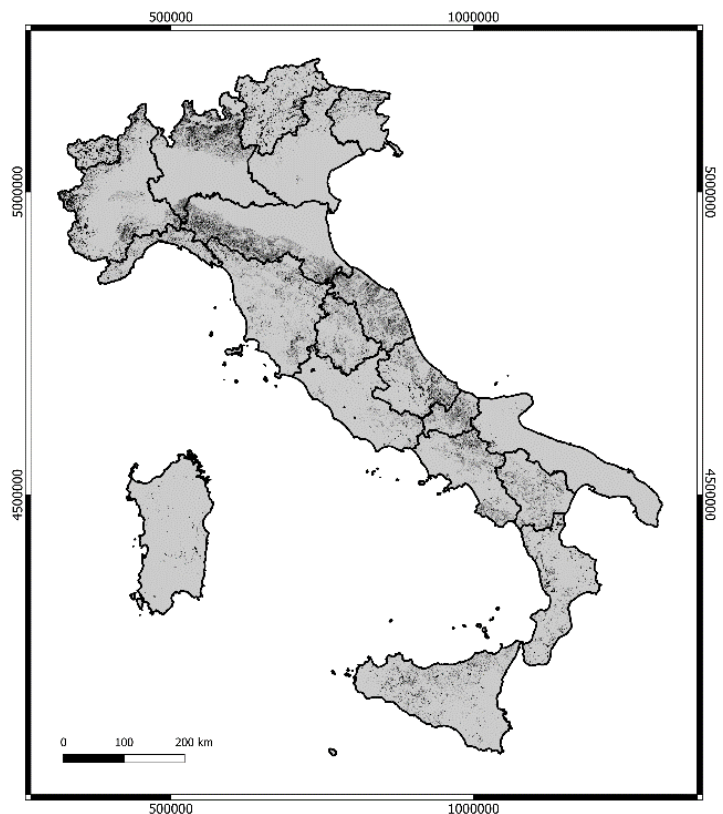


Figure 2 The map shows the IFFI landslide data (black polygons) for the Italian regions (black lines).

equal to 7.9% of the national territory. Landslides are available in vector format, as polygons with several associated information (e.g., locality, date, and type of landslide).

An analysis carried out by Trigila et al. (2010) attempted to verify the completeness and homogeneity of this national landslide map using three different methods of analysis: (a) areal frequency statistics; (b) analysis of the proximity of surveyed landslides to urban areas; and (c) analysis of the variation of the landslide index within the same lithology. The analysis revealed that IFFI is highly heterogeneous, with areas that are representative in terms of homogeneity and reliability and that can potentially be used for further assessment (for example, as training and calibration data for landslide susceptibility modelling) and areas where the collected information is underestimated or inaccurate. The IFFI data aim to facilitate the widest dissemination and use of landslide information to local governments, research institutions, technicians working in the field of land use design and planning, and citizens. Figure 2 shows the spatial distribution of the IFFI inventory for the entire national territory.

The PAI landslide hazard maps

The PAI landslide hazard maps (Fig. 3) were prepared for the Italian regions in the framework of a national project (www.isprambiente.gov.it) that was focused on identifying areas of possible evolution of existing landslides and areas where new landslides potentially may occur. In some regions, the original PAI maps prepared by the regional

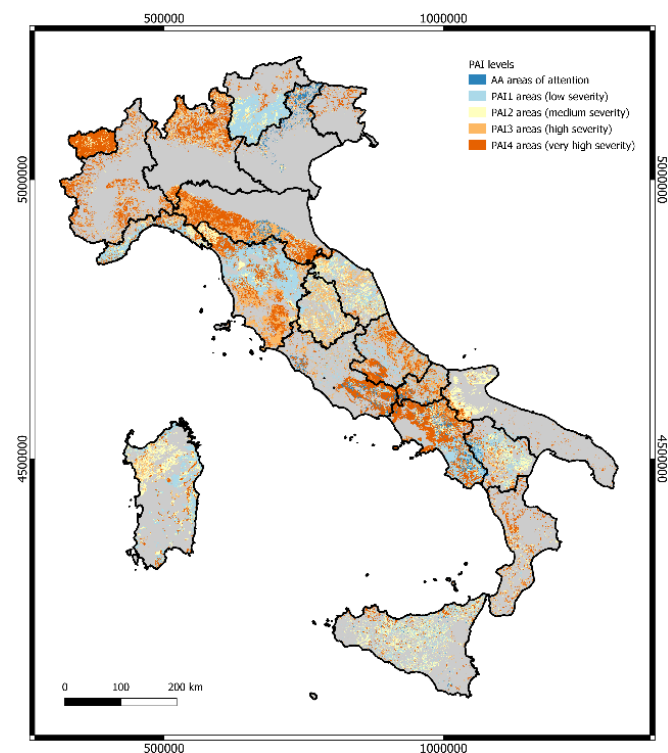


Figure 3 The map shows the distribution of the five PAI hazard levels (AA, H₁, H₂, H₃, and H₄) for the Italian regions (black lines).

administrations were updated with local studies and investigations, recent landslide occurrences, and structural risk mitigation interventions. The PAI mapsshow polygons classified in five levels of severity: AA (area of attention), PAI₁ (low), PAI₂ (moderate), PAI₃ (high), and PAI₄ (very high). Figure 3 shows the spatial distribution of each level for Italy.

The PAI maps were carried out, according to the criteria of the Act of Guidance and Coordination of the DPCM of 29/09/1998, by the Basin Authorities (now merged into the Hydrographic District Authorities according to the provisions of Law No. 221 of December 28, 2015), for the preliminary design of soil defence interventions and infrastructure networks and the drafting of Civil Protection Emergency Plans.

Large-scale landslide susceptibility maps

Another important information for land management and planning is the susceptibility map that subdivides the territory according to the probability of landslide occurrence across a given geographic space (Reichenbach et al., 2018). This probability is usually estimated by using a binary classifier which is informed of landslide presence/absence data and associated landscape characteristics. In Italy, the IFFI landslide inventory map was used to prepare slope-unit based landslide susceptibility maps. For each type of mass movement of the IFFI inventory (Complex, Deep Seated Gravitational Slope Deformation, Diffused Fall, Fall, Rapid Flow, Shallow, Slow Flow, Translational), a different susceptibility zonation was prepared using a Bayesian version of a Generalized Additive Model. The landslide susceptibility maps were prepared considering the following three aspects: (a) spatial homogeneity/heterogeneity of landslide inventories, (b) a solid approach to the susceptibility estimation, and (c) the use of SU as geomorphologically sound mapping units (Loche et al., 2022).

SANF system - example of the use of landslide maps

In the context of the scientific activities carried out for the Italian National Department for Civil Protection, IRPI has designed and implemented an early-warning system to forecast the possible occurrence of rainfall-induced landslides in Italy. The system named SANF (an Italian acronym for National Early Warning System for Rainfall Induced Landslides), forecasts the possible occurrence of landslides by comparing rainfall measurements and forecasts with rainfall thresholds for the possible occurrence of landslides (Fig. 4). For this purpose, a national rain gauge network provides rainfall measurements, and numerical weather models provide synoptic-scale quantitative rainfall forecasts. The landslide forecasts are based on rainfall thresholds of the mean Intensity-Duration type that are used to define critical levels for the possible occurrence of landslides, in different classes (Rossi et al., 2012).

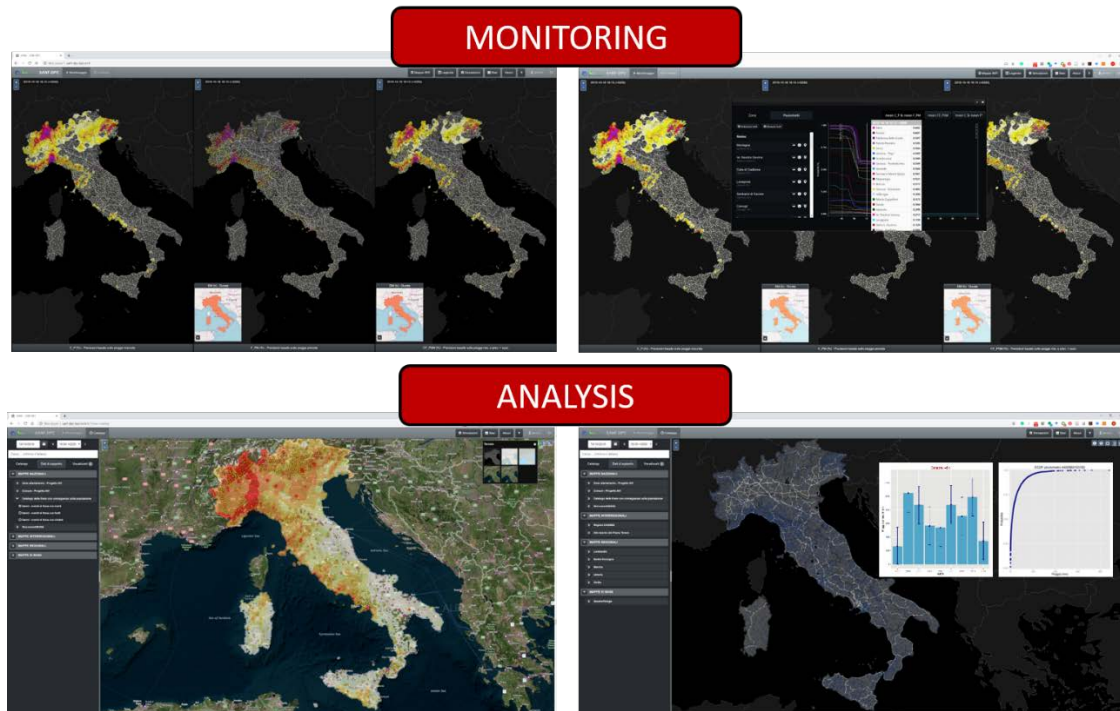


Figure 4 Monitoring and analysis interfaces of the SANF system designed and implemented to forecast the possible occurrence of rainfall-induced landslides in Italy.

Discussion and conclusions

Landslide mapping and zoning can be prepared at national, regional, and local levels using different and heterogeneous approaches, depending on techniques and methods used for landslide data collection (i.e., inventory maps) and hazard and risk assessment. Landslide inventory maps are important to document the extent of landslide phenomena in a region, to investigate the distribution, types, pattern, recurrence, and statistics of slope failures, to determine landslide susceptibility, hazard, vulnerability, and risk, and to study the evolution of landscapes dominated by mass-wasting processes (Guzzetti et al., 2012). Moreover, high-quality landslide inventory maps have positive effects on all derivative products and analyses, including erosion studies and landscape modelling (Tucker and Hancock, 2010), susceptibility and hazard assessments, and risk evaluations.

A critical literature review on landslide susceptibility modelling (Reichenbach et al., 2018) revealed a considerable heterogeneity of the landslide and thematic data types and scales, the modelling approaches, and the criteria used to evaluate the model performance, which highly influence the zonation. The quality of the susceptibility models has improved over the years, but top-quality assessments are still not common. In addition, common standards and recommended practices to construct, validate, and evaluate the susceptibility models and the associated zonation are not available.

The presented cartographic products from Italy encompass the following: national landslide inventory maps (IFFI inventory), regional landslide hazard maps

(PAI maps), and large-scale landslide susceptibility zonation maps for different landslide types. The current practice shows the use of maps at national, regional, and local levels for water management (through soil defence interventions), infrastructure management and civil protection, including landslide forecasts at the national level (SANF system). The different cartographic products described above may constitute a starting point for landslide hazard and risk analysis at the national level and an important tool to support mitigation policies through the identification of intervention priorities, allocation of funds, programming of mitigation measures and planning of civil protection measures.

The presented cartographic products from Croatia encompass the following prototypes of landslide maps developed through scientific projects: mosaicked regional landslide susceptibility maps (scale 1:25,000); large-scale landslide susceptibility maps (scale 1:5,000); and large-scale landslide inventory maps (scale 1:2,000). The recommended use of all maps in spatial planning is derived from research conducted with numerous spatial planners dealing with the creation and implementation of spatial plans at national, regional, and local levels. The main purpose of the Croatian large-scale maps is to obtain special restrictions for the development and implementation of spatial plans. All presented maps are also important tools to support mitigation policies through the identification of intervention priorities, allocation of funds, programming of mitigation measures through water and infrastructure management, as well as planning of civil protection measures.

From the two multi-level landslide mapping approaches and experiences carried out in Croatia and Italy, the following points can be derived:

- 1) Landslide maps and zonation are still not associated with regulations/laws, and consequently, they are rarely considered by planners. This hampers the distribution of these cartographic products among professionals and private companies dealing with spatial planning.
- 2) Inventory and susceptibility maps need to be associated with different levels/types of regulation/restriction because of different types of information (i.e., evidence vs prediction).
- 3) Landslide maps (landslide inventory, landslide susceptibility, landslide hazard and risk maps) prepared at small, medium and large scale, cannot be used for construction design or other engineering purposes that require engineering-geological mapping at a detailed scale.
- 4) The interaction between the scientific community and spatial planning institutions/actors is of crucial importance, and it needs to be strengthened both in Croatia and Italy because of the relevant use of landslide inventory and zonation maps in spatial planning.
- 5) Stakeholders require regulations/restrictions associated with the recognized landslide phenomena and the classes of the zonation maps that can only be achieved through the cooperation of scientists and spatial planners.
- 6) The two different scientific experiences can be used to start a discussion on the use/application of landslide maps.

Acknowledgements

The data collection and analyses for Croatia were carried out in the framework of the scientific projects: PRI-MJER Project funded by the European Union (KK.05.1.1.02.0020; <https://pri-mjer.hr/>) and LandSlidePlan Project funded by the Croatian Scientific Foundation (HRZZ IP-2019-04-9900, <https://landslideplan.eu/>). We thank the members of the projects: Marko Sinčić, Junior Researcher – Assistant PhD fellow; Assoc. Prof. Martin Krkač; Assist. Prof. Petra Jagodnik; Full Prof. Željko Arbanas; and Hrvoje Lukačić, Assistant. An important contribution was made by leading spatial planner Gorana Ljubičić.

References

- Bernat Gazibara S (2019) Methodology for landslide mapping using high resolution digital elevation model in the Podsljeme area (City of Zagreb). Faculty of Mining, Geology and Petroleum Engineering of the University of Zagreb. 257p. (In Croatian)
- Bernat Gazibara S, Sinčić M, Krkač M, Jagodnik P, Mihalić Arbanas S (2023) Guidelines for preparation of landslide maps in Republic of Croatia. Faculty of Mining, Geology and Petroleum Engineering of the University of Zagreb. 60p. (In Croatian)
- Bernat Gazibara S, Mihalić Arbanas S (eds) (2023) Atlas of landslide maps of the PRI-MJER project. Cartographic data and information on landslides for responsible management. Faculty of Mining, Geology and Petroleum Engineering of the University of Zagreb, Faculty of Civil Engineering of the University of Rijeka. 34p.
- Domlija P (2018) Identification and classification of landslides and erosion phenomena using the visual interpretation of the Vinodol Valley digital elevation model. PhD thesis, Faculty of Mining, Geology and Petroleum Engineering of the University of Zagreb, Zagreb, Croatia. 475p.
- Guzzetti F, Mondini A C, Cardinali M, Fiorucci F, Santangelo M, Chang K T (2012) Landslide inventory maps: New tools for an old problem. *Earth-Science Reviews*, 112(1-2), 42-66.
- Iadanza C, Trigila A, Starace P, Dragoni A, Biondo T, Roccisano M (2021) IdroGEO: A collaborative web mapping application based on REST API services and open data on landslides and floods in Italy. *ISPRS International Journal of Geo-Information*. 10(2): 89.
- Jagodnik P, Bernat Gazibara S, Sinčić M, Lukačić H, Arbanas Ž, Mihalić Arbanas S (2023) Geomorphological settings and types of landslides in the City of Buzet identified using LiDAR digital terrain model. In Fio Firi K (ed) Book of Abstracts of the 7th Croatian Geological Congress with international participation. Croatian Geological Survey, Zagreb, pp 79-79.
- Krkač M, Bernat Gazibara S, Sinčić M, Lukačić H, Šarić G, Mihalić Arbanas S (2022) Impact of input data on the quality of the landslide susceptibility large-scale maps: A case study from NW Croatia. In Alcántara-Ayala I et al. (eds) *Progress in Landslide Research and Technology*, Volume 2 Issue 1. Springer, Cham, pp 135-146. https://doi.org/10.1007/978-3-031-39012-8_4
- Loche M, Alvioli M, Marchesini I, Bakka H, Lombardo L (2022) Landslide susceptibility maps of Italy: Lesson learnt from dealing with multiple landslide types and the uneven spatial distribution of the national inventory. *Earth-Science Reviews*. 104125.
- Mihalić Arbanas S, Arbanas Z, Bernat Gazibara S, Ljubičić G, Krkač M, Jagodnik P (2023) Guidelines for the application of landslide maps in the Republic of Croatia. Faculty of Mining, Geology and Petroleum Engineering of the University of Zagreb and Faculty of Civil Engineering of the University of Rijeka. 32p. (In Croatian)
- Mihalić Arbanas S, Krkač M, Bernat Gazibara S (2016) Application of advanced technologies in landslide research in the area of the City of Zagreb (Croatia, Europe). *Geologia Croatica*. 69(2): 179-192.
- Reichenbach P, Rossi M, Malamud B D, Mihir M, Guzzetti F (2018) A review of statistically based landslide susceptibility models. *Earth-science reviews*. 180: 60-91.
- Rossi M and the SANF team (2012) SANF: National warning system for rainfall-induced landslides in Italy. In: *Landslide and Engineered Slopes. Protecting society through improved understanding*. 2: 1895-1899.
- Salvati P, Bianchi C, Rossi M, Guzzetti F (2010) Societal landslide and flood risk in Italy. *Natural Hazards Earth System Science*. 10: 465-483, <https://doi.org/10.5194/nhess-10-465-2010>.
- Trigila A, Iadanza C, Guerrieri L (2007) The IFFI project (Italian landslide inventory): Methodology and results. *Guidelines for mapping areas at risk of landslides in Europe*. 23: 15.
- Trigila A, Iadanza C, Spizzichino D (2010) Quality assessment of the Italian Landslide Inventory using GIS processing. *Landslides*. 7: 455-470.
- Tucker G E, Hancock . R (2010) Modelling landscape evolution. *Earth Surface Processes and Landforms*, 35(1), 28-50.

Rock collapse structure on the Liburnian coast (Rijeka Bay, NE Adriatic)

Čedomir Benac⁽¹⁾, Sanja Dugonjić Jovančević^{(1)*}, Martina Vivoda Prodan⁽¹⁾, Lovro Maglić⁽²⁾

1) University of Rijeka, Faculty of Civil Engineering, Rijeka, Croatia, +385 265 937 (sanja.dugonjic@uniri.hr)

2) University of Rijeka, Faculty of Maritime Studies, Studentska 2, 51000 Rijeka, Croatia

Abstract The studied rock collapse structure is located on the Liburnian coast (Rijeka Bay, channel zone of the NE Adriatic). The relief of the southern part of this coast, with a length of 6.5 km, is a large escarpment with very steep to vertical slopes reaching heights of 100 m above sea level, as a result of tectonic movements along the Kvarner fault zone. These events probably led to a sudden relaxation of the highly fractured rock mass. The progressive extension occurred in places where previously favourably oriented paraclases of faults and fissures had formed a very large and complex rock collapse. The width of the displaced mass along the coast is 375 m and the estimated total volume of the displaced rock mass is 2,400,000 m³. The lower part of the instability phenomenon lies 40 m below MSL and it was submerged during the Holocene sea level rise. A large part of the displaced rock mass was in a stable position, with sporadic rock falls. Recent techniques to survey the instability site and to analyse the evolution of the rupture surface and its dimensions above and below the sea level were used and combined (Unmanned Aerial Vehicles, and Remotely Operated Vehicles).

Keywords coastal instability, tectonic movements, rock collapse, marine erosion, SfM-MVS photogrammetry, underwater survey

Introduction

The Liburnian coast is located on the western coast of the Rijeka Bay. It is part of the Kvarner channel zone of the northeastern Adriatic. The relief of the southern part of this coast looks like an escarpment. This 6.5 km long escarpment, is characterized by very steep to vertical slopes, that reach a height of 100 m above mean sea level. The submarine slopes are also very steep, so that the isobaths of -50 m run close to the coastline (Figure 1).

The terrain is extremely inaccessible, so that the use of modern research techniques was necessary. The aforementioned scarps were surveyed using an Unmanned Aerial Vehicle (UAV) and the 3D point cloud was generated using the Structure from Motion (SfM) with Multi-View Stereo (MVS) photogrammetry. The submarine zone was surveyed using scuba-diving equipment and Remotely Operated Vehicles (ROVs). Using these methods, successful research was carried out on a large rock slide in the southern part of the aforementioned escarpment (Benac et al., 2023).

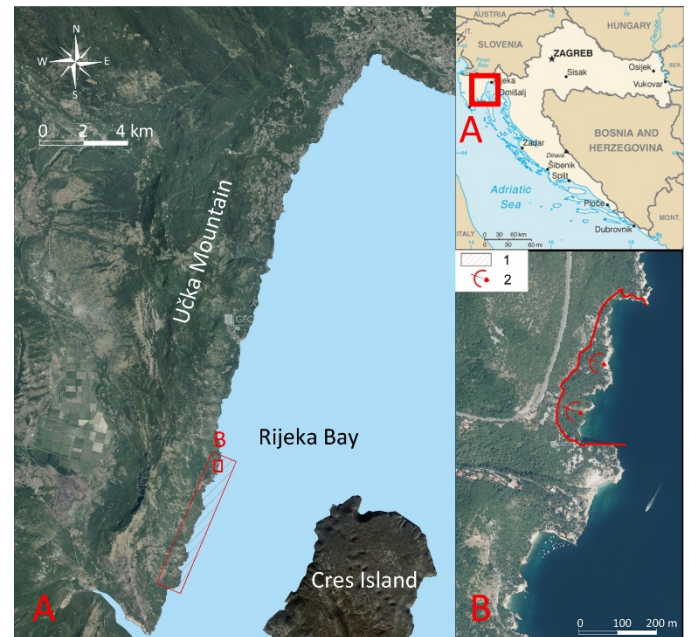


Figure 1 Location and simplified geological maps A) the Liburnian coast: 1- position of escarpment B) study area: 2 - studied collapse structure.

The instability studied in this paper is one of the largest and most interesting instability phenomena on the aforementioned part of the Liburnian coast. Based on the results obtained with the proposed methodology and the analyses presented in this paper, the origin and geomorphologic evolution of the investigated rock collapse are presented and discussed.

Geological setting and geomorphological evolution

The wider study area is part of the lower (southern) overthrust of the ridge of the Učka Mt. Overturned folds and reverse faults of the paraclasis dipping to the northeast, are common within the lower overthrust. Upper Cretaceous rudist limestone predominate in the southern Liburnian coastal zone. The limestone rock mass is tectonically strongly deformed and exhibit distinct bedding. The bedding planes are mostly inclined to the east and southeast. The layers are 10 to 100 cm thick. The flysch rock mass is squeezed between the carbonate rocks and is mostly covered by younger colluvial deposits. Tectonic breccias have been found near reverse faults (HGI, 2009).

During the first phase of the Dinaridic compression, the Istrian peninsula was separated from the strongly deformed Adriatic segment by the Kvarner fault zone and rotated towards the northeast where it is underthrusting beneath the External Dinarides (Placer et al., 2010). During the second phase of the orogeny, the principal regional stress changed to a N-S direction and the Učka Mt. ridge acquired its present NNE-SSW (meridional) strike (Marinčić & Matičec, 1991). Transpression and radial extension during the last phase of regional stress caused the deformation of younger diagonal and transverse dextral strike-slip faults and opposite vertical tectonic movements on the eastern slopes of Učka Mt. The key prerequisite for the appearance of today's very steep southern Liburnian coast is the structural arrangement of the discontinuities in the carbonates along the Kvarner fault zone (Mihljević, 1996). The relatively rectilinear extension of the Liburnian coast is a consequence of the Kvarner fault zone. The interruption of the geological structures of the Kvarner islands towards the northwest is visible on geological maps (Korbar, 2009).

A relatively narrow and elongated karst plateau is located between the ridge of the southern Učka Mt. and Rijeka Bay. This plateau is slightly inclined towards Rijeka Bay and is strongly limited by the escarpment along the

Liburnian coast. Intense morphogenetic processes caused by neotectonic movements and sea level oscillations, as well as climatic changes, have shaped the present form of the Kvarner area, and also the relief of the studied area (Benac & Juračić, 1998; Juračić et al., 2009). Several large rockslides have been recorded on this coast (Benac et al., 2023).

Results

The studied collapse structure is separated from the edge of the karst plateau by a system of fractures (faults and fissures) that form an irregular elongated outline of the main escarpment. Three normal faults with almost parallel extensions are visible above the main scarp of the landslide (Figure 2).

The collapse structure consists of two lithologic types. Cataclastic breccia is found in the southern part of the studied instability. This rock mass consists of angular fragments originating from limestone. The range of fragments is a few centimeters to blocks with a diameter of one meter. The matrix is calcitic reddish clay (Figure 3). A strongly fractured and karstified limestone rock mass there is in the central and northern parts of the collapse structure (Figure 4).

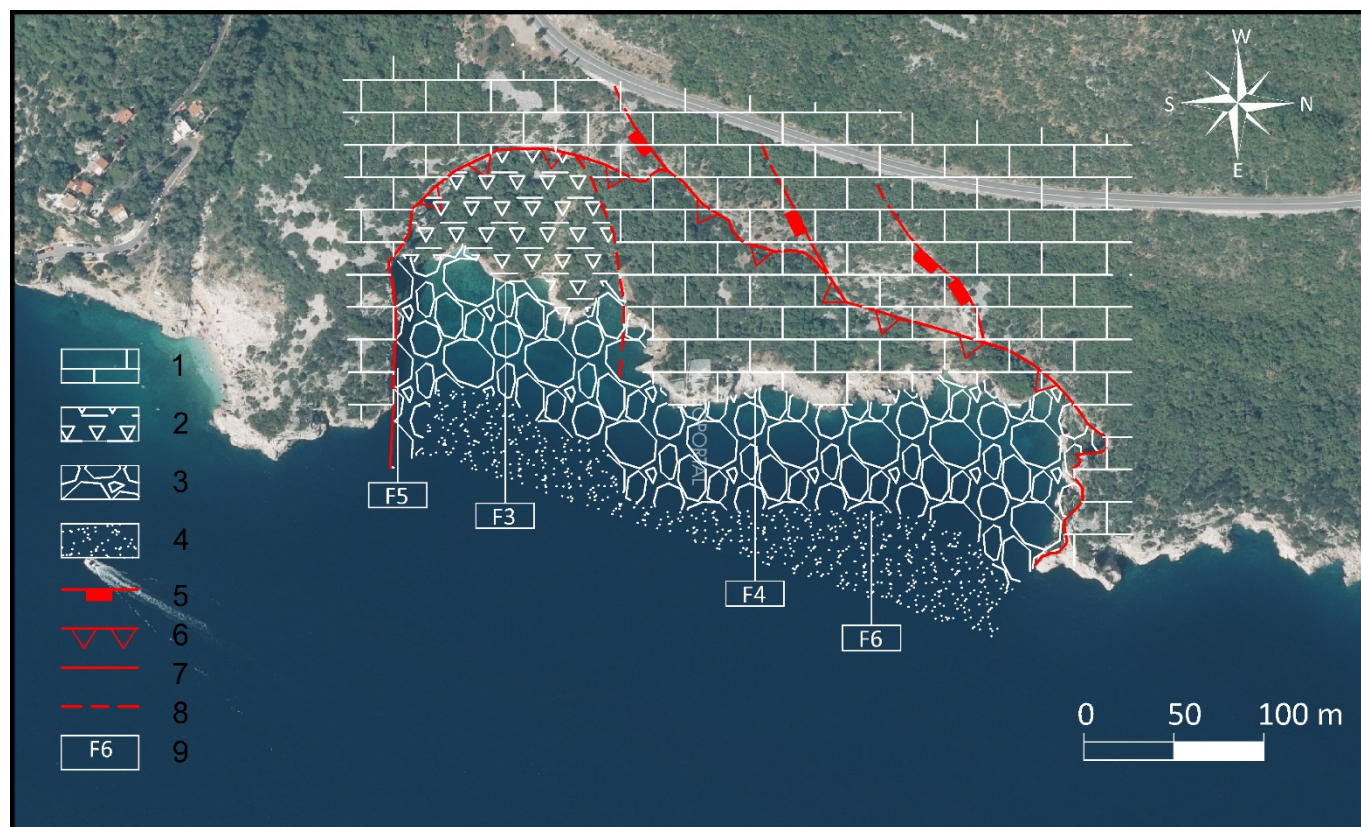


Figure 2 Geological map of collapse structure 1-Upper Cretaceous limestone, 2-cataclastic breccias, 3-colluvial cobbles, and boulders, 4 coarse sand and silty sand, 5-normal fault with a position of hanging wall, 6-main scarp, 7-lateral discontinuities, 8-approximate geological boundary, 9-position of photos.



Figure 3 Tectonic breccia on the southern edge of collapse structure (Photo: D. Kalajžić).



Figure 4 Strongly fractured and karstified limestone rock on the northern side of the collapse structure (Photo: D. Kalajžić).

The shallow part of the bottom near the coastline has a gentle slope inclination. Marine erosion is more pronounced on the coast, which consists of cataclastic breccias. A narrow marine terrace and a pocket beach have formed there (Figure 3). Tidal notches are formed due to the bioerosion of limestone rocks, predominating on the central-northern part of studied collapse structure. (Figure 4). Based on the underwater survey insight, the bare rock mass is visible on the lateral side of the investigated instability (Figure 5). Boulders with a diameter of up to 50 cm are located at a depth of 40 m (Figures 2 and 6). The deeper part of the bottom is slightly inclined and covered with sandy sediments. The landslide toe is located at a depth of about 40 m below mean sea level. The total volume of the displaced rock mass as about 2,400,000 m³.

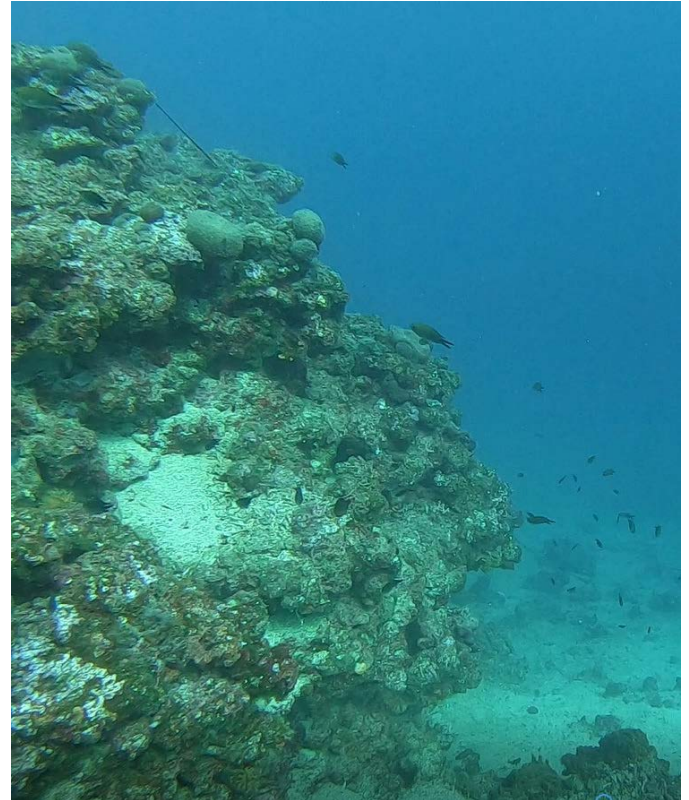


Figure 5 Rock mass on the southern edge of collapse structure (Photo: L. Maglić).



Figure 6 Boulders on the foot of sliding body 40 m deep (Photo: L. Maglić).

The total height (from the crown to the landslide toe) is up to 140 m. The geometry of the studied instability was described according to the nomenclature for landslides proposed by WP/WLI (IAEG, 1990):

- the length of the displaced mass: $L_d = 130$ m;
- the width of the displaced mass: $W_d = 375$ m;

The investigated collapse structure cannot be strictly classified into one type of landslide (Hung et al., 2014). In

the initial phase of development, it was a rock collapse, because sliding of a rock mass occurred on a rupture surface consisting of several planes. Rock collapse occurred on an irregular rupture surface consisting of many randomly oriented joints, separated by segments of intact rock. In the second phase, lasting until the present day, rock falls are still occur.

Discussion and conclusion

Several large instabilities have been recorded on the escarpment along the southern part of the Liburnian coast. The rock collapse studied in this article, together with the instability analysed by Benac et al., 2023, is one of the most interesting phenomena on this part of the coast

During the last phase of the tectonic evolution of the Istrian peninsula and the Kvarner area, tectonic movements along the Kvarner fault zone may have been active. The mentioned instabilities were formed during the transpressive deformation along the Kvarner fault zone (Korbar, 2009; Placer et al., 2010). Recent tectonic activity in the wider area (Markušić et al., 2019) probably triggered collapse events and caused the displacement of large blocks of cataclastic breccias and limestone (Figure 2). The present form of the described collapse structure has the shape of a rock slump, however, as described earlier, it can be classified as a rock collapse with characteristics of a compound rock slide (Hungar et al., 2014).

The morphological evolution of the instability probably took place in several phases. Due to the subsidence of the seabed in the present Rijeka Bay, the formation of initial scarps occurred in the first phase. This event led to a relaxation of the rock mass. The progressive extension took place at the site of the previously formed and favourably oriented paraclases of faults and fissures. In the second phase, the detachment of blocks of the cataclastic breccia and limestone from the main slope and the beginning of a rock collapse or compound rock slide occurred. The disintegration of the front part of the sliding body of the detaching large rocky blocks and the onset of periodic rock falls occurred in the third phase. Sea flooding of the lower part of the displaced material occurred in the last phase, allowing the influence of marine erosion, partial rock fall and debris fall, and the sedimentation of fine-grained sediments.

Intertidal notches are visible in relatively resistant limestone rocks mass (Figures 2 and 4). The measurements in other locations show that the elevation points are located at similar depths of elevation points that have been found elsewhere on the Liburnian coast (Benac et al., 2004). Therefore, it can be assumed that the upper part of the sliding body was in a relatively stable position before the Late Pleistocene-Holocene sea level rise (Benac et al., 2023). The measurement of elevation points of the tidal notches at the location analysed in this paper could provide interesting data on the recent stability of the collapsed structure.

Since the beginning of instrumental measurements, sea level rise in the northern Adriatic has been recorded in the range of $2.0 \pm 0.9 - 3.4 \pm 1.1$ mm/year (Surić et al., 2014; Tsimplis et al., 2012). New climate models predict extreme wave storms (Bonaldo et al., 2017) and increased marine erosion in the Adriatic Sea (Gallina et al., 2019). Because of this, wave attacks could be stronger and higher in the future on this studied coast. Marine erosion could be especially expressed in These lees-resistant cataclastic breccias (Figures 2 and 3). It can be a triggering effect for increasing landslide hazard increase.

It will be necessary to carry out detailed research in the future using modern techniques. In this way, they will be able to perform a structural analysis of the rock mass, as well as locate the exact position of the toe of the sliding body. The results of a new investigation, , would therefore be an important step towards a better understanding of the geomorphological evolution of the studied collapse structures and similar structures on escarpments around the Kvarner area. This could significantly change the current reconstruction not only of coastal evolution in the Kvarner area but also in other parts of the Adriatic channel zone.

Acknowledgements

The authors would like to thank their colleague Duje Kalajžić for excellent photos using UAV technique and for help with terrain analysis using SfM-MVS photogrammetry. This research has been partially financed by the University of Rijeka (Uniri-tehnic-18-97, Uniri-zip-2103-6-22 and Uniri-iskusni-tehnic-23-191).

References

- Benac, Č., Dugonjić Jovančević, S., Navratil, D., Tadić, A., & Maglić, L. (2023). Large gravitational collapse structure on a rocky coast (Kvarner, NE Adriatic Sea). *Geologia Croatica*, 76(3), 105–112. <https://doi.org/doi:10.4154/gc.2023.10>
- Benac, Č., & Juračić, M. (1998). Geomorphological indicators of the sea-level changes during Upper Pleistocene (Wuerm) and Holocene in the Kvarner region. *Acta Geographica Croatica*, 33(1), 27–42.
- Benac, Č., Juračić, M., & Bakran-Petricioli, T. (2004). Submerged tidal notches in the Rijeka Bay NE Adriatic Sea: indicators of relative sea-level change and of recent tectonic movements. *Marine Geology*, 212(1), 21–33. <https://doi.org/https://doi.org/10.1016/j.margeo.2004.09.002>
- Bonaldo, D., Bucchignani, E., Ricchi, A., & Carinel, S. (2017). Wind storminess in the Adriatic Sea in a climate change scenario. *Acta Adriatica*, 58(2), 195–208.
- Gallina, V., Torresan, S., Zabeo, A., Rizzi, J., Carniel, S., Sclavo, M., Pizzol, L., Marcomini, A., & Critto, A. (2019). Assessment of Climate Change Impacts in the North Adriatic Coastal Area. Part II: Consequences for Coastal Erosion Impacts at the Regional Scale. *Water*, 11(6). <https://doi.org/10.3390/w11061300>
- HGI. (2009). *Geološka karta Republike Hrvatske 1:300.000 [Geological map of Republic of Croatia 1:300.000 – in Croatian]*. Hrvatski geološki institut.
- Hungar, O., Leroueil, S., & Picarelli, L. (2014). The Varnes classification of landslide types, an update. *Landslides*, 11(2), 167–194. <https://doi.org/10.1007/s10346-013-0436-y>

- IAEG. (1990). Suggested nomenclature for landslides. *Bulletin of the International Association of Engineering Geology - Bulletin de l'Association Internationale de Geologie de l'Ingenieur*, 41(1), 13–16. <https://doi.org/10.1007/BF02590202>
- Juračić, M., Benac, Č., Pikelj, K., & Ilić, S. (2009). Comparison of the vulnerability of limestone (karst) and siliciclastic coasts (example from the Kvarner area, NE Adriatic, Croatia). *Geomorphology*, 107(1), 90–99. <https://doi.org/https://doi.org/10.1016/j.geomorph.2007.05.020>
- Korbar, T. (2009). Orogenic evolution of the External Dinarides in the NE Adriatic region: a model constrained by tectonostratigraphy of Upper Cretaceous to Paleogene carbonates. *Earth-Science Reviews*, 96(4), 296–312. <https://doi.org/https://doi.org/10.1016/j.earscirev.2009.07.004>
- Marinčić, S., & Matičec, D. (1991). Tektonika i kinematika deformacija na primjeru Istre [Tectonics and kinematics of deformations, an Istrian model – in Croatian. *Geološki Vjesnik*, 44, 257–268.
- Markušić, S., Stanko, D., Korbar, T., & Sović, I. (2019). Estimation of near-surface attenuation in the tectonically complex contact area of the northwestern External Dinarides and the Adriatic foreland. *Natural Hazards and Earth System Sciences*, 19(12), 2701–2714. <https://doi.org/10.5194/nhess-19-2701-2019>
- Mihljević, D. (1996). Strukturno-geomorfološke značajke i morfotektonski model razvoja gorskog hrpta Učke [Structural-geomorphological Characteristics and Morphotectogenetic Evolution Model of the Učka Mountain Range (Croatia) – in Croatian]. *Hrvatski Geografski Glasnik*, 58, 33–39.
- Placer, L., Vrabec, M., & Celarc, B. (2010). The bases for understanding of the NW Dinarides and Istria Peninsula tectonics. *Geologija*, 53(1), 55–86. <https://doi.org/10.5474/geologija.2010.005>
- Surić, M., Korbar, T., & Juračić, M. (2014). Tectonic constraints on the late Pleistocene-Holocene relative sea-level change along the north-eastern Adriatic coast (Croatia). *Geomorphology*, 220, 93–103. <https://doi.org/https://doi.org/10.1016/j.geomorph.2014.06.001>
- Tsimplis, M. N., Raicich, F., Fenoglio-Marc, L., Shaw, A. G. P., Marcos, M., Somot, S., & Bergamasco, A. (2012). Recent developments in understanding sea level rise at the Adriatic coasts. *Physics and Chemistry of the Earth, Parts A/B/C*, 40–41, 59–71. <https://doi.org/https://doi.org/10.1016/j.pce.2009.11.007>

Geological-Geotechnical Exploration for the Landslide mitigation Section at the Old Cemetery in Smederevo

Ivica Tornjanski^{(1)*}, Aleksandar Tokin⁽²⁾, Nemanja Stanić⁽²⁾

1) Urban Planning Institute of Belgrade

2) Hidrozavod DTD a.d. Novi Sad

Abstract: The slope where the Old Cemetery in Smederevo is situated has been shaped by landslide processes. These are most likely deep but dormant landslides with the failure surface of over 20 m. Active landslides occur in shallow, near surface areas, with the failure surface of about 2 m. In addition to present exogenic processes, human activities such as cutting, filling, land development etc. also impact the landscape. The study microlocation occupies the slope section in the Old Cemetery northern boundary area from Karadorđeva Street to Koče Kapetana Street. The slope gradient in this section is about 45°. The slope stretches to the Danube river alluvial plain, with elevations ranging from 74 to 74,5 m, whereas the elevations in the slope section under consideration range from 77 to 90 m. Overall stability of the slope is ensured by an RC retaining system – a concrete diaphragm wall built at the slope toe, whereas traces of active landslide and failures with their effects are clearly visible in higher sections of the slope. The study area is made up of the sediments of various compositions and ages. The bedrocks represented by the Neogene sediments are overlain by the Quaternary delluvial sediments. The proposed solution involves construction of the retaining system comprised of Ø800 mm piles with a capping beam. The piles will be 10 m long, with the pile base elevation at 72,0 m. The capping beam elevation will be at 83,0 m. The spacing between the piles depends on the static calculation, with an assumption that Ø800 mm piles with the spacing of 2,0 m can provide stability. The gap between the piles (from the surface of the ground to the capping beam) will be protected by horizontal sheet piling. Drains that will allow water drainage should be provided for at the sheet piles. The pile retaining wall length is 54 m. Terramesh gabion wall filled with sand will be constructed after the pile retaining wall has been completed. The gabion walls will be supported by the pile capping beam and installed by stepping back by 0,5 m. In case the gabions have cross section of 1,0 x 1,0 m, the retaining wall face will have a gradient of 2:1. The elevation of the top the Terramesh gabion retaining wall will range from 86,0 to 89,0 m, depending on the elevation of the slope in the back. The surface layer of the sand fill should be covered with topsoil and grassed.

Keywords: the Old Cemetery, Smederevo, landslide, piles

Geomorphological characteristics

The study area occupies the border between southern Banat plains and the hills of Smederevo. Present landscape patterns have mostly been shaped by the Danube river together with present exogenic landslide processes. A number of landslides is a one of the outstanding characteristics of the right bank of the Danube river along its entire flow through Serbia. The tendency of the river course to shift southward is the primary cause of the landslide processes.

The slope where the Smederevo Old Cemetery is situated has been shaped by landslide processes. These are most likely deep landslides with the failure surface of over 20 m however, with the suspended landslide process. Active landslides occur in shallow, near surface areas, with the failure surface of about 2 m.

In addition to present exogenic processes, human activities such as cutting, filling, land development etc. also impact the landscape.

The The study microlocation occupies the slope section in the Old Cemetery northern boundary area from Karadorđeva Street to Koče Kapetana Street. The slope gradient in this section is about 45°. The slope stretches to the Danube river alluvial plain, with elevations ranging from 74 to 74,5 m, whereas the elevations in the slope section under consideration range from 77 to 90 m. Overall stability of the slope is ensured by an RC retaining system – a concrete diaphragm wall built at the slope toe, Figure 1, whereas traces of active landslide and failures with their effects are clearly visible in higher sections of the slope, Figure 2.



Figure 1. A section of the existing retaining system at the slope toe



Figure 2. Landslides and failures in higher sections of the slope

Geological characteristicsThe study site is made up of sediments of various composition and ages. The Quaternary diluvial sediments overlie the Neogene bedrocks.

The Neogene (Lower Pliocene – Pl_1)

$Pl_1(lg, ug, p)$ – a complex of marly and coaly clays with sand interbeds

A complex of coaly (ug) and marly (lg) clays represented by clays with lenticular interbeds of coal and sands overlie the floor sands. Thickness of coaly clays ranges from 40 to 60 m. Coaly clays are always highly jointed, with a number of tectonic joints dividing the rock mass into irregular blocks. The coal is of a variable thickness. It is faulted and contorted due to tectonic movements. Relatively closely spaced faulting in coals as marking beds virtually produce discontinuities in the horizontal direction of the bed.

In general, the clay-sandy complex is a product of lacustrine sedimentation, where the sand and the clay belong to shallow and deep facies, respectively. Their relationship corresponds to the shallowing process in the Pannonian Sea accompanied by many movements in the tectonically mobile basin (which is indicated by several beds of coal). The Pliocene lake retreat along its boundary resulted in formation of abrasion terraces. Steep scarps – cliffs and plateaus were formed in sands and marly clay, respectively.

The Neogene sedimentary rocks are gently undulating, dipping northeast at an angle of 5 to 15°.

Two groups of discontinuities are present in a broad area:

The first group includes the faults that strike approximately parallel to the Danube river, with the dip direction ranging from 15° to 205° (with a relatively steep

dip westward), along which individual blocks moved up or down).

The second group of faults have the direction of 135° to 315°, with the dip southwestward. Their strike is diagonal to the strike of the first group of faults, and subsequent movements occurred along the faults. Reverse rise of the coaly clays in relation to the roof sands occurred along the faults.

The Quaternary (Q)

The Quaternary sediments are the most widespread stratigraphic member on the surface and are represented by the heterogenous fill material (n) that makes up the surface portions of the slope toe and bottom portions of the site, diluvial deposits (dl) composed of clayey silty-sandy sediments that make up the surface portions of the unstable slope.

Hydrogeological characteristicsLithology and porosity conditions determine hydrogeological properties of the study site. The diluvial deposits have pseudointerparticle and fine fissure porosity. The fill material and Pliocene sands are mostly of interparticle porosity. Due to their different porosity types and distribution on the site, the identified sediments can be classified in the following groups according to their geologic function:

- hydrogeologic conductors of water – the fill material and diluvial deposits,
- hydrogeologic accumulator aquifers – the Pliocene sands.

In the Pliocene sands, an aquifer has been formed in which the water table was not discovered to a depth of 15 m during borehole drilling. During periods of high precipitation, the water table in the aquifer is always much higher and estimated to be up to 2 – 3 m from the surface of the ground.

Seismic characteristicsNo detailed microseismic zoning of the area studied has been performed. The seismicity parameters have been taken from the website of the Seismological Survey of Serbia (<http://www.seismo.gov.rs/>). The maximum intensity earthquakes can be expected according to the seismic hazard maps for peak horizontal ground acceleration for the bedrock – $Acc(g)$ and a maximum macroseismic intensity – I_{max} in units specified by the European Macroseismic Intensity Scale (EMS-98) within the return periods of 95, 475 and 975 years and are represented in Table below.

Table 1. Seismicity parameters for return periods.

Seismicity Parameter	Return Period (in years)	
	95	475
Acc(g) max	0.06	0.10
I _{max} (EMS-98)	VI-VII	VII-VIII

Basic characteristics of landslideThe process of initiation and development of landslide on the location considered is both complex and specific. Main prerequisites for slope instability are the site geologic structure, morphology, hydrogeological properties and poor physical and mechanical properties of the rock masses (marly clays, marls and sands). Human activities such as improper, usually unplanned cuttings, damages to water and sewer systems, and similar activities can be a contributing factor in causing landslides.

The wider area is affected by the process of instability. These are most likely deep landslides with the failure surface of over 20 m however, with the suspended landslide process. Active landslides and failures occur in shallow, near surface areas in the top portion of the steep slope spreading along the Cemetery northern boundary. The estimated failure surface is about 2 m, and the landslide future activity can directly threaten and restrict the use of the Cemetery area.

Landslide mitigation measuresThe engineering solution to the repair of the part of the Old Cemetery landslide in Smederevo has been proposed taking into account the results of investigations and surveys.

The proposed solution will provide stability of the top portions of the steep slope in the north part of the Cemetery in Karađorđeva Street, and prevent any further slides of the surface portions of the site. In addition, the steep slope will be permanently stabilized and its potential failures prevented.

The proposed solution involves construction of the retaining system comprised of Ø800 mm piles with a capping beam. The piles will be 10 m long, with the pile base elevation at 72,0 m. The capping beam elevation will be at 83,0 m. The spacing between the piles depends on the static calculation, with an assumption that Ø800 mm piles with the spacing of 2,0 m can provide stability. The gap between the piles (from the surface of the ground to the capping beam) will be protected by horizontal sheet piling. Drains that will allow water drainage should be provided for at the sheet piles. The pile retaining wall length is 54 m.

Terramesh gabion wall filled with sand will be constructed after the pile retaining wall has been completed. The gabion walls will be supported by the pile capping beam and installed by stepping back by 0,5 m. In case the gabions have cross section of 1,0 x 1,0 m, the retaining wall face will have a gradient of 2:1. The elevation of the top the Terramesh gabion retaining wall will range from 86,0 to 89,0 m, depending on the elevation of the slope in the back.

Stability of the existing RC diaphragm wall may not be compromised during construction works. This particularly applies to pile driving machine moves on the site. In addition, the use of bored pile walls is proposed because the method of drilling bored piles produces the least vibration.

The back of the gabion wall (the section between the the gabion and the existing slope) will be filled with

sand. The sand should be compacted in layers of up to 30 cm by manual vibro compactors (tamping rammer). Sand layers compaction should be minimum $E_{vd} = 15$ MPa.

The surface layer of the sand fill should be covered with topsoil and grassed.

Slope stability analysisGeostatic calculations have been used in stability analysis of the soil and the proposed retaining system.

Geostudio 2012 – *Slope/W* software and *the Morgenstern-Price* limit equilibrium method were used in the analyses. The geoen지니어ing model at the cross section 1-1' was adopted in the analyses (Figure 3).

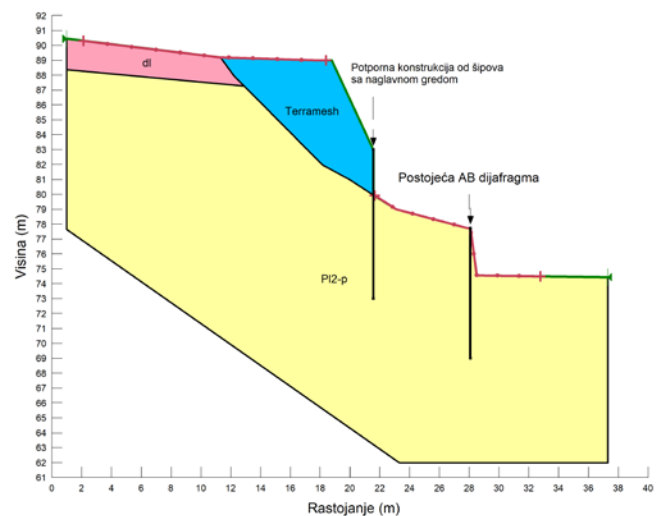


Figure 3. Geoen지니어ing model at GT cross section 1-1'

The first step involved the analysis of the overall stability after the repair that is, construction of the retaining system from the piles and "terramesh" gabion wall.

Strength parameters (for terramesh) for the structure were provided by the material supplier, and they apply to the fill excluding geomesh for reinforcement. The equivalent parameters for the terramesh structure are the following:

- $\gamma = 18,5$ kN/m³;
- $\phi = 35^\circ$;
- $c = 10$.

The above parameter values apply to the case where sand materials are used for filling.

Shear strength is 300 kN, with the pile spacing of 2,0 m.

Stability analyses have been made for regular conditions and for horizontal ground acceleration of $Acc(g) = 0,1$. The results are represented in Figures 4 and 5.

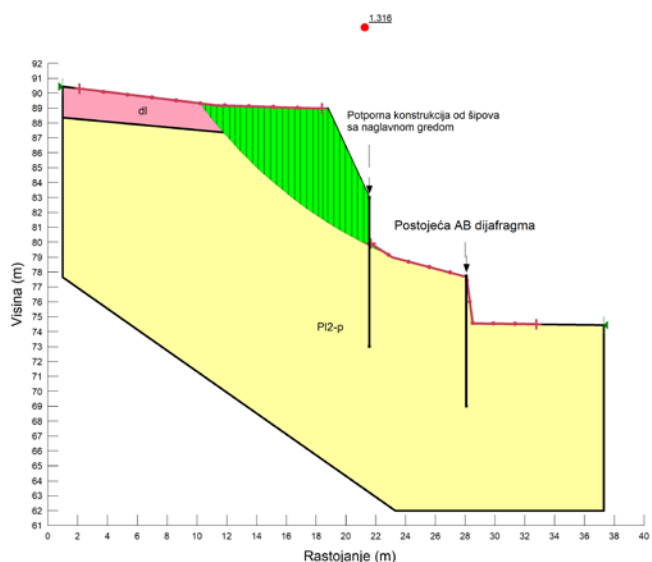


Figure 4. Slope stability analysis in the area of the retaining system

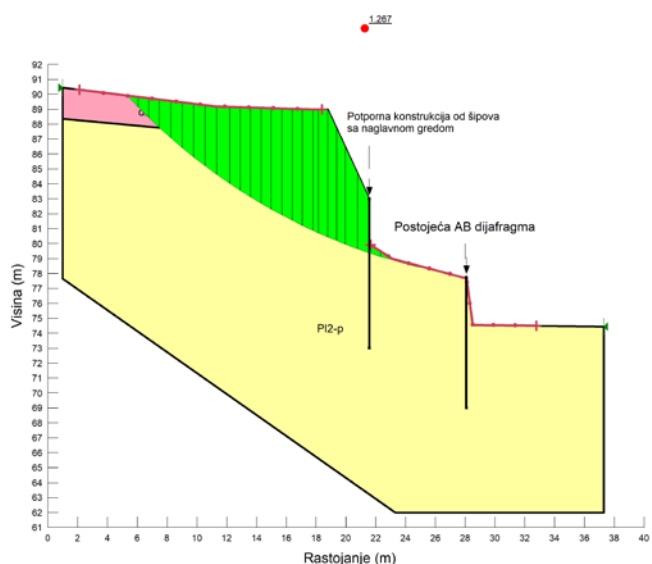


Figure 5. Slope stability analysis in the area of the retaining system – including the peak horizontal ground acceleration for the return period of 475 years

The factors of safety for the critical slip surface are $F_s = 1.316$ (excluding the ground acceleration) and $F_s = 1.267$ (including the ground acceleration), respectively. The estimated factors of safety can be considered satisfying for the structure type studied. Since estimation for the cross section analyzed is the most critical given the position of the retaining system in relation to the slip surface, it can be considered relevant for the entire retaining system.

The analysis has also been made for the effects the retaining system has on the landslide in the surface portions of the site (Figure 6).

Since it was not possible to reconstruct the soil conditions before the landslide occurrence, back-analysis has been used to determine stability along the slip surface, with an assumption that the sliding body is currently in the limit equilibrium state ($F_s \approx 1.0$).

The analysis resulted in the following conditional strength parameters along the slip surface:

- $\gamma = 21,0 \text{ kN/m}^3$;
- $\phi = 11,2^\circ$;
- $c = 0 \text{ kN/m}^2$.

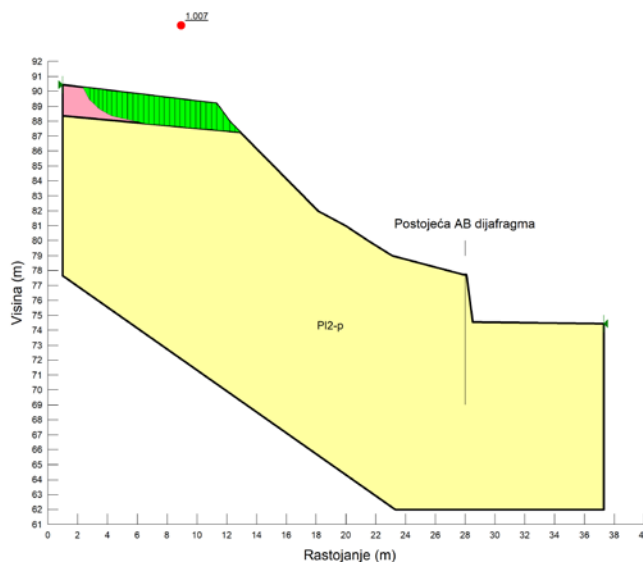


Figure 6. Back-analysis

The effects of the retaining system on the landslide stabilization are demonstrated in an increase of the factor of safety from $F_s = 1.0$ to $F_s = 3.58$ (excluding the horizontal ground acceleration for the return period of 475 years) that is, $F_s = 2.15$ (including the horizontal ground acceleration for the return period of 475 years) – Figures 7 and 8.

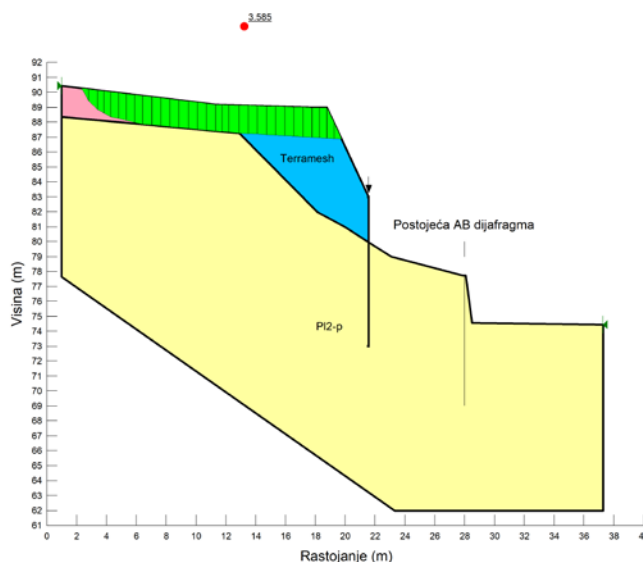


Figure 7. The analysis of stability in the landslide area – excluding the peak horizontal ground acceleration for the return period of 475 years

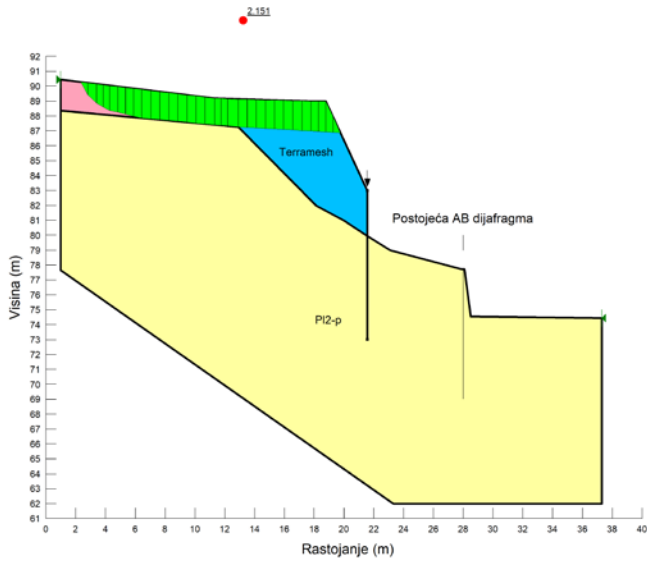


Figure 8. The analysis of soil stability in the landslide area – including the peak horizontal ground acceleration for the return period of 475 years.

Slope stabilization and erosion control using a Naturally based solution with Biopolymers

Aleksandra Nikolovska Atanasovska^{(1)*}, Josif Josifovski⁽²⁾

1) M.Sc., University "Ss. Cyril and Methodius", Faculty of Civil Engineering - Skopje, Department of Geotechnics, N. Macedonia, (nikolovskaaleksandra189@gmail.com)

2) Prof. Ph.D., University "Ss. Cyril and Methodius", Faculty of Civil Engineering - Skopje, Department of Geotechnics, N. Macedonia

Abstract: Climate change, usually manifested by frequent and intense rainfalls, can be a main contributing factor for soil instabilities, in the form of landslides, and soil erosion. Thus, it is crucial to comprehend the process of atmospheric interaction responsible for the stability of natural and man-made slopes, the water infiltration, and shallow (local) instabilities which over time most certainly can develop into global slope instability. Nowadays, the usage of environmentally friendly materials for soil improvement has become very popular with the increased environmental awareness. The biopolymers are processed from a biodegradable substance, thus they are safe for the environment or people. The paper presents the results of research on the use of biopolymers as naturally based solutions for soil treatment and improvement. The biopolymer acts as a binding viscous agent with the soil particles providing additional adhesion, thus provides more resistance to the erosion process. The research methodology was organized into two stages, laboratory testing followed by experimental testing on a large-scale physical model. First, strength-deformation properties and saturated coefficient of permeability of the natural (untreated) and improved (treated) soil were defined. Hence, through comparison, the improvement effects or the degree of the improvement has been defined. Second, experimental tests on an untreated and biopolymer-treated slope with a slope of 1:1.5, on which rainfall of 10 liters per hour was applied for 180 minutes were performed. The results have shown that the natural polymer improves not only the mechanical but also the hydraulic soil parameters by forming a viscous gel matrix with a reinforcing bond between the soil grains that fills the pores. In dry conditions, the treated soil forms a solid surface crust that prevents evapotranspiration. When it rains, it becomes hydrophobic and allows the run of water without significant soil erosion. All test results confirm the efficiency of the biopolymer as an additive to the soil for stabilizing the slopes subjected to atmospheric actions.

Keywords: Slope stability, Erosion resistance, Naturally-based solution, Biopolymer stabilization.

Introduction

The influence of climate change in the infrastructure sector is becoming ever more visible and should not be

ignored. Climate change creates several challenges for infrastructure that can affect their lifespan and transport safety. The high-temperature variations and intense rainfall affect the stability of soil slopes. Increased rainfall and dry periods have a great impact on slope stability because over time they cause erosion, cracking, local instabilities, and even trigger landslides.

Soil erosion is a process of detachment and transport of soil particles caused by water and wind (Song et al. 2005). Soil erosion occurs once shear stress exerted by moving fluids exceeds a critical value, referred to as critical erosion shear stress (Soo-Min et al. 2018). Generally, erosion is considered that can not affect the stability of the slope. However, this research shows that the rainfall-runoff rate and soil erodibility initiate erosion which reduces the shear capacity while increasing the pore pressure which ultimately results in erosion sometimes even sliding. Some soils are more erodible than others, but climate change may bring more frequent and more intense rainfall that will cause increased soil erosion regardless of soil type (Nikolovska et al. 2023)

In reality, the berms are partially or completely filled with eroded soil material, as shown in Fig. 1, thus runoff water flows down the slopes and creates paths that can be quite deep and over time result in surface instabilities. To prevent such situations and reduce their occurrence in the future, it is necessary to take prevention measures during the design phase, directed to increase the resistance to erosion and improve infiltration.

Some soils are more erodible than others, but in general climate change brings more frequent and intense rainfall which causes increased soil erosion regardless of soil type.

Soil water content is an important element for the growth of vegetation. Vegetation dynamics largely depend on soil water availability, which, in turn, results from several complex and mutually interacting hydrologic processes (Chen et al. 2007). Different vegetation and soil types have different water infiltration capacities. Root systems make the soil more resistant to external influences. Hence, climate change causes severe dry periods that create difficult conditions for vegetation to



Figure 1 Soil slope with expressed erosion of the Highway Miladinovci – Shtip, R.N. Macedonia.

thrive, which emphasizes the need to take measures for surface stability at the slopes in the design phase.

Today, many natural soil improvement techniques that increase erosion resistance by improving their mechanical and hydrological properties (Ham et al. 2018) are available. One of them is the biopolymeric material produced by microorganisms, algae, plants, etc., which are considered ecological and sustainable materials for soil improvement. In the past decade, natural polymers have been identified as highly effective polymers that stabilize soil surface structure and improve infiltration (Lentz et al. 1997). Natural polymers are water soluble and when mixed with soil, they can produce increased soil strength, improve cohesion, and reduce water permeability, but also retain soil moisture, and produce greater resistance to erosion forces.

Natural polymer solution

A biopolymer product is an aqueous solution containing a binding agent for soil stabilization. The product is obtained by processing a biodegradable substance of natural origin, specially designed for application on slopes exposed to climate changes and atmospheric actions (Nikolovska et al. 2022).

Fig. 2 shows the erosion resistance model of polymer-treated soil. The gel structure of the natural solution fills the pores and cavities, which reduces the potential for infiltration, and coats the grains, improving their mutual adhesion and connection, which increases the strength of the material (Ivanov et al. 2008). Soils treated with polymer solutions form a solid surface crust that prevents water infiltration and allows free surface runoff without soil erodibility (Cheng et al. 2015). Polymer-treated soils have an additional positive effect on plant life, primarily due to the absorption of moisture and its retention in the soil, which supports and stimulates the growth of vegetation for a longer period (Chung et al. 2018).

Testing methodology

The testing in this study was organized into two phases: the first phase where the physical, strength-deformation characteristics and coefficient of the permeability were determined for the untreated and biopolymer-treated soil, and the second phase, when

experimental testing on physical models was performed for the untreated and biopolymer-treated slope subjected to intense rainfall

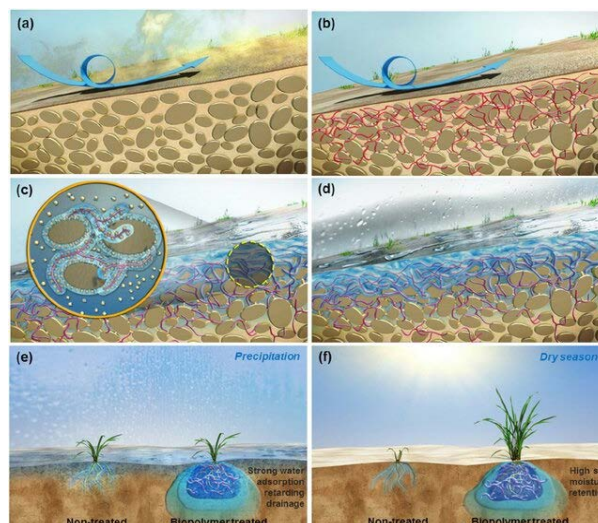


Figure 2 Erosion resistance model of polymer-treated soil (Chang et al. 2015).

Laboratory testing

To determine the physical and mechanical properties of the soil around 60 laboratory tests have been performed. Fig. 3 shows the grain size distribution curve of the investigated soil, which is classified as silty sand soil (SM according to the USCS).

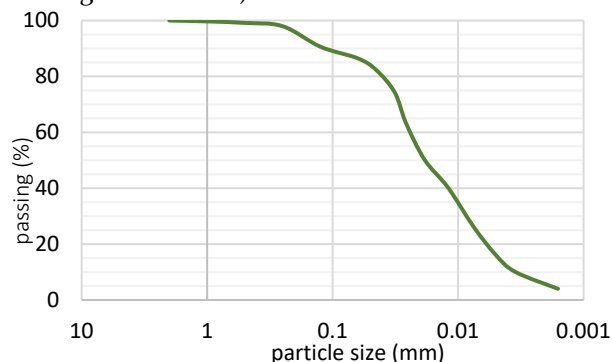


Figure 3 Grain size distribution curve.

The strength and compressibility parameters were obtained through the Uniaxial Compressive Strength (CEN ISO TS 17892-7), Direct shear (MKTC CEN ISO/TS 17892-10), and Oedometer tests (MKTC EN ISO/TS 17892-5), respectively. The coefficient of water permeability (CEN ISO TS 17892:11) is determined for a constant pressure of 0.5 bar for samples saturated with water from top to bottom.

Experimental testing

The physical model was built in a box 0.5m in length 0.5m in height, and 0.1m. For better contact with the soil on the bottom, the model has an adhesive mesh positioned (see fig. 5). Also, drainage holes were used to simulate water flow out when the soil is saturated. The model was placed at an angle representing a slope with an inclination

of 1:1,5. The untreated and biopolymer-treated slopes were subjected to rainfall with an intensity of 10 l/h for 180 minutes. Additionally, untreated and biopolymer-treated slopes with an inclination of 1:2 were planted with vegetation and subjected to rainfall intensity of 12 l/h after 27 days of curing time (Fig. 8).

Results

Laboratory results

In Tab. 1 are presented results of the physical properties of surface layer soil characterized as silty sand (SM).

Table 1. Physical properties of silty sand soil.

Classification tests			Proctor test	
Natural moisture ω [%]	Natural unit weight γ [kN/m ³]	Specific gravity Gs [/]	Optimal moisture ω_{opt} [%]	Max dry unit weight γ_d [kN/m ³]
23.62	18.82	2.67	17.60	15.20

Strength-deformability properties

The representative values of the angle of initial friction and cohesion were calculated as the average value of two series with three samples for untreated and biopolymer-treated soil.

Tab.2 presents the results of strength-deformation parameters, the angle of initial friction, and cohesion, where an improvement ratio of 9.52 % and 7.5 % is registered, respectively. The compressibility modulus has been calculated for 240 kPa load and represents an improvement ratio of 36.64 % compared with the modulus of untreated soil, under saturated conditions.

Table 2 Strength-deformable properties.

Natural soil			Polymer-improved soil		
ϕ [°]	c [kPa]	M_v [kPa]	ϕ [°]	c [kPa]	M_v [kPa]
29.2	25.9	4648	32.3	28.0	2945

The uniaxial compressive strength (UCS) was determined on samples with dimensions of 5.0 cm by 10.0 cm in series on 1, 7, 14, and 28 days. In Fig. 4 the biopolymer-treated sample before and after testing is shown, while in Tab. 2 and Tab.3 the results of untreated and treated samples are presented.

Table 3 Compressive strength parameters of natural samples.

Day of testing	Normal stress σ [kPa]	Deformation ϵ [%]
1	435.3	4.0

Table 4 Compressive strength parameters of treated samples.

Day of testing	Normal stress σ [kPa]	Deformation ϵ [%]
1	257.1	3.5
7	1749.9	2.9
14	1132.4	2.6
28	2000.6	2.9



Figure 4 Compressive strength of treated samples before and after testing, series of 28 days old.

Water permeability

The volume of infiltrated water in the treated sample was 6.71 cm³ /day, which is 6 times higher than the amount of the untreated sample, 1.06 cm³/day. Hence, biopolymer-treated soil has hydrophobic effects on the soil that allow free flow, unlike natural soil where the water is retained. Therefore, the water coefficient was tested where the following values of the coefficient were obtained: for treated soil, the coefficient is 2.20×10^{-6} m/s and for the natural soil is 3.47×10^{-7} m/s.

Experimental results

In the second phase, experimental testing (Fig. 5) of erosion was performed on an inclined slope of treated and untreated soil after 24 hours of needed time for the biopolymer solution to bond with the soil, Fig. 5.

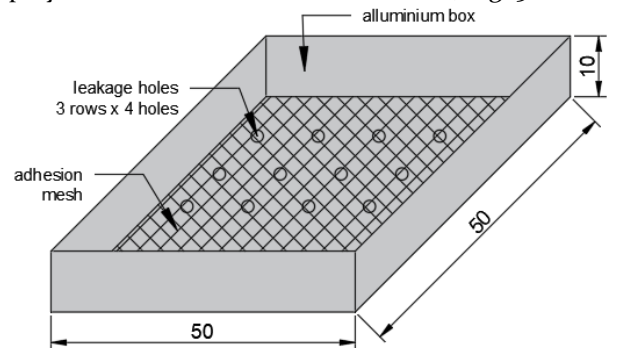


Figure 5 Experimental model

The biopolymer solution was applied by spraying evenly over the surface of the slope. The solution with a high viscosity fills the pores and cavities in the soil while the grains are coated with a bio-film creating a surface crust. The duration of the rainfall was 180 minutes, while every 60 minutes snapshots were made to register the changes on the surface of the slopes. The rainfall was simulated through a system of sprinklers which were installed above the model and connected to the water supply system.

Before the test began, there was no visual difference between the treated and untreated slopes. The interaction between the biopolymer solution, soil, and water creates a specific soil rheology characterized by hydrophilic absorption, and binding of water molecules. In contact with water, the surface crust becomes a hydrophobic surface that allows surface water to flow freely with high

resistance against the erosive forces of water visible in Fig. 5 where practically no erosive changes were observed on the polymer-treated slope in 180 minutes (Nikolovska et al. 2022).

During the test, it was observed how the surface crust absorbs the water, thus becoming a hydrophobic surface, after which the surface water starts to run freely over the surface without causing surface erosion (Nikolovska et al. 2022). After the soil was completely saturated, the water started to drain through the boreholes at the base, and movement paths of the eroded soil were observed on the surface. After 180 minutes, there was muddy water with

fine fractions in the base of the slope, which was not the case with the treated slope. The eroded soil is shown in Fig. 7 with the granulometric content: 69.4% silt, 21.2% sand, and 9.0% clay. In the following series of tests untreated and treated slopes with vegetation grown were tested on 120 minutes of rainfall with an intensity of 12 l/h. During the rainfall, no erosion was observed on the treated slope, hence, the biopolymer-treated slope has a higher stability and resistance to erosive force (Nikolovska et al. 2023). Moreover, the water absorption of the viscous solution proves to have a positive effect on vegetation growth (Fig. 7).

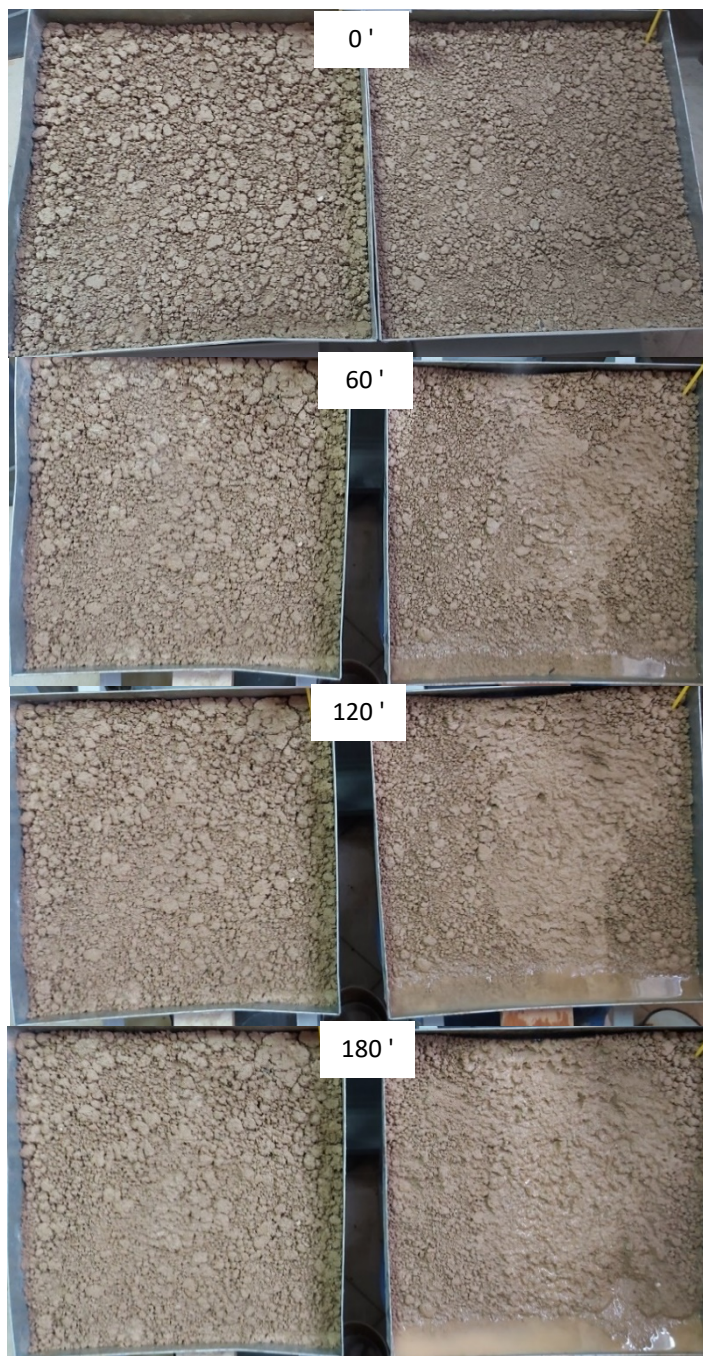


Figure 6 Erosive changes of polymer-improved slope (left side) and natural slope (right side).



Figure 7 Eroded soil in 180 minutes of rainfall for polymer-improved slope (left side) and natural slope (right side).



Figure 8 Erosive changes of slopes with vegetation, polymer-improved slope (left side), and natural slope (right side)

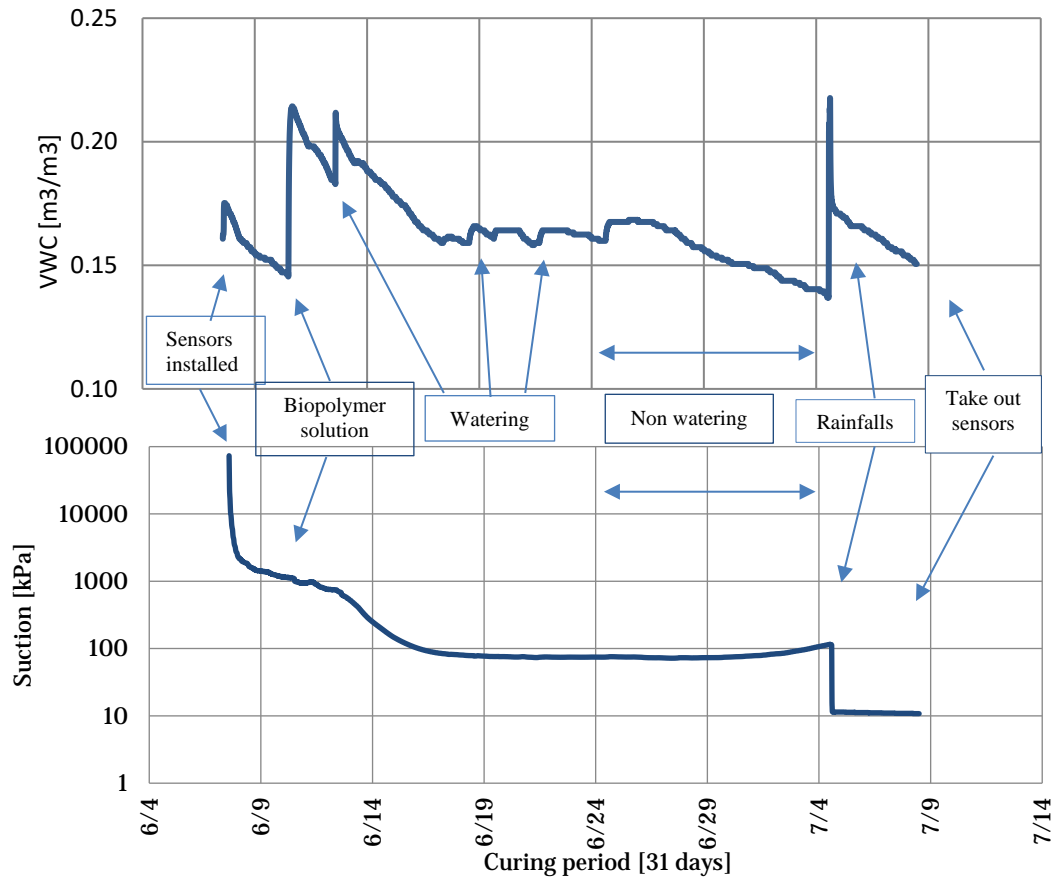


Figure 9 Results of Volumetric water content and suction for silty sand soil

The biopolymer-treated slopes with vegetation were tested after 27 days of curing period. The curing period is a needed time when vegetation roots create a strong connection with the soil and hydrophobic layer. In these slopes, were installed sensors that measured volumetric water content, suction, and temperature. The sensors were taken away after 31 days, were that period all laboratory conditions were registered, such as watering, non-watering, laboratory works, temperature changes, etc. When watering the curve for volumetric soil moisture has an increase. When the rainfall was applied, the value of the volumetric water content from $0.137 \text{ m}^3/\text{m}^3$ increased to $0.218 \text{ m}^3/\text{m}^3$. Inversely of volumetric water content, in the periods when there is non-watering for vegetation, a decrease in suction is registered. When rainfall was applied, the suction value of 110.1 kPa decreased to 11.3 kPa , or a that is decrease of 98.8 kPa .

Conclusions

The use of biopolymers has proven to be an effective measure to improve and stabilize soil material. The surface crust formed by the polymer reduces erosion and restricts the runoff water from infiltrating into the ground, thus providing surface stability to the slopes and promoting the growth of vegetation. The biopolymer as a high viscosity solution fills the pores and clogs the soil particles with biofilms thus creating a 1-2 cm thick surface crust. Thus, layer improves infiltration and creates hydrophobic flow ways which provide greater resistance of erosion. Hence, adhesion between the soil grains reduces the infiltration of water into the soil.

The polymer solution improves the deformation and strength parameters of the soil. The laboratory tests have shown not just an increase in the cohesion of the treated soil, but also in the friction angle and modulus of compressibility. Moreover, the experimental tests treated and untreated material subjected to rainfall had also visibly shown the effects and the efficiency of the biopolymer solution. The use of biopolymers as a naturally based solution for erosion control, has great potential because of represents an efficient, economical, and environmentally sustainable engineering.

References

- Chang I, Jeon M, Cho G-Ch (2015) Application of microbial biopolymers as an alternative construction binder of earth buildings in underdeveloped countries. *International Journal for Polymer Science*, Volume 2015, Article ID 326745, 9p.
- Chen L, Huang Z, Gong J, Fu B, Huang Y (2007) The effect of land cover/vegetation on soil water dynamic in the hilly area of the loess plateau, China. *Journal of Soil Science, Catena*, 70(2):200-208.
- Chun G, Chang I (2018) Cementless soil stabilizer – biopolymer. *The 2018 World Congress on Advances in Civil, Environmental, & Materials Research (ACEM18)*, Incheon, Korea, 29 p.
- Ham S M, Chang I, Noh D H, Kwon T H, Muhunthan B (2018) Improvement of surface erosion resistance of sand by microbial biopolymer solution. *Journal of Geotechnical and Geoenvironmental Engineering*. 144(7): 06018004.
- Ivanov V, Chu J (2008) Applications of microorganisms to geotechnical engineering of bioclogging and biocementation of soil in situ. *Reviews in Environmental Science and Bio/Technology* 7(2):139-153.
- Josifovski J, Nikolovska A, A (2022). Biopolymer soil stabilization as protection from slope erosion and shallow sliding. *EGU General Assembly 2022*, EGU22-4236
- Lentz R D, Sojka R E (1994) Field results using polyacrylamide to manage furrow erosion and infiltration. *Soil science*, Vol, 150, No. 4.
- Nikolovska A, Josifovski J (2023). Experimental and numerical soil stability analysis of biopolymer-treated slope. 2nd International conference of civil engineering ICCE 2023, Tirana Albania.
- Nikolovska A, Josifovski J, Susinov B, Abazi S (2022). Erosion of soil slopes under the influence of atmospheric actions and stabilization with natural polymer solutions. *Second Macedonia Road Congress*.
- Nikolovska A, Josifovski J (2022). Biopolymer stabilization on soil slopes from surface erosion. *Fifth symposium of the Macedonian Association for Geotechnics*.
- Nikolovska A, Josifovski J, Susinov B (2022) Atmospheric effects of soil erosion and slope stabilization with natural polymer solution. *17th International Symposium on Water Management and Hydraulic Engineering*.
- Song Y, Liu L, Yan P, Cao T (2005) A review of soil erodibility in water and wind erosion research. *Journal of Geographical Science*, Vol. 15, 167-176p.
- Soo-Min H, Chang I, Dong-Hwa H, Tae-Hyuk K, Balasingam M (2018) Improvement of surface erosion resistance of sand by microbial biopolymer formation. *Journal of Geotechnical and Geoenvironmental Engineering*, 144 (7)p.

Slope stability back analysis and a proposition for rehabilitation of landslide on the road section Gornji Milanovac – Klatičevo

Dragana Slavković^{(1,2)*}, Milan Kandić⁽¹⁾, Ivan Stefanović⁽¹⁾, Vladimir Filipović⁽¹⁾

1) Institute of Transportation CIP Ltd, 6/IV Nemanjina street, Belgrade, Serbia; email: dragana.slavkovic@sicp.co.rs

2) University of Belgrade, Faculty of Mining and Geology, Department of Geotechnics, Belgrade, Serbia

Abstract: During the construction on the section of the designed road Gornji Milanovac - Klatičevo (Gornji Milanovac Bypass), in the period from November 2022 to April 2023, there was an occurrence of slope instability on the right side of road cut from km 0+910 to km 0+950 i.e., terrain sliding in the form of soil creep. A landslide occurred on the part of the constructed cut slope, which extends over a total length of approximately 125 m. The surface layer of soil affected by sliding (colluvium) is made of silty-sandy clay, soft to medium hard consistency and increased water content. This material was originally created by the decomposition of the basic rock mass (bedrock) and the deposition of material from the higher parts of the slope by planar erosion (diluvium). Bedrock under the diluvium layer consists of the Neogene (Miocene) complex of red sandstones. For the purposes of defining the natural conditions in the terrain under which the terrain sliding process was activated, a slope stability back analysis was performed for the Mohr-Coulomb Failure Criterion and the state of effective stresses. Defining the cause of the soil failure is imposed as the primary goal of paper, considering that during the engineering geological mapping of the terrain in the design phase, no phenomena were observed that would indicate soil instability. In addition, before the activation of the landslide, slope stability analysis with the influence of groundwater in design phase was performed in order to simulate extreme conditions during exploitation and a satisfactory safety factor was obtained. After defining the cause of landslide activation, the paper proposed the use of several remedial measures as well as their mutual combination to completely rehabilitate the landslide.

Keywords: landslide, slope stability back analysis, rehabilitation of landslide.

Introduction

On the section of road under construction Gornji Milanovac-Klatičevo, as a part of bypass around Gornji Milanovac, from km 0+910 to km 0+950 on the right side of the projected road, slope instability, i.e. terrain sliding, occurred. Landslides occurred on the part of the derived slope of the cut, which extends over a total length of about 125 m (from km 0+900 to km 1+025). The process of terrain sliding occurred in the period November 2022 - April 2023.

The width of the landslide was about 40 m, and the length varied from 15 to 35 m (Figure 1). Taking into account the results of engineering geological mapping of the terrain and the results of previously performed research and tests, for the purposes of creating a project for a construction permit, an appropriate geotechnical model of the terrain with the position of the sliding plane was formed.

The surface layer of the soil affected by sliding - colluvium (Ko) is made of dusty-sandy clay, soft to medium hard consistency and increased humidity. This material was originally created by the decomposition of the bedrock mass and the deposition of material from the higher parts of the slope by planar erosion (deluvium). Within these deposits, local weak aquifer with slow drainage due to uneven drainability may occur.

Deluvial deposits (dl) are lithologically represented by dusty and dusty sandy clays, medium hard to hard consistency, low to high plasticity. Within the layer of deluvial clay, the presence of interlayers of sandy gravel was registered. Deluvial deposits are characterized by an intergranular type of porosity and low to medium water permeability. According to the GN-200 classification, these materials can be classified in II-III category.

The main rock mass under the deluvium layer is built by the Neogene (Miocene) complex of red sandstones. It is characterized by great facies diversity. The rock mass is represented by red sandstones and siltstones, with varying degrees of fracturing and alteration. Gradually changing of harder, less degraded zones with zones of a higher degree of alteration is characteristic (Figure 2).

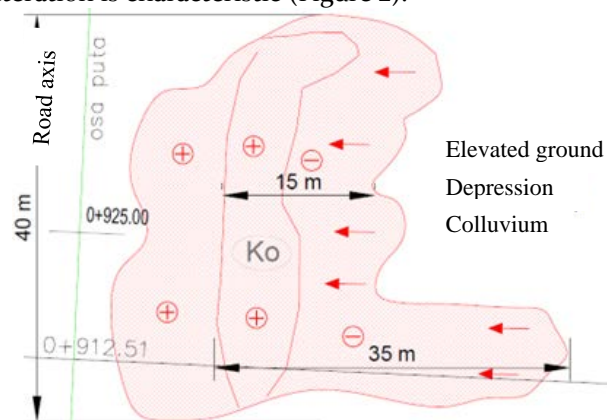


Figure 1. Situational plan of landslide from km 0+910 to km 0+950

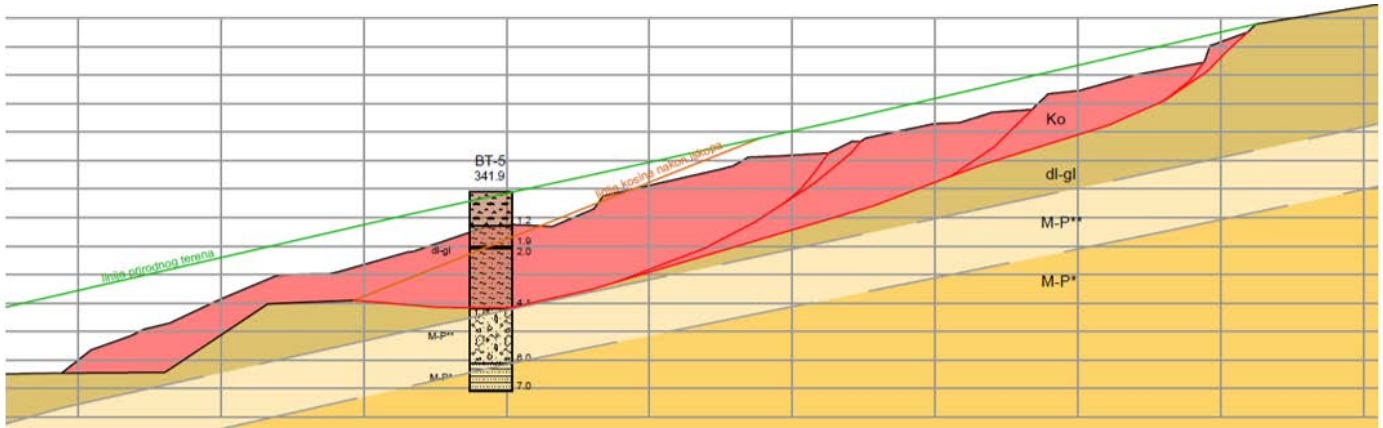


Figure 2. Engineering-geological cross section (km 0+912)

Slope stability back analysis

Slope stability back analysis was done for the Mohr-Coulomb failure criterion and the state of effective stresses, where the value of unit weight $\gamma=19.0 \text{ kN/m}^3$ was adopted. Stability calculations were done in the RocScience’s Slide software (Figure 3).

Since at the moment of activation of the landslide, the terrain is in a state of limit equilibrium, the average values of the mobilized shear strength parameters along

the critical sliding plane were obtained by slope stability back analysis:

- Friction angle (ϕ_m') = 17 °
- Cohesion (c_m') = 4 kPa

The mobilized strength represents the shear stress required to maintain the equilibrium of the sliding body. The parameters obtained by the back analysis are authoritative for the calculation of the effect of forces from the sliding body.

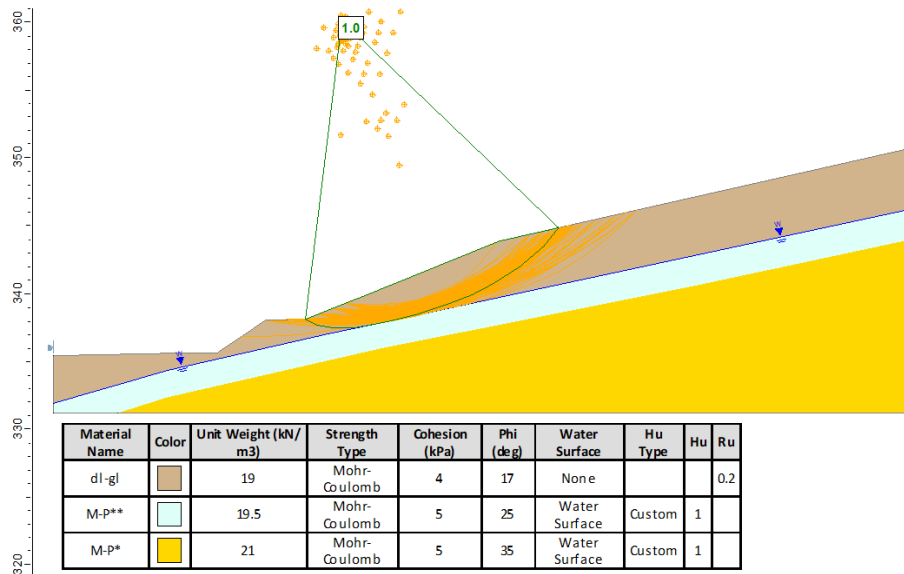


Figure 3. Slope stability back analysis (cross section on km 0+912)

Scope and type of exploration before and after landslide activation

For the purposes of designing the subject slope, in the slope zone detailed geotechnical investigations of the terrain were carried out in August 2019, April and May 2021, which included:

- engineering geological mapping of the terrain,
- exploratory drilling in the slope zone and engineering geological mapping of the borehole core,

- observation of the occurrence and level of underground water in the borehole
- laboratory geomechanical testing of soil samples

The engineering geological mapping of the terrain at the subject location was carried out in August 2019, for the purposes of designing the preliminary project, as well as in the period April - May 2021, for the purposes of developing the project for the construction permit. During the mapping of the terrain, no phenomena were observed that would indicate instability of the soil under natural conditions.

Exploratory drilling was carried out on the subject slope on chainage km 0+910, that is on the part of the constructed slope where the landslide occurred. The depth of the exploratory borehole was 7 m, and the drilling was completed in a layer of solid rock mass. During the execution of the exploratory borehole, engineering geological mapping of the core was carried out, i.e. identification and classification of lithological units.

Observation of the occurrence and level of underground water in the borehole: during the exploratory drilling in borehole in the slope zone was no occurrence of underground water.

Laboratory geomechanical testing of soil samples: One soil sample from the deluvial clay layer (dl-gl), also the layer in which the landslide occurred, was tested from the exploratory borehole drilled at the site in question. The examined sample was taken from a depth of 3.1-3.4 m. A total of 28 soil samples were examined from the layer of deluvial clay in the narrower and wider research area. All these results were used in the analysis and adoption of relevant soil strength parameters. The samples were tested according to valid standards.

Checking of the limit equilibrium of the cut slope was made according to SRPS EN 1997-1, using partial safety factors. Approach 3 was used, according to which partial factors were adopted for soil strength parameters: for the friction angle $\gamma_\phi=1.25$ and for cohesion $\gamma_c=1.25$.

The incline of the slope is designed so that in the lower part of the slope the initial incline is 1:1.5 (33°) up to a height of 3 m, and the incline at a height of over 3 m is 1:2.5 (22°). The slope stability analysis was done with the influence of groundwater in order to simulate extreme conditions during exploitation. The influence of water was introduced into the calculation through the level of underground water in the layer of sandy clay debris (M-P**) and the coefficient $R_u=0.2$ in the layer of deluvial clay (dl-gl). The stability analysis was performed for the section at the chainage km 0+950, where the height of the slope was the highest (10.7 m) and a satisfactory safety factor was obtained ($F_s=1.13$) (Figure 4). The required value of the minimum global safety factor in calculating according to the Eurocode is $F_s>1$.

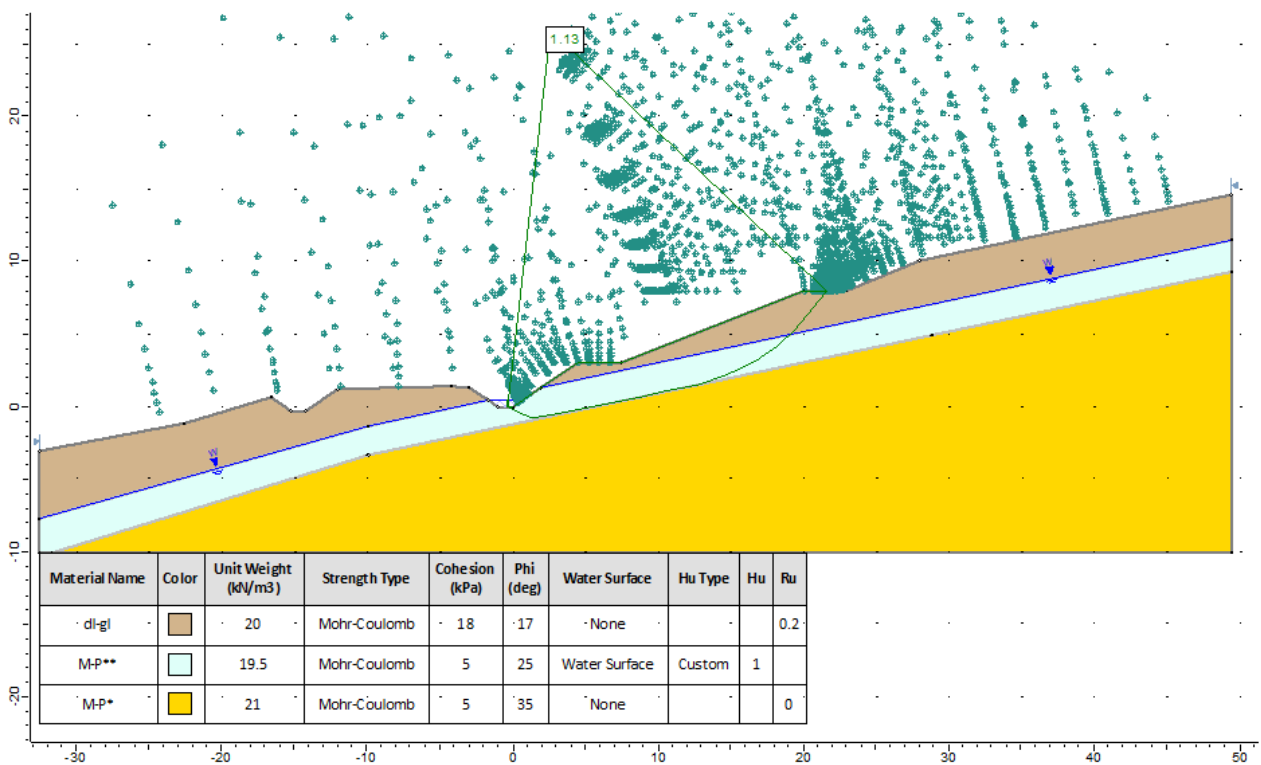


Figure 4. Cut stability analysis on km 0+650 (Geotechnical Report, CIP, 2022.)

In order to define in more detail the construction of the terrain and the geotechnical conditions for the rehabilitation of the unstable slope, in August 2023, additional geotechnical investigations and tests were carried out, which included the following investigations:

- Exploratory drilling and engineering geological mapping of the borehole core,
- Installation of piezometer construction
- Observation of occurrences and levels of underground water in boreholes,
- Laboratory geomechanical testing of soil samples.

Exploratory drilling was carried out on the subject slope from chainage km 0+850 to km 1+035. A total of 6 exploratory boreholes were drilled, 7.0 - 10.0 m deep, total drilling length 57.0 m (Figure 5). During the execution of the exploratory boreholes, engineering geological mapping of the core was carried out, i.e. identification and classification of lithological members (Figure 5).

Installation of a piezometer construction: in order to be able to monitor changes in the groundwater level in the area of the slope in question, a piezometer construction was installed in the exploratory borehole.

Observation of the occurrence and level of underground water in the borehole: during the exploratory drilling in the exploratory boreholes, there was no occurrence of underground water.

Laboratory geomechanical testing of soil samples: 8 soil samples were tested from the exploratory boreholes

carried out at the site in question. Of these, 2 samples from the layer of deluvial clay (dl-gl) - the layer in which the landslide occurred and 6 samples from the sandstone decay zone (M-P**). Identification and classification tests, peak and residual direct shear tests and oedometer compressibility tests were performed on the samples.

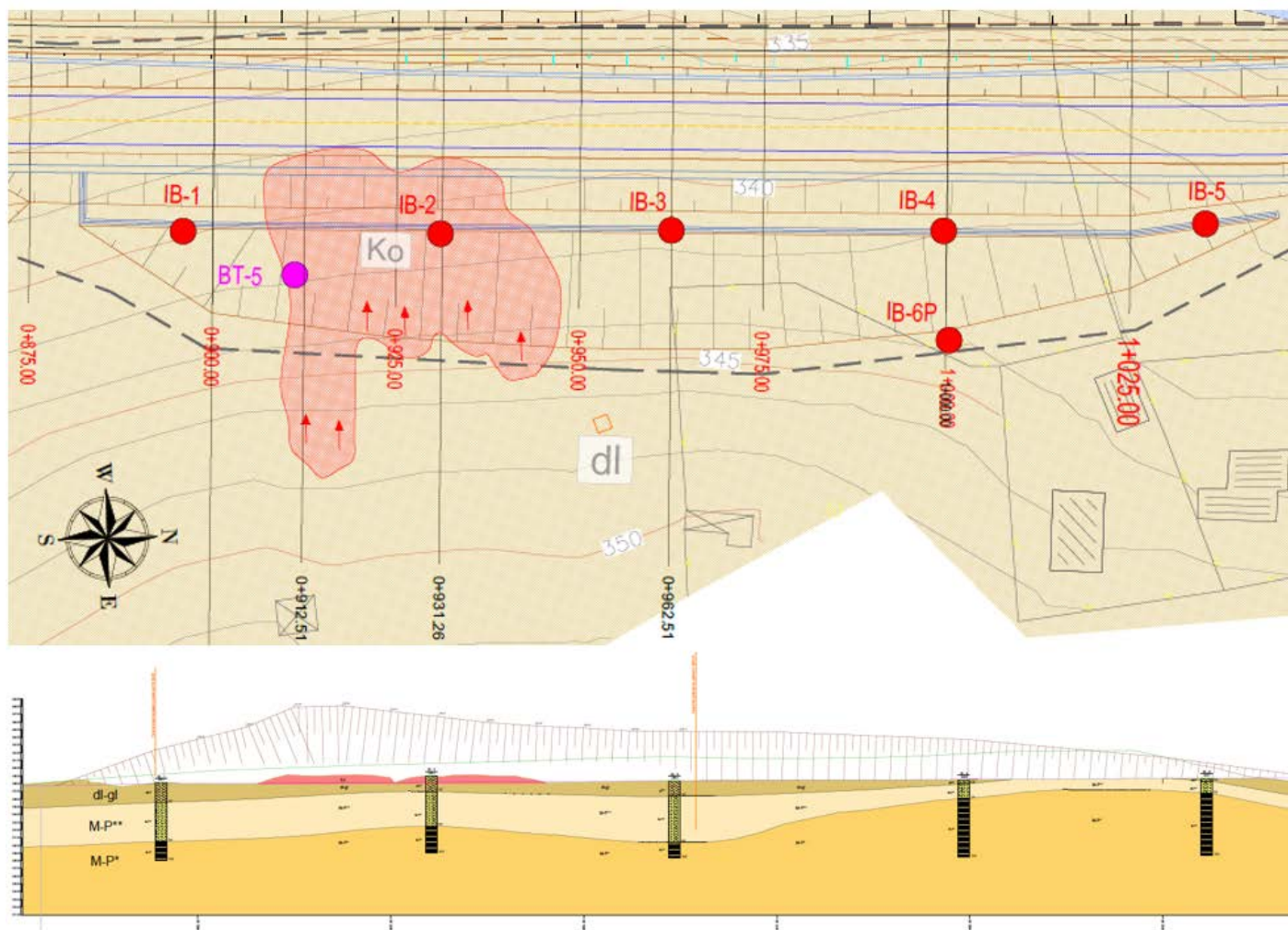


Figure 5. Engineering geological map with position of additional investigation works and an engineering geological section of terrain

Causes of slope instability

The instability of part of the slope occurred in the period november 2022 - april 2023. First, fissures and fractures appeared in the ground, and over time, a landslide occurred that gradually spread. The surface layer of deluvial clay (dl-gl) was affected by sliding to a depth of 1-3 m. The width of the landslide is about 40 m, and the length varies from 15 to 35 m.

After heavy rains in the winter period, there was an increased inflow of water into the soil and the formation of a local aquifer, which is fed by the infiltration of surface and seepage waters from the higher parts of the slope. The influence of this water is one of the causes that led to the instability of the constructed slope. The water affected the soil on the slope in different ways and led to a decrease in its shear strength. Also, a factor that significantly influenced the occurrence of landslides is the

heterogeneity of the material affected by the slide, that is, the presence of sandy-gravelly interlayers in the clayey soil. These interlayers enabled seepage of underground

water from the higher parts of the slope and the formation of compact aquifers in the clay layer, local wetting of the soil and reduction of soil strength parameters.

A set of immediate causes that appeared as a consequence of the action of water, and which, through combined action, led to the instability of the slope are:

- Increase in pore pressure of groundwater: Due to the saturation of the soil with groundwater, there is an increase in pore pressure, a decrease in normal effective stresses and a decrease in the shear strength of the soil. The influence of pore pressure was analyzed during the design process and was included in the slope stability calculation via the groundwater level and the Ru factor (Ru=0.2).

- Sufosis: internal erosion that occurs when water moves through the soil. Water causes fine particles of material to be carried out, which leads to the destruction of the natural structure of the soil and the gradual reduction of its shear strength.

- Influence of surface and atmospheric water: During excavation, there is a reduction of horizontal stresses in the soil. When the terrain is built of hard highly plastic clays, reduced horizontal stresses can cause fissures to appear on the surface of the terrain. If the slope is open for a long time and there is a possibility of infiltration of surface and atmospheric water into the resulting fissures, there is a softening of the soil, a decrease in strength over time and a gradual shear deformation that leads to the progressive collapse of the slope. Touring the field in april 2023 it was observed that surface water was constantly flow in the body of the landslide on the part of the slope that is most affected by the slide around the chainage km 0+912.

- The impact of wastewater discharge: By visiting the field in april 2023, it was determined that the households located in the upper part of the slope, in the immediate vicinity of the landslide, do not have a connection to the city's sewerage network, and that they discharge waste water into septic tanks. Underground discharge of wastewater can contribute to additional wetting of the surrounding soil and decrease its shear strength.

Extreme conditions during stability analysis

During the analysis of the stability of the subject slope in the design process, critical (extreme) conditions that may occur during exploitation were assumed. Although there was no water in the soil during the research, underground water in the soil was assumed during the analyses. The influence of water was introduced into the calculation through the level of underground water in the layer of sandy clayey debris (M-P**) and the coefficient $R_u=0.2$ in the layer of deluvial clay (dl-gl). The adopted soil strength parameters are close to the minimum parameters obtained by laboratory tests. The samples tested in laboratory conditions were previously completely saturated with water during the shear strength test, according to current standards, so the negative influence of water on soil strength parameters is already included.

In order to demonstrate that the occurrence of a landslide (unstable slope) could not be predicted during the design process, we reduced the soil strength parameter to values lower than the minimum obtained by laboratory tests. We also included in the calculation the maximum hydrostatic influence of groundwater in the clay layer. By lowering the strength parameters of the deluvial clay layer (dl-gl) with cohesion values $c=10$ kPa and the friction angle $\phi=17^\circ$, as well as adopting the coefficient $R_u=0.5$, a satisfactory safety factor ($F_s>1$) is obtained (Figure 6).

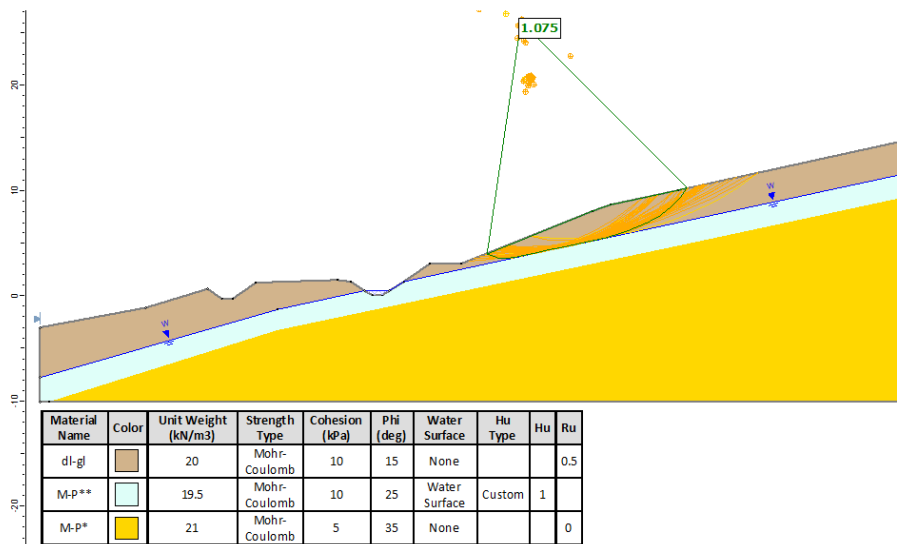


Figure 6. Cut slope analysis of the stability at km 0+950 with reduced soil strength parameters and complete saturation of the deluvial clay layer $R_u=0.5$

The stability analysis with reduced strength parameters shows that the occurrence of landslides could not be predicted because even with the adoption of significantly lower strength parameters than those obtained from laboratory tests (including parameters obtained from additional research), as well as the maximum hydrostatic influence in the deluvial clay layer, satisfactory factor of safety is obtained.

If during the design assumed that the influence of water that appears in the soil during a short period of time will

lower the soil parameters to values close to the residual $c_r=3$ kPa and $\phi_r=12^\circ$ (the values of the strength parameters $c=4$ kPa and $\phi=17^\circ$), most of the slopes that were designed on the route would have to be protected by supporting structures.

The instability occurred in the part of the slope from km 0+910 to km 0+950, with a total length of about 40 m, while the entire slope of the cut is about 125 m long (km 0+900 to km 1+025).

On the route of the Gornji Milanovac-Klatičevo road section, from km 0+000 to km 4+675, about 1200 m of road was designed/constructed in cuts in the same or similar clay materials (dusty clay, degraded marl, sandy marl) that occur on unstable part of the slope. The incline of the slopes are designed with the same inclines so that in the lower part of the slope the initial incline is 1:1.5 (33°) up to a height of 3 m, and the incline above 3 m is 1:2.5 (22°) with berms every 5 m height. The maximum slope height in the cuts is 4.8 - 11.5 m

Geotechnical recommendation for landslide rehabilitation

It is recommended to rehabilitate the unstable slope by creating a support structure in the lower part of the landslide or by replacing the clay material in the part of the unstable slope. It is also recommended to protect the part of the slope that is stable with geogrids in order to prevent the eventual occurrence of instability on that part of the slope as well. The recommended values of geotechnical parameters required for stress-deformation analyzes and stability calculations, when developing a landslide rehabilitation project, are shown in table 1.

Table 1. Recommended geotechnical parameters

Layer mark	Unit weight (kN/m ³)	Cohesion (kPa)	Friction angle (°)	Compressibility modulus (MPa)	Deformation modulus (MPa)
k _o	19.0	3	12	7 - 8	-
dl-gl	19.0	13	17	9 - 11	-
M-P**	19.0	18	25	10 - 14	-
M-P*	21.0	51-64	28-30	-	62 - 85

Conclusion

For the purposes of designing the subject slope, detailed geotechnical investigations of the terrain were carried out, which included: engineering geological mapping of the terrain, exploratory drilling in the slope zone and engineering geological mapping of the borehole core, observation of the occurrence of groundwater in the borehole and laboratory geomechanical testing of soil samples.

The slope stability analysis during design was done with soil strength parameters that are close to the minimum parameters obtained by laboratory tests and with the influence of groundwater, in order to simulate extreme conditions during exploitation. The stability analysis was performed for the section at the chainage km 0+950 (the highest part of the slope) and a satisfactory safety factor was obtained ($F_s=1.13$).

The water affected the soil on the slope in different ways and led to a decrease in its shear strength. Also, a factor that significantly influenced the occurrence of landslides is the heterogeneity of the material affected by the slide, that is, the presence of sandy-gravelly interlayers in the clayey soil. These interlayers enabled seepage of underground water from the higher parts of the slope and

the formation of compact aquifer in the clay layer, local wetting of the soil and reduction of soil strength parameters.

In order to define in more detail the construction of the terrain and the geotechnical conditions for the rehabilitation of the unstable slope, additional geotechnical investigations were carried out in August 2023. Additional geotechnical investigations yielded very similar geotechnical parameters of the soil layers to those used in slope design. There was no underground water in the ground during the investigation.

The subsequent stability analysis with reduced strength parameters shows that the occurrence of landslides could not be predicted because even with the adoption of significantly lower strength parameters than those obtained from laboratory tests (including parameters obtained from additional research), as well as the maximum hydrostatic influence in the deluvial clay layer, satisfactory factor of safety is obtained.

The conditions that led to the instability of the slope are of a local nature and could not be foreseen during the design, which can be seen from the fact that the instability occurred in a part of the slope with a length of about 40 m, while the entire slope of the cut is about 125 m long. Also, on the route of the Gornji Milanovac-Klatičevo road section, about 1200 m of the road was designed / constructed in cuts in the same or similar clay materials that occur on the unstable part of the slope.

On the basis of everything previously stated, it can be concluded that the design of the subject slope is in accordance with all relevant standards and rules of the profession and that the occurrence of instability could not be predicted, i.e. that the occurrence of landslides occurred due to unforeseen underground conditions that occurred locally in the part of the designed slopes.

References

- Kandić M. (2020) Report of geotechnical conditions of municipal road construction Gornji Milanovac - Klatičevo (Gornji Milanovac Bypass); Municipality of Gornji Milanovac: cadastral municipality of Gornji Milanovac, cadastral municipality of Velereč, cadastral municipality of Klatičevo (preliminary project). Institute of Transportation CIP Ltd. Belgrade, Serbia
- Kandić M. (2022) Report of geotechnical conditions of municipal road construction Gornji Milanovac - Klatičevo (Gornji Milanovac Bypass); Municipality of Gornji Milanovac: cadastral municipality of Gornji Milanovac, cadastral municipality of Velereč, cadastral municipality of Klatičevo (project for a construction permit). Institute of Transportation CIP Ltd. Belgrade, Serbia
- Kandić M. (2023) Geotechnical report with the suggestion of remedial measures unstable slopes from km 0+910 to km 0+950. Institute of Transportation CIP Ltd. Belgrade, Serbia

Addressing Rockfall Challenges in flysch environment - A case study from Greece

Themistoklis Chatzitheodosiou^{(1)*}, Ioannis Farmakis⁽²⁾, George Prountzopoulos⁽³⁾, George Stoumpos⁽¹⁾, Dimitra Papouli⁽¹⁾, Thomas Thomaidis⁽¹⁾, Vassilis Marinos⁽¹⁾

1) National Technical University of Athens, School of Civil Engineering, Geotechnical Division, Athens, Greece, (chatzitheodosiou@mail.ntua.gr)

2) University of Newcastle, School of Engineering, Newcastle, Australia

3) Independent Geotechnical Engineering Consultant, Athens, Greece

Abstract Rockfalls pose a significant hazard in mountainous regions, affecting infrastructure, obstructing roads, and posing a risk to human life. This hazard is particularly high in flysch environments, marked by a heterogeneous composition of rock formations of varying strengths, prone to erosion that compromises the stability of slopes. This paper examines an engineering geological investigation addressing rockfall hazards on a mountainous provincial road in central Greece. Utilizing traditional in-situ geological studies and remote sensing technologies, primarily Structure-from-Motion (SfM) photogrammetry and also Light Detection and Ranging technology (LiDAR), the research team has identified the engineering geological factors influencing rockfall incidents, delineated hazardous zones, and predicted possible rockfall paths through physically-based modeling. SfM photogrammetry monitoring and change detection analysis revealed detachments, while trajectory analysis, updated by volumetric measurements, highlighted areas of significant danger. Our workflow contributes to understanding the instability mechanisms and directly support engineers in designing strategies to mitigate rockfall hazards, thereby increasing safety on this crucial transport route. This study demonstrates the power of combining geospatial technologies with engineering geological expertise to enhance public safety along transportation routes in mountainous regions prone to rockfalls.

Keywords flysch rock masses, SfM photogrammetry, TLS LiDAR mapping, rockfall monitoring, rockfall modeling.

Introduction

Rockfalls pose a critical hazard to transportation networks and public safety in mountainous regions, particularly where human development intersects with natural landscapes. These hazards are pronounced in flysch environments, where unique geomorphological conditions and the heterogeneity of flysch formations—comprising low-strength materials and structures affected by tectonic activity—increase the risk of slope failures (Marinos, 2019).

Building on the foundation of traditional engineering geological survey methods, the integration of remote sensing technologies, such as Structure-from-Motion (SfM) photogrammetry (Westoby et al., 2012) and TLS LiDAR, has revolutionized rockfall assessment and monitoring by providing high-resolution spatial data. This data enables the detailed analysis of complex topographies, deformation detection, and the precise estimation of rockfall events, including their precursors (Abellan et al., 2014; Kromer et al., 2019). The integration of these technologies with surface reconstruction algorithms allows for the automated addition of critical rockfall features to digital databases, enhancing our understanding of rockfall dynamics (DiFrancesco et al., 2021). Detailed 3D surface models generated from remote sensing technologies provide crucial inputs for numerical simulations. These simulations accurately depict rock face geometry, enabling physically-based modeling of the entire rockfall process – initiation, propagation, and deposition. Factors like trajectory energy, velocity, and potential reach are considered. However, identifying rockfall sources and obtaining accurate geotechnical parameters remains a challenge for creating realistic, high-resolution models. As demonstrated by Farmakis et al. (2023), data-driven models offer significant potential for improved rockfall susceptibility assessment, advancing our ability to predict and manage these hazards. Within this context, the presented case in the Valaora-Stavros village region in central Greece, demonstrates an integrated approach to addressing and mitigating rockfall hazards. This study, focused along a critical provincial mountainous route in a flysch environment, integrates SfM photogrammetry, Terrestrial Laser Scanning (TLS), and advanced digital tools for several key advancements.

High-resolution topographic data and engineering geological mapping are used to identify rockfall source areas, characterize failure mechanisms, and quantify rockfall volumes. Physically-based trajectory modeling, calibrated with monitoring data, pinpoints high-hazard zones and provides essential insights into rockfall dynamics. The integration of engineering geological and geomorphological analyses, alongside precise modeling, enables the development of targeted mitigation strategies

specifically tailored to the constraints and failure modes of the Valaora flysch terrain. This multi-faceted approach enhances rockfall hazard analysis. It accounts for spatial limitations and complex failure mechanisms, typical in mountainous flysch environments, ensuring that mitigation measures are strategically designed for maximum effectiveness.

Study Area Overview

The Valaora region, situated in the western part of the Evritania prefecture near Greece's artificially created Kremaston Lake, is characterized by its steep and precipitous slopes (Fig. 1,2). Recognized as one of the most susceptible areas to landslides in Greece, the mountainous terrain of Evritania necessitates a thorough engineering geotechnical analysis to secure infrastructure and public safety in this high-hazard zone (Marinos et al., 2015).

Predominantly composed of Gavrovos flysch, the geologic structure of the Valaora region features a sequence of sandstone, clay, siltstone layers, and an underlying limestone base. The complexity of this stratification plays a crucial role in defining the area's stability, influencing erosion patterns and the effectiveness of any mitigation strategies implemented.

Stability challenges in the area are significant, with rockfalls posing a severe threat to the adjacent provincial road. Medium to large boulders ranging from approximately 5 to 10 m³, often detach from the upper slopes, posing hazards due to the lack of protective infrastructure. Erosion and shallow slides, especially towards the area's northeastern parts, further contribute to the instability, undermining the surface layer and leading to potential road safety threats. Moreover, rockfalls occurring directly above the road (Fig. 3), amplify these dangers, compounded by the slope's steepness and the lack of catchment barriers.

The mechanisms behind rockfall failures, are intricately linked to their geological makeup, especially the presence of sandstone masses overlying weaker siltstones at various elevations. Erosion's role in undercutting the sandstone, along with the creation or

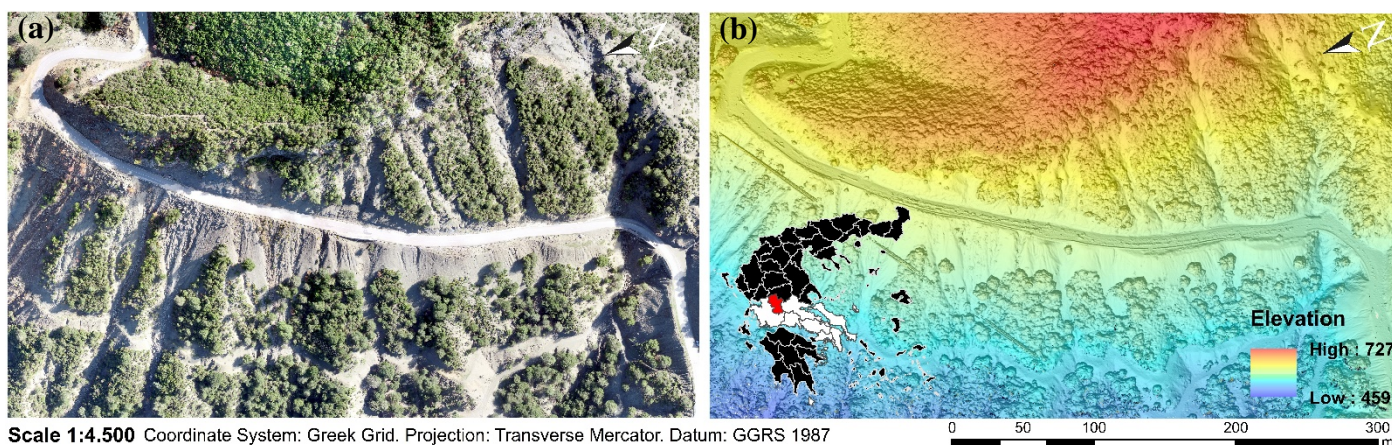
expansion of tensile cracks within these layers, greatly accelerates the failure process. This issue becomes even more critical when water applies hydrostatic pressure within the rock's open discontinuities.



Figure 2 Aerial view of the Valaora region illustrating steep terrain where rockfalls threaten the road and public safety. Visible scars across the landscape mark recent rockfall events, underlining the need for continuous monitoring and mitigation. The potential trajectories of rockfalls from the upper sections of the slope, through thalwegs, to the road level are of particular concern.



Figure 3 Significant rockfalls involving sandstone at the slope NE edge, directly above the provincial road. This activity is intensified by the undercutting of sandstone caused by the differential erosion of siltstone beneath it.



Scale 1:4.500 Coordinate System: Greek Grid. Projection: Transverse Mercator. Datum: GGRS 1987

Figure 1 The Valaora study site in Evritania, Greece, featuring: (a) an orthomosaic and (b) a Digital Surface Model (DSM) (Surveyed on 15 September 2021) [For an interactive exploration and visual representation visit the latest digital twin (Chatzitheodosiou, 2023)].

Materials and Methods

Engineering geological Investigation

This study commenced with detailed in-situ engineering geological mapping, including identification of tectonic structures to gain insights into the overall stability of the rock masses and identify potential sources of failure. Field investigations were followed by the classification of flysch formations into four distinct types based on sandstone-siltstone composition and tectonic disturbances, employing a modified Geological Strength Index (GSI) for heterogeneous rock masses like flysch (Marinos, 2019). Subsequent laboratory tests, including Point Load Tests (PLT), Brazilian tests, and direct shear tests on discontinuities, were conducted to determine key physical and mechanical properties of the intact rock, rock mass and joint strength.

While these initiatives significantly advanced comprehension of the geological context and mechanical properties of the study area, the complex nature of rockfall hazards demands a more in-depth analysis. Addressing these complexities requires an understanding of source areas, as well as estimations of potential volumes, magnitudes, and trajectories of rockfall events. This necessitated a shift towards the collection of high-resolution topographic data and the creation of advanced digital tools for a more detailed and accurate analysis of rockfall hazards.

High Resolution Topographic Data Acquisition

Following the groundwork established through initial engineering geological surveys, this investigation utilized Unmanned Aerial Vehicles (UAVs), notably a DJI Phantom 4 RTK and a DJI Mavic 3 Enterprise, to capture the dynamic landscape of the area under study. These UAVs, armed with high-definition cameras, undertook multiple flights to perform aerial photogrammetry. Coupled with an RTK base station, this approach ensured centimetre-level accuracy in the reconstruction of the terrain through SfM, facilitating the creation of detailed point clouds DSMs, and orthomosaics (Fig.1).

To enhance the detail on rock outcrops, especially in areas susceptible to structurally controlled failures, TLS LiDAR was implemented. The accuracy of LiDAR, which measures distances using light beams, yielded point cloud datasets with millimetre-level precision. This detailed topographic data offered a detailed perspective of the terrain's features and structures, crucial for identifying potential slope failure mechanisms.

Digital Tools Development

Utilizing the Leica ScanStation P40 TLS LiDAR system, precise orientation measurements and geometric characteristics (spacing, persistence) of discontinuity surfaces were captured for detailed kinematic analyses. This system's long-range capability (up to 270m), high-speed scanning (1 million points per second), and low noise ensured the acquisition of detailed 3D data essential

for rock mass structural analysis. Joint surfaces were extracted by locally applying Principal Component Analysis (PCA) on the XYZ space of the 3D points and subsequently forming individual clusters through Density-Based Spatial Clustering (DBSCAN) (Farmakis et al., 2020) (Fig.4).

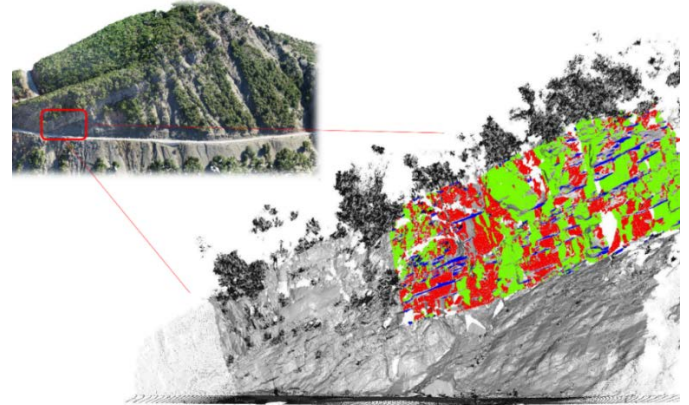


Figure 4 Digital Analysis of Discontinuity Sets in structurally controlled sandstone. Featured is a slope segment assessed using TLS LiDAR digital data for accurate orientation measurements of discontinuities. Geological compass data at the base of the slope, served for cross-verification of the digital analysis.

Concurrently, the generation of Digital Depth Maps from UAV and LiDAR datasets provided a granular visualization of the terrain's surface variations, highlighting both potential rockfall sources and areas of instability indicated by undercuts (Fig.5).

Further advancing the project's capabilities, development efforts focused on creating computer vision solutions for the semantic segmentation of three-dimensional data. This approach aims to accurately categorize key terrain features such as vegetation, bedrock, and human infrastructure, within the point cloud data (Fig. 6).

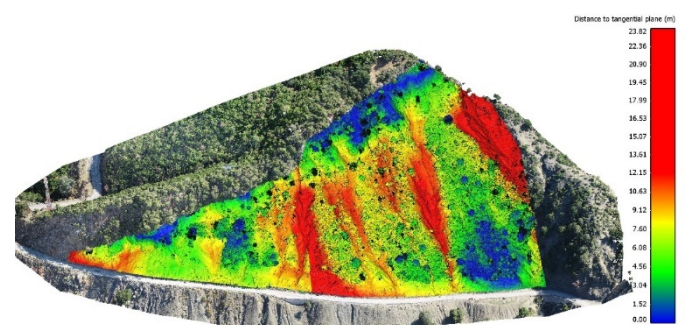


Figure 5 Depth map of the slope. This digital depth map renders the slope's surface against a reference plane, with a blue-to-red scale indicating distance from the reference. Overhangs and undercuts are clearly marked in blue and red, respectively.

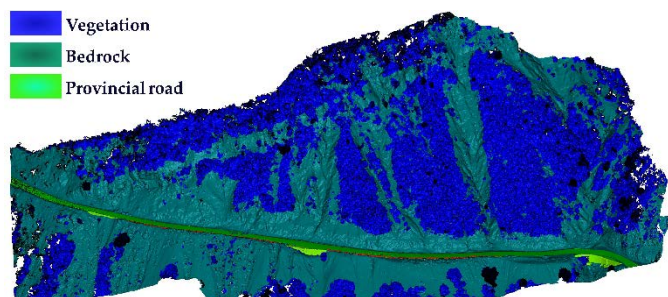


Figure 6 Point cloud after semantic segmentation, divided into three primary categories: ground, vegetation, provincial road.

Point cloud analyses were conducted primarily using Python programming mainly based on the Open3D library. Additionally, open-source software such as CloudCompare was employed for visualization and basic measurements.

Rockfall Monitoring – Rockfall Database

Throughout the study, SfM photogrammetry monitoring played a pivotal role, providing time-series data on terrain evolution in the Valaora region. Employing high-resolution UAV imagery to systematically generate precise point clouds, this approach facilitated the detection and analysis of geomorphological changes over time.

The deployment of the Multiscale Model to Model Cloud Comparison (M₃C₂) algorithm (Lague et al., 2013) stood out by enabling accurate identification and quantification of alterations such as rockfalls and slope deformations (Fig. 7). By methodically comparing sequential point cloud datasets, the research team was able to detect instability zones and track the dynamic changes within the landscape.

This ongoing monitoring effort, essential for revising and refining assessments, continues to inform our understanding of landslide behaviour and hazards within the region. Further depth in analysis was facilitated by the adaptation of the DBSCAN algorithm (Ester et al., 1996) clustering spatial changes. Also, the Iterative Alpha Shape algorithm, as suggested by DiFrancesco et al. (2021), was used for volumetric calculations of these changes.

Volumetric measurements were also conducted on the blocks that had fallen onto the slope's face and the roadway, including overhanging blocks and grooves formed from detachments on the slope. A digital rockfall database was then developed, cataloguing attributes of each rockfall incident, including its location, volume, shape, and the timing of occurrence.

Physically-based Model - Trajectory Analysis

The final phase of this research involved the creation and application of a physically-based model to simulate rockfall trajectories. The 3D surface model created using UAV photogrammetry significantly benefited from implementing semantic segmentation. This technique enhanced the terrain representation by accurately removing vegetation and filling in data gaps across two distinct steps.

The model's accuracy in predicting rockfall trajectories in the Valaora area was ensured through careful calibration using two years of monitoring data and change detection techniques. This calibration process utilized in-depth knowledge of the starting points, end zones, mechanisms of failure, and volume of rockfalls, which was gathered from both monitoring and geological engineering evaluations. This allowed for the precise adjustment of the model's restitution coefficients for both normal and tangential impacts on slope materials, vital for replicating actual conditions.

By integrating volumetric information into the simulations, the model could make detailed forecasts about the movement of rockfalls, including impact energy calculations, marking areas at high hazard.

Key Findings

An engineering-geological map was created, categorizing rock masses into four types (Fig. 9). The primary source of rockfalls was identified in moderately disturbed sandstones with thin layers of siltstones, classified based on GSI (Marinos, 2019) as **Type III**.

In the northern section of the study area, Flysch Type III is positioned at a modest elevation above the road, reaching a maximum of 25 m above a highly disturbed-folded rock mass (Fig.8). This underlying mass, not significantly deformed or sheared, consists of siltstone with layers of sandstone (**Type VIII**). Moving southward, the Type III Flysch formation is found at a higher altitude, above moderately disturbed siltstone with thin layers of sandstones (**Type VI**), and in the southern part, it reaches a maximum height of 90 m above a highly disturbed-folded rock mass (Fig.2). This mass retains its structure and is made up of alternating siltstones and sandstones (**Type VII**).

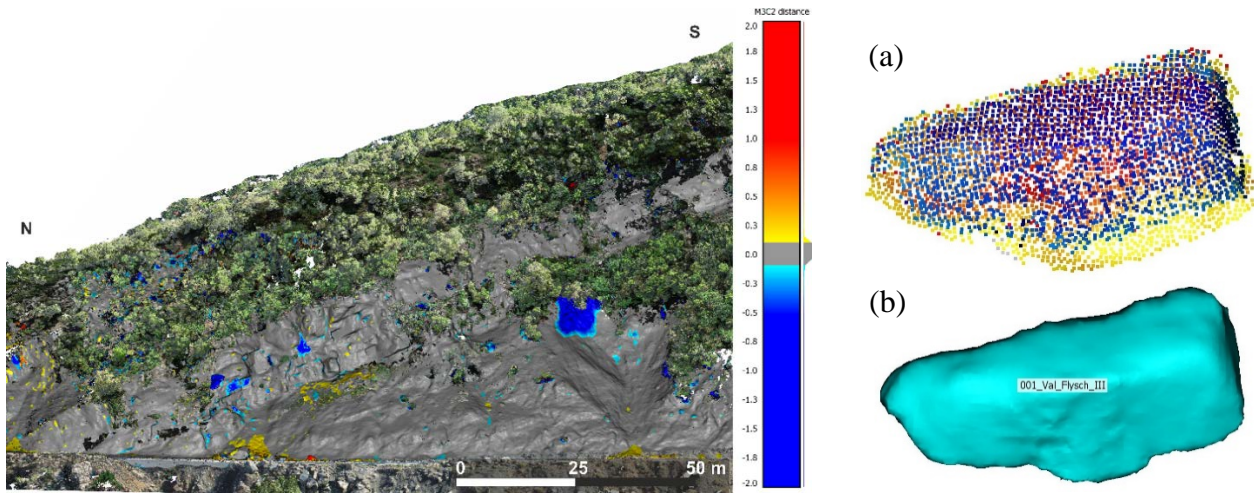


Figure 7 Left: M₃C₂ change detection output, depicting negative (loss) and positive (gain) changes presented by cooler and warmer colours, respectively. Right: An example of a rockfall detection presented: (a) as a point cloud and (b) as a 3D surface model.

The potential trajectories of rockfalls from the Flysch Type III either land directly on the roadway in the northern section or in the southern section travel through thalwegs from the higher parts to the road level.



Figure 8 The northern section of the slope clearly reveals the origin of rockfalls in Type III flysch above Type VIII. The failure mechanism is evident, characterized by the undercutting of the sandstone as a result of the differential erosion of the underlying siltstone. a) the main rockfall source with 13 m³ volume, measured by digital reconstruction of the detachment geometry, and b) a 6.5 m³ block from this detachment, located on the slope side.

Assessing this rockfalls, RocFall₃ software of Rocscience Inc., was used to complement a trajectory analysis. Its methods for calculating runout distances (Runout Total – 3D, Runout XY – 2D, Runout Z – vertical) and algorithms for impact and sliding dynamics matched the physical principles of the developed model well.

The calibration of the model and the accurate calculation of restitution coefficients involved determining the initial positions of rockfall events using change detection data. Initial velocities for detachments were assumed, and a back trajectory analysis for deposit sources was conducted, utilizing change detection and reports from local authorities. After determining the restitution coefficients, simulations of trajectories were

conducted. These simulations were followed by a statistical evaluation of the outcomes, focusing on the final impact spots and energy.

Results highlighted significant concerns regarding vertical trajectories towards road infrastructure in the northern sector dominated by Type III flysch (Fig. 10,11). Peak kinetic energies at the road level were estimated to be between 6200-6500 kJ, for rockfall volumes of approximately 13 m³, originating from a detachment height of around 20-30 m. However, the potential rock fragmentation during descent indicates that actual impact energies could be lower.

The southern sector appeared safer, with most trajectories ending in thalwegs and fewer reaching roads having lower bounce heights and speeds. The safety of this area was enhanced by the higher elevation of Type III flysch, requiring rockfalls to cover a larger distance before reaching the roadway, thus reducing their energy and hazard potential. Trajectory analyses for wedge-type slides in siltstone (Types VII and VIII) were excluded due to their tendency for immediate disintegration upon detachment.

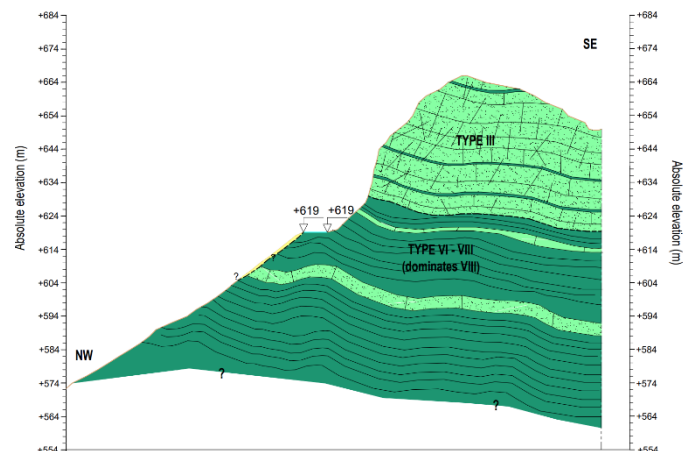


Figure 10 Engineering Geological Section: This section is illustrated in red on the engineering geological map (Fig.9).

Mitigation Strategies

Upon identifying failure mechanisms and rockfalls trajectories along the road's slopes, the study area was divided into two distinct regions (Fig. 9), spanning a total of 435 m. These sections necessitated different mitigation

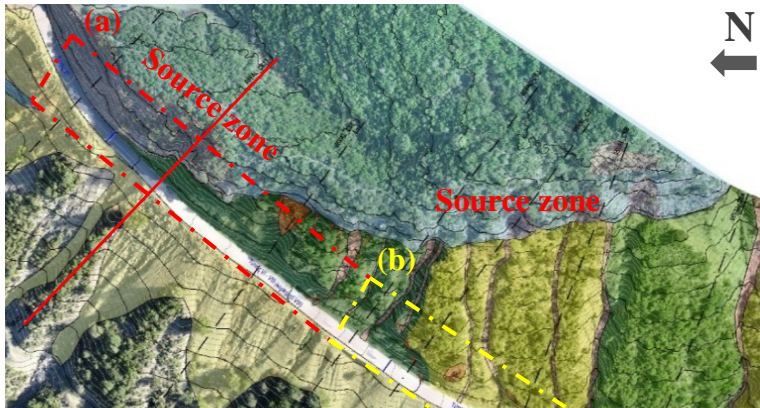


Figure 9 Engineering-geological map of the study area showing: (a) the high-risk northern area and (b) the safer southern area.

The southern section, characterized by rockfall sources at higher altitudes and increased slope height, exhibited a more favourable setting. In this section, most rockfalls end up in talwegs, with a reduced probability of affecting the road and presenting lower impact energies.

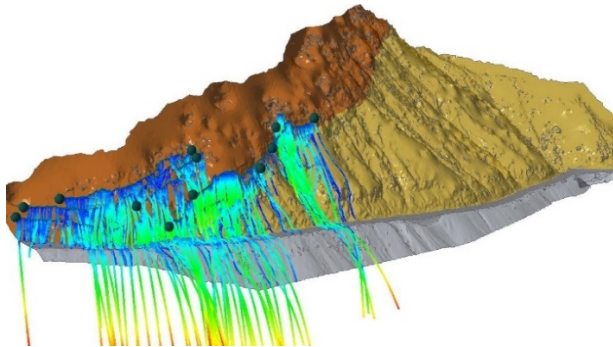


Figure 11 Trajectory analysis on the northern slope reveals high-hazard areas due to significant impact energies. Rockfalls originating from Type III flysch, marked in orange, display steep trajectories toward road infrastructure, with some impacts on Type VIII flysch, shown in yellow.

To address these hazards, a combination of active and passive stabilization methods was proposed. In the northern section, applying bolting techniques to sandstone benches in the upper sections of the slope above the road was limited due to accessibility challenges. Similarly, the implementation of passive measures, like barriers, was constrained by the lack of available space at the base of the slopes.

In light of these limitations, a reinforced concrete protective road shelter was the central proposed solution, featuring an internal width of 9m to accommodate traffic lanes, barriers, and sidewalks, adhering to road-cross-section standards. The shelter's design included a minimum free height of 5m which is supported by piles for stability (Fig. 12).

strategies due to limitations regarding the applicability of various technical solutions. The northern section faced significant large-scale rockfall issues (Fig. 11), with sandstone rock masses exhibiting a layered structure and minimal fragmentation.

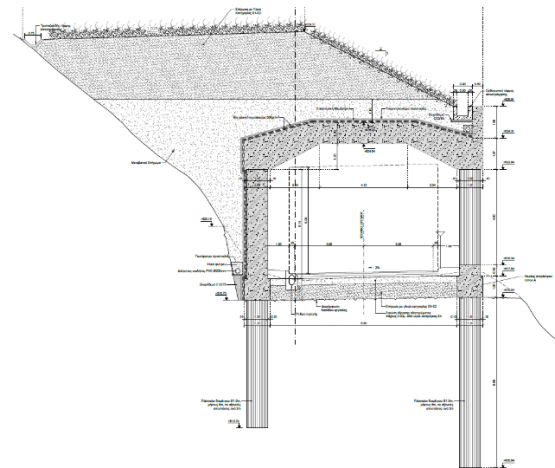
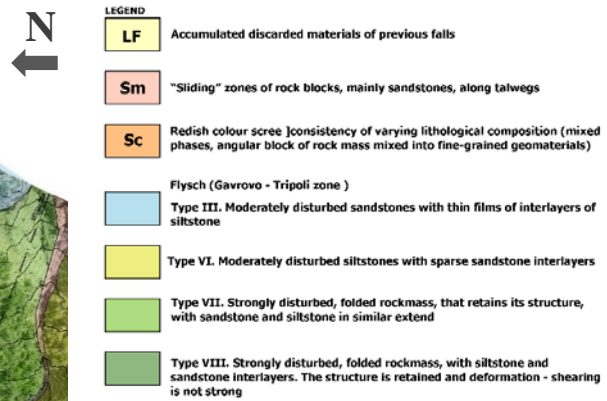


Figure 12 Typical cross-section of the proposed concrete road shelter in the northern part of the slope (Fig.9 a).

The decision for the selection of the shelter as the best technical solution, although costly for the category of the specific road, was based on certain particularities. These mainly concerned environmental restrictions for the excavation of high open cuts and the disposal of excavated materials in the nearby area. Additionally, technical solutions consisting of rock fall barriers were not preferable to the Client, due to its practical inability to properly maintain the barriers after a rockfall.

Conclusions

This engineering geological study of rockfall hazards along a provincial road in Valaora, Evritania, Greece, highlights the challenges of geotechnical characterization and mitigation in flysch terrains. The inherent heterogeneity and structural disturbances of flysch formations require advanced techniques to understand failure mechanisms and develop effective countermeasures.

The study combined traditional engineering geological mapping with remote sensing technologies (SfM photogrammetry, TLS LiDAR) along with innovative digital workflows, leading to significant advancements. High-resolution 3D models were instrumental in identifying rockfall sources and analysing structurally controlled failures. Insights from SfM monitoring and change detection algorithms enhanced the understanding of rockfall dynamics, enabling precise identification of detachment locations and a deeper comprehension of behaviour. Monitoring outputs and volumetric measurements supported the calibration of physically-based trajectory modeling, which accurately depicted potential rockfall paths and impact energies, identifying high-hazard zones.

The engineering geological and geomorphological insights, along with the modeling outputs, informed the development of targeted mitigation strategies for the complex flysch failure modes.

References

- Abellan, A.; Oppikofer, T.; Jaboyedoff, M.; Rosser, N.J.; Lim, M.; Lato, M.J. (2014) Terrestrial laser scanning of rock slope instabilities. *Earth Surf. Process. Landf.* 39, 80–97.
- Chatzitheodosiou, T. (2023). "One rock at a time" 3D Geology Mini Series. Available at: <https://sketchfab.com/themisto123> [Last accessed: 02/2024].
- DiFrancesco, P.M.; Bonneau, D.A.; Hutchinson, D.J. (2021) Computational geometry-based surface reconstruction for volume estimation: a case study on magnitude-frequency relations for a LiDAR-derived rockfall inventory. *ISPRS Int. J. Geo-Inf.* 10.
- Ester, M.; Kriegel, H.P.; Sander, J.; Xu, X. (1996). A density-based algorithm for discovering clusters in large spatial databases with noise. In *Proceedings of the KDD-96 Proceedings*, Portland, Oregon, 2–4 August.
- Farmakis, I.; Hutchinson, D.J.; Vlachopoulos, N.; Westoby, M.; Lim, M. (2023). Slope-scale rockfall susceptibility modeling as a 3D computer vision problem. *Remote Sensing*. 15(11): 2712.
- Farmakis, I.; Marinos, V.; Papathanassiou, G.; Karantanellis, E. (2020). Automated 3D Jointed Rock Mass Structural Analysis and Characterization Using LiDAR Terrestrial Laser Scanner for Rockfall Susceptibility Assessment: Perissa Area Case (Santorini). *Geotech. Geol. Eng.* 38, 3007–3024.
- Kromer, R.; Walton, G.; Gray, B.; Lato, M.; Group, R. (2019). Development and optimization of an automated fixed-location time lapse photogrammetric rock slope monitoring system. *Remote Sens.* 11.
- Lague, D.; Brodu, N.; Leroux, J. (2013). Accurate 3D Comparison of Complex Topography with Terrestrial Laser Scanner: Application to the Rangitikei Canyon (N-Z). *ISPRS J. Photogramm. Remote Sens.* 82, 10–26.
- Marinos, V.; Papathanassiou, G.; Vougiouka, E.; Karantanellis, E. (2015). Towards the Evaluation of Landslide Hazard in the Mountainous Area of Evritania, Central Greece. In: *Engineering Geology for Society and Territory*, Lollino et al. (eds.), Published by Springer – Volume 2, pp. 989-993,
- Marinos, V. (2019). A revised, geotechnical classification GSI system for tectonically disturbed heterogeneous rock masses, such as flysch. *Bulletin of Engineering Geology and the Environment*, 78(2), 899–912.
- Westoby, M.J.; Brasington, J.; Glasser, N.F.; Hambrey, M.J.; Reynolds, J.M. (2012). "Structure-from-Motion" Photogrammetry: A Low-Cost, Effective Tool for Geoscience Applications. *Geomorphology* 179, 300–314.

Geotechnical Conditions, Stability Analysis and Remedial Measures of Višnjička 74 Landslide in Belgrade

Uroš Đurić ^{(1)*}, Sanja Jocković ⁽¹⁾, Miloš S. Marjanović ⁽¹⁾, Veljko Pujević ⁽¹⁾, Ksenija Micić ⁽¹⁾, Zoran Radić ⁽¹⁾, Milena Raković ⁽¹⁾

1) University of Belgrade, Faculty of Civil Engineering, Bulevar kralja Aleksandra 73, Belgrade, udjuric@grf.bg.ac.rs

Abstract This paper presents the results of geotechnical investigations, stability analysis and urgent remedial measures of the landslide at Višnjička 74 street in Belgrade. The area under study is located at the foot of an old fossil landslide. The landslide was activated due to excavation of the foundation pit in June 2023. Due to large displacements of the retaining structures and the surrounding objects, urgent remedial measures were proposed. Following these measures, further sliding was prevented. Additional geotechnical investigations were performed (geophysical investigations, inclinometer measurements, boreholes, soil sampling, laboratory tests, piezometers), to obtain more comprehensive insight into the processes responsible for sliding. Residual shear parameters were determined by laboratory tests, and back calculated using numerical analysis and inclinometer readings. Very complex geotechnical conditions were determined on-site and thus presented in the light of future construction works.

Keywords landslide, foundation pit, inclinometer, back analysis, stability analysis

Introduction

The site is located at the bottom of the residential area and the identically named natural slope Karaburma at Višnjička 74 street in Belgrade. It is bordered by the streets: Višnjička, Vojvode Micka Krstića, and Triglavska (Figure 1). The wider area is densely urbanized and represents a zone of combined activities (industrial, commercial, and residential). On the north side, the site is bordered by Višnjička Street, and on the south, there is a zone with objects for individual housing and the residential-business complex "Danube Terraces". To the east and the west, there are workshop halls and warehouse spaces.

The original design included the construction of two underground parking levels, and a piled retaining structure for excavation protection was already in place at the site. The terrain at the site is not flat and is arranged for mechanization access.

The site is situated at the border between the Danube's highest river terrace and the Karaburma slope's bottom part. Within the site, the elevation of the terrain ranges from 70 to 80 m above sea level.

Excavations of the foundation pit were performed during June 2023, reaching a depth of approximately 6-7 meters. Due to the excavation procedure, combined with intensive rainfall during May and June 2023, significant displacements of the piled retaining structure occurred at the end of June 2023. According to the Expert Opinion of the Faculty of Civil Engineering in Belgrade, extensive displacements were caused by activating a part of the fossil landslide in the wider area of the location. These landslide movements threatened the neighbouring objects and the site itself. As a recommended measure for landslide remediation, - urgent, intensive, and therefore uncontrolled (in terms of compaction by standard procedures) filling of the foundation pit using predominantly earth material, and occasionally with construction debris, was done in the first half of July 2023. After the refilling of the pit, the landslide was stabilized.



Figure 1. Site map (the site is marked by 74)

Previous geotechnical investigations

Last time, the site underwent geotechnical investigations in 2019 for a commercial-residential building design (manually drilled 4 boreholes, reaching up to 12 m in depth, each). Additionally, the area and its surroundings have been systematically investigated over the past 50 years. A major geotechnical study was conducted in 1975 for an industry hall construction, including 12 boreholes. In 1961, investigations were done to design a residential block (Dunavski Venac), uphill. Further studies occurred in 1989 for the "Stara Karaburma" urban plan. There were at least four archive boreholes

close to the site. Detailed investigations were also conducted around Višnjička Street, with only one borehole near the site itself.

Additional investigations were necessary due to several factors. First, the previous studies were conducted decades ago, and geological conditions may have changed over time due to natural processes and human activities. Second, the reactivation of the fossil landslide that has occurred on the site required additional investigation to safeguard the site and the surroundings, since the results of the ground investigation campaign from 2019 were not adequate for this task.

Geological and geomorphological setting

The study area, situated on the right bank of the Danube, has previously undergone extensive earthworks, including levelling, excavation, filling, and material rearrangement. It features complex geomorphological and geological structures, primarily composed of Quaternary sediments from abrasion-erosion terraces. These terraces were covered by layers of loess deposited during the Quaternary period. Marly clays and Marls represent the oldest sediments identified via borehole core logging.

Variations in climatic conditions during the Quaternary era resulted in diverse sediment deposition, leading to challenges in delineating precise lithological boundaries. From the lithological point of view, these sediments range from gravel to sand, silt, and clay, with varying percentages of each component and predominantly fine to occasionally medium-grained texture. Sedimentological analyses indicate angular or weakly rounded grains, suggesting minimal transportation during the deposition time.

Engineering geological & Geotechnical investigations

Field investigations were conducted by the University of Belgrade - Faculty of Civil Engineering during the period from July to August 2024.

The following engineering-geological and geotechnical investigations and tests were carried out in the research area (Figure 2):

- Engineering-geological and geotechnical reconnaissance of the terrain;
- Borehole drilling with the installation of piezometer and inclinometer constructions;
- Engineering-geological mapping of the borehole core with soil/rock sampling;
- Geodetic and geotechnical monitoring of retaining structure and terrain;
- Geophysical investigations.

Engineering-geological reconnaissance

The reconnaissance included inspections of all structures on adjacent parcels as well as on the slope near the residential-business complex "Danube Terraces". During this process, the degree of damage to the constructed retaining structure, surrounding infrastructure and buildings was visually assessed.

Locations for new investigation works (borehole drilling and geophysical surveys) were also identified. Given that the terrain is significantly urbanized, and that substantial backfilling of the previously excavated foundation pit has been carried out on the site itself, it was not possible to conduct geological surface analysis.

Geotechnical borehole core drilling

The borehole drilling was conducted using continuous coring to investigate subsurface geology, sediment properties, and hydrogeological characteristics. Six new boreholes, reaching depths of up to 36 meters (totalling 186.9 meters), supplemented previous investigations. Special attention was given to obtaining undisturbed core samples to identify potential landslide slip surface zones by reducing the drilling pressure and without using additional fluids. Detailed engineering-geological core logging aided in defining geological layers, while core samples were tested in geotechnical labs to determine soil physical and mechanical properties. Piezometers were drilled and installed close to the borehole positions to monitor groundwater levels and assess their influence on terrain deformation and nearby structures. Besides the piezometers, existing depression wells were also used for this purpose (Figure 2).

Geodetic and geotechnical monitoring

A geodetic monitoring network was set up to track deformations in the retaining structure, neighbouring objects, and terrain surface. It included 55 stabilized points, using bolts or reflective markers. Typically, points were monitored once per day, but in cases of heavy rainfall or controlled excavation, monitoring was conducted twice daily, before and after the excavation completion.

Geophysical investigations

Geophysical investigations were undertaken at the site by seismic refraction profiling along six profiles (Figure 2). Their positions and lengths were customized based on site conditions. The aim was to identify geological layers with varying primary seismic wave velocities, that could indicate diverse lithological environments, and to ascertain the presence of a solid rock mass. Across 5 of 6 profiles, four different layers were identified, with three boundaries that delineate them. Despite the efforts, the presence of a solid rock mass within the investigation area could not be confirmed. The south-eastern border zone with a piled retaining structure including the RC pile cap disabled its confirmation. Contour maps of identified geological unit borders were generated to determine spatial positioning and quantify angle variations, crucial for assessing potential instability or slip surface zone.

Geotechnical laboratory testing

Laboratory tests of the physical-mechanical properties of soil were conducted at the accredited Laboratory for Soil Mechanics at the University of Belgrade, Faculty of Civil Engineering, as well as at the

accredited Laboratory for Roads and Geotechnics at the Institute for Testing of Materials Serbia (IMS), Belgrade. Tests were conducted on 43 representative samples. Additionally, 65 additional samples were taken from the boreholes for testing the soil moisture content.

The results of these laboratory tests provided valuable data to define representative soil profiles for slope stability analysis and to assess and mitigate landslide hazards.

Results of the geological & geotechnical investigations

The wider area surrounding the site is characterized by the terrain surface that has varying surface slopes, composed of colluvial loess, diluvial clays, and other Quaternary sediments overlaying Neogene marly clays, clayey marls, and marls interbedded with layers of limestone (Figure 4). The marly clays in the subsurface zone are weathered and prone to volumetric changes (swelling). Such terrains are characterized by slow movements of soil masses, affecting degraded diluvial clays in the slope.

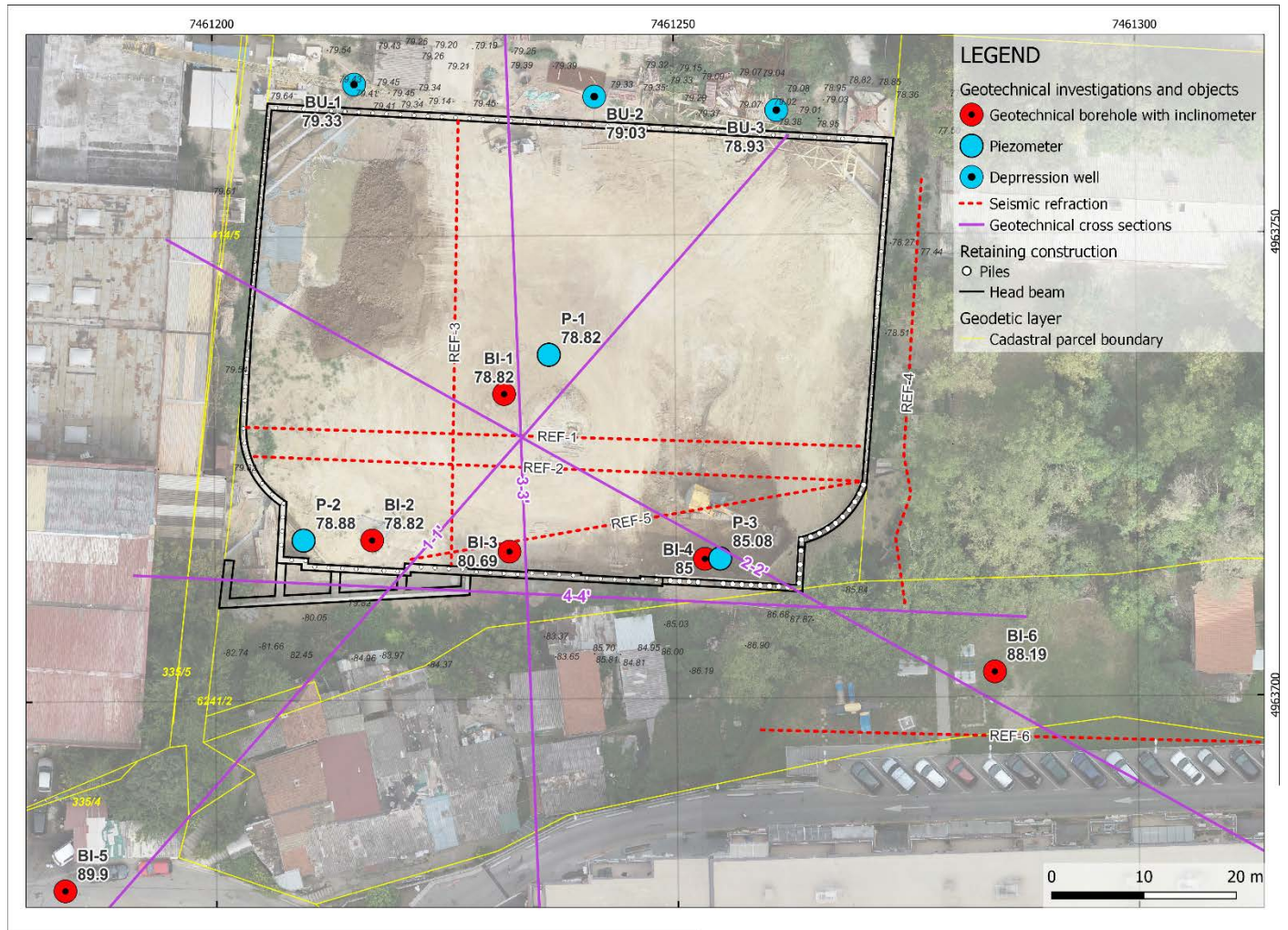


Figure 2. Situation of newly conducted geotechnical investigations

The engineering-geological conditions in such environments, which need to be thoroughly and comprehensively investigated beforehand, require complex geotechnical measures to enable rational space utilization for construction purposes. In such terrains, measures such as proper drainage system and slope stabilization are necessary, involving the design and construction of massive protective or retaining structures using piles (or diaphragm walls) and landslide remediation based on detailed geotechnical terrain investigations and intensive and continuous geotechnical monitoring.

The stability of the slope extending from the site foundation pit across the “Danube terraces” is influenced by the specific natural terrain configuration. The most significant geological-morphological-hydrogeological factors stem from the interaction and disposition of Quaternary and Tertiary sediments, represented by weathered diluvial and marly clays, terrain inclination, and the geological history of Tertiary substrates (paleo-shorelines and adverse hydrogeological conditions).

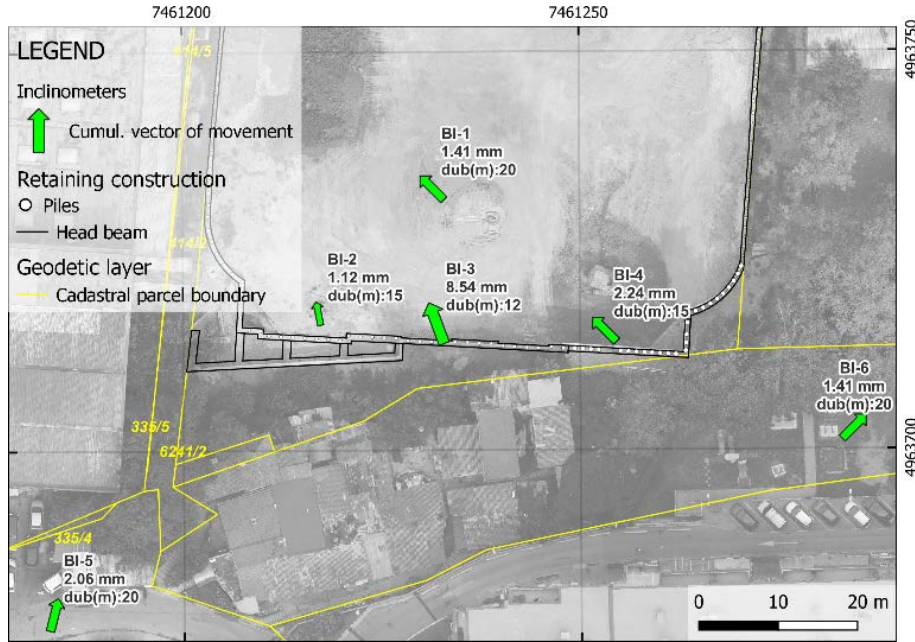


Figure 3. Vectors of maximum (cumulative) inclinometer displacements

A crucial factor in assessing the stability of the subject slope, as well as the broader surroundings, is the urbanization of the area - the impact of human activities, primarily unplanned or unprofessional earthworks, which often lead to the reactivation of certain parts of landslides or the formation of new local terrain instabilities. It is worth noting that during the construction of facilities in the immediate vicinity, relatively significant ground movements have occurred in the wider area, indicating potential fossil landslide (re)activations. These circumstances required redesign of the mentioned facilities, as well as the implementation of additional, non-planned measures for remediation and stabilization

compared to the initial design solutions, which all led to significant construction delays.

From the perspective of slope stability, based on the results of engineering-geological and geotechnical investigation results (such as geotechnical monitoring, analysis of available technical documentation, and adopted engineering-geological and geotechnical terrain models), it has been determined that there is a direct correlation between the slope and the hillside sliding above the site, even during shallow excavations or the incision of the slope and hillside toe that is situated in the foundation pit of the site.

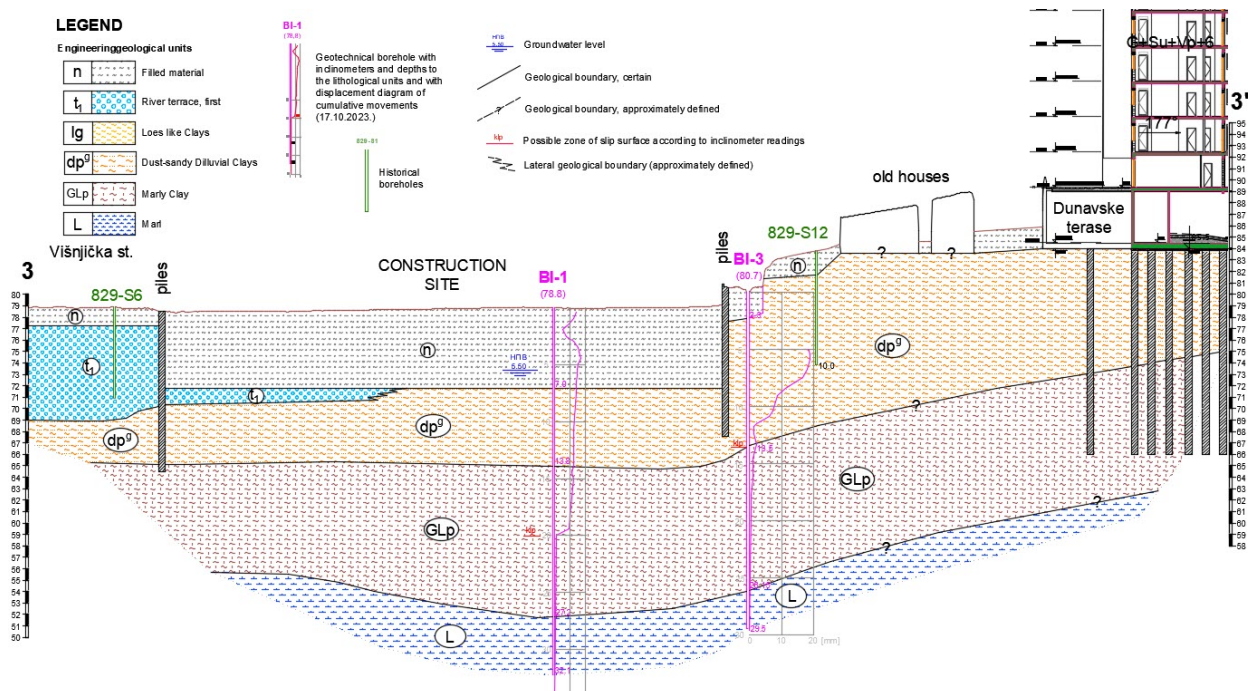


Figure 4. Geotechnical cross-section 3-3'

The ground investigations revealed a relatively high groundwater level (2 to 5 m below surface level, as shown in Figure 4), compared to the original excavation plan (up to 72 m above sea level), accompanied by occurrences of seepage and pressurized groundwater in soil fissures. A wet period from May to June 2023 coincided with excavation, leading to a rise in groundwater levels and unfavourable hydrological conditions. The hydrological state resulted in high pore pressures within the soil mass, contributing to the formation of deep sliding surfaces in the marly clays. These high pore pressures represent a significant geotechnical constraint for slope stability at the site location.

During the active mechanical excavation, the maximum daily value of displacements ranged from approximately 5 to 10 mm. These observations characterize the slope as a slow-moving landslide, with the slope currently considered to be in the intermediate stage of failure according to literature recommendations (Maksimović, 2008).

A total of 6 inclinometers were installed at the site. Based on the inclinometer readings, the sliding surface is detected at various depths, ranging from 13 to 20 m. Initially, all inclinometers showed zero movements, and therefore the controlled excavation in the southern part of the foundation pit was done, to "trigger" reactivation of the previously stabilized landslide. After the controlled excavation, all installed inclinometers showed movements. Final inclinometer readings are given in Figure 3. In this figure, only the cumulative vector of movements is depicted at depths corresponding to the highest movement rates identified in the analyzed incremental graphs.

Displacement values (> 2 mm) and landslide activity directions were recorded in inclinometers BI-3 (Figure 5) and BI-4 at depths of 12-15 m. Although the displacements near the precision limit (< 2 mm) were detected in inclinometers BI-1, BI-2, and BI-6, they cannot be disregarded, as their activity coincided temporally and occurred at similar depths as those in inclinometers BI-3 and BI-4. Clear determination of the depth and shape of the landslide surface was not feasible without additional inclinometer movements and prolonged monitoring, risking the stability of adjacent structures, particularly the residential business complex "Danube Terraces".



Figure 5. Photograph of BI-3 borehole core log in the zone of the slip surface (yellow arrow)

Conservative values were adopted for the shape and depth of the landslide slip surface, resulting in an irregular shape and block-like movement mechanism, categorizing

the landslide as deep. The surface affected by sliding remains uncertain due to the inability to systematically monitor the wider area.

Numerical Analysis

Based on the results of the field and laboratory geotechnical investigations and inclinometer monitoring, it was concluded that the construction of a residential and commercial building in the considered location has an impact on neighbouring buildings and the global stability of the slope. Therefore, computational profiles of the terrain were formed and a numerical analysis of stability with back-analysis was performed. Analysis was performed on 2D models, using the limit equilibrium method in Rocscience Slide 6. Morgenstern-Price slice method was used, which simultaneously satisfies all equilibrium conditions. The global safety factor was adopted as a stability criterion. The piled retaining structure is modeled as a very high-strength material. Analysis was done on 2 representative 2D cross-sections.

First, the back analysis based on the inclinometer observations was done. According to these measurements, it was concluded that the sliding mechanism is block-like and the sliding zones are mainly in the layer of marly clay (in contact with laminar clays, in the contact zone with deluvial clay and in the contact zone with limestones). Therefore, two sliding surfaces (shallow and deeper) of the block type (slip zone) with residual shear strength parameters were assumed. The calculation was made assuming residual shear strength parameters for the entire layer of marly clay. Results of the numerical back analysis are in line with laboratory values of residual angle of internal friction, and the same values are obtained for both analyzed cross sections.

After the back analysis, the following situations (scenarios) were simulated:

- Backfilled foundation pit (after large displacements in the end of June 2023);
- Complete foundation pit excavation (with berms), according to the original design (Figure 6);
- Controlled excavation to "trigger" reactivation of the previously stabilized landslide, September and October 2023 (Figure 7);
- Excavation of 1-1.2 m - alternative design with shallow mat foundations.

Obtained results show that complete foundation pit excavation, as well as controlled excavation, leads to a factor of safety lower than 1, which is in line with the field observations and inclinometer readings. Also, surrounding objects are in the zone of critical sliding surfaces. With an unexcavated foundation pit, factors of safety range between 1.2-1.5, which is considered acceptable. Therefore, an alternative design solution with a shallow mat foundation is checked, and this scenario leads to the factors of safety 1.18-1.4, which is considered acceptable.

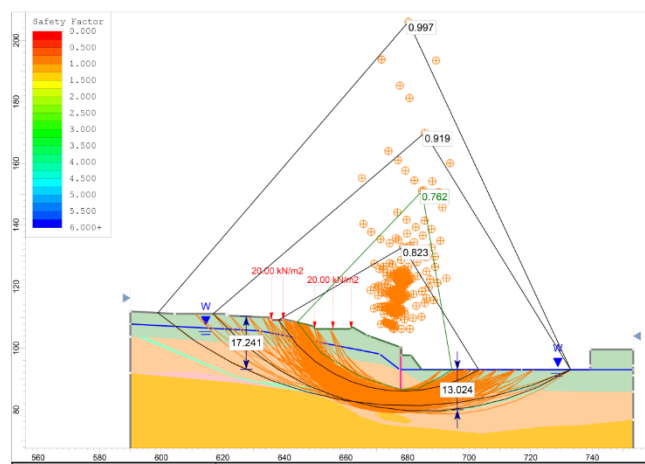


Figure 6. The factor of safety for complete foundation pit excavation (with berms), according to the original design (section 1-1). Both assumed sliding surfaces are critical

For the numerical back analysis profiles shown in Figures 6 and 7, we did not consider the load from the “Danube terraces” because the observed domain does not extend to the retaining structure on the construction site. On the other hand, the “Danube terraces” are founded on piles resting on a layer of marl that is considered as geotechnical bedrock.

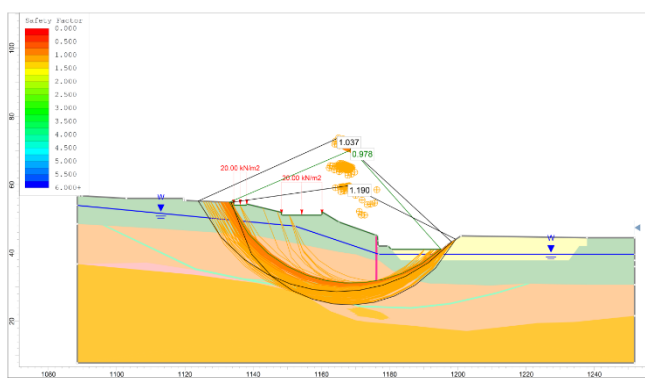


Figure 7. Factor of safety for controlled excavation to "trigger" reactivation of the previously stabilized landslide (section 1-1). Factor of safety ~1.0

Remediation Measures

As previously shown, foundation pit excavation would lead to a large movement of a landslide. Therefore, to proceed with an excavation, the very expensive retaining structure must be constructed first. Due to high costs, an alternative solution without underground floors is adopted. First, the shallow mat foundation is considered. However, due to the urgent and uncontrolled filling of the foundation pit, a very soft and thick (6-8 m) fill was formed, which made the shallow foundations impossible to construct. Estimated settlements of the shallow foundations on fill are in the range of 30-40 cm, which is considered unacceptable.

Due to the very high compressibility of the fill, ground improvement methods using jet-grouting or vibro-

compactions were proposed. As an alternative, deep-piled foundations could also be a possible solution. In this case, the pile base should remain above the slip surface, to increase the normal pressure on the slip surface.

Before any further work on the foundation design and execution, an additional geotechnical study including CPT or DPHS testing of the fill is recommended. Due to the high heterogeneity of the backfill, there's a possibility that the coarse-grained components may restrict the effectiveness of such testing, necessitating caution in interpretation. Geotechnical and geodetic monitoring should be continued during all of the further works.

Conclusions

The landslide on the Višnjička 74 street was activated due to an excessive excavation of the foundation pit in June 2023. Urgent remedial measures and additional geotechnical investigations were executed. Ground investigations have shown very complex geotechnical conditions. Numerical analysis shows that the excavations of the foundation pit are impossible without placing a very expensive retaining structure. Therefore, alternative foundation solutions were proposed.

Acknowledgements

This work is supported by the Serbian Ministry of Science, Technological Development and Innovation via Project 200092. The support of the INGRAP-OMNI d.o.o., ZIDAR d.o.o and EFFECTOR PLUS d.o.o is acknowledged.

References

- Elaborat o geotehničkim uslovima izgradnje stambeno-poslovnog objekta na KP 6241/1 KO Palilula, ul. Višnjička 74, sa osvrtom na stabilnost susednih objekata i terena usled nastalih pomeranja (in Serbian). Univerzitet u Beogradu – Građevinski fakultet (Technical documentation / in Serbian)(2023)
- Elaborat o geotehničkim istraživanjima terena za potrebe izgradnje stambeno-poslovne zgrade u ul. Višnjička br. 74 na KP 6241/1 KO Palilula. Geobiro-Va, Valjevo (Technical documentation / in Serbian) (2019)
- Elaborat geotehničkog izveštaja o dopunskim istražnim radovima na lokaciji centar „Belgrade Plaza“. Institut za puteve, Beograd (Technical documentation / in Serbian) (2016)
- Elaborat o geološkim istraživanjima za potrebe ocene stabilnosti padine u sklopu razrade projekta izgradnje „Plaza“ centra u Višnjičkoj ulici. Institut za ispitivanje materijala, Beograd (Technical documentation / in Serbian) (2012)
- Maksimović M. (2008) Mehanika tla. AGM knjiga, Beograd. (ISBN 978-86-86363-07-7) 510p
- Stručno mišljenje o globalnoj stabilnosti na gradilištu stambeno-poslovnog objekta na KP6241/1 KO Palilula, Ul. Višnjička 74 i susednih objekata (terena) usled nastalih pomeranja sa predlogom hitnih sanacionih mera. Univerzitet u Beogradu Građevinski fakultet (Technical documentation / in Serbian) (2023)

Landslide mapping for the regional gas pipeline construction near Priboj (Serbia)

Katarina Andrejev⁽¹⁾, Miloš Marjanović^{(2)*}, Rastko Petrović⁽¹⁾

1) Taš Grupa, Kraljice Marije 9, Belgrade, Serbia

2) University of Belgrade, Faculty of Mining and Geology, Belgrade, Djusina 7, milos.marjanovic@rgf.bg.ac.rs

Abstract The on-going gas pipeline design in Serbia is currently reaching its apex, and therein, extensive investigation and planning had to be undertaken to ensure its safe execution and long-term exploitation. Therein, engineering-geological conditions play important role and at the stage of preliminary design directly imply the alinement of the future pipeline route. This paper is focused on Zlatibor-Prijepolje pipeline branch in SW Serbia, which is further split into Priboj and Prijepolje sections. The former, Priboj section, is the subject of this work. The mapping methodology included: preparation of the base maps, field mapping, and data interpretation. Preparation stage was extensive and included acquisition of earlier investigations and maps at larger scale, primarily Engineering-geological map of Prijepolje at 1:300,000 scale, which was digitized in GIS environment, and converted into mobile GIS formats for field work. The entire route was scanned using airborne LiDAR, which resulted in a dense point cloud and Digital Terrain Model of 25 cm resolution. It was used for delineating landslides, proluvial fans, riverbeds, gullies, and other relevant morphological phenomena that indicate poor stability. This interpretation was also digitized in the GIS environment and prepared for mobile GIS application. After compiling all engineering-geological data, mobile base maps were created for field work, where additional forms were digitized on-spot. General characteristics of the area can be deducted as follows. The ophiolitic mélange is dominant and hosts most instabilities, due to its high weathering grade and unfavourable hydrological conditions. All landslides are predominantly deep-seated, and mostly of earth slide type. In total, 37 landslides are identified in the area, 12 of which along the current route. Based on their spatial extents further recommendations are given regarding particular locations and segments of the Priboj section in order to optimize its rout. It has been demonstrated how integrative approach is essential to gather relevant data and characterize the terrain appropriately, for further, more detailed design stages.

Keywords landslides, LiDAR, DTM, pipeline, Priboj

Introduction

A new gas pipeline route has been included in the Spatial plan of Serbia, and its western branch Zlatibor-Prijepolje,

contains several sections, one of which connects Priboj and Nova Varoš, i.e., Pribojska Banja – Rutoši, to be more specific (Fig. 1). The target pipeline segment is at its preliminary design stage, and its route totals 13.6 km. It will service installation with working pressure of 16-50 bars and will be installed at 1.5 to 2.0 m depth, depending on the terrain conditions. The primary objective was to compile engineering-geological map with focus on current and potential instabilities along the corridor that encloses 500 m left and right along the pipeline route (approximately 14 km²).

Study area

Seated in the SW Serbia, the wider area of interest belongs to a hilly-mountainous region with continental to sub-alpine climate. It has a distinct river system subdued to the Lim River watershed. The centreline is the Rutoška River valley, tightened in the W-E direction between the foothills of the Zlatibor Mt. to the north and Zlatar Mt. to the south. High relative elevations (840 m) and large variation in slope angles ranging from very gentle along the riverbed to subvertical in the gorge part of the valley, suggest a terrain which is very discontinuous and drastically different conditions. It is sparsely populated, mainly rural area, but industrially important with numerous objects of the hydro energetic Lim River system, and regional level roads. Geologically, it belongs to a highly complex and intensively tectonized zone on the contact of two major formations, Mesozoic limestones and Jurassic ophiolitic mélange, suggesting complex geological conditions during the closure of the Thetis ocean, delineated along transform SW-NE trending faults. Its continental development is seized during Miocene, when a basin was form, comprising of typical lacustrine sedimentation, which transited into the current fluvial development, and associated quaternary deposits (Dimitrijević et al., 1980). The entire area is in neo-tectonic uplift along the SW-NE trending faults, although seismic activity is not particularly pronounced. The most distinct geological feature is the ophiolitic mélange itself, as it comprises of various rock types with significantly different characteristics (Jevremović and Sunarić, 2009). It includes clastic, volcanic and metamorphic constituents, but diabase predominates, covering 46% of the area of interest, while serpentinites, cherts and sandstones are subordinate as isolated masses, totalling about 14% altogether.

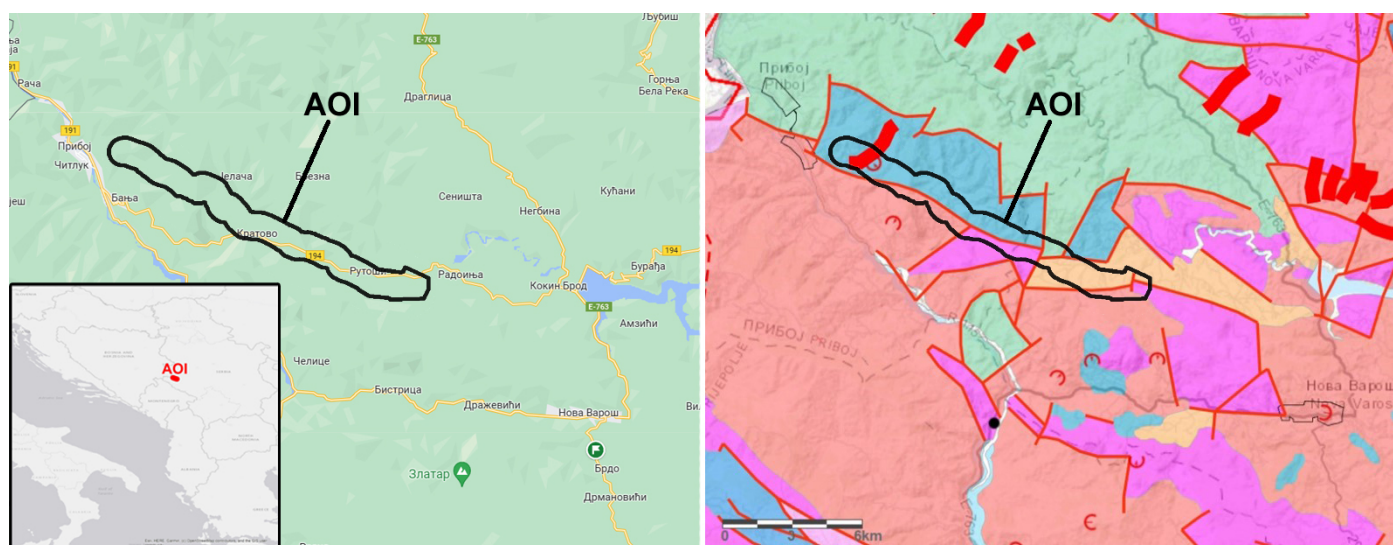


Figure 1 Location of the study area (to the left) and engineering-geological map (to the right).

Such lithological variability and tectonic distress suggest that this complex is highly susceptible to weathering, with very thick crust of frail and loose material. The main counterpart of this unit is represented by Miocene clastic sequence, covering about 25% of the area. Remaining 15% is covered by isolated limestone masses, and alluvial and proluvial deposits enclosed in the area of interest.

Different types of instabilities are rather frequent in this area, ranging from earth slides to rockfalls (Hungur et al., 2014). They are traditionally interpreted as deep seated rotational slides hosted in the thick weathered crust of the ophiolitic *mélange* unit, but also as shallow translational slides in the Miocene clayey deposits. As limestone masses are locally thrust over ophiolitic *mélange*, the groundwater conditions are also unfavourable, and traditionally considered as one of the principal factors of deteriorating rock and soil strength at expense of pore pressure. The draw-down effect is also a possibility, given the close allocation of several artificial lakes within the hydro-energetic powerplant system. The natural trigger is the intensive rainfall and snow thaw in the highlands, which is customary in spring and autumn season.

Materials and methods

The task required compiling all valuable data together and delivering an up-to-date interpretation of the ground conditions in the area. It was conducted through several phases, preparation of the base maps, field work and their final compilation and interpretation. The footprint of the area of interest is generated as a buffer of 500 m around the pipeline route, covering approximately 14 km². For desktop GIS environment ArcMap 10.4 was used, with standard file formats (shp. for vector and .tiff for raster data), while MapitGIS android application (using the .mbtiles file format for raster and vector data) was used for mobile GIS environment installed on a tablet device Lenovo S5000-F with Android OS.

Preparation of the base maps

The base maps included several sources (Tab. 1) and each one of them was used to compile a master base map which was interactively used in the field (Fig. 2).

The Digital Terrain Model (DTM) was created by using the airborne RIEGL VUX-40 sensor on payload (flight conducted in 2022), with the initial point density of 50/m². The last reflection points were used to generate a point cloud stripped from the vegetation. The raw point cloud was decimated to 25 cm resolution and regular spacing. It was used to interpolate the DTM by spline function with default setting, from which a *Hillshade* model was created, using default sun incidence and azimuth angle (315° and 45° respectively). Simultaneously, the terrain was imaged using a high definition photogrammetric camera and appropriate *Orthophoto* was created in .ecw format matching the DTM 25 cm resolution. The LiDAR *Hillshade* at such resolution can be considered as a powerful tool for landslide mapping (Bernat Gazibara et al., 2017). Therein, a shade effect that simulates 3D visual impression can indicate fresh footprints of the landslide elements (scars, foots, tension cracks, etc.) and imply the status of the landslide activity (Fig. 3). The *Orthophoto* base map was used to append the *GoogleEarth* historical imagery to visualize ground changes linked to landslides (Fig. 3).

Table 1 Data sources.

Base map	Data source	Scale/ resolution
Digital Terrain Model	Airborne LiDAR survey	25 cm
Orthophoto image	Airborne Photogrammetric survey	25 cm
Engineering-geologic map	https://geoliss.mre.gov.rs	1:300k
Engineering-geologic map sheet Prijepolje	https://gzs.gov.rs/	1:100k
Depth to bedrock	https://soilgrid.org	250 m
Historical Satellite Images	https://earth.google.com/	NA

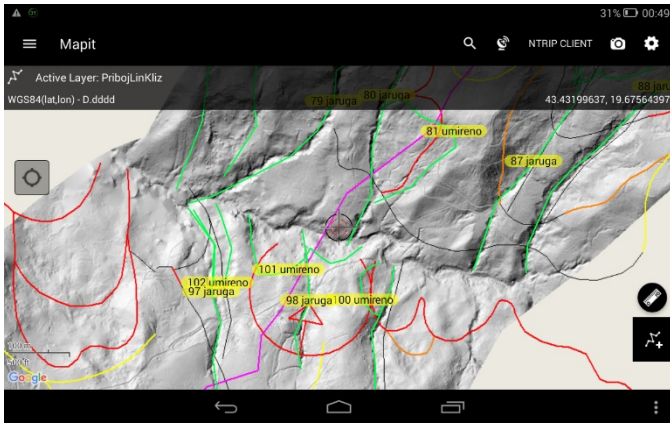


Figure 2 MapitGIS display for interactive use during the field work (*Hillshade* base map and on-spot digitized content). Red lines represent content from Engineering-geological map, while other lines are digitized on-spot while using the app.

Engineering-geological map of Prijepolje at 1:100 000 scale (Jevremović and Sunarić, 2009) was digitized in desktop GIS environment and converted to mobile format for field use (Fig. 2). All instabilities were grouped into active and dormant landslides and marginally stable slopes, while gullies and fluvial fans are also outlined.

Finally, depth to bedrock base map was created using the coarse resolution source map from *Soilgrid* portal (250 m). To make it more suitable for the application in the field it was converted from raster to the 250 x 250 m point grid. Subsequently, these points were used to interpolate depths by using spline interpolation tool (at default settings) in desktop GIS environment (Fig. 4). The interpolated raster was then converted to contour lines with 2.0 m vertical spacing.

Field work

Conventional field mapping was conducted along the route, covering about 14 km². Due to time limitation it was undertaken during the vegetated season which reduced the visibility of fresh landslide footprints. The mapping included direct classification of encountered units, mainly in accordance with the engineering-geological base map, whereas greater attention was dedicated to mapping of instabilities, and their state of activity (by direct and indirect indicators, such as morphological features, but also hydrological, damaged objects, tilted trees, etc.).

Incision depths at gullies and other open scarps was also recorded and levels of groundwater table at available wells and streams. The existing (base map) instabilities were checked for their current status, whereas new instabilities were directly digitized on-spot by using the MapitGIS app, which has offline mode of geo-locating, allowing for a seamless field logistics (Fig. 2). Analogue field log was also kept and field photographs taken for relevant details.

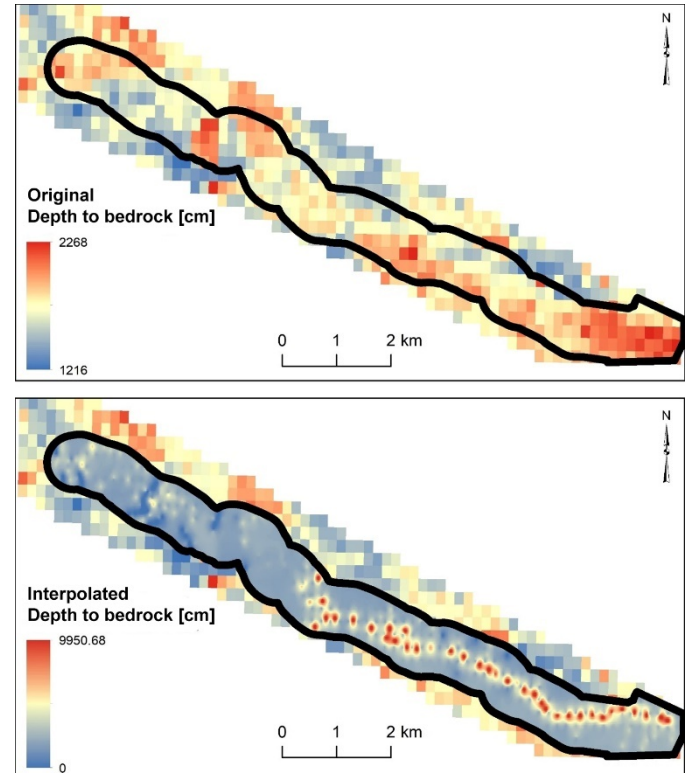


Figure 4 Depth to bedrock base map before (upper) and after (lower) spline interpolation.

Data compilation

All collected data were combined in a desktop GIS environment. Typical cross sections were traced across the main landslides, 17 in total. Due to an elongated shape, the area of interest was split into 8 frames suitable for visualizing in 1:5000 scale.



Figure 3 Detail of the *Hillshade* base map clearly delineating landslide elements (left); GoogleEarth footage of the same location from 2019 (middle); Orthophoto base map of the same site in 2022 with indicated destruction of vegetation possibly due to landsliding (left).

Results

The entire area can be roughly halved into western highland and the eastern valley, which matches the hypsometric and lithological difference.

The landslides are more abundant in highland part (Fig. 5-6), composed primarily of ophiolitic mélangé wherein weathered diabase ($\beta\beta$) predominate. These host deeper landslides, ranging from 5 to 15 m (Fig. 6). Locally, the unit containing clastic component (PŠGA), a mixture of sandstone transiting to siltstone and claystone. The landslides within this unit, are smaller and slightly shallower. The least susceptible is the chert unit (R). The preconditions to sliding is primarily related to the groundwater table, which is in this area relatively shallow, as indicated in numerous contact springs and observed wells. Springs are arrayed around the periphery where water bearing Triassic carbonates thrusting the ophiolitic mélangé below, as less conductive.

The valley stretches eastward firstly with steep slopes, and the second half of the valley, further upstream has much more gentle slopes. The steeper end is composed of ophiolitic mélangé (PŠGRK $\beta\beta$) on the right valley side, while left slopes are made of massive carbonates (LK). The gentler upstream part is entirely made of loose clastic sediments, primarily marls and clay (LCLG), deformable and weathered, covered with thick deluvial crust. Landslides are less prominent and mainly shallow. Fluvial fans edging the valley plain and several deep gullies are present as the valley is the dominant erosion basis from highland downslope.

There are 18 distinct landslide bodies, 3 of the flow type, while 6 are rotational (deep-seated) and 9 translational (shallow) earth slides. Their size varies,

especially lengths which are ranging from 100 to 500 m, but mostly are 200-300 m long. There are 6 active landslides, with fresh footprints recognized on the field or remotely, while remaining are dormant.

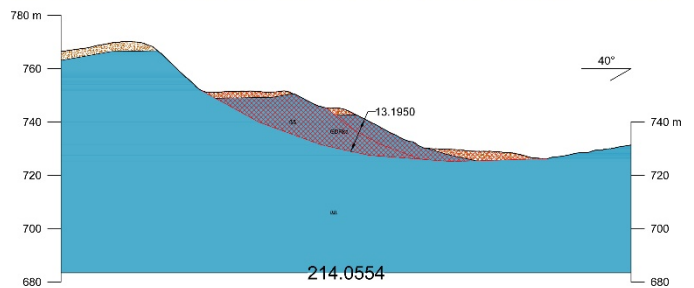


Figure 6 A field photo (above) and the cross-section No. 8 (below), depicting deep-seated rotational landslide (visualized also in Fig. 3) with typical hummocky ground in the foot area.

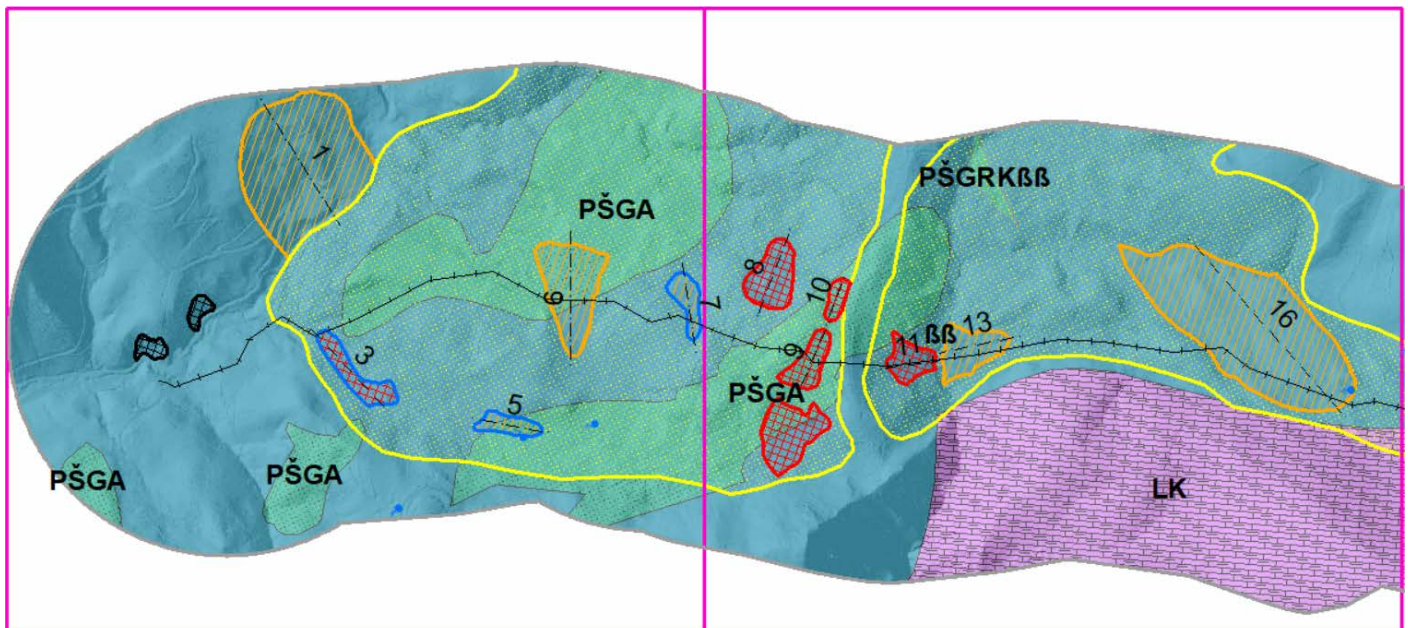


Figure 5 The two most critical and most westward frames of the engineering-geological map (crossed black line – designed pipeline; dashed line – cross section; red polygons – active landslides; orange polygons – dormant landslides; yellow polygons – marginally stable slope; $\beta\beta$ – diabase; PŠGA – clastic mélangé; PŠGRK $\beta\beta$ – undifferentiated mélangé; LK – marly limestone;).

Table 2 Engineering geological complexes and basic properties.

Complex	Depth to bedrock [m]	Elastic moduli [GPa]
Cemented soft rock	5-10	2.0-5.5
Cemented carbonate	2-3	5.0-10.0
Cemented volcanoclastic	5-10	0.2-3.0
Cemented hard igneous	10-15	0.5-3.0
Cemented metamorphic	3-5	1.0-3.0

Earlier interpretations suggest considerable overestimation of the number of active landslides, although it is important to mention again that the field work was conducted during the vegetated season. Considerable portion of the terrain remained categorized as marginally stable slope, approximately 4 km², while all other instabilities combined occupy 0.7 km². It suggests that any type of engineering work undertaken could cause new landslides enclosed in this zone. There are also 3 larger fluvial fans which are also considered as inconvenient.

The gas pipeline is routed through 11 landslides, two of which are active, and one fluvial fan. These suggest that rerouting should be taken to account, before moving to the next design stage, or undertake the necessary remediation measures.

As for the engineering geological classification (Tab. 2), all units can be separated into: cohesionless soil complex (sand and gravel of the fluvial origin); poorly cemented complex (clayey-silty sand of deluvial and proluvial genesis); complex of cemented soft rock (marlstones, sandstones etc.); complex of well cemented carbonate rocks (limestone and marly limestones); complex of well cemented volcanoclastic rock (chert, siltstone, etc.); complex of cemented hard igneous rock (diabase); complex of cemented hard metamorphic rock (serpentinite). Each of these complexes, except for the cohesionless and poorly cemented, have their weathered and fresh counterparts (of varying depth), and in Table 2 their generalized engineering-geological properties are given.

Conclusion

This work shows a successful example of integrated approach combining various source of data and state-of-the-art field and desktop technics for combining them. Relying solely on earlier findings was deemed unjustified. Instead, a thorough LiDAR mapping and field check are to be used as standard of practice for objects of such importance and longevity since it is important for them to remain in stable grounds not as of current but for decades to come. For this reason, all earlier findings, e.g., former active landslides, should be considered dormant and susceptible to reactivation. In addition, all further engineering work might open new instabilities within the zone of marginally stable slopes, possibly during the execution of pipeline groundworks itself. Groundwater influence is predominant in weakening the topmost weathered layers and are responsible for most of the

anticipated instabilities. Most landslides are occurring on the interface of saturated weathered layer and its fresh rock counterpart. The most critical are pipeline segments passing through the active landslides in the westernmost frame, where surface ground de-stripping (and other groundworks such as re-sloping) or retaining and draining structures are in order. Alternatively, the rerouting is also a viable option, if other gas pipeline standards are met (ground stability is only one of them).

Further design stages imply more detailed analysis of focused areas, including explorational drilling to proposed depths (based on estimated slip surface depths), sampling and lab testing for determining strength properties of materials in weathered and fresh zones, etc. For further project development monitoring of the site, is also in order, and it can be easily continued by further sequences of LiDAR scanning, whereas focused areas of active landslides can be further instrumentally monitored.

References

- Bernat Gazibara, S., Krkač, M., Sečanj, M., & Mihalić Arbanas, S. (2017). Identification and mapping of shallow landslides in the City of Zagreb (Croatia) using the LiDAR-based terrain model. In *Advancing Culture of Living with Landslides: Volume 2 Advances in Landslide Science* (pp. 1093-1100). Springer International Publishing.
- Jevremović D, Sunarić D (2009) Tumač za osnovnu inženjerskogeološku kartu 1:100 000, list Prijepolje K34-16. University of Belgrade, Faculty of Mining and Geology, Belgrade. 57p. (in Serbian)
- Dimitrijević M, Karamata S, Petrović B, Sikošek B, Veselinović D (1980) Tumač za osnovnu geološku kartu 1:100 000, list Prijepolje K34-16. National Geological Survey, Belgrade. 55 p. (in Serbian)
- Hungar O, Leroueil S, Picarelli L (2014) The Varnes classification of landslide types, an update. *Landslides*. 11: 167-194.

Failure estimation of the Majdanpek open pit east face based on inverse velocity model

Miloš Marjanović⁽¹⁾, Stefan Milanović⁽¹⁾, Nikola Simić⁽¹⁾, Lazar Kričak⁽¹⁾

1) University of Belgrade, Faculty of Mining and Geology, Belgrade, Djusina 7, milos.marjanovic@rgf.bg.ac.rs

Abstract The Majdanpek open pit mine south district is currently active mining prospect of copper ore exploitation in eastern Serbia. Its depth is approaching the termination depth and occurrences of large-scale instabilities and global instability of the final pit slope is possible. These can generate catastrophic mass movement inside an area that encloses a regional road route and the Pek River bed which is channelled along the outer contour of the pit. The displacements that were noted in early 2023, in the eastern face of the pit draw further concern and required a detailed monitoring campaign to be undertaken quickly. It included several approaches, but in this work focus was on surveying on 5 static benchmarks through the period January-July 2023. Due to the unknown status of the displacement acceleration or deceleration on its progressive failure path, the inverse velocity calculation of the entire series was undertaken. The series involved surveying of benchmarks using the absolute coordinates measured manually by a total station every 4-5 days. Displacements trends indicated constant cumulative increment with different rates at different benchmarks with periods of acceleration and deceleration. Long-term trend suggests that steep part of the progressive failure curve is not reached. However, inverse velocity trend in most benchmarks suggests slight decrease, indicating possible global progressive failure. Other monitoring approaches confirmed only local failures, while limit equilibrium stability models suggest both, presence of local failures and marginally stable slopes with safety approaching one. Inverse velocities estimated failure by the end of 2023. Extensive precaution measures were undertaken to avoid such scenario, including constant early warning evacuation system, as well as immediate remediation measures on reshaping the slope.

Keywords displacement, survey, inverse velocity, open pit

Introduction

The Majdanpek south district open pit mine (Fig. 1), one of the many in the realm of eastern Serbia copper mines is located within the outskirts of the Majdanpek town. The Pek River crosses through the upper horizons of the pit, as well as the regional road No. 33. After more than 60 years of exploitation, the current pit elevation is at about 100 m ASL and its crest at 620 m ASL suggests that it is soon to be approaching its terminal depth of 550 m, as further deepening is considered a bad practice, both economically

and for safety reasons (Read and Stacey, 2009). Further deepening below elevation 120 m, as well as tailing atop the crest is working twice-fold to reach that limit, while at the same time it creates stability problems due to mass removal in the base and increase of the mass on top of the slope. In addition, the mine contour has nowhere to spread further, which significantly reduces options regarding the slope engineering (reducing the slope angle and increasing the number of benches cause extension of the pit contour which cannot be suited due to infrastructural constraints). Another potential concern is possible transition to the underground excavation, which raises new stability issues, especially regarding yielding at such higher stresses (creep) or sudden and quick failures along larger structural interfaces (Brummer et al., 2006). The north face of the pit was notorious for its constant displacements and constant need for mitigation and remediation. However, the displacements have been visualized in the east face as well, firstly as subtle tension cracks in the tailing material, but subsequently as gaping cracks several meters deep (Fig. 2). Although displacement tolerance is considerably larger than in urban and infrastructural Geotechnical practice, quick development of these disturbing features opted for a comprehensive monitoring project in January-July 2023. There are alerting examples of large-scale slope failures in open pits, especially in the cases of transiting to underground excavation and further disturbing of rock masses by blasting and stress concentration along discontinuities, e.g., Palabora mine (Stewart et al., 2001). They result in millions of cubic meters of materials and immense material damage, which is especially concerning given the site's disposition (vicinity to urban, natural and infrastructure domains).



Figure 1 Plan view of the Majdanpek south district open pit (red).



Figure 2 Gaping cracks and local benching between conjugated failure planes on the abandoned tailing horizon 550 m.

Methodology

Management of landslides, especially at the open pit slopes require constant displacement monitoring, to avoid any incidents that might affect staff and equipment. Cumulative displacements, with appropriate frequency of measurements, are one good indicator, but assuming the stage of the curve is difficult in an on-going survey. The same applies for velocity derived as displacement per temporal frequency of measurements (mm/day), although acceleration and deceleration phases can be recognized. An alternative is to use inverse velocity, i.e., temporal frequency vs. displacement (day/mm) as its threshold cut-off is zero, when theoretically the velocity of failure approaches infinity. Once day/mm trend is established (usually following the linear fashion) it is possible to linearly extrapolate the trend and determine the time when it will reach zero, i.e., the moment of failure.

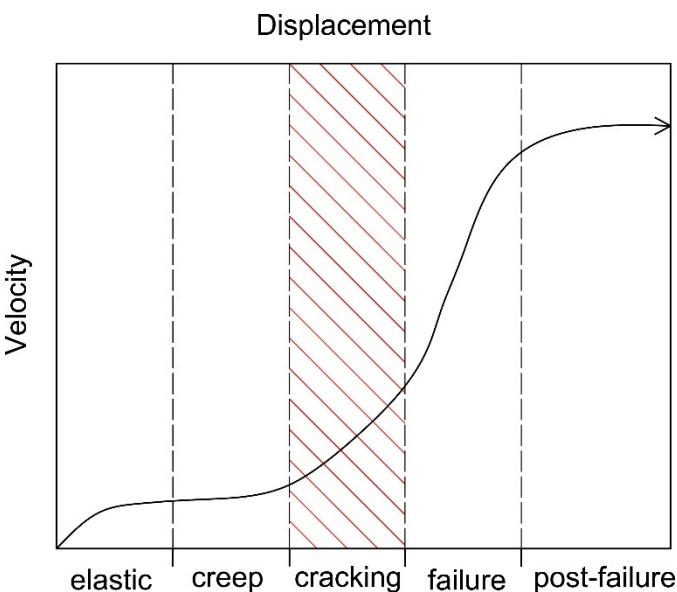


Figure 3 Schematic progressive failure curve and phases of deformation, with current slope state (shaded area).

The concept of inverse velocity to predict slope failure time are dating back to the 80's (Fukuzono, 1985) and have been perfected and updated more recently (Rose and Hungr, 2007; Carlà et al., 2017; Zhou et al., 2020). There are some important assumptions and limitations involved. Firstly, it assumes the creep motion along a progressive failure curve, which has several states with increasing acceleration, but the last stage is mainly linear (Fig. 3). Secondly, it presumes several invariants, and constant conditions slope conditions. Consequently, it is not suitable for structurally controlled and brittle failure modes, nor it is utterly realistic for open pits where significant slope profile change is common, hydrogeological conditions change, loading and unloading is taking place, as well as blasting and other mining activities. However, there are reports on successful estimation and avoiding of catastrophic scenarios using the inverse velocity approach (Rose and Hungr, 2007).

The open pit was monitored by various techniques:

- conventional fixed benchmarks survey;
- photogrammetric imaging using drone;
- terrestrial radar interferometry;
- piezometer water table surveillance
- visual inspection.

In this work, the focus is on the results of surveying measurements which have been undertaken from January to July 2023, with average frequency of 4-5 days. Absolute coordinates in Gaus-Kruger Zone 7 reference system were determined in each visit manually, using a total station. Nine benchmarks were initially installed, but four of them succumbed to local instabilities and were not monitored throughout the entire period. Their spatial positioning was arrayed in a 3x3 grid covering the central part of the eastern face of the pit (Fig. 4). The benchmarks are allocated in rows following the bench geometry, so all three in a row are more-or-less of same elevation. They are labelled R1-9 starting from the lower towards the upper positions. Although not in focus, other techniques were used to cross-compare with results of surveying.

Results and discussion

The main issue in interpreting the surveying results is whether the slope is globally or locally unstable, and whether failures are structurally controlled. The initial stability analysis suggests fair factors of safety in range 1.3-1.4, but these were not conducted in saturated nor in seismic conditions, and major structures were not taken into account. When all these additional factors are introduced, the factor of safety drops to one, which is marginally stable case, open to interpretation in favour of global slope failure. Alongside, the stability model identifies many local failures in the upper horizons, hosted in the tailing material. Due to intensive activities in the lower horizons, three lower (labelled R1-3) and one middle (labelled R7) benchmarks were compromised, leaving five in the upper part functional through the entire observation period.

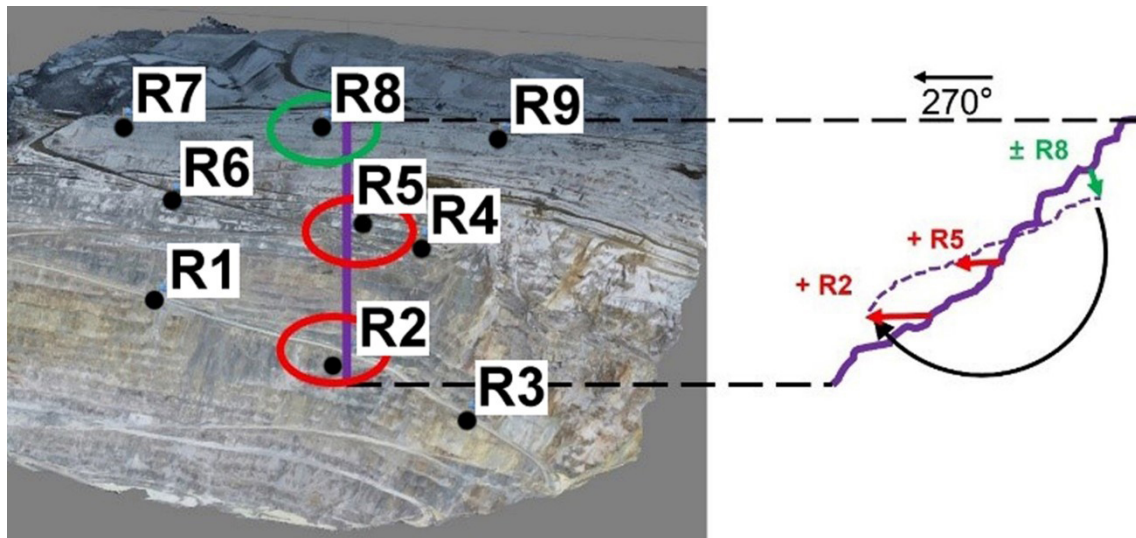


Figure 4 Schematic display of global rotational failure based on initial benchmark measurements.

Initially, during the first month of the survey, the lower benchmarks R1-3 showed indications of more dominant horizontal component vs. vertical displacement (~30 mm/day vs. ~10 mm/day, respectively), whereas the topmost benchmarks showed twice larger vertical displacements than horizontal (~20 mm/day vs. ~10 mm/day, respectively). This is an indication for global rotational slip, which has been further measured (Fig. 5). After this period, in March 2023 the lower benchmarks were destroyed and became inaccessible, partly due to regular mine operations, but partly due to deformations.

Cumulative displacement suggests that there are periods of acceleration and deceleration, which are synchronized across all benchmarks (Fig. 5), indicating that global failure is possible, and that inelastic creep is in progress. Displacement rate is the highest in benchmark R 8, reaching 60 mm/day. Smaller accelerations were obvious in Jan-Feb (ranging between 10-20 mm/day), and Apr-May (ranging between 20-30 mm/day), while the most prominent one is in Jun-July (ranging between 30-40 mm/day). In between, the displacement rate is constant at about 5-10 mm/day. Such rate corresponds to Slow to Moderate landslides according to conventional classification (Hungri et al., 2014), while in domestic mining legislation they can be considered level 4 of 5, which is an alerted stage, just before immediate actions.

Despite the heavy rainfall which was often in first part of the 2023, causing flooding in the Pek River area. there was no direct correlation of these accelerations with the rainfall. as R^2 value was as low as 0.3. Mining activities were also uncorrelated, due to simultaneous unloading of the lower horizons and loading of the upper ones. In addition, the unloading was undertaken on the in the upper horizons comprising of the tailing material, to prevent local failures.

All these findings cannot unambiguously eliminate possibility that benchmarks are related to several independent local failures, but it is likely that the failure is

not structurally controlled, as accelerations are subtle and synchronized across large area.

Displacement rates are calculated for Northing, Easting and Z directions and total vector. Given the slope orientation, the total horizontal vector more-or-less coincides with westward movement. Therefore, the most interesting are findings for -Y and -Z (vertical) directions. The inverse velocity linear trends (Fig. 6) are suggesting that the creep is still not in the final acceleration phase, as the trend gently declines towards the horizontal axis for all benchmarks. Benchmark R9 is showing biased values as it has both uplift and subsiding, so its general trend is parallel to horizontal axis. In other words, there are no accelerations and decelerations at R9 position, and its overall displacement rate is minor in comparison to other benchmarks, which is also apparent from the cumulative plot (Fig. 5). For this reason, R9 is not visualized in Fig. 6.

All linear trends are calculated using least square method. Their linear extrapolations (Fig. 6) are not ideally aligned, but all indicate failure by the end of 2023 or beginning of 2024.

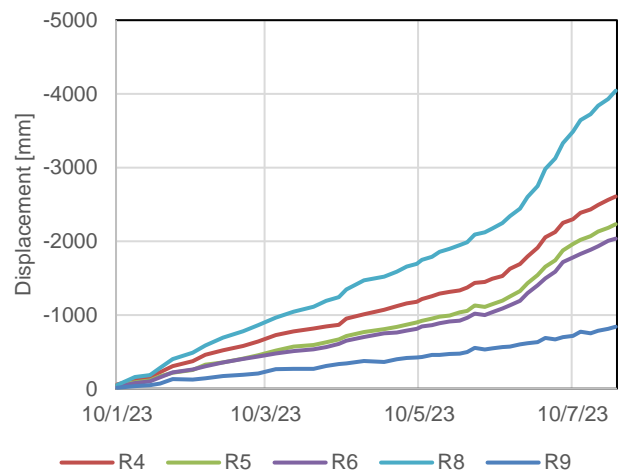


Figure 5. Cumulative vertical displacement for Jan-Jul 2023 on benchmarks R4-9.

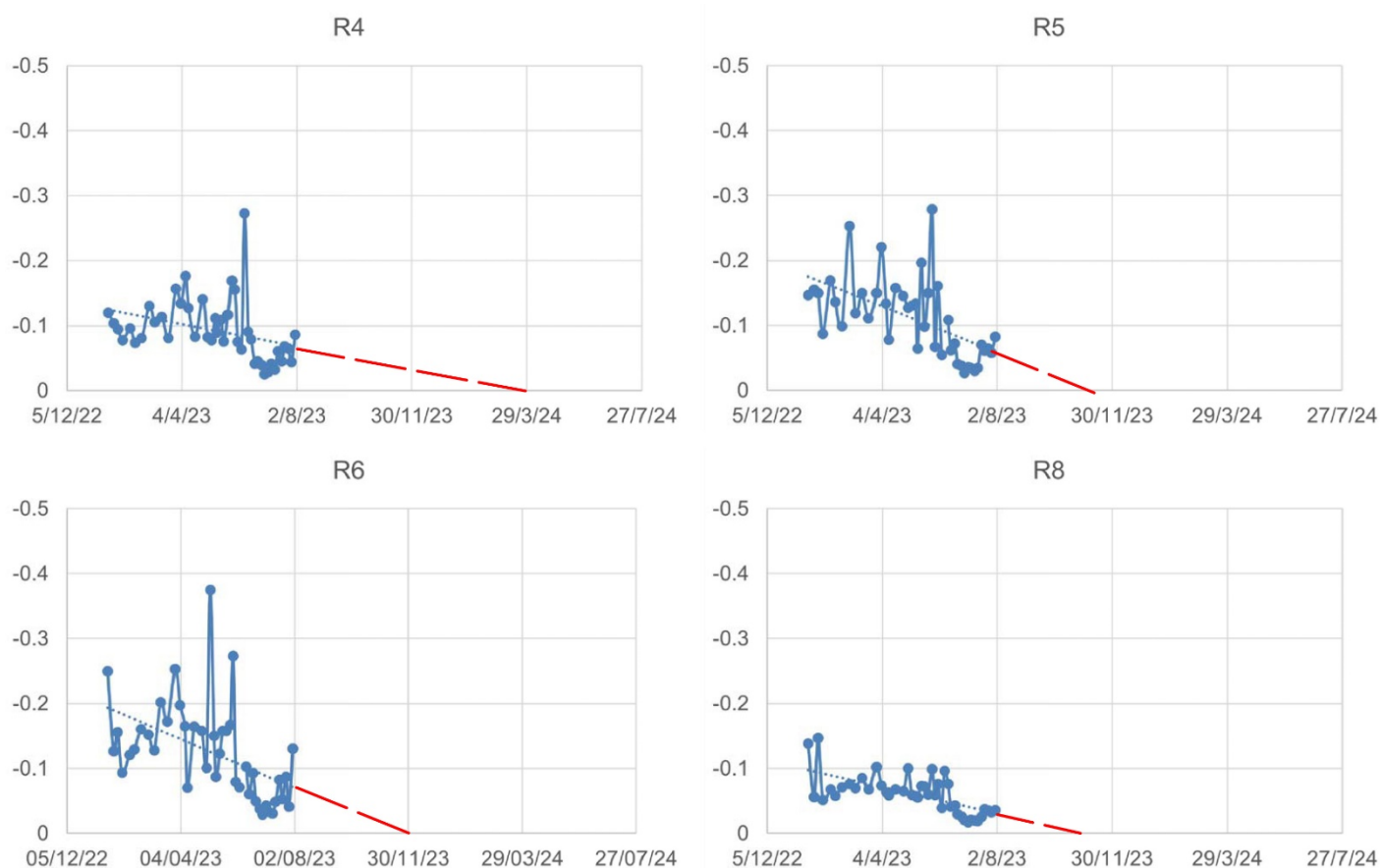


Figure 6 Inverse velocity plots of vertical displacements and extrapolated time of failure (red dashes).

As the immediate measures were undertaken to prevent further displacement acceleration (including reshaping of the slope geometry and draining), this pessimistic estimation was luckily never confirmed, although it remains a big question whether the failure would follow the estimated linear trend or curve back upward and decelerate to a new steady state, as previously seen in some examples (Carlà et al., 2018). It is likely that a simple creep mechanism cannot entirely approximate the behaviour of a large rock slope, and that other complexities and additional factors were more influential than anticipated.

Conclusion

This work describes a case study of an open pit mine and its unstable slope, which was potentially facing a global failure. With factors of safety approaching one and visually observed cracks and dislocations in the beginning of 2023, a monitoring system was engaged using several techniques, acquiring data from hourly to weekly basis. The purpose of these measurements was to determine the current state of the slope and predict further displacement behaviour. In this work, the focus was on benchmark survey, including 9 positions in total, 5 of which survived the monitoring period. All analysis showed periods of considerable accelerations, within six-month period and implied undertaking of immediate actions to increase the

slope stability. Accordingly, the slope was reshaped and drained, while further long-term stability plans were underway. The inverse velocity model was showing rather pessimistic estimation, which included a pessimistic outcome of global slope failure on 4 of 5 surveying benchmarks, by the end of 2023, while one benchmark indicated failure in March 2024. It is also important to mention that theoretically the moment of failure takes place even sooner than the trend reaches zero. Such scenarios were luckily avoided, but the analysis was used to persuade immediate actions and plan future long-term slope stability, especially in case the exploitation transits to underground excavation. Even more elaborate monitoring system is therein required, with operative early warning system installed to set alarms when thresholds are reached.

References

- Brummer R K, Li H, Moss A (2006) The transition from open pit to underground mining: an unusual slope failure mechanism at Palabora. In Proceedings International Symposium on Stability of Rock Slopes in Open Pit Mining and Civil Engineering, Cape Town. The South African Institute of Mining and Metallurgy. pp. 411-420.
- Carlà T, Intrieri E, Di Traglia F, Nolesini T, Gigli G, Casagli N (2017) Guidelines on the use of inverse velocity method as a tool for setting alarm thresholds and forecasting landslides and structure collapses. *Landslides*. 14: 517-534.
- Carlà T, Macciotta R, Hendry M, Martin D, Edwards T, Evans T., Farina P., Intrieri E., Casagli N (2018) Displacement of a landslide retaining wall and application of an enhanced failure forecasting approach. *Landslides*. 15: 489-505.
- Fukuzono T (1985) A method to predict the time of slope failure caused by rainfall using the inverse number of velocity of surface displacement. *Landslides* 22(2): 8-13.
- Hungr O, Leroueil S, Picarelli L (2014) The Varnes classification of landslide types, an update. *Landslides*. 11: 167-194.
- Read J, Stacey P (2009) Guidelines for open pit slope design. CSIRO publishing Collingwood, Australia. 495p.
- Rose N D, Hungr O (2007) Forecasting potential rock slope failure in open pit mines using the inverse-velocity method. *International Journal of Rock Mechanics and Mining Sciences*. 44(2): 308-320.
- Stewart A, Wessels F, Bird B (2001) Design, Implementation, and Assessment of Open Pit Slopes at Palabora over the Last 20 Years. In: Hustrulid, McCarter, Van Zyl (eds.) *Slope Stability in Surface Mining*. Society for Mining, Metallurgy and Exploration. Littleton, USA. pp. 177-181.
- Zhou X P, Liu L J, Xu C (2020) A modified inverse-velocity method for predicting the failure time of landslides. *Engineering geology* 268: 105521.

Geotechnical conditions of cut 5 on the highway A1, section Gornje Polje-Caričina Dolina

Lazar Jovanović⁽¹⁾, Biljana Abolmasov⁽²⁾

1) The Highway Institute, Bul. Peka Dapčevića 45, Belgrade, Serbia

2) University of Belgrade, Faculty of Mining and Geology, Đušina 7, Belgrade, Serbia

Abstract This study focuses on the Serbian Crystalline Core, a region characterized by shale formations susceptible to erosion. Recognized as a priority area for erosion control by state authorities, the region has undergone substantial soil conservation efforts. The research investigates slope 5 on highway A1, section Grdelica- Vladičin Han, impacted by landslides triggered not only by construction activities but also by erosive rainfall affecting the vulnerable shale formations. The slope's instability prompted state intervention, leading to three sets of structural reinforcements, each consisting of two rows of piles. Post-mitigation monitoring, including inclinometer readings, indicates no further movement. The study provides a comprehensive analysis of the geological and geotechnical aspects, rainfall-induced erosion, and the effectiveness of mitigation measures.

Keywords slope stability, landslide, Serbian Crystalline Core

Introduction

Located within the Grdelica Gorge (Figure 1), a critical juncture in European corridors linking Central Europe to Athens, this region faces erosion challenges, prompting its designation as a priority zone for erosion control. According to Engineering-geological basis for the general plan of the Grdelica Gorge and Vranje Valley (1956), the historical impact of geological processes on transportation infrastructure was exemplified by the 1948 traffic disruption through the Grdelica Gorge for 14 days.

The A1 highway section, specifically Grdelica – Vladičin Han, LOT 1: Gornje Polje – Predejane Tunnel, witnessed landslide activation in cut 5 in October 2014, affecting planned retaining walls 12 and 14. Remediation efforts included implementing a supportive structure featuring two rows of micro piles with two levels and anchor tensioning. Further geotechnical investigations in 2018-2019 informed the design of a new supportive structure using reinforced concrete piles (K1), and subsequent studies in 2019 defined parameters for two additional structures (K2 and K3).

To comprehensively understand the geological and geotechnical characteristics, various investigations were conducted. Geodetic terrain surveying and mapping provided a detailed topographical overview. Investigative

drilling involving 96 boreholes with a total depth of 2358.5 m offered insights into subsurface conditions. Geophysical investigations encompassed 5 profiles covering 1295 m, contributing to a better understanding of geological features. Geotechnical monitoring involved the installation of 45 inclinometers and 25 piezometers to monitor ground movements and water table fluctuations. Additionally, geodetic field observations at 26 locations and surface measurements of characteristic points on the slope face provided valuable data for assessing terrain stability. Laboratory testing included the analysis of 217 samples, contributing to a comprehensive understanding of material properties and supporting geotechnical assessments.

With these extensive investigations, the study aims to conduct a detailed analysis of existing research results to define the geotechnical model of the landslide zone. This involves specifying geometric characteristics, groundwater conditions, spatial distribution, mutual relationships of engineering-geological elements, and the mechanism and dynamics of sliding. The study concludes that implemented remediation measures are adequate for ensuring seamless traffic on the A1 highway. The slope remediation plan is phased to ensure the stability of the future highway and enhance overall slope safety, including the alignment, in subsequent phases.



Figure 1 Geographical location of Grdelica Gorge

Field conditions

The broader research area belongs to the Serbian crystalline core. Cvijić (1924) referred to this terrain as a sizeable ancient core around which smaller mountains formed and attached to the old mass. A part of this formation constitutes the Vlasina Complex. The Vlasina Complex, to which the lower part of the research area belongs, originated as a volcano-sedimentary association formed on the periphery of an island arc. The rock masses underwent metamorphism during the Lower Carboniferous, resulting in the formation of green shale facies. The thickness of crystalline shales reaches up to 5 km. The minerals that make up the shale of the wider research zone are albite, chlorite, and muscovite. Orogenic movements before the Permian broke the crystalline shales, creating a "parquet" relief block structure. This block structure facilitated further development of epirogenic Tertiary and Quaternary movements. Two solid domes, Vljajna to the west and Oštrozub to the east formed, uplifting the space between them through epirogenic uplift movements. Under conditions of significant lateral compression, blocks descended along discontinuities, forming basins, among which is the Grdelica Gorge.

Within these discontinuities are related to rhyolite breakthroughs within the Surdulica granodiorite massif. The fractures to which the breakthroughs are connected stand out in two zones: they start west of Čemernik and merge into one near Predejane, which runs through the valley of South Morava. Movements along these dislocations have been restored, therefore the rhyolites are significantly damaged. The seismic zone within the research area requires extra caution in the design process due to the potential impact of earthquakes.

During the Oligocene-Miocene period, tectonic basins formed within the current domain of the South Morava Valley. The Miocene transgression transformed the Grdelica Basin into a lake. The Pliocene lake levels served as the erosion base for rivers incising during the Quaternary. The Morava River inherited its lake-shaped form, which was shaped depending on the structure. Within the Basic Geological Map of Vlasotince (1966) (Figure 2), environments related to the fluvial processes of the South Morava are distinguished – alluvium and three river terraces. Vertical movements are still active in this area today, resulting in very intense erosion.

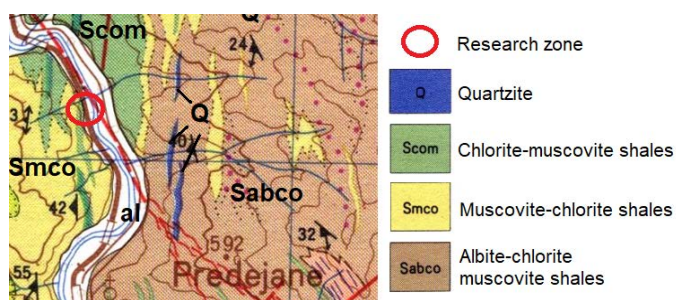


Figure 2 Part of the Basic Geological Map of Vlasotince

In the Grdelica Gorge area, covering an area of 3000 km², 5737 active gullies have been recorded, ranging in length from 100 to 200 meters and depths from 1 to 20 meters. According to data from 1955, 760 active and 140 dormant landslides were documented. Due to these challenges, the Directorate for Erosion Control in Serbia prepared a comprehensive plan for developing Grdelica and Vranje basins (1956). Despite steep slopes and intense rainfall, the plan recognized that areas with preserved forests, showed minimal signs of erosion. Accordingly, afforestation measures were implemented, and ravines were lined with large blocks to prevent further erosion.

After the initial incision of slope 5, through engineering-geological mapping of the open parts of the slope and the area above it, the presence of the following contemporary geodynamic processes was identified: surface weathering, gullying, and sliding.

Landslide description

Long-term processes led to a rapid decline in safety factors over time. Initially, the surface weathering of parent rocks created conditions for further activity. Excessive and average rainfall weakened the physical and mechanical characteristics of the terrain surface and eroded at the bottom of the slope during the South Morava River. Through an analysis of topographic maps suggesting subtle signs of the landslide toe, later confirmed by drilling activities with GBK-1 borehole, where older shale layers above alluvial deposits and strata inversion provide conclusive evidence, it becomes evident that the studied area corresponds to a paleo landslide (Figure 3).

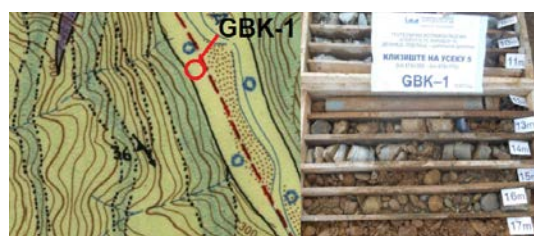


Figure 3 Evidence of paleo landslide

The combined effects of slope incision in cut section 5 and heavy atmospheric rainfall, leading to a 2 m increase in the water level of the South Morava River, resulted in the reactivation of colluvial processes in initial zone (Figure 4).



Figure 4 Initial zone

According to Geotechnical report on the results of supplementary investigations on the slope 5 section (2015), the activated landslide is characterized by translational movement and numerous tension cracks, with 100 m in length and width. The maximum surface of rupture is 6 m, and the movements are planar along the contact between debris and shale. The landslide covers an area of 7.000 m², with a total volume of 25.000 m³. After the construction of supporting structures (walls 12 and 14) and the implementation of micropiles in the active landslide zone, movements in this area were significantly reduced. However, as determined by subsequent geodetic measurements, the landslide continued to expand towards the left wing, covering an area five times larger than the initial landslide. In that zone, within the inclinometers Ipb-13 and GIK-7, movements were observed at depths of 15, and 17 meters (Figure 5).

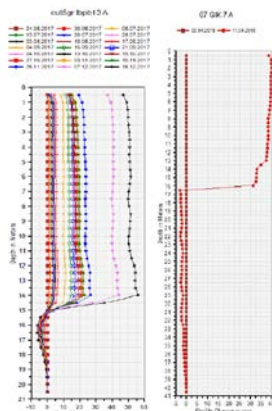


Figure 5 Inclinometer readings of Ipb13 and Gik-7

Analyzing the results of the Report on conducted supplementary geotechnical field investigations and laboratory tests of slope no. 5 section (2018, 2019), landslide has been categorized into three zones: source area (beneath the frontal scarp), main body (beneath the secondary scarp), and accumulation area. Landslide zones with scarp images and ERT-4 geophysical profile are shown in Figure 6.

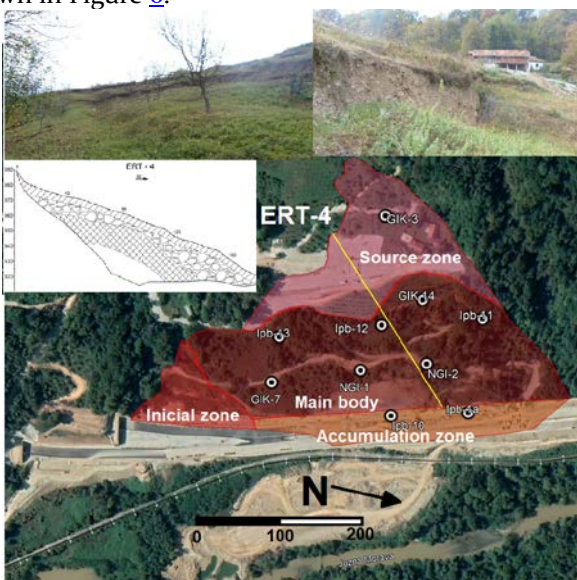


Figure 6 Landslide zones with scarp images and ERT-4

The frontal scarp is 3,5 m high. Within the source area, Quaternary deposits are 17,5 m thick, formed by diluvial processes and sedimentation within the highest third river terrace. Besides the Quaternary deposits, inclinometer movements are within completely altered shales, reaching a depth of 25,5 m. The dimensions of this zone are 300 m in width and 110 meters in length, resulting in an area of 20.000 m². The core of the borehole GIK-3 is shown in Figure 7.



Figure 7 The core of the borehole GIK-3

Two secondary scarps, a meter in height, have been observed in the middle of the active slope. Their continuation at greater depths is noticed within the inclinometer borehole GIK-14, 12, and 15 m; Ipb-12 13, and 16 m and Ipb-11 17, and 19 m (Figure 8).

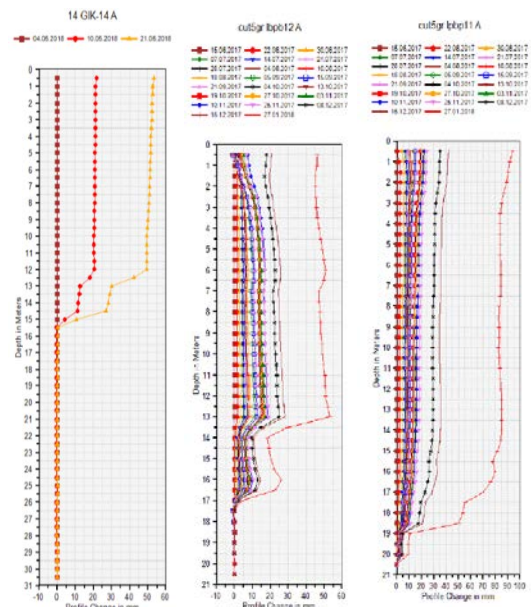


Figure 8 Inclinometer readings above two secondary scarps

In the central part of the main body, two movement zones converge into one. Here, the deepest surface of rupture was measured within the NGI-2 inclinometer at a depth of 21 m. To determine if the highway is affected by sliding, the ipb10 and ipb11 inclinometer, installed directly above the planned route, provides an answer.

Inclinometric measurements revealed movements at 18 m depth, indicating the presence of the landslide in the highway zone at a depth of 7 m. The inclinometer readings above the planned route are shown in Figure 9.

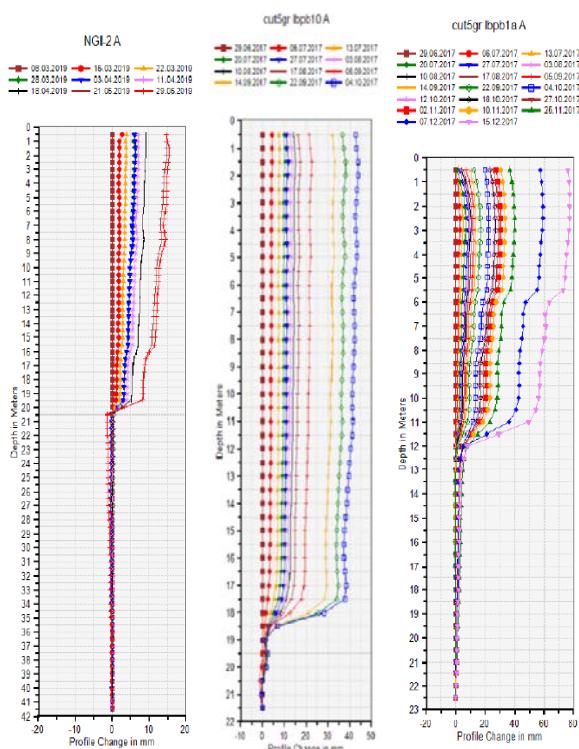


Figure 9 Inclinometer readings above the planned route

The depth of the landslide surface of rupture is 25.5 m, which is classified as a moderately deep landslide according to IAEG classification. The affected area is approximately 75 000 m², and the mobilized material volume is 875 000 m³. Based on these parameters, the landslide belongs to the large landslides (IAEG) group. With a slope angle of 23-28°, the landslide belongs to slopes of moderate inclination. In horizontal projection, the shape of the landslide is isometric. Regarding the material type, the landslide predominantly consists of moistened debris in a clayey matrix. The location of the landslide is above the erosion base. The development of the process occurred in two directions: towards the left wing and above the initial one. According to the IAEG classification based on the manner of enlargement, it belongs to the retrogressive group of multiple landslides. Movement occurred in zones of totally altered shales where movements are mixed translational and rotational.

The geotechnical model

Considering the composition and determined properties of the identified geotechnical environments, a stability analysis for the limit equilibrium state ($F_s=1$) was conducted using the Morgenstern-Price method. The terrain model at the moment of instability occurrence was analyzed under increased moisture conditions, with water in the terrain represented by the pore pressure coefficient

depending on the geotechnical environment. The geotechnical model of the main body at the moment of activation is illustrated in Figure 10. The resulting shear angle is 28°.

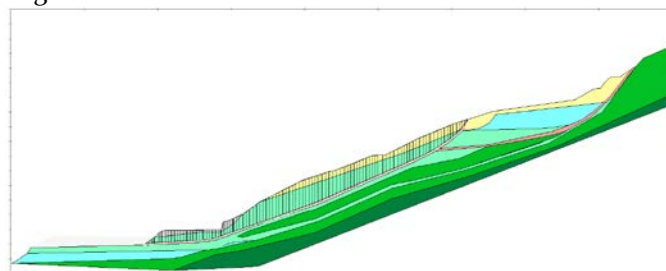


Figure 10 Geotechnical model of the main body

By activating the main body, conditions for activating a landslide along the slope (source area) had been created. The already affected terrain has been included in the stability analysis as a point load. The geotechnical model in the source body at the moment of activation is illustrated in Figure 11. The angle of the activated landslides shear is 23°.

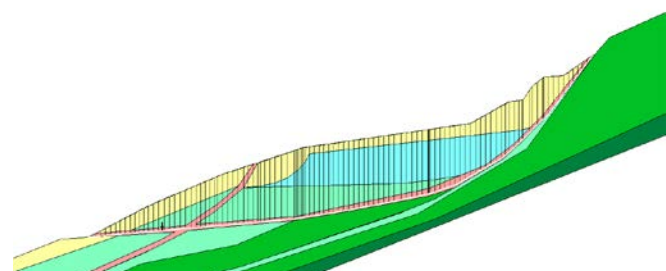


Figure 11 Geotechnical model in the source area of landslide

These calculations were performed with a defined surface of rupture using parameter values for the identified lithological units, as given in Table 1.

Table 1 Values of parameters for lithological units

Lithological units	Cohesion	The angle of shearing
Compact shales	350 kPa	40°
Altered shales	200 kPa	34°
Totally altered shales	10 kPa	28°
Alluvial deposits	10 kPa	22°
Diluvial deposits	15 kPa	21°
Embankment	0 kPa	35°

Under identical conditions, except that the totally altered shales have a cohesion of 5 kPa in the sliding zone, stability analysis was conducted for the possibility of landslide activation with the deepest surface of rupture using the Morgenstern-Price method. The geotechnical model for the deepest possible surface of rupture is shown in Figure 12. The obtained Factor of Safety for the landslide with the deepest surface of rupture is 1.25. Since the safety factor is less than 1.4, this option must also be considered for remediation.

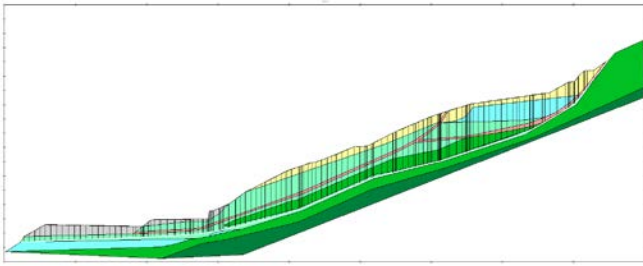


Figure 12 Geotechnical model for the deepest surface of rupture

Landslide remediation

The landslide remediation and slope stabilization solution was carried out in phases. In the first phase, a new structure, K₁, was constructed to ensure the stability of the future highway and the surrounding terrain. In the second phase of the work, according to the project task, it is necessary to stabilize the entire slope above the K₁ structure by implementing the K₂ and K₃ structures and other stabilization measures to increase the stability factor of the K₁ structure and the entire slope. The position of remediation structures are shown in Figure 13.

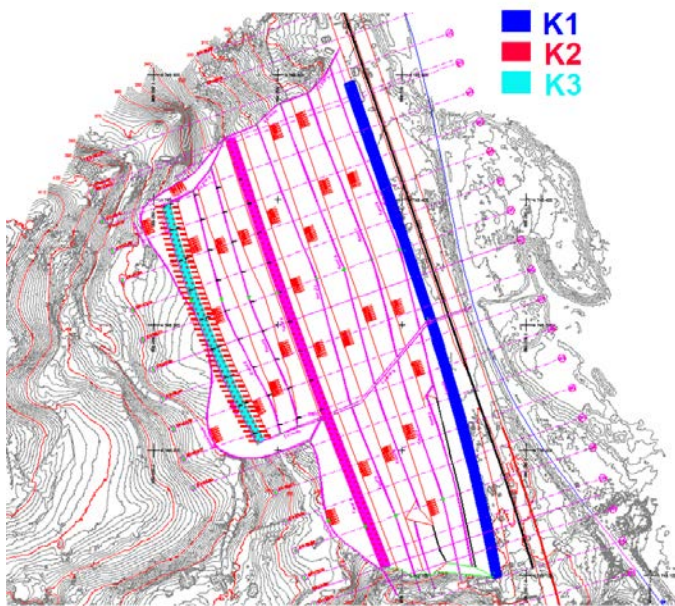


Figure 13 The position of remediation structures

In the first phase of landslide remediation, the construction of structure K₁ is planned for 411.48 m, aimed at partially stabilizing the slope with a safety factor 1.2. The construction works for structure K₁ consist of two rows of drilled piles with a diameter of Ø 1500 mm, totaling 181 piles. The length of the piles for structure K₁ is 16.18 or 20 m, depending on the position and the condition to ensure a minimum foundation depth of 5 m in altered shales zone. The upper and lower rows of piles are spaced at an axial distance of 4.5 m. All piles are connected by a head beam (slab) with a thickness of 1.2 m and a width of 6 m.

Additional stability of structure K₁ is provided by two rows of electro-insulated pre-stressed anchors with a length of 20+15=35 m and a load capacity of 1075 kN. The construction project includes the installation of 361 anchors, with their length at the anchor head being 15 m., A wall with a height of 5.92 m is constructed on the slab, with buttresses every 2.25 m of the wall's length. The main body profile with structures K₁, and K₂ are shown in Fig 14.

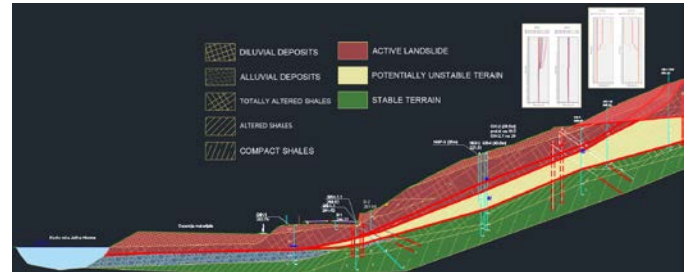


Figure 14 The main body profile with structures K₁ and K₂

In the second phase of landslide remediation, the construction of structure K₂ is planned to protect the main body area, while structure K₃ aims to halt movement in the source zone. These structures consist of two rows of alternately installed Ø 1500 mm piles. The piles are designed at a spacing of 4.50 m. The length of the piles for Additional stability for retaining structures K₂ and K₃ is provided by permanent 863 electro-insulated geotechnical anchors. The source area profile with K₃ structure are shown in Figure 15.

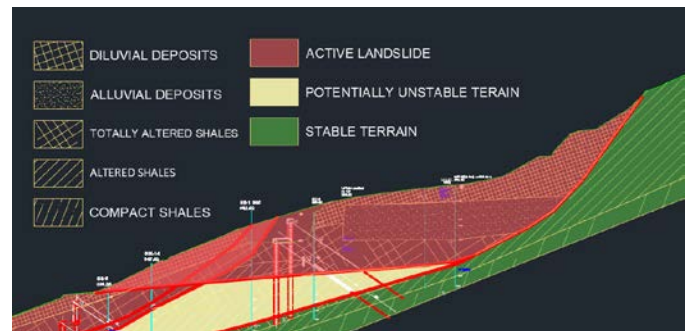


Figure 15 The source area profile with K₃ structure

After constructing structures K₂ and K₃, a final treatment of the slopes behind structures K₂ and K₃ is planned as an additional remediation measure, including installing protective erosion control mesh, which serves as a good basis for surface greening. The remediation measures are executed at greater depths than the deepest sliding surface. By inclinometer measurements and geodetic measurements of markers within the structures (2019), it was determined that the landslide had been stabilized. According to Integral inženjering (2024) the cost of landslide remediation is 35.6 million euros. The remediation is shown in Figure 16.



Figure 16 Landslide remediation

References

- Civil Engineering Institute Macedonia (2018) Highway E-75, Belgrade - Niš - border with the Republic of North Macedonia, LOT 1: Gornje Polje - Caričina Dolina, km 873+719.94 - km 885+522.78, Report on Conducted Supplementary Geotechnical Field Investigations and Laboratory Tests of Slope No. 5 Section.
- Civil Engineering Institute Macedonia (2019) Highway E-75, Belgrade - Niš - border with the Republic of North Macedonia, LOT 1: Gornje Polje - Caričina Dolina, km 873+719.94 - km 885+522.78, Report on Conducted Supplementary Geotechnical Field Investigations and Laboratory Tests of Slope No. 5 Section.
- Cvijić J. (1924) Geomorphology I. Vasiljević M. Serbian Academy of sciences and arts, Knez Mihajlova 35, Belgrade. 585p.
- Federal Geological Institute (1966) Basic geological map 1:100,000, sheet Vlasotince K 34-45 with Explanation.
- Highway Institute (2015) Highway E-75, Section: Gornje Polje - Predejane, LOT 1, Geotechnical Report on the Results of Supplementary Investigations on the Slope 5 Section, from km 879+350 to km 879+775.
- Institute for Geological and Geophysical Research, Department for Engineering and Hydrogeology, (1956) Engineering-geological basis for the general plan of the Grdelica Gorge and Vranje Valley.
- Integral Engineering (2019) Highway E-75, Belgrade - Niš - border with the Republic of North Macedonia, LOT 1: Roads and Bridges from Grdelica to Predejane Tunnel, Geodetic Report on Monitoring of Structure K1 on Slope No. 5 Section.
- Integral inženjering (2024) Execution of Works on the New Remediation of Cut Section 5 from km 879+350 to km 879+775 as Part of the Highway Construction Project E75, Section: Grdelica (Gornje Polje) - Caričina Dolina, LOT 1: Roads and Bridges from Grdelica to Predajane Tunnel (Serbia) URL: <https://integral.ba/izvodjenje-dijela-radova-na-novoj-sanaciji-usjeka-5-od-km-879350-do-km-879775-u-sklopu-projekta-izgradnje-autoputa-e75-dionica-grdelica-gornje-polje-caricina-dolina-lot-1-put-i-mosto/> [Last accessed: 02.14.2024].

Second phase of Landslide stabilisation on Cut 3, LOT 1, Motorway E75, section Gornje Polje – Caričina dolina

Marina Janković^{(1)*}, Marija Bakrač⁽²⁾

1) WOLF PROJECT d.o.o., Belgrade, Kraljevačka 64, Serbia, +381 60 7001 248 (marina.jankovic357@gmail.com)

2) GEOESTETIKA d.o.o., Belgrade, Serbia

Abstract Landslide stabilization works in the zone of Cut 3 were divided into 3 phases. The scope of this paper is to provide detailed information on the Phase 2 of the designed stabilization measures. These works consisted of constructing the Reinforced Soil Embankment (RSE), up to 12.5 m height in the zone of the toe of the landslide. The embankment contributed to the stabilization of the slope as a ballast, as well as redistribution of the mass after the excavation necessary for the road deviation. The design envisaged the use of flexible geogrid which had to be manufactured from high-modulus polyester (PET) yarns with low creep by knitting production technique. The construction of the piles over which rockfill and concrete have been placed up to a height of 5.8 served as stable foundation for the RSE. After the execution, Reinforced Soil Embankment increased safety factor against sliding of the Cut 3 and, due to its flexible type of construction, complex geometry that fits very well into natural surroundings has been achieved. The paper also gives a short overview on related literature and explains the beneficial effect of a high alignment capacity of reinforcement products on the performance of the composite material “reinforced soil”.

Keywords landslide, slope stabilisation, flexible geogrids, interaction flexibility, geosynthetics.

Introduction

During the execution of works on the E-75 highway, Belgrade-Niš - the border with FYR Macedonia, on section Gornje Polje - Caričina Dolina, LOT 1, on the Cut 3 from km 876+325 to km 876+825 there was a violation of the stability of a conditionally stable slope that jeopardizes the highway route (Fig.1). By analyzing the results of observing the geodetic benchmarks on the slope, as well as the results of the observation of the displacement in the inclinometer constructions, it can be said that it was a huge landslide with a complex slip mechanism. The sliding process involves the surface sediments, as well as the deeper areas within the shale. Landslide stabilization works in the zone of Cut 3 were divided into 3 phases.

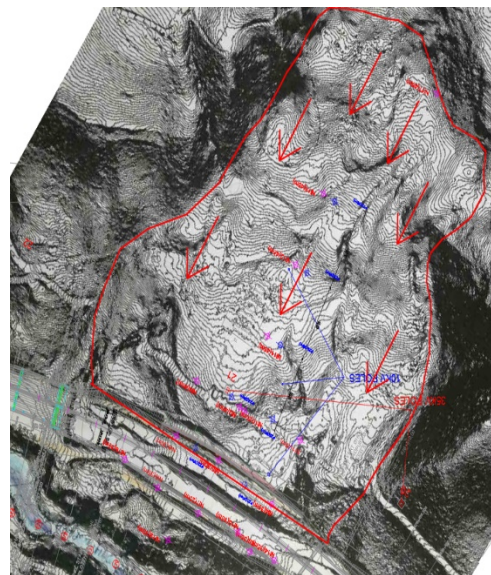


Figure 1 Landslide on the Cut 3

Stabilisation works Phase I

Within the Phase 1 of works for landslide stabilization in the zone of CUT 3 – LOT 1, works on the excavation of the terrain behind the existing structure of micro-piles and works on the surface drainage are foreseen. The excavation works envisage considerable relief of Cut 3, which will greatly contribute to the stabilization of the slope, and the development of surface drainage will provide lower groundwater level.

The design envisaged the construction of transversal drainage trenches (channels) of two different types in several layers and perimeter channel. Also, on every newly formed berm, the precast concrete channels for collecting atmospheric waters has been constructed.

Stabilisation works Phase II

Within the Phase II of works for landslide stabilization in the zone of CUT3 - LOT1, works on the stabilization of the landslide toe in the zone of the left bank of the South Morava River, in the length of 300,50 m, from km 3 + 592 to km 3 + 900.35 (along the axis of the river), or from km 876 + 739,23 to km 876 + 485 (along the axis of the highway) were foreseen. These works consisted of constructing the Reinforced Soil Embankment, up to

12.5 m height in the zone of toe of the landslide. The embankment contributes to the stabilization of the slope as a ballast, as well as redistribution of the mass after the excavation necessary for the road deviation.

As the river is very near the embankment, the embankment was founded on the construction of the piles over which rockfill and concrete were placed up to a height of 5.8 m as a measure to improve the weak subsoil. In this way, a stable base for the embankment was made. The height of the embankment is 10,5-12,5 m, up to the level of the road.

The protective structure from piles has been performed from two rows of bored piles Ø900 mm, 15 m long, on a distance of 2.5 m, transverse and longitudinal. The piles have been connected with a pile cap beam of dimensions 5,0 x 1,0 m and 300,50 m long. Working dilatations on the pile cap beam is on every 9-12 m.

The reinforced concrete wall of 3 m high and a width of 80 cm, has been constructed over the pile cap beam. The face of the wall is vertical, while on the back it is in an inclination of 10: 1. Behind the wall s a rockfill in concrete in layers have been placed, up to a full height of 5.8 m. For rockfill in concrete, a stone of fractions of 50-100 cm swere used, and filling of caverns between the rock was done by concrete C25/30. The alignment of the protective structure and RSE can be seen on Fig 2.



Figure 2 Alignment of the RSE on top of protective structure

Reinforced Soil Embankment with high flexible PET geogrids

The embankment from reinforced soil has been constructed with a green face in the slope of 60° after the completion of the works on the protective structure from piles and rockfill in concrete. The embankment was constructed using material from the local excavation from Cut No.3 for which laboratory tests have been carried out to prove the material is suitable for the construction of the reinforced soil embankments. The filling were placed in layers up to a maximum of 30 cm, until the total height of the layer is 60 cm, after which the corresponding row of the high flexible PET geogrid has been placed, and this procedure repeated until the full height of the embankment is reached. For this type of construction, compaction of 98% of dry bulk density is required.

The construction of the embankment can be done in a classic way except in the zone od 1.5 m behind the embankment face with spreading by the lightweight bulldozer and compaction with the smooth vibration roller of maximum 8 tons in weight, in layers up to maximum 30 cm. In the zone 1.5 m behind the embankment face, spreading shall be done by hand in 30 cm thick layers. The main compaction will be done by 40/50 cm wide vibration plate near the embankment face. After stabilizing the material, 60/70 cm wide vibration roller of a maximum weight of 1 tone can be used.

The design envisages the use of flexible geogrid which has to be manufactured from high-modulus polyester (PET) yarns with low creep by knitting production technique. According Stability calculations, geogrids with long-term design strength of 34kN/m – 64 kN/m were used. Required length of geogrids varied between 9-12 m. On the face of the embankment, the geogrid has been folded and anchored inside the embankment.

Considering that high embankment was designed on a stabilised landslide, design adopted green facing as the most favorable type of finish for the RSE slope. In general, if there is sufficient available space, green facing is the most flexible and economically advantageous way of finishing RSE slope.

The use of flexible geogrids ie. geogrid without memory effect was of great importance in order to perform the designed geometry of the reinforced embankment with maximum precision and quality. In this way, the construction time of the reinforced embankment is reduced by 30-50% and thus the construction costs by >20% compared to RSE with stiff geogrids.

Importance of Interaxtion Flexibility

It is the general understanding that the three main characteristics of geosynthetic reinforcement products, which dominate the performance of the compound material “geotextile reinforced earth”, are the tensile strength, tensile modulus as well as the interaction behavior with the soil.

Interaction behaviour is capability of the geogrid to take forces from the soil and to transfer forces into the soil.

Different publications report on research results regarding the different geosynthetic characteristics influencing the interaction behavior such as geometrical factors, mechanical factors, and adaptability of the geogrid to the soil and all it's particles of a different sizes and shapes. Contribution of geogrid geometrical proprieties were analyzed for more than 20 years, by for example Sarsby (1985th) and Zigler and Timmers (2004th). The importance of geogrid crossmembers and its contribution the pull-out behavior has been emphasized in various papers. The influence of the surface roughness has been noticed and analyzed already at the early days of geosynthetics by Schlosser and Elias (1978th). They found direct correlation between surface roughness and transfer of shear stresses from the soil to the geogrid, so the higher surface roughness the better transfer of shear stresses.

O'Rourke et al (1990) concluded that harder surface of geosynthetic decreases shear strength at the contact between geosynthetic and soil. Several other researchers found that increased flexibility and surface friction of geogrids have positive influence on the interaction between geosynthetic product and soil. So it can be said that geosynthetic products with higher Interaction flexibility have better interaction with soil. Positive contribution of Interaction flexibility can be simply explained by Euler Effect as shown on the Figures 3.

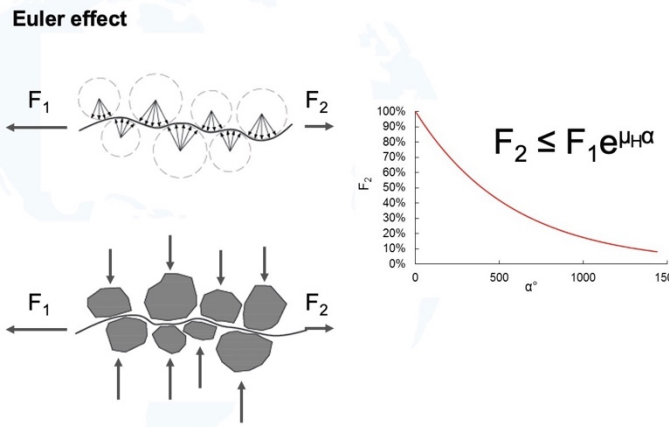


Figure 3 Euler Effect and Interaction flexibility of geogrids

Flexible geogrids allow denser compaction of soil, which results in larger contact surface between geogrid and soil and better transfer of the shear forces among them. This can be explained by the Euler-Eytelwein formula shown on the Figure 3 in which force F₂ can be balanced with smaller force F₁ due to contribution of friction over contact surface between rope and for example bar or coil. Lower value of Flexural Rigidity of geosynthetic product means higher Interaction Flexibility.

Flexural Rigidity of geosynthetic products can be measured according to ASTM D7748 Standard Test Method for Flexural Rigidity of Geogrids, Geotextiles and Related Products.

Stability Analyses

Stability analysis of slope and protective structure is performed in phases of work execution. Phases are modeled according to the technology of work execution.

For the purposes of the stability analysis, additional geotechnical investigations were performed. Based on the results of these investigations, a geotechnical profile on km 876+625.0 was created. The level of the sliding surface, underground water and layers of soil/rock is imputed in the calculations exactly as the ones measured really. Since there was no laboratory testing in the additional geotechnical investigations, soil parameters that were used for calculations are taken from the original geotechnical report from the main design of Highway. Residual strength parameters for the sliding surface are determined by back analysis search for the safety factor of Fs=1.0 in the phase of excavation for the Highway, which

is in accordance with the phase when the sliding started. According to the used methodology, the obtained values for a sliding surface layer and parameters for other layers are presented in Table. 1.

Table 1. Soil/Rock parameters used for the calculations

Material	γ [kN/m ³]	φ [°]	c [kPa]
S***	22	27	15
S**	24	27	25
S*	26	40	100
Ka	22	19	0

An analysis of internal stability was performed to define the characteristic geometry and type of the geogrid.

This analysis was carried out in accordance with the Recommendations for the design and analysis of reinforced earth constructions - EBGEO [1] and DIN 1054 (1976) [2]. The GGU Stability software is used. To ensure sufficient stability, the degree of exploitation is required η ≤ 1. As a seismic load, the horizontal acceleration kh = 0.15 was taken.

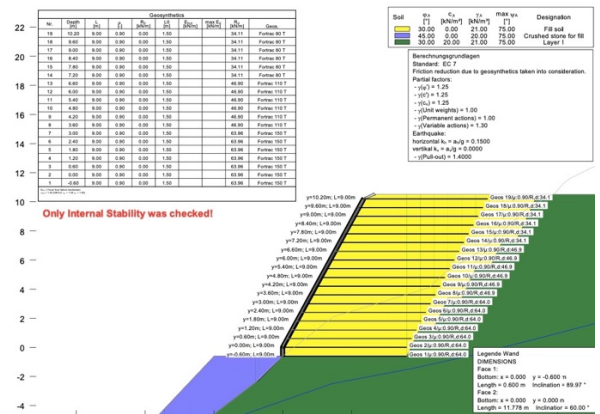


Figure 4 Internal Stability Calculation Results

The maximum coefficient of utilization μ = 0.88 was obtained during the internal stability check using the Vertical slices method for the combination of permanent+variable+seismic loads. The minimum required geogrid length of 9.00m was obtained.

The results of the combined and global stability analysis gave slightly higher minimum required lengths of the most heavily loaded geogrids. The maximum coefficient of utilization μ = 0.98 was obtained by calculation according to Bishop, also for the load combination that includes seismic.

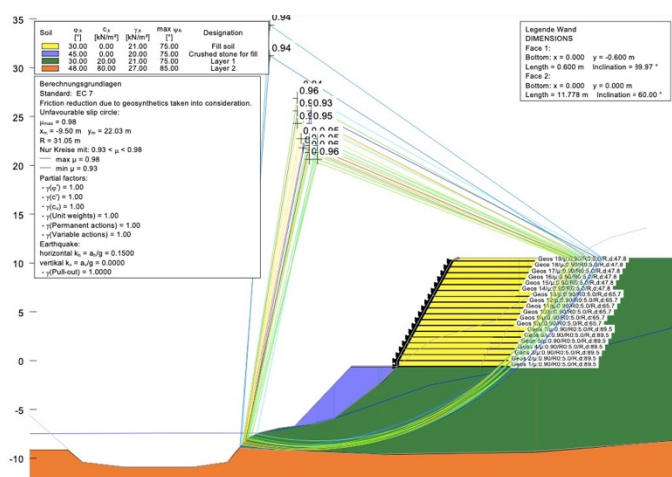


Figure 5 Compound Stability Calculation Results

Three different types of geogrids are adopted, with design tensile strengths ($R_{B,d}$) of min 64kN/m, 47kN/m and 34kN/m, and lengths varying from 9m-12m.

In accordance with EB GEO, the Design tensile strength $R_{B,d}$ is obtained by reducing the nominal tensile strength $R_{B,k0}$ by partial factors A_1 - A_5 related to the specific geogrid, and a partial safety factor.

$$R_{B,d} = R_{B,k0} / (A_1 * A_2 * A_3 * A_4 * A_5 * g_M)$$

The greatest influence on the tensile strength of a certain type of geogrid for a design life of 60 or 100 years has the partial creep factor A_1 . Fortrac T geogrids with which the designer performed stability calculations have partial creep factors certified by BBA as well as in accordance with ISO/TR 20432, for different design lives and for different temperatures

An analysis of global stability of the embankment and the protective structure is also performed in phases of work execution according to the technology of work execution. The calculation is performed in FEM software Plaxis 2D. This calculation is based on the finite element method, using an incremental iterative process. As this construction is linear it is justified to analyze it in a cross section in the conditions of a flat state of deformation. The stability factor in the Plaxis 2D program was obtained according to a process called Phi-C Reduction, which was adopted as very good for this type of calculation. For the purposes of this design, one characteristic cross section in the Plaxis 2D program was modeled. After analyses, based on obtained values of safety factors for sliding it can be concluded the proposed and analysed measures with the protective structure and the embankment are satisfactory.

Construction of Reinforced Soil Embankment

Backfilling was done in soil layers up to a maximum of 30 cm, until the total layer thickness of 60 cm was reached, after which the corresponding geogrid was placed and the procedure was repeated until the full height of the embankment was reached. The embankment layers were compacted until a compaction of at least 95% of dry soil

density was achieved. The construction of the embankment was done in usual way, except in the 1.5 m zone along the face of the embankment, where fill soil was spread with a light bulldozer, compacted with a vibrating smooth roller weighing a maximum of 8 tons, in layers of a maximum of 0.30 m thickness.

In a zone up to 1.5 m wide from the face of the embankment, spreading was done manually in layers up to 30 cm thick. Primary compaction was done with a 40/50 cm wide vibrating plate directly next to the face of the slope of the embankment, and once the soil was sufficiently stabilized, a light vibrating roller with a width of 60/70 cm and a maximum weight of up to 1 ton was used.

In addition to the Fortrac T geogrid, whose type and length were determined by stability calculations and which were installed perpendicular to the direction of the embankment with 20 cm overlaps, a protective geogrid type HaTe 23.142 GR was installed on the face of the embankment as erosion protection layer, which can be seen in Figure 6.



Figure 7 Installation of geosynthetic materials

The design has envisaged the green face of the embankment. Greening of the face was achieved by the installation of a mixture of humus, appropriate mixture of seed for planting and filling material in the thickness of 20-30cm along the face of the embankment to allow the vegetation growth.

Various mixtures of seeds should be selected depending on exposure to sun, soil, altitude and precipitation. Help of local vegetation specialist was recommended as always in similar cases.

The final aesthetic appearance of the reinforced soil embankment is completely integrated into the surroundings, Figure 7.



Figure 7 Finished RSE with green facing

Stabilisation works Phase III

Within the Phase III of works for landslide stabilization in the zone of CUT₃ - LOT₁, works are estimated on stabilization of existing support structure on the right side of right half profile, in the length of 300,50 m, from km 3 + 592 to km 3 + 900.35 (along the axis of the river), or from km 876+525 to km 876+725 (along the axis of the highway). These works consist of constructing additional pretensioned anchors, RC beams which are positioned as stiffeners on the slope berm, under the existing structure, gabion wall on the platform above the berm and additional drainage hole.

Conclusions

An embankment built using locally available soil that would otherwise end up in a landfill with all the costs and negative impacts that this brings, reinforced by high strength PET geogrids with very high Interaction Flexibility became instead an integral part of Landslide Stabilization measures. Reinforced Soil Embankment with a green facing due to the flexibility of its structure is also a very good choice in areas where foundation settlements can occur same as in the areas with high seismic activities.

References

- Deutsche Gesellschaft für Geotechnik, Recommendation for Design and Analysis of Earth Structures using Geosynthetic Reinforcement-EBGEO (2011), Translation of 2nd German Edition DIN 1054 (1976)
- Sarsby, R.W. (1985): The Influence of Aperture Size/Particle Size on the Efficiency of Grid Reinforcement. 2nd Canadian Symposium on Geotextiles and Geomembranes, Edmonton, Canada
- Schlosser, F.; Elais, V. (1978). Friction in reinforced Earth. Proceedings ASCE Symp. Earth Reinforcement, Pittsburgh
- Ziegler, M., Timmers, V. (2004). A new approach to design geogrid reinforcement. EuroGeo3, München
- O'Rourke, T.D.; Druschel, S.J.; Netravali, A.N. (1990). Shear strength characteristics of sand-polymer interfaces. Journal of geotechnical engineering, Vol. 116

On the Performance and Related Design Considerations of Geosynthetic Reinforced Soil Structures under Seismic Conditions

Ehsan Bordbar^{(1)*}, Viktor Poberezhnyi⁽¹⁾, Thomas Hasslacher⁽¹⁾, Marija Bakrač⁽²⁾

1) HUESKER Synthetic GmbH, Gescher, Fabrikstrasse 13, Germany, + +492542 701-311 (bordbar@huesker.de)

2) GEOESTETIKA D.O.O., Cetinjska24, Beograd, Serbia

Abstract This paper focuses on the methodology of geosynthetic reinforced soil (GRS) used in the construction of retaining structures in seismically active regions. The use of GRS in the construction of steep slopes, retaining walls and bridge abutments is well established with many successful examples around the world. These structures show favourable performance under complex boundary conditions such as extremely dynamic loads. Compared to conventional retaining walls, GRS resist seismic loads with less deformation and less risk of failure due to their flexible and ductile nature. Seismic shake table tests on a block wall reinforced with woven geogrids were carried out by Ling et al. (2003). The test setup, program and main results of this study are summarised. The second part is devoted to the seismic geotechnical design of GRS. Established design approaches are presented and the normative requirements of Eurocode 7, Eurocode 8 and some national annexes are outlined. The paper concludes with two case studies in seismically active regions.

densely populated urban areas or mountainous regions (Alexiew and Hangen 2012). According to Tatsuoka et al. (1998), they exhibit exceptional behaviour during earthquake-induced seismic loading events. Even if subjected to extreme seismic events, such structures demonstrate the ability to absorb seismic energy and act as a coherent structure, minimizing the resulting deformations (Ling et al. 2005).

Seismic hazards in Serbia

All critical infrastructure projects, including transport routes, bridges, dams, and structures of civil defence, shall be adequately designed to withstand ground shaking without collapse. The impact of seismic activity on both ultimate and serviceability states of the designed structures should be considered. In the Balkan Peninsula, as well as in Serbia, seismicity needs to be properly considered. Fig. 1 shows the gravitational acceleration for Serbia for a return period of 475 years with a probability of exceedance of 10% in 50 years (SSS 2018).

Keywords geosynthetic reinforced soil, Earthquake, Block wall, geogrid

Introduction

In the construction industry, geosynthetics are often used for the construction of embankments on soft soils, base courses, protective barriers or retaining structures. Their good performance, distinctive properties, wide range of applications and cost effectiveness are the main reasons for their use. Numerous case studies reflect their exceptional load-bearing capacity, stability and effectiveness under challenging conditions such as progressive settlement or slope deformation (Alexiew and Silva 2007; Detert and Fantini 2017).

When exposed to large ground movements (such as large settlements on compressible soils, or even larger and more abrupt movements as can occur in mining subsidence areas), reinforced earth structures are known to respond effectively (BS 8006-1:2010). The remarkable flexibility of geosynthetic retaining structures allows them to be built in very confined spaces and under challenging conditions, such as

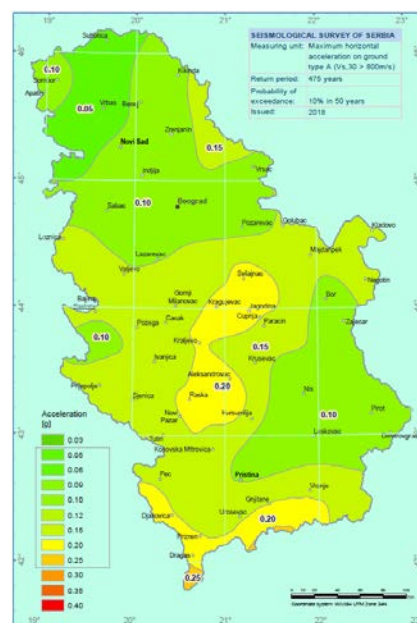


Figure 1 Seismic hazard map of Serbia showing the probability of exceedance of 10% in 50 years (Seismological Survey of Serbia 2018).

Furthermore, Fig. 2 shows the earthquake zonation in Serbia based on macroseismic intensity. As can be seen, the whole terrain of Serbia can be seismically active. However, the distribution is not uniform (SSS 2018). A comprehensive study on the seismic situation of Serbia has been done by Blagojevic et al. (2023). Blagojevic et al. (2023) have worked on the classification of residential buildings in Serbia and in the seismic areas. In this study it has been shown that for the return period of 475-year PGA values between 0.05 g to 0.25 g can be expected in Serbia depending on the region. Moreover, for the two populated cities of Belgrade and Novi Sad PGA values of 0.10-0.14 can be expected. Therefore, it can be concluded that the design of retaining structures in Serbia should be conducted with careful consideration of the related codes for seismic design.

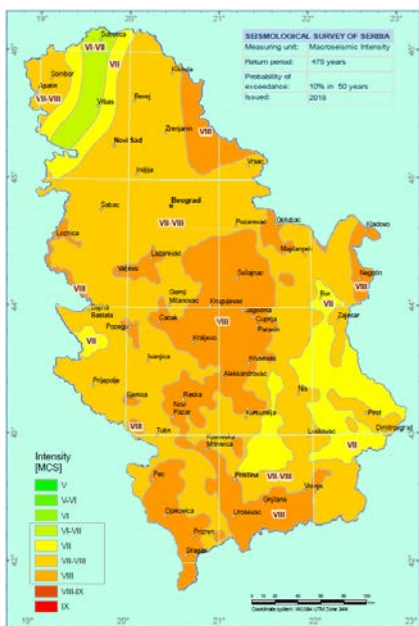


Figure 2 Seismic hazard map of Serbia showing the intensity zones (Seismological Survey of Serbia 2018).

Seismic design methods and standards

There are various methods used to design GRS structures used worldwide. Both analytical and numerical tools can be used for the design purposes. Three categories can be constructed from the existing methods:

- Pseudo-static methods (based on Mononobe-Okabe approach)
- Pseudo-Dynamic methods
- Displacement methods (based on Newmark sliding block models)

The pseudo static design approach is used in the Eurocode and in most standards dealing with seismic design. The effects of the earthquake are represented by a force applied to the structure. This force is often applied as a percentage of the gravity force. The design acceleration differs in different parts of the world and is defined by standards of national origin.

Consideration of GRS in seismic design

The conditions under which the horizontal k_h and vertical ground acceleration coefficients k_v are considered simultaneously vary around the world. Since the vertical coefficient is more important for the foundation systems, the horizontal coefficient will undoubtedly have a greater impact on the stability design of retaining structures (Detert and Russo 2019).

As with a static design, a seismic design of a GRS retaining wall must satisfy both external and internal stability requirements. Sliding, overturning (eccentricity), global stability and bearing capacity are external failure modes. Rupture, pull-out, stripping of reinforcement or failure of other structural elements such as facing are internal modes of failure.

The most relevant properties of the geosynthetic reinforcement materials used in GRS retaining structures that need be considered in a seismic design are:

- Long-term tensile strength
- Load-strain behavior Interaction with surrounding soil.

Consideration of tensile strength

The seismic action on GRS retaining walls consists of the inertial load on the wall itself, the seismic active load from the retained soil and surcharge loads. The tensile strength of the reinforcement must be sufficient to resist the tensile forces produced by seismic and static actions.

Consideration of load-strain behavior

Load-strain properties of the reinforcement are important for correct modelling since they determine the deformation behaviour of GRS (El-Emam and Bathurst 2004).

Numerical analysis data on the performance of GRS under seismic conditions indicate that, under static conditions, total wall displacements decrease with increasing reinforcement stiffness. Among other factors, foundation conditions, i.e., whether the reinforced soil system is free to slide or restricted to rotation at the toe, have a significant effect on wall displacements for structures subjected to harmonic ground motions. As the stiffness of the reinforcement increases, the effect of the toe constraint on wall displacements decreases (Bathurst and Hatami 1998).

Consideration of interaction in GRS

The interaction between the geosynthetic and the soil as well as the interaction between a reinforced soil block and the retained soil, is critical for seismic design. For cohesionless soils, it is assumed that there is no change in the peak friction angle due to seismic excitation. For internal stability analysis (facing-to-GRS), the interfacial friction angle δ is assumed to be equal to $2\phi/3$. For external stability analysis (GRS-to-retained soil) the interface friction angle is assumed to be equal to ϕ (Bathurst and Cai 1995).

As another advantage of the geogrids in the seismic situation, the flexibility of the geogrids can be named. The flexibility of geogrids allows them to deform under loading, redistributing stresses and effectively dissipating seismic forces. Detert and Lavasan (2018), investigated the interaction relevant characteristics of geosynthetics under static and dynamic loading. The authors showed that the geogrids with very high bending stiffness absorb the compaction energy and may reduce the resistance of the soil particles due to an elastic rebound from the stiff geosynthetic which consequently can cause small cavities in the compacted soil. In contrast a higher density and consequently higher shear strength can be achieved using geogrids with relatively low bending stiffness due to the higher adaptability of the geogrid between soil particles. This fact causes higher confinement effect which results in lower deformations in the structure. This matter becomes more significant in the case of the dynamic loading and in the seismic situations since the stress state, changes permanently in the system and the soil particles require a permanent confinement. In the same way the rebounding effect of stiff geogrids can be more extreme in the dynamic loading situation (Detert and Lavasan 2018).

Large-scale seismic shaking table tests

In the last years several studies on the performance of GRS retaining walls under seismic loading were carried out using shaking table technique. A series of tests were performed on a half-scale shaking table test model of a metal strip-reinforced earth wall by Chida et al. (1985). A numerical model created by Segrestin and Bastick (1988) using finite element modelling (FEM) showed good agreement with the findings of Chida et al. (1985). The results of shaking table testing on a reinforced embankment confined by two 2.5 m high walls made of gabion baskets and an outer continuous concrete panel were published by Murata et al. in 1994. Sakaguchi (1996) tested a 1.5-meter-tall model of a reinforced wall on a shaking table (Hatami and Bathurst 1998). Seven reduced-scale GRS models were investigated by Cubrinovski, Bowman and Jackson under seismic excitation using the University of Canterbury shake-table (2010). As part of TRB's National Cooperative Highway Research Program (2012), a large-scale shake table test was conducted to investigate the performance of a GRS-supported bridge abutment.

Although, the test programmes mentioned above confirm the favourable findings by Tatsuoka et al. (1998), the small number of experimental and numerical studies, the limited nature of each study, and the wide range of results do not allow for a precise quantification of the seismic response of GRS retaining structures.

Full Scale Seismic Testing by Ling et al.

In 2003, the University of Columbia conducted full-scale seismic testing of a block wall reinforced with woven PET geogrids to assess its performance in heavy seismic loads.

The testing aimed to analyze the internal and external behavior, evaluate the frictional bond between geogrid and concrete blocks, and compare actual behavior and loads with design predictions (Ling et al. 2005). Three 2.8 m high retaining walls were tested using fine sand as the backfill material and two types of woven geogrid with different tensile strengths and made of different raw materials. The hollow core concrete blocks used weighed 34 kg each and were 200 mm high, 300 mm deep, and 450 mm wide. The detail of the connection between the Allan Blocks and the Huesker geogrid is shown in Fig. 3.



Figure 3 Blocks to geogrids connection detail (Ling et al., 2005).

Three tests were carried out using horizontal and vertical excitations with different peak accelerations. The peak was scaled to 0.4g in the first shaking and 0.8g in the second. The results showed that the block wall system with woven geogrid reinforcement performed effectively under seismic conditions.

Settlement was detected after the second excitation and reducing the vertical space between geogrid layers from 60 cm to 40 cm greatly reduced settlement. Horizontal displacement was less than 10 mm after the first stimulus, but was greater during the second stimulus, with test walls 1, 2, and 3 being displaced by a maximum of 100 mm, approximately 80 mm, and slightly less than 80 mm, respectively. The horizontal displacements induced in test 1 are shown in Fig. 4.

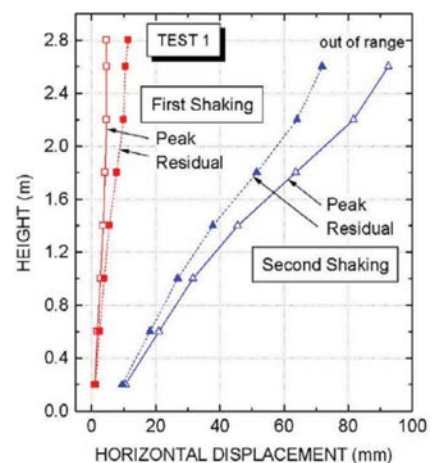


Figure 4 Horizontal displacements at Test 1 (Ling et al., 2005).

Even at very high seismic accelerations of around 0.8g, none of the three walls failed. With a vertical acceleration of 50% of the horizontal acceleration in test 3, no failure occurred. It was found that a closer spacing of the geogrid layer significantly improved the deformation behaviour of the wall. At a maximum acceleration of 0.4g,

the measured deformation was insignificant. At a significant acceleration of 0.8g, good performance was still recorded. No collapse of the frictional bond between the blocks and the geogrid layers was observed during the test.

Case study in seismically active regions

Many GRS retaining walls, steep slopes and bridge abutments have been built in recent years in seismic regions, e.g., on the Balkan Peninsula. Due to the high attractiveness of these structures in terms of construction speed and cost, adaptability, low environmental impact, excellent performance under seismic loads, etc., their number is constantly increasing.

One of the most recent projects in the Balkan Peninsula is the Vlora bypass in Albania. It is part of the Adriatic-Ionian Highway and is one of the most important national infrastructure projects in Albania. Its purpose is to improve the flow of traffic along the Ionian coast for travelers and tourists heading for the Riviera. The project consists of 29 km of dual carriageway, including 5 bridges, 2 underpasses, 15 interchanges and 3.6 km of retaining walls, most of which were constructed using GRS. An overview of one of the sections with GRS is shown in Fig. 5.

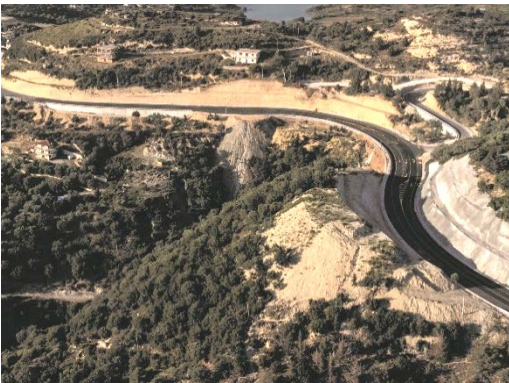


Figure 5 Overview of one of the GRS sections (WBIF, www.wbif.eu).

The site extends over mountainous terrain and is characterized by complex topography with steep irregular slopes, challenging geological and hydrological conditions and a lack of access for construction. There is also a high level of seismic activity in the area. With PGA values of 0.2g and a 475-year return period, a seismic design had to be carried out alongside the static design (Pagani et al. 2018).

Due to the specific topography of the site, with steep mountain slopes, all the retaining structures had to be constructed in a very confined space, with little access for the delivery of materials and construction equipment. Some slopes had to be cut and excavated, while other parts of the designed road had to be backfilled. GRS retaining walls were used to maintain the required geometry, retain soil masses, and ensure the stability of the road structures. Fig. 6 shows some of the cut and fill sections of the road.



Figure 6 Cut and fill sections (TIRANA post, www.tiranapost.al).

Fortrac Natur facing system, developed by Huesker, was used because it allows the GRS retaining walls to be constructed quickly and cost-effectively. The system consists of the following components:

- Flexible geogrids for reinforcement, i.e., to provide tensile strength and improve the stability and serviceability of the wall
- Soil as fill material
- Erosion protection grids or mats to protect the fill from erosion
- Temporary frontal formwork made of bended steel mesh with bracing bars to facilitate installation of the geogrids

Fig. 7 shows a typical cross-section detail of Fortrac Natur facing system.

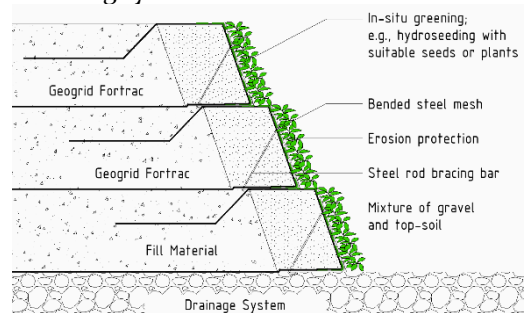


Figure 7 Fortrac Natur facing system detail (Huesker).

The slope to the vertical of the facing was set at 70°. The flexibility of the GRS solution allowed elements such as concrete culverts or bridge abutments to be easily integrated into the retaining walls. One of the GRS retaining walls is shown in Fig. 8.



Figure 8 GRS retaining wall (Huesker).

The GRS retaining walls were designed in accordance with the requirements of Eurocode 7 (EN 1997-1:2004) and Eurocode 8 (EN 1998-1:2004, EN 1998-5:2004)

using the partial safety factor approach. Both static (permanent) and seismic design situations were analysed. Internal, compound and external (global) stability were estimated using the Bishop circular slice method (Fig. 9) and the vertical slice method, which analyses polygonal slip planes similar to the Janbu approach, but taking into account the shear resistance between the blocks. Bearing capacity, sliding, and overturning checks were also carried out.

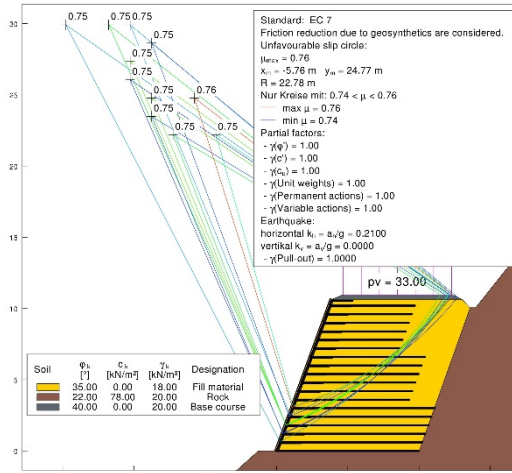


Figure 9 Stability analysis, Bishop method (Huesker).

Coefficient of horizontal acceleration for internal forces k_h was estimated to be equal to 0.21. The calculation was carried out according to §4.1.3.3 of EN 1998-5:2004 for a PGA value of 0.3g, an importance factor of 1.4 (importance class IV, Table 4.3 EN 1998-5:2004) and a soil factor of 1.0 (ground type A, Table 3.2 EN 1998-5:2004).

A large part of the project (approx. 85%) was successfully completed in 2021 and 2022. The simplicity and low equipment requirements of the GRS principle allowed the retaining walls to be constructed quickly, facilitating access to other road sections or structures.

As another example of the constructed projects in the Balkan Peninsula, the geogrid retaining structure within the Sofia ring road project can be named. The Sofia ring road surrounds the Sofia city and has a total length of 61.8 km and is divided into four arcs (subsections). Some arcs of the road have been upgraded in the last years and several subsections need to be still improved. The purpose of the road is to improve the traffic flow between different parts of the city. The project consists of dual carriageway, including bridges, underpasses, interchanges and retaining walls, constructed using GRS retaining walls. The retaining structure was constructed using Fortrac block facing.

In May 2012 an earthquake occurred in Sofia with an intensity of Mw5.6. The earthquake was felt in entire Bulgaria and the neighboring countries. The earthquake had no casualties but several moderate damages to some building in Sofia and the cities around it were reported (Rykova et al. 2017). Investigation after the earthquake have shown that no damage occurred in the GRS retaining structure or its facing (Fig. 10).



Figure 10 Fortrac Block GRS retaining wall in Sofia ring road project after earthquake in 2012 (Huesker).

Conclusion

Both experience and research results indicate that GRS retaining walls have excellent performance under seismic conditions. Although there are many different approaches to the seismic design of GRS retaining walls, a sound and safe design is possible. Conducted shaking table and numerical studies have shown high stability and low deformation of these structures even when significant ground motions are applied, e.g., in the case of the simulated Kobe earthquake. The application of GRS principles to the construction of retaining walls offers high feasibility in challenging conditions, including the potential for high seismic effects or complex environments, e.g., mountainous regions or limited space. Furthermore, the flexibility of the geogrid which provides a good soil-geogrid interaction can support higher confinement of the compacted soil particles which causes lower deformations. This fact also plays an important role in the stability of the GRS retaining structures in seismic area.

Acknowledgement



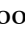







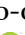

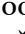











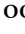
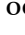

















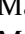
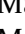



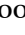






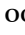


The authors like to thank all the associates, including the investor, consultants, and contractors, for their exceptional and professional cooperation throughout all project phases.





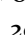







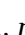






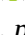



References

Alexiew, D., Silva, A. E. F., (2007). Load tests on a 1:1 model of a geogrid-reinforced bridge abutment. Darmstadt Geotechnics, No. 15, Proc. 14th Darmstadt Geotechnical Conference, Darmstadt, Germany.
 Bathurst, R., Hatami, K., (1998). Seismic Response Analysis of a Geosynthetic-Reinforced Soil Retaining Wall. Geosynthetics International, Vol. 5, Nos. 1-2, pp. 127-166.
 Blagojević, N., Brzev, S., Petrović, M., Borozan, J., Bulajić, B., Marinković, M., Hadzima-Nyarko, M., Koković, V., Stojadinović, B., (2023). Residential building stock in Serbia: classification and vulnerability for seismic risk studies, Bulletin of Earthquake Engineering, pp. 4315-4383.

- BS 8006-1 (2010). Code of practise for strengthened/reinforced soils and other fills. British Standards Institution, United Kingdom.
- Chida, S., Minami, K., Adachi, K., 1985. Tests with Regard to the Stability of the Fill Constructed by the Reinforced Earth Technique (unpublished report translated from Japanese).
- Detert, O., Fantini, P., (2017). High geogrid-reinforced slopes as flexible solution for problematic steep terrain: Trieben-Sunk project, Austria. Proc. 4th World Landslide Forum (WLF), Ljubljana, Slovenia.
- Detert, O., Lavasan, A., (2018). Relevant properties of geosynthetic reinforcements on the interaction behavior under static and cyclic load conditions. Proceedings of the 11th International Conference on Geosynthetics, Seoul, Korea.
- El-Emam, M., Bathurst, R., (2004). Experimental Design, Instrumentation and Interpretation of Reinforced Soil Wall Response Using a Shaking Table. International journal of Physical Modelling in Geotechnics, pp. 13-32.
- EN 1997-1 (2004). Eurocode 7: Geotechnical design – Part 1: General rules. CEN, Brussels, Belgium.
- EN 1998-1 (2004). Eurocode 8: Design of structures for earthquake resistance – Part 1: General rules, seismic actions and rules for buildings. CEN, Brussels, Belgium.
- EN 1998-5 (2004). Eurocode 8: Design of structures for earthquake resistance – Part 5: Foundations, retaining structures and geotechnical aspects. CEN, Brussels, Belgium.
- Fundo, A., Duni, L., Kuka, Sh., Begu, E., Kuka, N., (2012). Probabilistic seismic hazard assessment of Albania. Acta Geodaetica et Geophysica Hungarica.
- Homepage - European Union and the Western Balkans. (n.d.). Retrieved January 30, (2023), from <https://www.wbif.eu>.
- Homepage - Seismological Survey of Serbia. Interactive seismic hazard map of Serbia https://www.seismo.gov.rs/Seizmichnost/Karte_hazarda_e.htm
- Jackson P., (2010). An experimental study on geosynthetic reinforced soil walls under seismic loading. ME Thesis, University of Canterbury, Christchurch, New Zealand.
- Ling, H., Asce, M., Mohri, Y., Leshchinsky, D., Burke, C., Asce, A., Matsushima, K., Huabei, L., (2005). Large-Scale Shaking Table Tests on Modular-Block Reinforced Soil Retaining Walls. Journal of Geotechnical and Geoenvironmental Engineering.
- Pagani, M., Garcia-Pelaez, J., Gee, R., Johnson, K., Poggi, V., Styron, R., Weatherill, G., Simionato, M., Viganò, D., Danciu, L., Monelli, L., (2018). Global Earthquake Model (GEM) Seismic Hazard Map.
- Rykova, P., Solakov, D., Slavcheva, K., Simeonova, S., Aleksandrova, I., (2017). The 2012 Mw5.6 earthquake in Sofia seismogenic zone – is it a slow earthquake, EGU General Assembly, Vol 19.
- Segrestin, P., Bastick, M., (1988). Seismic Design of Reinforced Earth Retaining Walls - the Contribution of Finite Element Analysis, Theory and Practice of Earth Reinforcement, Proceedings of the International Geotechnical Symposium on Theory and Practice of Earth Reinforcement, Fukuoka, Kyushu, Japan, pp. 577-582.
- Sakaguchi, M., (1996). A Study of the Seismic Behavior of Geosynthetic-Reinforced Walls in Japan. Geosynthetics International, Vol. 3, No. 1, pp. 13-30.
- Tatsuoka, F., Koseki, J., Tateyama, M., Munaf, Y., Horii, N., (1998). Seismic stability against high seismic loads of geosynthetic-reinforced soil retaining structures. Keynote Lecture, Proc. 6th Int. Conf. on Geosynthetics, Atlanta, USA. Vol. 1, pp. 103–142.
- TRB's National Cooperative Highway Research Program (NCHRP) Web-Only Document 187, (2012). Seismic Design of Geosynthetic-Reinforced Soil Bridge Abutments with Modular Block Facing
- TiranaPost, (2022), 5 December: View from the Vlora Bypass that opens this tourist season. Aktualitet. Retrieved January 30, (2023), from <https://tiranapost.al/english/aktualitet/pamje-nga-bypass-i-i-vlores-qe-hapet-kete-sezon-turistik-i514659>
- Website, www.tiranapost.al [Last accessed: 02.02.2024]

AUTHOR INDEX

- Abolmasov B.  0000-0002-5439-2893, *pg. 231, 309*
 Aleksić D., *pg. 121*
 Amin Khalili M.  0000-0001-9671-761X, *pg. 107*
 Andreevska N. M., *pg. 157*
 Andrejev K., *pg. 297*
 Apostolidis E., *pg. 193*
 Arbanas Ž.  0000-0002-5736-6746, *pg. 73, 219, 225*
 Babović N., *pg. 121*
 Bajović A., *pg. 203*
 Bakrač M., *pg. 315, 321*
 Bar N.  0000-0001-7948-2468, *pg. 89*
 Begović N., *pg. 203*
 Benac Č.  0000-0002-2961-5485, *pg. 259*
 Bernat Gazibara  0000-0002-5530-4381, *pg. 99, 143, 149, 213, 253*
 Bojadjieva J.  0000-0003-4047-7500, *pg. 175*
 Bordbar E., *pg. 321*
 Borrelli L.  0000-0003-2833-788X, *pg. 1, 169*
 Bufeov F., *pg. 243*
 Calcaterra D.  0000-0002-1407-9368, *pg. 107*
 Capparelli G.  0000-0003-3324-8224, *pg. 187*
 Chatzitheodosiou T., *pg. 283*
 Čeh N.  0000-0003-4903-9769, *pg. 73, 219*
 Di Martire D.  0000-0003-0046-9530, *pg. 107*
 Di Muro C.  0009-0008-4692-4651, *pg. 107*
 Dugonjić Jovančević S.  0000-0002-0242-7409, *pg. 259*
 Đurić U.  0000-0002-1171-8419, *pg. 291*
 Edip K.  0000-0003-3394-510X, *pg. 175*
 Farmakis I.  0000-0001-7066-7845, *pg. 283*
 Ferlisi S.  0000-0003-0500-3369, *pg. 1, 169*
 Filipović V., *pg. 277*
 Fiorucci F.  0000-0003-0570-8297, *pg. 99*
 Fornaro G.  0000-0002-1679-607X, *pg. 1, 169*
 Garaeva A., *pg. 243*
 Gjorgiev G., *pg. 55, 157*
 Gorobtsov D.  0000-0002-1232-6652, *pg. 239*
 Gudoshnikov K., *pg. 243*
 Guerriero L.  0000-0002-5837-5409, *pg. 107*
 Gullà G.  0000-0003-1165-4782, *pg. 1, 169*
 Hasslacher T., *pg. 321*
 Hoxha N., *pg. 203*
 Ivanovski I., *pg. 127*
 Jaboyedoff M.  0000-0002-6419-695X, *pg. 9*
 Jagodnik P.  0000-0002-0056-2076, *pg. 99, 149*
 Jagodnik V.  0000-0003-1331-8002, *pg. 219, 225*
 Janevski B.  0000-0002-3767-5840, *pg. 37*
 Janković M., *pg. 315*
 Jemec Auflič M.  0000-0002-3642-6092, *pg. 199*
 Jež J.  0000-0002-1438-6480, *pg. 199*
 Jocković S.  0000-0002-3896-4791, *pg. 291*
 Josifovski J.  0000-0001-9771-8331, *pg. 271*
 Jovanović L., *pg. 309*
 Jovanovski M.  0000-0002-6261-3721, *pg. 37, 55, 127, 157*
 Kandić M., *pg. 277*
 Katić J., *pg. 213*
 Kavoura K.  0000-0002-0736-3803, *pg. 193*
 Kitanović O.  0000-0002-7571-2729, *pg. 181*
 Kokkali P., *pg. 193*
 Korolev A., *pg. 243*
 Krautblatter M.  0000-0002-2775-2742, *pg. 207*
 Kričak L., *pg. 303*
 Krkač M.  0000-0002-0232-3394, *pg. 143, 149, 213*
 Kumelj Š.  0000-0003-1618-9736, *pg. 199*
 Lapčević V.  0000-0003-2338-1718, *pg. 81*
 Latypov A.  0000-0001-9584-4676, *pg. 243*
 Loche M.  0000-0002-0756-2175, *pg. 247*
 Luigi Gariano S.  0000-0002-1605-7701, *pg. 19*
 Lukačić H.  0000-0002-5079-932X, *pg. 143, 149, 213*
 Luongo D.  0009-0005-6735-991X, *pg. 1, 169*
 Maglić L.  0000-0002-7923-0938, *pg. 259*
 Marinos V.  0000-0001-7575-7006, *pg. 283*
 Marjanović M.  0000-0002-9675-1401, *pg. 181, 203, 231, 297, 303*
 Marjanović M. S.  0000-0002-7968-3873, *pg. 291*
 Marušić D.  0000-0002-8775-677X, *pg. 163, 219*
 Micić K.  0000-0002-4101-4412, *pg. 231, 291*
 Mihalić Arbanas S.  0000-0003-4036-3722, *pg. 143, 149, 213, 253*
 Miladinović A., *pg. 121*
 Milanović S.  0000-0003-4761-8716, *pg. 303*
 Milinković A., *pg. 133*
 Naumov M., *pg. 239*
 Nedelkovska N., *pg. 55, 127, 157*
 Nicodemo G.  0000-0002-3512-8405, *pg. 1, 169*
 Nikolovska Atanasovska A.  0000-0002-3387-1158, *pg. 271*
 Nikolovski D., *pg. 175*
 Nikolovski T., *pg. 127*
 Novak A.  0000-0001-9859-0413, *pg. 199*
 Onder Cetin K.  0000-0003-0540-2247, *pg. 27*
 Papouli D., *pg. 283*
 Peduto D.  0000-0003-3435-642X, *pg. 1, 55, 169*
 Pejić M.  0000-0002-6367-6943, *pg. 47*
 Peranić J.  0000-0002-2574-6349, *pg. 73, 219, 225*

- Peshevski I.  0000-0002-2748-5795, *pg. 37, 55, 127, 157*
- Peternel T.  0000-0003-4280-6953, *pg. 199*
- Petrov G.  0009-0005-8278-0710, *pg. 127*
- Petrović R.  0009-0006-7979-3569, *pg. 297*
- Poberezhnyi V., *pg. 321*
- Prountzopoulos G., *pg. 283*
- Pujević V.  0000-0001-8417-9594, *pg. 291*
- Radić Z., *pg. 291*
- Raković M.  0000-0001-9670-1677, *pg. 291*
- Ramondini M.  0000-0003-0671-965X, *pg. 107*
- Reale D.  0000-0001-7027-5227, *pg. 1, 169*
- Reichenbach P.  0000-0003-0787-4459, *pg. 253*
- Rossi M.  0000-0002-0252-4321, *pg. 143, 149, 253*
- Salčin N.  0009-0002-3884-616X, *pg. 115*
- Salic Makreska R.  0000-0003-3571-1139, *pg. 175*
- Sandić C.  0000-0002-8858-0526, *pg. 139*
- Santangelo M.  0000-0003-1299-9192, *pg. 99*
- Scaringi G.  0000-0003-3505-7456, *pg. 247*
- Setiawan H.  0000-0003-2048-2791, *pg. 225*
- Shubina D.  0000-0003-2161-2500, *pg. 239*
- Simić N.  0000-0002-7823-5868, *pg. 303*
- Sinčić M.  0000-0003-4252-3523, *pg. 143, 149*
- Slavković D., *pg. 277*
- Spanou N., *pg. 193*
- Spina D., *pg. 187*
- Stanić N., *pg. 265*
- Stefanović I., *pg. 277*
- Stepanović G., *pg. 133*
- Stevanović I., *pg. 203*
- Stoumpos G., *pg. 283*
- Šegina E.  0009-0001-4433-4171, *pg. 199*
- Škuflić R., *pg. 73*
- Thomaidis T., *pg. 283*
- Todorović S., *pg. 181*
- Token A., *pg. 265*
- Torbica S., *pg. 81*
- Tornjanski I., *pg. 265*
- Turk D., *pg. 199*
- Umut Ayhan B.  0000-0002-1000-1678, *pg. 27*
- Versace P., *pg. 187*
- Vivoda Prodan M.  0000-0003-0464-2687, *pg. 73, 219, 225, 259*
- Vučković D., *pg. 203*
- Vujadinović Mandić M.  0000-0001-9583-5067, *pg. 65*
- Yunatci A., *pg. 27*